SEPTEMBER 1977

analytical chemistry

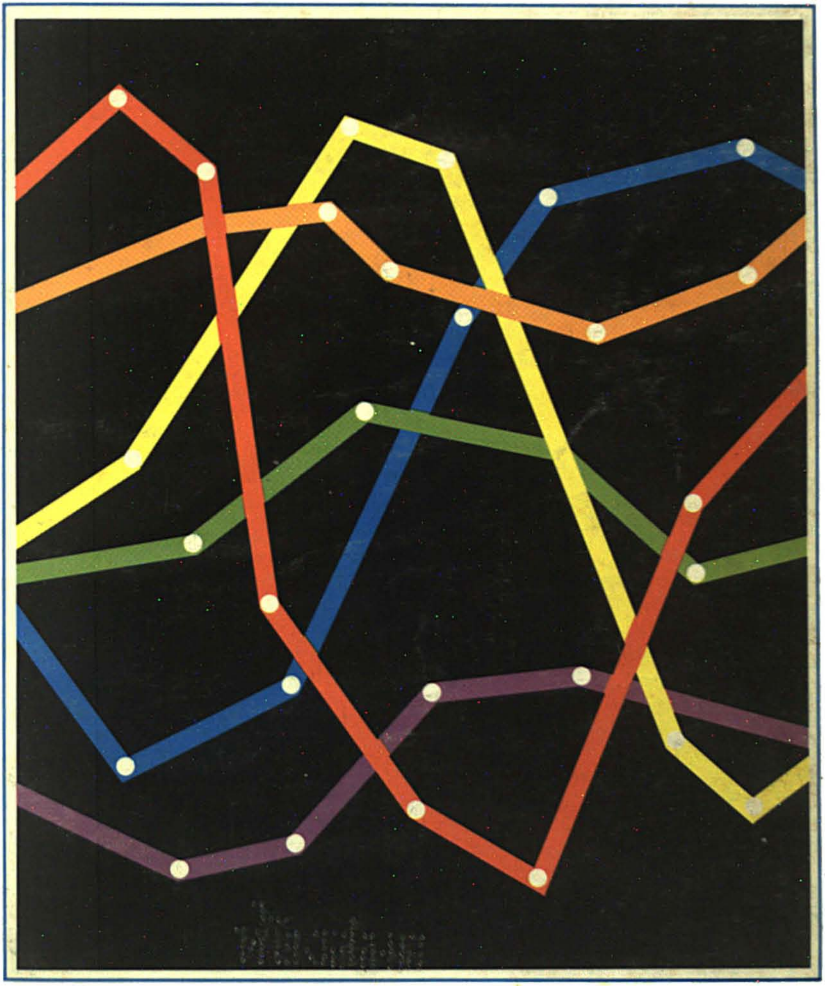

Digital Analysis of Spectra

KMX-6 APPLICATION #5

KMX-6+Hi-Temp GPC= Absolute MW of Polyolefins

A new KMX-6 heated sample cell accessory makes possible the coupling of a high temperature gel permeation chromatograph with the KMX-6 Light Scattering Photometer to provide rapid direct measurement of absolute molecular weight and molecular weight distributions of polyolefins. This technique eliminates the problems of GPC column calibration and variations in column retention characteristics.

Molecular weight parameters are calculated from the solute excess Rayleigh factor (a function of the intensity of the scattered light as measured by the KMX-6) and the solute concentration (as measured by an infrared detector or other hi-temp GPC detector).

Diagrammed at right is an analysis performed in cooperation with Dr. T. B. MacRury (Union Carbide Technical Center, South Charleston, W. VA), of NBS 1484, a high density polyethylene. Measurements were performed in 1, 2, 4-trichlorobenzene at 135°C.

The calculated value for the weight-average molecular weight is 109,000 and the number-average molecular weight is 99,000. The NBS value for the weight-average molecular weight is 119,600 ±13,000 and the number-average molecular weight is 100,500 ±4,000.

In addition to the high temperature capability described here, a low dead-volume test cell is available for measurements at ambient temperatures. For complete information on this and other KMX-6 applications, call or write Chromatix.

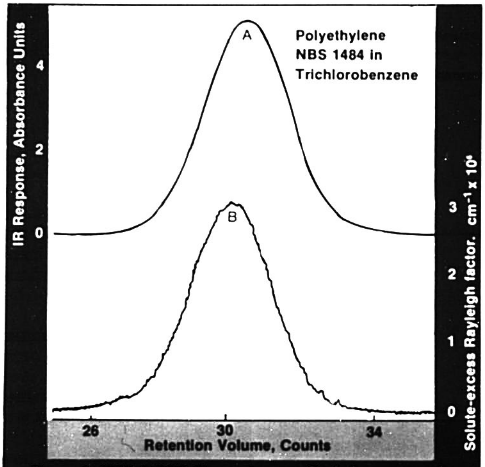

Figure 1. KMX-6/GPC Chromatogram. Peak A corresponds to IR detector response; Peak B to KMX-6 response for 3.87 mg of NBS 1484 polyethylene.

chromatix

1145 Terra Bella Avenue
Mountain View, CA 94043
Phone (415) 969-1070
Telex 910-379-6440

D6903 Neckargemund 2
Unterestrasse 45a
West Germany
Phone: (06223) 7061/62
Telex: 461691

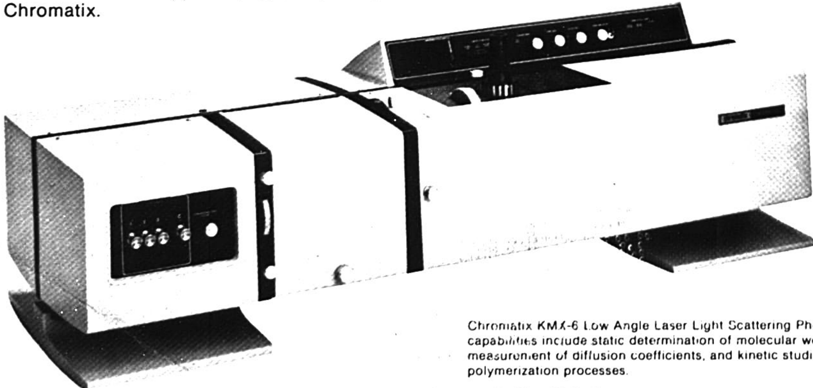

Chromatix KMX-6 Low Angle Laser Light Scattering Photometer. Other capabilities include static determination of molecular weight, measurement of diffusion coefficients, and kinetic studies of polymerization processes.

CIRCLE 34 ON READER SERVICE CARD

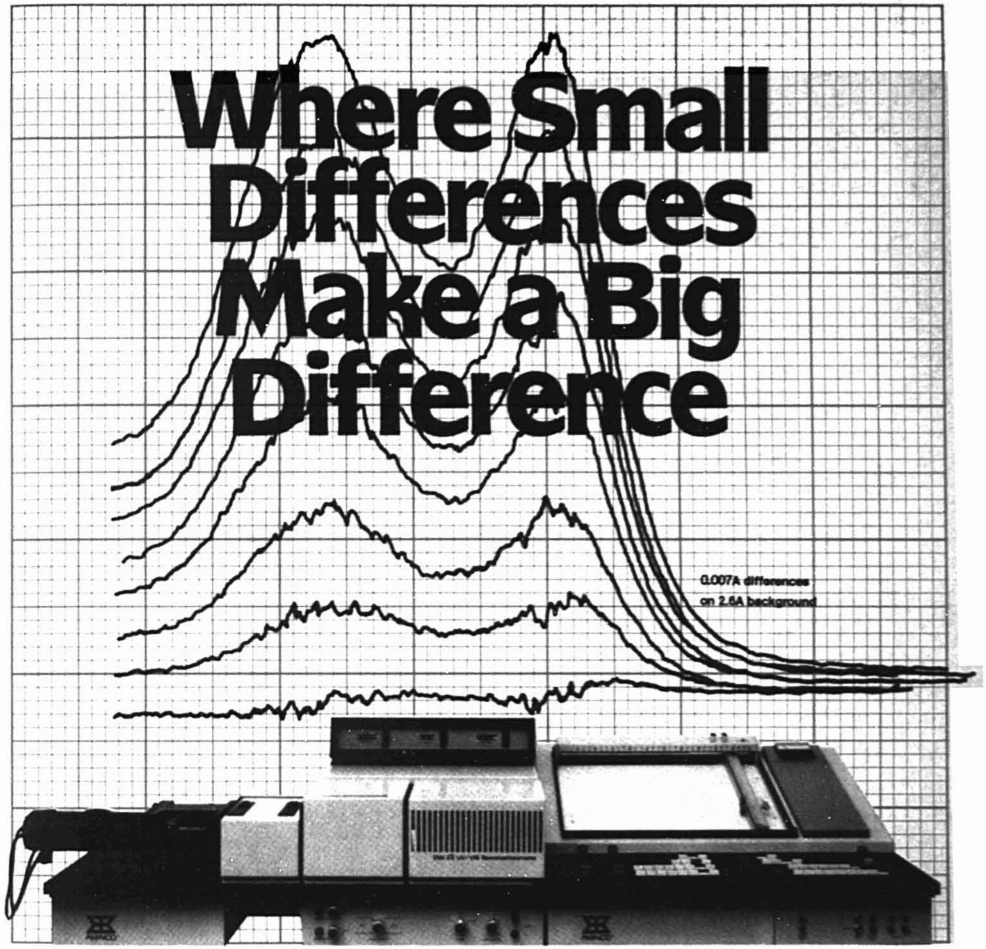
Where Small Differences Make a Big Difference
0.007A differences on 2.6A background

The DW-2a™ UV-VIS Spectrophotometer Extends the Range of Sample Investigations!

With our new DW-2a spectrophotometer, small differences can lead to new research territories in UV-VIS spectrophotometry. The reason? Our painstaking improvements in such parameters as photometric accuracy, stability, and system versatility lead to substantial increases in overall system performance. Now, you can reliably record and reproduce absorbance differences as small as 0.0005A, even with extremely concentrated samples. This means that trace components can be easily detected in near-opaque samples.

And consider that Aminco offers one of the largest selections of compatible and convenient accessories for UV-VIS research. With this comprehensive system, you can extend the range of sample investigations to include extremely turbid samples, frozen samples, solids, anaerobic samples, fluorescing samples and many others.

For more information on the Aminco DW-2a Spectrophotometer, contact American Instrument Company, 8030 Georgia Avenue, Silver Spring, MD 20910. Phone: (301) 589-1727.

Write for your free copy of "Selected Applications for the DW-2®/DW-2a™ Spectrophotometer"—over 500 references listed.

AMINCO®
DIVISION OF TRAVENOL LABORATORIES, INC.

© 1977, Travenol Laboratories, Inc.

Circle No. 7 For more information

Circle No. 8 To have sales representative call

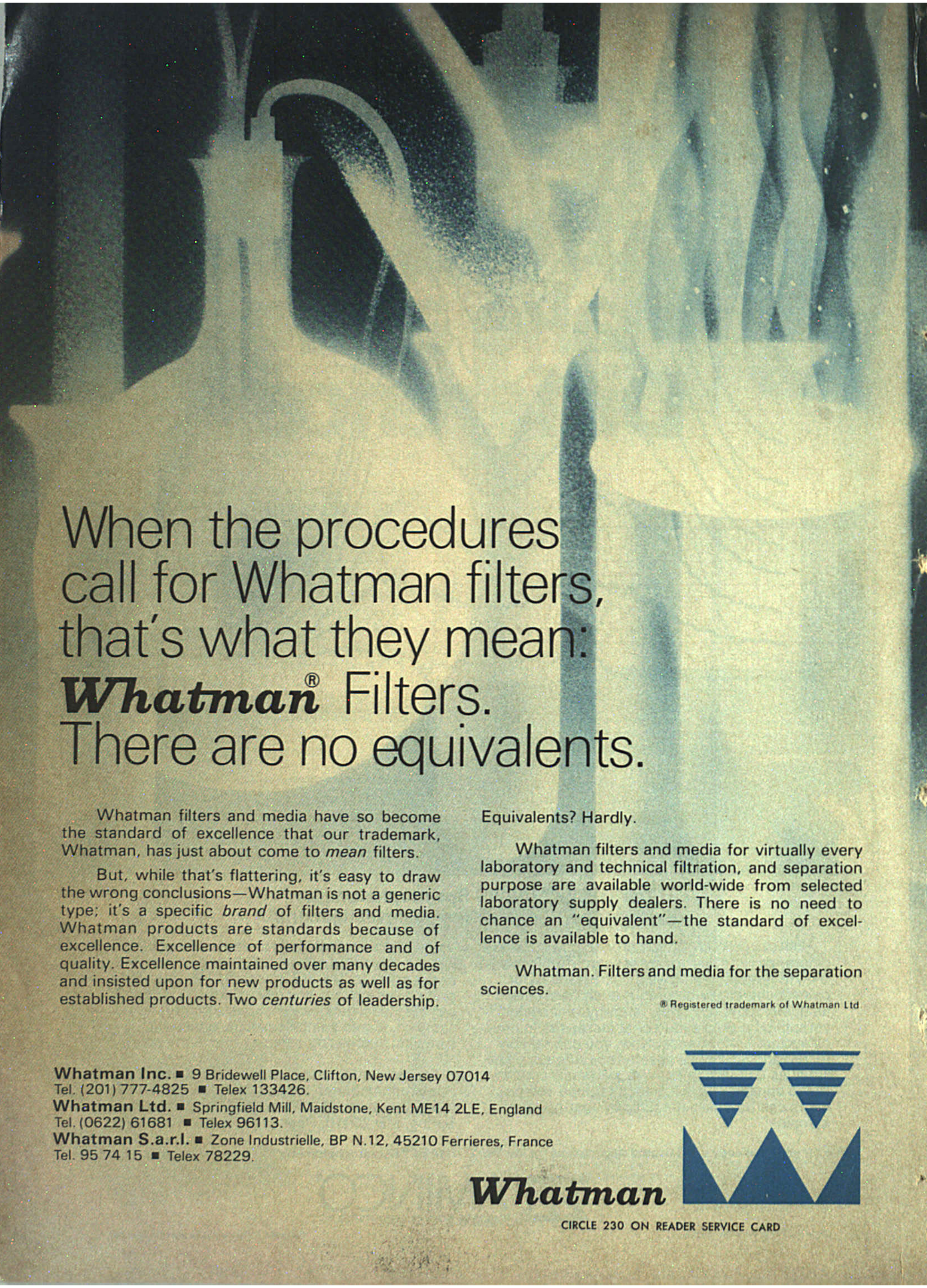

When the procedures call for Whatman filters, that's what they mean: **Whatman**® Filters. There are no equivalents.

Whatman filters and media have so become the standard of excellence that our trademark, Whatman, has just about come to *mean* filters.

But, while that's flattering, it's easy to draw the wrong conclusions—Whatman is not a generic type; it's a specific *brand* of filters and media. Whatman products are standards because of excellence. Excellence of performance and of quality. Excellence maintained over many decades and insisted upon for new products as well as for established products. Two *centuries* of leadership.

Equivalents? Hardly.

Whatman filters and media for virtually every laboratory and technical filtration, and separation purpose are available world-wide from selected laboratory supply dealers. There is no need to chance an "equivalent"—the standard of excellence is available to hand.

Whatman. Filters and media for the separation sciences.

® Registered trademark of Whatman Ltd

Whatman Inc. ■ 9 Bridewell Place, Clifton, New Jersey 07014
Tel. (201) 777-4825 ■ Telex 133426.
Whatman Ltd. ■ Springfield Mill, Maidstone, Kent ME14 2LE, England
Tel. (0622) 61681 ■ Telex 96113.
Whatman S.a.r.l. ■ Zone Industrielle, BP N.12, 45210 Ferrieres, France
Tel. 95 74 15 ■ Telex 78229.

Whatman

CIRCLE 230 ON READER SERVICE CARD

Volume 49, No. 11, September 1977
ANCHAM
49(11) 843A–964A/1473–1648 (1977)
ISSN 0003-2700

analytical chemistry

© Copyright 1977
by the American Chemical Society

No part of this publication may be reproduced in any form without written permission from the American Chemical Society

Published monthly with review issue added in April and Laboratory Guide in August by the American Chemical Society, from 20th and Northampton Sts., Easton, Pa. 18042. Executive and Editorial headquarters, American Chemical Society, 1155 16th St., N.W., Washington, D.C. 20036 (202) 872-4600. Second class postage paid at Washington, D.C., and at additional mailing offices.

1977 Subscription rates—including surface postage

	1 yr	2 yr	3 yr
MEMBERS:			
Domestic	$ 9.00	$16.00	$22.00
PUAS	17.00	32.00	46.00
Canada, Foreign	18.00	34.00	49.00
NONMEMBERS:			
Domestic	12.00	21.00	29.00
Canada	21.00	39.00	56.00
PUAS	23.00	43.50	64.00
Foreign	24.00	45.50	67.00

Airmail and air freight rates are available from Membership & Subscription Services, ACS, P.O. 3337, Columbus, Ohio 43210, (614) 421-7230.

New and renewal subscriptions should be sent with payment to the Office of the Controller at the ACS Washington address.

Subscription service inquiries and changes of address (include both old and new addresses with ZIP code and *recent mailing label*) should be directed to the ACS Columbus address noted above. Please allow six weeks for change of address to become effective.

Claims for missing numbers will not be allowed if loss was due to failure of notice of change of address to be received in the specified time: if claim is dated (a) North America: more than 90 days beyond issue date, (b) all other more than one year beyond issue date; or if the reason given is "missing from files"

Microfiche subscriptions, one year only, are available at the same rates but are mailed first class domestic and airmail foreign.

Microfiche subscriptions, for inquiries and payments
Single issues, current year, $2.50 except review issue, $4.00
Back issues and volumes
Microfilm editions from Vol. 1 to present

Write or call

Special Issues Sales
American Chemical Society
1155 16th St., N.W.
Washington, D.C.
20036
202-872-4364

Advertising Management: Centcom, Ltd., 25 Sylvan Road South, Westport, Conn. 06880 (203) 226-7131

CONTENTS

REPORT

The methods currently available for analysis of spectra recorded in digital form are summarized by D. E. Metzler, C. M. Harris, R. L. Reeves, W. H. Lawton, and M. S. Maggio **864 A**

INSTRUMENTATION

R. G. Griffin presents three approaches for obtaining high resolution NMR spectra in solids and considers how useful information can be obtained from these spectra **951 A**

THE ANALYTICAL APPROACH

M. G. Heydanek describes the analytical approach taken in tracing the origin of an off-flavor found during quality assurance examination of a breakfast cereal **901 A**

LETTERS

An INSTRUMENTATION article on microscopes and an editorial on single atom detection are amplified **858 A**

NEWS

Technical programs for the ORNL Conference on Analytical Chemistry, the 12th International Symposium on Advances in Chromatography, and the 91st Annual Meeting of AOAC are listed. The celebration marking the installation of Du Pont's 1000th automatic clinical analyzer is discussed in Analytical Chemistry at Work **879 A**

BOOKS

Books on luminescence, thermal analysis, and minicomputers are reviewed by R. J. Hurtubise, Bernhard Wunderlich, and S. P. Perone **931 A**

EDITORS' COLUMN

Data gathered from a survey on the peer review process have been analyzed for NSF. Results of this analysis are given **945 A**

EDITORIAL

Meetings in the USA would benefit from increased participation by foreign scientists. Thoughts on the mechanism for such participation are presented **1473**

Technical Contents/Briefs **846 A**
Author Index **IBC**
Future Articles **IBC**
Meetings **886 A**
Short Courses **894 A**
New Products **910 A**
Chemicals **918 A**
Manufacturers' Literature **923 A**

Our cover illustrates this month's REPORT, *"Digital Analysis of Electronic Absorption Spectra". Cover artist: Sharon Harris*

ห้องสมุด กรมวิทยาศาสตร์
11.พ.ย.2520

Briefs

Spectroscopic System for the Study of Fluorescent Lanthanide Probe Ions in Solids 1474

A laser spectroscopic system is developed to enable the use of lanthanide probe ions for detailed fundamental studies of defects in solids and for qualitative and quantitative determinations of trace ion concentrations.

Marvin P. Miller, David R. Tallant, Frederick J. Gustafson, and John C. Wright,* Department of Chemistry, University of Wisconsin, Madison, Wis. 53706 *Anal. Chem., 49 (1977)*

Determination of Porphyrins at Low Concentration Using Porphinatocopper(II) Phosphorescence 1482

The method, which determines concentration of free porphyrins by phosphorescence of the copper(II) complex, is intended for use in accurate biomedical studies rather than as a screening technique.

David K. Lavallee* and James Andrew, Department of Chemistry, Colorado State University, Fort Collins, Colo. 80523 *Anal. Chem., 49 (1977)*

Multielement Trace Analysis of Geological Materials with Solvent Extraction and Flame Atomic Absorption Spectrometry 1485

The development of a precise analytical method is reported for the determination of Cu, Ni, Co, Cr, Ag, Pb, Bi, Cd, Zn, Mn, Au, Tl, Sb, Ga, and Mo in geological materials with limits of detection better than 0.5 ppm.

P. Hannaker and T. C. Hughes,* Department of Geology, School of Earth Sciences, University of Melbourne, Parkville, Victoria 3052, Australia *Anal. Chem., 49 (1977)*

Enhancement of Emission by Potassium Chloride in the Low-Pressure Microwave-Induced Plasma Emission Spectrometer 1489

Potassium chloride, added to microvolume samples, enhances the emission lines of many elements excited in the low-pressure microwave-induced plasma emission spectrometer.

Ikuo Atsuya, Hiroshi Kawaguchi, Claude Veillon, and Bert L. Vallee,* Biophysics Research Laboratory, Department of Biological Chemistry, Harvard Medical School, and the Division of Medical Biology, Peter Bent Brigham Hospital, Boston, Mass. 02115 *Anal. Chem., 49 (1977)*

Determination of Phosphorus in Milk Powders by Optical Emission Spectrometry with a High Frequency Inductively-Coupled Argon Plasma Source 1492

A detection limit of 0.1 μg/mL P at the phosphorus 213.62-nm line is obtained, with a relative standard deviation of 2% for the complete analytical procedure.

A. M. Gunn, G. F. Kirkbright,* and L. N. Opheim, Department of Chemistry, Imperial College, London, SW7, U.K. *Anal. Chem., 49 (1977)*

Colorimetric Determination of Hippuric Acid in Urine and Liver Homogenate 1494

The sample containing hippuric acid (1 to 100 μg), acetic anhydride, *p*-dimethylaminobenzaldehyde, and pyridine is allowed to react to 40 °C for 1 h and hippuric acid is determined by measuring the absorbance at 458 nm.

Shinji Ohmori* and Mikiko Ikeda, Faculty of Pharmaceutical Sciences, Okayama University, Okayama 700, Tsushima-Naka-1, Japan, and **Shohei Kira and Masana Ogata,** Department of Public Health, Okayama University Medical School, Okayama 700, Shikata 2-5, Japan *Anal. Chem., 49 (1977)*

New Drift-Tube Source for Use in Chemical Ionization Mass Spectrometry 1497

Varying the electrostatic field strength in the drift region changes the extent of fragmentation on the quasi-molecular ions in a way which mimics changing source temperature or reagent gas.

P. C. Price, H. S. Swofford, Jr., and S. E. Buttrill, Jr.,* Department of Chemistry, University of Minnesota, Minneapolis, Minn. 55455 *Anal. Chem., 49 (1977)*

Negative Ion Chemical Ionization Mass Spectrometry of Volatile Metal Chelates 1501

Negative chemical ionization mass spectra are reported for a series of metal complexes together with sensitivity measurements for several chromium *tris*-β-diketonates using a gas chromatograph chemical ionization mass spectrometer computer system.

S. R. Prescott, J. E. Campana, and T. H. Risby,* Department of Chemistry, The Pennsylvania State University, University Park, Pa. 16802 *Anal. Chem., 49 (1977)*

Predicting Absolute Sensitivity and Limit of Detection for X-ray Analysis of Pollution Samples 1505

Absolute sensitivity of XRF pollution analysis for all elements is predictable from tabulated parameters. This allows selection of optimum experimental conditions and direct comparison with other analytical techniques.

L. S. Birks, Naval Research Laboratory, Washington, D.C. 20375 *Anal. Chem., 49 (1977)*

Determination of Fluorine by Neutron Activation Analysis 1507

A procedure for the activation analysis of fluorine in a thermal neutron flux of 1.2×10^{12} neutrons/cm^2-s is described which permits a minimum detectable weight of 14 μg of fluorine.

H. Gene Knight,* A. Keith Furr, and T. F. Parkinson, Neutron Activation Analysis Laboratory, Virginia Polytechnic Institute and State University, Blacksburg, Va. 24061 *Anal. Chem., 49 (1977)*

---

* Corresponding author.

How do you run an analysis you've never done before?

Running a new (and unfamiliar) analysis can be a real hassle. Rounding up all the apparatus and reagents you need. Getting results that don't make sense, or won't reproduce. Everything seems to work one day, but not the next. Finding that you can do it, but nobody else in the lab can — or vice versa.

At ORION we're working hard to take the aggravation out of running inorganic analyses with new measuring technology that's simple and easy-to-learn. Our Analytical Methods Guide outlines hundreds of analyses with sample preparation steps, recommended equipment, and literature references.

ORION'S Technical Service Group can send you more detailed information on the methods listed in the Guide, and they'll be delighted to help unscramble any problems you may encounter. We've put "Tech Service" as close as your telephone with our toll-free numbers. In the U.S.A. (outside Massachusetts), call 800-225-1480. In Canada, call 800-363-9270.

CIRCLE 156 ON READER SERVICE CARD

ORION RESEARCH
analytical methods guide
ORION IONALYZER
INSTRUCTION MANUAL cupric ion electrode model 94-29
chloride ion electrode
thiocyanate electrode
nitrate ion electrode
halide electrode
divalent cation electrode
calcium ion electrode
cyanide activity electrode
fluoride electrode

Now available — the new 1977 edition of the Guide. For a free copy write:
ORION RESEARCH
380 Putnam Avenue,
Cambridge, MA 02139

Briefs

Determination of 13 Elements with Atomic Numbers between 12 and 47 by 14-MeV Helium-3 Activation Analysis 1510

The interference-free detection limits are in the range of 1–500 ppb for a 2 μA irradiation of 1 h or 1 half-life, whichever is shorter depending on the product nuclide.

C. S. Sastri, H. Petri, and G. Erdtmann,* Zentralabteilung für Chemische Analysen, Kernforschungsanlage Jülich GmbH, 5170 Jülich, West Germany *Anal. Chem., 49 (1977)*

Determination of the Surface Predominance of Toxic Elements in Airborne Particles by Ion Microprobe Mass Spectrometry and Auger Electron Spectrometry 1514

Multitechnique approaches involving surface analysis, bulk analysis, and solvent leaching are used to characterize particulate pollutants.

R. W. Linton, P. Williams, and C. A. Evans, Jr.,* School of Chemical Sciences and Materials Research Laboratory, University of Illinois at Urbana—Champaign, Urbana, Ill. 61801 and **D. F. S. Natusch,** Department of Chemistry, Colorado State University, Fort Collins, Colo. 80523 *Anal. Chem., 49 (1977)*

X-ray Photoelectron Spectroscopic Studies of Iron Oxides 1521

Core line x-ray photoelectron spectra are reported for the iron compounds αFe_2O_3, γFe_2O_3, $\alpha FeOOH$, $NiFe_2O_4$, $CoFe_2O_4$, Fe_3O_4, and FeO.

N. S. McIntyre* and D. G. Zetaruk, Analytical Science Branch, Whiteshell Nuclear Research Establishment, Pinawa, Manitoba, Canada *Anal. Chem., 49 (1977)*

Sampling Error in Ion Microprobe Analysis 1529

Sampling constants are derived and applied to in-situ microanalysis to estimate and limit sampling error.

G. J. Scilla and G. H. Morrison,* Department of Chemistry, Cornell University, Ithaca, N.Y. 14853 *Anal. Chem., 49 (1977)*

Qualitative Analysis of Thin Gallium Nitride Films with Secondary Ion Mass Spectrometry 1536

Secondary ion mass spectrometry provides a convenient direct qualitative chemical analysis of thin semiconducting GaN films. The technique identifies Ga and the traditionally difficult N as well as oxygen and carbon impurities.

J. Edward Andrews,* A. P. Duhamel, and Michael A. Littlejohn, Department of Electrical Engineering, North Carolina State University, Raleigh, N.C. 27607 *Anal. Chem., 49 (1977)*

Characterization of Lignites by Pyrolysis–Gas Chromatography 1540

A technique is developed for the rapid characterization and "screening" of lignite samples by pyrolysis–gas chromatography. The production of C_1–C_5 n-paraffins and 1-olefins is monitored.

C. S. Giam,* T. E. Goodwin, P. Y. Giam, K. F. Rion, and S. G. Smith, Department of Chemistry, Texas A&M University, College Station, Texas 77843 *Anal. Chem., 49 (1977)*

Generation of Nitrosamines for Gas Chromatographic Analysis via Direct Injection 1544

Techniques for in-situ generation of nitrosamines for chromatographic analysis are described with high and reproducible yields in the 10- to 100-ng range.

D. J. Freed* and A. M. Mujsce, Bell Laboratories, 600 Mountain Avenue, Murray Hill, N.J. 07974 *Anal. Chem., 49 (1977)*

Determination of Intact Oxazepam by Electron Capture Gas Chromatography after an Extractive Alkylation Reaction 1545

The N_1, O_3-dimethyl derivatives of oxazepam and lorazepam are determined down to 1 ng/mL serum. At 25 ng/mL, 98.4 ± 3.2% is recovered.

Jörgen Vessman,* Margareta Johansson, Per Magnusson, and Signhild Strömberg, AB KABI, Research Department, Analytical Chemistry, Fack, S-112 87 Stockholm, Sweden *Anal. Chem., 49 (1977)*

Ion-Exchangers for Gas–Solid Chromatography 1549

The use of lightly sulfonated porous polymers as efficient and selective stationary phases is described.

Roland F. Hirsch,* Chemistry Department, Seton Hall University, South Orange, N.J. 07079, and **Courtenay S. G. Phillips,** Merton College, Oxford, England *Anal. Chem., 49 (1977)*

Determination of Ethyl and Methyl Parathion in Runoff Water with High Performance Liquid Chromatography 1551

Determination of ethyl and methyl parathion at the ppb level yields relative standard deviations of 1–6% and an accuracy of ±2%.

Daniel C. Paschal,* Richard Bicknell, and David Dresbach, Department of Chemistry, Illinois State University, Normal, Ill. 61761 *Anal. Chem., 49 (1977)*

Matheson has

189 Flowmeters

Specialty Gas Handling equipment is our business. Matheson has engineered 189 different flowmeters, all of which feature accuracy, precision, quality and durability. When you buy from Matheson, our experience and technology allow you to measure the flow of over 130 different gases.

Electronic Mass Flow Controllers And Flowmeters

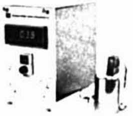

These electronic units sense the mass flow of gas by measuring the differential cooling between two points. They are dependent on heat capacity and provide accurate readings regardless of temperature and pressure changes in the gas stream. All meter circuitry is solid state. The long list of units includes over 30 linear models ideal for use with integrators, totalizers and computer data reduction equipment.

Mass flow controllers incorporate a valve controlled by the flow transducer to reduce or increase flow to maintain a constant stream.

CIRCLE 142 ON READER SERVICE CARD

150mm Flowmeter Units, 7600 Series

Matheson's most versatile rotameter series. Can be panel or bench mounted with the valve on the outlet or inlet. Accuracy of 3% and 5% of full scale depending upon the rate of flow. The series offers a wide selection of flowmeter tubes with ranges from 0.0084 SCFH to 104 SCFH. Floats of glass, stainless steel, and tantalum. Accessories of brass, stainless steel, and Monel. Available with various needle valves including Matheson's new PC metering valve. Typical calibration curves for many gases available. 24 basic models to choose from.

CIRCLE 146 ON READER SERVICE CARD

The Gas Proportioner

A 2-component mixture with component accuracy to ±5% can be made with this unit. Most simply it consists of 2-150mm tubes, a mixing tube, valves (we recommend high accuracy valves) and is compensated for back pressure by outlet valves. A high sensitivity regulator (Matheson's No. 8) is a necessary accessory. You specify the mixture you need — Matheson does the rest.

CIRCLE 143 ON READER SERVICE CARD

Acrylic Purge Meters, 7260 Series

These have an accuracy of 10% full scale. They are low-priced units for use with non-corrosive gases. Direct reading scales indicate maximum flows from 0.01 to 50 SCFH of air. This series can by easily panel mounted. The acrylic body is protected by an aluminum frame. Pressure is rated at 100 psig, temperature to 150°F. Four standard ranges available.

CIRCLE 147 ON READER SERVICE CARD

150mm Four Tube Flowmeter Units, 7400 Series

Four tube units can produce 3 and 4 component gas mixtures, or permit metering of 4 separate streams of gases by changing the configurations. You can specify 3 tube mixers and a mixing tube to produce a homogeneous mixture of 3 gases. Or, 4 tubes and one discharge port to produce a 4 component mixture. Four tubes and 4 outlets permit the monitoring of 4 separate streams. Specifications are the same as those for the 150mm Series. Two models available in brass and 316 stainless steel.

CIRCLE 144 ON READER SERVICE CARD

65mm Flowmeter Units, 7200 Series

This glass flowmeter is accurate to 5% of full scale. It possesses a single float and is calibrated to read directly in SCFH of air (the series range is 0.2 to 45 max SCFH air). Correction factors for many gases are available. Fittings are of aluminum and stainless steel. Pressure to 200 psig; temperature to 250°F. Five standard ranges are available.

CIRCLE 148 ON READER SERVICE CARD

Flowmeter Calibration Services

Calibration of *all* Matheson flowmeters can be provided for virtually any gas and pressure. An actual flowmeter calibration can increase accuracy of your flow measurements. The gases shown are a partial listing of some past calibrations. Air, argon, 1,3-butadiene, butane, carbon dioxide, carbon monoxide, cyclopropane, dimethyl ether, ethane, ethylene, helium, hydrogen, isobutane, isobutylene, methane, methyl acetylene, nitrogen, nitrous oxide, oxygen, propane, propylene, refrigerants, sulfur hexafluoride and vinyl chloride.

CIRCLE 145 ON READER SERVICE CARD

Matheson®

Lyndhurst, N.J. 07071

East Rutherford, N.J. 07073
Morrow, Georgia 30260
Bridgeport, N.J. 08014
Gloucester, Massachusetts 01930
Joliet, Illinois 60434
La Porte, Texas 77571
Cucamonga, California 91730

Newark, California 94560
Hanover, Maryland 21076
Whitby, Ontario, Canada L1N 5R9
Edmonton, Alberta Canada T5B 4K6
B 2431 Oevel, Belgium
6056 Heusenstamm, West Germany

Briefs

Laser Two-Photon Excited Fluorescence Detection for High Pressure Liquid Chromatography 1554

A selective detection method with sub-ppm detection limits for the oxadiazoles PPD, PBD, and BBD is described and compared with conventional UV detectors.

Michael J. Sepaniak and Edward S. Yeung,* Ames Laboratory–ERDA and Department of Chemistry, Iowa State University, Ames, Iowa 50011 *Anal. Chem., 49 (1977)*

Trace Chloride Determination by Rate Controlled Coulometric Titration 1557

Trace chloride determinations down to 1 ppm (2.8×10^{-5} M) are performed easily and rapidly with deviations from known values of no more than 5%. The precision of the method is within a few percent of the relative standard deviation.

Michael J. Zetlmeisl* and David F. Laurence, Tretolite Division, Petrolite Corporation, 369 Marshall Avenue, St. Louis, Mo. 63119 *Anal. Chem., 49 (1977)*

Study of the Steady-State Current at Tubular Electrodes in the Micromolar Concentration Region

1563

Current vs. flow rate data are used to distinguish flow dependent and flow independent current components. A pulsed flow procedure for measuring submicromolar concentration levels is suggested.

W. J. Blaedel* and D. G. Iverson, Department of Chemistry, University of Wisconsin, Madison, Wis. 53706 *Anal. Chem., 49 (1977)*

Mechanism of Neutral Carrier Mediated Ion Transport through Ion-Selective Bulk Membranes 1567

The mechanism of the cation selectivity of neutral carrier based solvent polymeric membranes is elucidated using tracer techniques. Their cation permselectivity is due to the presence of immobile anionic sites.

A. P. Thoma, A. Viviani-Nauer, S. Arvanitis, W. E. Morf, and W. Simon,* Department of Organic Chemistry, Swiss Federal Institute of Technology, Universitätstrasse 16, CH-8092 Zurich, Switzerland *Anal. Chem., 49 (1977)*

Redox Thermodynamics and Electron Transfer Reactivity of Heme by Enthalpimetry and Voltammetry 1573

Results of thermometric enthalpy titration, polarography, and cyclic voltammetry are reported. ΔH, ΔG, and ΔS assignments are determined in nonaqueous and mixed solvents.

Raymond Bury and Joseph Jordan,* Department of Chemistry, The Pennsylvania State University, 152 Davey Laboratory, University Park, Pa. 16802 *Anal. Chem., 49 (1977)*

Assay of Phenobarbital with an Ion-Selective Electrode 1577

A rapid and reliable assay method is developed based on the potentiometric sensing of the phenobarbital anion with a coated wire electrode. The results obtained are in agreement with the standard USP method.

Gary D. Carmack and Henry Freiser,* Department of Chemistry, University of Arizona, Tucson, Ariz. 85721 *Anal. Chem., 49 (1977)*

Silver-110 Microgram Sulfate Analysis for the Short Time Resolution of Ambient Levels of Sulfur Aerosol

1579

Atmospheric particulate samples collected on quartz or glass fiber filters are analyzed for total sulfur at the microgram level with a precision of ±3%.

Joseph Forrest* and Leonard Newman, Atmospheric Sciences Division, Department of Applied Science, Brookhaven National Laboratory, Upton, N.Y. 11973 *Anal. Chem., 49 (1977)*

Determination of Acid POH Groups of Hydrolysis-Susceptible Esters of Phosphorous Acid 1584

The procedure described has an accuracy of better than 1% in samples of about 10–20 mg H_3PO_3.

Robert Siegfried, Federal Research Centre for Nutrition, D-75 Karlsruhe, West Germany *Anal. Chem., 49 (1977)*

Reaction-Rate Method for the Determination of Hydrocortisone 1586

A rapid, 30-s method is described based on the blue tetrazolium reaction. Relative standard deviations less than 1% are obtained on commercial samples.

R. M. Oteiza, D. L. Krottinger, M. S. McCracken, and H. V. Malmstadt,* School of Chemical Sciences, University of Illinois at Urbana—Champaign, Urbana, Ill. 61801 *Anal. Chem., 49 (1977)*

Cyclic and Differential Pulse Voltammetric Behavior of Reactants Confined to the Electrode Surface 1589

Cyclic and differential pulse voltammetric behavior of reactants attached to the surface of graphite electrodes are examined experimentally and theoretically. The surface activities of the attached reactants differ appreciably from their surface concentrations.

Alan P. Brown and Fred C. Anson,* A. A. Noyes Laboratory, California Institute of Technology, Pasadena, Calif. 91125 *Anal. Chem., 49 (1977)*

FLUOROMETRY MADE EASY

Analysis is simple, quick, and accurate with this sophisticated, ratio recording Spectrofluorometer from BAIRD...

Providing sensitivities in the low parts-per-trillion, Baird's Model SFR-100 is a versatile, state-of-the-art instrument that can speed routine work and simplify the most complex analysis.

A double-beam ratio system for corrected spectra, together with excellent long-term stability, provides outstanding accuracy. A high signal-to-noise ratio assures clear, unambiguous results. Readout of reference, emission and ratio signals can be selected on an integral panel display and separate XY recorder. An analog panel meter facilitates set-up, and BCD output is available for simple computer interfacing. Many other advanced operating features are included.

Send today for complete SFR-100 specifications and operating details, together with data on a broad range of accessory equipment and devices.

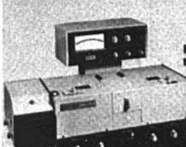

FLUORICORD — Exceptional versatility for research and difficult routine analysis. Easy to operate, with excellent resolution and accuracy . . . high repeatability and sensitivity.

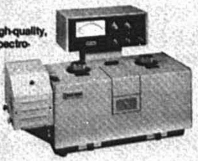

FLUORIPOINT — A high-quality, automatic scanning, spectrofluorometer at a surprisingly modest price. Ideal for the small laboratory.

Let us demonstrate the SFR-100 in your own laboratory. We will leave you a free copy of "Practical Fluorescence Theory, Methods, and Techniques," by G. G. Guilbault, for giving us a chance to show what this unique instrument can do.

B A **BAIRD-ATOMIC**

Home Office: Baird-Atomic, Inc.
125 Middlesex Tpk., Bedford, MA 01730
Tel. (617) 276-6000 — Telex: 923491 —
Cable: BAIRDCOBFRD

CIRCLE 24 ON READER SERVICE CARD

Briefs

Ion-Exchange Separation and Determination of Calcium and Magnesium 1595

Magnesium(II) and calcium(II) are separated by ion-exchange chromatography using a sulfonated macroporous resin, ammonium chloride, or ethylenediammonium chloride eluent and automatic detection with a color-forming reagent.

Michael D. Arguello and James S. Fritz,* Ames Laboratory—ERDA and Department of Chemistry, Iowa State University, Ames, Iowa 50011 *Anal. Chem., 49 (1977)*

Automated Atomic Absorption Spectrometric Determination of Total Arsenic in Water and Streambed Materials 1599

Ultraviolet radiation or acid–persulfate digestion is used to decompose organic arsenic compounds.

Marvin Fishman* and Roberto Spencer, U.S. Geological Survey, Mail Stop 407, Box 25046, Denver Federal Center, Denver, Colo. 80225 *Anal. Chem., 49 (1977)*

Determination of Ethylene Oxide in Gas Sterilants by Fourier Transform Infrared Spectrometry 1602

The FTIR method gives accurate results between 5 and 25%, calculated on a weight basis. A brief study of difference spectrometry shows promise for this technique in quality control.

P. V. Allen and A. J. Vanderwielen,* Control Analytical Research and Development, The Upjohn Company, Kalamazoo, Mich. 49001 *Anal. Chem., 49 (1977)*

Enhancement of the Fluorescence Intensity of Derivatives of Amino Acids in Mixed Solvent Systems 1606

Mixed solvent systems containing DMSO are found to greatly enhance the fluorescence intensity of *o*-phthaldehyde, dansyl chloride, and fluorescamine derivatives of amino acids, leading to the possibility of more sensitive analytical procedures.

Peter M. Froehlich* and Larry D. Murphy, Department of Chemistry, North Texas State University, Denton, Tex. 76203 *Anal. Chem., 49 (1977)*

Multichannel Pipet for Parallel Aliquoting of Samples and Reagents into Centrifugal Analyzer Minidiscs 1608

A multichannel pipet designed for use with a minidisc centrifugal analyzer aliquots and delivers eight solutions in parallel in 30 s with 0.5% reproducibility.

R. P. Gregory IV, J. D. Lowry, and H. V. Malmstadt,* School of Chemical Sciences, University of Illinois, Urbana, Ill. 61801 *Anal. Chem., 49 (1977)*

Determination of Low Levels of Sulfur in Organics by Combustion Microcoulometry 1615

The limit of detection is 0.2 ppm by weight and the standard deviation at the 1- to 2-ppm level is 0.1 ppm by weight.

D. C. White, British Petroleum Company Limited, Group Research and Development Department, Analytical Branch, Sunbury-on-Thames, Middlesex, England *Anal. Chem., 49 (1977)*

Weak Peak Enhancement by Selective Ion Trapping in a Quadrupole Ion Storage Source 1619

The combination of a three-dimensional quadrupole ion storage source with a conventional quadrupole mass filter is shown to provide a means of enhancing the intensities of weak mass spectral peaks.

G. Lawson and J. F. J. Todd,* Chemical Laboratory, University of Kent, Canterbury, Kent, CT2 7NH, U.K. *Anal. Chem., 49 (1977)*

Quantitative Comparison of Combined Chromatographic/Mass Spectrometric Profiles of Complex Mixtures 1623

An automated method is described for quantitative comparison of GC/MS profiles of complex mixtures with historical libraries of previous results.

Dennis H. Smith* and Michael Achenbach, Departments of Genetics and Chemistry, Stanford University, Stanford, Calif. 94305, and **William J. Yeager, Patricia J. Anderson, William L. Fitch, and Thomas C. Rindfleisch,** Department of Genetics, Stanford University, Stanford, Calif. 94305 *Anal. Chem., 49 (1977)*

Correspondence

Radiofrequency Oxygen Plasma Treatment of Pyrolytic Graphite Electrode Surfaces 1632

John F. Evans and Theodore Kuwana,* Department of Chemistry, The Ohio State University, Columbus, Ohio 43210 *Anal. Chem., 49 (1977)*

Rate of Extraction of Copper from Aqueous Solutions 1636

Stephen J. Kirchner and Quintus Fernando,* Department of Chemistry, University of Arizona, Tucson, Ariz. 85721 *Anal. Chem., 49 (1977)*

Corrosion of Stainless Steel by Organic Solvent Mixtures 1637

Alice Y. Ku and David H. Freeman,* Department of Chemistry, University of Maryland, College Park, Md. 20742 *Anal. Chem., 49 (1977)*

Find the 2 membrane filters you use the most, and you'll see our point. And get free samples.

The point you'll see is that S&S offers more different types of membrane filters or laminates (over 115!) for microfiltration or ultrafiltration than anybody else.

For instance, just about every nitrocellulose membrane listed below is available in the following formats: white, black or green; with low extractables for gravimetrics; plain or with a 3.1mm or 5mm grid; hydrophobic or hydrophobic-edged; air-side up for leukocyte chemotaxis assays; pre-sterilized with ETO gas or packaged for use in the autoclave. Plus — as we are sure our samples will prove — they're of the highest quality and uniformity.

This list shows some of our best-sellers. Find the two different membrane types you use most, check the size you want, fill in your name and address, and mail the form to us. Your free samples will be on their way to you quickly. If you don't see the membrane type you need, indicate what you do need in the blank space at the bottom — we probably have it, too. And if the size you want isn't here, we'll supply any standard size up to 50mm—just indicate which one.

What does it mean to you if S&S makes so many different filters and you may use only two? It means that if you start with S&S you can stay with S&S, no matter how your membrane filter applications might change. One brand, one source, one high level of quality.

Check your two choices now and get your free samples.

SCHLEICHER & SCHUELL

Keene, New Hampshire 03431
Schleicher & Schuell GmbH, D-3354, Dassel, West Germany
Schleicher & Schuell AG, 8714, Feldbach ZH, Switzerland

S&S GRADE #	PORE SIZE (µm)	DESCRIPTION	DIAMETER		
			25mm	47mm	Other (Up To 50mm)
AE 100/LK	12	Nitrocellulose, white, specially packaged for leukocyte chemotaxis assays			
AE 99	8	Nitrocellulose, white, plain			
AE 98	5	Nitrocellulose, white, plain			
AE 98/LK	5	Nitrocellulose, white, specially packaged for leukocyte chemotaxis assays			
AE 97	3	Nitrocellulose, white, plain			
AE 95	1.2	Nitrocellulose, white, plain			
AE 91	0.8	Nitrocellulose, white, plain			
BC 07/21GAP	0.7	Nitrocellulose, white 3.1mm black grid, autoclave pack, 10 envelopes, 10 filters and 10 nutropads per envelope, for fecal coliform analysis			
BA 90	0.6	Nitrocellulose, white, plain			
BA 90/21	0.6	Nitrocellulose, white 3.1mm black grid			
BA 85	0.45	Nitrocellulose, white, plain			
BA 85/21	0.45	Nitrocellulose, white 3.1mm black grid			
BA 85/21GAP	0.45	BA85 autoclave pack, 10 envelopes, 10 filters & nutropads per envelope			
BA 83	0.2	Nitrocellulose, white, plain			
BA 80	0.15	Nitrocellulose, white, plain			
PH 79	0.1	Nitrocellulose, white, plain			
EI 41	<0.005	Nitrocellulose, transparent, plain, furnished moist			
ST 69	1.2	Cellulose acetate, white, plain			
OE 67	0.45	Cellulose acetate, white, plain			
OE 66	0.2	Cellulose acetate, white, plain			
AC 62	0.010-0.005	Cellulose acetate, transparent, plain, furnished moist			
AC 61	<0.005	Cellulose acetate, transparent, plain, furnished moist			
RC 59	0.6	Regenerated cellulose, white, plain			
RC 58	0.2	Regenerated cellulose, white, plain			
RC 57	0.15	Regenerated cellulose, white, plain			
RC 51	<0.005	Regenerated cellulose, transparent, plain, furnished moist			
TE 39	15.0	PTFE on non-woven polypropylene, white, plain			
TE 38	5.0	PTFE on non-woven polypropylene, white, plain			
TE 36	0.5	PTFE on non-woven polypropylene, white, plain			
TE 35	0.2	PTFE on non-woven polypropylene, white, plain			
TE 30	0.02	PTFE on non-woven polypropylene, white, plain			

Send to Schleicher & Schuell, Inc., Keene, N.H. 03431

AC-9

Name________________ Institution/Company________________

Address________________ City__________ State__________ Zip__________ Phone (   )__________

CIRCLE 191 ON READER SERVICE CARD

6 Channel Recorders

- Up to 6 continuously overlapping records
- Electronic linearization for direct recording in engineering units
- Plug-in amplifiers for easy span change
- Color coded linear ribbon indicators easily read at a distance
- High precision and reliability for laboratory and industrial use

Chessell Model 320 potentiometric recorders provide 6 channel continuous, fully overlapping records across 250 mm (10 inches) of calibrated chart width. All inputs are electronically linearized and recorded as linear functions for easy interpretation. Direct measurement of AC or DC electrical parameters is possible by use of plug-in modular input amplifiers which provide flexibility for quick span changes. No calibration is required. Stacked pen trays and plug-in drive PCB's permit easy field expansion up to 6 channels.

Operational versatility is enhanced by bold, clear, color coordinated linear ribbon scale indicators that allow observation of pen position at a distance. A wide selection of chart speeds permits chart life up to 2000 hours. Options include 10 speed electronic chart drive, event marker, individual channel high/low alarms and fan fold charts.

Call or write for free product guide.

Chessell

EI
A Eurotherm
International
Company

Data Collection Recording Systems

Isaac Newton Center, Reston, VA. 22090
Telephone: (703) 471-4830 • Telex: 899449

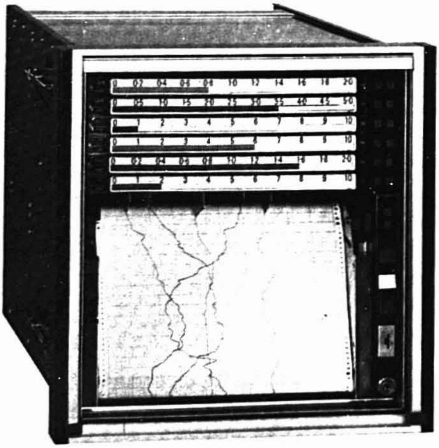

CIRCLE 40 ON READER SERVICE CARD

Briefs

Sheet Resistivity Measurements of Chemically Modified Electrodes by Four-Point Probe Method 1639

Vakula S. Srinivasan* and Walter J. Lamb, Department of Chemistry, Bowling Green State University, Bowling Green, Ohio 43403 *Anal. Chem., 49 (1977)*

Aids for Analytical Chemists

Photographic Techniques for Fluorescent Spots on Thin-Layer Chromatographic Plates 1640

P. W. Rulon* and M. J. Cardone, Norwich Pharmacal Company, Norwich, N.Y. 13815 *Anal. Chem., 49 (1977)*

Determination of Mercury in Edible Oils by Combustion and Atomic Absorption Spectrophotometry 1641

Wei-Chong Tsai and Lih-Jiuan Shiau, Food Industry Research and Development Institute, P.O. Box 246, Hsinchu, Taiwan, Republic of China *Anal. Chem., 49 (1977)*

Dry Ashing of Animal Tissues for Atomic Absorption Spectrometric Determination of Zinc, Copper, Cadmium, Lead, Iron, Manganese, Magnesium, and Calcium 1644

E. E. Menden, D. Brockman, H. Choudhury, and H. G. Petering,* Kettering Laboratory, Department of Environmental Health, University of Cincinnati College of Medicine, Cincinnati, Ohio 45267 *Anal. Chem., 49 (1977)*

Small Volume, High Performance Cell for Nonaqueous Spectroelectrochemistry 1646

Fred M. Hawkridge,* Department of Chemistry, Virginia Commonwealth University, Richmond, Va. 23284, and **Jeanne E. Pemberton and Henry N. Blount,*** Brown Chemical Laboratory, The University of Delaware, Newark, Del. 19711 *Anal. Chem., 49 (1977)*

Correction. Studies on the Mechanism of Atom Formation in Graphite Furnace Atomic Absorption Spectrometry 1647
R. E. Sturgeon, C. L. Chakrabarti, and C. H. Langford

Correction. Gel Permeation Chromatography of Low Molecular Weight Materials with High Efficiency Columns 1647
Anoop Krishen and Ralph G. Tucker

Correction. Determination of Thorium and Uranium in Ores and Mill Tailings by Alpha Spectrometry 1648
C. W. Sill

While you're working in the foreground*.. your FX is working in the background*

examples:
- fourier transformation
- data massage
- basic programming
- $T_1/T_{1}\rho$ calculation
- plot/print/CRT display
- spin simulation

examples of acquisition:
- $T_1/T_1\rho$
- auto stacking
- multi-mode
- pulse programmed
- kinetic
- long term

* **Foreground/Background system**

Comprehensive 60 and 100 MHz Systems

The FX60Q & FX100 features:
- (DQD) DIGITAL Quadrature Detection System
- Multi-Frequency TUNEABLE Probe observation
- Dual Frequency probes
- 4-channel DIGITAL phase shifters (DPS)
- Comprehensive auto-stacking system
- * Foreground/Background system
- Computer based pulse programmer with Multiple Pulse Sequence Generator
- CPU Expandable to 65K words (MOS)
- 2-channel 12 bit AD/DA
- $T_1\rho$/spin locking system
- Disc storage systems
- Multi-Mode HOMO/HETERO decoupling capabilities
- Multi-Mode TRIPLE Resonance
- Programmable Variable Temperature Unit
- Simplex Y/Curvature gradient controller

JEOL

Analytical Instruments, Inc.

235 Birchwood Ave., Cranford, NJ 07016
201—272-8820

CIRCLE 105 ON READER SERVICE CARD

Photon counting: when light measurement is difficult—and crucial.

Few developments have so greatly enhanced light measurements as photon counting. By increasing sensitivity and stability, photon counting has opened the way to a wide range of high-precision applications.

For example: At Case Western Reserve University Hospital, the Department of Neurology has been using fluorometric techniques in the analysis of biogenic amines and their metabolites in biologic material of diverse origin.

Dr. Mars comments, "With low concentrations and conventional analog techniques, it became apparent that differences between sample and reagent blank were frequently too small to permit adequate confidence in the procedures." Now, since the installation of an Ortec photon-counting system, ". . . photon counting has extended our capabilities in the measurement of low sample concentrations, has significantly enhanced the ease and reliability of processing large numbers of samples, and has eliminated human error in recording the results."

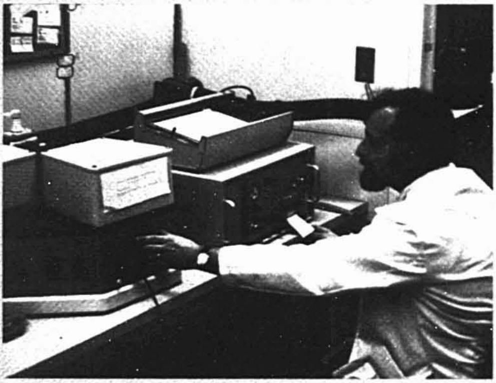
Dr. H. Mars, University Hospital, Case Western Reserve University.

For complete information on Ortec photon-counting systems, write or call Life Sciences Division, Ortec Incorporated, 100 Midland Road, Oak Ridge, TN 37830; (615) 482-4411. Worldwide sales and service.

Providing solutions. ORTEC®

AN EG&G COMPANY
76 OFFICES IN 49 COUNTRIES

©Ortec

6851

CIRCLE 157 ON READER SERVICE CARD

*Extra Precision, Extra Performance in Liquid Chromatography

EXTRA PRECISION
Philips NEW XP Digital Programmer is microprocessor controlled for extra precision, so that resolution of % B in A is controlled to ± 0.5% to give the highest repeatability of retention times. The Gradient Programmer requires only one pump for simplicity and economy, provides 9 segments each up to 99 minutes and each capable of being programmed with a choice of 99 curve shapes plus a step function. This XP series flexibility always assures the proper program for your problem rather than a compromise.

EXTRA PERFORMANCE
The XP Digital Solvent Delivery System gives smooth, pulse-free operation up to 10,000 PSI with flow rates up to 10 ML. This high pressure capability shortens analysis time and pulse-free operation allows operation at higher sensitivity for higher performance.

To complete the total LC System Philips offers a wide range of XP Detectors to assure the highest level of performance in liquid chromatography. You have a choice of four detectors to let you select the correct one for the job:

1. Fixed Wavelength UV Detector
Operates at 254 NM;

2. Variable Wavelength UV Detector
Operates to 190 NM;

3. Unique Electron Capture Detector
Is available for those compounds with electron affinity. (It's selective response allows detection of electron capturing compounds down to 25 picograms while ignoring non electron capturing species.);

4. Universal Flame Ionization Detector
Is available when little is known about the sample. It gives a universal and linear response for all organic compounds.

The NEW Philips XP Series brings together microprocessor controlled Gradient System, a high performance Solvent Delivery System, and the widest available range of Detectors to provide the best solution to your LC problems. For more information call or write today to: Philips Electronic Instruments, 85 McKee Drive, Mahwah, N.J. 07430 • (201) 529-3800.

INTRODUCING THE PHILIPS XP*-LC

PHILIPS

PHILIPS®

Circle #162 for literature requests

Circle #163 for demonstration requests

Letters

Single Atom Detection

Sir: The points you raise in your editorial of April 1977 (*1*) about problems arising in projected applications of single atom analytical techniques are well taken. There have been three laser-based methods that have demonstrated sensitivities of 1–100 atoms/cm^3 (*2–4*). All of these methods make use of the ability of lasers to deliver large optical powers into atomic linewidths at resonant frequencies. As a result, they depend on wavelength tunable devices and/or fortuitous sets of energy levels. Molecular species can only be detected at much reduced sensitivities.

We have developed a method that has demonstrated detectivities of 10^4 atoms/cm^3 with the promise of a very wide generality (*5*). The probability of covering ⅔ or more of the periodic table is very good. In addition, there is abundant evidence that many molecular species are susceptible to detection by this technique (*6*). Our method requires quantitative optical detection of fluorescence excited by energy transfer from "active" nitrogen. We call it "analytical photon catalysis" since the sample species acts as a catalyst for photon production from the energetic metastable nitrogen species.

Due to the simplicity, generality, low cost, and extreme sensitivity of the technique, we feel it is a serious candidate to occupy a prominent place "in the kit bag of the profession". In addition to the above advantages, the method has a large dynamic range. This is clearly demonstrated (*5*) when the concentration of Bi atoms is measured over six orders of magnitude in a single run.

These comments are in no way meant to detract from the detection of single atom events at Oak Ridge. The paper of Hurst and coworkers (*4*) reports on an unequivocal achievement of one of physics' illusive, long-standing goals. We merely want to point out the ultimate utility of our technique to the readers of ANALYTICAL CHEMISTRY.

References

(1) H. A. Laitinen, *Anal. Chem.*, **49,** 529 (1977).
(2) W. M. Fairbank, Jr., T. W. Hansch, and A. L. Schawlow, *J. Opt. Soc. Am.*, **65,** 199 (1975).
(3) J. A. Gelbwachs, C. F. Klein, and J. E. Wessel, *Appl. Phys. Lett.*, **30,** 489 (1977).
(4) G. S. Hurst, M. H. Nayfeh, and J. P. Young, *ibid.*, p 229.
(5) G. A. Capelle and D. G. Sutton, *ibid.*, p 407.
(6) A. N. Wright and C. A. Winkler, "Active Nitrogen", Academic Press, New York, N.Y., 1968; G. A. Capelle, unpublished data.

David G. Sutton
Aerophysics Laboratory
Aerospace Corp.
Los Angeles, Calif. 90045

Microscopes

Sir: I feel that your readers deserve some amplification of Dr. McCrone's article [*Anal. Chem.*, **49,** 659A–664A (1977)], "How to Buy a Microscope".

Although Dr. McCrone is widely knowledgeable regarding polarizing microscopes and microscope training courses, he unaccountably fails to mention that Vickers manufactures a complete range (student through research) of polarizing microscopes, available worldwide, and, in England, offers a rather good program of intensive courses in microscopy.

G. R. Osgood, Jr.
Vickers Instruments, Inc.
Woburn, Mass. 01801

Dr. McCrone replies: I was embarrassed to be reminded of the Vickers polarizing microscopes, but their catalog was missing from my library of catalogs sent regularly by the other manufacturers. This library was used in preparation of the article.

Vickers does have a wide range of polarizing microscopes very competitive with those I did cover. Their M-70b student microscope is comparable to the corresponding Nikon, Olympus, Hacker, Kent, and Unitron instruments with the advantage of an inclined bodytube. They also have a more sophisticated model with a large ball-bearing stage with binocular inclined bodytube for about $1600. This and all Vickers microscopes are designed to accept vertical illuminators to be used for opaque specimens and especially ore mineral analysis.

Finally, they have a large modular polarizing microscope in the $6000–7000 range, the M-41. Mr. Osgood tells me that this instrument is about to be phased out in favor of a new M-17 with DIN optics and other improvements including planachromats. Apoplans will also be available although not initially, at least, strainfree. This is no serious drawback, however, since planapos (or apoplans) are not generally necessary for polarized light observations. Contrariwise, crossed polars are not ordinarily used for observation or photomicrography at the highest resolving power. This latter instrument will fall in the range of the Leitz Orthoplan or Nikon Apophot.

DEXSIL®

High Temperature
GC Phases

Extended column life at 400°
and beyond

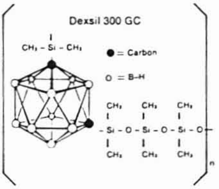

Separate amino acids, drugs, paraffins, hydrocarbons, natural waxes, pesticides, fatty acids, steroids, alcohols, etc. – at column temperatures of 400° C and more. Routinely. With outstanding selectivity.

Columns packed with Dexsil 300GC have shown negligible bleed from 20° to 450° C. Limited life applications can be performed at temperatures to 500° C. Two other Dexsil polymers – 400GC and 410GC – can be selected according to application, and used at temperatures to 400° C.

When used at lower temperatures up to 350° C, the Dexsils offer the advantages of using more sensitive GC settings and increasing column life because of the Dexsils' low bleed. Users report column life under routine conditions at 2, 3, 4 years and more.

Dexsil is available NOW, either directly or from your regular supplier. Write for details, and an exhaustive bibliography of over 200 Dexsil applications.

DEXSIL
295 Treadwell Street • Hamden, CT 06514
(203) 288-3509

® Registered Trade Mark Dexsil Chemical Corporation Hamden CT.

CIRCLE 50 ON READER SERVICE CARD

COMPARE YOUR IDEA OF A WORKHORSE RECORDER TO OURS.

The rugged Gould 105 General Purpose Strip Chart Recorder delivers such reliable performance, with so many unexpected features, that it goes beyond the traditional definition of a workhorse unit.

Die-cast to handle the day-to-day rigors industrial analytical instrumentation must face, the 105 still offers you a full complement of features you might not expect on such a competitively priced recorder.

Full scale accuracy is ± 0.1%. Rectilinear data presentation is available on either single or dual 10-in. channels. Response time (10% to 90% full scale) is less than 350 ms.

The Model 105 uses disposable felt tip pens available in four colors. It easily takes Z-fold or roll paper without modification. Chart speeds range from 1 in./hr. to 20 in./min. It even makes chart annotation simpler with a flatbed, "write-on" design and event marking standard.

And of course you have the Gould/Brush sales and service organization should you ever need us. Check Gould's 105 — a workhorse of a recorder with a tradition of thoroughbreds.

For a detailed brochure, contact Gould, Inc., Instrument Systems Division, 3631 Perkins Ave., Cleveland, Ohio 44114. Or call toll free at (800) 325-6400, Ext. 77. In Missouri: (800) 342-6600.

CIRCLE 82 ON READER SERVICE CARD

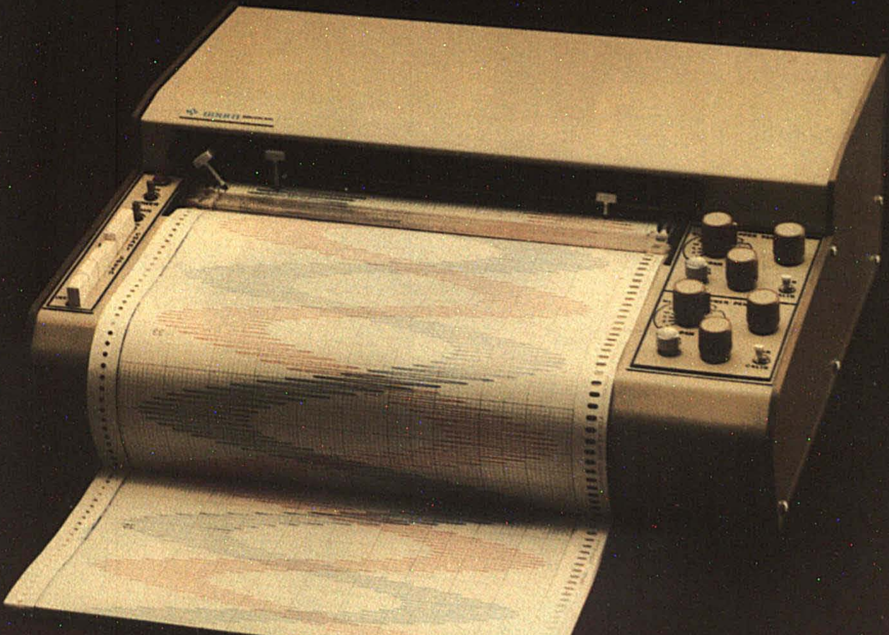

GOULD

SYSTEM
TN-2000

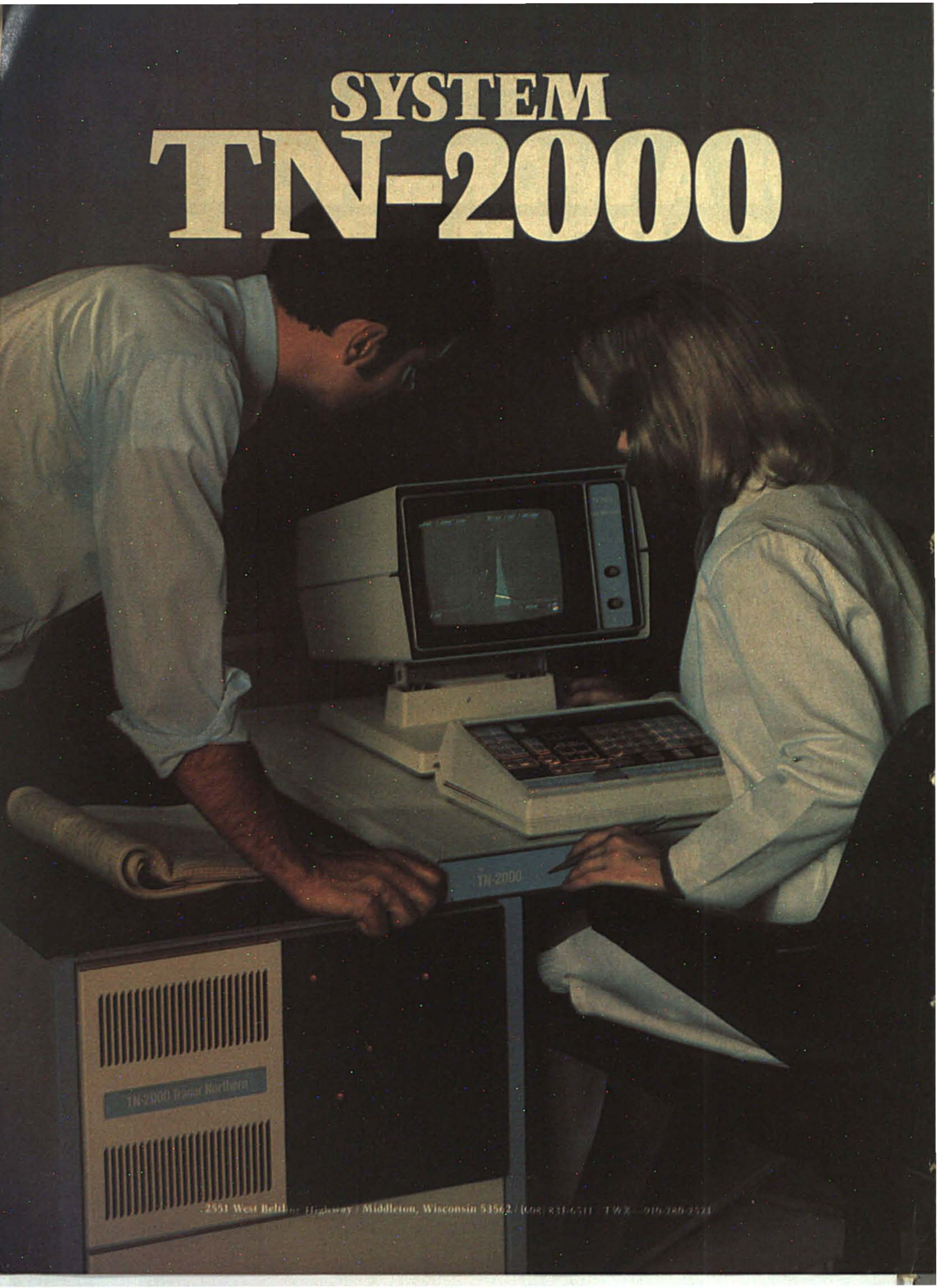
TN-2000
TN-2000 Tracor Northern

2551 West Beltline Highway / Middleton, Wisconsin 53562 / (608) 831-6511 / TWX—910-280-2521

The new generation X-ray analysis system from TracorNorthern.

At Tracor Northern we've established a reputation for leadership in developing innovative analytical instrumentation.

Five years ago we introduced the NS-880, the first truly computer-based X-ray elemental analysis system. The NS-880 has gained world-wide acceptance and is today the premier quantitative analysis system.

Tracor Northern now proudly introduces System TN-2000, a new microcomputer-based system with the exceptional performance you've come to expect from our instruments. System TN-2000 offers human-engineered convenience and simplified operation at a modest price, while maintaining our tradition of uncompromising quality and unmatched verstility.

System TN-2000 is totally human-engineered for convenience and ease of operation. The modular backlighted control keypad and large-screen high-resolution display can be individually placed to optimally suit your working environment.

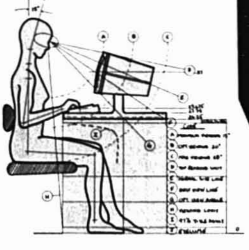

System TN-2000's superior display is controlled by its own microprocessor to provide comprehensive visual information with unparalleled clarity and versatility. Labeled keypad functions and unique OMNI control provide instant interaction with all display features.

TN-2000
Tracor Northern
TN-2000 Tracor Northern

System TN-2000

12.7 cm.
17.8 cm.

A uniquely new, elegantly simplified approach to operation setup and control allows you to perform complete analyses with unprecedented ease. You simply select desired operations from displayed choices, with current selections identified by complete and lucid text.

TN-2000
Tracor Northern

Efficient operation is ensured by permitting operating parameters to be individually modified.

System TN-2000 is more than an innovative instrument. It is a state-of-the-art computer-based system whose capabilities can grow with your needs.

If you are interested in rapid and reliable X-ray elemental analysis, you must see System TN-2000 in action. Contact us now.

Tracor Northern

Tracor Europa B.V. / Schiphol Airport Amsterdam / Building 106, The Netherlands / Telephone (020) 41 1865 / Telex 13695

CIRCLE 204 ON READER SERVICE CARD

AND NOW SIGMA:

The first complete GC line with consistent excellence in performance, adaptable to any analytical need and budget. The SIGMA series from Perkin-Elmer is entirely new, entirely unified. It includes gas chromatographs, lab data systems, and accessories. Incorporating the latest chromatographic technology and the most recent advances in microprocessors, SIGMA presents major improvements in system control and detector performance.

SIGMA is unique for another important reason. You get identical chromatographic performance from every instrument in the series because they're all assembled from common components and accessories. You can transfer most methods developed on one SIGMA gas chromatograph to any other in the series, with no deterioration in performance. Even the column can be transferred.

Optional SIGMA accessories include an Autosampler for liquid sampling, and various systems for gas sampling and column switching. An Automatic Environmental Sample System enables air samples to be analyzed with any of the detectors. There's also a solid sampling system. You can get a wide selection of standard interchangeable columns, both metal and glass – capillary and packed. Everything has been incorporated in the SIGMA concept.

Ask your Perkin-Elmer representative for all the facts on the SIGMA series. Contact him now, or write Perkin-Elmer Corp., Mail Station 12, Main Ave., Norwalk, CT 06856.

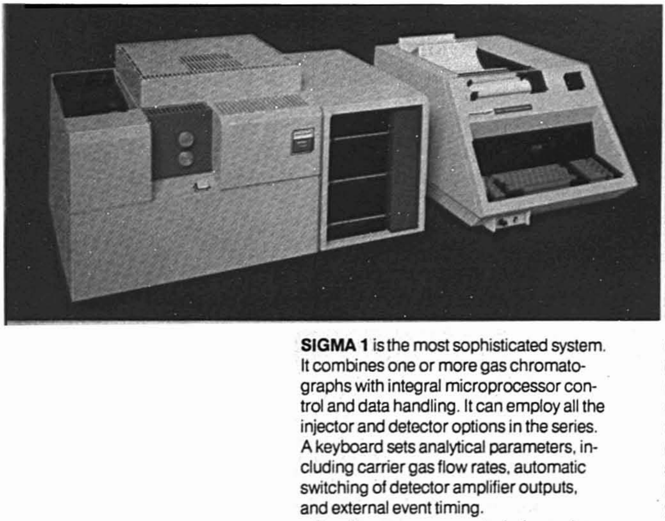

SIGMA 1 is the most sophisticated system. It combines one or more gas chromatographs with integral microprocessor control and data handling. It can employ all the injector and detector options in the series. A keyboard sets analytical parameters, including carrier gas flow rates, automatic switching of detector amplifier outputs, and external event timing.

Its microprocessor controls the analyzer units and reduces data for as many as four detectors at once. An internal printer/plotter gives you the chromatogram, analytical conditions, and results.

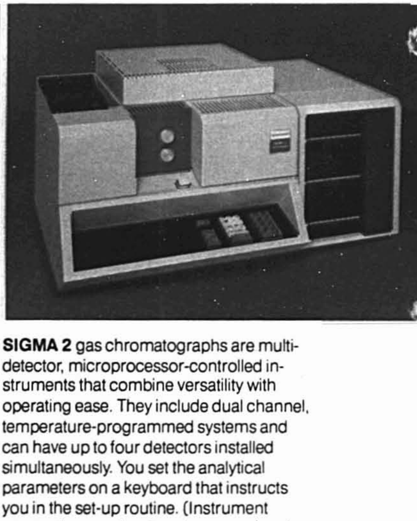

SIGMA 2 gas chromatographs are multi-detector, microprocessor-controlled instruments that combine versatility with operating ease. They include dual channel, temperature-programmed systems and can have up to four detectors installed simultaneously. You set the analytical parameters on a keyboard that instructs you in the set-up routine. (Instrument parameters can be stored on a card and entered through a Card Reader Accessory.) The microprocessor also provides multi-level temperature programming, digital setting of carrier gas flow rates, and digital reporting of all set and actual values.

A NEW ERA IN GC

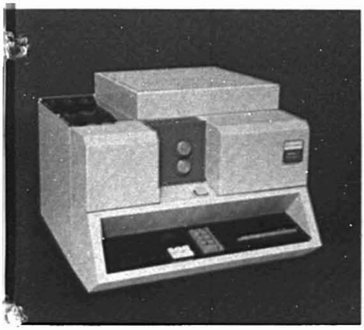

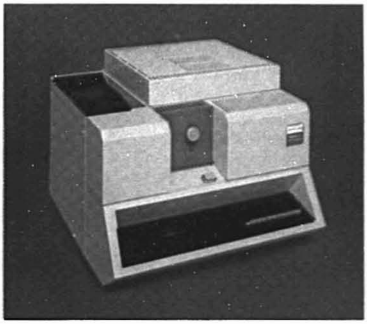

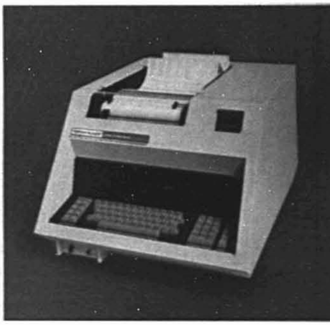

SIGMA 3 gas chromatographs are modestly priced, but exceptionally versatile, single or dual channel temperature-programmed instruments. They come with a wide choice of detectors: flame ionization; electron capture; nitrogen/phosphorous; flame photometric; or hot wire. Accessory amplifiers are available for simultaneous multi-detector operation. A simple numerical keyboard sets parameters while the microprocessor controls the routine, so no "impossible" values can be entered.

SIGMA 4 gas chromatographs are excellent for routine applications and teaching. They are dedicated isothermal instruments designed for single column, single detector operation. They are also available with a wide choice of detectors: flame ionization; electron capture; nitrogen/phosphorous; flame photometric; and the new thermistor thermal conductivity for rugged routine operation. Injectors, gas controls and other accessories and options are identical to those used throughout the entire SIGMA series.

SIGMA 10 Lab Data System handles data from any gas or liquid chromatograph. Annotated chromatograms can be obtained for any one of the four active channels connected to it, and multiple data files and methods can be stored. Six time-controlled relays are standard on every channel, and ready signals from gas chromatographs and Autosamplers can be fed back to the system for complete synchronization of automatic analysis. With the optional programmability accessory, you can write programs in standard BASIC. A cassette accessory provides additional storage space for programs, and there's also an RS-232C input/output accessory.

PERKIN-ELMER

CIRCLE 180 ON READER SERVICE CARD

ห้องสมุด กรมวิทยาศาสตร์

Digital Analysis of

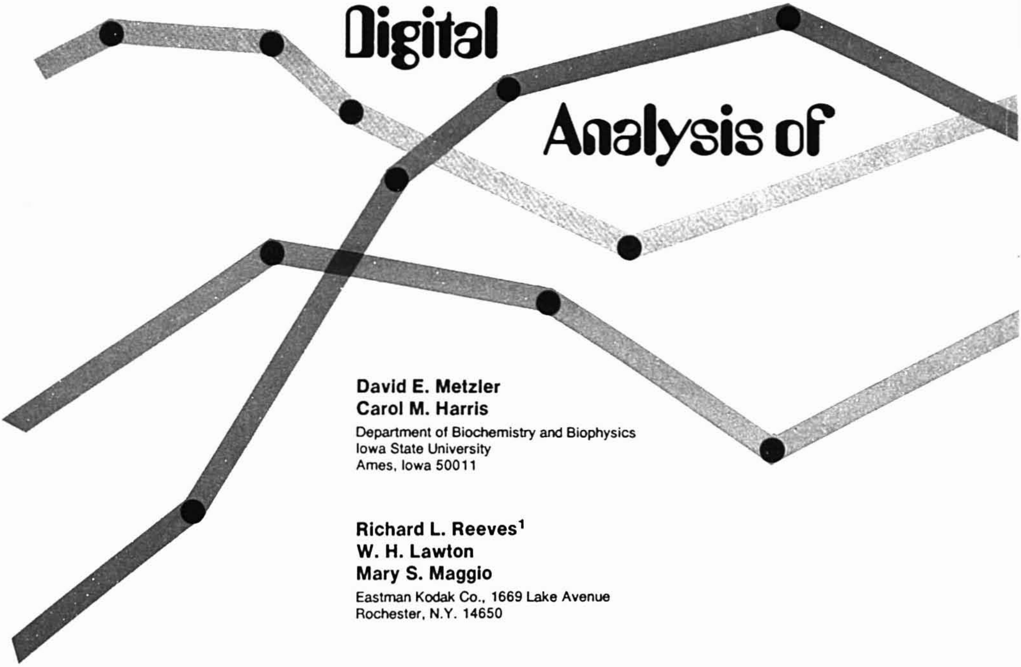

David E. Metzler
Carol M. Harris
Department of Biochemistry and Biophysics
Iowa State University
Ames, Iowa 50011

Richard L. Reeves[1]
W. H. Lawton
Mary S. Maggio
Eastman Kodak Co., 1669 Lake Avenue
Rochester, N.Y. 14650

The wide use of spectrophotometry in chemical analysis results from the fact that electronic spectra of substances in solution are easy to measure with high precision and at relatively low concentrations. Despite the ease of measurement, a large amount of the information contained in the original spectra is seldom used in analyses and is almost never reported. As a result, the conventional use of data at a few wavelengths requires relatively large spectral changes for a given precision, whereas use of the information in the entire absorption curve would allow small changes to be analyzed with the same precision. Attempts at empirical correlations are made difficult by the fact that the literature contains the scantiest of data: ϵ_{max}, λ_{max} (±1–2 nm), and perhaps an indication of the existence of a "shoulder" at some approximate wavelength.

Substantial improvements in methods of collecting, analyzing, and reporting spectrophotometric data are available. The precision of modern spectrophotometers permits band positions to be located more accurately than the customary ±1 nm. With a small amount of effort, information about band shapes can be obtained. Such data are often more useful with broad-band spectra than are changes in ϵ_{max}. Since the information in an entire curve can be reduced to a few parameters, changes in curve shape induced by changes in experimental conditions can be studied by examining the variation in these parameters rather than the variation of the entire curve. Use of direct-reading digital output systems together with computer-assisted analysis of band shape provides further improvement in precision and saving of time. It is the purpose of this review to summarize the methods that are currently available for analysis of spectra recorded in digital form and to illustrate them with appropriate examples.

Digital Recording

Consider a simple spectrum such as that of 1-methylcytosine (Figure 1) which consists of two overlapping bands. A spectrum of this type can be described by specifying the position, height, and shape of each of the two bands. Band shape can often be expressed in terms of width and skewness together with a description of the vibronic fine structure. In many spectra of organic and inorganic substances, no fine structure is evident and a spectrum such as that in Figure 1 can be described accurately by recording the coordinates of perhaps 20 points. If vibronic fine structure is present, 100–200 points will usually suffice to convey all of the available information. In other cases, e.g., benzene in the vapor phase, a much larger number of points is needed. A desirable approach is to record the coordinates of the necessary number of points directly in a form convenient for computer processing (*1-4*). Alternatively, data from carefully recorded graphs can be digitized manually (*2*) or by machine (*4*).

Collection of data in digital form provides the following advantages: (a) Repeated scans can be averaged easily to provide a lower noise level, corrections can be applied, and molar absorptivities can be calculated automatically. (b) Spectra of individual ionic and molecular forms in equilibrium mixtures can be evaluated precisely. (c) Band shapes can be analyzed readily. (d) Processed data constitute

---

[1] To whom correspondence should be addressed.

Electronic Absorption Spectra

a library of data in digital form. (e) Spectra may be replotted readily in any desired format, e.g., for publication, at a nominal cost. (f) The redundancy of data affords a sensitive means to test the correctness of a chemical model. A two-component mixture can be analyzed at two wavelengths, but there are no degrees of freedom remaining to test for additional components if they exist. In our own experience, the existence of a third minor component in an assumed two-component product mixture would have been overlooked without digital treatment of the spectrophotometric data (*5*). (g) Digital acquisition of data is also useful in very rapid spectrophotometry (*6*).

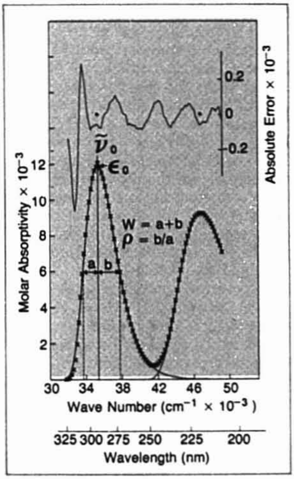

Figure 1. Absorption spectrum of 1-methylcytosine

Spectrum recorded with Model 1501 Cary spectrophotometer equipped with Cary Datex digital output system interfaced to IBM keypunch. Absorbances recorded at intervals of 200 cm^{-1}. Symbols: experimental points; solid lines: summation of two lognormal distribution curves fitted to points. Plot at top is difference (in units of molar absorptivity) between experimental points and corresponding points on fitted curve

Resolution of Spectra of Multicomponent Linear Systems

One is usually interested in analyzing mixtures characterized by spectra containing overlapping bands from several absorbing species. The computer is uniquely suited for simplification of the labor involved in studying such systems.

A simple application is analysis of a mixture of components where spectra are known. Spectra of the pure components are recorded, and these "library spectra" are then used together with those of the unknown mixtures to compute the composition (*7*). It is assumed that the spectra of the mixtures are linear combinations of those of the individual components, and a simple least-squares procedure is used. In this approach the absorption curve of a single unknown mixture may be resolved.

In many instances, spectra of individual species are unknown, but it may be assumed that the system is linear—that changes in experimental variables alter only the concentrations of absorbing species. It is possible to resolve families of spectral curves obtained as a function of some experimental variable and to obtain equilibrium or rate constants as well as the spectra of the individual species. Two methods for solving this type of problem will be discussed.

The first method is a general one that will be illustrated by an example (*8*). The six curves plotted in Figure 2B were obtained by mixing various concentrations of a nonabsorbing component, A, and an absorbing component, B. It was proposed that the system be described by the following chemical model

$$A + B \overset{K}{\rightleftarrows} AB$$

$$K = [AB]/[A][B] \qquad (1)$$

Since only B and AB absorb in the wavelength region of interest, the observed curves A_i should be given by

$$A_i(\lambda) = [B]_i\epsilon_B(\lambda) + [AB]_i\epsilon_{AB}(\lambda) \qquad (2)$$

A convenient and useful approach treats spectra as vectors (*9*). A digital recording of a spectrum consists of a record of the absorbances at a finite number of wavelengths; thus, it is a set of p numbers. Such a set may be regarded simply as a single point located in p-dimensional space so that the p coordinates of the point are, numerically, the p absorbances of the spectrum. The point may be conceived of as the end of a vector from the origin; thus, a complete spectrum may be regarded as a single vector $\mathbf{A}_i$. If it is now postulated that the observed spectrum is that of two absorbing

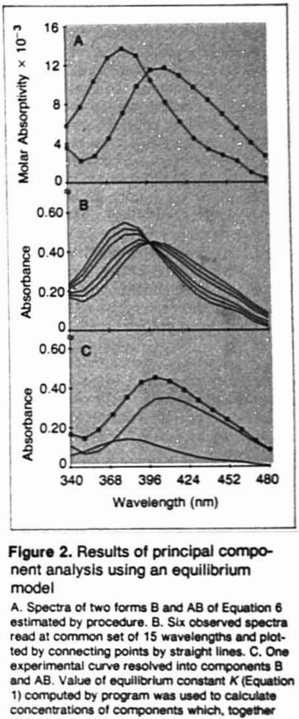

Figure 2. Results of principal component analysis using an equilibrium model

A. Spectra of two forms B and AB of Equation 6 estimated by procedure. B. Six observed spectra read at common set of 15 wavelengths and plotted by connecting points by straight lines. C. One experimental curve resolved into components B and AB. Value of equilibrium constant *K* (Equation 1) computed by program was used to calculate concentrations of components which, together with curves of 2A, were used to graph components and summation curve (upper solid line) components—a linear combination of two component spectra—the vector representing the observed spectrum may be thought of as the resultant of two component vectors in the p-dimensional space.

The next step in the analysis is to describe the two component p-dimensional vectors as vectors in *two*-dimensional space. This can be done since two vectors constitute three points, defining a plane. It follows that all vectors representing spectra of mixtures of the two components will be resultants of the two component vectors and, therefore, must all lie in one plane. All points in a plane may be located by two coordinates; therefore, all spectra of a two-component system may be represented by pairs of coordinates, that is, they may be represented as vectors in a plane plot. It would seem as if p-2 bits of information have been lost, but such is not the case, since the plane plot has been oriented in the p-dimensional space so that each vector in the plane implicitly represents all p bits of information. The eigenvectors provide a set of two orthogonal unit vectors which represent the coordinates of the plane plot. The analysis of a three-component system involves description of the spectra in terms of three eigenvectors, and so on.

To verify the two-component assumption suggested by Equation 2, one need only show that the observed $\mathbf{A}_i$ are linear combinations of the first two eigenvectors of the second moment matrix:

$$\mathbf{A}_i = \alpha_{1i}\mathbf{V}_1 + \alpha_{2i}\mathbf{V}_2 \qquad (3)$$

where $\mathbf{V}_1$ and $\mathbf{V}_2$ are the eigenvectors of the second moment matrix

$$M = [A'A]/n \qquad (4)$$

associated with the two largest eigenvalues of M. In Equation 4, A denotes the n by p data matrix

$$A = \begin{bmatrix} A_1(\lambda_1) \cdots A_1(\lambda_p) \\ \cdots\cdots\cdots\cdots \\ A_n(\lambda_1) \cdots A_n(\lambda_p) \end{bmatrix} \qquad (5)$$

[see Anderson (*10, 11*)] and A' is the transpose of A. If the reconstruction in Equation 3 is not within experimental error, then the presence of more than the assumed number of component species or of nonlinear effects such as peak shifts or bandwidth changes is indicated.

Once the two-component assumption is verified, we proceed to the second stage of the analysis—estimation of the shapes of these components. Note that their spectra must also be some (as yet unknown) combination of the eigenvectors:

$$\epsilon_B = \eta_{11}\mathbf{V}_1 + \eta_{12}\mathbf{V}_2$$
$$\epsilon_{AB} = \eta_{21}\mathbf{V}_1 + \eta_{22}\mathbf{V}_2 \qquad (6)$$

Solving for the ϵ's at some p wavelengths is reduced to the problem of solving for the η's.

A straightforward manipulation of Equations 1, 2, and 4 results in an expression for $\mathbf{A}_i$ as a linear combination of the vectors, the coefficients being functions of the initial concentration ($[A]_{0i}$ and $[B]_{0i}$), K, and the η's. Identification of these coefficients with the α's in Equation 3 results in a relationship of the form

$$\alpha = \sum_{i=1}^{2}\sum_{j=1}^{2} \eta_{ij}F(K; [A]_0, [B]_0) \qquad (7)$$

and K and the η's can be solved for by regression.

Figure 2A shows the resulting estimates for $\epsilon_B(\lambda)$ and $\epsilon_{AB}(\lambda)$. These estimates together with the calculated value of K were then used to reconstruct the $\mathbf{A}_i$ for comparison with the appropriate experimental curve. Figure 2C shows a comparison of the experimental points from one curve and the calculated curve (solid line) obtained by addition of the two resolved components. Significant lack of fit would have indicated that although the two-component assumption was correct, the proposed chemical scheme (Equation 1) was incorrect.

The method just described is applicable to any system in which a relationship between the concentrations of the absorbing species and the experimental variables is known. The principal advantages are that it provides a step-by-step method of testing hypotheses about the system being studied, and that the number of unknowns to be estimated (vector amounts rather than ϵ at each wavelength) is greatly reduced.

As an alternate approach, it is possible to proceed directly to the evaluation of the constants and the spectra of the individual species. In this case, the ϵ at each wavelength for each absorbing component is estimated by regression.

An example is the evaluation of multiple overlapping pK_a values for acids or bases (*1*). A more complex example (*1, 2*) is illustrated in Figure 3. An aldehyde, 5-deoxypyridoxal (designated P), and an amino acid, alanine (designated L), combine reversibly to form a Schiff base which has acid-base properties. Figure 3A is a diagram of the equilibria. Spectra were measured for various mixtures of the aldehyde and amino acid in the pH range 5–12. In separate experiments the spectra and pK_a values of 5-deoxypyridoxal were determined. By use of the latter "library data" together with the experimental spectra, a nonlinear least-squares procedure was used to find the values of the formation constant and the two pK_a values for the Schiff base (enclosed in boxes in Figure 3A). At the same time the spectra of the three ionic forms of the Schiff base (H_2PL, HPL, and PL) indicated in Figure 3A were estimated by linear least squares and are plotted in Figure 3B. Comparison plots of the type shown in Figure 3C are generated automatically by the computer program used.

These plots compare observed spectra from the input data (points x, O, etc.) with calculated curves (solid lines) based on the computed spectra of individual forms and calculated pK_a values. Small experimental errors (in pH or concentration) will appear as small systematic deviations. Any serious deviation may indicate that the chemical model used (the scheme in Figure 3A) is incorrect or incomplete. Failure may be due to the presence of more than the expected number of components or from nonlinear effects such as changes in band shape with changes in ionic composition. General programs able to accommodate equilibria of various types and capable of providing treatment of data similar to that in Figure 3 are available (*12*).

Nonlinear Systems

The methods described are applicable to many systems in which experimental variables alter the concentration of absorbing species without introducing nonlinear perturbations of the underlying shape functions such as peak shifts and changes in bandwidth. There are equilibria, however, such as tautomerism (*3, 4, 13, 14*) or solvation (*14, 15*) in which the position of equilibrium is shifted by changing the medium or temperature. These changes introduce nonlinear effects and the equilibria must be studied by resolution of experimental spectra into components as described in the next two sections.

Description of Spectra with Lognormal Distribution Curves. A useful approach to resolution of spectra is to fit each absorption band with a mathematically defined function. For example, spectra of inorganic complexes and the ultraviolet spectrum of the iodide ion are fitted well by Gaussian distribution curves (*16, 17*) as a function of wave number. However, most absorption bands of organic substances are distinctly skewed, and the Gaussian curve does not describe them accurately. The lognormal function (*2, 3, 18, 19*) often provides an excellent fit (*2, 3, 19–24*) as illustrated in Figures 1 and 5. For a Gaussian band, three parameters, the peak position ($\tilde{\nu}_o$), the height (ϵ_o), and width ($W = 2\sigma$), describe the curve. For lognormal an additional parameter, a dimensionless number ρ (Figure 1), defines the skewness. It can be shown that ρ, usually positive, approaches 1.0 as the lognormal approaches the Gaussian. Thus, the lognormal can be regarded as a skewed Gaussian. The lognormal is also very similar to the Poisson distribution, which might be expected to fit well on the basis of theory, but which is awkward to use (*25*).

At the top of Figure 1, the differences between the lognormal curve, which has been fitted to the spectrum of 1-methylcytosine and the experimental points, have been graphed. This difference plot, useful in visually evaluating the goodness of fit, shows that the maximum misfit in this curve is not much more than 1% of the peak height. While the lognormal is not always appropriate, we have applied it with excellent results to a large variety of compounds, including pyridine, phenol, benzoic acid, purines, pyrimidines, flavins, and aromatic amino acids (*23*). Band parameters used in obtaining the fits in Figures 1 and 5–7 are given in Table I.

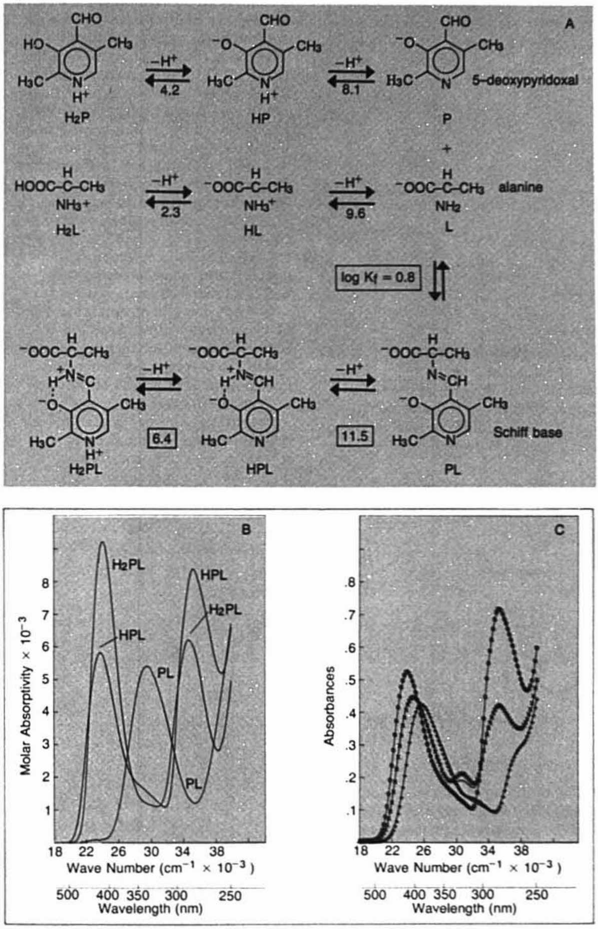

Figure 3. Evaluation of constants and spectra of 5-deoxypyridoxal and alanine

A. Equilibria involved in formation of Schiff base (PL) between aldehyde (P) and amino acid (L). Numbers below horizontal arrows give pK_a values for dissociations shown; K_f is pH-independent formation constant. Values enclosed in boxes found by computer-assisted, data-fitting procedure. B. Spectra of three ionic forms of Schiff base. These spectra are those computed for ionic forms shown in Figure 3A. Input data were 18 experimental spectra of solutions containing 1×10^{-4} M aldehyde and varying concentrations of amino acid and varying pH values, namely: pH 4.26, 6.18, 11.88, and 12.76 at 1.17 M amino acid; pH 5.02, 6.21, 11.92, and 13.00 at 0.5 M; pH 6.00, 6.77, 7.71, 8.89, 9.31, 10.20, and 12.44 at 0.05 M; pH 9.21 at 0.001 M; pH 9.45 at 0.01 M; pH 9.59 at 0.02 M amino acid. Values of log K_f and of pK_a's for Schiff base given in Figure 3A found by same computer program used to evaluate these spectra. C. Comparison plots generated by using spectra shown in Figure 3B together with equilibrium constants of Figure 3A to generate predicted spectra (solid lines). These are compared for three experimental solutions: (x) pH 6.77; (O) pH 9.31; (+) pH 12.44; all at 0.05 M alanine

Shape Functions from Self-Modeling. Not all absorption bands are fitted well with lognormal curves. The narrow, highly skewed low energy bands of the chlorophylls and of many dyes are examples. In the field of infrared spectroscopy, a variety of functions and empirical combinations of functions have been used to describe band shapes (*18*). The self-modeling of Lawton et al. (*26*) can also be used to obtain an empirical shape function. The shape function obtained may be shifted, stretched, or compressed to accommodate changes in amplitude, peak position, and width of spectral bands induced by changes in experimental conditions.

A series of spectra containing a mixture of components in varying ratios is required. The spectra of a two-component system could be described by Equation 8:

$$A_i(\lambda) = \epsilon_{1i} f_1\left(\frac{\lambda - \gamma_{1i}}{W_{1i}}\right) + \epsilon_{2i} f_2\left(\frac{\lambda - \gamma_{2i}}{W_{2i}}\right) \quad (8)$$

A_i is the measured absorbance of the i'th curve, f_1 and f_2 are the component shape functions to be determined, ϵ_{1i} and ϵ_{2i} are the absorbances or absorptivities at the maxima, γ_{1i} and γ_{2i} are the wavelengths or wave numbers of maximum absorbance, and W_{1i} and W_{2i} are the bandwidths at half peak height.

The method produces the shape functions common to the entire family of curves and peak locations, bandwidths, and amplitudes for each of the components corresponding to each individual curve in the family. The estimated shape functions are cubic splines (*27*) that are able to assume effectively any shape with relatively few parameters. The method is equally applicable to data recorded on a wavelength or wave number base. Note that the transformation of the axis in Equation 8 is arbitrary. Any transformation could be chosen.

In theory, one is not limited as to the number of component shape functions to be determined. In practice, however, due to the large number of unknown parameters, one is usually limited to one or two *different* shapes. It is often true, however, that all *n* components in a multicomponent system have the same shape. If the

Table I. Parameters Describing Shapes and Positions of Absorption Bands in Figures 1 and 5–7

Compound	Position, $\nu_0 \times 10^{-3}$ cm^{-1}	Height, $\epsilon_0 \times 10^{-3}$ L mol^{-1} cm^{-1}	Width, W × 10^{-3} cm^{-1}	Skewness, ρ
1-Methylcytosine (cationic)				
Band 1	35.35	11.95	4.12	1.44
Band 2	46.87	9.28	6.80	1.47
Schiff base of alanine and 5-deoxypyridoxal (low energy bands)				
Cationic (H_2PL) form	24.11	9.27	3.64	1.48
Neutral (HPL) form	23.85	5.83	4.23	1.39
5-Deoxypyridoxal cationic form				
Aldehyde, 2.4 °C	29.26	1.39	4.49	1.27
Hydrate, 2.4 °C	34.02	6.92	3.10	1.45
Aldehyde, 67.7 °C	29.36	3.01	4.70	1.24
Hydrate, 67.7 °C	34.01	3.87	3.25	1.45
Pyrazine	31.27	0.67	3.04	2.32
	38.74	4.95	3.20	1.42
Ribonuclease, pH 6.8	35.87	7.94	3.65	2.01
	44.87	11.19	6.90	1.26

shapes are different, frequently $n - 1$ of the component shape functions are accessible. The one unknown shape function can be estimated by the self-modeling method, and the positions, amplitudes, and bandwidths of all the n functions can be allowed to vary independently.

Systematic Studies of Effects of Temperature and Solvent Changes. Changing temperature or solvent usually causes nonlinear effects on band shapes. Medium effects also include changes in microscopic environment such as those that accompany the partitioning of absorbing species between solution and micelles or solution and polymers in aqueous media. The nonlinear effects have proved to be quite troublesome in measuring concentration ratios of indicator species for defining acidity functions in aqueous mineral acids (*28*). If one wishes to measure concentrations as a function of solvent or temperature, the changes in band shape must be taken into account. Fortunately, the area under an absorption band remains constant even though the molar absorptivity at a single wavelength does not, so long as the absorbing species is in molecular dispersion. The constancy of molar area, $a°$, represents an extension of the Beer-Lambert law and has been used to advantage in spectral studies of potassium iodide (*17*) and substituted 3-hydroxypyridines (*3*).

The constancy of $a°$ with changes in temperature or solvent, together with the ability to describe band shapes precisely, has provided a reliable method for evaluation of the tautomeric equilibria of the azo dye, 4-phenylazo-1-naphthol-2,4′-disulfonate (PND) (*4*).

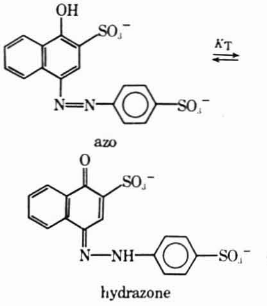

(9)

The tautomerization constant, K_T, is equal to [hydrazone]/[azo]. The hydrazone form predominates in water and water-rich binary mixtures, whereas the azo tautomer is the exclusive species in aprotic solvents. Changing solvent at a fixed temperature or changing temperature in a given solvent changes the band positions and bandwidths of the component curves as well as K_T. Since the shape functions of the two species are not changed and molar areas could be assumed constant, K_T could be determined in any solvent and at several temperatures by nonlinear regression from the ratio of areas under the resolved curves. The band parameters ($\tilde{\nu}_0$ or λ_0, ϵ_0, and W) were allowed to vary freely. The empirical shape functions used for resolving the experimental curves are shown in Figure 4A. The shape function for the pure azo form was determined from the experimental curve in an aprotic solvent. The function for the hydrazone was computed by the self-modeling method from families of experimental curves of varying tautomeric ratios.

Both of the curves shown in Figure 4 show contributions at short wavelengths from overlapping bands. These contributions have to be approximated by addition of more bands to resolve the curves with analytical functions (Gaussian, lognormal, etc.). Resolution with the empirical functions is simpler since the latter are not required to approach zero absorbance at any wavelength. The experimental curves in Figure 4 could be resolved by lognormal functions when plotted as a function of $\tilde{\nu}$, provided the curves were truncated at 380 nm to eliminate the contribution from the overlapping high frequency band.

Solvent-dependent tautomerization of 3-hydroxypyridines has been described by resolution of the low energy end of the spectrum with lognormal curves—one set for each of the two tautomers (*3*).

Solvation. Another type of pH-independent equilibrium is reversible solvation. An example is hydration of an aldehyde such as 5-deoxypyridoxal or pyridoxal phosphate:

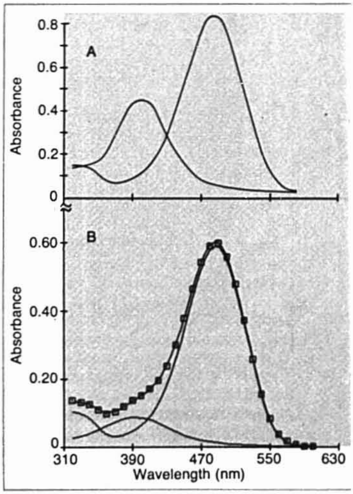

Figure 4. A. Empirically determined shape functions for hydrazone (long wavelenth band) and azo forms of dye PND (Equation 9). B. Resolution of mixture spectrum measured in 1.76 mol % *tert*-butyl alcohol in water at 25°

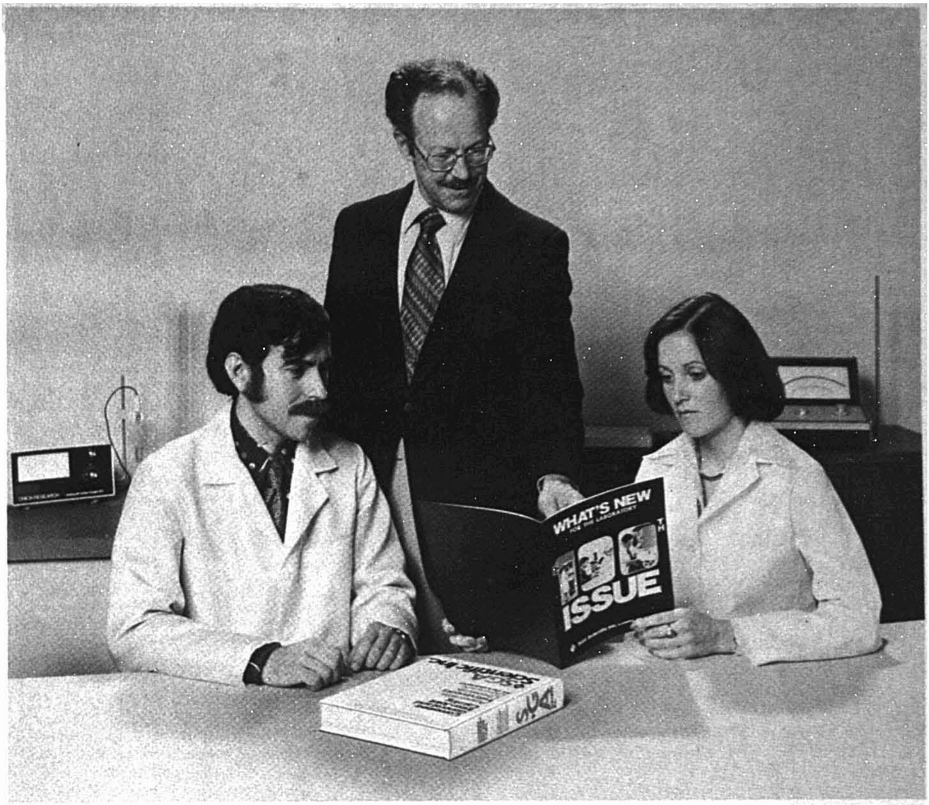

Something new for everyone.

That's how we look at "What's New for the Laboratory"

SGA Scientific has brought newsworthy product information to laboratory people for more than 30 years through our house publication.

We review what's new for the laboratory from a wide range of distinguished manufacturers, bringing together a variety of instruments, equipment and supplies in every issue. If it's new . . . if it fills a need in your laboratory . . . chances are it will appear in "What's New for the Laboratory."

Our readers are researchers, administrators, planners, and technical specialists; people like you who recommend, specify, approve and buy for the laboratory. "What's New for the Laboratory" is our way of keeping in touch. And of course, it serves as a continuing update for our General Catalog.

If you would like to receive the 100th Issue of "What's New for the Laboratory", just let us know. Write to SGA Scientific in Bloomfield, New Jersey, or to any of our branches.

SGA Scientific Inc.
735 Broad Street
Bloomfield, N.J. 07003

Branches: Boston, Mass./Elmhurst, Ill./Fullerton, Calif./New Haven, Conn./Philadelphia, Penna./Silver Spring, Md./Syracuse, N.Y.

CIRCLE 189 ON READER SERVICE CARD

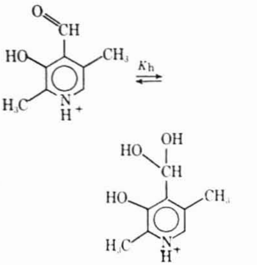

(10)

In this case, the equilibrium can be altered easily by changing the temperature as illustrated in Figure 5. The aldehyde cation is represented by a band at 29.4×10^3 cm^{-1}, and the hydrate by a band at 34.0×10^3 cm^{-1}. The bandwidths vary significantly with temperature, but if the molar areas (integrated intensities) are constant with temperature, the following relationship holds:

$$K_h = \text{fraction hydrate/fraction aldehyde} = \frac{a_h a^\circ_a}{a_a a^\circ_h} = -\frac{a_h}{a_a}\frac{\Delta a_a}{\Delta a_h} \quad (11)$$

Here, a_h and a_a are the measured areas of hydrate and aldehyde bands, and a°_h and a°_a are the molar areas for the individual components—areas which cannot be measured directly. However, the ratio a°_a/a°_h is equal to the ratio of the *changes* in area $\Delta a_a/\Delta a_h$ at any two temperatures (or different set of solvents). Hence, Equation 11 can be solved. Thus, for the data of Figure 5, $K_h = 2.2$; $a^\circ_a = 294$ km mol^{-1}; $a^\circ_h = 326$ km mol^{-1}. Because band width and skewness parameters can be fixed at preselected values appropriate for the compounds and conditions used, it is possible to resolve complex equilibria involving three or more tautomers and hydrates (e.g., in the neutral form of pyridoxal 5′-phosphate) with considerable confidence. Application to complex spectra of enzyme-substrate complexes is anticipated (*29*).

Solvent effects on the absorption curve of methyl orange dye in the visible region of the spectrum have been interpreted in terms of changing ratios of two unresolved bands (*15*). The low frequency component, which is predominant in water, was assigned to a hydrogen-bonded hydrate. Since neither pure component could be measured, identical shape functions were assumed, and resolution was accomplished by self-modeling nonlinear regression.

Vibronic Fine Structure. If a spectrum contains intense vibronic fine structure, as does that of pyrazine (Figure 6), band parameters are harder to define, but using a computer-assisted least-squares method, it is possible to find the lognormal parameters reproducibly. A difference plot showing the difference between each experimental point and the corresponding point on the mathematically fitted curve (sum of lognormals), when plotted against wave number, provides a striking display of the fine structure (Figure 6). This figure illustrates the vibronic structure of both the $\pi - \pi^*$ transition centered at 38.7×10^3 cm^{-1} and the $n - \pi^*$ transition at 31.3×10^3 cm^{-1} in hexane and with a prominent spacing at approximately 500 cm^{-1}. In derivatives of benzene the intensity of the fine structure changes with changes in the nature of the solvent. The positions of the peaks in the difference plot vary in almost the same way as the value of $\tilde{\nu}_0$ on the wave number scale.

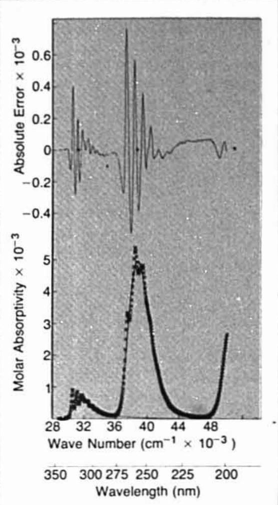

Figure 6. Spectrum of pyrazine in hexane

Both $n - \pi^*$ transition at 31.3×10^3 cm^{-1} and the $\pi - \pi^*$ transition at 38.7×10^3 cm^{-1} fitted with lognormal curves. Difference plots (computed as in Figure 1) provide convenient display of vibronic fine structure across entire widths of bands

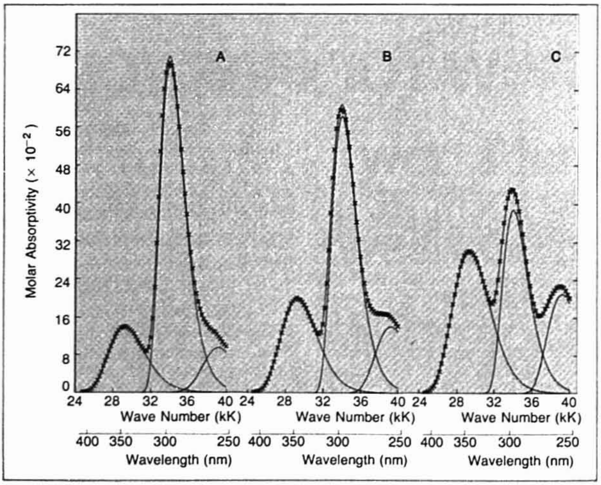

Figure 5. Spectrum of cation of 5-deoxypyridoxal in 0.1 M HCl at three temperatures (left to right, 2.4, 18.8, and 67.7 °C)

Spectra resolved with lognormal curves into bands representing aldehyde (unshaded) and covalent hydrate (shaded)

Spectra such as that of 1-methylcytosine (Figure 1) appear very smooth. However, the difference plots, shown at the tops of the figures, contain reproducible features that are directly related to underlying vibronic structure. These "fine structure plots" can sometimes be used to locate approximate positions of major sub-bands, and observation of their alterations with changes in environment may be useful.

Since electronic spectra are composites of many transitions arising from excitation of various vibrational modes in the ground and the excited states of the molecule, a logical possibility is to describe the spectrum as the summation of at least all of the principal vibronic sub-bands, each band being represented by a narrow Gaussian. This approach has become popular with the availability of analog computers of the "curve analyzer"

© 1977 MARKAD SERVICE CO./all rights reserved C-50

You can't mis-connect this QUICK-CONNECT!

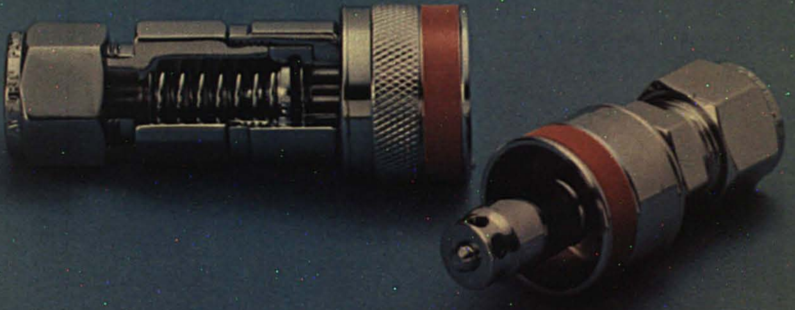

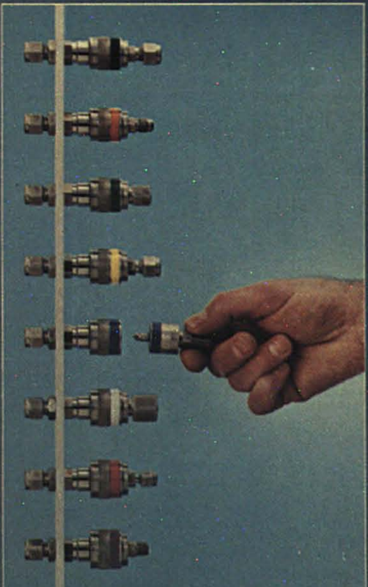

Patented

Swagelok® "Keyed" Quick-Connects prevent accidental intermixing of fluids in multiple line systems. Bodies and stems are "keyed," numbered and color coded to guarantee proper connections.

Eight different "keys" are available. Each "key" has a positive mechanical lockout system to prevent stems and bodies of unmatched "keys" from coupling with each other, or interchanging with any other type of quick-connect.

Automatic shut-off minimizes pressure loss or fluid spillage during uncoupling. An attempt to couple unlike "keys" will not open the shut-off valve and allow accidental flow.

Available in brass or 316 stainless steel, with tube connections or NPT pipe ends in 1/8", 1/4", 3/8" and 1/2" sizes. Immediate availability from local distributor stocks.

Swagelok®

CRAWFORD FITTING COMPANY
29500 Solon Road, Solon, Ohio 44139
Crawford Fittings (Canada), Ltd., Ontario

CIRCLE 32 ON READER SERVICE CARD

type. However, it is usually deemed impractical to use more than a small number of vibronic sub-bands. While the approach may be valid, we note that the first electronic absorption band of benzene contains over 80 sub-bands whose height is 1% or more of the maximum (*30*). Thus, in our minds, it is questionable whether attempts to sum the vibronic sub-bands are better than our method of portraying fine structure. In any event, if a digital output system is available, the method which we have described is simpler. We also note that the combination of band parameters tabulated, together with the fine structure plot, contains all of the information originally present in the spectrum. None is thrown away.

The spectra of a number of cationic dyes in aqueous solution present an interesting problem in curve resolution that is handled readily by digital methods. Spectra of monomeric cyanine dyes contain a single sharp, intense peak representing the 0–0 transition and a shoulder about 1200 cm^{-1} away on the high frequency side (*31*). The spectra can be described either by using analytical functions for the individual sub-bands or with empirical shape functions that include both sub-bands. West and Pearce (*31*) have described a monomer-dimer equilibrium for a cyanine dye in aqueous solution. They showed that the dimeric form of the dye absorbs in the same region as the high energy shoulder in the monomer spectrum. For resolution of spectra of such mixtures into mathematical components related to the two chemical components, empirical shape functions are superior to analytical functions because an absorption curve containing unresolved sub-bands can easily be described by a single spline function.

Difference Spectra and Proteins

The most popular way of examining small changes in spectra is to measure the difference between spectra of two solutions that are matched except for a difference in solvent composition, temperature, pH, etc. Unfortunately, no matter how careful the measurements, difference spectra give an incomplete picture. Without knowing one of the absolute spectra from which the difference was obtained, it is impossible to state what changes in the spectrum gave rise to the difference curve. In contrast, fine structure plots of the type shown in Figures 6 and 7 can be directly and easily understood. Experiments done at different times in different laboratories and on different compounds can all be compared, one with another.

Spectra of proteins have been studied most commonly by difference methods (*32, 33*) and at low temperatures (*34*). First derivative spectroscopy has also been used (*35*). Our methods of band shape analysis provide a fourth alternative. In one approach the 280-nm (35.7×10^3 cm^{-1}) band of proteins is fitted by a single lognormal band, and a second lognormal is used to fill in the valley up to $41–42 \times 10^3$ cm^{-1} (~240 nm) (*18*). The method gives a set of parameters giving the overall shape of the 35.7×10^3 cm^{-1} band plus a fine structure plot which often contains sharp peaks (Figure 7). Perturbation of a spectrum (as caused by pH changes or denaturation) can be recorded as a change in band parameters together with a change in fine structure. The peaks in the fine structure plot can often be related directly to those of the component aromatic amino acids. Thus, in a tryptophanless protein such as pancreatic ribonuclease, two peaks can be associated with tyrosine and up to five with phenylalanine (Figure 7).

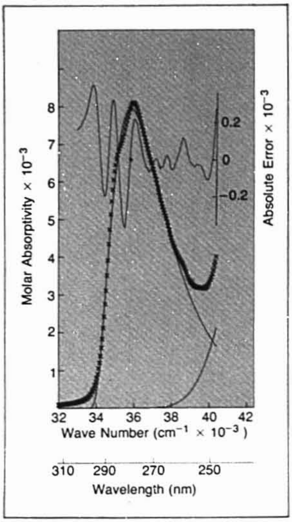

Figure 7. Spectrum of protein ribonuclease (lacking in tryptophan) at pH 6.8 fitted with two lognormal curves

Difference plot shows three high peaks (to left) resulting from vibronic structure in tyrosine bands and four lower peaks with characteristic spacing (to right) representing structure in very weak phenylalanine bands

A second approach to protein spectra is to assign separate lognormal bands to each amino acid. Then, by examining shifts, broadening, and other changes in band parameters, it may be possible to make more definite interpretations of spectral perturbations. This more complex approach is still under development. Similar methods are undoubtedly applicable to nucleic acids, e.g., to analysis of "melting" behavior.

Summary

The advantages of digital acquisition of spectrophotometric data and methods of computation are reviewed. The analysis of multicomponent spectra is considered for the following cases: (a) Spectra of all pure components of a mixture are known, and only their concentrations are unknown. (b) Spectra of one or more components and one or more equilibrium constants are unknown. A chemical model is used to relate the concentrations. The correctness of the chemical model can be tested, and the constants and spectra evaluated. (c) Nonlinear effects such as band broadening, frequency shifts, and changes in molar absorptivity occur along with changes in concentrations. Quantitative descriptions of such spectra using analytical functions such as the lognormal distribution curve or empirical spline functions are presented. The various cases are illustrated by examples published from the authors' laboratories.

Acknowledgment

We thank A. E. Cahill for assistance in preparation of the manuscript and D. Clark Bennett for technical assistance.

References

(1) K. Nagano and D. E. Metzler, *J. Am. Chem. Soc.*, **89**, 2891 (1967).
(2) R. J. Johnson and D. E. Metzler, *Methods Enzymol.*, **18A**, 433 (1970).
(2a) C. S. French, *Proc. Nat. Acad. Sci. USA*, **68**, 2893 (1971).
(3) D. E. Metzler, C. M. Harris, R. J. Johnson, D. B. Siano, and J. A. Thomson, *Biochemistry*, **12**, 5377 (1973).
(4) R. L. Reeves, M. S. Maggio, and L. F. Costa, *J. Am. Chem. Soc.*, **96**, 5917 (1974).
(5) K. T. Finley, R. S. Kaiser, R. L. Reeves, and G. Wernimont, *J. Org. Chem.*, **34**, 2083 (1969).
(6) J. A. Miller, P. Levoir, J. C. Fontaine, F. Garnier, and J. E. Dubois, *Anal. Chem.*, **47**, 29 (1975).
(7) J. M. Arends, H. Cerfontain, I. S. Herschberg, A. J. Prinsen, and A.C.M. Wanders, *ibid.*, **36**, 1802 (1964).
(8) E. A. Sylvestre, W. H. Lawton, and M. S. Maggio, *Technometrics*, **16**, 353 (1974).
(9) W. H. Lawton and E. A. Sylvestre, *ibid.*, **13**, 617 (1971).
(10) T. W. Andersen, "Introduction to Multivariate Analysis", Wiley, New York, N.Y., 1958.
(11) T. W. Andersen, *Ann. Math. Stat.*, **34**, 122 (1963).
(12) D. J. Leggett and W.A.E. McBryde, *Anal. Chem.*, **47**, 1065 (1975).
(13) R. L. Reeves and R. S. Kaiser, *J. Org. Chem.*, **35**, 3670 (1970).
(14) C. M. Harris, R. J. Johnson, and D. E. Metzler, *Biochim. Biophys. Acta*, **421**, 181 (1976).
(15) R. L. Reeves, R. S. Kaiser, M. S. Maggio, E. A. Sylvestre, and W. H. Lawton, *Can. J. Chem.*, **51**, 628 (1973).

REALLY!...

Time Saving is just the "tip of the iceberg" in Automatic Titration . . .

11798
PHM64 RESEARCH pH METER
TTT61 DIGITAL TITRATOR
AUTOBURETTE ABU13

Computerized Systems

Radiometer gives you so much more!

Radiometer's titration systems take the tedium out of titration, making more productive time available to you . . . as you enjoy the convenience of an automated, precise system that provides reliable results day after day after day.

Precision

Radiometer systems add titrant incrementally . . . rapid when it should be, then in decreasing quantities as the end-point is approached, until mere 10-thousandths of an ml. (or less) are being added . . . all automatically! Results are consistent — these systems eliminate overshoot.

Confidence & Dependability

When you specify Radiometer, you're selecting equipment which has proven itself worldwide for over 30 years. Radiometer's high standards of quality and workmanship ensure many years of reliable performance.

Versatility

Radiometer's modular approach to titration offers a broad selection of burettes, reaction vessels, pH meters, controllers and recorders — assuring the right combination for your applications and budget . . . today and tomorrow. Buy the capability you need . . . expand it as you need it.

Let us tell you how a Radiometer titration system can save you time and provide much more. For complete information and FREE Titration Appraisal Brochure contact:

Recording Systems

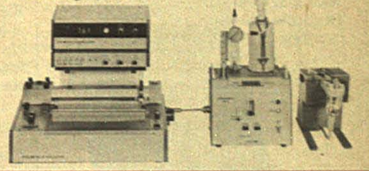

End-Point Systems

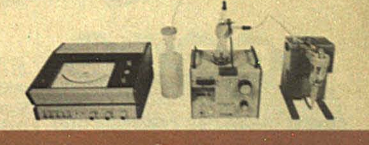

RADIOMETER COPENHAGEN

THE LONDON COMPANY
U.S. Representative for Radiometer-Copenhagen
811 Sharon Drive
Cleveland, Ohio 44145
Telephone (216) 871-8900

Radiometer . . . Innovators in Titration since 1941.

CIRCLE 129 ON READER SERVICE CARD

132
SOLUTIONS
FOR
TITRATION
PROBLEMS
CORCO

At Corco, we make 132 standard solutions — and uncounted special or custom solutions. Volumetric. Percentage. For Aqueous and nonaqueous titrations. Special solutions to meet ACS and ASTM requirements. Indicators. Buffers. Clinical reagents. All within an accuracy to 0.05%.

As many companies come to Corco for normal solutions as those for special normalities. We make them just as easily and just as well. Because Corco makes only reagent-grade solutions. (Reagent acids, bases, and specialty chemicals, too.)

Corco has the solutions — special or standard — in pints, gallons, five-gallons and drums. Write or call for your copy of our booklet with that title. Or circle the number.

CORCO
HAS THE
SOLUTIONS

CORCO

CORCO CHEMICAL CORPORATION
Manufacturers of
Reagent & Electronic Chemicals
Tyburn Road & Cedar Lane • Fairless Hills, Pa. 19030
(215) 295-5006

CIRCLE 35 ON READER SERVICE CARD

(16) C. K. Jørgensen, "Absorption Spectra and Chemical Bonding in Complexes", pp 91–3, Pergamon, Elmsford, N.Y., 1962.
(17) D. B. Siano and D. E. Metzler, *J. Chem. Soc. Faraday Trans.*, **268**, 2042 (1972).
(18) R.D.B. Fraser and E. Suzuki, *Anal. Chem.*, **41**, 37 (1969).
(19) D. B. Siano and D. E. Metzler, *J. Chem. Phys.*, **51**, 1856 (1969).
(20) D. B. Siano, *J. Chem. Educ.*, **49**, 755 (1972).
(21) I.-Y. Yang, R. M. Khomutov, and D. E. Metzler, *Biochemistry*, **13**, 3877 (1974).
(22) I.-Y. Yang, C. M. Harris, D. E. Metzler, W. Korytnyk, B. Lachmann, and P.P.G. Potti, *J. Biol. Chem.*, **250**, 2947 (1975).
(23) D. E. Metzler, C. M. Harris, I.-Y. Yang, D. Siano, and J. A. Thomson, *Biochem. Biophys. Res. Commun.*, **46**, 1588 (1972).
(24) R. Miura and D. E. Metzler, *Biochemistry*, **15**, 283 (1976).
(25) A. L. Koch, *J. Theor. Biol.*, **23**, 251 (1969).
(26) W. H. Lawton, E. A. Sylvestre, and M. S. Maggio, *Technometrics*, **14**, 3 (1972).
(27) S. Wold, *ibid.*, **16**, 1 (1974).
(28) R. L. Reeves, *J. Am. Chem. Soc.*, **88**, 2240 (1966).
(29) M. L. Fonda and R. J. Johnson, *J. Biol. Chem.*, **245**, 2709 (1970).
(30) L. Lang, "Absorption Spectra in the Ultraviolet and Visible Region", Vol I, p 367, Academic Press, New York, N.Y., 1961.
(31) W. West and S. Pearce, *J. Phys. Chem.*, **69**, 1894 (1965).
(32) J. W. Donovan, *Methods Enzymol.*, **27D**, 497 (1973).
(33) J. W. Donovan, in "Physical Principles and Techniques of Protein Chemistry", S. J. Leock, Ed., Part A, p 101, Academic Press, New York, N.Y., 1969.
(34) J. Horwitz, E. H. Strickland, and C. Billups, *J. Am. Chem. Soc.*, **92**, 2119 (1970).
(35) J. F. Brandts and L. J. Kaplan, *Fed. Proc.*, **30**, 1108 (1971).

Work supported by Grant AM-1549 from the U.S. Public Health Service.

Metzler

Harris

Reeves

Lawton

Maggio

David E. Metzler is professor of biochemistry at Iowa State University. His research interests are in the areas of biological catalysis, mode of action of vitamin-containing coenzymes, and spectroscopy of biochemical substances.

Carol M. Harris is a research technician at Iowa State University. Her interests are in spectroscopy, computer programming, and enzyme chemistry.

Richard L. Reeves is a research associate in the Kodak Research Laboratories. His present research interests include the physical and colloid chemistry of aqueous dye solutions, mixed micelles involving dyes, dye–dye and dye–polymer interactions, and the spectrophotometric analysis of dye solutions.

William H. Lawton is supervisor of the Applied Mathematics Section, a consulting unit of the Eastman Kodak Co. His publications have been mainly concerned with modeling of physical processes, with special emphasis on estimation involving nonlinear models, curve resolution, and spectral analysis. He has also published papers in both photographic theory and spectrophotometric analysis. Dr. Lawton is editor of *Technometrics*, a statistical journal of applications in chemistry, physics, and engineering.

Mary S. Maggio is a senior analyst in the Applied Mathematics Section of the Eastman Kodak Co. She has coauthored numerous papers on statistics and its applications to the physical and chemical sciences. Her special interest has involved nonlinear estimation and principal components analysis.

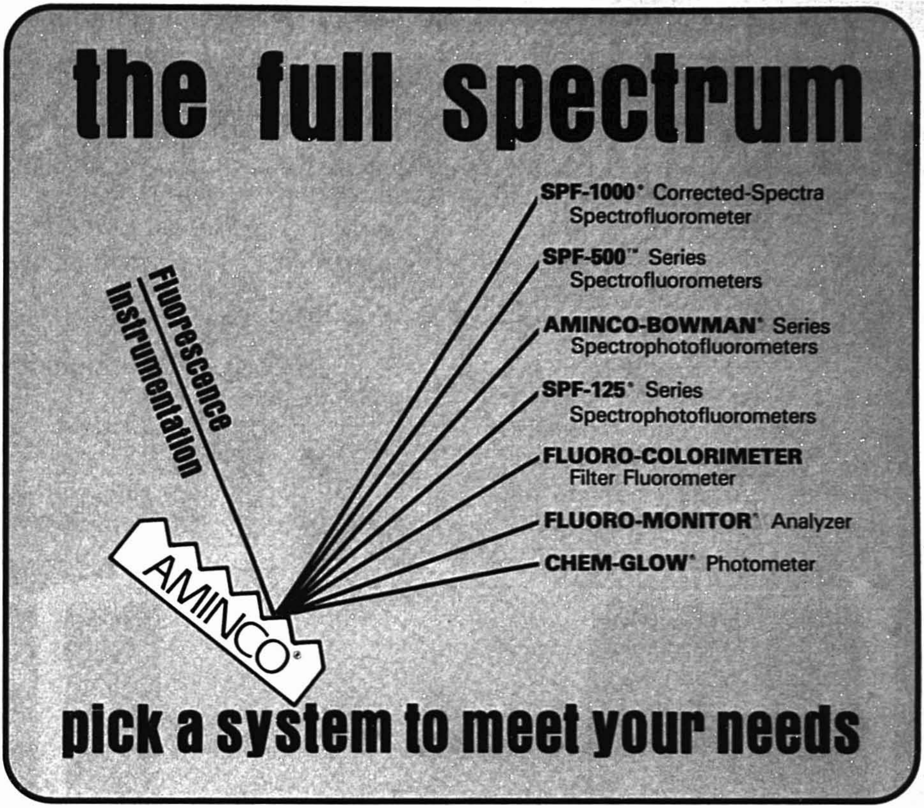
the full spectrum
Fluorescence Instrumentation
SPF-1000* Corrected-Spectra Spectrofluorometer
SPF-500™ Series Spectrofluorometers
AMINCO-BOWMAN* Series Spectrophotofluorometers
SPF-125* Series Spectrophotofluorometers
FLUORO-COLORIMETER Filter Fluorometer
FLUORO-MONITOR* Analyzer
CHEM-GLOW* Photometer
AMINCO®
pick a system to meet your needs

SPF-1000 CORRECTED-SPECTRA SPECTROFLUOROMETER — top-of-the-line instrument for the most sophisticated research applications.

SPF-500 SERIES SPECTROFLUOROMETERS — quality grating instruments for today's research needs with a sensitivity and resolution comparable to the SPF-1000 instrument.

AMINCO-BOWMAN SERIES SPECTROPHOTOFLUOROMETERS — provide wavelength scanning with high-quality grating separation of wavelength. Over 5,000 units are currently in use.

SPF-125 SERIES SPECTROPHOTOFLUOROMETERS — for non-scanning or scanning applications using grating separation of wavelength.

FLUORO-COLORIMETER — for filter fluorometry, colorimetric, tubidimetric, and nephelometer applications.

FLUORO-MONITOR ANALYZER — for high-performance liquid chromatography fluorescence applications.

CHEM-GLOW PHOTOMETER — for bioluminescent and chemiluminescent applications.

See us at the **FACSS Meeting and the A.O.A.C. Meeting, Booth No. 11.**

For further details, contact your local representative or

AMINCO® AMERICAN INSTRUMENT COMPANY
DIVISION OF TRAVENOL LABORATORIES, INC.
Silver Spring, Maryland 20910 · Phone: 301-589-1727

©1977 Travenol Laboratories, Inc.

CIRCLE 3 ON READER SERVICE CARD

The first family of Microprocessor GC's starts at

$7500*

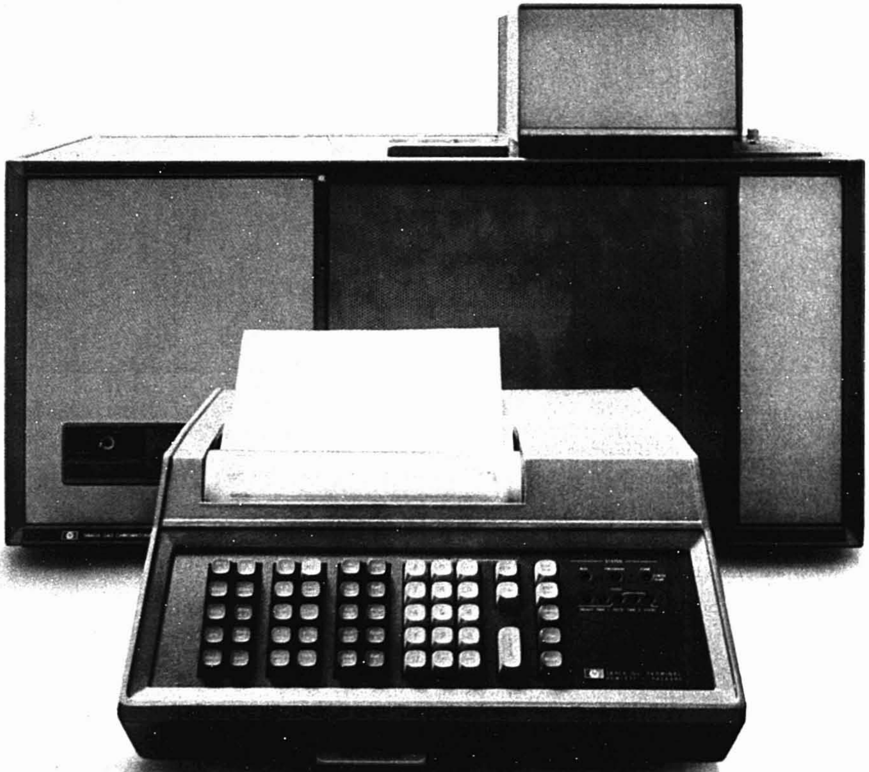

*U.S. Domestic Price Only

$7500* buys you HP 5800 series high performance chromatography with integrated keyboard control, printer/plotter output, peak area integration, area percent calculation, autoranging FID and power fail protection. Save operator time and improve the precision of your lab.

In addition, you get the ability to expand directly to...

Complete Methods Calculations

Automatically performs normalization, internal standard, or external standard calculations saving you from this routine task.

Internally Controlled Automatic Sampling Systems

No operator required. After initial setup, the processor takes over and frees you from button pushing.

Time Programming

Analysis parameters are adjusted throughout the run removing the need for a standby operator.

Run Programming

Autorecalibration and parameter changes between injections without the need for your intervention.

Magnetic Card Programming

Provides infinite method storage and data entry eliminating tedious keyboard reentry with possible error introduction.

Amplified-Autoranging TCD

Provides high sensitivity without operator concern for amplifier range.

External Alarm

Monitors your analysis to assure that a critical component is within specified levels.

Processor Controlled Automated Valving

Allows on stream analysis of multiple sample streams and column switching for complex analyses.

Standard Analyzers for Special Applications

Tailored solutions for the analysis of refinery gas, transformer oil gas, trace organics in water, atmospheric contaminants and other separation problems.

Glass Capillary System

May be used as a splitter or in a fully-automated purged/splitless mode.

Post Run Custom Calculations

When you require special calculations, they are performed automatically at the end of every run by an HP calculator or data system.

Hewlett-Packard offers the GC system to fit your needs with price/performance to fit your budget.

43703

HEWLETT hp PACKARD

Route 41, Avondale, Pennsylvania 19311

For assistance call: Washington (301) 948-6370, Chicago (312) 255-9800, Atlanta (404) 955-1500, Los Angeles (213) 877-1282

CIRCLE 96 ON READER SERVICE CARD

Look twice.

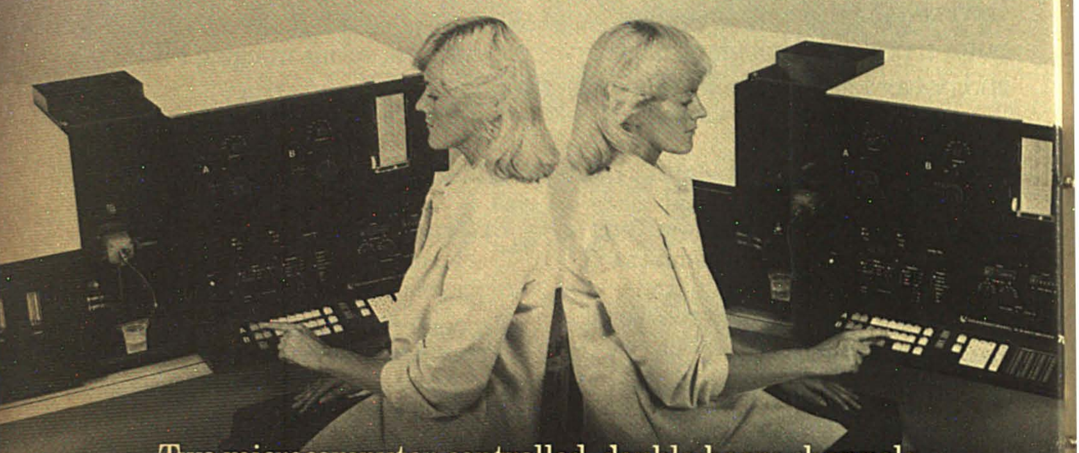

Two microcomputer-controlled, double-beam channels make the new IL751 Atomic Absorption Spectrophotometer your best buy.

The **IL751 Atomic Absorption Spectrophotometer**, with its two microcomputer-controlled double-beam channels, can determine twice as many elements in a given time. You can also use the second channel for an internal standard to get vastly improved accuracy. The microcomputer is by far the most powerful now built into any AA instrument.

At first sight, you might think that you'd have to pay dearly to get an IL751. Look again. *The base price is only $16,000.00.**

The $16,000 base price of the IL751 is only about 20% higher than that of top-of-the-line competitive instruments that do far less. The price is comparable to the lowest-priced double-beam instruments around, if you figure it at $8,000 per channel. And what channels!

Internal Standard, Statistics, Speed, Simplicity.

- Two channels mean two simultaneous elements, twice the analytical speed. Especially important with furnace atomizer.
- Calibration is exact and permanent. The first time, you can use up to five standards, in any order, each run several times. After that, you don't need to do it again. Just enter the values from the keyboard, run one standard once only, and press "Auto-Cal".
- Get superior accuracy by using "internal standard" mode to compensate for sample viscosity, dilution errors, or changes in flame conditions.
- Read statistics — mean, standard deviation, and relative standard deviation — on up to 99 determinations.
- Analyst calibrates it, anybody runs it. In Format Lock mode, keyboard is immune to changes. The only keys left alive are "Auto-Zero", "Auto-Cal" and "Read".

A 16-page technical article describes successful analyses.

Not everybody understands the ability of the internal standard mode to improve accuracy and simplify sample preparation. Now, it is clearly explained in a 16-page article, with examples from cement and steel analysis. The article also gives data on a cross-section of important analyses, including dual-element flame analyses of waters, steel, ores, and fertilizers; background correction in emission; and simultaneous determinations with the furnace atomizer of As/Se, and Pb/Cd in waters, and Ba/Sb in gunshot residues. Ask for Reprint 84.

The atomic absorption leader has a new name. It's . . .

Instrumentation Laboratory
Analytical Instrument Division
Jonspin Road, Wilmington, MA 01887
CIRCLE 104 ON READER SERVICE CARD

*U.S. price. Subject to change without notice.

ORNL Conference on Analytical Chemistry in Energy Technology

Gatlinburg, Tenn.
October 4–6, 1977

Analytical Chemistry in Nuclear Fuel Processing will be the topic of the 21st Conference on Analytical Chemistry in Energy Technology, October 4–6, 1977, in Gatlinburg, Tenn. This annual conference is sponsored by Oak Ridge National Laboratory and its Analytical Chemistry Division. The conference will emphasize the role of the analytical chemist in solving problems arising from new directions in energy research. One entire day's session is devoted to accountability and safeguards, and another full day's session is concerned with nondestructive methods of analysis. Other subjects include instrumental methods for determination of uranium and plutonium, and in-line and effluent analysis. The $35 registration fee includes a copy of the proceedings to be published in early 1978 and an outdoor mountain cookout, complete with clog dancing, on October 5. For those not registering for the entire conference, there will be a charge of $10 per day. Reservations for lodging should be made directly with the Riverside Motor Lodge, Gatlinburg, Tenn. 37830. Other inquiries should be directed to L. J. Brady, ORNL, P.O. Box X, Oak Ridge, Tenn. 37830. The detailed preliminary program appears below. In addition to the technical sessions, there will be an exhibition in the lobby of the Riverside Motor Lodge.

Tuesday, October 4

Accountability and Safeguards: Session I

Chairman: C. D. Bingham, ERDA

9:00 Welcome. W. D. Shults, ORNL

9:15 Enrichment of Safeguards. H. E. Lyon, ERDA

9:45 Some Aspects of Analysis for Accountancy at Windscale. I. R. McGowan, England

10:05 Analytical Chemistry Needs for Safeguards in Nuclear Fuel Reprocessing. E. A. Hakkila, LASL

10:45 Significance of Nuclear Material Assay Methods for Safeguards. Joseph Goleb, ERDA

11:05 HEDL Safeguards NDA Programs. Paul Goris, Dennis Fazzari, HEDL

11:25 Mission and Responsibility of a National Safeguards Laboratory. C. D. Bingham, ERDA

Accountability and Safeguards: Session II

Chairman: J. A. Carter, ORNL

1:30 U.S. Technical Assistance to IAEA in Safeguards. H. Kouts, BNL

1:50 Role of Destructive Analysis in IAEA Safeguards. Stein Deron, IAEA

2:10 Preparation and Isotopic Analysis of U and Pu for Safeguards. J. A. Carter, R. L. Walker, ORNL

2:30 Laboratory Quality Assurance and Its Role in Nuclear Fuel Reprocessing and Refabrication. W. L. Delvin, HEDL

3:10 Verification of Reprocessing Plant Input and Output Analyses: Practical Experiences in Reprocessing of Lightwater Reactors with Burn-ups up to 39 GWD/KG. Rolf Berg, Germany

3:30 Accountability Methods for Plutonium and Uranium: NRC Manuals. R. G. Gutmacher, F. B. Stephens, LLL

3:50 Barnwell Nuclear Fuels Plant Material Accounting and Control System. G. D. Workman, G. A. Huff, D. G. Hill, C. Joseph, AGNS

4:10 Uranium Mass Analysis for Accountability Purposes. E. E. Fylby, R. L. Hand, M. A. Wade, Allied Chemical

Wednesday, October 5

Instrumental Analysis for Uranium and Plutonium

Chairman: G. R. Waterbury, LASL

8:30 Determination of Submilligram Amounts of Uranium with LASL Automated Spectrophotometer. D. D. Jackson, R. M. Hollen, S. F. Marsh, M. R. Ortiz, J. E. Rein, LASL

8:50 Evaluation of Automated Titration System for Determination of Uranium. K. Lewis, D. L. Colwell, C. G. Goldbeck, ERDA; J. E. Harrar, LLL

9:10 Improved Technique for Controlled Potential Coulometric Determination of Plutonium. M. K. Holland, J. R. Weiss, C. E. Pietri, ERDA

9:30 Highly Selective Coulometric Method and Equipment for Automated Determination of Plutonium. D. D. Jackson, R. M. Hollen, F. R. Roensch, J. E. Rein, LASL

10:10 System of Plutonium Analyses in PNC Plutonium Fuel Fabrication Facilities. T. Itaki, K. Onishi, H. Isagawa, M. Aoki, Japan

10:30 Automated Fluorometer for Uranium Analysis. R. J. McElhaney, J. D. Caylor, S. H. Cole, T. L. Futrell, UCND

10:50 Calorimetric Assay of Plutonium. W. W. Rodenburg, D. R. Rogers, Mound Laboratory

11:10 Conceptual Description of Real-Time Computerized Laboratory Instrumentation System-22-S Laboratory, Rockwell Hanford Operations. D. L. Anderson, Rockwell

In-Line and Effluent Analysis

Chairman: B. L. Vondra, ORNL

1:30 In-Line and Off-Line Destructive Chemical Analysis in Nuclear Fuel Reprocessing. B.-G. Brodda, Germany

1:50 In-Line Measurements for Fuel Reprocessing Plant. M. H. Campbell, H. M. Jones, Exxon

2:10 Discussion of Remote Techniques Used in Analysis of Irradiated Fuel Processing Streams. D. N. LeMaire, D. R. Trammell, J. P. Henscheid, M. A. Wade, Allied Chemical

2:30 Remote Sampling System and On-Line Analytical Monitors in Barnwell Nuclear Fuels Reprocessing Plant. W. L. Belew, G. A. Huff, L. F. Sears, AGNS

3:10 Automated Particle Size Analysis of Sol-Gel and HTGR Fuel Microspheres. J. E. Mack, ORNL

3:30 Radioactive Particulate Studies in Gaseous Effluents at Nuclear Fuels Reprocessing Facility. R. C. Girton, A. K. Herbst, Allied Chemical

3:50 Actinide Analytical Program for Characterization of Hanford Waste. S. J. Johnson, W. I. Winters, Rockwell

4:10 Determination of Tritium in Solutions from Nuclear Fuel Reprocessing. E. W. Baumann, K. W. MacMurdo, SRL

Thursday, October 6

Nondestructive Analysis: Session I

Chairman: G. R. Keepin, LASL

8:30 Process Control in Fuel Reprocessing—Applying Destructive and Nondestructive Nuclear Physics Determination Techniques. P. Filss, H. Kirchner, Germany

8:50 On-Line Measurement of Total and Isotopic Plutonium Concentrations by Gamma-Ray Spectrometry. K. J. Hofstetter, G. A. Huff, AGNS; R. Gunnink, J. E. Evans, A. L. Prindle, LLL

9:10 Nondestructive Determination of Burn-up by Gamma-Scanning: Examination of ^{144}Ce/Pr and ^{134}Cs/^{137}Cs as Fission Monitors in Candu Fuels. J. D. Chen, D. G. Boase, R. B. Lypka, D. G. Zetaruk, Canada

9:30 Neutron Methods for Assay of Fissionable Material in Presence of Fission Products. T. Crane, D. A. Close, M. S. Krick, H. O. Menlove, LASL

9:50 Nondestructive Analysis of Rover Fuel Using Isotopic Source Assay System. L. E. Trejo, Allied Chemical

10:30 Assay of Fissionable Isotopes in Aqueous Solution by Pulsed Neutron Interrogation Method. P. Campbell, D. G. Boase, E. M. Gardy, Canada

10:50 Nondestructive Assay Instruments for LASL Dymac Program. R. S. Marshall, LASL

11:10 Measurement of Special Nuclear Material Concentrations in Solution by Absorption Edge Densitometry. T. R. Canada, D. G. Langner, J. L. Parker, J. W. Tape, LASL

11:30 Close-Coupled X-ray Analysis of Mixed Oxide Fuels. M. C. Lambert, M. W. Goheen, M. W. Urie, N. Wynhoff, HEDL

Nondestructive Analysis: Session II

Chairman: D. A. Costanzo, ORNL

1:30 Statistically Designed Experiment to Determine Effect of Nonhomogeneity on NDA Measurements for Plutonium. L. P. McRae, D. F. Shepard, A. E. Schilling, G. T. Furner, D. A. Sebelien, Rockwell

1:50 Preparation of Test Materials for Interlaboratory Comparison Program on NDA Physical Standards. A. M. Voeks, N. M. Trahey, J. M. Scarborough, ERDA

2:10 Analysis of Refabricated Fuel: Determination of Carbon in Uranium Plutonium Mixed Carbide. S. Huwyler, Switzerland

2:30 Detection of Carbon Dioxide in Gases Evolved During Hot Extraction Determination of Hydrogen in Ingot Uranium Metal. Milton L. Jursik, J. D. Pope, National Lead

2:50 Predictive Thermogravimetric Technique for Close-Coupled Oxygen-to-Metal Ratio Analysis of Uranium-Plutonium Oxide. G. C. Swanson, HEDL

3:10 Nondestructive Analysis of Plutonium Contaminated Soil. H. E. Smith, L. H. Taylor, Rockwell

12th International Symposium on Advances in Chromatography

November 7–10, 1977

The Twelfth International Symposium on Advances in Chromatography will be held November 7–10, 1977, at the International Congress Centre RAI, Amsterdam, The Netherlands. A

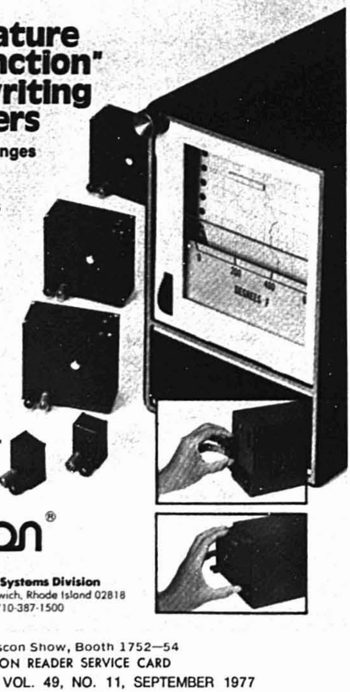

Rustrak miniature "plug-in-a-function" continuous writing servo recorders

Buy one . . . Plug in 100 Ranges
With one recorder you can record ac and dc volts and amps, temperature, process data and more. Owning the versatile, direct-writing Rustrak 400A is like having 100 recorders. In stock at your local authorized Rustrak distributor.

Attention OEM's. Custom mounting arrangements, colors, nameplates, chart paper and scales available.

New 32 Page Catalog.
Provides details on DC, AC, Temperature, Servo, Multichannel, Event and a variety of special recorder types.

gulton®
Measurement & Control Systems Division
Gulton Industries Inc., East Greenwich, Rhode Island 02818
401-884-6800 • TWX 710-387-1500

See us at Wescon Show, Booth 1752—54
CIRCLE 83 ON READER SERVICE CARD

Get the most consistent chromatography with more consistent Chromosorb® supports.

Whether you're doing gas or liquid chromatography, the consistency of your results often depends on the consistency of your support material. For the most uniform results time after time, specify Chromosorb. Only Chromosorb diatomite supports are quality controlled from the ground up by one manufacturer. Only Chromosorb offers you three types of column packings to fit your needs.

For Liquid Chromatography

(Circle 107)

The Chromosorb LC-Series is the newest of the Chromosorb lines. Currently two supports are available. LC-1 is the first diatomite-based support compatible with all liquid phases. LC-2 is a pellicular packing specifically developed for high-speed, high-efficiency liquid-solid chromatography. LC-3, 4, 5 and 6 will be available in the very near future.

For Gas Chromatography
Diatomite Supports

(Circle 108)

Johns-Manville has a complete line of diatomite supports for gas chromatography too. Chromosorb A, G, P and W are specially processed diatomite supports available acid washed or non-acid washed for a variety of analyses. Chromosorb G, P and W can be ordered with a DMCS treatment. Chromosorb 750 and high performance grades of W and G are highly efficient diatomite-based supports specifically designed for biomedical and pesticide analysis. A fluorocarbon resin, Chromosorb T, is used for separation of highly polar or reactive compounds.

Porous Polymers

(Circle 109)

The Chromosorb Century Series consists of eight porous polymer packing materials made of cross-linked resin with a uniform rigid structure of a distinct pore size and having different surface characteristics. They have found wide application in a number of difficult separations, i.e., water, gases, alcohols, fatty acids, glycols, etc.

For technical assistance about any chromatographic situation, contact Jack Denboske, Johns-Manville, Box 5108-FM, Denver, CO 80217. Count on his support, count on our more consistent supports.

CIRCLE 110 ON READER SERVICE CARD

JM
Johns-Manville

Johns-Manville
JM
Chromosorb
750
Johns-Manville
JM
Chromosorb LC-1
LIQUID CHROMATOGRAPHIC SUPPORT
Johns-Manville
JM
Chromosorb® 102

total of 84 papers representing contributions from 20 countries will be presented at the symposium. A special feature of the meeting will be an exposition of the latest instrumentation and books. In addition to the six formal symposia sessions entitled New Horizons, Gas Chromatography, Environmental Problems, Biochemical Gas Chromatography, Thin-Layer Chromatography, and High-Performance Liquid Chromatography, there will be two poster sessions and six informal discussion groups. The proceedings of the symposium will be published in the *Journal of Chromatography* in a single issue. Registration should be made in advance. The programs, registration forms, and hotel reservation cards can be obtained from Organisatie Bureau Amsterdam b.v., International Congress Centre RAI, P.O. Box 7205, Europaplein 14, Amsterdam, The Netherlands; or A. Zlatkis, Chemistry Department, University of Houston, Houston, Tex. 77004. The technical sessions are scheduled as follows:

Monday, November 7, *Morning:* New Horizons. *Afternoon*: Gas Chromatography, Environmental Problems

Tuesday, November 8, *Morning*: Biochemical Gas Chromatography. *Afternoon*: Thin-Layer Chromatography

Wednesday, November 9, *Morning*: Informal Discussion Groups on High-Performance Thin-Layer Chromatography, Environment, Selective Detectors. *Afternoon*: Informal Discussion Groups on Liquid Chromatography, Biomedical Gas Chromatography, High-Resolution Columns; Poster Sessions on Gas Chromatography, Liquid Chromatography

Thursday, November 10, *Morning and Afternoon*: High-Performance Liquid Chromatography

Compare Balances . . .
Sauter has a broader range of electronic and mechanical balances; far heavier, sturdier construction; and better prices.

Electronic Precision Balance Typ RS 25

SAUTER RS 25

Electronics
12 Capacities
Dual ranges. Automatic Tare. Analog and Digital outputs. Readings to 10 mg. Capacities from 80 g to 1200 kg.

Analyticals
18 Models
Readability to 1 microgram, capacities from 2 mg to 200 grams. Tare, pre-weigh, hydraulic release, high weighing chambers, etc.

Top Loaders
20 Models
Digital and „hands-off" Analog models with capacities from 160 g to 20 kg. Readability to 1 mg. Interchangeable pans. Tare. Auto-Levelling, etc.

Compounding? Batching?
Be sure with Sauter!
Three digital readouts give an overview of the whole operation. Read the weight of each ingredient as you add it. And also read the total weight of all the ingredients previously added. All electronic, 1 gram precision, 25 kg capacity.

For a catalog describing the extensive Sauter Lab Balance line, write or call:

SAUTER

August Sauter of America, Inc.
80 Fifth Avenue
New York, N. Y. 10011
Phone (212) 685-6659
Telex 421790

CIRCLE 188 ON READER SERVICE CARD

When you choose Precision you get something extra... S/P

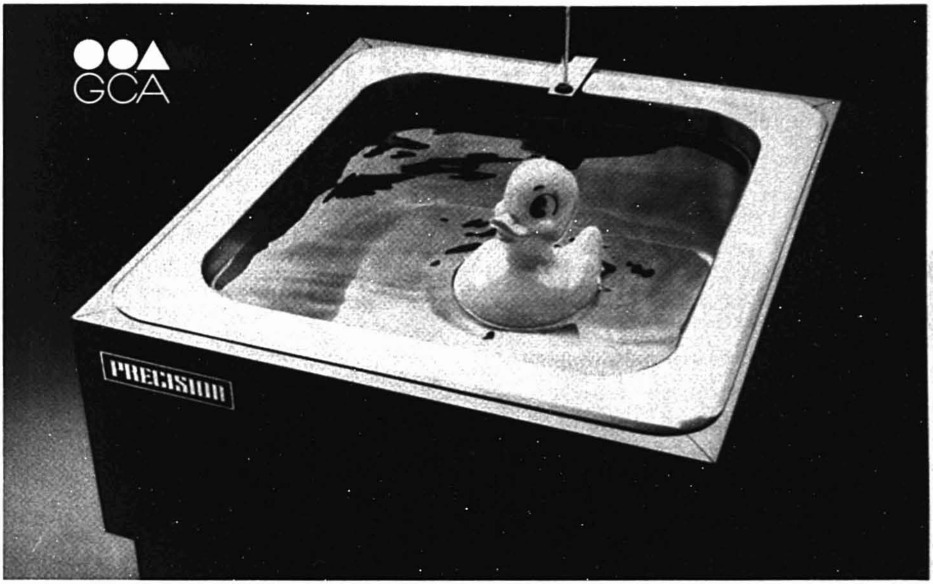

Buy a lab bath the way you buy a people bath. Buy it to last 20 years, to work reliably under daily use.

Buy it for temperature uniformity. On the Model 184 shown here, PRECISION *guarantees* uniformity throughout the bath to ±0.15°C. at 37°C. and at 57°C. (with cover in place).

Buy it for quality construction, for PRECISION'S one-piece, deep-drawn, stainless steel chamber, with no welds or seams to wear or weaken.

Buy it for the name you can trust. In forty years PRECISION has built more lab baths than all other manufacturers—that includes the whole flock. Quack.

Ask your S/P Representative for the free catalog of PRECISION Laboratory Baths.

PRECISION™

Something extra... S/P

S/P carries a lot of laboratory items. But, then, S/P is a leading distributor for more than 550 top manufacturers. To handle this huge inventory smoothly, we have 25.4 million cubic feet of warehousing space, 1.9 million cubic feet of chemical vaults, and 25 strategically located stocking centers. You benefit with a wider choice in all grades and price ranges. And we're flexible enough to stock any laboratory supply items and chemicals used in research, quality control or production specifically for you. It's all part of the S/P Responsive System of service for professionals like you. Call your S/P Representative and take stock of him.

S/P®

scientific products
distributor of chemicals, laboratory supplies
and scientific instruments
Division of American Hospital Supply Corporation
1430 Waukegan Road, McGaw Park, IL 60085

CIRCLE 190 ON READER SERVICE CARD

91st Annual Meeting of AOAC

October 17–20, 1977

The Association of Official Analytical Chemists expects more than 1300 attendees for its 91st Annual Meeting to be held October 17–20, 1977, at the Marriott Hotel, Twin Bridges, Washington, D.C. Over 240 scheduled presentations will cover the areas of new techniques, methods, and instrumentation for analysis of foods, drugs, pesticides, cosmetics, forensic materials, hazardous substances, feeds, fertilizers, and other materials related to agriculture and public health and welfare.

Three symposia and two workshops are scheduled to take place during the four-day meeting. Topics of these symposia and dates are: drug residues in animal tissues, Monday, October 17, and Tuesday, October 18; high-pressure liquid chromatography, Wednesday, October 19; and environmental pollutants, Thursday, October 20. A thin-layer chromatography workshop conducted by Kontes Glass Co. will be held Tuesday evening, October 18. An automated analysis workshop run by Technicon Industrial Systems, Tarrytown, N.Y., will be held Wednesday evening, October 19.

Immediately before the meeting, on October 15 and 16, the American Chemical Society will hold a course on "High-Pressure Liquid Chromatography" conducted by David H. Freeman of the University of Maryland (for more information see page 896 A).

A reception on Monday evening, October 17, at 6:30 p.m. will be followed by the Harvey W. Wiley banquet at 7:30 p.m. The highlight of the banquet will be the presentation of the Wiley Award to Gunter Zweig, Environmental Protection Agency, Office of Pesticide Programs, for his outstanding contributions to the development of chromatographic techniques for pesticide analysis.

Nearly 40 firms will exhibit laboratory equipment and supplies. Registration will be from 1 p.m. Sunday, October 16–Thursday morning, October 20. The fee is $10 for one day or $20 for two or more. For further information, contact L. G. Ensminger, AOAC, Box 540, Benjamin Franklin Station, Washington, D.C. 20044.

Steven Dal Nogare Award

The Delaware Valley Chromatography Forum invites nominations for the Steven Dal Nogare Award. The award, consisting of $500 cash and an inscribed plaque, is given annually for significant contributions to chromatographic theory, instrumentation, or applications. The award will be presented at the Pittsburgh Conference on Analytical Chemistry and Applied Spectroscopy in Cleveland, February 27–March 3, 1978. The recipient will be expected to give an award address.

Nominations including a brief bibliography and a list of accomplishments related to chromatography should be submitted before November 15 to Lyle H. Phifer, Chem Service Inc., P.O. Box 194, West Chester, Pa. 19380.

"OSHA & US"

A new 17-min, 16-mm color film entitled "OSHA & US" has been produced by the University of Michigan Television Center in cooperation with the National Institute for Occupational Safety and Health. The intent of the film is to make people in academic, research, and medical institutions,

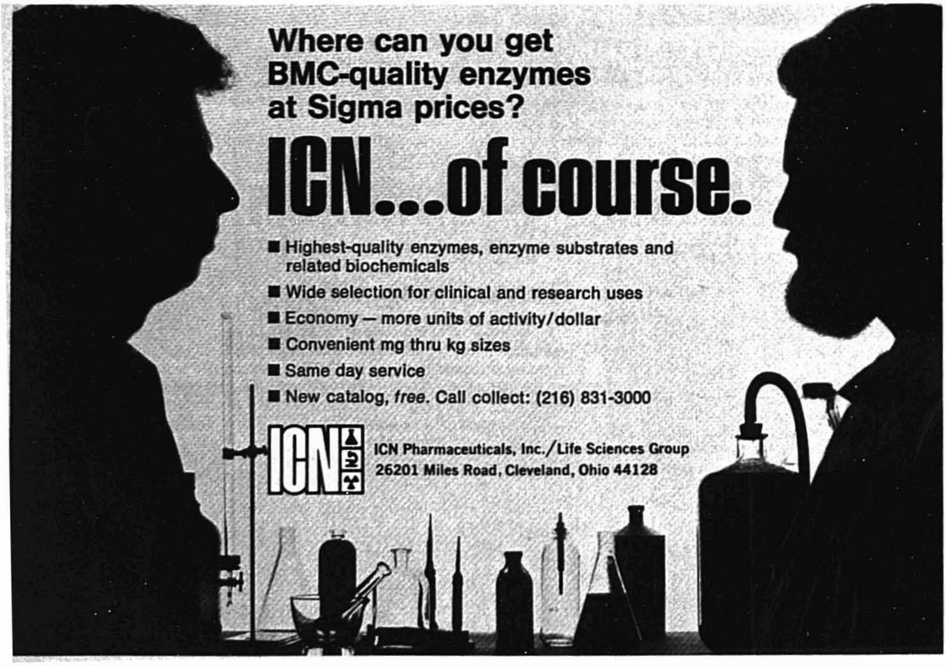

Where can you get BMC-quality enzymes at Sigma prices?

ICN...of course.

- Highest-quality enzymes, enzyme substrates and related biochemicals
- Wide selection for clinical and research uses
- Economy — more units of activity/dollar
- Convenient mg thru kg sizes
- Same day service
- New catalog, *free*. Call collect: (216) 831-3000

ICN

ICN Pharmaceuticals, Inc./Life Sciences Group
26201 Miles Road, Cleveland, Ohio 44128

CIRCLE 111 ON READER SERVICE CARD

Our gases are rare. Our hardware is not.

AIRCO
Rare and Specialty Gases
1
Pure Gases
2
Mixed Gases
3
Equipment
AIRCO
AIRCO

Every rare and specialty gas you'll ever need—from Argon and CO to SO_2 and Xenon. Plus every piece of hardware and equipment you'll ever need to use them. Like these valves, for example. Plus flowmeters, regulators and aluminum sample cylinders—the works. For your *free* copy of our new 1977 catalog listing them all, and including complete physical properties and equipment recommendations, call Hank Grieco at (201) 464-8100. Or send this coupon to Airco Industrial Gases.

Name____________________ Title____________________

Company____

Address____

City__________________ State____________ Zip____________

Airco Industrial Gases, Rare & Specialty Gases Dept., 575 Mountain Ave., Murray Hill, NJ 07974.

CIRCLE 4 ON READER SERVICE CARD

as well as other organizations with a research laboratory environment, aware of the impact of the Occupational Safety and Health Regulations. It is designed to help these workers understand what the regulations mean, why it is important to understand them, and what an individual's responsibilities and obligations are under OSHA regulations. The film can be obtained from Josephine Wenk, Business Manager, University of Michigan Television Center, 400 Fourth St., Ann Arbor, Mich. (313-764-8298), for: film rental for one week, \$40; cassette rental for one week, \$40; film purchase, \$180; and video cassette ¾-in. U-matic purchase, \$125.

Analytical Chemistry at Work

Du Pont Installs 1000th aca

Officials of Du Pont and Western Pennsylvania Hospital (West Penn) recently celebrated the installation of the 1000th automatic clinical analyzer (aca) with ceremonies in Pittsburgh. The first aca, put into service at the University of Wisconsin in 1970 following five years of research and development, is still operating. Today, combined sales of instruments and test packs for use with the analyzer are approaching \$100 million annually.

With a basic capacity of any 30 different test methods, the aca offers unusual versatility. The most significant advantages of this particular instrument setup are the discrete selection of available tests for each patient, the ability to run any number of tests in any order, and presentation of the results in less than 8 min after the first reagent pack is inserted in the instrument. The aca can be used 24 h a day and is particularly economical for regular runs of small batch, STAT, and special tests.

Du Pont continues to develop new methods for use with the aca and recently introduced four new methods at the American Society of Medical Technologists national convention. These new methods, gamma glutamyl transferase, amylase, ammonia, and phosphorus, bring the total number of methods to 32. The special analytical test packs for use with the instrument serve both as reaction chambers and cuvettes for photometric analysis.

Test pack operation of Du Pont's aca is discussed by (left to right) Sylvan M. Sax, chief biochemist; Arthur B. Blackburn, lab supervisor; and John J. Moore, assistant biochemist, all of West Penn Hospital in Pittsburgh. Officials at West Penn expect to provide better patient care, improved lab service around the clock, and overall reduced costs with the installation of the aca

Meetings

- **26th IUPAC Congress.** Sept. 4–10. Tokyo. *Contact: 26th Congress of IUPAC, P.O. Box 56, Kanda Post Office, Tokyo 101-91, Japan*
- **MCA Workshop on Safety & Health in the Chemical Industry.** Sept. 8. Marriott Hotel, New Orleans. *Contact: Milton Freifeld, Manufacturing Chemists Assoc., 1825 Conn. Ave., N.W., Washington, D.C. 20009*
- **Internal Solvent Extraction Conference, ISEC 77.** Sept. 9–16. Toronto, Ontario. Sponsored by the Canadian Institute of Mining and Metallurgy, the Canadian Society for Chemical Engineering, and the Society for Chemical Industry. The program includes analytical sessions. *Contact: M.H.I. Baird, Secretary, ISEC 1977, Chemical Engineering Dept., McMaster U., Hamilton, Ont. L8S 4L7, Canada*
- **Scanning and Transmission Electron Microscopy Meeting.** Sept. 12–14. U. of Glasgow, Scotland. Sponsored by the Electron Microscopy and Analysis Group of the Institute of Physics. *Contact: Meetings Officer, The Institute of Physics, 47 Belgrave Square, London SW1X 8QX, UK*
- **7th International Vacuum Congress and 3rd International Conference on Solid Surfaces.** Sept. 12–16. Vienna, Austria. *Contact: Nancy Hammond, Executive Secretary, American Vacuum Society, 335 East 45th St., New York, N.Y. 10017*
- **1977 General Assembly of Gesellschaft Deutscher Chemiker.** Sept. 12–16. München, West Germany. Includes Analytical Chemistry Division sessions. *Contact: GDCh-Geschäftsstelle, Postfach 90 04 40, D-6000 Frankfurt/Main 90, West Germany*
- **Third Symposium on Environmental Aspects of Fuel Conversion Technology.** Sept. 13–16. Diplomat Hotel, Hollywood, Fla. Sponsored by the U.S. Environmental Protection Agency's Industrial Environmental Research Laboratory/RTP. *Contact: Franklin A. Ayer, Research Triangle Institute, P.O. Box 12194, Research Triangle Park, N.C. 27709. 919-541-6260*
- **50th Anniversary of the Discovery of Electron Diffraction Meeting.** Sept. 19–21. Imperial College, London. Organized by the Institute of Physics in collaboration with the Royal Microscopical Society and the Faraday Division of the Chemical Society. *Contact: Meetings Office, The Institute of Physics, 47 Belgrave Square, London SW1X 8QX, England*
- **6th International Conference of the IMEKO Technical Committee on Measurement of Force and Mass.** Sept. 20–22. Odessa, USSR. *Contact: IMEKO Secretariat, H-1371, Budapest, POB 457, Hungary. Page 202 A, Feb.*
- **7th North American Thermal Analysis Society Conference.** Sept. 26–28. St. Louis, Mo. *Contact: D. W. Brazier, NATAS Conference*

In metal analysis, Jarrell-Ash has the tool you need— whatever the workload

Atomic absorption for normal workloads...

Analyzing a few samples for many trace metals? Or perhaps many samples for a few trace metals? Our Model 850, world's only totally automated AA spectrophotometer, is the answer. Provides 6-digit accuracy. Integral computer controls all functions, cuts set-up time by a factor of 10. Pre-programming too, if you wish. Guarantees procedural uniformity— whether you're in the lab or not. Want ultra-trace? Merely snap on our flameless accessory head to convert to 10^{12} to 10^{14} gram range.

For bulletin, circle 78.

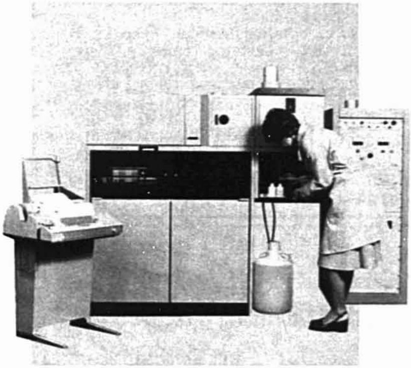

Plasma spectrometry for extra-large workloads...

Inundated with high-throughput tests? Many samples for many trace metals each? Our Plasma AtomComp is the answer. An emission unit that equals a squadron of AAs. Thanks to its inductively-coupled argon plasma source, this direct-reading spectrometer matches AA in detection sensitivity. But has remarkable capacity. Determines up to 48 elements simultaneously, in any combination, any concentration, in less than two minutes. Prints out results in ppb or %. Computer-controlled, hence easy to operate.

For bulletin, circle 79.

Jarrell-Ash Division,
trace metals problem-solver.

Fisher Scientific Company
711 Forbes Avenue
Pittsburgh, PA 15219
(412) 562-8300

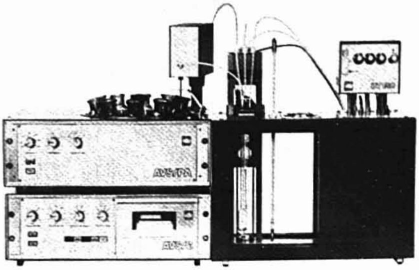

Save Lab Time

Automatic Viscosity Measuring Systems — AVS — Automates Capillary Viscosity Measurements.
System AVS/PA with 10 sample capacity employs one capillary viscometer and performs selected test programs of testing single or repeat measurements, discharge, rinsing and sample change automatically.
AVS/G base unit in conjunction with AVS/PA provides a seven digit tape print out with a 0.01 sec resolution.
Efflux time is measured opto-electronically resulting in accuracy of measurement of 0.1%. Covers measuring range of 0.3 to 30.000 cSt at temperatures up to +150°C.
AVS systems for single and serial measurement also available.

Send for descriptive color brochure now.

SCHOTT
JENAER GLASWERK SCHOTT & GEN., Inc.
11 East 26th Street • New York, New York 10010 • (212) 679-8535

CIRCLE 106 ON READER SERVICE CARD

NEW SLM 8000
Photon Counting Spectrofluorometer

With Corrected
Polarization Accessory

New 8-page brochure tells in detail the remarkable efficiency of this innovative lab instrument that performs direct photon counting with ultimate sensitivity in light detection (10^{-12} Molar Quinine Sulfate) accompanied by the lowest possible "dark count" drift and highest gain stability.

☐ Please send SLM 8000 brochure.
Other SLM High Performance Instruments:
☐ SLM 4000 Precision Corrected Polarization Fluorometer
☐ SLM 4800 Subnanosecond Fluorescence Lifetime Instrument

NAME ____________________
AFFILIATION ____________________
ADDRESS ____________________
CITY ____________ STATE ______ ZIP ______

SLM
INSTRUMENTS, INC.
1101 East University Avenue • Urbana, IL 61801 • Phone (217) 384-7730

CIRCLE 195 ON READER SERVICE CARD

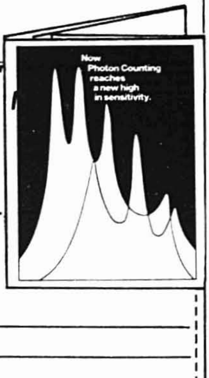

Chairman, 1977, Dunlop Research Centre, Sheridan Park Research Community, Mississauga, Ont. L5K 1Z8, Canada. Page 202 A, Feb.

- **2nd International Symposium on Aquatic Pollutants.** Sept. 26–28. Noordwijkerhout (near Amsterdam), The Netherlands. Approximately 30 papers on transport, transformation, identification, and biological effects of aquatic pollutants will be presented by invited speakers from 10 different countries. *Contact: George L. Baughman, Environmental Research Lab, U.S. Environmental Protection Agency, College Station Rd., Athens, Ga. 30601. 404-546-3145*
- **9th Meeting of the British Mass Spectroscopy Group.** Sept. 27–29. U. of Swansea, Wales. *Contact: J. R. Chapman, Secretary, British Mass Spectroscopy Group, AEI Scientific Apparatus Ltd., Barton Dock Road, Urmston, Manchester M31 2LD, England*
- **3rd International Symposium on Column Liquid Chromatography.** Sept. 27–30. Salzburg, Austria. *Contact: Verein Österreichischer Chemiker, Eschenbachgasse 9, A1010 Vienna 1, Austria*
- **2nd International Symposium on Polynuclear Aromatic Hydrocarbons.** Sept. 28–30. Battelle's Columbus Laboratories, Columbus, Ohio. *Contact: Peter W. Jones, Battelle's Columbus Laboratories, 505 King Ave., Columbus, Ohio 43201*
- **Arnold O. Beckman Conferences in Clinical Chemistry.** Sept. 28–30. Hilton Inn, Annapolis, Md. Sponsored by the American Association for Clinical Chemistry. Topics to be covered are: Basis for Laboratory Testing, Screening for Disease, Strategies for Laboratory Testing, Response to Abnormal Test Data, and Education in Laboratory Utilization. *Contact: David Uddin, Naval Medical Research Institute, Bethesda, Md. 20014*
- **16th Annual Meeting of ASTM Committee E-19 on the Practice of Chromatography.** Oct. 2–5. San Francisco. *Contact: Gerald Dupre, Bio/dynamics, Inc., Box 43, Mettlers Rd., East Millstone, N.J. 08873*
- **21st Annual ORNL Conference on Analytical Chemistry in Energy Technology.** Oct. 4–6. Riverside Motor Lodge, Gatlinburg, Tenn. *Contact: L. J. Brady, Anal. Chem. Div., Oak Ridge National Laboratory, Oak Ridge, Tenn. 37830. Page 879 A*

Now there are TWO price/performance leaders..

The new, compact HP 1081 high performance liquid chromatograph performs routine LC functions with a precision inherited from HP 1084–the first microprocessor-based liquid chromatograph. Its performance and price will appeal to research chemists who previously built their own LC systems. Its convenience and reliability will satisfy the demands of industrial chemists. Those just starting with LC will find it includes exactly the basic elements they require.

HP 1081 has a high-performance reciprocating diaphragm pump with in-line pulsation damping–new design principles proven in HP 1084. Samples are injected at full column pressure through a six-port valve (seven-port is optional). Separation columns locate in a protected compartment. A UV detector–one of the finest available–provides exceptional sensitivity and interfaces with strip-chart recorders, integrators and computer-based data systems (other detectors can also be fitted).

Push-buttons and a digital readout provide instant checks of pump setting or column pressure.

HP 1081 is the solution for isocratic LC applications under routine analysis conditions–where quantitative precision, ease of operation, simplicity and reliability are key factors. In method development its low pump volume makes solvent changes fast and simple. HP 1081 is a complete, ready-to-use HPLC system–engineered to Hewlett-Packard standards and supported by Hewlett-Packard services worldwide.

Hewlett-Packard is setting new standards in HPLC instrumentation. Get the full details today.

The HPLC choice

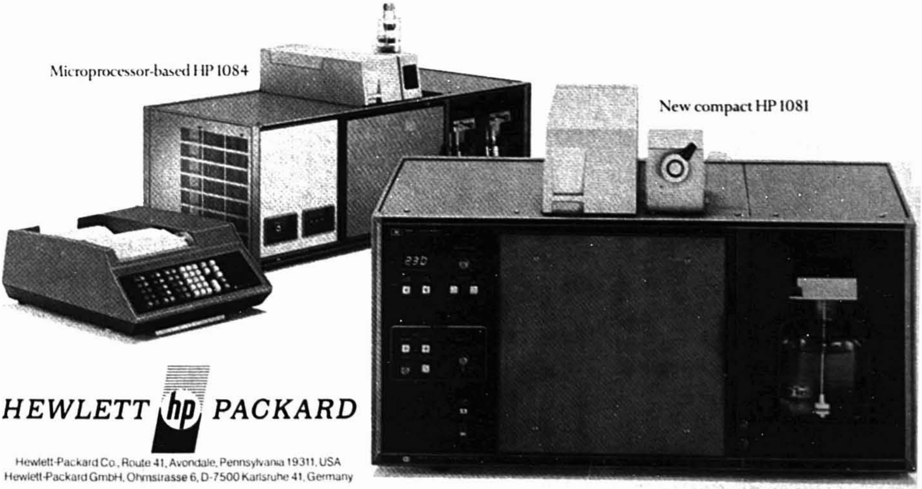

HEWLETT *hp* PACKARD

Hewlett-Packard Co., Route 41, Avondale, Pennsylvania 19311, USA
Hewlett-Packard GmbH, Ohmstrasse 6, D-7500 Karlsruhe 41, Germany

CIRCLE 94 ON READER SERVICE CARD

- **2nd Annual Symposium on Analytical Instrumentation.** Oct. 6–7. Hilton Inn at Corporate Square, Baton Rouge. *Contact: Larry Cattran, BRAIDG, Box 14233, Baton Rouge, La. 70808*
- **152nd National Meeting of the Electrochemical Society.** Oct. 9–14. Hyatt Regency Hotel, Atlanta, Ga. *Contact: The Electrochemical Society, Inc., P.O. Box 2071, Princeton, N.J. 08540*
- **Third International Conference on Nuclear Methods in Environmental and Energy Research.** Oct. 10–12. U. of Missouri-Columbia. *Contact: James R. Vogt, General Chairman, Nuclear Methods in Environmental and Energy Research, Environmental Trace Substances Research Center, U. of Missouri, Route 3, Columbia, Mo. 65201*
- **1977 Annual Meeting of the Optical Society of America.** Oct. 10–14. Royal York Hotel, Toronto, Ont., Canada. Organized in cooperation with the Atomic and Molecular Physics and the Optical Physics Divisions of the Canadian Association of Physics. *Contact: Optical Society of America, 2000 L St., N.W., #620, Washington, D.C. 20036*
- **3rd Annual Conference on New Advances in Separation Technology.** Oct. 11–12. Cherry Hill Hyatt House, Cherry Hill, N.J. *Contact: W. F. Heneghan, 289 Greenwich Ave., Greenwich, Conn. 06850*
- **ACS 9th Central Regional Meeting.** Oct. 12–14. Charleston, W. Va. *Contact: J. J. Smith, R&D Dept., Union Carbide Corp., P.O. Box 8361, South Charleston, W. Va. 25303*
- **ACS 13th Western Regional Meeting.** Oct. 12–14. Sheraton Anaheim Hotel, Anaheim, Calif. *Contact: M. M. Owens, Atlantic Richfield Co., 1801 E. Sepulveda Blvd., Carson, Calif. 90745*
- **Symposium on Biological/Biomedical Applications of Liquid Chromatography.** Oct. 13–14. Boston. *Contact: Gerald L. Hawk, Waters Associates, Maple St., Milford, Mass. 01757*
- **Annual Meeting of the Society of Forensic Toxicologists.** Oct. 14–17. Aboard S.S. Emerald Seas Miami/Nassau. *Contact: Leonard Bednarczyk, 1050 N.W. 19th St., Miami, Fla. 33136*
- **ISA/77 Conference & Exhibit.** Oct. 16–20. International Convention Center, Niagara Falls, N.Y. *Contact: Instrument Society of America/77—Niagara Falls, P.O. Box 34093P, Pittsburgh, Pa. 15230*
- **91st Annual Meeting of the Association of Official Analytical Chemists.** Oct. 17–20. Marriott Hotel, Twin Bridges, Washington, D.C. *Contact: Luther G. Ensminger, AOAC, Box 540, Benjamin Franklin Station, Washington, D.C. 20044. Page 884 A*
- **24th Canadian Spectroscopy Symposium.** Oct. 23–26. Conference Centre, Ottawa, Canada. *Contact: T. R. Churchill, Canmet, 555 Booth St., Ottawa, Ont., Canada K1A 0G1*
- **Midwest U. Analytical Chemistry Conference.** Oct. 27–29. Cornhusker Hotel, Lincoln, Neb. *Contact: James D. Carr, Dept. of Chemistry, U. of Nebraska, Lincoln, Neb. 68588*
- **ASTM Symposium on Aquatic Toxicology.** Oct. 31–Nov. 1. Holi-

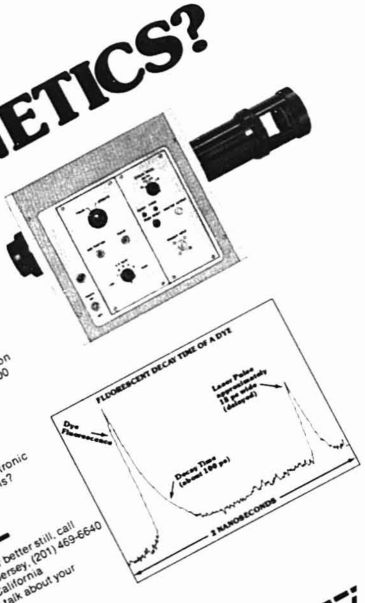
FLUORESCENT DECAY TIME OF A DYE
Dye Fluorescence
Laser Pulse approximately 15 ps wide (delayed)
Decay Time (about 100 ps)
2 NANOSECONDS

ARE YOU IN FAST KINETICS?

IF YES—
Do you need a Temporaldisperser (former name: Streak camera) to incorporate into your Temporalphotometer or Temporalspectrophotometer?

IF YES—
Can you use a 10 picosecond resolution multialkali cathode, with less than 100 picosecond jitter?

IF YES—
Would film or (optional) electronic output suit your applications?

IF YES—
Send the coupon. Or better still, call Ralph Eno in New Jersey, (201) 469-6640 or Herb Haber in California (415) 965-2300 to talk about your specific needs.

IF NO—
Request our latest catalog showing the world's most complete line of photosensitive devices.

HAMAMATSU

HAMAMATSU CORP.
120 WOOD AVENUE
MIDDLESEX, NEW JERSEY 08846
(201) 469-6640

International Offices in Major Countries of Europe and Asia

☐ YES! Send me information about the Temporaldisperser right away.
☐ NO, but send me your complete catalog.

NAME
TITLE
PHONE
COMPANY
ADDRESS
CITY STATE ZIP

AC 97

CIRCLE 99 ON READER SERVICE CARD

Thinking about buying an LC column?

Think MicroPak.™

A new universal design makes it possible for everyone to enjoy the high performance of Varian MicroPak columns. This universal design couples 4 mm i.d. tubing with 1/16" standard compression fittings for use with almost any liquid chromatograph. The advantages of MicroPak columns are significant.

High efficiency

Every MicroPak column will provide in excess of 10,000 plates per meter. Varian tests to this high standard at flow rates that chromatographers use in the real world, not at ultra-low flow rates used only in theoretical studies to get high but unrealizable plate counts. MicroPak efficiencies really do make it easier to get better separations.

Wide selection of bonded phases

MicroPak columns are offered in a wide selection of bonded phases: CH, CN, NH_2, and MCH. Non-polar and moderately polar compounds can be handled by reverse phase on CH and MCH columns. In addition, MCH is ideal for ion pairing work.

Assured performance

Complete customer satisfaction is assured. If the column should fail to perform during its normal lifetime, the user can return it and receive a proportionate credit on a new column. You can't lose. You always get full value.

Now, with the universal design, it's easy to give these great columns a try. For full details write Varian Instrument Division, Box D-070, 611 Hansen Way, Palo Alto, CA 94303, or circle *Reader Service Number 218.*

To have a Varian representative contact you, circle *Reader Service Number 219.*

varian

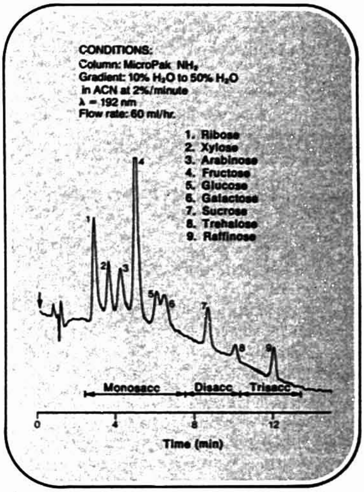

Saccharides. Separated on a MicroPak NH_2 column.

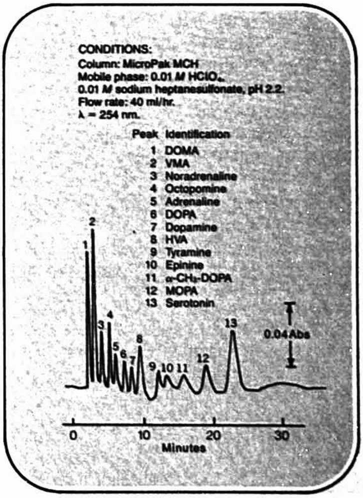

Catecholamines. Separated on a MicroPak MCH column.

Computerization of a 4260 Infrared Spectrophotometer.

Several months prior to the 1977 Pittsburgh Conference, Beckman technical staff began private demonstrations of their new Infrared Spectral Information System. Fully integrated were a basic computer, a research grade 4260 instrument, a complete signal interface box, and applications software on floppy disc storage.

Then in Cleveland, workshops and seminars were held to introduce formally IRSIS capabilities to the public. And now, Beckman is ready to put users nationwide on line with a fully tested, turnkey IR system that can digitize and store spectra on floppy disc, process the data fully through 12 operational programs, and output results to a printer or plotter for final answers.

Typical all computer-controlled operations include spectral subtraction, addition, ordinate expansion and averaging, along with a peak pick/search/match routine for compound identification.

Spectra comparison operations have been designed to be completely flexible. For this latter purpose, each user can build a high speed personalized data file to do the exact identification required.

Then, all an operator need do is place the sample in the 4260. Final answers to complex identifications appear in minutes.

So, don't wait a minute longer to get complete information on true IR computer capability. To talk to the experts, contact your local Beckman representative or Scientific Instruments Division, Beckman Instruments, Inc., P.O. Box C-19600, Irvine, CA 92713.

BECKMAN®

CIRCLE 25 ON READER SERVICE CARD

day Inn Cleveland Airport West, Cleveland, Ohio. *Contact: Leif L. Marking, Fish Control Laboratory, P.O. Box 862, LaCrosse, Wis. Page 316 A, Mar.*

- **ACS 13th Midwest Regional Meeting.** Nov. 3–4. U. of Missouri, Rolla. *Contact: S. B. Hanna, Dept. of Chemistry, U. of Missouri, Rolla, Mo. 65401*
- **4th Joint Conference on Sensing of Environmental Pollutants.** Nov. 6–11. Hilton Hotel, New Orleans. *Contact: V. E. Derr, National Oceanic & Atmospheric Administration, Environmental Research Lab, Boulder, Colo. 80303*
- **1977 International Symposium on Chromatographic Analysis of Polymers and Related Materials.** Nov. 7–10. Chicago. *Contact: Jack Cazes, Waters Associates, Inc., Maple St., Milford, Mass. 01757*
- **12th International Symposium on Advances in Chromatography.** Nov. 7–10. International Congress Centre RAI, Amsterdam. *Contact: Organisatie Bureau Amsterdam b.v., International Congress Centre RAI, P.O. Box 7205, Europaplein 14, Amsterdam, The Netherlands; or Prof. A. Zlatkis, Chemistry Department, U. of Houston, Houston, Tex. 77004. Page 880 A*
- **Fourth Annual Meeting of the Federation of Analytical Chemistry and Spectroscopy Societies.** Nov. 7–11. Convention Center, Detroit, Mich. *Contact: Mitch Kapron, Ethyl Corp., 1600 W. Eight Mile Rd., Ferndale, Mich. 48220. 313-542-6940*
- **15th Conference on Vacuum Microbalance Techniques.** Nov. 8–11. Boston. *Contact: Nancy Hammond, AVS, 335 E. 45th St., New York, N.Y. 10017*
- **Conference on National Understanding for the Development of Reference Materials and Methods for Clinical Chemistry.** Nov. 16–17. Atlanta. *Contact: Adrian Hainline, Clinical Chemistry Div., Bureau of Laboratories, Center for Disease Control, Atlanta, Ga. 30333*
- **Advances in Photon-Excited X-ray Fluorescence Analysis.** Nov. 27–Dec. 2. San Francisco. Sponsored by the Isotopes and Radiation Div. of the American Nuclear Society (ANS) and held in conjunction with the ANS winter meeting. *Contact: Enzo Ricci, Analytical Chemistry Div., Oak Ridge National Laboratory, P.O. Box X, Oak Ridge, Tenn. 37830*
- **33rd Congress of the G.A.M.S. on Analytical Chemistry.** Nov. 29–Dec. 2. Paris. *Contact: Secretariat du G.A.M.S., 88 Blvd. Malesherbes, 75008 Paris, France*
- **1977 Eastern Analytical Symposium.** Nov. 30–Dec. 2. Americana Hotel, New York City. Sponsored by American Chemical Society, Society for Applied Spectroscopy, and American Microchemical Society. *Contact: G. W. Ewing, Chemistry Dept., Seton Hall U., S. Orange N.J. 07079. Page 316 A, Mar.*
- **Chemical Applications of Lasers—Present Status.** Nov. 30–Dec. 2. U. of North Carolina at Chapel Hill. *Contact: C. S. Johnson, Jr., Dept. of Chemistry, U. of North Carolina, Chapel Hill, N.C. 27514*
- **ACS 33rd Southwest Regional Meeting.** Dec. 5–7. Little Rock, Ark. *Contact: A. B. Gosnell, Henderson State U., Arkadelphia, Ark. 71923*
- **36th Exposition of Chemical Industries.** Dec. 5–8. McCormick Place, Chicago. *Contact: International Exposition Co., 200 Park Ave., New York, N.Y. 10017*
- **Meeting on Infrared and Raman Spectrometries.** Dec. 5–17. U. de Bordeaux, France. *Contact: P. Pineau, Laboratoire de Spectroscopie Infrarouge, 351 Cours de la Liberation, 33405 Talence Cedex, France*
- **Symposium on Applications of Electroanalytical Sensors.** Dec. 6–8. The City University, London. Organized by Sira Institute. The technical program will concentrate on developments in the application of pH and ion-selective electrodes, ion-selective fet's, and other electrochemical sensors. *Contact: R. G. Keiller, Sira Institute Ltd., South Hill, Chislehurst, Kent BR7 5EH, England*
- **2nd Annual Toxic Substances Control Conference & Exposition.** Dec. 8–9. Shoreham Americana Hotel, Washington, D.C. *Contact: Government Institutes, Inc., 1733 Bethesda Ave., N.W., Washington, D.C. 20014. 301-657-2922*
- **International Conference on Monitoring of Hazardous Gases in the Working Environment.** Dec. 12–14. The City University, London, England. Organized by the Chemical Society in conjunction with the Health & Safety Executive, the Electrical Research Association, and the City University. *Contact: John F. Gibson, The Chemical Society, Burlington House, London, W1V 0BN, England*
- **CLEOS '78—IEEE/OSA Conference.** Feb. 7–9, 1978. San Diego, Calif. Organized by the Institute of

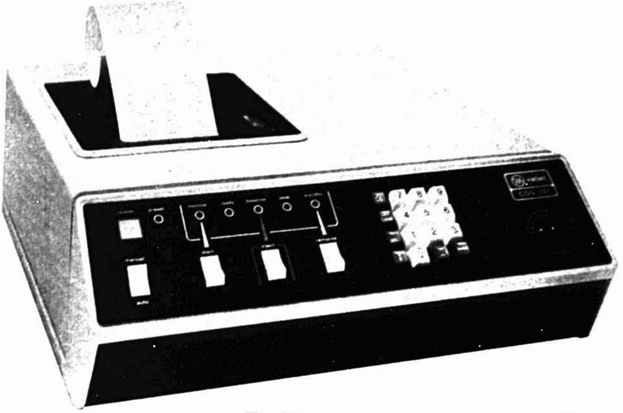

A better, easier way to quantitate your chromatograms... the new Varian CDS-111 Chromatography Data System

The CDS-111 is more than a powerful chromatography data system. It will automatically quantitate most chromatograms completely on its own. It will control an entire chromatography system — chromatograph, AutoSampler, valving, external events — in automatic closed-loop operation. It has large-computer power to store, for use on command, up to 9 (nine) complete method files each of which can be tailored to automatically control a complex analysis from start to finish. It will even link method files so that a single chromatogram can be automatically edited and calculated up to nine different ways. And the CDS-111 Chromatography Data System makes it all easy.

It automatically quantitates most chromatograms entirely on its own. You don't have to punch in sets of prerun instructions. The CDS-111 already knows what to do. All the critical measuring parameters are factory preset and the CDS-111 automatically updates the parameters throughout the run to accurately quantitate most types of chromatograms. For unusual, or complex analyses, you can easily override the presets and set whatever values you need.

It accurately measures the areas of all types of peaks, simple and complex. For accurate, precise measurement of all true peaks, the CDS-111 continuously filters the noise from the chromatographic signal and keeps the peak detection threshold-to-noise ratio constant throughout the analysis.

The CDS-111 automatically calculates the results according to any of 6 (six) different methods: internal standard, external standard, calibration factor, relative response factor, area % and normalized area %. Through powerful file linking, any combination of these methods can be automatically applied to the data from a single injection and the results automatically reported in more than one form, e.g., weight %, mole %, and volume %.

The CDS-111 stores, for immediate use, up to 9 (nine) complete method files, each tailored to control a specific analysis. Files can be simple, using only their presets which will handle most analyses. Or they can be sophisticated, controlling the entire chromatographic process — the AutoSampler, the Model 3700 chromatograph, external devices, data acquisition, calculations and final report. You don't have to set up the CDS-111 every time you run a different sample. You can call up your stored file at the touch of a button.

The CDS-111 controls are simple. Four switches, a small keyboard and 6 (six) indicator lights give you complete control and you don't really need the keyboard at all unless you want to override the automatic settings, edit a report, or build or alter a method file.

The CDS-111 makes chromatography automation available to every lab. It interfaces simply with both gas and liquid chromatographs. Two different basic models are available, so you can choose a system that best meets your particular needs and budget.

To have a Varian technical representative contact you circle ***Reader Service No. 220.***

For more information circle
Reader Service No. 221.

Varian Instrument Division
611 Hansen Way, Box D-070
Palo Alto, California 94303

varian

Electrical and Electronics Engineers and the Optical Society of America. *Contact: CLEOS, c/o Optical Society of America, Suite 620, 2000 L St., N.W., Washington, D.C. 20036. Page 612 A, June*

- **29th Pittsburgh Conference on Analytical Chemistry and Applied Spectroscopy.** Feb. 27–Mar. 3, 1978. Cleveland Convention Center, Cleveland, Ohio. *Contact: Edwin S. Hodge, Carnegie-Mellon U., Mellon Institute, 4400 5th Ave., Pittsburgh, Pa. 15213. Page 802 A, Aug.*
- **175th ACS National Meeting.** Mar. 12–17, 1978. Anaheim, Calif. *Contact: A. T. Winstead, ACS, 1155 16th St., N.W., Washington, D.C. 20036*
- **ACS 12th Middle Atlantic Regional Meeting.** Apr. 5–7, 1978. Hunt Valley Inn, Hunt Valley, Md. *Contact: F. Gornick, Dept. of Chemistry, U. of Maryland, Baltimore, Md. 21228*
- **8th Annual Symposium on the Analytical Chemistry of Pollutants.** Apr. 5–7, 1978. Geneva, Switzerland. *Contact: Congress Secretariat, P.O. Box 182, CH-4013, Basle, Switzerland. Page 708 A, July*
- **9th Materials Research Symposium on Trace Organic Analysis: A New Frontier in Analytical Chemistry.** Apr. 10–13, 1978. Gaithersburg, Md. Sponsored by the National Bureau of Standards. *Contact: Stephen Chesler or Harry Hertz, Chemistry Bldg., Room A105, National Bureau of Standards, Washington, D.C. 20234. 301-921-2153. Page 708 A, July*
- **American Nuclear Society Topical Conference on Computers in Activation Analysis and Gamma Ray Spectroscopy.** Apr. 23–26, 1978. Mayaguez, Puerto Rico. Sponsored by NBS, American Chemical Society, American Nuclear Society, Energy Research and Development Administration, U. of Puerto Rico, and Puerto Rico Nuclear Center. *Contact: B. S. Carpenter, Bldg. 235, NBS, Washington, D.C. 20234. 301-921-2167*
- **Canadian Chromatography Conference.** Apr. 27–28, 1978. Hotel Bonaventure, Montreal, Ontario. *Contact: V. M. Bhatnagar, P.O. Box 1779, Cornwall, Ont. K6H 5V7, Canada*
- **3rd Annual Regional Spring Training Conference and Exhibition of AOAC.** May 1–3, 1978. Marriott Hotel, Atlanta. *Contact: Sol Cohen, Assistant Director for Research and Instrumentation, FDA, 60 Eighth St., N.E., Atlanta, Ga. 30309. 404-881-2131*
- **International Conclave on Analytical Chemistry.** May 9–16, 1978. Louisiana State U., Baton Rouge. *Contact: J. W. Robinson, Louisiana State U., Baton Rouge, La. 70803*

Short Courses

ACS Courses. For more information, contact: Department of Educational Activities, American Chemical Society, 1155 16th St., N.W., Washington, D.C. 20036. 202-872-4508

Thin-Layer Chromatography
Washington, D.C. Sept. 28–29. Victor Rodwell and Donald McNamara. $195, ACS members; $235, nonmembers

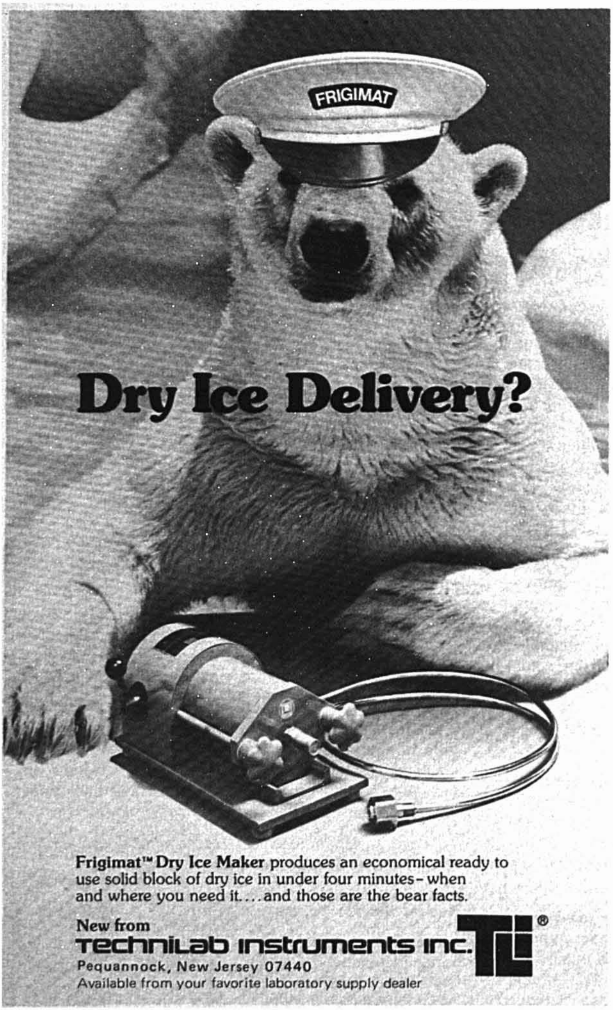

Frigimat™ Dry Ice Maker produces an economical ready to use solid block of dry ice in under four minutes–when and where you need it....and those are the bear facts.

New from
technilab instruments inc.
Pequannock, New Jersey 07440
Available from your favorite laboratory supply dealer

CIRCLE 203 ON READER SERVICE CARD

When you choose EM Laboratories you get something extra... S/P

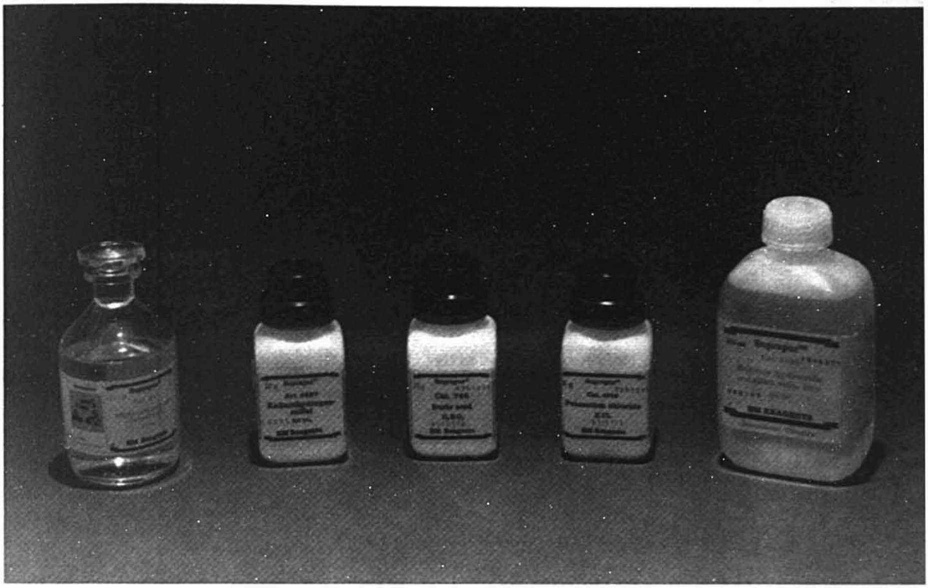

Finally, there's a line of ultrapure reagents which won't cost you a fortune. They're Suprapur® reagents. EM Laboratories' ideal combination of price and purity.

Suprapur® reagents are manufactured by and are a trademark of E. Merck, Darmstadt, Germany. Each container carries a guaranteed minimum assay of impurities—often in the range of $10^{-6}\%$... and less.

For a variety of analytical and research techniques. Atomic Absorption instrumental analysis. Emission Spectrography. X-Ray Fluorescence analysis of particulate matter. Materials Research. Think Suprapur® reagents.

EM Laboratories, Inc.
associate of
E. Merck, Darmstadt, Germany

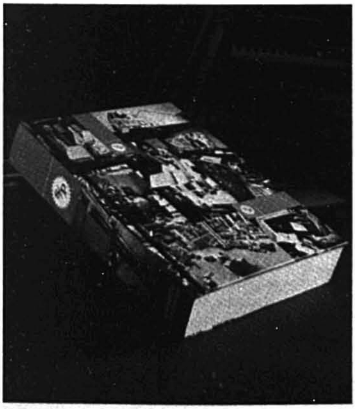

Something extra... S/P

S/P carries a lot of laboratory items. But, then, S/P is a leading distributor for more than 550 top manufacturers. To handle this huge inventory smoothly, we have 25.4 million cubic feet of warehousing space, 1.9 million cubic feet of chemical vaults, and 25 strategically located stocking centers. You benefit with a wider choice in all grades and price ranges. And we're flexible enough to stock any laboratory supply items and chemicals used in research, quality control or production specifically for you. It's all part of the S/P Responsive System of service for professionals like you. Call your S/P Representative and take stock of him.

scientific products
distributor of chemicals, laboratory supplies
and scientific instruments
Division of American Hospital Supply Corporation
1430 Waukegan Road, McGaw Park, IL 60085

CIRCLE 192 ON READER SERVICE CARD

Bio-Rad AG® resins

unparalleled after more than 2 decades for purity and uniformity.

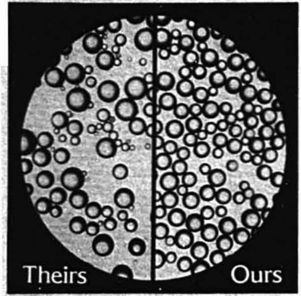

The purity and sizing of ion exchange resins play the key roles in reliability and reproducibility of results. Bio-Rad AG resins are purified by several steps to very low levels of heavy metals. And we size our resins until microscopic examination shows that 95% of the resin beads are within the specified range. The photomicrograph clearly shows the difference painstaking sizing makes.

Oddly enough, you pay little or nothing more for these superior resins! Why not get the best?

To help you select the proper AG resin for the application, Bio-Rad has prepared a massive (70x100 cm) full color wall chart that is both useful and attractive. Your inquiry will speed a copy to you. Contact:

BIO·RAD Laboratories
2200 Wright Avenue
Richmond, California 94804
Phone (415) 234-4130

Also in: Rockville Centre, N.Y.; Toronto, Ontario; London; Milan; Munich; Sao Paulo; Vienna.

CIRCLE 27 ON READER SERVICE CARD

Chromatographic Maintenance and Troubleshooting Workshop
San Francisco. Oct. 1–2. John Walker, Minor Jackson, and M.P.T. Bradley. $195, ACS members; $235, nonmembers

High-Pressure Liquid Chromatography
Washington, D.C. Oct. 15–16. David H. Freeman. Given in conjunction with 91st AOAC Meeting. $195, ACS members; $235, nonmembers

Laboratory Safety: Recognition and Management of Hazards
Detroit. Nov. 4–6. Norman Steere and Maurice Golden. Given in conjunction with the FACSS Meeting. $255, ACS members; $305, nonmembers

Column Selection in Gas Chromatography
Detroit. Nov. 10–11. Harold McNair and Walter Supina. Given in conjunction with the FACSS Meeting. $165, ACS members; $205, nonmembers

Thermal Methods of Analysis
Detroit. Nov. 10–11. Wesley Wendlandt and Ilya Sarasohn. Given in conjunction with theFACSS Meeting. $195, ACS members; $235, nonmembers

Electroanalytical Chemistry
New York City. Nov. 17–19. Dennis Evans and Paul Whitson. $255, ACS members; $305, nonmembers

Laboratory Safety: Recognition and Management of Hazards
San Francisco. Dec. 7–9. Norman Steere and Maurice Golden. $255, ACS members; $305, nonmembers

Thin-Layer Chromatography
San Francisco. Dec. 8–9. Victor Rodwell and Donald McNamara. $195, ACS members; $235, nonmembers

---

Hazardous Chemical Safety School
Conducted by J. T. Baker Chemical Co. Attendance is limited to 50. Boston, Sept. 8–9; Buffalo, Oct. 13–14; Chicago, Sept. 29–30; Cleveland, Sept. 22–23; Detroit, Sept. 26–27; Kansas City, Oct. 27–28; Los Angeles, Oct. 17–18 and Oct. 20–21; Minneapolis, Oct. 3–4; Pittsburgh, Sept. 19–20; St. Louis, Oct. 24–25; Toronto, Oct. 10–11. $185 (includes two-volume manual and meals). *Contact:* Carol Morris, Office of Safety Training, J. T. Baker Chemical Co., Phillipsburg, N.J. 08865. 201-859-2151, ext. 262

A Guide to Gas Chromatographic Columns
O'Hare Marriott Motor Hotel, Chicago. Sept. 30. Harold McNair and Joel Yancey. $60. *Contact:* Howard Novitch, Course Coordinator, Analabs, 80 Republic Dr., North Haven, Conn. 06473. 203-288-8463

Gas Chromatography
Florham Park, N.J. Oct. 12–14. $155, lecture only; $225, lecture and laboratory. *Contact:* Varian Instruments, Training Dept., D-430, 611 Hansen Way, Palo Alto, Calif. 94303

Practical Mass Spectrometry
Pittsburgh. Nov. 1–4. *Contact:* Jodi Kelsey, Manager, Dept. of Admin., Extranuclear Laboratories, Inc., P.O. Box 11512, Pittsburgh, Pa. 15238. 412-782-3884

Atomic Absorption
Florham Park, N.J. Nov. 2–4. $125, lecture only; $225, lecture and laboratory. *Contact:* Varian Instruments, Training Dept., D-430, 611 Hansen Way, Palo Alto, Calif. 94303

Symposium on Clinical Toxicology, Pharmacology, and Carcinogenic Hazards
San Francisco. Dec. 9–11. Bruce Ames, Samuel S. Epstein, Irving Sunshine, Donald S. Young, and Paul L. Wolf. $150. *Contact:* Medical Symposia, Division of Letters and Sciences, University of California Extension, Berkeley, Calif. 94720. 415-642-1061

For Your Information

Fisher Scientific Co., Pittsburgh, Pa., has agreed in principle to acquire the business of the Diagnostics Department of Cyanamid's Lederle Laboratories Division. The acquisition includes the marketing, sales, research, and development operations, but not manufacturing facilities and related personnel. The agreement provides for a two-phased transfer. Initially, Lederle will continue to manufacture products for Fisher with both companies' names appearing on the serological, immunological, and chemical products. During the second phase, Fisher will begin operating its own manufacturing facilities at a site to be selected and will market the diagnostic products under its own name.

International Laboratory Exhibition

(Salon du Laboratoire 1977)

Paris, porte de Versailles

Nov.29 **Dec. 3** **1977**

9:30 a.m.
TO
6:30 p.m.

Energy
Environment
Quality of Life
Research
Teaching
Innovation
Health

These are the goals of Laboratoire.

The 67th Physics Exposition will take place jointly with the Laboratory Exhibit. The two exhibitions will have a common entrance.

The Congress of Analytical Chemistry—33rd Congress of G.A.M.S.—will take place at the same location and dates as the exhibition.

The Exhibit is organized by l'Association pour le Salon du Laboratoire régie par la loi de 1901
12, rue Chabanais—75002 PARIS—France—Tel. 742.79.00

For further information contact:
International Trade Shows in France, 1350 Avenue of the Americas, New York, N.Y. 10019
Tel. (212) 582-4960 Telex: FREN 237 757

CIRCLE 128 ON READER SERVICE CARD

QUALITY LABORATORY APPARATUS

muffle furnace

WITH NEW

INSU-LIGHT

DIAL YOUR TEMPERATURE WITH BUILT-IN AUTOMATIC PROPORTIONING CONTROL

Increased heating efficiency with Insu-Light insulation . . . heat-up, cool-down and recovery times reduced by as much as 20% over previous models. Lighter insulation improves portability . . . reduces shipping charges. Automatic solid-state controller . . . controls to ±1% of full scale reading. "Low-mass" heating elements respond quickly to minimize temperature variations. Counter-balanced door maintains cool side toward operator. Models are available in . . . three voltages . . . two temperature ranges to a maximum of 2150°F (1177°C). Type 2000 available where greater chamber depth is required . . . three voltages . . . two temperature ranges.

Write for Laboratory Apparatus Catalog #3000.

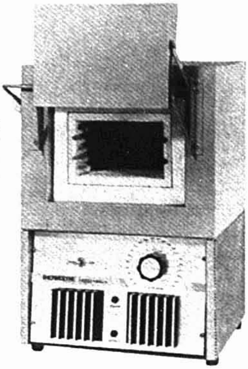

Type 10500

SYBRON | Thermolyne

Thermolyne Corp., a subsidiary of Sybron Corp., 2555 Kerper Blvd., Dubuque, IA 52001

CIRCLE 200 ON READER SERVICE CARD

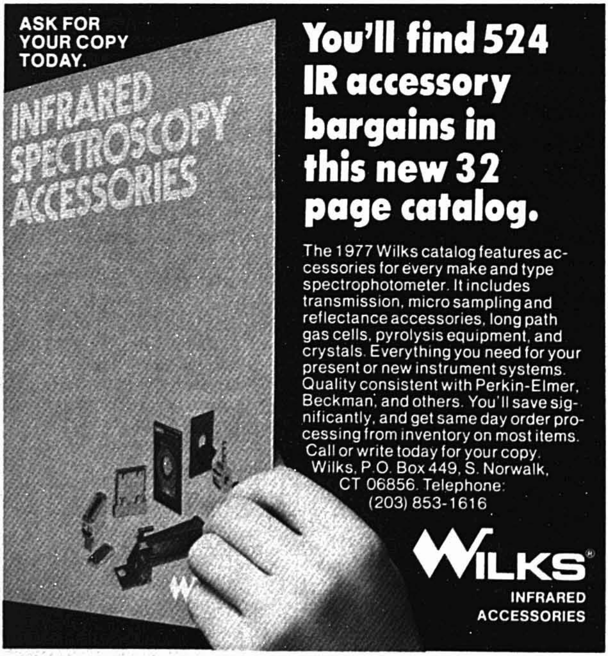

ASK FOR YOUR COPY TODAY.

You'll find 524 IR accessory bargains in this new 32 page catalog.

The 1977 Wilks catalog features accessories for every make and type spectrophotometer. It includes transmission, micro sampling and reflectance accessories, long path gas cells, pyrolysis equipment, and crystals. Everything you need for your present or new instrument systems. Quality consistent with Perkin-Elmer, Beckman, and others. You'll save significantly, and get same day order processing from inventory on most items. Call or write today for your copy. Wilks, P.O. Box 449, S. Norwalk, CT 06856. Telephone: (203) 853-1616

WILKS®

INFRARED ACCESSORIES

CIRCLE 232 ON READER SERVICE CARD

News

The National Bureau of Standards (NBS) in cooperation with the National Institutes of Health (NIH) is offering a new **computerized data base for the electron impact ionization mass spectra** of 25 600 compounds. The data base can be used to identify these compounds in studies of environmental pollutants, food additives, and similar investigations requiring mass spectrometric techniques. The data were compiled jointly by the National Heart, Lung, and Blood Institute of NIH, the Environmental Protection Agency, and the United Kingdom's Mass Spectrometry Data Centre. The NIH/EPA/MSDC Mass Spectral Data Base is available under a one-year renewable lease from the Office of Standard Reference Data, NBS, A-537 Administration Bldg., Washington, D.C. 20234.

The **"NBS Metric Kit"**, a publication of the National Bureau of Standards, contains valuable information on the metric system. The kit consists of a copy of "What About Metric", a consumer-oriented explanation of the metric system; a booklet listing references on metric information; a brief history of measurement systems and a color chart of the modernized metric system; a wallet-sized conversion card; a 15-cm ruler; and a metric conversion status reprint from DIMENSIONS/NBS, the Bureau's monthly magazine. Introduced in 1975, the kit has now been revised to reflect the passage of the Metric Conversion Act. Kits may be purchased for $2.00 each from Superintendent of Documents, U.S. Government Printing Office, Washington, D.C. 20402. Order by Stock No. SN003-003-01736-1.

Digilab, Inc., the leading manufacturer of infrared Fourier transform spectrometers with headquarters in Cambridge, Mass., has opened a regional sales office to serve the area from southern New Jersey to South Carolina. The new office is located at Wilde Lake Village Green, Suite 200, Columbia, Md. 21044 (301-596-5700).

The Institute for Scientific Information (ISI) will introduce a new index that offers current, comprehensive coverage of published conference proceedings. Beginning in 1978, the ***Index to Scientific & Technical Proceedings*** will annually cover around 3000 proceedings and the more than 80 000 individual papers published in them. Proceedings that appear in book form as well as those from the journal literature will be included. The index will appear monthly, with semiannual cumulations. For further information, contact: ISI, 325 Chestnut St., Philadelphia, Pa. 19106.

In a license agreement with The Upjohn Co., **LC Instruments Co.,** a subsidiary of Lachat Chemicals, Inc., has acquired exclusive worldwide patent, manufacturing, and marketing rights for an automated high-performance liquid chromatographic system. The intricate timers and circuitry control developed by The Upjohn Co. allow the entire liquid chromatographic system to operate without the attention of an operator for a number of test samples. Lachat Chemicals, Inc., headquartered in Mequon, Wis., manufactures and markets medical and laboratory instruments through its subsidiary, LC Instruments Co.

Shimadzu Scientific Instruments, Inc., is a newly incorporated U.S. subsidiary of Shimadzu Seisakusho, Ltd. of Japan. The company, which formerly operated under its parent company name from the Silver Spring, Md., location, is now situated at 9147-H Red Branch Road, Columbia, Md. 21045. The complete line of its gas chromatographs, accessories, and parts will be marketed directly by the subsidiary and also through American Instrument Co.

Heyden & Son Ltd., worldwide publishers of scientific and technical books and periodicals, announces the opening of its U.S. office at Kor-Center East, Bellmawr, N.J. 08030. The new U.S. operation is equipped with complete warehouse facilities for distribution and will handle all marketing and sales promotions for the United States and Canada.

On the occasion of his **90th birthday celebration,** Professor **Hans Lieb** of Graz, Austria, was given an Honorary Dr. Med. title at the University of Graz, on June 17, 1977. Professor Lieb is the oldest living pioneer in elementary microanalysis.

The National Committee for Clinical Laboratory Standards (NCCLS) announces the publication of PSI-6, **Guidelines for Service of Clinical Laboratory Instruments.** The standard recognizes that the proper use of clinical laboratory instruments requires adequate operator training, installation, preventative maintenance, and repair when needed. Copies are available at $4.00 each postpaid from NCCLS, 771 E. Lancaster Ave., Villanova, Pa. 19085.

From Buchler...keeping pace with the age of discovery:

An ALL NEW digital power supply.

Buchler introduces the first laboratory power supply with large, bright L.E.D. digital readout and instant pushbutton selection of constant-*power*, constant-*voltage*, or constant-*current* modes.

The bright L.E.D. display means easy reading, even from across the room, without the distraction of dual or multifunction scales.

Overvoltage and overcurrent protection are built in; control circuits operate at low voltage for long life and reliability.

This is the only truly contemporary power supply. It's new from Buchler. Available through your leading laboratory supply house.

SEARLE

Buchler Instruments
Division of Searle Diagnostics Inc.
1327 Sixteenth Street
Fort Lee, New Jersey 07024 U.S.A.
201-224-3333

Buchler 3-1500
Power Supply
835
DANGER HIGH VOLTAGE

Buchler Instruments: made in the United States, sales and service worldwide.

CIRCLE 18 ON READER SERVICE CARD

Three ways to improve your testing quality

From no one else but Bausch & Lomb

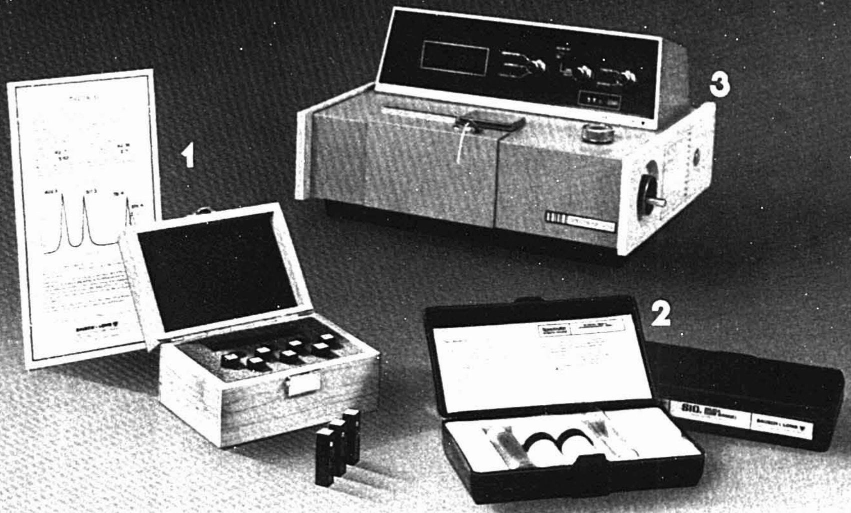

1 Bausch & Lomb's exclusive Spectronic™ Standards filter set. An NBS traceable set of filters that checks the accuracy of your spectrophotometer. Tests for stray light, wave length accuracy, and spectrophotometric accuracy. Each Spectronic Standards set is tested and certified by Bausch & Lomb. At last, you'll know if your spectrophotometer is up to your quality control standards.

2 Bausch & Lomb Spectro-Kit™ Reagent Systems to assure you of reagent quality water. Because you can't always be certain you have Class I reagent water, we offer these spectrophotometric tests for *Silica* and *Permanganate Time.* Both are easy to use and have illustrated instructions. They enable you to test reagent water as suggested by NCCLS, CAP, and ACS.

3 Bausch & Lomb Spectronic® Spectrophotometers—one of many we manufacture. All share one capability, and that is performance quality. Quality backed by over a quarter century of spectrophotometer experience and a nationwide network of field support and service.

You have to sell quality.
So do we.
We're Bausch & Lomb.

BAUSCH & LOMB
ANALYTICAL SYSTEMS DIVISION
ROCHESTER, NEW YORK 14625

Call your nearest B&L representative. Or call us at 716-385-1000, ext. 325.

CIRCLE 16 ON READER SERVICE CARD

Menard G. Heydanek, Jr.
Flavor Technology
John Stuart Research Laboratories
The Quaker Oats Co.
617 W. Main Street
Barrington, Ill. 60010

The Analytical Approach

Edited by Claude A. Lucchesi

Tracing the Origin of Off-Flavors in a Breakfast Cereal

During the routine quality assurance examination of a packaged ready-to-eat breakfast cereal, a piney-spruce off-flavor was found. These quality assurance examinations routinely monitor all aspects of food products, such as package appearance, fill weight, product appearance, flavor, and odor, and usually total 25 or more attributes. These examinations or audits of product quality are designed to locate problems in production that may go unnoticed for some period of time if they are not monitored. They usually are most important in locating subtle, esthetic quality differences which, when absent or changed, will not present the food manufacturer's best tasting product to the consumer. The observation of this piney off-flavor in the cereal product was very important since subsequent taste panels showed that it contributed a highly undesirable flavor character. Location of the source of this adverse flavor and its quick removal were of paramount importance because of present day methods of manufacturing large amounts of food products at a single location.

Scheme A shows the steps taken to locate the piney off-flavor source. There were three possible sources:

- The ingredients of the cereal product
- The process, i.e., odor development during cooking
- The package or the external environment.

One advantage in the development of an analytical approach to this type of problem is that the off-flavor can be traced organoleptically with the nose as well as with analytical instruments. In fact, the nose is probably the most important analytical tool an analytical flavor chemist uses. Each of the ingredients used in the cereal manufacture was smelled, and no source of piney odor was found. The processing system, especially the water sources, was examined, and no piney odor source found. This was probably the least likely source of the off-flavor but could not be ruled out completely until the system was checked. When the packaging material used for the outer boxes was examined, it was not piney but the inner glassine liner contained a piney odor. A similar procedure was used to find the piney source in the components of the glassine liner. The liner is composed of two sheets of Kraft paper laminated with a resin in microcrystalline wax and overwaxed on both sides with paraffin wax. As seen in Scheme A, the resin used in bonding the paper layers is the obvious culprit.

Since the resin contains an odorous material, the method of choice for isolation of these components was a distillation technique. Vacuum distillation of the resin at 175 °C and $0.5\text{-}\mu$ pressure was used to strip the volatile odor from the resin, and collection of the volatiles was accomplished in cold-finger traps cooled with dry ice–acetone baths.

The collected volatile material was rinsed from the traps with pentane, and the resulting solution produced the typical piney odor that was noted in the glassine liner and off-flavored product when examined organoleptically on perfume blotters (thick filter paper).

To determine precisely what chemical components were responsible for the off-flavor, a further fractionation of the distillate was undertaken (Scheme B). Again, with organoleptic evaluation as the criteria for following the piney off-flavor, gas chromatography was used to fractionate the components into discrete flavor entities. Gas chromatography was carried out

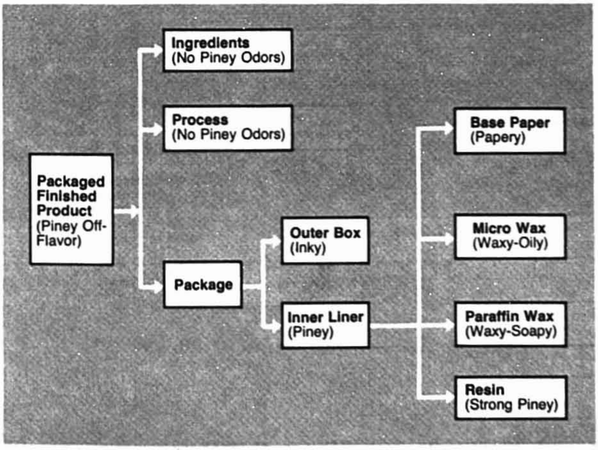

Scheme A. Odor source of piney off-flavor
Odor descriptions in parentheses

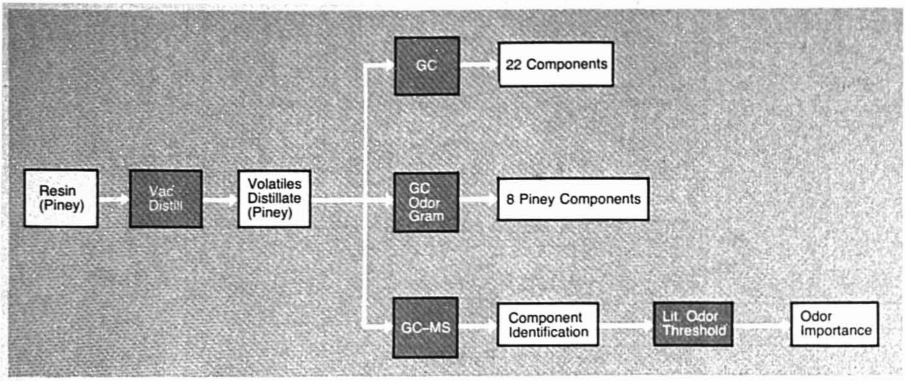

Scheme B. Evaluation of individual component/odor importance

on a Carbowax 20M column, and the separate components were organoleptically evaluated at the end of the column. The use of 3/1 exit splitter attached to a heated collection vent and exit sniffing port allowed each component to be organoleptically evaluated as it exited from the column.

From the chromatogram (Figure 1), at least nine of the separated peaks, including most of the major peaks, had odors associated with a piney character. Since more than one component had piney character, the identity of the piney odor components was needed to evaluate their individual thresholds. GC–MS analysis yielded the component identifications shown in Table I. All the components identified were common to pine oil or could be derived via hydrogenation of pine oil during resin processing and had published odor thresholds in the 1 to 8 ppb range (*1*).

At this point, even with the identities established, it was not known which of these components had a pronounced flavor effect in the finished product. Several avenues were now available to determine which of the chemicals or group of components were responsible for the off-flavors. Since there are ranges of flavor thresholds covering six orders of magnitude, it is not a safe assumption to regard the most abundant as the most odorous. One approach would be to obtain each of the chemicals and determine their odor thresholds in the product. Then one must determine the amount of transfer from the package to the product and limit the package to those levels or below for complete flavor compatibility. This would be a long and time-consuming task that would not necessarily yield any more practical results than the alternate approach we chose to use. The objective of our approach was to develop an appropriate quality control method and define specification limits for the purchase of the waxed glassine liner material. Since the ultimate desire was to prevent odor/flavor transfer to the product, we took advantage of this transfer property to help define the specification limits of the piney odor components.

To develop the appropriate flavor-instrumental correlations as outlined in Scheme C, samples of waxed glassine with varying levels of pine odors were subjected to organoleptic analysis for their ability to produce off-flavor in ready-to-eat cereals. They were ranked by a panel of expert judges into two classes: acceptable (no foreign flavor imparted) and unacceptable (definite foreign odor or flavor) resulting in substandard finished product. The latter category was subdivided into levels designated as weak,

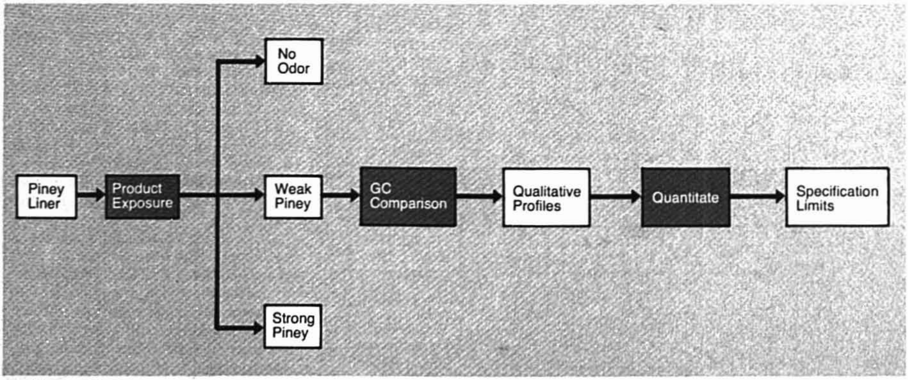

Scheme C. Determination of component limits in glassine liner for product compatibility

Distilled Water-The Weak Link in Your AA and LC Analyses!

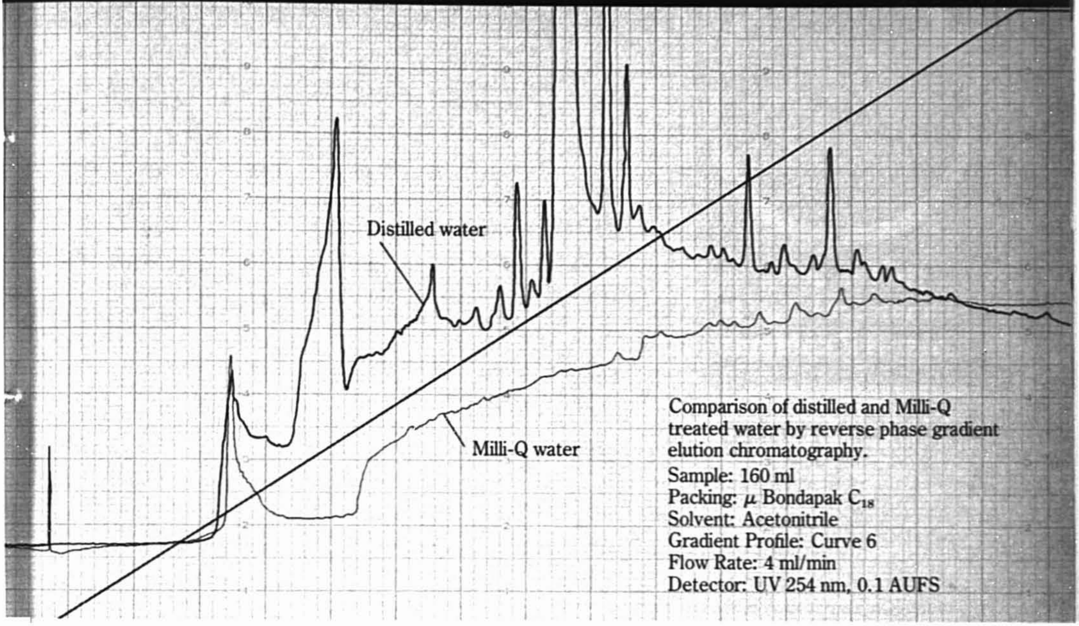

Comparison of distilled and Milli-Q treated water by reverse phase gradient elution chromatography.

Sample: 160 ml
Packing: μ Bondapak C_{18}
Solvent: Acetonitrile
Gradient Profile: Curve 6
Flow Rate: 4 ml/min
Detector: UV 254 nm, 0.1 AUFS

Distilled water has too many trace organics—even when triple distilled. Also inorganics, particles, and if you store it, bugs!

But a Milli-Q™ system will always deliver the purity you need, on demand at your point of use.

It removes dissolved organics by carbon adsorption; dissolved inorganics by ion-exchange; and particles and microorganisms by 0.22 micron Millipore membrane filtration. Maintenance is just a disposable cartridge change.

You can use your still to feed the Milli-Q. But our Milli-RO™ reverse osmosis system is more dependaable, more economical, and like the Milli-Q maintenance free.

Why not have the water purity you need, consistently? A Milli-Q/Milli-RO combination costs far less to operate than a still. Call 800-225-1380 toll free for a copy of our descriptive bulletin. (In Canada 800-261-0961; in Mass. 617-275-9200.) Water Systems Division, Millipore Corporation, Bedford, Mass. 01730.

CIRCLE 138 ON READER SERVICE CARD

MILLIPORE®

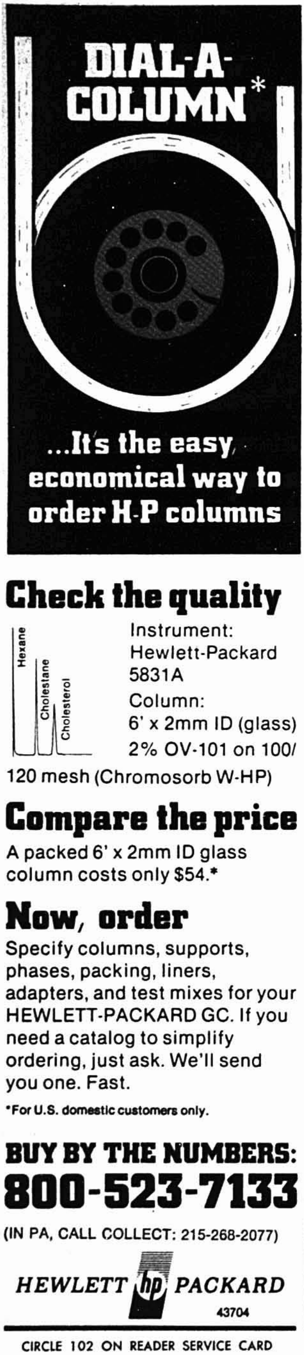
DIAL-A-COLUMN*

...It's the easy, economical way to order H-P columns

Check the quality

Hexane
Cholestane
Cholesterol

Instrument: Hewlett-Packard 5831A

Column: 6' x 2mm ID (glass) 2% OV-101 on 100/120 mesh (Chromosorb W-HP)

Compare the price

A packed 6' x 2mm ID glass column costs only $54.*

Now, order

Specify columns, supports, phases, packing, liners, adapters, and test mixes for your HEWLETT-PACKARD GC. If you need a catalog to simplify ordering, just ask. We'll send you one. Fast.

*For U.S. domestic customers only.

BUY BY THE NUMBERS: 800-523-7133

(IN PA, CALL COLLECT: 215-268-2077)

HEWLETT hp PACKARD

43704

CIRCLE 102 ON READER SERVICE CARD

Table I. Component Identifications

Figure 1 pk. no.	Odor	Identification by GC–MS	Retention time of authentic compound
1	Weak pine	Menthane	
2	Weak pine	Menthane	
3	Slightly strong pine	Camphene	+[a]
4	Pine tree	8-*p*-Menthene	
5	Camphor	Limonene	+
6	Camphor	1,8-Cineol	+
7	Fragrant	*P*-cymene	
8	Sweet, pleasant	1,4-*p*-Menthadiene	
9	Sour, camphor	Camphor	+
10	Very strong pine	Fenchyl alcohol	
11	Licorice	*p*-Isopropyl anethole	
12	Fatty-citrus	. . .	
13	Flowery, green	. . .	
14	Pine, chestrub, strong	Borneol	+
15	Resinous, pine pitch	Borneol acetate	
16	Foul, acidic	. . .	

[a] + = authentic compound matches unknown retention time. Others were not compared or not available.

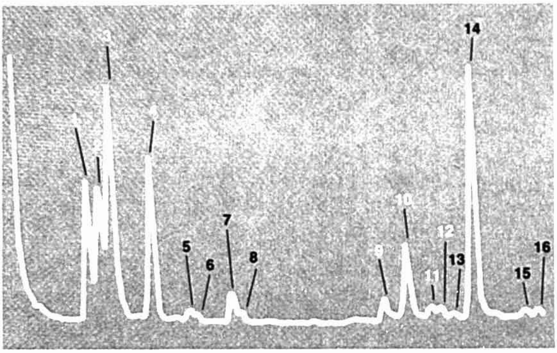

Figure 1. Gas chromatogram of resin volatiles

moderate, and strong. Also, 100 g of these same waxed glassine samples were subjected to hot jar-headspace analysis by the ASTM F-151 procedure. This method involves heating the sealed sample container, withdrawing a constant volume of headspace sample via syringe, and injecting it into a gas chromatograph. The gas chromatography procedure was calibrated by using α-pinene and borneol as standards for terpene hydrocarbons and oxygenated terpenes, respectively. The results showed a general increase in the level of pine components as the relative organoleptic strength of the product off-flavor increased.

From this type of data, the correlation between organoleptic analysis and objective gas chromatography can be established. In this case, there was good correlation between the detection of piney off-flavor and the presence of the major terpenes (peaks 1 to 4, Figure 1) and oxygenated species, borneol and fenchyl alcohol (peaks 10 and 14, Figure 1), at levels of 80 ppb or greater for each component. Therefore, routine quality control testing of incoming liner shipments with GC was initiated, and levels of these components were routinely determined with the understanding that at 80 ppb each or higher, the product might be subjected to off-flavor development during distribution.

The net result of instituting these tighter and more specific controls on the glassine liner was a marked reduction in the incidence of these piney odors in our standard packaging material. Several suppliers sought and found acceptable substitute resins that did not have this inherent odor and thus were more easily controlled. Others have met the specified levels, and very few problems have been seen since.

References

(1) Compilation of Odor and Taste Threshold Values Data, W. H. Stahl, Ed., DS48, 05-048000-36 ASTM Publications, 1973.

INDEX TO ADVERTISERS IN THIS ISSUE

CIRCLE INQUIRY NO.	ADVERTISERS	PAGE NO.
4	* **Airco Industrial Gases** Hammond Farrell, Inc.	885A
5	* **Alltech Associates, Inc.** Chromad	947A
3, 7–8	* **American Instrument Company** Industrial Advertising Associates	843A, 875A
6	* **Anachemia Chemicals, Inc.** Brand Advertising Limited	938A
24	**Baird-Atomic, Inc.** Buck & Berglund, Inc.	851A
17, 19	**J.T. Baker Chemical Company** Naimark & Barba, Inc.	929A, 947A
26	**Barnes Engineering Company** Jarman, Spitzer & Felix, Inc.	940A
16	* **Bausch & Lomb** Blair Advertising	900A
25	* **Beckman Instruments, Inc.** N. W. Ayer ABH International	892A
27	***Bio-Rad Chemical** Fred Schott & Associates	896A
20	* **Brinkmann Instruments, Inc.** Blatt Advertising, Inc.	OBC
18	**Buchler Instruments** Fletcher-Walker-Gesell, Inc.	899A
22	* **Burdick & Jackson Laboratories, Inc.** Studio 5 Advertising, Inc.	922A
21	**Burrell Corporation** The Agency of Pittsburgh	938A
39	* **Cahn Instruments, Division of Ventron** Marketing Directions, Inc.	926A
38	* **Carle Instruments** Marketing Directions, Inc.	913A
40	**Chessell Recorders** Tech-Lit Services, Inc.	854A
34	* **Chromatix, Inc.** David R. McClurg	IFC
35	**Corco Chemical Corporation** Sit/Com Corporation	874A
36, 37	**Corning Glass Works** Winterkorn, Hammond & Lillis, Inc.	960A, 961A
32	* **Crawford Fitting Company** Falls Advertising Company	871A
50	**Dexsil** Kenyon Hoag Associates	858A
51, 52	* **E.I. DuPont de Nemours & Co., Inc., Photo Products/Instruments** N. W. Ayer ABH International	932A
63	* **EM Laboratories, Inc.** Langeler-Mason Inc.	909A
76	**Fischer & Porter Company** Furlong Promotions, Inc.	944A
75, 77, 78–79	* **Fisher Scientific Company** Tech-Ad Associates	887A, 915A, 939A
85	**Galileo Electro-Optics Corp.** Schneider Parker, Inc.	941A
84	* **Gilford Instrument Laboratories Inc.** Oberlin Industrial Advertising	963A
81	* **Glenco Sciencific, Inc.** Cooley & Shillinglaw	940A
82	**Gould, Inc.** Carr Liggett Advertising, Inc.	859A
80	**Gow-Mac Instrument Company** Kenyon Hoag Associates	918A
83	**Gulton Industries, Inc., M&CS Division** AC Incorporated	880A
99	**Hamamatsu Corporation** Mandabach & Simms, Inc.	890A
100	* **Hamilton Company** Mealer & Emerson, Inc.	935A
97	* **Hellma International, Inc.** Miller Advertising Agency, Inc.	929A
95	* **Hewlett-Packard** Dancer Fitzgerald Sample, Inc.	933A
94	**Hewlett-Packard** Dorland Advertising Limited	889A
96, 101, 102, 116	**Hewlett-Packard** Reese, Tomases & Ellick, Inc.	876A–877A, 904A, 920A–921A
103, 111	**ICN Pharmaceuticals, Inc.** Bayless-Kerr Company	889A, 907A
104	**Instrumentation Laboratory, Inc.** Aries Advertising, Inc.	878A
115	* **International Plasma Corp.** Paul Pease Advertising, Inc.	922A
106	**JENAer Glaswerk, Schott & Gen, Inc.** Bloom Advertising Company, Inc.	888A

LABORATORY SERVICE CENTER

GAS ANALYSES
Mass Spectrometry • Gas Chromatography
• Leak Detection
• Vacuum and Inert Gas Fusion
GOLLOB ANALYTICAL SERVICE
46 Industrial Road, Berkeley Heights, N.J. 07922
201-464-3331

LAB SAFETY
Send for 1977 Catalog
LAB SAFETY SUPPLY CO.
P.O.Box 1422, Janesville, WI 53545

Allylthiourea • p-Aminohippuric Acid • Ammonium Reineckate • Aurin
1-Benzyl-4-piperidone • Cellobiose • α-Chloralose • Diacetyl Monoxime
Dimethylamine HCl • 2,2′-Dipyridyl • Esculin • Ethyl Levulinate
Fructose • Inulin • o-Iodobenzoic Acid • L-Malic Acid • Maltose
DL-Mandelic Acid • Mercuric Potassium Iodide • o-Nitrobenzaldehyde
Orcinol • Orcein • P.A.N. • pH Indicators • L-Rhamnose • Salicin
Sodium Diethyldithiocarbamate • Sodium Dithionate • Succinimide
Thiosemicarbazide • Triphenylphosphine • o-Vanillin • Xylitol • Xylose

Write for our Products List of over 3000 chemicals

Tel: 516-273-0900
TWX: 510-227-6230

EASTERN CHEMICAL
Division of GUARDIAN CHEMICAL CORP.
BOX 2500 K
HAUPPAUGE, N. Y. 11787

Manufacturers' Representative, twenty-five years experience in field, desires lines in Washington, D.C., Maryland and Virginia area. Will consider dealerships. Write **Box 9-77-1, ACS, 1155 16th St. N.W., Washington, D.C. 20036.**

ANALYTICAL CHEMIST (experienced) needed by western agency to administer and operate small efficient laboratory specializing in water, mineral, and rock analyses; knowledge of and ability to operate electronic analysis equipment essential. MS or MA preferred. Salary negotiable. Apply by October 1 to Director, MONTANA BUREAU OF MINES AND GEOLOGY, Montana Tech, Butte, MT 59701. We are an Affirmative Action, Equal Opportunity employer.

USE LABORATORY SERVICE CENTER

INDEX TO ADVERTISERS IN THIS ISSUE

CIRCLE INQUIRY NO.	ADVERTISERS	PAGE NO.
105	**JEOL Analytical Instruments, Inc.** Weinrich Associates, Inc.	855A
107–110	* **Johns-Manville** Frye-Sills, Inc. Advertising	881A
112	* **Kewaunee Scientific Equipment Corporation** Phillipps Associates, Inc.	941A
113, 114	* **Kontes** Aitkni-Kynett Company, Inc.	964A
127	**Laboratory Data Control** Kelleher, Bamberger, Terry	957A
128	**Laboratoire** Sepic	897A
129	* **The London Company** Jaeger, Inc. Advertising	873A
201	**3M** Martin-Williams Advertising	959A
142–148	* **Matheson** Kenyon Hoag Associates	849A
149	* **Mettler** Harris D. McKinney, Inc.	953A
140–141	* **Micromeritics Instrument Corporation** Ad Graphics	955A
138	**Millipore Corporation** Schneider Parker, Inc.	903A
139	* **Mitsubishi Chemical Industries Ltd.** Global Advertising Company, Ltd.	945A
156	* **Orion Research, Inc.** OBC Advertising	847A
157	**Ortec Inc.** Thomas R. Sundheim, Inc.	856A
174	**Parr Instrument Company** F. Willard Hills Advertising Agency	922A
173	* **Pennsylvania Glass Sand Corporation** Marsteller, Inc.	937A
164, 167, 168, 169, 180	* **Perkin-Elmer Corporation** Marquardt & Roche, Inc.	862A–863A, 916A, 927A, 943A, 948A–949A
177	**Petrolite Instruments** Boone Advertising Inc.	950A
163	* **Philips Electronic Instruments, Inc.** Dobbs Advertising Company, Inc.	857A
165, 166	** **Philips Industries** Vaz Dias Internationaal bv	928C, 928G
170	**Pierce Chemical Company** Advertising Design	923A
182–183	* **Princeton Applied Research Corporation** The Message Center	925A
175	** **Pye Ether Ltd** C. J. Nicholl & Associates Ltd.	928B
171, 172	** **Pye Unicam, Ltd.**	928D, 928F
181	**Rheodyne** Bonfield Associates, Inc.	934A
194	* **Sargent-Welch Scientific Company** Polytech Advertising	911A
188	* **August Sauter** Planen & Werben	882A
191	* **Schleicher & Schuell, Inc.** Jarman, Spitzer & Felix	853A
190, 192 193	* **Scientific Products** Mitchel Suttner McPhilliamy Inc. Advertising	883A, 895A, 930A
189	* **SGA Scientific Company** Lakewood Advertising Agency	869A
195	**SLM Instruments, Inc.** Grubb, Graham & Wilder, Inc.	888A
187	**SPEX Industries, Inc.** Seymour Nussenbaum	908A
203	**TechniLab Instruments, Inc.** D & S Marketing Associates, Inc.	894A
200	**Thermolyne Corporation** E. R. Hollingsworth & Associates	898A
202	**Thermoplastic Processes, Inc.** Gilbert, Whitney & Johns, Inc.	929A
204	**Tracor Northern** Dave Carman & Associates, Inc.	860A–861A
223	* **Valco Instruments Company** Cooley & Shillinglaw	916A
218–219, 220–221	* **Varian** Ahern Advertising Agency	891A, 893A
222	**Varian-MAT** Shepherd, Tibball, Galog Associates	917A
231	* **Waters Associates** Edward W. Fischer & Associates	952A
230	* **Whatman, Inc.** J. S. Lanza & Associates	844A
232	* **Wilks Scientific Corporation** WILSCI Advertising	898A
243	* **Carl-Zeiss, Inc.** Michel-Cather, Inc.	919A
242	** **Carl Zeiss, Inc.** Werbedienst fur Markenwaren GmbH	928E

** See ad in ACS Laboratory Guide*

*** Company so marked has advertisement in the foreign regional edition only*

Advertising Management for the American Chemical Society Publications

CENTCOM, LTD.

Thomas N. J. Koerwer, President: Clay S. Holden, Vice President: Benjamin W. Jones, Vice President; Robert L. Voepel, Vice President; C. Douglas Wallach, Vice President, 25 Sylvan Rd. South, Westport, Connecticut 08880 (Area Code 203) 226-7131

ADVERTISING SALES MANAGER
James A. Byrne

SALES REPRESENTATIVES

Atlanta, GA . . . Robert E. Kelchner, CENTCOM, Ltd. Telephone: 203-226-7131

Boston, MA . . . Don Davis, CENTCOM, LTD. Telephone 203-226-7131

Chicago . . . Thomas Hanley, CENTCOM, LTD., 540 Frontage Rd., Northfield, Ill. 60093. 312-441-6383.

Cleveland . . . James Pecoy, CENTCOM, LTD., Suite 205, 18615 Detroit Ave., Lakewood, Ohio 44107. 216 228-8050.

Houston . . . Robert LaPointe, CENTCOM, LTD., 415-692-0949.

Denver . . . Clay S. Holden, CENTCOM LTD., 213-776-0552.

Los Angeles 90045 . . . Clay S. Holden, CENTCOM, LTD., Newton Pacific Center, 3142 Pacific Coast Highway, Suite 200, Torrance, CA 90505, 213-325-1903

New York 10017 . . . Don Davis, Richard L. Going, CENTCOM LTD., 60 East 42nd St., 212-972-9660

Philadelphia . . . Richard L. Going, CENTCOM LTD., GSB Building, Suite 510 1 Belmont Avenue Bala Cynwyd, Pa. 19004. Telephone: 215-667-9666

San Francisco, CA . . . Robert LaPointe, CENTCOM, LTD., Room 235, 1499 Bayshore Highway, Burlingame, CA 94010. Telephone: (415) 692-0949

Westport 06880 . . . Don Davis, CENTCOM, LTD., 25 Sylvan Rd. So., 203-226-7131.

Manchester, England . . . Jill E. Loney, Technomedia Ltd., 216, Longhurst Lane, Mellor, Stockport, SK6 5PW, Telephone: 061-427-5660

Reading, England . . . Malcolm Thiele, Technomedia Ltd., Wood Cottage, Shurlock Row, Reading, RG10 OOE. Telephone 073-581-302

Paris, France . . . Patric B. Hale, Technomedia Ltd., 18 Rue Gounod, 92 Saint-Cloud, Paris. Telephone: 602-24-79

Tokyo, Japan . . . Haruo Moribayashi, International Media Representatives Ltd., 2-29 Toranomon 1-chome Minato-ku, Tokyo 105, Japan. Telephone: 502-0656

PRODUCTION DEPARTMENT

Production Director
Joseph P. Stenza

Advertising Production Assistant
Barbara Aufderheide

PRODUCT CAPSULES

Scan this list for products of interest. Then, circle the indicated numbers on the adjacent reply card and selected literature from advertisers in the previous issue will be sent to you

No.	Product Capsules
301	Balances
302	Baths; Circulators
303	Biological Analyzers
304	Books; Periodicals; Catalogs
305	Centrifuge Equipment
306	Chemicals; Reagents; Gases
307	Chromatography, Gas
308	Chromatography, Liquid
309	Chromatography, Thin Layer
310	Computers; Calculators
311	Coolers; Freezers
312	Densitometers
313	Electrical Equip: Amplifiers; Power Supplies; Voltmeters; etc.
314	Electrochemical: pH Meters; Ion Meters; Titrators; Electrodes
315	Electrophoresis
316	Elemental Analyzers
317	Environmental Analyzers
318	Fourier Transform Data Systems
319	Furniture; Fume Hoods
320	Gas Chrom/Mass Spec Systems
321	Labware: Glass; Plastic; Metal
322	Lasers
323	Mechanical Equip: Presses; Mills; etc.
324	Microscopes
325	Mixers; Stirrers; Blenders; Shakers
326	Nuclear Instruments
327	Oscilloscopic Instruments
328	Ovens; Furnaces; Heaters
329	Photometers; Colorimeters
330	Pipets; Samplers; Dispensers
331	Pumps; Flowmeters
332	Recorders; Integrators
333	Services, Analytical; Consultants
334	Signal Averagers
335	Spectro, AA
336	Spectro, Fluorescence
337	Spectro, Infrared
338	Spectro, Mass
339	Spectro, NMR
340	Spectro, UV/Vis
341	Spectro, X-Ray
342	Stills; Demineralizers
343	Supplies: Lubricants; Detergents; etc.
344	Thermal Analyzers
345	Valves; Fittings; Tubing
346	Vacuum Equipment

"TEK-CHROM" Pre-Coated TLC Plates from ICN

featuring

- Uniform coating for analytical or preparative work. **No edge effects! No ridge effects!**
- Controlled narrow particle size for high resolution. **Better separations.**
- Unique inert organic binder. **Plates can be washed with polar solvents. Particularly useful for Silver Nitrate impregnation.**
- New "Rapid Plates". **Cuts analysis time. Simplifies transferring data to LC and HPLC.**
- Economically priced! **Reduces your overall costs for thin layer Chromatography.**

Making your own plates? ICN offers a full line of bulk Silica and Alumina adsorbents for TLC. Binder and fluorophors optional.

Send for ICN CHROMATOGRAPHY catalog now.

For Immediate Action. . .
Call collect **216/831-3000**
. . .ask for
Chromatography Product Manager.

ICN

ICN Pharmaceuticals, Inc.
Life Sciences Group
26201 Miles Road
Cleveland, Ohio 44128

See us at FASEB.

CIRCLE 103 ON READER SERVICE CARD

FIRST CLASS
Permit No. 25682
Philadelphia, Pa.
19101

BUSINESS REPLY CARD

No postage stamp necessary if mailed in the United States

POSTAGE WILL BE PAID BY

ANALYTICAL CHEMISTRY
P. O. Box #8660
Philadelphia, Pennsylvania 19101

Analytical Chemistry

SEPTEMBER 1977

Valid through January 1978

NEW PRODUCTS, CHEMICALS, LITERATURE: 401 402 403 404 405 406 407 408 409 410 411 412 413 414 415
416 417 418 419 420 421 422 423 424 425 426 427 428 429 430 431 432 433 434 435 436 437 438 439 440 441 442
443 444 445 446 447 448 449 450 451 452 453 454 455 456 457 458 459 460 461 462 463 464 465 466 467 468 469
470 471 472 473 474 475 476 477 478 479 480 481 482 483 484 485 486 487 488 489 490 491 492 493 494 495 496

ADVERTISED PRODUCTS: 1 2 3 4 5 6 7 8 9 10 11 12 13 14 15 16 17 18 19
20 21 22 23 24 25 26 27 28 29 30 31 32 33 34 35 36 37 38 39 40 41 42 43 44 45 46
47 48 49 50 51 52 53 54 55 56 57 58 59 60 61 62 63 64 65 66 67 68 69 70 71 72 73
74 75 76 77 78 79 80 81 82 83 84 85 86 87 88 89 90 91 92 93 94 95 96 97 98 99 100
101 102 103 104 105 106 107 108 109 110 111 112 113 114 115 116 117 118 119 120 121 122 123 124 125 126 127
128 129 130 131 132 133 134 135 136 137 138 139 140 141 142 143 144 145 146 147 148 149 150 151 152 153 154
155 156 157 158 159 160 161 162 163 164 165 166 167 168 169 170 171 172 173 174 175 176 177 178 179 180 181
182 183 184 185 186 187 188 189 190 191 192 193 194 195 196 197 198 199 200 201 202 203 204 205 206 207 208
209 210 211 212 213 214 215 216 217 218 219 220 221 222 223 224 225 226 227 228 229 230 231 232 233 234 235
236 237 238 239 240 241 242 243 244 245 246 247 248 249 250 251 252 253 254 255 256 257 258 259 260 261 262

PRODUCT CAPSULES: 301 302 303 304 305 306 307 308 309 310 311 312 313 314 315 316 317 318 319 320 321 322 323
324 325 326 327 328 329 330 331 332 333 334 335 336 337 338 339 340 341 342 343 344 345 346

Name________________________________ Position________________

Company____

Street________________________________ City________________

State________________ Zip________________ Telephone________________

30-ton
motorized
hydraulic press
for safe, fast
reproducible pressing
of pellets 13-mm to
44-mm in diameter.

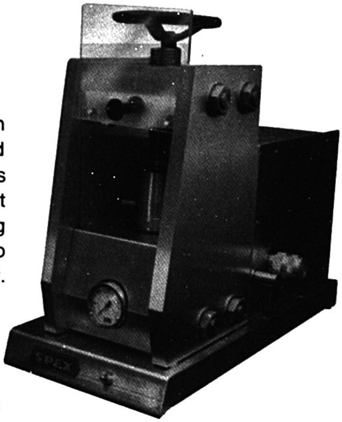

SPEX INDUSTRIES INC.
P.O.BOX 798, METUCHEN, N.J. 08840
(201) 549-7144
CIRCLE 187 ON READER SERVICE CARD

Analytical Chemistry SEPTEMBER 1977 Valid through January 1978

NEW PRODUCTS, CHEMICALS, LITERATURE: 401 402 403 404 405 406 407 408 409 410 411 412 413 414 415
416 417 418 419 420 421 422 423 424 425 426 427 428 429 430 431 432 433 434 435 436 437 438 439 440 441 442
443 444 445 446 447 448 449 450 451 452 453 454 455 456 457 458 459 460 461 462 463 464 465 466 467 468 469
470 471 472 473 474 475 476 477 478 479 480 481 482 483 484 485 486 487 488 489 490 491 492 493 494 495 496

ADVERTISED PRODUCTS: 1 2 3 4 5 6 7 8 9 10 11 12 13 14 15 16 17 18 19
20 21 22 23 24 25 26 27 28 29 30 31 32 33 34 35 36 37 38 39 40 41 42 43 44 45 46
47 48 49 50 51 52 53 54 55 56 57 58 59 60 61 62 63 64 65 66 67 68 69 70 71 72 73
74 75 76 77 78 79 80 81 82 83 84 85 86 87 88 89 90 91 92 93 94 95 96 97 98 99 100
101 102 103 104 105 106 107 108 109 110 111 112 113 114 115 116 117 118 119 120 121 122 123 124 125 126 127
128 129 130 131 132 133 134 135 136 137 138 139 140 141 142 143 144 145 146 147 148 149 150 151 152 153 154
155 156 157 158 159 160 161 162 163 164 165 166 167 168 169 170 171 172 173 174 175 176 177 178 179 180 181
182 183 184 185 186 187 188 189 190 191 192 193 194 195 196 197 198 199 200 201 202 203 204 205 206 207 208
209 210 211 212 213 214 215 216 217 218 219 220 221 222 223 224 225 226 227 228 229 230 231 232 233 234 235
236 237 238 239 240 241 242 243 244 245 246 247 248 249 250 251 252 253 254 255 256 257 258 259 260 261 262

PRODUCT 301 302 303 304 305 306 307 308 309 310 311 312 313 314 315 316 317 318 319 320 321 322 323
CAPSULES: 324 325 326 327 328 329 330 331 332 333 334 335 336 337 338 339 340 341 342 343 344 345 346

Name__________ Position__________

Company__________

Street__________ City__________

State__________ Telephone__________

FIRST CLASS
Permit No. 25682
Philadelphia, Pa.
19101

BUSINESS REPLY CARD
No postage stamp necessary if mailed in the United States

POSTAGE WILL BE PAID BY

ANALYTICAL CHEMISTRY
P. O. Box #8660
Philadelphia, Pennsylvania 19101

PRODUCT CAPSULES

Scan this list for products of interest. Then, circle the indicated numbers on the adjacent reply card and selected literature from advertisers in the previous issue will be sent to you

No.	Product Capsules
301	Balances
302	Baths; Circulators
303	Biological Analyzers
304	Books; Periodicals; Catalogs
305	Centrifuge Equipment
306	Chemicals; Reagents; Gases
307	Chromatography, Gas
308	Chromatography, Liquid
309	Chromatography, Thin Layer
310	Computers; Calculators
311	Coolers; Freezers
312	Densitometers
313	Electrical Equip: Amplifiers; Power Supplies; Voltmeters; etc.
314	Electrochemical: pH Meters; Ion Meters; Titrators; Electrodes
315	Electrophoresis
316	Elemental Analyzers
317	Environmental Analyzers
318	Fourier Transform Data Systems
319	Furniture; Fume Hoods
320	Gas Chrom/Mass Spec Systems
321	Labware: Glass; Plastic; Metal
322	Lasers
323	Mechanical Equip: Presses; Mills; etc.
324	Microscopes
325	Mixers; Stirrers; Blenders; Shakers
326	Nuclear Instruments
327	Oscilloscopic Instruments
328	Ovens; Furnaces; Heaters
329	Photometers; Colorimeters
330	Pipets; Samplers; Dispensers
331	Pumps; Flowmeters
332	Recorders; Integrators
333	Services, Analytical; Consultants
334	Signal Averagers
335	Spectro, AA
336	Spectro, Fluorescence
337	Spectro, Infrared
338	Spectro, Mass
339	Spectro, NMR
340	Spectro, UV/Vis
341	Spectro, X-Ray
342	Stills; Demineralizers
343	Supplies: Lubricants; Detergents; etc.
344	Thermal Analyzers
345	Valves; Fittings; Tubing
346	Vacuum Equipment

New HPLC Column News

EM LABORATORIES VOL. I, NO. 1

NEW HIBAR®-II

ELMSFORD, NY (EM)
EM Laboratories has just introduced a brand new, totally different line of prepacked columns for HPLC – Hibar-II.

BRAND NEW HIBAR®-II HARDWARE

The Hibar-II columns are 25 cm long and have an inside diameter of 4.6 mm. Hibar-II columns are adaptable to all modular or unitized HPLC systems, featuring zero dead volume fittings. Each column contains removable/cleanable frits for extended life.

WIDE RANGE OF PREPACKED SORBENTS

But the best news is that Hibar-II columns are prepacked with the entire line of great sorbents from E. Merck, Darmstadt, Germany. That means convenience and versatility like you've never before enjoyed in HPLC. Sorbents for partition, adsorption, gel permeation, and ion exchange chromatography. Two different particle shapes: irregular shaped, totally porous (LiChrosorb®) and totally spherical shaped porous (LiChrospher®), and two different particle sizes . . . 5 and 10 micron.

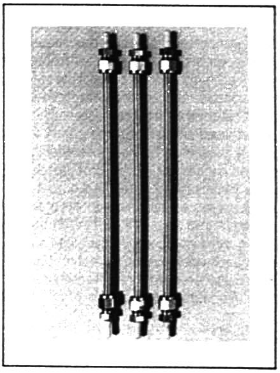

For your price convenience and service, Hibar-II columns are available from selected nationwide scientific supply houses.

You need all the facts on this important development in our industry, so write today for complete technical information and the name of your nearest stocking distributor.

Products for HPLC

CIRCLE 63 ON READER SERVICE CARD

EM Laboratories, Inc.
associate of
E. Merck, Darmstadt, Germany
500 Executive Boulevard
Elmsford, N.Y. 10523
(914) 592-4660

Pure Consistency...

◆ laboratory reagents and indicator strips ◆ sorbents, plates and columns for chromatography
◆ biochemical specialties ◆ instrumentation chemicals

New Products

Pollution/Gas Analyzer

The instrument uses a unique mass spectrometer principle that affords ppm range sensitivity, gas selectivity, ruggedness, and ease of maintenance. The system can continuously monitor any number of preselected gases for quantitative measurements including carbon monoxide, sulfur dioxide, and basic hydrocarbons in room or outside atmospheric environments. An alarm unit may also be purchased with the unit to alert an operator that any particular gas level is unacceptably high. Oscilloscope presentation is optional. CVC Products, Inc. 413

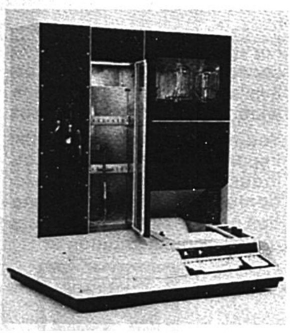

SP8000 high-performance liquid chromatograph contains a powerful microprocessor that both monitors operation of the LC components and provides users with the ability to preprogram series of different chromatographic tasks. The SP8000 incorporates a unique ternary gradient system that independently controls three solvents for both isocratic and gradient work. Other advances include a single pump providing pulse-free, constant flow, and a self-contained helium degas system that is easy to use and allows uninterrupted chromatographic operation. Other features include full alphanumeric keyboard with LED display, printer/plotter, temperature-controlled column compartment, automatic sample injector, multiple-wavelength absorbance detector, and dual-channel data system. Spectra-Physics, Inc. 402

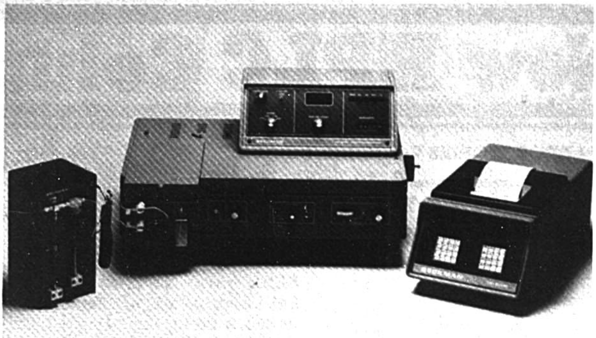

Trace I and Trace II spectrophotometer systems are based on the Model 34 UV/VIS spectrophotometer with final answer computer, printer, and special accessories for automatic calculation of clinical chemistries based on kinetic and end-point analyses of enzymes. Trace I and II simplify STAT and routine chemistries and enzyme immunoassays of analyses such as drugs of abuse and anticonvulsant drugs. Results are computed, displayed, and printed out in absorbance, rate, or concentration, as selected. The Trace I system consists of the Model 34 UV/VIS spectrophotometer with heated "sipper" (low-volume heated flow cell), the DP-3000 microprocessor/computer, and a pipetor/diluter. The DP-3000 is preprogrammed to handle 13 standard chemistries and has 25 additional user-programmable chemistries. The Trace II system is comprised of the Model 34C UV/VIS spectrophotometer, which includes a heated "sipper" and a compatible printer. It is specifically designed to perform virtually all clinical chemistry analyses and features a substrate depletion warning. Beckman Instruments, Inc. 401

Gas Chromatograph/ Mass Spectrometer

HP 59993A fully integrated GC/MS incorporates all-digital electronics, a microprocessor-controlled GC, electron ionization source, hyperbolic quadrupole mass filter, electron multiplier detector, power supply, analyzer vacuum system, inlet vacuum system, and a GC/MS membrane interface. The data system includes an HP 21MX E-Series microprogrammable 16-bit computer with 32K words of memory and an HP 7900A dual-disc drive with 5 megabytes of data storage. Ions are detected by the continuous dynode electron-multiplier detector. Sensitivity is rated at 10 to 1 on 1 ng of methyl stearate, scanned at 300 amu/s. The mass range is 10–800 amu. Optional features include a jet or membrane separator; a capillary injection system that operates in the splitless mode; Aldermaston, EPA/NIH, and contributed spectral libraries; and a data communications interface to allow transmission between the GC/MS and the Cornell or Cyphernetics timeshare systems. Basic system, excluding the CRT terminal, is priced at $70 000. Hewlett-Packard Co. 415

For more information on listed items, circle the appropriate numbers on one of our Readers' Service Cards

---

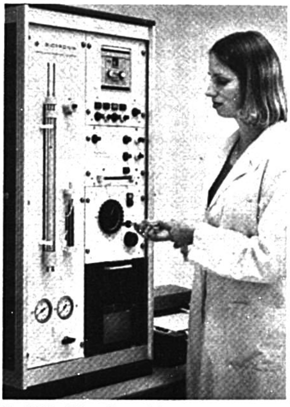

Model D-400 amino acid analyzer separates and measures amino acids in protein hydrolyzates and biological fluids by single-column, high-resolution ion-exchange chromatography. As many as 24 samples can be injected. The narrow diameter column increases the sensitivity of analysis to 0.5 nm each component and reduces the consumption of reagent and buffers. An integral ammonia filter continuously removes contaminating amines from all buffers. Linear absorbance detection of ninhydrin-positive components in the sample is displayed on a two-pen continuous writing recorder. Chromatographic procedures are time directed by a 15-channel programmer that can select six buffers and two column temperatures plus control accessories including an optional calculating integrator. Durrum Instrument Corp. 407

Schott—the glass makers for Abbe and Zeiss—bring you...

the THALAMID® combination electrode

A superior electrode exemplifying not only the expertise in scientific glassmaking originated at Schott & Gen. in the days of Ernst Abbe and Carl Zeiss, but, as well, the innovative approach to all details of a product which has characterized Schott's contributions to the laboratory.

In this combination electrode, scientifically designed pH-sensitive glasses are combined with a unique, high-performance electrochemical system, a superior reference junction and sound, time-tested construction to provide accuracy, stability, durability and reliability.

The outstanding features of this electrode are detailed below; and we'll be happy to send you a bulletin on the entire Schott electrode line, available exclusively from Sargent-Welch.

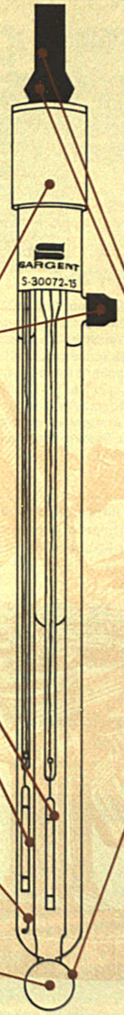

Stainless steel (18-8-2) cap resists corrosion and provides mechanical strength for secure clamping.

Refill aperture for reference electrode has a rubber cap to provide a tight seal against electrolyte leakage or creepage and a side tube for connection to a remote reservoir.

THALAMID® (thallium amalgam) cartridge form internal elements are characterized by stability, absence of thermal decomposition and low hysteresis at temperatures up to 135°C, by freedom from complex formation with sample components (including cyanide), by indifference to the KCl electrolyte and polarization currents and by a long service life. In these respects the THALAMID system is superior to one or both of the calomel and silver-silver chloride systems. Identical elements in glass and reference electrodes provide thermal and electrical symmetry to speed temperature equilibrium and reduce asymmetry potential.

Liquid junction comprises a platinum filament sealed through the glass wall of the reference electrode. This junction provides low resistance, a low electrolyte leak rate, a constant junction potential, good performance in samples with very high and very low salt contents, and resistance to clogging by slurries or viscous solutions. It is located just above the pH-sensitive bulb to minimize sample volume demand. For difficult samples requiring large electrolyte flow and frequent purging, a combination electrode with ground junction is available.

Internal buffer is specially compounded for stability with temperature change and with time, and for compatibility with the glass surface. Nominal pH is 7, suited to all common pH meters.

Special coaxial cable shields the glass electrode conductor from electromagnetic and capacitive interference and has a tough, waterproof cover. It is non-microphonic and does not affect the meter reading when moved.

Hermetic seal between cap and cable is made by vulcanizing to exclude moisture and relieve mechanical strain on the internal elements of the electrode.

Only two membrane glasses cover all applications: Type N (general purpose) and Type H (high temperature-high alkalinity): **Type N**—Suitable for all uses except those involving high temperature and/or high sodium ion concentrations (high alkalinity). Response is very close to Nernstian and linear even in highly acid solutions. Na^+ ion response is very low (insignificant below pH 12.5 at 25°C) and, even more important, it is stable where significant. Type N glass electrodes can be used continuously from 0° to 80°C, intermittently to 100°C. Low specific resistance allows a 0.5 mm wall with a total resistance of only 100 megohms (10 mm bulb) at room temperature. The heavy wall, high inherent glass strength and careful fabrication result in a strong, shock resistant construction. **Type H**—In contrast with Type N glass, Type H has a lower sodium ion error, improved chemical resistance, and a longer life expectancy at high pH and/or elevated temperature, and a higher electrical resistance. It is the glass of choice for measurements at a pH above 1 in solutions with high alkali metal content and for use in photographic developers and nonaqueous systems. With Type H glass, can be used at temperatures up to about 110°C, the boiling point of the reference electrolyte, or, with suitable pressurizing, to 135°C.

SARGENT-WELCH SCIENTIFIC COMPANY

7300 NORTH LINDER AVENUE • SKOKIE, ILLINOIS 60076 • (312) 677-0600

Anaheim/Birmingham/Chicago/Cincinnati/Cleveland/Dallas/Denver/Detroit/Springfield, N.J./Toronto/Montreal

CIRCLE 194 ON READER SERVICE CARD

NMR Spectrometer

Model PMX60 proton NMR spectrometer is a high-performance (30:1 S/N on 1% EB), permanent-magnet system and features the latest in solid state circuitry. It features a color-coded keyboard to simplify operation. Optimum parameters can be selected automatically, or specific conditions can be selected. A visual meter for tuning resolution also allows observation of lock and signal intensity. A hold button facilitates simple integration control and can be used to eliminate unwanted solvent or water peaks from the spectra. Internal lock and homo nuclear decoupling is built into the console. A compressed air device simplifies sample tube insertion and removal as well as minimizes abrupt temperature changes within the magnet console during sample tube exchange. Jeol Analytical Instruments **410**

Colored Glass Filters

Seventy-eight individual 50-mm square colored glass filters are supplied with individual spectrophotometer curves. Surface parallelism and finish are held to high standards. Each filter is marked with an identifying portion of the catalog number for permanent recognition. Available in protective plastic display pages that can be incorporated into a storage binder. Melles Groit **420**

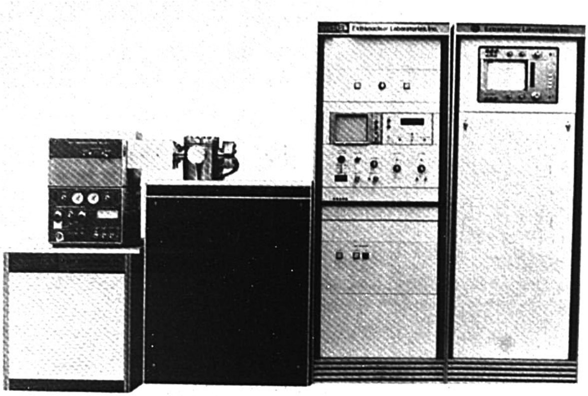

SpectrEL Simulscan 200 GC/MS offers simultaneous analysis by chemical ionization and electron impact ionization methods in one instrument. In addition to time savings and convenience, this simultaneous scanning provides the certainty that the CI and EI spectra come from the exact same sample. The two spectra can be obtained at scan rates of 2 ms/amu. The Simulscan systems are available with either the Varian or HP Series GC's or can incorporate the GC best suited to the customer's individual needs. The standard system includes positive ion mass spectrometry, analog detection, and operates to mass 1000. Options available include the addition of negative ion mass spectrometry, pulse counting detection, and a mass range to 1200 amu. Extranuclear Laboratories, Inc. **404**

For more information on listed items, circle the appropriate numbers on one of our Readers' Service Cards

The PW 1410/20 AHP x-ray spectrometer/desk calculator system offers users an automatic machine producing fast results at a moderate price. The spectometer incorporates a microprocessor that can accept and store a large number of analytical programs. The operator simply loads the sampie and selects the desired program via the calculator keyboard. Analysis is performed entirely automatically, and the calculator, an HP 9814A, converts the received intensities into element concentrations, which it then prints out. It is ideal for both production-line quality control and laboratory research application. Philips Industries, Scientific and Analytical Equipment Dept., Lelyweg 1, Almelo, The Netherlands **405**

Dye Lasers

The DL-II series of dye lasers includes the DL12 with oscillator, the DL14 with oscillator/amplifier, and the DL14P with oscillator/amplifier with pressure-scanned etalon for 0.0006-nm resolution at 460 nm. The range of the DL-II series is 217–930 nm when nitrogen laser pumped, and 324–930 nm when Nd:YAG pumped. Synchronized frequency doubling is achieved with a new desk calculator accessory that permits selection of scanning either linear in wavelength or wavenumber as well as data acquisition. Similarly, the wavelength range to be scanned and the ordinate expansion may be simply programmed to suit specific requirements. Price of the DL12 is $7950, the DL14 is $9250, and the DL14P is $9750. Molectron Corp. **411**

Liquid Chromatography System

This "bench-top" system for low-pressure applications contains a Mixograd gradient former, Minipuls peristaltic pump, chromatographic spectrophotometer, column, valve, fittings, shut-off valve, and Race Track fractionator. Components can be substituted or eliminated to meet particular applications—ion exchange, gel permeation, absorption, HPLC, etc. Gilson Medical Electronics **417**

Carle Puts A Price On Simultaneous TCD/FID Analysis of Refinery Gases

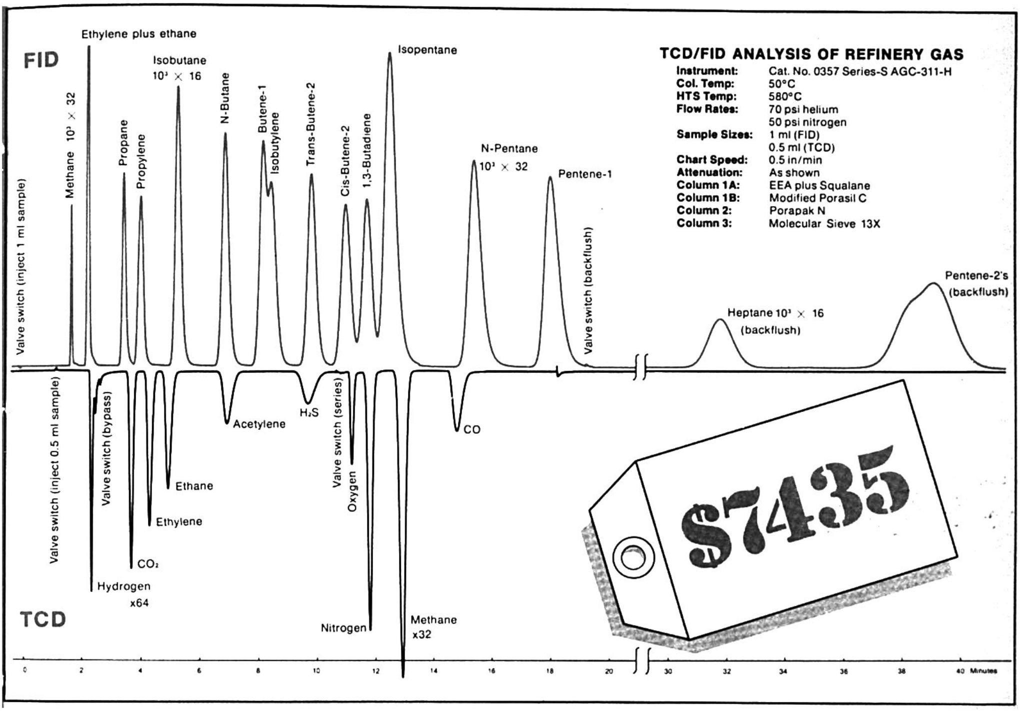

TCD/FID ANALYSIS OF REFINERY GAS

Instrument:	Cat. No. 0357 Series-S AGC-311-H
Col. Temp:	50°C
HTS Temp:	580°C
Flow Rates:	70 psi helium 50 psi nitrogen
Sample Sizes:	1 ml (FID) 0.5 ml (TCD)
Chart Speed:	0.5 in/min
Attenuation:	As shown
Column 1A:	EEA plus Squalane
Column 1B:	Modified Porasil C
Column 2:	Porapak N
Column 3:	Molecular Sieve 13X

Interested in a complete GC analysis of refinery gas? Shown above is one answer to that knotty problem, accomplished automatically with the latest Carle Series-S Analytical Gas Chromatograph. This instrument performs trace level hydrocarbon measurement with a sensitive FID, while simultaneously measuring inerts with a TCD.

Each one of Carle's Series-S AGCs is factory-dedicated to perform a specific analysis automatically. That's how Carle puts a price on the answer. Every Series-S AGC is ready to go to work on your problem right out of the box. There's nothing more to buy, no more column engineering necessary—Carle's already done it.

Each Series-S AGC incorporates Carle's unique multi-column sequencing techniques. With just one sample these multiple columns produce a complete, sensitive analysis impossible to duplicate with old-fashioned single column techniques.

This new refinery gas analysis is just one of the Series-S answers available from Carle. There are a dozen more, such as natural gas, combustion gas and hydrogen product gas. For a concise description of these Series-S answers, and an Application Data Sheet detailing this new refinery gas analysis, call or write today.

CARLE
INSTRUMENTS, INC.

1141 East Ash Avenue, Fullerton, CA 92631 714-879-9900

CIRCLE 38 ON READER SERVICE CARD

Algorithms for Chemical Computations

ACS Symposium Series No. 46

Ralph E. Christoffersen, Editor
The University of Kansas

A symposium sponsored by the Division of Computers in Chemistry of the American Chemical Society.

This multidisciplinary collection of state-of-the-art papers assesses significant developments in algorithms for several important areas of chemistry and pinpoints places where currently available algorithms are inadequate.

Leading experts not only evaluate the tremendous opportunities for progress in chemical research that algorithms provide but also analyze the substantial difficulties that algorithms may present.

Topics covered include those of particular interest to scientists doing significant amounts of computing in the fields of quantum chemistry, scattering, computer handling of chemical information, and solid state theory.

CONTENTS

Graph Algorithms in Chemical Computation • Algorithm Design in Computational Quantum Chemistry • Rational Selection of Algorithms for Molecular Scattering Calculations • Molecular Dynamics and Transition State Theory • Newer Computing Techniques for Molecular Structure Studies by X-ray Crystallography • Algorithms in the Computer Handling of Chemical Information

151 pages (1977) Clothbound $12.75
LC 77-5030 ISBN 0-8412-0371-7

SIS/American Chemical Society
1155 16th St., N.W./Wash., D.C. 20036

Please send ______ copies of *SS 46 Algorithms for Chemical Computations* at $12.75 per copy.

☐ Check enclosed for $________ . ☐ Bill me.
Postpaid in U.S. and Canada, plus 40 cents elsewhere.

Name

Address

City State Zip

Model SF-330 spectrofluorometer, designed for operational simplicity and user convenience, is intended for food processing, drug manufacturing, biological, and chemical laboratory applications that require a moderately priced sensitive instrument for analysis of trace concentrations of organic and inorganic chemicals. Features include two photomultiplier detectors, a 150-W xenon lamp source, two concave grating monochromators, selectable spectral bandwidth combinations, scan speeds of 25 or 50 nm/min, and digital readout. $5795. Varian Instrument Div. **406**

Dual-Wavelength Detector

System D-137 is designed to be added to the Durrum-Gibson stopped-flow mixing chamber. It employs split-beam dual-detection optics to measure fast reactions at two wavelengths simultaneously. The two signals are then processed by solid state electronics to provide the ratio and difference of the two signals. By selecting appropriate wavelengths, small absorbance changes of fast reactions can be measured in turbid solutions where single-wavelength measurements are hampered by effects of scattered light. Durrum Instrument Corp. **418**

Carbon Analyzers

These carbon analyzers use a new coulometric carbon dioxide titrator to provide high accuracy in a wide variety of carbon analyses including mineral carbon, total carbon, and organic carbon in water, oils, and solids. Carbon levels from sub ppm to 100% can be determined. The coulometer can also be used for other high-accuracy CO_2 measuring applications. Coulometrics Inc. **419**

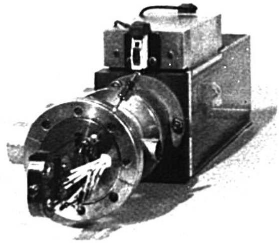

An interface to combine liquid chromatograph and mass spectrometer systems permits mass spectral analysis of those chemicals difficult to identify with a GC/MS. Among its features, the interface allows free choice of electron impact or chemical ionization and does not interfere with GC/MS or solid probe operation. It provides high sensitivity LC detection, high sample yield, and high chromatographic integrity. It is particularly useful in mass spectral analysis of mycotoxins, polycylic aromatic compounds, pesticides, steroids, triglycerides, coumarins, and many drug metabolites, and will have wide applications in pharmaceutical and biomedical research, and in petroleum, energy, pollution, and pesticide studies. The interface can be added to any Finnigan mass spectrometer with a differential pumping system. It can be installed on a new mass spectrometer or retrofitted to an existing system. Finnigan Corp. **403**

Try our it-can't-be-a-balance balance

[There's never been anything quite like it.]

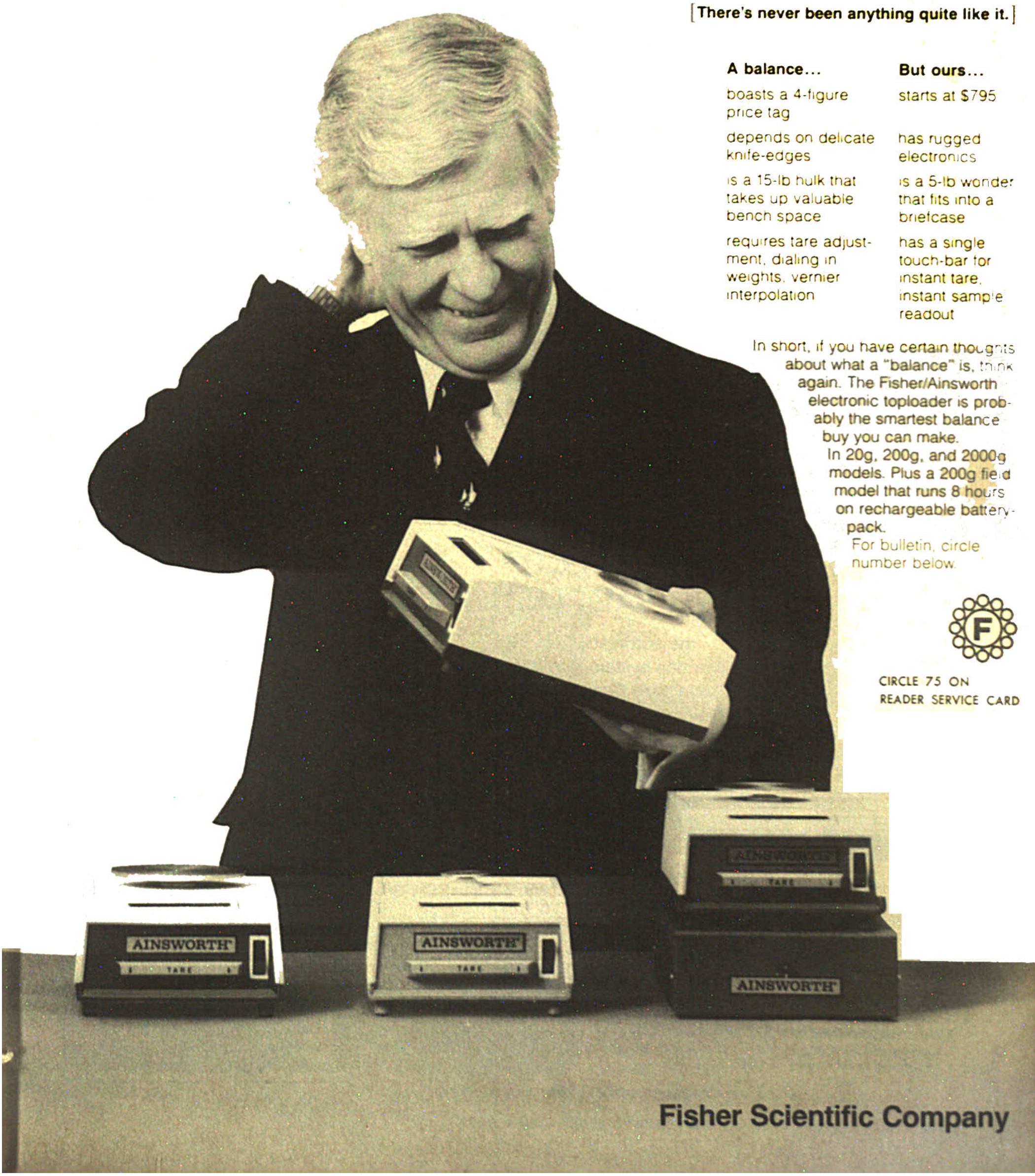

A balance...	But ours...
boasts a 4-figure price tag	starts at $795
depends on delicate knife-edges	has rugged electronics
is a 15-lb hulk that takes up valuable bench space	is a 5-lb wonder that fits into a briefcase
requires tare adjustment, dialing in weights, vernier interpolation	has a single touch-bar for instant tare, instant sample readout

In short, if you have certain thoughts about what a "balance" is, think again. The Fisher/Ainsworth electronic toploader is probably the smartest balance buy you can make.

In 20g, 200g, and 2000g models. Plus a 200g field model that runs 8 hours on rechargeable battery-pack.

For bulletin, circle number below.

CIRCLE 75 ON READER SERVICE CARD

Fisher Scientific Company

The most intelligent microbalance

The new AD-2Z Autobalance with both Autoranging and Autozero

It can set zero, balance the beam, select the best range, shift the decimal, display the weight on a large digital readout, print it (with an optional printer) and much more . . . all automatically and within seconds. That's what all microbalances should do, but only the AD-2Z does. 5 gram capacity, 0.1 microgram sensitivity. Recording and vacuum models available.

Call your local Perkin-Elmer sales office, or write Instrument Division, Perkin-Elmer Corporation, Main Avenue, Norwalk, CT 06856.

PERKIN ELMER

CIRCLE 168 ON READER SERVICE CARD

For Liquid Chromatography

VALCO'S MULTI LOOP AUTO SAMPLER . . .

the automatic sample injection system that lets you Minimize Sample Waste, Maximize System Efficiency

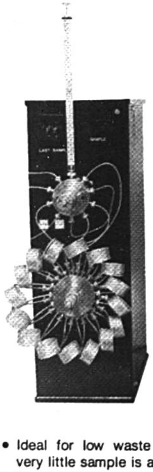

All for under $3,000.

- Ideal for low waste applications where very little sample is available
- Small uniform bore minimizes error due to sample carry-over
- Improves repeatability of recorded area and retention times
- Up to 150° continuous operation in high temperature GPC (optional)
- No pressurized gas required for sample loading into injection valve
- No bottles to fill, break, or lose
- All Hastalloy C and nickel flow path available for reactive samples (optional)
- BCD samples number identification for use with computers or integrators
- Pulse and continuous contact closures available
- Up to 4 injections per sample
- Simplicity of operation

VALCO instruments co
P O Box 19032 Houston, Tx 77024
713-688-9345
TWX 910-881-5500
Telex 79-0033

CIRCLE 223 ON READER SERVICE CARD

New Products

UV–VIS Spectrophotometer

Model 576 scattered transmission spectrophotometer is designed specifically to handle turbid, scattering samples. Automatic digital background correction compensates for initial differences between cells. The background corrector automatically plots out the flattened spectrum, and necessary corrections are stored in digital memory. A modified sample can then be run, and the difference spectrum superimposed. Repetitive scanning capability is also a standard feature. Data can be either superimposed or presented sequentially on the instrument's Format recorder. The instrument sample compartment can accommodate all of the sampling accessories developed for the 57 Series. Perkin-Elmer Corp. **412**

Preparative Gel Electrophoresis

The vertical column system accepts sample loads up to 5 times greater than those accepted by existing systems and can easily handle up to 20 times that amount when fitted with a larger optional inner column. Recovery rate typically exceeds 80%, and the design minimizes eluate dilution. No pumps or cooling systems are needed. The cylindrical design eliminates leakage and consequent sample loss and makes the cell easy to use and clean. Camag Inc. **416**

Differential Corrected Spectra Unit

The differential corrected spectra unit, a digital microprocessor system designed for use with the Model MPF-44A fluorescence spectrophotometer, can store in memory all of the correction factors needed to correct excitation of emission spectra. This is an electronic feature equivalent to the optical function of a double-beam spectrophotometer. Applications include detection of small differences in samples for compound identification in quality control, elimination of fluorescing solvents or blanks, screening unknowns, elimination of Raman bands, and storage of original spectra of unstable samples. Another mode of operation of the unit provides a combined excitation emission scan of a sample of interest. Perkin-Elmer Corp. **421**

For more information on listed items, circle the appropriate numbers on one of our Readers' Service Cards

It's now this convenient to get superior GC/MS analyses.

With the Varian MAT 44 Quadrupole GC/MS, operation is as straightforward as entering a few keyboard commands. You get qualitative and quantitative results with unprecedented ease, sensitivity and precision. The MAT 44 provides full microprocessor control, EI/CI operation, capillary or packed columns and real-time TV display.

The data below give a brief indication of the many capabilities of this exceptional instrument system. For complete information or to arrange a demonstration call or write today. (201) 822-3700. Varian MAT Mass Spectrometry, 25 Hanover Road, Florham Park, New Jersey 07932.

varian

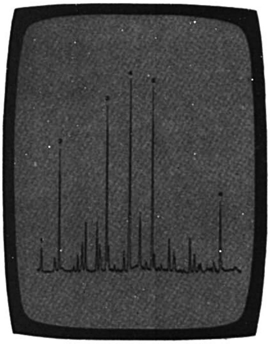

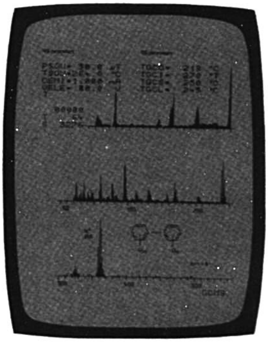

PCB ANALYSIS

The data shown opposite are taken from a capillary column run of a PCB mixture. The glass column was directly connected to the ion source and the total ion chromatogram is shown at the left. An example of the TV display during analysis is given at the right. The spectra are normalized and have the mass scale identified before output as hard copy or further processing via the data system.

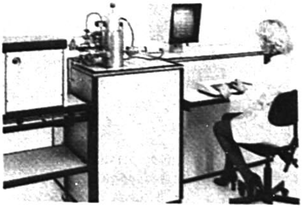

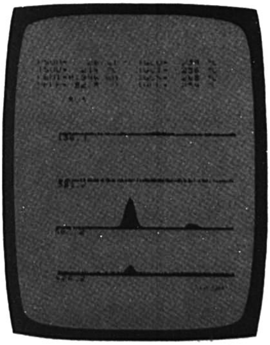

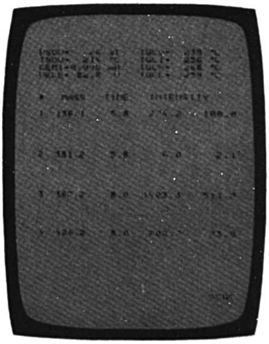

DRUG ANALYSIS

The data opposite shows the quantitative analysis of the drug Vincamine in an animal urine extract. To the left is the TV display during the elution and monitoring of peaks from the drug (m/e 367, m/e 426) and the reference standard (m/e 136, m/e 381). At the end of the run, the quantitation is automatically completed and peak intensity ratios displayed relative to the standard as shown at the right.

CIRCLE 222 ON READER SERVICE CARD

GOW-MAC
the T.C. Detector
Specialists
can keep your GC
in business.

The best way to save money is preventive care of your T.C. detector. A cell using hot wire filaments operates at elevated temperatures, the wires, too, are hot due to the current passed through them, therefore subject to oxidation. Many things can oxidize the detector elements: samples, leaks, inadequate purge. When filaments are oxidized their resistance will change and the bridge is out of balance. Certain filaments resist oxidation more than others under different conditions. Other things which unbalance bridge circuits are corrosion, vibration, column bleed, carbon deposits, etc. GOW-MAC can help by the availability of numerous filament materials and years of experience in solving such problems. Thermistors are also available in various resistance ranges. GOW-MAC can supply detector elements for most of the gas chromatographs in production as well as those that are no longer manufactured.

Four ways to solve the problem and save time and money:

1. Purchase detector elements in pairs. If you have several T.C. instruments and want to re-filament your own detector this is fast and the least expensive approach. You can have elements in stock or, we can ship from stock. Even our representatives have emergency stock for customers in trouble.
2. Purchase a quad. (four matched elements). This is for those who have one or two units and want to re-filament the cell themselves. With a quad. anyone can re-filament his own detector. All four elements are matched so you don't have to pick two matched pairs to make a well-balanced bridge.
3. The easiest, not the quickest or least expensive, is to take the cell block out of the detector oven and send it to us. We will clean, refilament, check for leaks, drift and noise for $110.00*. This takes at least 48 hours, so allow one week for us to receive and return.
4. You can also purchase a spare detector and keep it on the shelf. Most detectors can be supplied by GOW-MAC for about $150.00.

Take your pick, by ordering directly from GOW-MAC you can save either money, time, or both.

We're prepared to send time and money saving information:

1. Filament Bulletin listing 8 different materials available for detector elements including thermistors.
2. Cell Bulletin which lists 12 T.C. detectors from process to micro, 4 types of Gas Density Detectors.
3. Our Filament Replacement Chart. This lists all major GC manufacturers, instrument models and the GOW-MAC replacement elements.
4. General Service Bulletin—tells how to re-filament a cell, discusses maintenance and trouble shooting as well as recommended operating conditions for T.C. cells.
5. Price List—this will save you money.

We'll even throw in the booklet, "Selecting a GC Column" written for GOW-MAC by Dr. H. McNair. DON'T WAIT!

*W or WX filaments for most detectors.

GOW MAC

GOW-MAC INSTRUMENT CO.
100 Kings Road, Madison, N.J. 07940
Telephone: 201/377-3450 Telex: 136331
Shannon Free Airport, Co. Clare, Ireland

CIRCLE 80 ON READER SERVICE CARD

Spectrum Analyzer

Model FFT 512/S-20 spectrum analyzer incorporates an all-digital range translator that enables the analyzer to magnify the resolution in any selected region of a spectrum by factors of 8, 16, 32, 64, or 128. If the magnified portion is of much lower amplitude than parts of the original spectrum, additional gain of ×2, ×4, and ×8 is provided. With this feature, resolution to within 2 Hz is provided in the 0–100 kHz range, and within 0.4 mHz in the 0–20 Hz range. Additional features include vertical scale calibration in arbitrary engineering units over wide ranges, and display on command of the ratio: active spectrum/stored spectrum. Rockland Systems Corp. **414**

Chemicals

Ethyl Fluorescein

Kromex fluorescein, ethyl ester, is a fluorescent agent potentially useful in biomedical and biochemical research studies where fluorescein has proved valuable. This high-purity compound has a quantum yield of greater than 0.95 and is believed to have greater membrane permeability. It is characterized by a broad-based actual lot analysis, and a certificate of the analysis is supplied. Available in 2-g size. J. T. Baker Chemical Co. **424**

Immobilized Proteolytic Enzymes

Sorbazyme-Q series of immobilized enzymes consists of a variety of proteolytic enzymes attached to an inert matrix of cellulose with retention of catalytic properties and improved stability. They are supplied as a white, dry powder, can be recovered at the end of a reaction and reused many times, and can be packed in columns and used in a continuous flow reactor. Quantimetrix Medical Industries **425**

Ultrapure Elements

Antimony, arsenic, bismuth, cadmium, copper, gold, indium, lead, selenium, silver, sulfur, tellurium, thallium, and zinc are offered at 99.999+% purity. Quantities available range from hundreds of grams to kilograms and are available in various bulk forms including shot, rods, and fragments. Each shipment includes information on impurities, toxicity, and handling. Reactor Experiments, Inc. **426**

Accuracy is easy with . . .

the compact Zeiss PM 6 Spectrophotometer with double-grating monochromator and automatic blank reference.

It's so simple, it's foolproof. All you do is:

1 put your blank in the first position;
2 place samples in the other three positions, or a known standard in the #2 position;
3 set the display to absolute absorbance or the desired concentration value;
4 push the button for the sample position you want, and the results will be displayed directly either in absorbance or concentration. Kinetic determinations are just as simple.

And it's accurate. You can sample volumes from 20ml to 0.2ml without loss of sensitvity. Read out digitally from −0.300 to 3.000 Absorbance and 0-10,000 Concentration, and expand the scale 10X with great accuracy. Spectral range is 200-800nm with high photometric linearity.

No other instrument in its price range offers a double-grating monochromator.

The PM 6 comes with 4-position motorized and programmable sample changer, or a unique funnel cell for rapid routine determinations. Accessories include a new, inexpensive gel scanner, a thermo-electric temperature control, a multi-speed recorder and a printer.

Write today for complete details and a demonstration.

Nationwide sales and service direct and only from Zeiss.

Carl Zeiss, Inc., 444 5th Avenue, New York, N.Y. 10018 (212) 730-4400. Branches in: Atlanta, Boston, Chicago, Columbus, Houston, Los Angeles, San Francisco, Washington, D.C. In Canada: 45 Valleybrook Drive, Don Mills, Ont., M3B 2S6. Or call (416) 449-4660.

Spectrophotometer PM6
2 7 8
1.246

ZEISS
THE GREAT NAME IN OPTICS
CARL ZEISS
WEST GERMANY
CIRCLE 243 ON READER SERVICE CARD

Modular hardware.
Flexible software.

The 3350 Series gets you into lab automation for less than you think ...and lets you grow easily and economically.

The Hewlett-Packard 3350 Series Laboratory Automation Systems protect your investment by providing answers to today's needs while assuring the versatility required to meet tomorrow's. The Series can satisfy your combined data handling, control, and reporting needs — whether you're a chemist or a lab manager.

Here's Where You Start Growing

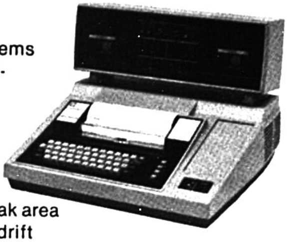

The Hewlett-Packard 3351A offers full data systems capability at a multi-channel integrator price. Configured for your laboratory, it is ready to:

- Integrate total peak area
- Correct baseline drift
- Detect low slow peaks
- Perform tangent skims
- Allocate fused peak areas
- Correct for tangent baseline penetration
- Average response factors
- Define multiple reference peaks
- Predetermine how specific peaks will be integrated
- Override decision logic of the standard software integrator

The standard system includes all calculation procedures commonly used by chromatographers, and can generate final reports with retention time, response factor, area, amount, and peak name included.

The 3351 can be expanded to add:

- Time of day
- LAB BASIC
- Sampler control software
- Interface to 30 instruments
- External events control
- Slice width integration
- Data file and peak summing software
- Systems software loading from cassettes
- Simulated distillation software for D-2887 and crude oil analysis

The most significant addition you can make is the Hewlett-Packard 2645 CRT with data cartridges — a high speed, silent data terminal for keyboard entry, system operation monitoring, and data results inspection.

The CRT with cartridges offers many of the capabilities of a large disc system.

- Data cartridges provide automatic data storage and retrieval for statistic analysis, trend reporting, shift summary logs, long-term data storage, and report retrieval.
- Data cartridges also offer storage and automatic calling of LAB BASIC programs for each analysis to generate special report formats, to perform special calculation procedures, and to access and execute additional programs for other instruments (gel permeation, auto analyzers, atomic absorption).

If you require capability greater than the 3351, there are expanded systems, including a disc-based version, in the 3350 Family designed to handle larger applications and provide additional data storage.

The Hewlett-Packard 3350 Series Assures You Cost-Effective Answers as You Grow!

Hewlett-Packard 2645 CRT with dual cartridges to optimize software flexibility.

HEWLETT hp PACKARD

Route 41, Avondale, Pennsylvania 19311

For assistance, call: Washington (301) 948-6370, Chicago (312) 255-9800,
Atlanta (404) 955-1500, Los Angeles (213) 877-1282.

43705E

CIRCLE 116 ON READER SERVICE CARD

Three new reasons why your department should

TAKE ANOTHER LOOK AT PLASMA ASHING

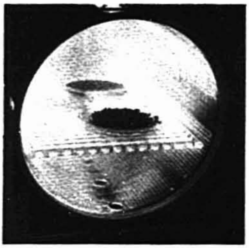

1. New End-of-Ashing Detector. We've incorporated an optical feedback mechanism that uses spectral analysis to determine if any ashing is going on. If the sample is entirely ashed, or needs stirring, your IPC system will let you know.

2. New Temperature Control. Transferring technology we developed in maintaining a critical temperature envelope for semiconductor manufacturing, we have built a sophisticated temperature probe into our ashing chamber for real-time control over temperature *at the sample*.

3. New Heat Lamps. Until now, the only benefit you derived from plasma ashing was its speed at low temperatures. Now you can enjoy plasma's cleanliness, safety and inexpensive unattended operation and get rid of your expensive and hazardous perchloric acid. These are important advantages when you need speed and are ashing a lot of samples. Now you can do high temperature ashing simply with our efficient new built-in heat lamps.

So: Three good new reasons. And there are many more that won't fit this space. Please let us tell you our complete story and show what other chemists and spectroscopists are doing in the **QC Laboratory** with our ashers . . . Analyzing plastics, paints, foods, drugs and more. Call or write Dick Bersin; ask for IPC Bulletin 4802.

International Plasma Corporation, 31159 San Benito Street,
Box 4136, Hayward, CA 94544.
(415) 489-3030.

CIRCLE 115 ON READER SERVICE CARD

Solvents so pure one grade fills all your exacting needs . . .

DISTILLED IN GLASS™

from BURDICK & JACKSON LABORATORIES

Ask for Data Sheet BJ-25
Distilled in Glass Solvents
BJ-21 Liquid Scintillation Counting

BURDICK & JACKSON LABORATORIES, INC.
MUSKEGON, MICHIGAN 49442 (616) 726-3171

CIRCLE 22 ON READER SERVICE CARD

ACID DIGESTION BOMBS

The rapid and safe way to dissolve inorganic samples in HF, HC1 or HNO_3, or to digest organic materials in strong alkalis or oxidizing acids with complete sample recovery.

Now available in two models: a **general purpose bomb** for temperatures to 150° C and pressures to 1200 psig, and a new **high pressure bomb** for samples which require dissolution temperatures up to 285° C and pressures to 5000 psig.

Both have removable, 25 ml Teflon cups with convenient closures, long-taper seals and other exclusive Parr features. For details, write or phone: Parr Instrument Co., Moline, Ill. 61265. Telephone 309/762-7716

CIRCLE 174 ON READER SERVICE CARD

Manufacturers' Literature

Nitrogen–Phosphorus Detector. Discusses the advantages of the nitrogen-phosphorus flame ionization detector in therapeutic drug monitoring. 4 pp. Hewlett-Packard Co. **430**

X-ray Fluorescence. Reports on the use of a newly developed energy-dispersive x-ray fluorescence technique for nondestructive chemical analysis of catalysts, pharmaceuticals, and pigments. Ortec Inc. **431**

Multichannel Analysis System. Describes the TN-1710 modular multichannel analysis system and provides a detailed description of the system's modular, microcomputer-based architecture, as well as system capabilities and operating features. 16 pp. Tracor Northern, Inc. **432**

TOC, TC, TOD Monitoring Equipment. Presents a comprehensive guide for the potential buyer of an on-line TOC, TC, or TOD analyzer. 14 pp. Ionics, Inc. **433**

Photomultiplier Tube Scintillation Applications. Contains information about detector tubes in scintillation applications, including emission spectra, photopulse shape, and intrinsic energy resolution relating to a specific scintillator as well as basic properties, circuits, and considerations of actual applications. Hamamatsu Corp. **434**

Analytical Services. Describes analytical services available for the monitoring of air, water, and wastewater samples. 6 pp. Nalco Chemical Co. **435**

Reporting Integrators. Describes features of three 3380 Series graphic integrators including the power of the built-in microprocessor, automation flexibility to control integration parameters, calculation of analytical results, time programming, and control of automatic samplers. 12 pp. Hewlett-Packard Co. **436**

Ion Lasers. Provides detailed information on argon and krypton ion lasers. The lasers operate CW from the ultraviolet to far red at output powers as high as 40 W, and they can also be pulsed for very high peak powers. 28 pp. Spectra-Physics **437**

Hollow Cathode Lamps. Lists over 60 element lamps for use in atomic absorption spectrometry. Sadtler Research Laboratories, Inc. **456**

Atomic Absorption Spectrophotometer. Details are given on a large number of two-channel analyses performed with the IL 751 AA spectrophotometer. Examples include analysis of water, blood serum, steel, ores, fertilizers, and gunshot residue. 16 pp. Instrumentation Laboratory Inc. **438**

High-Temperature Systems. Features standard combustion tube furnaces and design and manufacturing capability for custom heat treating equipment. 4 pp. Thermcraft, Inc. **439**

Liquid Chromatography. Two brochures describe the Model 601 liquid chromatograph and the LC-55 spectrophotometric detector. Perkin-Elmer Corp. **440**

Digital Thermometers. Complete information on full line of digital thermometers, including prices, options, and accessories. 8 pp. Omega Engineering, Inc. **445**

Chromatography Products. Features a new pure air generator for providing zero air for chromatographs as well as evaporators, gas dryers, capillary injection kits, and graphite ferrules. 12 pp. L. C. Co. **446**

Secondary Ion Mass Spectometer. Describes the "plus"-SIMS system of components for addition to existing Auger, ESCA, or other UHV systems to provide surface analysis and depth profiling for both positive and negative secondary ions over a mass range extending to 1000 amu. 6 pp. Extranuclear Laboratories **441**

Analytical Systems. Describes the company's range of analytical systems and fields of applications based on the quadrupole mass spectrometer. Examples include GC/MS with simultaneous CI/EI detection, high-sensitivity trace analysis with API, isotope ratio measurements, reactive species studies with modulated beam MS, and surface analysis with SIMS. Extranuclear Laboratories, Inc. **442**

Chromatography Newsletter. "The Chromatography Optimizer" informs chromatography users of latest advances in accessories and supplies for gas and liquid chromatography. Included in the first issue are such items as a digital stopwatch for laboratory use, a GC applications library, and a dual-flow calibration oven. 4 pp. Varian Instrument Div. Service Center **443**

NEW!

100 µl REACTI-VIAL™

makes small sample handling

EASIER THAN EVER BEFORE!

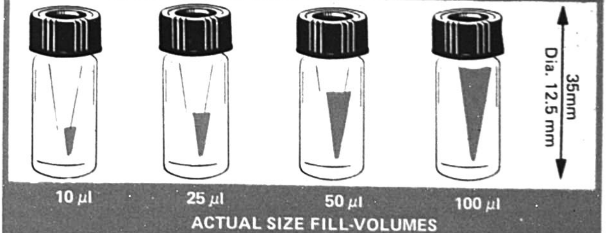

ACTUAL SIZE FILL-VOLUMES
TOTAL VISIBLE FILL-VOLUME = 200 µl

Made especially for trace sample isolation and storage and for small volume derivatizations, these new 100 µl Reacti-Vials make volumes as small as 10 µl easily manageable.

PIERCE
CHEMICAL COMPANY
Box 117, Rockford, Illinois 61105

CIRCLE 170 ON READER SERVICE CARD

Inspired by the 1976 ACS Centennial year

ACS Analytical Division

has published a unique book entitled

CENTENNIAL HISTORY of ANALYTICAL CHEMISTRY

Compiled from contributions made by many contemporary U.S. scientists, this book depicts the current field and its diverse origins. Stress is laid upon the American scene, but many foreign developments are included also.

EDITORS

H. A. LAITINEN
Graduate Research Professor
University of Florida

GALEN W. EWING
Professor of Chemistry
Seton Hall University

TOPICAL EDITORS

Chemical Methodology
Bruno Jaselskis
Professor of Chemistry
Loyola University, Chicago, Ill.

Electrochemistry
Robert A. Osteryoung
Professor of Chemistry
Colorado State University, Fort Collins

Spectrochemistry
James D. Winefordner
Graduate Research Professor
University of Florida, Gainesville, Fla.

Instrumentation
Galen W. Ewing
Professor of Chemistry
Seton Hall University, South Orange, N.J.

Separations
Donald A. Macnaughtan, Jr.
Senior Research Chemist
Mobay Chemical Co., New Martinsville, W. Va.

APPROXIMATELY 400 PAGES

Cost to ACS Analytical Division members	**$ 7.00**
Nonmembers	**10.00**

Postpaid to domestic subscribers. $1.00 additional for foreign postage.

TO ORDER

Send check or money order payable to ACS Division of Analytical Chemistry to

Dr. Frank A. Guthrie
Secretary, ACS Division of Analytical Chemistry
Department of Chemistry
Rose-Hulman Institute of Technology
Terre Haute, Indiana 47803

Name______________________________

Address____________________ **State**____________

Zip__________

No. of copies________

Manufacturers' Literature

Vacuum Process Equipment and Systems. Describes the company's capabilities in engineering and building customized vacuum systems. The range of these products includes environmental chambers, decorative metallizers, box coaters, roll coaters, drum coaters, custom sputtering systems, LCD evaporation systems, and in-line TV tube processing. 14 pp. CVC Products, Inc. **447**

Calibration Procedures for Vapor-Phase Analysis. Discusses calibration procedures for gas- and vapor-phase analysis by means of infrared absorption. Theoretical considerations required for understanding such analyses are presented in a simplified and concise manner. 14 pp. Wilks Scientific Corp. **448**

Analytical Methods Guide. Contains descriptions of documented uses of electrodes in approximately 300 different sample types. Explanations of electrode methodology and instrumentation accompany the methods. 34 pp. Orion Research Inc. **449**

Binding Analysis by Ultrafiltration. Presents alternative approaches to the use of ultrafiltration in binding analysis including a guide to selection of the best approach for specific applications. 8 pp. Amicon Corp. **450**

Moisture Tester. Describes a semiautomatic moisture tester for all types of solid, plastic, and viscous materials. 6 pp. C. W. Brabender Instruments, Inc. **451**

Ovens. Features the 1078 line of ovens and describes the basic types of chambers available, the control instrumentation suitable for them, and a verbal guide to the kind of chamber specified for different requirements. 8 pp. Blue M Electric Co. **452**

Vacuum Valves. Details the complete line of valves from $\frac{1}{2}$ to 4 in. including right angle, straight-through, safety, air inlet, and variable leak valves. 12 pp. Leybold-Heraeus Vacuum Products, Inc. **454**

Computing Controllers. Describes computing controllers, standard off-the-shelf interfacing cards, and built-in software for original equipment manufacturers. Explains how the HP 9815 and 9825 computing controllers may be used to enhance products and systems by providing data acquisition and analysis capability. 12 pp. Hewlett-Packard Co. **457**

In Polarography—We're Number One...

Here's The Reason Why...

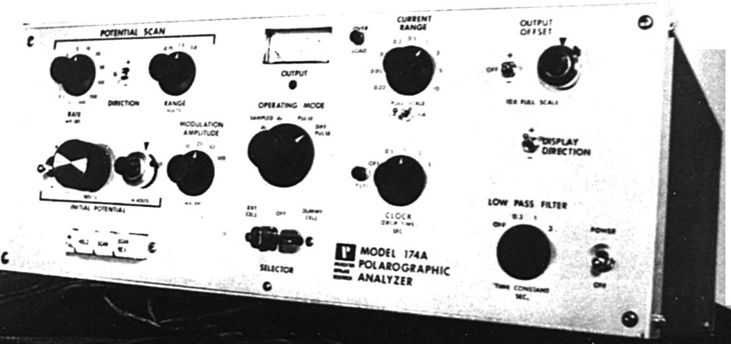
POTENTIAL SCAN
RATE
DIRECTION
RANGE
OUTPUT
OPERATING MODE
CURRENT RANGE
OUTPUT OFFSET
10X FULL SCALE
MODULATION AMPLITUDE
DISPLAY DIRECTION
INITIAL POTENTIAL
CLOCK
SELECTOR
MODEL 174A POLAROGRAPHIC ANALYZER
LOW PASS FILTER
TIME CONSTANT SEC.
POWER

And Here's What It Means To You...

MORE APPLICATIONS PUBLISHED AND PROVEN

Polarography, especially differential pulse polarography, is being used at an unprecedented rate everywhere for all kinds of analyses. Scan the table of contents of almost any analytical journal and you'll find papers describing the use of the 174A for analysis of metals, organics and anions. The papers are coming out so fast we're hard pressed to keep our bibliography and applications index TN-110 up to date (write for a free copy today).

MORE CUSTOMER SUPPORT

Our expert staff of applications chemists and field support specialists is always available to help solve your difficult problems. Our wide assortment of application notes, briefs and shorts can help get you started without fuss and bother. Our staff can provide suggestions, if you need them, on how to prep your sample for faster throughput. Of course there's no charge for any of this support or, for that matter, for detailed training at the factory.

MORE EXCELLENCE IN INSTRUMENT DESIGN

The Model 174A Polarographic Analyzer provides differential pulse polarographic capability at low cost. It's simple to operate and gives large, noise-free peaks for sub-ppm and even sub-ppb concentrations.

When sample throughput becomes important, the 315A Automated Electroanalysis Controller and the 316 Automated Cell Sequencer can be connected to the 174A for totally automated analyses. A full line of accessories for the 174A, 315A and 316 is available, including cells, electrodes, kits, and hardware. Everything to speed up your analyses and make the job easier.

For complete information or a demonstration, write or call:

Princeton Applied Research Corporation
AN EG&G COMPANY
Telephone: 609/452-2111
P. O. Box 2565 • Princeton, New Jersey 08540 • U.S.A.

Circle Reader Service Number 182 for TN 110
Circle Reader Service Number 183 for additional information

Cahn now makes it easier

with the

NEW

CAHN Series-20

Balances

The new Series-20 digital Balances automatically weigh up to 3.5g and offer sensitivity to 0.1μg. The new push-button tare system is unique and the only full-range tare system available. High sensitivity weighing is exceptionally fast and precise with these new Series-20 Balances. There is no doubt about it – Cahn Now Makes It Easier! There's a new Series-20 model for every requirement and price range.

CAHN 25 The full capability balance with portability; a unique push-button tare; full plus/minus ranges of 2, 20, 200 and 1000mg; widest range electrical zero; higher capacity of 3.5g; ultimate sensitivity and precision of 0.1μg.

CAHN 27 The full capability balance with a free-standing weighing chamber for remote and weigh-below applications.

CAHN 23 Users requiring only the more popular 20mg range, 1.5g capacity and 1.0μg sensitivity will benefit from this more economically priced model.

CAHN 21 For applications not requiring push-button tare even greater economy is found in this model. All other Series-20 features included.

For complete details ask your Cahn representative for the new Cahn Series-20 brochure or contact:

precision balances
for 100 grams and less.

CAHN Ventron

Cahn Instruments/A Division of Ventron Corporation
16207 South Carmenita Road/Cerritos, CA 90701 U.S.A.
Telephone 213-926-3378 ▪ TWX 910-583-4806

CIRCLE 39 ON READER SERVICE CARD

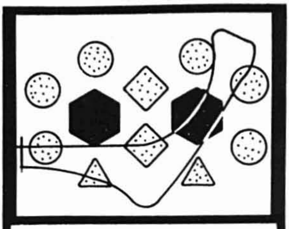

Electrochemical Studies of Biological Systems

ACS Symposium Series No. 38

Donald T. Sawyer, *Editor*
University of California

A symposium sponsored by the Division of Analytical Chemistry of the American Chemical Society.

The twelve papers in this significant new collection provide a representative cross section of the kinds of electrochemical methods used to characterize biological systems, as well as the kinds of biological problems that are being studied by such methods.

Several chapters in this important volume cover the development of improved electrochemical techniques and instrumentation. However, the principal emphasis is on the study of the redox properties of model compounds for biological systems.

CONTENTS

vitamin B_{12} and related cobalamins • bioelectrochemical modelling of cytochrome c • potentials of metal ion couples in complexes • metalloporphyrins in aprotic solvents • N-bridged dimer in nonaqueous media • reduction of nitrogenase substrates • manganese (II) and -(III) 8-quinolinol complexes • interfacial behavior of purines • coulometric titration of biocomponents • rotating ring disk enzyme electrode • left ventricle/aorta simulator • EDTA and NTA in phytoplankton media

216 pages (1977) clothbound $15.5C
LC 76-30831 ISBN 0-8412-0361-X

SIS/American Chemical Society
1155 16th St., N.W./Wash., D.C. 20036

Please send _____ copies of *SS 38 Electrochemical Studies of Biological Systems* at $15.50 per copy.

☐ Check enclosed for $ _______ . ☐ Bill me.
Postpaid in U.S. and Canada, plus 40 cents elsewhere.

Name

Address

City State Zip

X-Y Recorder. Covers in detail the general specifications, ordering information, OEM and control modules, and supplies and accessories for the Omnigraphic 2000 recorder. 8 pp. Houston Instrument 444

Thermal Analysis Application Studies. Four new application studies for the characterization and quality control of thermoplastics, thermosets, and films and two new application studies for the analysis of coal are available. Perkin-Elmer Corp. 453

Desktop Computer. Describes the Model 9831A Basic language desktop computer and its software and peripherals. Computer features twelve double-definable special function keys, 250K-byte high-speed tape drive, eight editing keys, upper and lower case alphanumeric keyboard and display, and optional plug-in read-only memories. 10 pp. Hewlett-Packard Co. 455

For more information on listed items, circle the appropriate numbers on one of our Readers' Service Cards

Catalogs

Surplus and Standard Stock Optics and Optical Filters. Contains an expanded line of surplus items including optical interference filters for UV, VIS, and IR; neutral density filters, mirrors, color glass filters, prisms, lenses, lamps, precision pinholes, filter storage boxes, fiber optics, and camera lenses. All surplus items are priced between 10–40% of original cost. 26 pp. Corion Corp. 459

Laboratory Products. Features new products available as well as sections on laboratory aids, chemical specialties, laboratory instrumentation, pumps, safety equipment, stainless steel lab ware, and stirrers. 40 pp. Cole-Parmer Instrument Co. 461

Microfiltration Products. Describes the full line of filtration products including nuclepore polycarbonate membranes, Toyo-cel cellulose membranes, supports and prefilters, general filter and test papers, filter holders, and accessory equipment. 48 pp. Nuclepore Corp. 462

Specialty Gases. Includes information on pure gases, mixed gases, and product and application descriptions for a complete line of equipment. 105 pp. Airco Industrial Gases 463

Electrodes. Features a wide assortment of ph, ORP, and process-type electrodes in various lengths, diameters, and prices. 16 pp. Chemtrix, Inc. 465

Laboratory Equipment and Reagents. Features expanded line of plasticware, circulators, melting point apparatus, jacks and timers, stirrers and spinbars, and other laboratory ware. 96 pp. J. & H. Berge, Inc. 466

Test Instruments. Includes frequency counters, generators, oscilloscopes, chart recorders, power supplies, distortion analyzers, learn-at-home electronics courses, and many other test instruments. 32 pp. Heath/Schlumberger Instruments 467

Recorders. Contains detailed information on four new X-Y recorders for OEM use, lab, medical, and industrial applications. 8 pp. Esterline Angus Instrument Corp. 468

TMA MADE PDQ

Thermomechanical analysis is the most sensitive way to measure a material's temperature-dependent properties. It's also simple, fast, and precise when you use the Perkin-Elmer TMS-2 Analyzer.

With the TMS-2 to gauge dimensional or viscoelastic changes, you can determine properties like expansion coefficient, heat distortion temperature, softening point, and heat shrink behavior. TMA measurements correlate well with many ASTM tests. What's more, the TMS-2 routinely performs them with much greater speed and precision.

Perkin-Elmer's unique *modular design* saves you money. The TMS-2 can be programmed simultaneously with the DSC-2 Differential Scanning Calorimeter or as an independent system with the UU-1 Temperature Program Control. In addition, the TMS-2 uses the same heater control unit and First Derivative Computer Accessory as the TGS-2 Thermogravimetric Analyzer. Hence, the TMS-2 can be added to or purchased with a TGS-2 at minimum cost.

Find out more about the TMS-2 from Perkin-Elmer, the leader in modern Thermal Analysis instrumentation. Write today to Perkin-Elmer Corporation, Main Avenue, Norwalk, CT 06856, or phone 203-762-6915.

PERKIN-ELMER

CIRCLE 169 ON READER SERVICE CARD

Special Centennial Tapes

4 Historic Symposia! 24 Speakers! Custom Packaging! Special Prices!

☐ Milestones in Physical Chemistry

8 Speakers — 315 Figures
Length: 5 Cassettes — 8 Hours
PRICE: $45 (postpaid)

The Speakers:

- G. T. Seaborg — 40 Years of Transuranium Elements
- D. Hodgkin — Structure of Molecules in Crystals
- G. Porter — Chemistry in Microtime
- P. J. Flory — Thermodynamics of Polymer Solutions
- W. O. Baker — Chemistry of the Solid State
- L. C. Pauling — Perspectives in Chemical Bonding & Structure
- H. Eyring — Reaction Rate Theory
- J. H. Van Vleck — Evolution of Theoretical Chemistry in America

☐ Structure and Quantum Chemistry + Evolution of Magnetic Resonance

8 Speakers — 210 Figures
Length: 4 Cassettes — 6 Hours
PRICE: $35 (postpaid)

The Speakers:

- J. A. Pople — Orbital Studies of Molecular Structure & Stability
- H. G. Drickamer — Pressure & Electronic Structure
- F. H. Stillinger — Quantum Chemistry & Eccentric Behavior of Liquid Water
- R. Zwanzig — Molecular Hydrodynamics
- H. S. Gutowsky — 30 Years of Relaxation
- J. S. Waugh — Alchemy of Nuclear Spins
- H. M. McConnell — Spin Labels
- F. A. Bovey — NMR of Macromolecules

☐ Evolution of Kinetics

8 Speakers — 140 Figures
Length: 4 Cassettes — 6 Hours
PRICE: $35 (postpaid)

The Speakers:

- B. S. Rabinovitch — Perspectives on Vibration Energy Relaxation in Unimolecular Reactions
- W. A. Noyes, Jr. — Photochemical Kinetics
- R. A. Marcus — Trends in Theoretical Chemical Kinetics
- K. F. Freed — Radiationless Processes in Polyatomic Molecules
- G. B. Kistiakowski — Early Years of Gas Phase Chemical Kinetics
- J. C. Polanyi — Recent Studies of Infrared Chemiluminescence & Fluorescence
- S. Claesson — Diffusion Rates & Chemical Reaction Kinetics
- J. Jortner — Intramolecular Dynamics in Excited Molecular States

— SPECIAL PRICE —

☐ BUY ALL THREE SETS — ONLY $85 (postpaid)

SAVE $30!

ORDER FROM:
American Chemical Society
1155 Sixteenth St., N.W.
Washington, D.C. 20036
ATTN: DEPT. AP

Name ____________________
Address ____________________
City ____________ State ________ Zip ________

(allow 4 to 6 weeks for delivery)

New plastic-membrane electrodes make Philips' PW/9414 Digital pH/Ion-Activity Meter

...EVEN BETTER!

It was already the finest digital pH and Ion Activity Meter you could own.

Accurate digital readings at a glance. Operation almost as simple as measuring pH. Push-button function selection. Precise manual or automatic temperature compensation. Isothermal intersection correction. Full alignment for asymmetry potential and sensitivity. Automatic polarity and decimal indication, readable from across the room. Standard recorder output. Optional BCD printer output.

Now we've made it even better. In place of liquid-membrane electrodes normally used for making K, Ca and NH_4 ion determinations we've developed a completely new range of **plastic-membrane** electrodes for K, NH_4, Na, Li, Ca, Ba and NO_3.

Result? For these important ions you now have better stability ... more dependable measurements ... better selectivity over the life of the electrodes ... less interference from other substances. Your electrodes last much longer ... and are even easier to use!

Wouldn't you like to see this improvement for yourself? Whether you're already a PW 9414 user or not, we'll be pleased to show you. Contact us now.

(Your enquiry will reserve free copies of our new publications "Instrumentation for the Modern Electrochemical Laboratory" and "Plastic-Membrane Electrodes".)

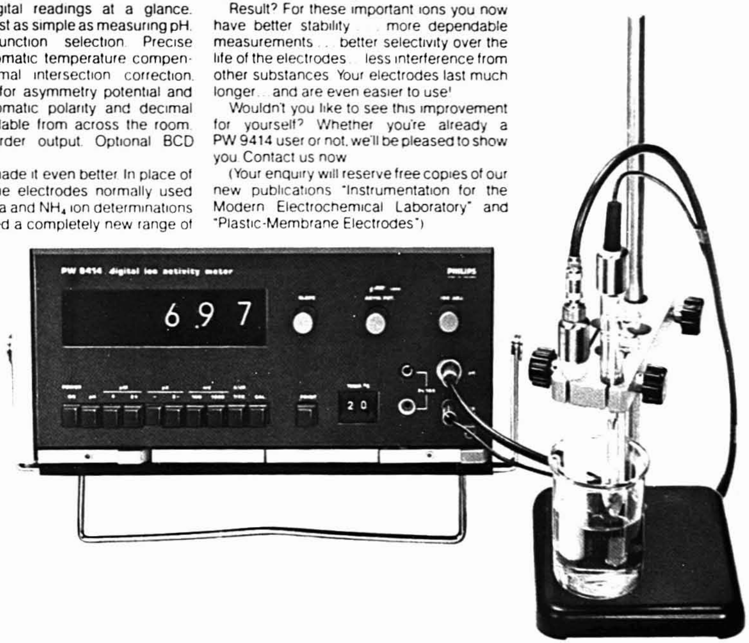

PHILIPS

Dear Sir, please send me full details of the Philips' PW 9414 plus your new publications "Instrumentation for the Modern Electrochemical Laboratory" and "Plastic-Membrane Electrodes".

Pye Ether Ltd.,
Caxton Way, Stevenage,
Herts., England SG1 2DG.
Tel: (0438) 4422 Telex: 82319 UKPSTVG

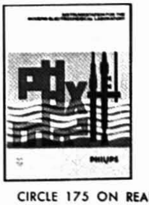

Name

Position

Company

Address

CIRCLE 175 ON READER SERVICE CARD

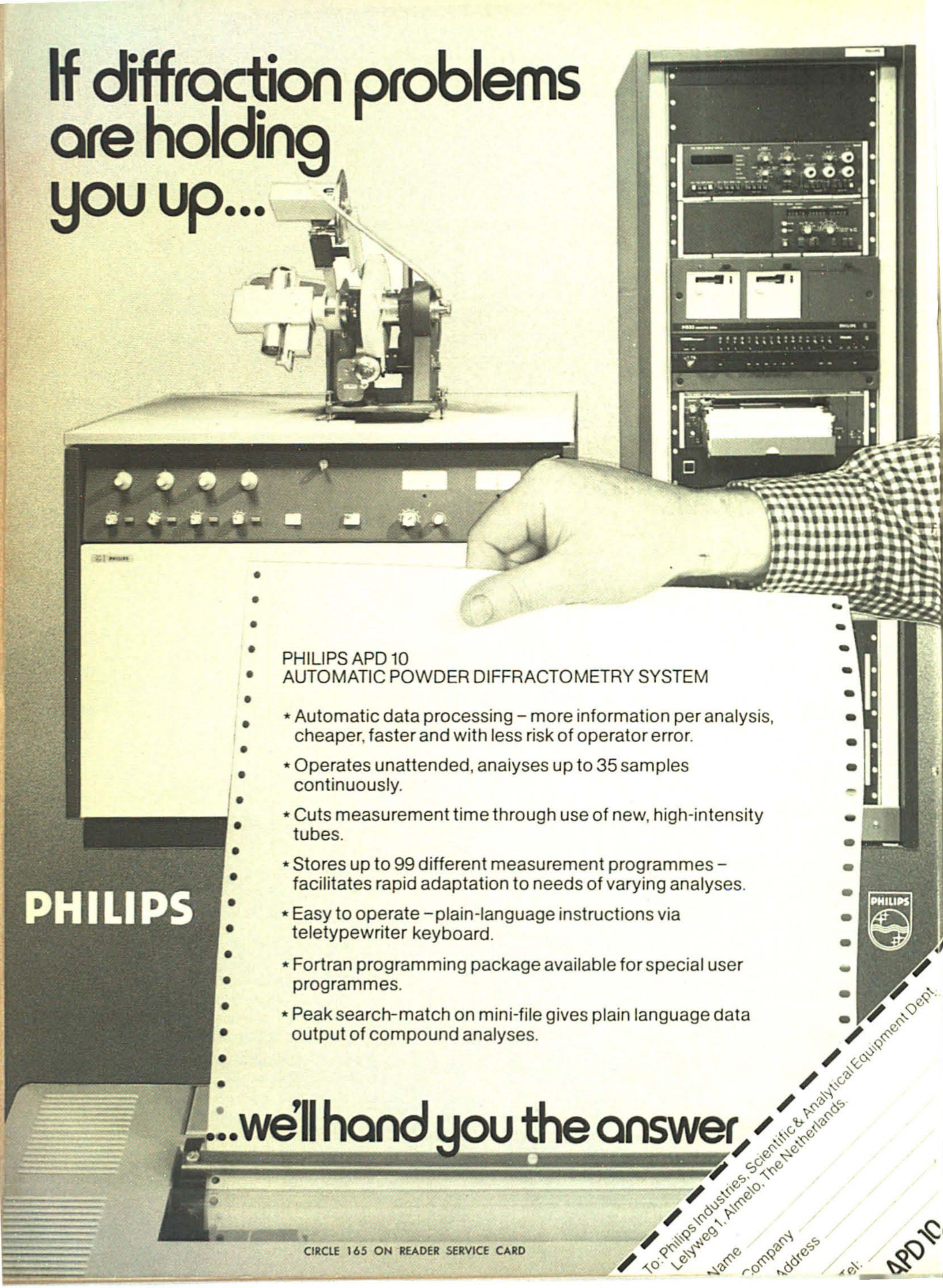

If diffraction problems are holding you up...

PHILIPS

PHILIPS APD 10
AUTOMATIC POWDER DIFFRACTOMETRY SYSTEM

- * Automatic data processing – more information per analysis, cheaper, faster and with less risk of operator error.
- * Operates unattended, analyses up to 35 samples continuously.
- * Cuts measurement time through use of new, high-intensity tubes.
- * Stores up to 99 different measurement programmes – facilitates rapid adaptation to needs of varying analyses.
- * Easy to operate – plain-language instructions via teletypewriter keyboard.
- * Fortran programming package available for special user programmes.
- * Peak search-match on mini-file gives plain language data output of compound analyses.

...we'll hand you the answer

To: Philips Industries, Scientific & Analytical Equipment Dept.
Lelyweg 1, Almelo, The Netherlands.

Name
Company
Address
Tel:

APD 10

CIRCLE 165 ON READER SERVICE CARD

AURA

is the world's most flexible, discrete, automatic chemistry system

AURA

for kinetic and end-point determinations -with speed and precision

AURA

the Automatic Reaction Analyser

From Pye Unicam – the ideal system for the hard-pressed clinical laboratory *and* for a wide range of other applications including biomedical research, pharmaceuticals, water analysis and feedingstuff manufacture.
AURA is flexible – because it can handle not only the present day tests, but will easily adapt to any future requirement.
AURA is modular. It incorporates a versatile sample preparation unit, a precision digital spectrophotometer and a powerful desk-top calculator – each of which can be used independently!

■ Get full information – just write, 'phone or use the reader reply card now!

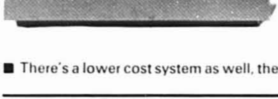

- **Kinetics – two integrating rate measurement programmes**
- **End-points – reagent and sample blank programme**
- **Sample Identification – rack and sample tube number printed with the result**
- **Audio-visual Alarms – warning messages on the printout for 'out-of-range' results; automatic shutdown and buzzer for fault conditions.**

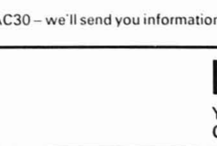

- **Quality Control – Statistics: means, S.D.s, C.V.s, printed automatically for controls and samples.**
- **Rapid Test Changeover – for increased throughput and efficiency.**
- **Low Running Costs – only 800 µl of sample and reagents.**

■ There's a lower cost system as well, the AC30 – we'll send you information on this also – automatically.

Pye Unicam Ltd

York Street, Cambridge, England CB1 2PX
Cambridge (0223) 58866. Telex: 817331

A member of the Pye of Cambridge Group

CIRCLE 172 ON READER SERVICE CARD

Analytical results must be correct: on no account should correctness be jeopardized by compromises in optics and electronics or operator errors.

Zeiss rules out such compromises: with the PM 6 spectrophotometer.

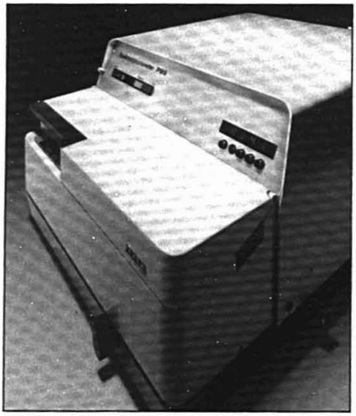

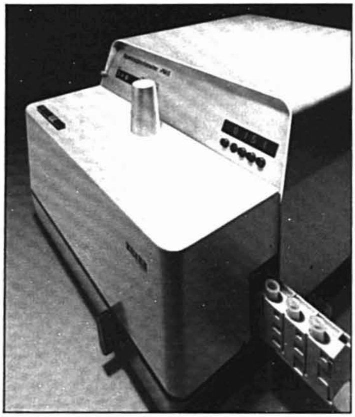

Results provided by any PM 6 spectrophotometer are correct. For:

The double grating monochromator is virtually free from straylight. Any wavelength between 200 and 800 nm can be set and read off to an accuracy of 0.1 nm. No filter and detector change. The band width of 2 nm is narrow enough even for more exacting samples.

Electronics replace controls for gain and exact cell transport. Concentrations or activity data are shown by the digital display with correct decimal point. With autosampler (PM 6P) the photometer analyzes up to 200 samples/hr absolutely unattended. It takes into account sample blanks or common reagent blanks and prints out a concentration report with magazine numbers, sample numbers and other identification data while the next samples are prepared. Photometric perfection without compromises.

Discuss the optimization potential of your lab with us. Even if your budget is tight. Come and see us or write to
Carl Zeiss, D-7082 Oberkochen

ZEISS
West Germany
Focus on the future

CIRCLE 242 ON READER SERVICE CARD

The Pye Unicam
SP 8-100

UV/Visible Spectrophotometer

The Pye Unicam SP8-100 is a major development in the design of precision instrumentation for applications which include scanning and reaction kinetics. High performance is combined with extreme simplicity of operation in a neat and compact package. Bench space is preserved by the built-in recorder and accessories which plug into the control console or fit within the vast sample compartment.

The unique 'Synchroscan' recording principle provides calibrated spectra automatically. 5 bandwidths, 5 chart speeds, 5 scan speeds and 9 recorder ranges from 0.05A give the flexibility required for any sample. High photometric accuracy up to 3A, low noise, fast response and superb stability add up to make the SP8-100 the highest performer in the medium price range.

The very wide selection of accessories includes quick-change attachments for colour measurement, fluorescence, densitometry, column monitoring, turbid samples and automated measurements.

So whatever your application, we're certain that you will discover an SP8-100 system that's Simply the Best for your needs.

Write, phone or use the reader reply service now for full details.

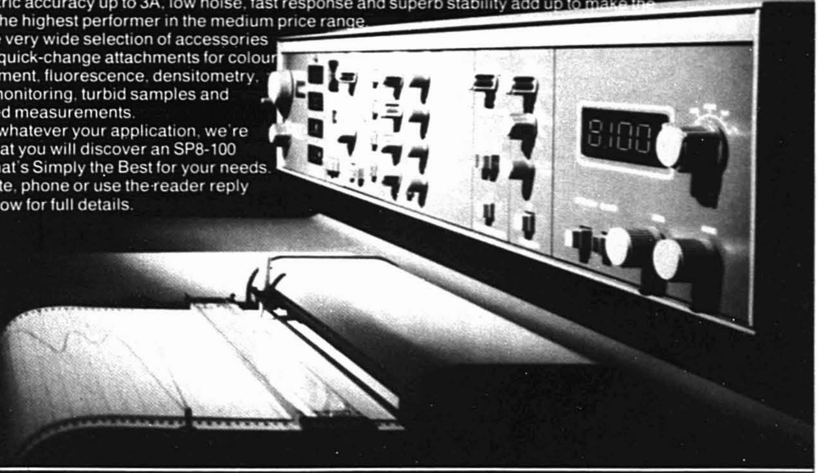

Pye Unicam Ltd
York Street, Cambridge, England CB1 2PX.
Cambridge (0223) 58866. Telex: 817331.

CIRCLE 176 ON READER SERVICE CARD

You told us.
"Make us a constant potential X-ray generator that can be used for single or two tube X-ray diffraction and X-ray spectrometry in sequential and simultaneous operation. Make it stable and precise, yet robust enough to work in almost any conditions. Allow for lots of work space on the table top and plenty of places to house electronics. One more thing, we don't want to have to see your service engineer too often either. Can you make it?"

We made it.
People who've seen it say: "That's the best constant potential generator you've ever made and you've made some good ones." We thought that a little too long for a name, not to say somewhat immodest, so we called it PW 1730.

PW 1730 won't make the coffee, sweep the laboratory floor or increase your chances of success with the opposite sex. It will just go on doing precisely what you tell it to, efficiently, quietly and honestly – for years to come.

PW 1730, the no-problem X-ray generator.
Send us your name and address and we'll send you its specifications.
Then we'll guarantee that it lives up to them.

Philips Industries, Scientific & Analytical Equipment Dept., Lelyweg 1, Almelo, The Netherlands.

PHILIPS

PHILIPS

CIRCLE 166 ON READER SERVICE CARD

stop vcm migration...

revolutionary lined tubing . . . clear, flexible . . . the new standard

If you're using clear, flexible tubing by any other name but BEV-A-LINE™ . . . your product may be exposed to vinyl chloride monomer and plasticizers and your "high purity" system is less than best.

Just compare new BEV-A-LINE Lined Tubing with the leading clear, flexible PVC tubing used in food, beverage, drug and medical device applications . . .

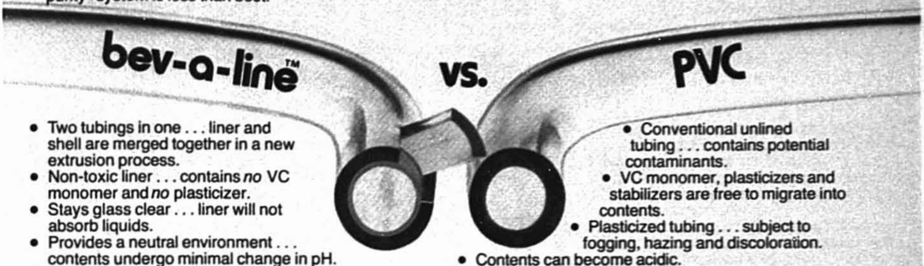

- Two tubings in one . . . liner and shell are merged together in a new extrusion process.
- Non-toxic liner . . . contains *no* VC monomer and *no* plasticizer.
- Stays glass clear . . . liner will not absorb liquids.
- Provides a neutral environment . . . contents undergo minimal change in pH.
- Excellent physical properties . . . all the advantages of PVC without the disadvantages.

Only one tubing carries this brand of purity:

BEV-A-LINE $\frac{PC}{VI}$ - $\frac{NVC}{L}$ - $\frac{N}{T}$ - $\frac{N}{F}$
$\frac{PC}{VI}$ = Non-Cytotoxic, meets or exceeds standards in Pharmacopeia XIX, Class VI, pages 644-647
$\frac{NVC}{L}$ = Non-Vinyl Chloride Lined
$\frac{N}{T}$ = Non-Toxic, meets standards per FDA reg. 121.2570, 121.2522, 121.2005, 121.2514
$\frac{N}{F}$ = Meets or exceeds standards in National Formulary. Vol. 14, pages 880 - 884, containers for injectables (plastics)

- Conventional unlined tubing . . . contains potential contaminants.
- VC monomer, plasticizers and stabilizers are free to migrate into contents.
- Plasticized tubing . . . subject to fogging, hazing and discoloration.
- Contents can become acidic.
- Good physical properties . . . but loss of plasticizer means loss of pliability.

Prove it to yourself . . . write for our free test kit and samples on your company letterhead. Or circle reader number for literature only.

THERMOPLASTIC PROCESSES, INC.
Distributed Nationally
Valley Road, Stirling, New Jersey 07980
N.J. (201) 647-1000 • N.Y. (212) 267-6220 • TWX 710-997-9583

CIRCLE 202 ON READER SERVICE CARD

HPLC Solvents by J. T. Baker

Maximum consistency lot-to-lot, bottle-to-bottle, lot-to-lot, bottle-to-bottle, lot-to-lot, bottle-to-bottle, lot-to-lot, bottle-to-bottle, lot-

Extremely tight specifications and superior product definition minimize the most frequent HPLC problems. 17 Baker HPLC solvents provide maximum reproducibility... total predictability... exceptional consistency. And actual lot analysis lets you verify this.

Write:
HPLC Dept. 7
J.T. Baker Chemical Company
Phillipsburg, N.J. 08865
(201/859-5411)

J.T.Baker®
CHEMICALS

CIRCLE 17 ON READER SERVICE CARD

HELLMA
. . . tomorrow's designs today!

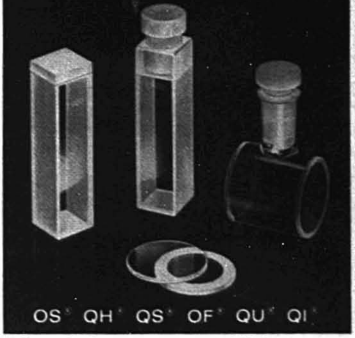

Hellma—the largest assortment of highest precision glass and quartz cells.
Standard · Flow-through · Constant-temperature
Anaerobic · Special Designs
Also available—ULTRAVIOLET LIGHT SOURCES
Deuterium Lamps · Mercury Vapor Lamps
Hollow Cathode Lamps · Power Supplies

HELLMA CELLS, INC.

Write for literature
Box 544
Borough Hall Station
Jamaica, New York 11424
Phone (212) 544-9534

CIRCLE 97 ON READER SERVICE CARD

When you choose Barnstead you get something extra...S/P

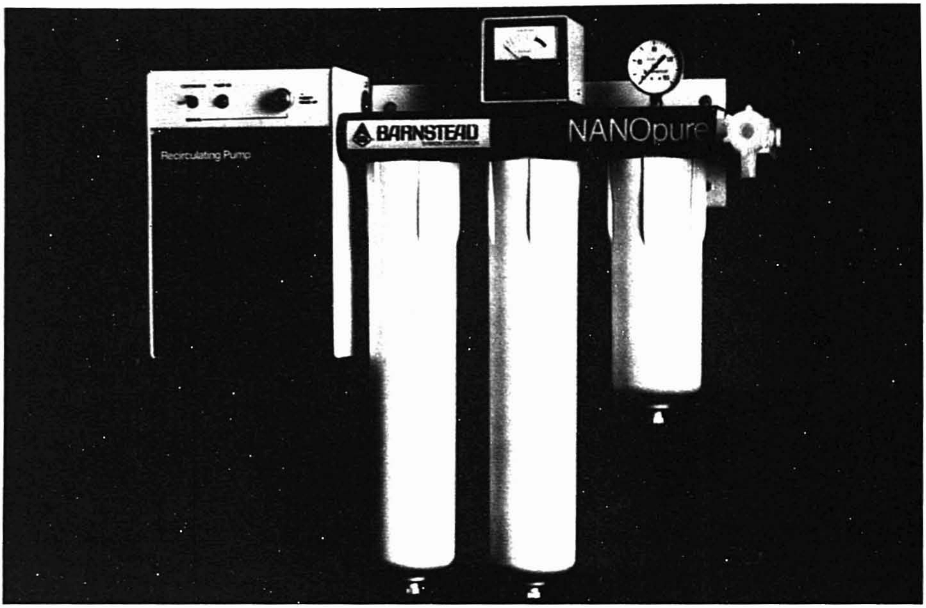

The New Standard for Reagent Grade Water

Barnstead's NANOpure deionization/submicron filtration system produces ultrapure water to meet all CAP/ASTM Type I reagent grade specifications. Long lasting cartridges deliver up to 3 liters per minute of pure water at exceptionally low cost. And replacement cartridges are always stocked by S/P for immediate delivery.

Designed for wall mounting, all NANOpure systems feature an in-line meter for quantitative recording of outlet purity.

Options include a recirculating pump to maintain constant outlet purity and ROpure reverse osmosis pretreatment to extend the life of cartridges by a factor of 10.

Write for the Barnstead Guide to Reagent Grade Water.

SYBRON | Barnstead

Barnstead Company
Division of Sybron Corporation

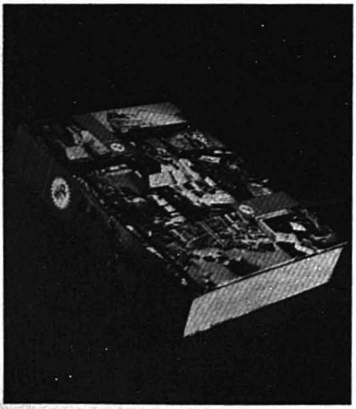

Something extra...S/P

S/P carries a lot of laboratory items. But, then, S/P is a leading distributor for more than 550 top manufacturers. To handle this huge inventory smoothly, we have 25.4 million cubic feet of warehousing space, 1.9 million cubic feet of chemical vaults, and 25 strategically located stocking centers. You benefit with a wider choice in all grades and price ranges. And we're flexible enough to stock any laboratory supply items and chemicals used in research, quality control or production specifically for you. It's all part of the S/P Responsive System of service for professionals like you. Call your S/P Representative and take stock of him.

S/p

scientific products

distributor of chemicals, laboratory supplies
and scientific instruments

Division of American Hospital Supply Corporation
1430 Waukegan Road, McGaw Park, IL 60085

CIRCLE 193 ON READER SERVICE CARD

Books

Fundamentals of Luminescence

Fluorescence and Phosphorescence Spectroscopy: Physicochemical Principles and Practice. Stephen G. Schulman. X + 288 pages. Pergamon Press Ltd., Headington Hill Hall, Oxford OX3 0BW, England. 1977. $20

Reviewed by Robert J. Hurtubise, Department of Chemistry, University of Wyoming, Laramie, Wyo. 92071

This book was written for the analytical chemist and biological scientist with a limited background in quantum mechanics, electronics, and optics and addresses those with a college background in physics and chemistry. The above scientists and others with an interest in the fundamentals of luminescence theory, instrumentation, and applications should welcome this well-written book. It can be a useful guide to more advanced treatments on luminescence because many topics are written in a way that stimulates the reader to pursue other references.

The chapters on photophysical processes in isolated molecules and molecules in solution make up roughly half the book. There is substantial information in these chapters for the nonspecialist to obtain a good grasp of the many interactions, intrinsic and extrinsic, that affect luminescence quantum yields. In one section, though on excited state proton transfer and fluorescence that occur at comparable rates, 26 equations are presented. The equations relate quantum yields of fluorescence of HA and A^- species with the concentrations of protonating and deprotonating species. It is somewhat cumbersome to wade through the equations, and it is doubtful whether the nonspecialist will be concerned with all of them.

In the chapter on instrumentation the components that make up commercial luminescence instruments are discussed, and an extensive table is given for solvent systems for phosphorimetric analysis. The chapter on applications emphasizes the analysis of biological samples, drugs, and metabolites; however, inorganic luminescence analysis is also discussed. A table at the end of the chapter gives a comprehensive listing of compounds that can be determined by luminescence methods. Of the 430 references at the end of this chapter, only three are from 1975 and the remainder from earlier years. In fact, in the entire book there are no references dated 1976 and very few dated 1975.

Some typographical errors appear. For example, on page 31 the time scale of a typical electronic transition is given as $\sim 10^{-5}$ s. Also, on page 125 in the discussion of polarization, "I" is used to represent both the light intensities emitted with electric vectors parallel to and perpendicular to the electric vector of the exciting light. The author occasionally uses very long sentences which detract slightly from the book. For example, the sentence on the bottom of page 101 and top of page 102 contains 68 words.

The author has addressed a sizable fraction of scientists that use luminescence analysis, and they are urged to have this book available because of the wide range of covered subjects which are presented in an interesting manner.

Thermal Analysis of Minerals. D. N. Todor. 256 pages. Distributed by ISBS, Inc., P.O. Box 555, Forest Grove, Ore. 97116. 1976. $32.50. Translated from the Romanian language by S. Marcus

Reviewed by Bernhard Wunderlich, Department of Chemistry, Rensselaer Polytechnic Institute, Troy, N.Y. 12181

The major attraction of this book lies in its section that describes in about 150 pages approximately 200 minerals and groups of minerals, including about 100 composite DTG, TG, and DTA curves of the Derivatograph type (without heating rates, endotherm direction, often without conditions such as atmosphere, etc.). The collection is based on 87 literature references of which less than half are after 1960, and of these, in turn, most are from Eastern European sources. The book is thus useful as a comparison guide for those who carry out thermal analyses on geological samples.

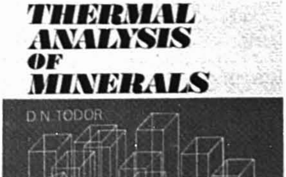

The further aims of the book—to help understand thoroughly the processes that arise when solid compounds are heated, which would make the book also useful among others for solid state physicists, chemists, metallurgists, and students in the field, as suggested in the Preface—are poorly served by the first 100 pages of the book. Many empirical facts are listed, but as soon as exact descriptions are required, the author falters. There are only severely abbreviated treatments of such important topics as heat conductivity, theory of DTA, and nonisothermal kinetics. Occasionally, quite wrong statements are made such as: fast heating can lead to an activation energy equal to the reaction enthalpy (Equation 42), and there is a wrong definition of entropy (Equation 54). The general style of the descriptions of the basic process of thermal analysis can be gained from the following excerpt from page 78:

"The melting process is briefly explained as follows: Thermal energy imports to the molecules an energy of agitation called *thermal agitation*. The mean amplitudes of the vibrations of atoms increase with rising temperature. When the temperature has reached values at which one may speak of a true collision between two neighbouring atoms, then the atoms generally fail to return to their initial positions of equilibrium; they mix instead, and the crystal lattice breaks down, the crystal melts. Hence, the melting process is nothing else but a breakdown of the crystal lattice."

It remains to be observed that SI-units are avoided in the book and that the more modern thermal analysis instruments which could increase the accuracy in temperature by at least one decade, such as DSC, are not mentioned. Heat of fusion, heat capacity, or glass transitions are not of interest in "Thermal Analysis of Minerals".

Because of the translation, there are some puzzling terms like heat transmission, unsteady state, range of temperature, T grad., thermal diffusibility, and most prominently the groove

THE LC COLUMN Sept./Oct.

Special discounts on new Zorbax™ column kits.

DuPont Instruments invites you to participate in a special trial offer that makes it economical for you to determine for yourself the quality and performance of our new Zorbax™ based columns. We've prepared kits that include Zorbax™ SIL, ODS and CN columns. These kits are available from our Technical Representatives at a special discount for a limited time (through November).

For more information contact your local representative or circle reader service card number 51. Or call (302) 772-5500, and your DuPont Technical Representative will be in touch with you within twenty-four hours.

Individual testing is behind guaranteed high performance of Zorbax™ columns.

To meet your HPLC separation needs steadily and reliably, high resolution and column-to-column reproducibility are essential. To achieve them, DuPont Instruments sets rigorous minimum standards for key column parameters. These include:

- Surface coverage (bonded phase)
- Theoretical plates
- Peak symmetry
- Selectivity
- Permeability

Each DuPont column is checked against these criteria and is guaranteed to meet or surpass them.

Figure 1 illustrates a representative quality control check. In this case, a Zorbax™ CN column was chromatographically tested under the conditions shown. Theoretical plates and peak symmetry were calculated on the phenylacetonitrile peak. Selectivity was judged between peaks 2 and 3. Column permeability is defined as a minimum acceptable flow rate at the given pressure drop for the column configuration.

As an example of typical control values, minimum theoretical plates specified for Zorbax™ columns are shown in Table 1.

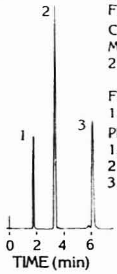

FIGURE 1
Column: Zorbax™ CN
Mobile Phase:
2% Isopropanol in Hexane
Flow Rate:
1.50 ml/min
PEAK IDENTITY
1. Toluene
2. Benzophenone
3. Phenylacetonitrile

In addition, elemental analyses are used to determine surface coverage for all bonded phase Zorbax™ packings. To assure maximum reproducible surface coverage, Zorbax™ bonded phases are produced with techniques that achieve bonding of all available sites. A high level of column-to-column reproducibility is dependent on this approach.

For all other key parameters as well, DuPont's challenging quality control standards assure you exceptional results in your separations. We'll be glad to send more information on the high performance of DuPont column products. Just circle reader service card number 52. Or write DuPont Instruments, Room 35922, Wilmington, DE 19898.

Table 1 Minimum Theoretical Plates

	4.6 mm X 25 cm	4.6 mm X 15 cm
Zorbax™ SIL	9000	5400
Zorbax™ ODS	8000	4800
Zorbax™ CN	9000	5400

Order DuPont columns and packings by toll-free telephone.

All DuPont instruments, HPLC columns and packings can be ordered by phone with a toll-free call (800-441-7508). This number is for the exclusive use of placing orders for HPLC columns, instruments and accessories. We hope you find this a convenient and time-saving way to purchase HPLC products from DuPont Instruments.

Du Pont Instruments

DU PONT

(sample holder). Although these terms do not detract the expert, I would not want my students to introduce them into their vocabulary. This leads me to the suggestion that this book be hidden on the shelves of specialized collections dealing with the analysis of minerals, but be kept away from students and workers in other fields. Thermal analysis is a much more precise science than one might guess reading this book.

The Minicomputer in the Laboratory: with Examples Using the PDP-11.
James W. Cooper. xvii + 365 pages. John Wiley & Sons, Inc., 605 Third Ave., New York, N.Y. 10016. 1977. $19.50

Reviewed by S. P. Perone, Department of Chemistry, Purdue University, West Lafayette, Ind. 47907

This book is most emphatically written for the user of a DEC PDP-11 minicomputer system in the laboratory. Chapters 3–14 provide almost exclusively the type of detailed operational and conceptual material one might expect to find in a well-written operating manual published by the computer manufacturer. Because this material is well-organized, readable, and embellished lightly with allusions to relevant data processing concerns—and because it contains materials extracted from several different DEC manuals—the PDP-11 user should find it very useful.

Chapter 1 provides a brief introduction to digital computer concepts, and Chapter 2 does a fine job of introduction to number systems and logical operations. Chapters 3–11 introduce the novice programmer to the principles and, more importantly, the nitty-gritty details of assembly language programming with the PDP-11 computer. These discussions include detailed instructions of the use of standard DEC software and peripherals. The coverage is complete, including interrupt handling, general input/output, and floating-point operations. Chapters 12 and 13 are particularly useful: one provides advanced programming concepts such as stack manipulation, reentrant, and recursive routines; the other provides an introduction to debugging operations using ODT-11.

Chapters 14–19 cover topics related to laboratory computer applications. Chapter 14 provides a functional and operational description of the LPS-11 laboratory data peripheral system offered by DEC. Chapters 15–19 cover the topics of signal averaging, data display methods, peak detection, Fou-

The new generation HP 5985 GC/MS Data System. Its price/performance capability is unprecedented.

New generation computer.
The built-in data system features a powerful computer that scans, processes and analyzes very fast (550 ns cycle time!). Batch processing and simultaneous acquisition/reduction programs are standard.

New generation GC.
This system includes our microprocessor-controlled HP 5840 GC, which many consider the finest money can buy.

New GC/MS interface.
Its three lines give you maximum flexibility. Any of them may be split in any ratio between the mass spec and GC detector (FID, EC, TC, N_2P, flame photometric).

Hyperbolic quadrupole.
For increased sensitivity at higher resolutions; sharp, consistent peak shapes.

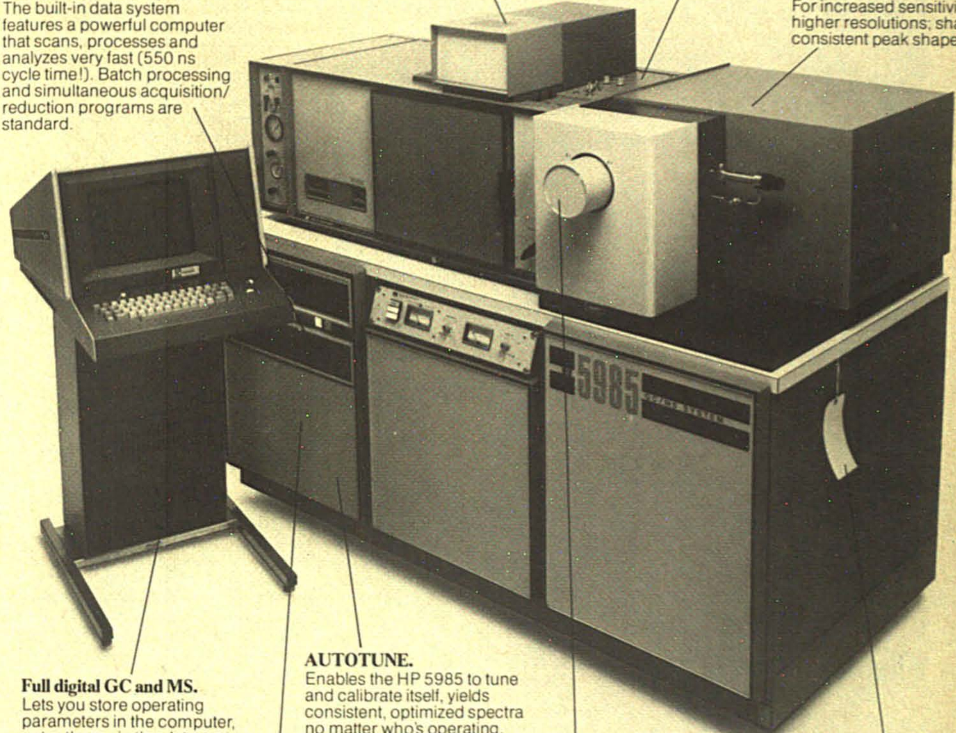

Full digital GC and MS.
Lets you store operating parameters in the computer, enter them via the data system. Saves time, reduces errors.

AUTOTUNE.
Enables the HP 5985 to tune and calibrate itself, yields consistent, optimized spectra no matter who's operating. Skeptics can override, but they'll quickly learn they don't have to.

Batch processor.
This powerful software enables the HP 5985 to collect, reduce and output data automatically for up to 36 samples, with a different set of GC and MS conditions for each. Saves man-hours, many man-hours.

CI/EI dual source.
Changes *both* conductance and configuration to achieve best results in both CI and EI operation.

More power for less money.
What real technological advancement is all about, what our new generation HP 5985 GC/MS is all about. Want proof? Call your local HP office, or write to the address below.

HEWLETT hp PACKARD

1507 Page Mill Road, Palo Alto, California 94304

For assistance call: Washington (301) 948-6370, Chicago (312) 255-9800, Atlanta (404) 955-1500, Los Angeles (213) 877-1282.

23702

CIRCLE 95 ON READER SERVICE CARD

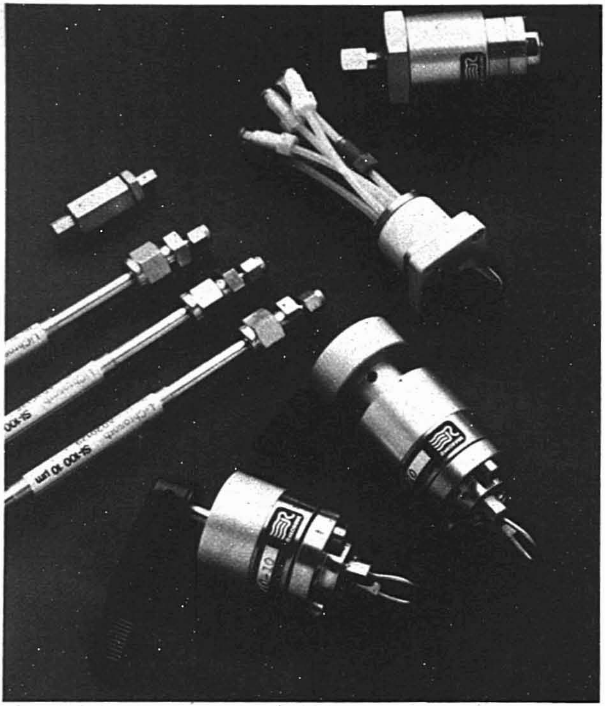

You can't get a good chromotogram without a great beginning.
We make it happen!

VALVES, WELL PACKED HPLC COLUMNS AND FILTERS

In a way, we're sort of the front-end company in high pressure liquid chromatography. Almost everything you need to make better chromatograms in the beginning is on our shelf. Here's our line to you:

The 70-10 Sample Injection Valve. For just $290 you can get our 6-port sample injection valve with a removable sample loop and 7000 psi pressure rating. Size, 10 μl to 2.0 ml.

The 7120 Syringe Loading Sample Injector. Fill loops conventionally or in the partial loop variable volume mode with only 0.5 μl sample loss.

Teflon Rotary Valves. For about half the cost you'd expecf to pay, we offer three, four and six way valves in 0.8 mm and 1.5 mm bores at $70 to $87. Features zero dead volume, chemical inertness and 300 psi rating.

HPLC Columns. Here are the columns with guaranteed peak symmetry and minimum plates per meter to doubly assure optimum column performance. Six columns currrently available priced from $180 to $240.

The Column Inlet Filter. It only costs a few dollars, but it can save you a boatload of trouble. Place this low dead volume filter between the injection valve and column to protect column inlet frits from plugging. Price, $40.

The Model 7037 Pressure Relief Valve. Protect your set-up against damage from over pressure (2000 to 7000 psi setting range).

Write or call for more information.
Address Rheodyne, Inc. 2809 Tenth Street, Berkeley, CA 94710. Phone (415) 548-5374.

RHEODYNE
THE LC CONNECTION COMPANY

CIRCLE 181 ON READER SERVICE CARD

rier transform applications, window functions, and phase correction methods. Chapter 15 is an excellent introduction to the principles of signal averaging with good illustrations. Chapter 16 on data displays is tied too closely to the LPS-11 hardware to be of general use. Chapter 17 on peak detection provides good insight to the problems and approaches for programmatic peak detection. Chapters 18 and 19 on the Fourier transform and various applications to NMR and IR data are the best of all. The author's considerable familiarity with this area lends authority and usefulness to these presentations.

There are several problems with this text. First and foremost is the fact that most of the material is useful only to a user of the DEC PDP-11. Because of the complexity of the PDP-11 instruction set and because of the attention to operational details, a reader with general interests would find only about five of the 19 chapters useful. It is disappointing that there is no general description of interfacing principles and hardware; Chapter 14 approaches this topic, but succeeds only in describing the functions of the LPS-11 data system. Finally, although the last two chapters, regarding Fourier transform applications, might be very useful to many readers, the book would be much more valuable if this level of presentation were extended to additional topics of interest, such as the application of smoothing algorithms, curve-fitting, peak deconvolution, and file searching.

Despite the problems mentioned above, the text does accomplish very well the major part of the author's goals—to provide a complete and useful guide to the implementation of a particular laboratory computer system. The many exercises and program illustrations are most useful for the novice programmer. It should be highly recommended to the many users of PDP-11 minicomputers.

New Books

Analytical Pyrolysis. C. E. Roland and Carl A. Cramers, Eds. ix + 424 pages. Elsevier Scientific Publishing Co., P.O. Box 211, Amsterdam, The Netherlands; 52 Vanderbilt Ave., New York, N.Y. 10017. 1977. $39.25

The proceedings of the Third International Symposium on Analytical Pyrolysis, held in Amsterdam, September 7–9, 1976, are presented. A total of 50 papers contributed by authors from the international commu-

SPECIALS... FROM THE SYRINGE SPECIALISTS.

Most people use our precision syringes for chromatography, but a lot of people need a unique syringe for a particular job. When you need that special syringe, chances are you will find it at Hamilton, the syringe specialists. We make over 240 different syringe models...many for specific applications. Like these syringes, for instance.

The one in the center is a push-button adjustable syringe with an unbreakable metal housing. You dial your desired volume on a micrometer setting device, cock the spring-driven plunger, and push the button. Presto, uniform injections, regardless of who operates it. The CR700 with a stainless steel plunger and Teflon sealing tip, is available in 20 μl, 50 μl and 200 μl capacities, with each syringe tested for ±1% repeatability.

On the right is our Carbon Analyzer Syringe with a special metal luer designed for the inlet of carbonaceous analyzers, 50 μl capacity. (The CR700 50 μl capacity also fits the C.A. inlet.)

On the left is a Teflon Syringe for highly reactive chemicals. Your sample only contacts Teflon in the syringe. The case acts as a protection from external damage and provides a means to see the volume indications. Teflon needles are available to provide a completely inert system.

You'll also find a syringe with a filter...one you can fill through the back of the plunger...high pressure syringes...one with a threaded plunger...super syringes up to 1.5 liters...automatic dispensers for a syringe...and many more. They are all described in our catalog. If you need a special syringe, write to the specialists, Hamilton Co., P.O. Box 10030, Reno, NV 89510.

HAMILTON

CIRCLE 100 ON READER SERVICE CARD

Marine Chemistry in the Coastal Environment

ACS Symposium Series No. 18

Thomas M. Church, *Editor*

A special symposium sponsored by the Middle Atlantic Region of the American Chemical Society.

Now available—a comprehensive volume containing the most recent advances in this new and increasingly important field.

The collection represents an indispensable source of information for every marine scientist. Emphasis is not merely on describing coastal problems but on showing the potential in applying the tools of modern oceanography and chemistry to solve these problems.

Forty-one chapters cover six major areas:

physical, organic, and tracer marine chemistry; estuarine geochemistry; hydrocarbons and metals in the estuarine environment; ocean disposal forum; applications and resources in marine chemistry; and organic and biological marine chemistry.

710 pages (1975) Clothbound $35.75
(ISBN 0-8412-0300-8) LC 75-28151

SIS/American Chemical Society
1155 16th St., N.W./Wash., D.C. 20036

Please send ______ copies of *No. 18 Marine Chemistry in the Coastal Environment* at $35.75 per book.

☐ Check is enclosed for $ ________ ☐ Bill me.
Postpaid in U.S. and Canada, plus 40 cents elsewhere.

Name

Address

City State Zip

nity embrace newly emerging pyrolysis GC and pyrolysis MS as a promising analytical technique. The varied areas of analytical applications of the technique include the analysis of materials such as rubber, polymers, textiles, biologically active compounds, and microorganisms. Also included are papers on laser-induced GC–MS and developments in the automation of analytical pyrolysis instruments. The book is a poor quality reproduction of author-furnished typewritten text.

Tabulation of Infrared Spectral Data. David Dolphin and Alexander Wick. xvi + 549 pages. John Wiley & Sons, Inc., 605 Third Ave., New York, N.Y. 10016. 1977. $19.50

This book tabulates infrared spectra of all of those organic functional groups for which characteristic frequencies have been established. These functional groups are classified according to the type of vibrations involved. Thus, starting with X—H single-bond vibrations in Chapter 1, the book continues with C—C, C—N, C—O, N—N, and N—O vibrations, respectively, in the following five chapters. Since the organic chemist now uses a wide variety of inorganic and organometallic intermediates, chapters on thionyl and phosphoryl compounds and on inorganic vibrations are also included. For each of the functional groups treated, there is a brief discussion on steric, electronic, and solute–solvent interactions that bring about changes in the characteristic group frequencies. The tables following the discussions show changes in group frequency as the electronic and steric environments around the group are varied. A total of 47 functional groups are covered.

Colloquium Spectroscopicum Internationale—XVIII. J. P. Robin, Ed. 105 pages. Pergamon Press Ltd., Headington Hill Hall, Oxford OX3 0BW, England. 1977. $8.00

The seven plenary lectures given at the XVIII Colloquium Spectroscopicum Internationale, Grenoble, France, 15–19 September 1975, are presented. Titles of the lectures and their respective contributors are: current capabilities and future goals in x-ray spectroscopy, L. S. Birks; effet Mössbauer et applications à la physique du solide, C. Janot; design of fluorometric analytical methods, D. N. Kramer; les propriétés spectrochimiques de certaines sources lumineuses, E. Plško; electron spectroscopy and molecular structure, K. Siegbahn; recent developments en spectroscopie instrumentale, M. Soutif; and some recent aspects in the structure elucidation of natural products, W. Voelter. Lectures are presented in the original language in which they were delivered.

Atlas of Thermoanalytical Curves, Volumes 1–5. George Liptay, Ed. Distributed by Sadtler Research Laboratories, Inc., 3316 Spring Garden St., Philadelphia, Pa. 19104. 1977. $175 ($35/volume)

This five-volume atlas published in London by Heyden & Sons, Ltd., presents DTA, DTG, and TG curves for 350 selected organic and inorganic compounds. The atlas is complete with references, notes on curve interpretation, and experimental data on the changing factors for analyses. Included with Volume five is a cumulative index for the entire set, consisting of an index to compounds, a chemical formula index, and a class index.

ASTM Publications

The following are available from the American Society for Testing and Materials, 1916 Race St., Philadelphia, Pa. 19103 (USA, Canada, and Mexico add 3% shipping charges. Other countries add 5%)

Methods for Emission Spectrochemical Analysis—1977 Supplement. 268 pages. 1977. Paperbound. $10.75

This supplement is published as a companion volume to the 1971 edition of "Methods for Emission Spectrochemical Analysis". The supplement consists of 21 new suggested methods, 3 new proposed methods, and 15 new or revised standard methods. Standards that have been reapproved without revision are not included.

Part 31 of 1977 Annual Book of ASTM Standards on Water. 1130 pages. 1977. $34

Part 31 on water analysis contains 139 ASTM standards that are new or changed in status since the 1976 edition. This book supersedes all previous editions and is brought up-to-date and published annually. Among the new standards are a test for evaluating water testing membrane filters for fecal coliform recovery; a test for polychlorinated biphenyls in water; tests for cadmium, cobalt, and lead in water by atomic absorption spectrometry; a test for oxygen demand in water by combustion-infrared analysis; tests for lithium, potassium, and sodium ions

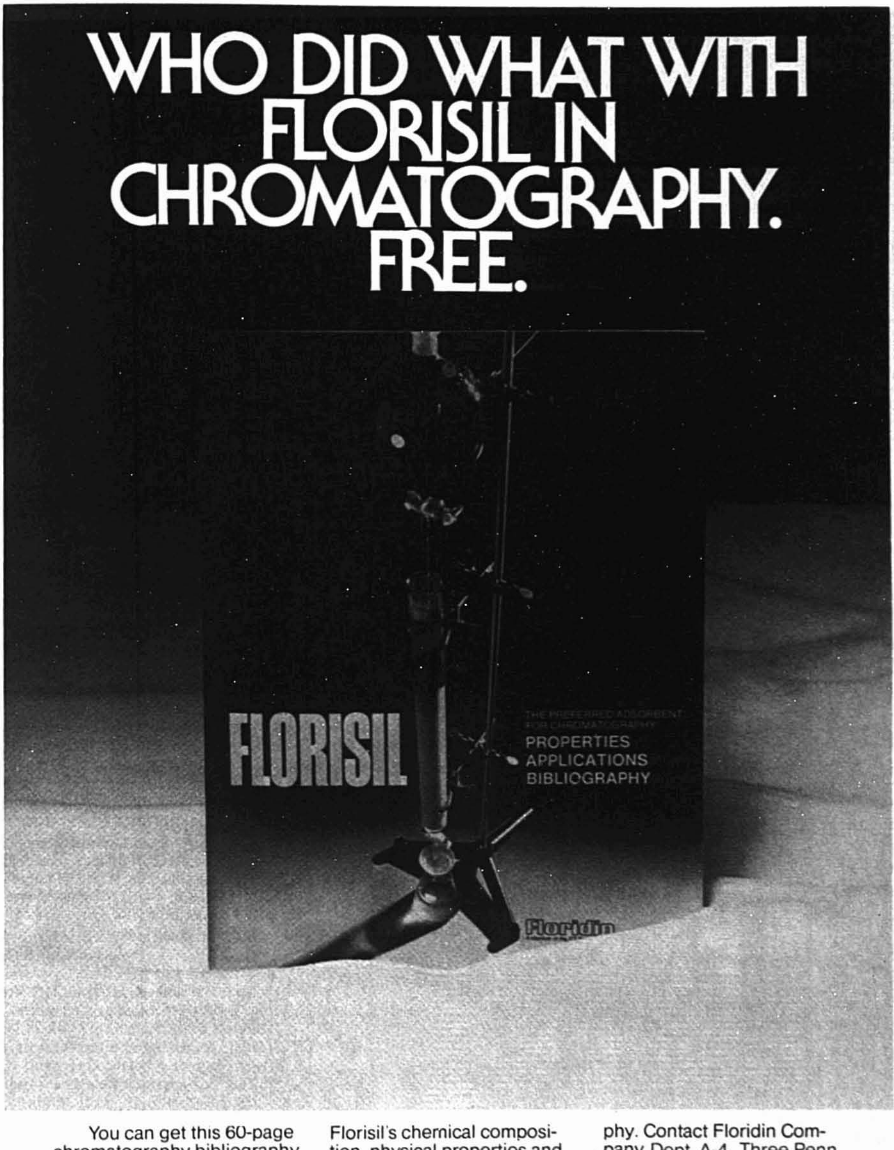
WHO DID WHAT WITH FLORISIL IN CHROMATOGRAPHY. FREE.
FLORISIL
THE PREFERRED ADSORBENT FOR CHROMATOGRAPHY
PROPERTIES
APPLICATIONS
BIBLIOGRAPHY
Floridin

You can get this 60-page chromatography bibliography free for the asking from Floridin. It'll tell you exactly why Florisil® is widely used to solve tough separation problems in column and thin layer chromatography.

The bibliography includes Florisil's chemical composition, physical properties and adsorptivity data. And a listing of who did what in chromatography with Florisil. Everything from Alkaloids to Thiosteroids.

Free for all. Floridin's Chromatography Bibliography. Contact Floridin Company, Dept. A-4, Three Penn Center, Pittsburgh, PA 15235. Phone: (412) 243-7500.

Floridin
A Member of the ITT System

CIRCLE 173 ON READER SERVICE CARD

PG-700

Reliable Shakers

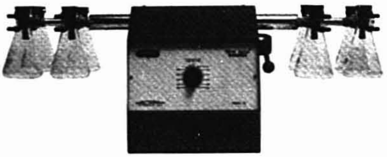

When it comes to reliable performance, you can count on Burrell Wrist-Action™ Shakers. They're ruggedly built for long life . . . some units have been in operation over forty years. Burrell Shakers duplicate a hand-mixing swirl with an even motion at all speeds for as long as necessary. And Burrell's unique Build-Up® System lets your Shaker grow as your lab grows . . . from a Shaker that holds 1 to 4 flasks to a Shaker that holds 24. Burrell parts and accessories are interchangeable. Burrell Wrist-Action Shakers with Build-Up design . . . the Reliable Shaker.

Write for our literature.

BURRELL
BURRELL CORPORATION
2223 Fifth Avenue, Pittsburgh, Pa 15219
Telephone 412-471-2527

CIRCLE 21 ON READER SERVICE CARD

ACCU-LUTE®

STANDARD
VOLUMETRIC
CONCENTRATES

$2.75 per unit
prompt delivery
made in U.S.A.

ANACHEMIA
CHEMICALS INC.
P.O. BOX 87 CHAMPLAIN, N.Y.
ZIP 12919 TEL.: (518) 298-9441

CIRCLE 6 ON READER SERVICE CARD

in brackish water, seawater, and brines by atomic absorption spectrometry. The contents include: definitions, specifications, reagents, and reporting results; sampling and flow measurements; general properties of water; inorganic constituents; organic constituents; radioactivity; bacteriological examination; water-formed deposits; and water treatment materials.

Compilation of ASTM Standards on Precision and Accuracy for Various Applications. 256 pages. 1977. Paperbound. $10.25

The need for precision and accuracy statements for standards has become so persuasive that this book has been issued to guide those concerned with the problem. Representation standards are presented as a guide to those who must prepare such material applicable to other materials. Among the topics considered are: determination of the precision of methods of committee D-19 on water; statements on precision and accuracy; rubber—precision statements for ASTM test methods; carbon black—stating the precision of ASTM test methods; defining a basis for petroleum product quality disputes; carbon black—measuring the precision of ASTM test methods; and use of the terms *precision* and *accuracy* as applied to measurement of properties of materials.

Continuing Series

Infrared and Raman Spectroscopy, Part B. Edward G. Brame, Jr., and Jeanette G. Grasselli, Eds. ix + 715 pages. Marcel Dekker, Inc., 270 Madison Ave., New York, N.Y. 10016. 1977. $37.50

This is the second of a new series entitled "Practical Spectroscopy Series" initiated in 1976. Part C, which is yet to be published, will complete Volume 1. Part B contains six chapters. The first chapter, written by R. P. Young, discusses computer systems. It describes data acquisition from offline and in-line spectrometers as well as the different methods of handling the acquired data for both qualitative and quantitative analysis. Chapter 2, coauthored by R. Nyquist and R. O. Kagel, demonstrates the successful application of infrared and Raman spectroscopy to analysis of organic materials. Chapter 3, by D. S. Lavery, covers the uses of infrared and Raman spectroscopy in environmental sciences. Topics discussed include sample handling, calibration methods, remote sensing, and multicomponent

The smartest label around.

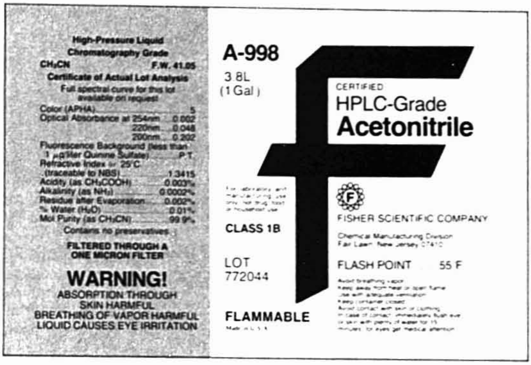

High-Pressure Liquid
Chromatography Grade
CH_3CN F.W. 41.05
Certificate of Actual Lot Analysis
Full spectral curve for this lot
available on request

Color (APHA) 5
Optical Absorbance at 254nm 0.002
220nm 0.048
200nm 0.202
Fluorescence Background (less than 1 μg/liter Quinine Sulfate) .... P.T.
Refractive Index @ 25°C (traceable to NBS) 1.3415
Acidity (as CH_3COOH) 0.003%
Alkalinity (as NH_3) 0.0002%
Residue after Evaporation 0.002%
% Water (H_2O) 0.01%
Mol Purity (as CH_3CN) 99.9%
Contains no preservatives

FILTERED THROUGH A
ONE MICRON FILTER

WARNING!
ABSORPTION THROUGH
SKIN HARMFUL
BREATHING OF VAPOR HARMFUL
LIQUID CAUSES EYE IRRITATION

A-998
3.8L
(1 Gal.)

CERTIFIED
HPLC-Grade
Acetonitrile

CLASS 1B

FISHER SCIENTIFIC COMPANY
Chemical Manufacturing Division
Fair Lawn, New Jersey 07410

LOT
772044

FLASH POINT 55 F

FLAMMABLE

Fisher Certified HPLC Solvents. Only label around that tells you everything you need to know.

Optical absorbance at a variety of wavelengths (full spectral curves on request). Refractive index directly traceable to NBS. Background fluorescence. Assay as mol % determined by GC. Water and preservative/inhibitor content. And much much more.

Fisher HPLC solvents are **distilled in glass.** Painstakingly filtered to eliminate particulates. And shipped by today's fastest distribution system.

After all, high-pressure liquid chromatography columns, detectors and samples are valuable things. They **deserve** the best. Only Fisher defines and certifies **every parameter** for their protection.

Only Fisher provides such tailormade services as Customer Reserve Quantity. Your nearest branch reserves your HPLC solvent needs for you alone, releasing them to your timetable. (Reserve an entire lot if you wish, assuring absolute uniformity month-to-month!)

Also: as today's largest lab supplier, Fisher provides an impressive selection of **auxiliary** HPLC materials — apparatus, appliances, supplies — to simplify your ordering.

Write for HPLC catalog **today!**

Fisher Scientific Company
711 Forbes Avenue Pittsburgh PA 15219

CIRCLE 77 ON READER SERVICE CARD

1 Quick Source

. . . for over 90 standard IR transmission windows.

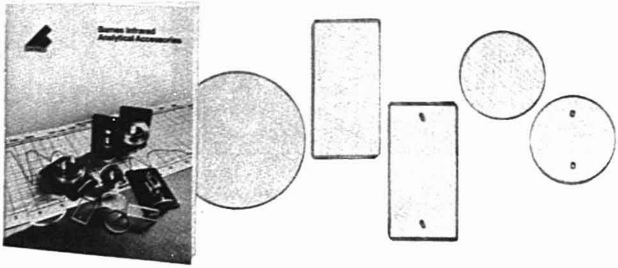

Barnes can be the single source of supply for all your crystal requirements. We provide discs, rectangles, and squares . . . drilled or undrilled . . . from NaCl to CsI. Over 90 different items . . . all available immediately from stock. We supply prompt price and delivery information on special orders.

And Barnes windows fit standard cells made by all manufacturers. Barnes crystals are a product of rigid manufacturing and quality control to assure flawless performance. And each window is individually wrapped to insure perfect condition.

For your crystal needs, check page 4 of our new 40-page catalog, "Barnes Infrared Analytical Accessories." Write or phone for your copy. Barnes Engineering Company, 30 Commerce Road, Stamford, Connecticut 06904. Call *toll free* (800) 243-3498, Ext. 281, or in Connecticut, (203) 348-5381, Ext. 281.

BARNES

Your IR Spectroscopy Source.

NOW GSA LISTED

CIRCLE 26 ON READER SERVICE CARD

Why sacrifice PERFORMANCE for ECONOMY?

THE GLENCO HPLC SYSTEM I

gives you both!

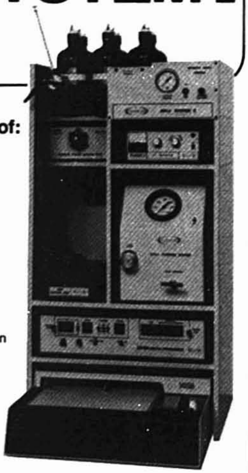

Glenco's System I is a complete, high-performance modular system consisting of:

- Pulse free liquid delivery system
- High pressure sample injection valve
- Exclusive sample loop filling syringe
- Prepacked high pressure column
- High performance UV detector
- 12 speed, 10" chart recorder
- Solvent reservoir
- Functional cabinet—chemical resistant finish
- HPLC System I—$3922.00

Gradient Elution Accessory $2045.

The Model GE 6 is a complete gradient elution system consisting of a solid state Digital Programmer (DP-410) and an automatically operated, six position stream selection valve (SSV-6). In addition to stream selection, three additional functions can be programmed at any time intervals (0-99 min/sec).

Typical Applications:

PTH amino acids, nucleotides, nucleosides, nucleic acids, vitamins, drugs, steroids, estrogens, pyrimidines, purines, phenols, esters and many others.

GLENCO SCIENTIFIC, INC.

2802 WHITE OAK DRIVE
HOUSTON, TEXAS 77007
(713) 861-9123

CIRCLE 81 ON READER SERVICE CARD

analyses. Chapter 4 on the use of infrared and Raman spectroscopy in food analysis is written by A. Eskamani. Chapter 5, written by P. B. Tooke, describes varied applications of infrared and Raman spectroscopy to the analysis of petroleum products. Finally, Chapter 6, authored by G. Celikiz, covers the use of infrared and Raman spectroscopy in textiles. The book is reproduced from typewritten text.

Comprehensive Analytical Chemistry, Vol. VI. G. Svehla, Ed. 555 pages. American Elsevier Publishing Co., Inc., 52 Vanderbilt Ave., New York, N.Y. 10017. 1976. $73.25

As in the previous volumes of the series, this text is designed as a self-sufficient reference. However, where complete details of methods are not given, full reference to the pertinent literature is provided. Volume VI is devoted solely to one subject: analytical infrared spectroscopy. As such the treatment of the subject is from the point of view of the practicing analytical chemist rather than from a theoretical aspect. The first two short chapters deal with historical survey, and symbols and abbreviations. The following five chapters are devoted to discussions of theory of infrared spectra, apparatus, experimental techniques, qualitative analysis, quantitative analysis, and applications, respectively. The last chapter contains the list of literature on infrared spectroscopy and collections of spectra.

Advances in X-Ray Analysis, Vol. 20. Howard F. McMurdie et al., Eds. xvii + 604 pages. Plenum Publishing Corp., 227 West 17th St., New York, N.Y. 10011. 1977. $42.50

Compiled in this volume are the proceedings of the 1976 Denver Conference on the Applications of X-Ray Analysis. This conference, 25th in the series, was jointly sponsored by the Joint Committee on Powder Diffraction Standards and the University of Denver. Fifty-five invited and contributed papers presented at the conference are arranged for this book under five general topics: x-ray powder diffraction (16 papers), x-ray topography (5 papers), x-ray diffraction stress analysis (13 papers), x-ray fluorescence (14 papers), and x-ray instrumentation (5 papers). Titles of those papers presented at the conference but not included in the book for various reasons are also listed. The book is a good quality photo-offset copy of author-furnished typewritten text.

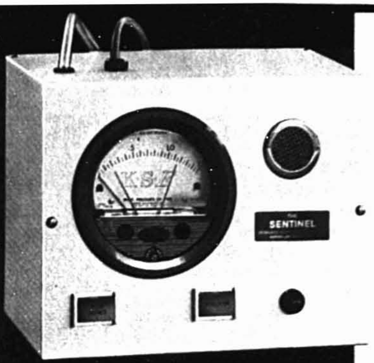

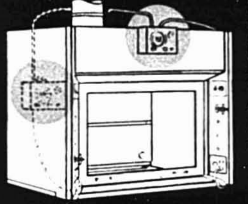

The alarm may be mounted on a shelf at the side of the hood, or on the top front hood panel. (Specify mounting location and the proper mounting bracket will be supplied.)

the Kewaunee
SENTINEL ALARM
maintains SAFE laboratory fume hood face air velocity

The Sentinel, as the name implies, effectively stands guard over the face velocity of fume hoods—If irregularities occur, it signals both audibly and visually. It is adaptable to all types and sizes of fume hoods and offers these and other advantages:

- Adjustable photo cell gauge triggers audible and visual alarms when fume hood face velocity falls below the safe operating level.
- Decreasing (or increasing) gauge pressure reading provides visual warning of deteriorating conditions before an unsafe face velocity level is reached.
- Conditions of exhaust fan, filters, exhaust duct and room air supply system are automatically monitored.

For more information call or write:

kewaunee
KEWAUNEE SCIENTIFIC EQUIPMENT CORP.
SPECIAL PRODUCTS DIVISION
4043 LOGAN ST., ADRIAN, MICH. 49221
Phone: 517/263-5731

CIRCLE 112 ON READER SERVICE CARD

WE'VE GIVEN RADIATION A BETTER IMAGE

Galileo's Channeltron® electron multiplier arrays can detect and image more kinds of radiation more accurately than anything else on the market.

Designed to fit your application, it detects ions, protons, electrons, UV photons, and soft X-rays. And the list goes on.

But even more important than its imaging versatility is the accuracy it offers. It possesses the lowest dark current available (<1 count/second/cm² in certain configurations).

What's more, all our detectors come to you with a warranty and all the engineering assistance you need.

For more information about our Channeltron electron multiplier arrays, our standard line of single channel detectors, or custom assemblies with associated electronics, write to Galileo Electro-Optics Corporation, Galileo Park, Sturbridge, MA 01518. Or better, call us at (617) 347-9191.

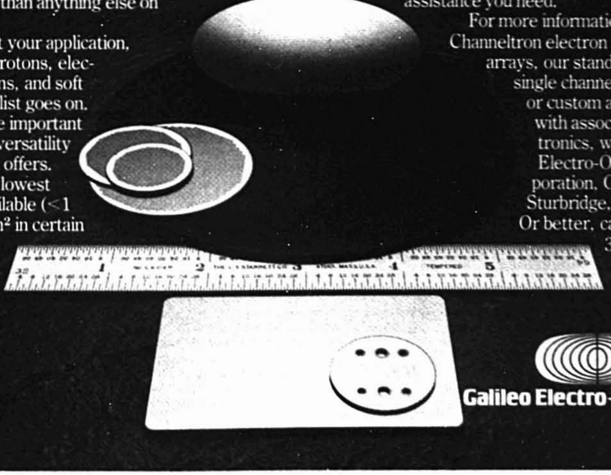

Galileo Electro-Optics Corp.

CIRCLE 85 ON READER SERVICE CARD

American Chemical Society

Advances
Symposia
Reprint
Collection

TITLES IN ENVIRONMENTAL CHEMISTRY

American Chemical Society, 1155 16th St., N.W./Wash., D.C. 20036

Removal of Trace Contaminants from the Air
Victor R. Deitz, Ed.
Sixteen chapters provide critical and in-depth coverage of air pollution characterization and removal. The collection stresses interactions among particulates and gas phase contaminants; pesticides; occupational contaminants; cigarette smoke and aerosol filtration; sulfur dioxide; trace gas adsorption; nitrogen oxides; and high ozone concentrations.
207 pages. Cloth. (1975) $17.25

Approaches to Automotive Emissions Control
Richard W. Hurn, Ed.
Nine chapters spotlight current developments toward the goals of lower emissions and greater fuel economy: the impact of automotive trends and emissions regulations on gasoline demand; gaseous motor fuels; fuel volatility, the pre-engine converter; and low emissions combustion engines.
211 pages. Cloth. (1974) $12.95

Air Pollution
Collected by D. H. Michael Bowen
Contains 38 articles from Volumes 3-6 of *Environmental Science & Technology*. Laws and regulations, specific pollutants and standards, monitoring, control methods, and transportation.
138 pages. Hard. (1973) $7.50
138 pages. Paper. (1973) $4.50

Solid Wastes—II
Collected by Stanton S. Miller
Thirty-three articles from Volumes 4-7 of *Environmental Science & Technology* report on federal, state, and local government projects; recycling and resource recovery; auto hulk disposal; plastics; scrap iron and tires; industrial sewage and sludge; and solid waste treatment technology.
"The book should be helpful to anyone who needs to be brought up to date in a hurry."
Reuse/Recycle (1975) **9**, 11
118 pages. Hardback. (1973) $7.50
118 pages. Paperback. (1973) $4.50

Pollution Control and Energy Needs
Robert M. Jimeson and Roderick S. Spindt, Eds.
Nineteen papers focus on energy demands vs. primary fuel supplies and the effectiveness of technologies that have been developed to meet environmental regulations. Topics include natural energy reserves, control of SO_x and NO_x, H-Oil desulfurization, sulfur oxides removal from stack gases, RC/Bahco system, effect of desulfurization methods on ambient air quality, and several available processes.
249 pages. Cloth. (1973) $16.95
249 pages. Paper. (1973) $9.95

Solvents Theory and Practice
Roy W. Tess, Ed.
Thirteen papers present the latest application formulas and techniques to combat pollution from solvents. Predicted compositions of resin solutions, solvent selection by computer, prediction of flash points for solvent mixtures, epoxy resin coatings, photochemical smog reactivity of solvents, solvents in electrodeposition coatings, polyamide resin solubility parameters, and solubility characteristics of vinyl chloride homopolymers, copolymers, and terpolymers.
227 pages. Cloth. (1973) $15.75

Catalysts for the Control of Automotive Pollutants
James E. McEvoy, Ed.
Current research by auto makers, catalyst companies, universities, and chemical and petroleum companies on all aspects of catalytic conversion to reduce automotive emissions. Emphasis is on analytical methods, mechanisms of catalytic removal, and catalysts themselves. Specific topics examined in fourteen papers include variation of selectivity, catalyst poisoning, the nature of the catalyst support, and others.
199 pages. Cloth. (1975) $19.95

Trace Elements in Fuel
Suresh P. Babu, Ed.
The latest research results on these often-toxic emissions cover their origin, the quantities in which they escape into the atmosphere, determination methods, and physiological effects. Specifically, fifteen chapters detail mineral matter and trace elements in coal; coal pretreatment and combustion; mercury and trace element mass balance; and environmental toxicology.
216 pages. Cloth. (1975) $16.50

Trace Elements in the Environment
Evaldo L. Kothny, Ed.
Nine chapters examine the geochemical cycle of trace elements in the environment. Boron, zinc, and selenium are discussed, as well as atmospheric pollutants, marine aerosol salt and dust, particulates, inorganic aerosols, S, V, Zn, Cd, Pb, Se, Sb, Hg. Includes methods of identification, separation, and measurement.
149 pages. Cloth. (1973) $12.50
649 pages. Paper. (1973) $7.25

Environmental Chemistry, Vol. 1
Senior Reporter: G. Eglinton
A review of the literature up to mid-1973 covering stable isotope studies and biological element cycling; environmental organic chemistry of rivers, lakes, bogs, marshes, swamps, oceans, fjords, anoxic basins; hydrocarbon distribution in the marine environment; DDT and PCB; organic chemistry of 2, 4-dichlorophenoxyacetic acid.
199 pages. Cloth. (1975) $22.00

Sulfur Removal and Recovery from Industrial Processes
John B. Pfeiffer, Ed.
Sixteen chapters form a consolidated reference source of sulfur removal and recovery methods concentrating on recovery techniques from sources other than power plant stacks. Emissions from smelter gas streams and Claus units are discussed, and seven scrubbing processes are described. Companion volume is No. 140.
221 pages. Cloth. (1975) $16.95

Marine Chemistry in the Coastal Environment
Thomas M. Church, Ed.
Forty-one chapters cover topics in six major areas: physical, organic, and tracer marine chemistry; estuarine geochemistry; hydrocarbons and metals in the estuarine environment; ocean disposal forum; applications and resources in marine chemistry; and organic and biological marine chemistry.
710 pages. Cloth. (1975) $35.75

Water Pollution
Collected by Stanton S. Miller
One-hundred-six articles from Volumes 4-7 of *Environmental Science & Technology* discuss federal and state policy; how, and to what extent military, business, and industrial communities are acting to implement new laws and standards; monitoring, specific pollutants, tertiary treatment, drinking water, microstaining, desalination, electrolysis, adsorption, and sewage treatment.
317 pages. Hardback. (1974) $15.00
317 pages. Paperback. (1974) $9.50

SIS/American Chemical Society
1155 16th St., N.W./Wash., D.C. 20036

Please send the following books:

____
____
____
____
____
____

☐ Check is enclosed for $ ________. ☐ Bill me.
Postpaid in U.S. and Canada, plus 40 cents elsewhere.

Name ______________________________

Address ______________________________

City __________ State __________ Zip __________

THE AA LEADER SETS THE PACE...AGAIN

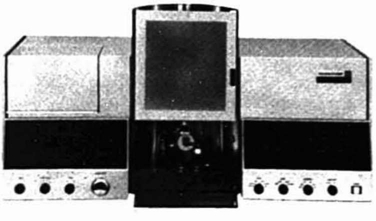

603

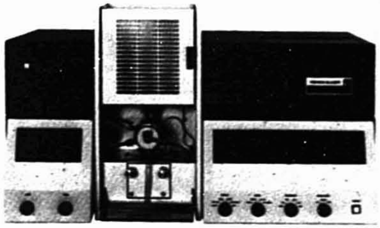

460

373

272

***Only* Perkin-Elmer can offer you a complete line of microprocessor atomic absorption spectrophotometers.** And all include built-in computer data handling; optical systems designed for both flame and flameless sampling; optional deuterium arc background correction; compatibility with Perkin-Elmer's complete line of AA accessories; and the unmatched technical backup you get only from the leader in atomic absorption.

The Model 603 is a double-beam instrument with unmatched performance, versatility, and ease of use. From its measured 0.03 nm resolution to its preprogrammed microcomputer, the 603 is the instrument against which all others must be compared.

Model 460 combines the 603's computer electronics with its own double-beam optical system, featuring automatic gain control and optional double-beam background correction at a moderate price.

Model 373 is a new mid-priced AA with a 460-type optical system and new microcomputer electronics offering many of the features of the Perkin-Elmer Models 603 and 460.

Model 372, another new one, is almost identical with the 373, differing primarily in its burner and gas control system.

Model 272 is a new low-cost AA with features and performance never before available in a single-beam AA instrument, regardless of price.

Whatever your needs in AA, Perkin-Elmer has exactly the right instrument for you. Talk to your Perkin-Elmer representative now, or write Perkin-Elmer Corporation, Main Avenue, Norwalk CT 06856.

CIRCLE 164 ON READER SERVICE CARD

PERKIN-ELMER

Lab-Crest® Low-Flow Rotameters

The New Performance Leader . . . By All Standards

Now you can get all the features and options that make a great low-flow rotameter, combined in one and the same instrument. Built by the industry's most experienced team of control engineers and glass craftsmen, the new Lab-Crest Low-Flow Rotameter features a unique precision valve that provides linear control throughout the range of flows . . . a new low-flow tube with ⅛-inch float that operates reliably in industrial environments . . . plus all the time-tested features that have made Fischer & Porter rotameters the standard of comparison since the birth of the industry:

- **Convenience.** Quick-release metering tubes with Viton cup seals are easily interchanged without tools.
- **Rangeability.** Eight interchangeable tubes provide a choice of flow ranges from 50 cc/min to 148 SCFH (air).
- **Accuracy.** Instantaneous readings are repeatable within ± ¼ %, a direct result of F&P's unsurpassed experience.
- **Visibility.** Ceramic scale with white background is easy to read, permanently fused into the borosilicate glass surface.
- **Versatility.** Choice of meter bodies with 3, 6 or 10-inch scale for in-line or panel-mounting . . . or with tripod mount.
- **Controllability.** Precision sixteen-turn valve with interchangeable stems and sleeves provides linear control at all flow rates, as well as positive shut-off; low-cost valve also available for less sensitive applications.
- **Corrosion Resistance.** Standard aluminum end fittings are also available with interchangeable brass or stainless steel inserts; stainless steel standard on models with precision valve.

More than ever, it makes sense to call us for all your rotameter needs, whether you are looking for OEM quantities or just one of a kind. We have the right type and the right options to meet your requirements exactly.

Call (215) 674-6000 and ask for Lab-Crest Scientific Division.
Fischer & Porter Company, County Line Road,
Warminster, Pa. 18974.

LAB-CREST
SCIENTIFIC
A DIVISION OF FISCHER & PORTER

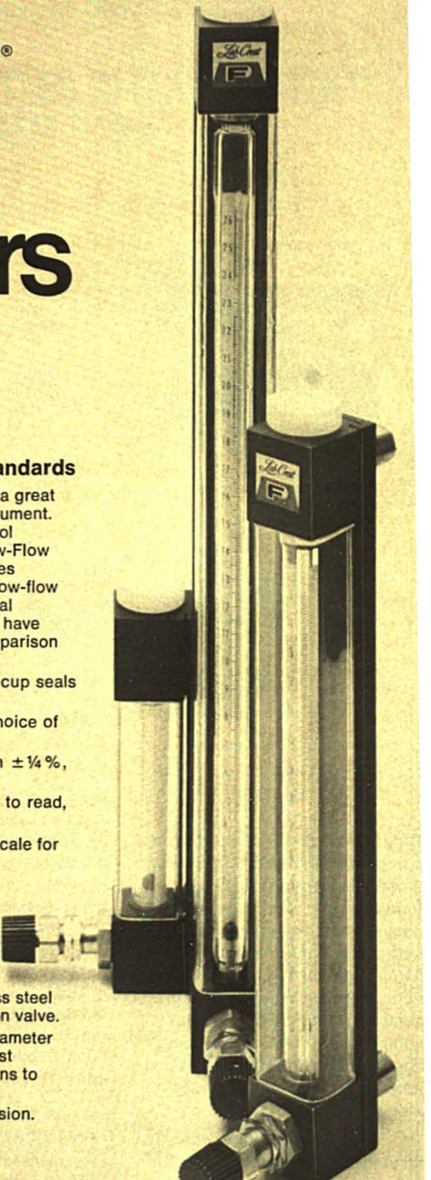

CIRCLE 76 ON READER SERVICE CARD

Editors' Column

NSF Peer Review

A survey of grant applicants and grant reviewers shows that the peer review system of the National Science Foundation (NSF) is judged to be quite adequate. Of the scientists who submitted research proposals to NSF during fiscal year 1975, 77% believe that the review procedures are appropriate. Somewhat predictably, nearly all applicants whose most recent proposal was funded believe that the review procedures are appropriate, whereas 50% of those whose most recent proposal was declined believe the procedures to be inappropriate. Among the scientists who participated in the review of research proposals by mail, 46% feel that the mail review process is sound, 50% believe that the process is acceptable, and only 4% feel that the process is questionable and includes many weaknesses.

The survey was initiated because of considerable discussion in the scientific community and in Congress of the peer review process. During the spring and summer of 1975, a series of Congressional oversight hearings on peer review was held by the U.S. House Committee on Science and Technology's subcommittee on Science, Research and Technology. Also, the National Science Board (NSB), which is the policy-making body of NSF, established a special task committee to study the process. In late 1975, NSB and the House subcommittee jointly commissioned a study to gather objective information about the scientific community's views on the peer review process. Originally, information was to be solicited from three groups: NSF reviewers, recent applicants for NSF funds, and scientific researchers who were neither reviewers nor recent applicants. Surveying the latter group was deemed not to be feasible, but from NSF files of reviews and proposal actions, it was possible to select independent samples of recent reviewers and applicants.

According to Deborah R. Hensler, consultant to NSB and author of a report presenting a detailed analysis of the survey data, the most serious criticism of the NSF peer review process is that it is biased against proposals from less prestigious institutions, proposals by younger researchers, and proposals that are innovative in character. Data from the surveys cannot be used to confirm or refute the charge of bias since no substantive or qualitative information about proposals was collected. However, both reviewer and applicant questionnaires included three questions to measure general perceptions of bias in the system. The questions were generally of the type: If two equally good proposals are submitted to NSF, one from A and one from B, do you think that each has an equal chance of being recommended for funding by the peer reviewers, or does one have a better chance than the other? A majority of reviewers and applicants believe that the NSF peer review process favors proposals from well-known institutions, proposals by older, well-established principal investigators, and proposals that are in the mainstream of thought rather than those which challenge current thinking.

Data from the survey also show that:

- Reviewers believe that strengths of the peer review system are the well-matched reviewers and proposals and the broad range of expert recommendations solicited.
- Reviewers feel that weaknesses of the system include lack of feedback and the opportunity for favoritism.
- A majority of both applicants and reviewers thought that NSF should require some type of peer review for all proposals. In selecting reviewers the majority favored continuance of a role for the NSF staff in reviewer selection; however, a significant minority favored random sampling techniques.
- Applicants and reviewers approve of the recent NSB policy of furnishing verbatim anonymous copies of reviews to grant applicants. They disapprove of providing the names of reviewers with their reviews.

Dr. Hensler's report, "Perceptions of the National Science Foundation Peer Review Process: A Report on a Survey of NSF Reviewers and Applicants", No. NSF 77-33, may be obtained from the Mail, Security, and Records Section, 1800 G Street, N.W., Washington, D.C. 20550.

A. A. Husovsky

Reliable. Fast and Easy.
MCI automatic analyzer.

Utilizes ASV method to simultaneously measure concentrations of 5 different trace heavy metals. Ultra-high sensitivity and automatic sample feed/discharge measuring cell assures fast, precise results. Reproducibility is 3-to-20%. Range: 0.1 PPB—10 PPM.

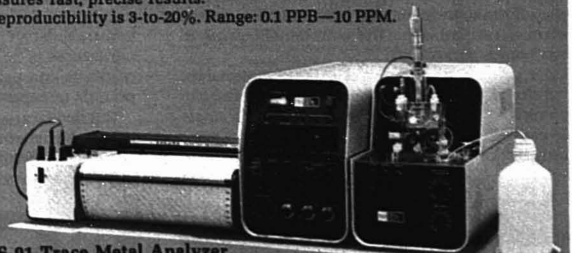

AS-01 Trace Metal Analyzer

MITSUBISHI CHEMICAL INDUSTRIES LIMITED
Instruments Dept., Mitsubishi Bldg., 5-2, Marunouchi 2-chome, Chiyoda-ku, Tokyo, 100 Japan Telex: J2490 Cable Address: KASEICO TOKYO

CIRCLE 139 ON READER SERVICE CARD

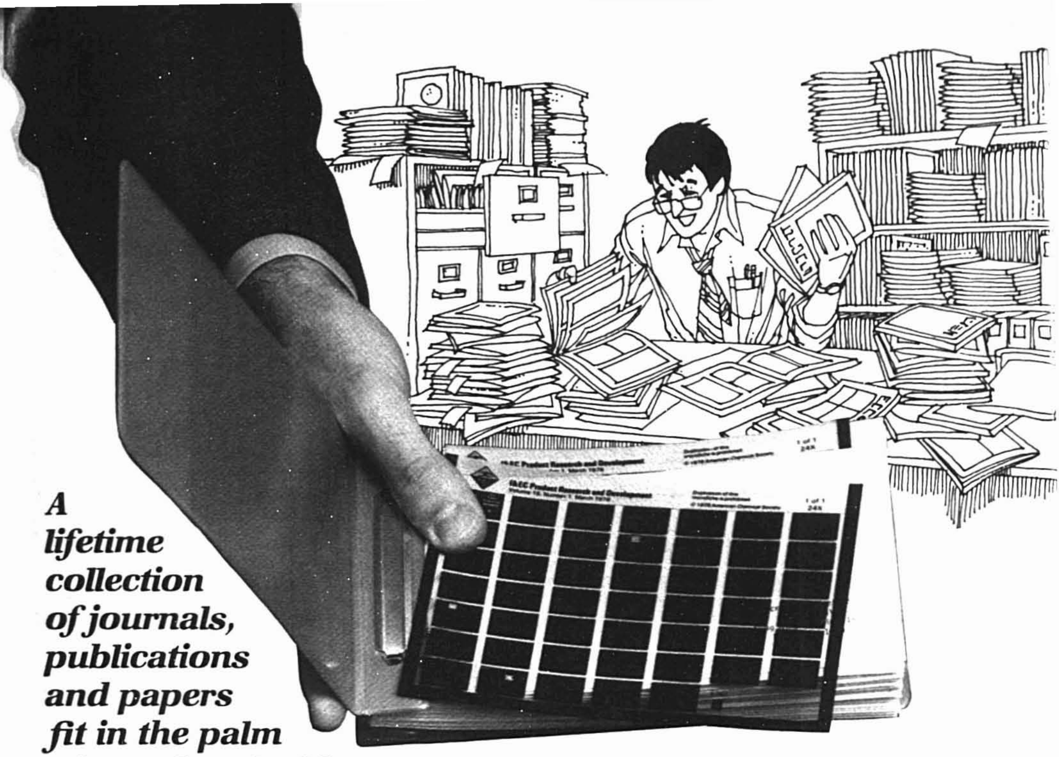

A lifetime collection of journals, publications and papers fit in the palm of your hand with

Microfiche

A MONEY SAVING, TIME-SAVING, SPACE-SAVING AID FOR YOUR HOME, OFFICE, WORKSHOP OR LAB

It started when big organizations found microfiche an efficient, low cost space-saver. Now many individual scientists, information managers, teachers, researchers and executives recognize that the same benefits apply in their own homes and offices.

Consider: you can store three file cases of materials in one small album you can carry in your hand. Yet, *you can buy a microfiche reader for less than the cost of a single good file cabinet.*

Not only is a large portion of current reference material (including *all* ACS journals) now available in microfiche, you can even arrange to have your own material put in microfiche form! *And subscriptions to many journals and other publications cost the same in microfiche or printed edition.*

If space is important where you work or live; if you like to refer to back issues of ACS journals and other periodicals; if you like material that is easily mailed and distributed—turn to microfiche. Not only is it easy to file and retrieve, ACS Microfiche is archival quality so your material will be in good shape for a lifetime.

Surprisingly, it's not only scholarly material that is available on microfiche, you'll find everything from catalogs to magazines, from news weeklies to computer information can be ordered on microfiche. Imagine the advantages of doing away with cumbersome computer readouts and using a tiny film to replace pounds and pounds of paper!

Cut down on wasted space, time and money—turn to the modern method of storing readily available information... turn to microfiche!

Call or write to us for more information on this important aid.

THIS PUBLICATION IS AVAILABLE ON MICROFICHE

ACS Microforms Program, Room 606
American Chemical Society,
1155 Sixteenth Street, N.W., Washington, D.C. 20036

(202) 872-4554

MODERN CLASSICS IN ANALYTICAL CHEMISTRY

Volume II

Edited by
Alvin L. Beilby

A selection from the best feature articles that appeared in issues of ANALYTICAL CHEMISTRY from 1970 through 1975.

Students
Instructors
Researchers
Problem-Solvers . . .

Particularly suitable as supplementary reading for the advanced student of analytical chemistry and for those who must keep up with the latest developments in analytical chemistry and instrumentation, this convenient collection of source material contains valuable information presented only in outline form in many modern textbooks.

Volume II 314 pages (1976) $8.50 paperbound
Volume I 268 pages (1970) $5.75 paperbound

Postpaid in U.S. and Canada, plus 40 cents elsewhere.

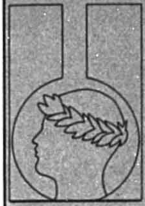

keep on top of recent advances in analytical chemistry.

CONTENTS (Volume II)

- Development of Analytical Chemistry
- Spectroscopy (11 articles)
- Electrochemistry (2 articles)
- Chromatography (3 articles)
- Automation and Instrumentation (6 articles)
- Measurement Techniques (7 articles)
- The Analytical Approach (9 articles)
- Art Conservation (2 articles)

Order from:
Special Issues Sales
American Chemical Society
1155 Sixteenth St., N.W.
Washington, D.C. 20036

ULTREX® Ultrapures

When you simply can't tolerate impurities or uncertainties in your starting materials.

Over 100 of the purest reagents and chemicals available anywhere in the world. Every product is accompanied by a detailed Certificate of Analysis of the actual lot supplied. In terms of spectrochemically detectable impurities, ULTREX products are typically 99.995% to 99.99995% pure. And the extremely low content of all impurities (often at the parts per billion level) satisfies the most rigid use requirements.

Whenever your requirements for purity and product definition are stringent, ULTREX ultrapures can indeed insure against loss of time, effort, and other expenses.

Consider ULTREX when you just can't afford to gamble with impurities or uncertainties.

Write for new ULTREX ultrapure
Reagent brochure

J. T. Baker Chemical Co.
Phillipsburg, N.J. 08865
201 859-5411

J.T.Baker®
CHEMICALS

CIRCLE 19 ON READER SERVICE CARD

Some interesting facts about a unique tubing material which you will find beneficial for the preparation of GC columns.

Nickel tubing is a fresh answer to the problems which have confronted the gas chromatographer for years.

ITS BENEFIT

First, it combines the chemical inertness of glass with the handling characteristics of metal tubing. No more struggling with fragile glass columns!

CHEMICAL INERTNESS

Comparison of separations of various classes of compounds known to be adversely effected by stainless steel columns were investigated. A typical series of chromatograms is shown.

****As can be seen, the results observed on a nickel column are comparable to those obtained on a glass column.****

UNIVERSAL APPLICABILITY

Alltech's technical Brochure No. 29 describes similar results for steroids, barbituates, catecholamines, amphetamines, pesticides and other difficult to chromatograph labile chemicals. The use of this tubing material as an alternative to glass for analysis of biological samples has been recently reported in literature.* It was this article which spurred Alltech's commercial offering of this material.

As more and more nickel tubing is being used, more and more separations are being reported almost as fast as the proverbial rabbit. If this tubing permits you to make a separation, we hope you will share it with us, hopefully to everyone's mutual benefit.

HANDLING ADVANTAGES

Nickel tubing handles just like metal tubing. Connections to your chromatograph are made with easy to assemble metal nuts and ferrules. No longer will you have to contend with difficult to connect glass columns or the fragility of glass which makes the packing and changing of columns a test of skill for even the most experienced user.

ENJOY THE CONVENIENCE

Enjoy the convenience of using this low cost material where you are now using glass columns. Please write us for our detailed Brochure No. 29. Perhaps the contents of this interesting brochure will stimulate an idea spinning in your head solving one of your nagging problems or just making your life a little easier.

**Journ. of Chrom., Vol. 140/#1/10-1-77/PP 9-15*

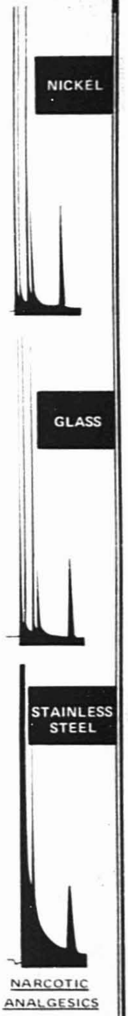

Alltech Associates

202 CAMPUS DR. • ARLINGTON HTS., IL. • 60004
312/392-2670 TWX 910 687 0425

CIRCLE 5 ON READER SERVICE CARD

TWO GIANT

Perkin–Elmer introduces two new groups of liquid chromatographs – Series 2 and Series 3. They give you the most advanced LC for your money.

All at once you have unprecedented alternatives in liquid chromatography. These instruments are all state-of-the-art, significant additions to the Perkin-Elmer line. They're not cost-burdened with features that should be options. Instead, they're an innovative concept in matching price to performance.

Series 2. Five modular units.

For economy and efficiency, any LC system you buy should be closely tailored to the work it must do. This is the main advantage of the Series 2 modular design. Begin with the simplest practical unit — add more modules and accessories later.

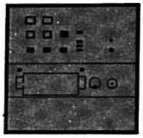

The Series 2/1, with a single pump, is the basic unit. It's compatible with all commercial LC detectors. The pumping system has only three moving parts, so it's dependable and exceptionally easy to maintain. Series 2/2 adds a second pump for more efficiency and output. Its basic linear gradient capability can quickly approximate solvent conditions necessary for isocratic separation.

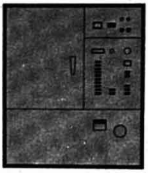

In the LC-65T Detector/Oven, superior UV/Visible detection is combined with temperature control. Series 2/1, combined with the LC-65T, joins the reliable, convenient solvent delivery of the one to the spectrophotometric detection and temperature control of the other. You get better quality separations with improved column efficiency, along with more readily optimized separation time. Series 2/2, combined with the LC-65T, has the additional pump that provides gradient and flow-programming capability, and the Detector/Oven for temperature control and UV/Visible detection.

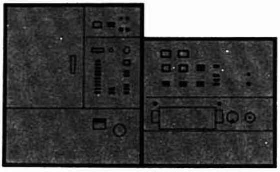

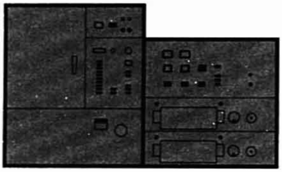

Series 3. Two units with microprocessor control.

Everything you need for highly precise qualitative and quantitative analyses is designed into these instruments. At the same time, they have all the convenience you need for routine problem solving. Both have their solvent delivery systems under microprocessor control. And both include high pressure capability and a wide flow rate range for analytical and preparative separations.

Series 3 adds the precision and convenience of microprocessor control to the dual-pump solvent delivery system of Series 2/2. It's also compatible with all commercially available LC detectors. Series 3 with the LC-65T adds up to the top of the line. It has the full solvent delivery capability of the Series 3 along with two other features for reliable problem solving: (1) temperature control and (2) UV/Visible spectrophotometric detection. The first results in excellent reproducibility. The second lets you check each step with confidence in developing a separation.

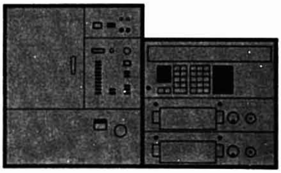

A wide choice of Perkin-Elmer accessories is available for all these instruments. Find out how efficiently Series 2 and Series 3 can fit all your liquid chromatography needs. Contact your Perkin-Elmer representative, or write Perkin-Elmer Corporation, Main Avenue, Norwalk, CT 06856.

CIRCLE 167 ON READER SERVICE CARD

PERKIN-ELMER

STEPS IN LC

Series 2/2 with LC-65T

Series 3 with the LC-65T

Push-button Titration.
No Burettes.
New Ion Trak™ II
by Petrolite®

Petrolite Ion Trak II does most of the work. All **you** do is put in the sample, push the button and read the answer.

There is no need for inconvenient and costly burettes. Ion Trak II automatically performs any titration where the titrant can be generated coulometrically and where the ion of interest can be detected by potentiometric or ion-selective electrodes.

It automatically regulates generation of the titrant and controls the rate of potential change at the sensing electrode. As the equivalence point is reached, the instrument slows down and automatically shuts off when titration is completed. The answer is displayed in equivalents of the ionic species of interest.

Ion Trak II eliminates the secondary steps necessary to conventional "automatic" titrators. Easy to use, versatile and low in cost, it dramatically enhances sensitivity at trace levels and reduces the need for back titration. And there's no warm-up period.

For more information about burette-less, push-button titrimetry, write or call Petrolite Instruments and ask about Ion Trak II.

CIRCLE 177 ON READER SERVICE CARD

PETROLITE INSTRUMENTS
PETROLITE CORPORATION
PETRECO DIVISION

4411 Bluebonnet Drive,
Suite C
Stafford, Texas 77477
713/494-7121
Telex: 774243

+2.68
REACTION
COMPLETE
µEq
VOLTS
mAmps
mV/Sec
PETROLITE INSTRUMENTS
ION TRAK™ II
SLOPE SELECT
POWER
BIAS
MODE SELECT
AUTO
BIAS POLARITY

Instrumentation

R. G. Griffin
Francis Bitter National Magnet Laboratory
Massachusetts Institute of Technology
Cambridge, Mass. 02139

High Resolution NMR in Solids

In the late 1960's the prevailing view among many NMR spectroscopists was that the field had reached maturity, and except for routine applications, few problems of real interest remained. This feeling led to an exodus of physicists and chemists from the field. Of those that continued to practice the art, many involved themselves in applications of the subject to problems in materials science or to chemical or biological problems. However, during that period several technical and scientific advances were made which opened new areas of scientific endeavor. Specifically, the development of superconducting solenoids, together with Fourier transform techniques (*1*), made observation of spectra of low abundance and/or sensitivity nuclei a routine matter. The most notable example of this is the observation of spectra of 1.1% abundant ^{13}C nuclei in liquids; the wealth of information on molecular conformation, dynamics, etc., available from these spectra is enormous.

In addition, during these and later years, techniques used for obtaining high resolution NMR spectra of solids were developed. It is these techniques and their present and future applications that we will discuss here. In Section I we outline the problem of high resolution NMR in solids; that is, we discuss the origin of the broad line spectra one customarily observes in solids and then outline three approaches to regaining resolution in the solid state. The approaches are considered in order of their chronological development, i.e., magic angle sample spinning, multiple pulse techniques, and magnetic dilution. Given that one can obtain high resolution spectra in solids, we consider in Section II what can be learned from such spectra. High resolution liquid NMR spectra are routinely employed in structural determinations and in the examination of chemical dynamics in solution. The observation of chemical shift, quadrupolar, and dipolar tensors in solids can also provide structural data, and when molecular motion is present in a solid sample, the spectra can, in principle, elucidate the rate and mechanism of that motion. In the final section, III, we discuss some new experiments which combine cross polarization, multiple pulse, and sample spinning techniques. Each of these experiments is designed to obtain a particular type of information, and these hybrid approaches may develop into the most exciting and generally applicable of the various experiments. We should mention at the outset of this review that in the last year two monographs concerned with this subject have appeared. One, by U. Haeberlen (*2*), is concerned primarily with multiple pulse techniques; the second, by M. Mehring (*3*), discusses both multiple pulse and magnetic dilution experiments. This author highly recommends both of these monographs to the serious student of solid state NMR. A review on sample spinning techniques by Andrew (*4*) appeared some time ago.

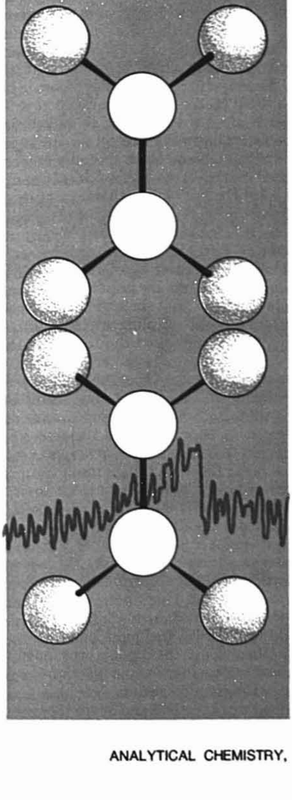

I. Approaches to High Resolution NMR in Solids

NMR spectra of solids are with few exceptions characterized by broad featureless lines. We can understand the source of this broadening and how to cope with it if we examine the size and form of the various terms in the nuclear spin Hamiltonian. A typical nuclear spin Hamiltonian is given in Equation 1 and contains four "interesting" terms:

$$\mathcal{H} = \mathcal{H}_{CS} + \mathcal{H}_J + \mathcal{H}_D + \mathcal{H}_Q \quad (1)$$

Liquids	10^3	10	0	0
Solids	10^3	10	5×10^4	10^5–10^6

The table indicates the expected sizes of the various interactions for liquids and solids in Hz; in liquids the dipolar ($\mathcal{H}_D$) and quadrupolar ($\mathcal{H}_Q$) terms vanish, and only chemical shift ($\mathcal{H}_{CS}$) and scalar coupling terms ($\mathcal{H}_J$) contribute. The reason that $\mathcal{H}_D$ (and likewise $\mathcal{H}_Q$) vanishes in liquids can be understood by examining Equation 2 which is the dipolar Hamiltonian

$$\mathcal{H}_D = \gamma^2\hbar^2 \sum_{i<j} -\frac{1}{r_{ij}^5}(\bar{r}_i \cdot \bar{r}_j - 3\, r_{iz} r_{jz}) \times (\bar{I}_i \cdot \bar{I}_j - 3\, I_{iz} I_{jz}) \quad (2)$$

for two like spins, for instance, two protons. Here $\bar{r}$ is the length of the internuclear vector, the I's are the spin operations, and γ and $\hbar$ are the gyromagnetic ratio and Planck's constant,

Send Today
for the new complete spectrum

Liquid Chromatography Packings, Packed Columns, and Chemicals
...aters, The Liquid Chromatography People

of Liquid Chromatography Packing Materials

This new catalog covers the complete spectrum of liquid chromatography packing materials, packed columns, and specialty chemicals from Waters — the world leader in liquid chromatography and its applications. Send today for your free copy of D13.

WATERS
137 Maple Street, Milford, MA 01757
Dial (617) 478-2000

CIRCLE 231 ON READER SERVICE CARD

respectively. Since $r_{iz} = r \cos \theta_{ij}$, where θ_{ij} is the angle between the laboratory field and the internuclear vector, we obtain an angular dependence for $\mathcal{H}_D$ of $(1 - 3 \cos^2 \theta_{ij})$. In liquids θ_{ij} is modulated by rapid isotropic molecular tumbling which causes $\langle 1 - 3 \cos^2 \theta_{ij} \rangle = 0$; thus, $\mathcal{H}_D = 0$. However, in solids θ_{ij} is fixed by the orientation of a crystallite in a magnetic field; thus, $\mathcal{H}_D \neq 0$. For two protons $\mathcal{H}_D$ is typically $\sim 5 \times 10^4$ Hz and is clearly larger than $\mathcal{H}_{CS}$ and $\mathcal{H}_J$; when there are many adjacent nuclei, there are many splittings, and these lead to the broad unresolved lines which are well known. Although $\mathcal{H}_Q$ is generally larger than $\mathcal{H}_D$ and thus resolvable, the lines in quadrupole spectra are typically several kilohertz wide for similar reasons, e.g., proton dipolar broadening.

The first attempts to reduce or eliminate $\mathcal{H}_D$ in solids were made independently and simultaneously by Lowe (*5*) and Andrew et al. (*6*) some years ago. These workers proposed that rapid spinning about an axis inclined at the "magic angle" of 54°44′ with respect to $\mathcal{H}_0$ would reduce or eliminate $\mathcal{H}_D$. This approach, which we call MASS (magic angle sample spinning), has been employed successfully in some instances, but in general it cannot remove homonuclear dipolar interactions. The reason for this is that one must spin rapidly compared to the magnitude of the interaction, $\sim 5 \times 10^4$ Hz for two protons, and at speeds of $\sim 4 \times 10^3$ Hz, one finds that the rotors begin to disintegrate due to centrifugal forces. With specially prepared materials one can reach speeds of $\sim 10^4$ Hz, but to date this seems to be the practical limit (*7*). Thus, because it is not generally possible to make $\nu_R \gtrsim 50$ kHz, one can employ MASS only in cases where relatively small interactions are present. We note, however, that since the chemical shift and scalar coupling are tensor interactions of rank two, they can, in principle, also be eliminated or reduced to their trace by MASS. We will see below that this is quite important for dilute spin double resonance experiments. In summary, MASS was thought to be useful only in special cases. For this reason high resolution NMR in solids was thought to be unachievable until about 1966.

At this time E. D. Ostroff, an electrical engineer designing pulse NMR spectrometers, did something no self-respecting NMR spectroscopist would do—he applied a high-power Carr-Purcell pulse train to a solid. The result was that the free induction was lengthened, i.e., the dipolar broadened lines narrowed (*8a*)! At about the same time similar results were obtained by Mansfield and Ware (*8b*). This experiment led J. S. Waugh and his coworkers, L. Huber and U. Haeberlen, to propose a pulse experiment referred to as WAHUHA which succeeded in reducing linewidths in rigid solids from 10^4 to $\sim 10^2$ Hz (*9*). The rationale for this experiment is quite similar to MASS in that it averages $\mathcal{H}_D$; however, this is accomplished by modulating the spin rather than the spatial factor. We have written Equation 2 in a form which emphasizes the mathematical similarity between the spatial and spin parts; in fact, multiple pulse experiments average about an axis inclined at the magic angle in analogy with MASS. However, this axis is the 111 direction in the rotating rather than the laboratory frame (*2,3*).

The third and final approach to high resolution in solids was suggested by A. Pines when he was a graduate student in the laboratory of J. S. Waugh. This approach utilizes the $1/r^3$ dependence of $\mathcal{H}_D$ to achieve narrow lines (*10*). Specifically, if two nuclei are separated by 10 Å rather than 1 Å, then $\mathcal{H}_D$ for these nuclei will be reduced by 10^3. Because of its 1.1% abundance, ^{13}C satisfies the conditions for being magnetically dilute; moreover, an additional reduction in the size of $\mathcal{H}_d$ occurs because of the relatively low magnetic moment of ^{13}C which enters Equation 2 as the factor γ^2. We will see below that low values of γ, together with "chemical" dilution, are sufficient to observe high resolution spectra from nuclei which are 100% abundant, e.g., ^{14}N and ^{31}P.

Dilute spin NMR in its pure form is, however, of little practical importance since most chemically interesting species contain protons as well as carbon, nitrogen, phosphorus, etc. Thus, proton-dilute spin broadening must be removed with large decoupling fields. In addition, T_1, which can be excruciatingly long in rigid solids, can be shortened in many instances by cross polarizing dilute and abundant spins in the manner suggested by Hartmann and Hahn (*11*). Pines et al. (*10*) recognized that cross polarization also enhances the dilute spin polarization by a factor of (γ_I/γ_S) where I and S refer to the abundant and dilute spins, respectively. Since the abundant spin is usually protons, the name given to this experiment is proton enhanced nuclear induction spectroscopy (*10*).

Finally, we should mention that two other double resonance schemes have been proposed for examination of rare spin species (*12*). These techniques rely on detection of changes in the abundant spin signal after cross polarization with rare spins and are referred to as "indirect detection" methods. While these approaches do not offer much advantage in terms of signal-to-noise over the direct method

Is the insecticide just as effective at a lower potency?

Extremely sensitive Mettler electronic microbalances can help you find the answer. Insects are weighed before and after feeding to determine how much insecticide was ingested. If the insects had a "full meal" and still survive, the potency can be increased until a single feeding is lethal. Mettler microbalances are so sensitive, they can detect microgram changes in weight.

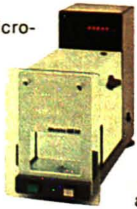

Mettler helps solve problems in analytical laboratories and on the production floors of industry. We market a variety of weighing and measuring instruments. All of them made with world-renowned Mettler craftsmanship. All of them backed by a worldwide team of service specialists who can be there when you need them. Mettler – instruments and people you can depend on.

Depend on Mettler for the answer.

Mettler

Electronic balances and weighing systems · Thermoanalytical instruments · Automatic titration systems · Laboratory automation

---

Mettler Instrumente AG, CH-8606 Greifensee-Zürich, Switzerland · Mettler-Waagen GmbH, D-63 Giessen 2, Postfach 2840, BRD
Mettler Instrumenten B.V., Postbus 68, Arnhem, Holland · Mettler Instrument Corporation, Box 100, Princeton, N.J. 08540, USA

CIRCLE 149 ON READER SERVICE CARD

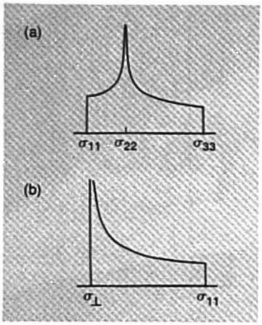

Figure 1. Absorption line shapes for polycrystalline samples with (a) axially asymmetric and (b) axially symmetric chemical shielding tensors

Principal values σ_{11}, σ_{22}, and σ_{33} [$\sigma_{11} = \sigma_{22} = \sigma_{\perp}$, $\sigma_{33} = \sigma_{11}$ in (b)] can be read off directly

Reprinted by permission of the American Institute of Physics

for nuclei such as ^{13}C, they may prove very useful for study of lower γ nuclei.

II. Anisotropic Magnetic Interactions

High resolution spectra of solids distinguish themselves from spectra of liquids in that they display the anisotropy of the chemical shift, dipolar, and quadrupolar tensors. We now discuss examples of each and what can be learned from the study of these interactions.

Chemical Shift Tensors. The first examples of chemical shift tensors were derived from multiple pulse studies of ^{19}F in powders (*13*) and single crystals (*14, 15*). Since then dilute spin double resonance and multiple pulse experiments have been used to study shift tensors of a number of nuclei including ^{13}C, ^{1}H, ^{15}N, ^{31}P, ^{29}Si, and ^{2}H. (For a summary of most of the available data, see Chapter 6 of ref. *2* and Chapter 5 of ref. *3*.) As an example, we discuss ^{13}C tensors of carbonyl and carboxyl groups, since at this time they are the most thoroughly investigated and illustrate the type of information that can be obtained.

In general, a symmetric second rank tensor possesses six independent elements: three principal values of the tensor and three Euler angles that relate the principal values to some reference frame, for instance, the unit cell axes. If the orientation of the molecules in the unit cell is known, then the tensor can be related to molecular axes. This requires a single crystal study, and we discuss below the manner in which one performs this experiment. In the event that single crystals are not available, then powder samples can be examined, although at a partial loss of information. Specifically, from powder spectra one obtains only the principal values of the tensor and not the orientation. Figure 1 illustrates a theoretical powder spectrum for an axially symmetric and axially asymmetric shift tensor. The theoretical analysis of these lineshapes has been dealt with elsewhere (*2, 3, 16*), and we simply note that one can obtain the principal values of the shift tensor directly from these spectra as shown in Figure 1. Figure 2 illustrates a series of ^{13}C powder spectra for a number of compounds containing carbonyl groups; in all of these compounds σ_{11} and σ_{33} are nearly identical, but σ_{22} moves from being equal to σ_{11} to being equal to σ_{33}. Thus, the reason that isotropic ^{13}C chemical shifts are different in these compounds is due to the fact that σ_{22} changes (*10*).

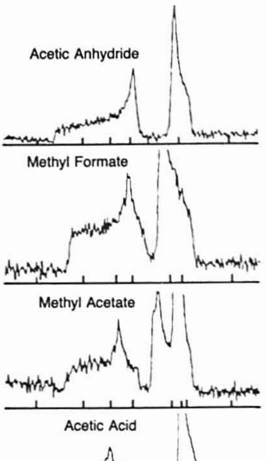

Figure 2. ^{13}C spectra of polycrystalline compounds containing carbonyl groups

Low field patterns from carbonyls, and high field from methyl groups. Temperatures: all ~77 K. Note sensitivity of σ_{22} to substituents. Horizontal axis calibrated in ppm relative to external C_6H_6 (23 °C)

Reprinted by permission of the American Institute of Physics

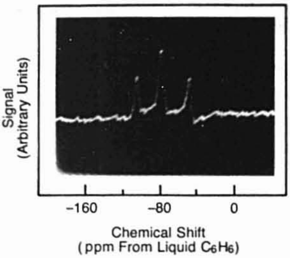

Figure 3. ^{13}C single crystal spectrum of AHOX taken with $C \perp \mathcal{H}_0$

Central line due to protonated carboxyl groups, and outer lines to ionic groups

Reprinted by permission of the American Institute of Physics

As mentioned above, a single crystal study is required for a complete determination of a chemical shift tensor. In such a study one measures line positions as the crystal is rotated in the magnetic field. Generally, three orthogonal crystal orientations are required. A typical ^{13}C spectrum of a single crystal of ammonium hydrogen oxalate hemihydrate (AHOX), $NH_4HC_2O_4 \cdot \frac{1}{2}H_2O$ (*17*), is shown in Figure 3. Rotation plots giving line position as a function of rotation angle for three different orientations are shown in Figure 4. The data of Figure 4 can be analyzed to yield not only the principal values of the shift tensor, but also its orientation in the molecular frame. Figure 5 illustrates the tensor orientations for the two different $—CO_2^-$ groups in AHOX. For the ionized CO_2 the σ_{11} element is almost along the C—C bond, but for the protonated CO_2, σ_{11} is rotated about 24° around σ_{33}, which is perpendicular to the O—C—O plane, so that σ_{22} is almost parallel to the C=O. The movement of the σ_{22} toward the C—O direction with increasing double bond character has been observed in a number of cases. In summary, then, we see that the reason carboxyl and carbonyl shifts are different in high resolution liquid spectra is that σ_{22} changes, and

measure
surface area,
pore structure
and do
chemisorption
studies

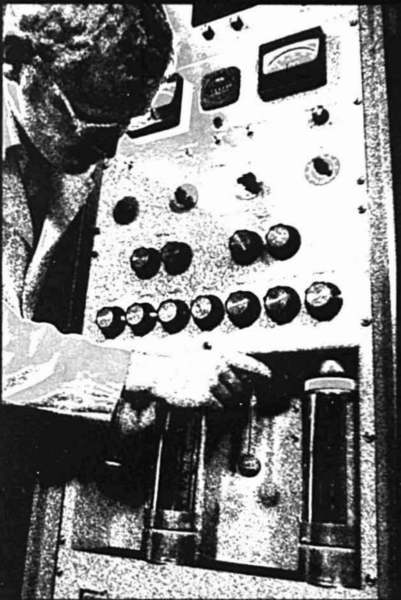

. . . characterizations of vital importance in determining the behavior of many materials and processes . . . with one of the quality instruments from Micromeritics, leader in the field of classical gas-adsorption analysis.

The instruments in our line range from a low cost, high-speed analyzer for process and quality control to the totally automated versatile system, capable of the most sophisticated R&D analyses.

We invite you to see why we're first in gas adsorption instruments. Ask for our literature package.

micromeritics®
instrument corporation
5680 goshen springs rd. • norcross, georgia 30093
U.S.A. • telephone: 404/448-8282 • telex: 70-7450

CIRCLE 140 ON READER SERVICE CARD

Unattended HPLC

Up to 192 injections
Up to 64 samples
Automatically . . .

- Microprocessor operation controls injections per sample, injection time, rinse between samples and automatic shutdown.
- Positive flow design requires only 0.75 ml of sample, allows precise, reproducible sample volumes.
- Adaptable to any HPLC pumping unit — can be externally controlled by computer integrator.

. . . with the model 725 automatic injector for HPLC

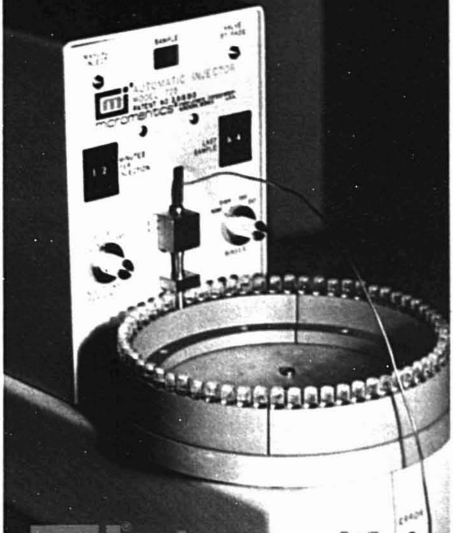

micromeritics®
instrument corporation
5680 goshen springs rd. • norcross, georgia 30093
U.S.A. • telephone: 404/448-8282 • telex: 70-7450

CIRCLE 141 ON READER SERVICE CARD

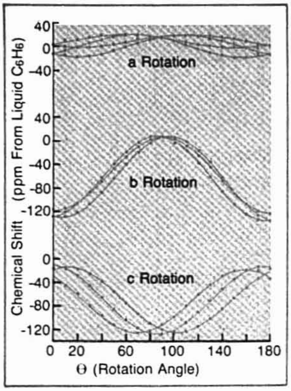

Figure 4. Rotation plots of AHOX obtained by rotating crystals about a, b, and c axes of unit cell

Reprinted by permission of the American Institute of Physics

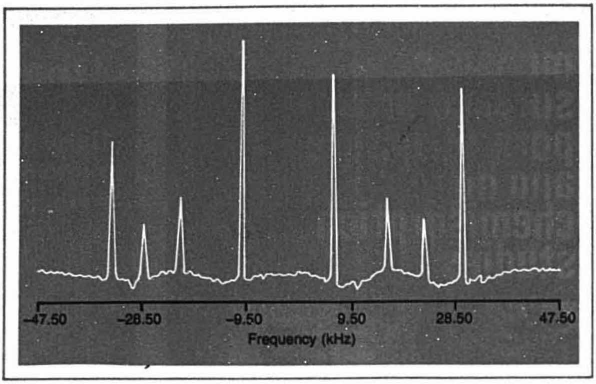

Figure 6. ^{14}N spectrum of NH_4^+ ions in AHOX

Despite 99.4% abundance of ^{14}N, lines are ~300 Hz full width. In other crystal orientations splittings reach ~500 kHz. C axis, 60°. $\nu_{^{14}N} = 21.200$ MHz

Reprinted by permission of the American Institute of Physics

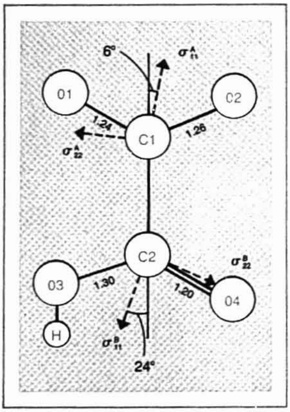

Figure 5. Schematic representation of AHOX molecule illustrating orientation of ionic and protonated carboxyl tensors

σ_{33} elements of both tensors perpendicular to plane of page (O—C—O plane)

Reprinted by permission of the American Institute of Physics

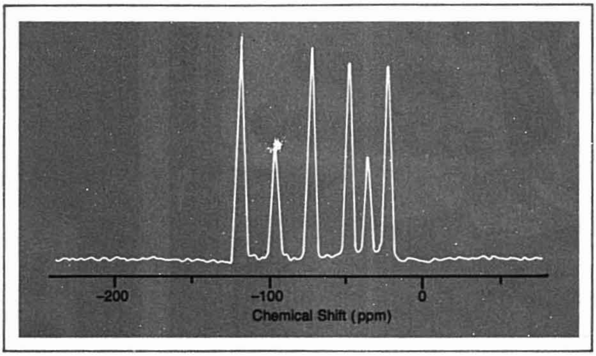

Figure 7. ^{13}C dipolar spectrum of DAOX

Weak lines due to 1.1% natural abundance ^{13}C; doublets centered around natural abundance lines due to ^{13}C—^{13}C dipolar splittings

concurrent with the change in σ_{22} is a change in the tensor orientation.

As data accumulate on shift tensors, trends such as were observed for —CO_2 groups are beginning to emerge. For instance, in aromatic carbons σ_{33} is always perpendicular to the aromatic ring (*18, 19*); in C═C tensors, σ_{22} is along the C═C direction (*20*). In PO_4 groups, σ_{11} is approximately perpendicular to the O—P—O plane formed by the shorter of the two P—O bonds, and σ_{22} approximately bisects the O—P—O angle (*21, 22*).

This invariance of shift tensors could be employed in structural studies. Perhaps the greatest potential lies in studies of disordered systems—liquid crystals (*23*), polymers (*24*)—where diffraction techniques yield only limited information.

Quadrupolar Tensors. Although nuclear quadrupole spectra in solids have been studied for many years with pure quadrupole resonance and conventional NMR techniques (*25, 26*), there are advantages to examining these nuclei by the techniques outlined in Section I. First, decoupling of abundant spins yields more well-resolved spectra. In addition, spins with $I \geq 1$ generally possess low gyromagnetic ratios; consequently, cross polarization and Fourier transform techniques are very helpful in obtaining the spectra. From the scientific point of view, the quadrupole interaction confers the advantage of increased resolution. For instance, quadrupole couplings for ^{2}H and ^{14}N are 10^5 and 10^5–10^6 Hz, respectively. With 10^2 Hz linewidths, this yields a resolution of 10^{-3}–10^{-4}, which compares favorably with resolution obtained in ^{13}C spectra of liquids at superconducting fields. This is illustrated in Figure 6 which is a typical spectrum of the $^{14}NH_4^+$ ions in a single crystal of AHOX (*27*). This spectrum was obtained in a crystal orientation where the lines were all within the 100-kHz spectral window of our spectrometer, but in a general orientation the splittings reach 500 kHz. The linewidths here are ~300 Hz full width, and the two sets of four strong and weak lines correspond to the two differently hydrogen-bonded $^{14}NH_4^+$ ions in the crystal lattice. The intensity difference arises because we were recycling

Chromatography News:

LDC Model 308
Computing Integrator

Sorry to have to tell you this, but your low cost computing integrator is already out of date.

Here's big news. LDC has developed a new microprocessor-based integrator so technologically advanced that it does remarkable things no other unit can. And all for $2,790. Just compare these exclusive features. You will recognize that they have been designed by chromatographers for chromatographers.

Continuous visual display of run progress. A real time display of operating mode by front panel mimic and LED always before your eyes.

Five baseline handling features. Including completely automatic correction of rising and falling baselines.

Built-in diagnostic center. Self testing de-bug programs permanently built into the memory.

Simplest unit in the world to service. Eliminates the most annoying complications of service and maintenance.

Permanent inked printer. No ribbons to change—ever.

Vertical design. Saves bench space.

Highly reproducible results. Achieves new levels of repeatable accuracy.

These are only the highlights. Send for the brochure, and see what a computing integrator can now offer you.

LABORATORY DATA CONTROL
Division of Milton Roy Co.
P.O. Box 10235, Riviera Beach, Fl. 33404
305/844-5241 Telex 513479

Send me the brochure describing the new Model 308 Computing Integrator. 141

Name ____________________

Address ____________________

Institution ____________________

City ____________________

State ____________ Zip ________

CIRCLE 127 ON READER SERVICE CARD

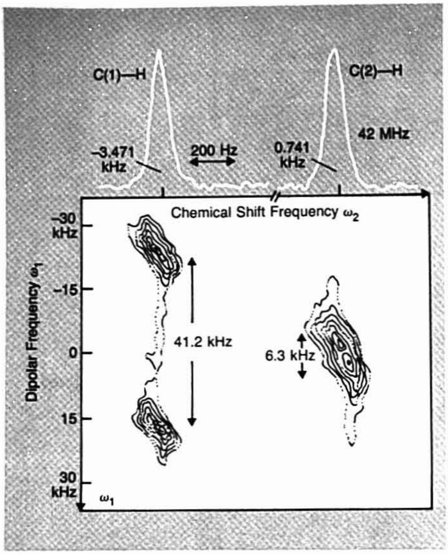

Figure 8. Two-dimensional local field spectrum of $Sr(HCO_2)_2 \cdot 2H_2O$

In this orientation C(1)—H and C(2)—H bonds make angles of $\theta_1 = 3.7°$ and $\theta_2 = 62.0°$ with $\mathcal{H}_0$, respectively; thus, C—H dipolar splittings are 41.2 and 6.3 kHz, respectively

Reprinted by permission of the American Institute of Physics

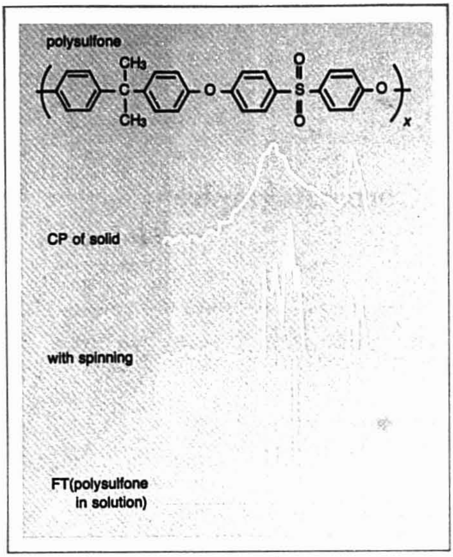

Figure 9. ^{13}C NMR spectra of polysulfone

Top: ^{13}C shift anisotropy powder spectrum obtained with dilute spin double resonance. Middle: ^{13}C spectrum obtained with double resonance and MASS. Bottom: Normal FT spectrum of polysulfone in solution

the experiment at a rate $\sim 1/T_1$. Because ^{14}N is 99.4% abundant one can obtain spectra like Figure 6 in a few minutes of signal averaging. To date, there have been only a few high resolution solid state studies of quadrupolar nuclei, but this promises to be a growing field of research. With these species one should be able to examine disorder and rates and mechanisms of molecular motion in single crystals; because the signal-to-noise is good, one can think of studying single crystals of relatively large molecules to partially determine their structure. Finally, we mention that elegant double quantum experiments may be used to decouple quadrupolar species from $I = ½$ nuclei—for instance, ^2H from ^1H (*28*)—and also to remove the quadrupolar interaction (*29*).

Dipolar Tensors. Early in the development of NMR, Pake (*30*) showed that dipolar splittings in NMR spectra would yield internuclear distances and directions. However, except in special cases, the multitude of such splittings led to an unresolved spectrum, and this approach quickly fell into disrepute. Today, with the development of high resolution solid state techniques, this type of experiment is again attractive as the spectrum of Figure 7 demonstrates. This spectrum is a ^{13}C single crystal spectrum of diammonium oxalate monohydrate (DAOX), $(NH_4)_2C_2O_4 \cdot H_2O$, which contains ~5 mol % doubly ^{13}C labeled oxalate ions, e.g., $^{13}CO_2$–$^{13}CO_2$. In the DAOX crystal lattice the oxalate molecule is nonplanar, i.e., the O—C—O planes are twisted by 28° with respect to one another (*31*). Consequently, the two ends of the molecule have different chemical shifts. Thus, the two weak lines in the spectrum are due to the two differently oriented 1.1% natural abundance CO_2 groups in the crystal. The four strong lines are due to the doubly enriched oxalate moieties and show dipolar splittings because each ^{13}C is adjacent to another. Thus, a study of the angular dependence of this splitting will yield the internuclear C—C distance and direction in the unit cell (*32*). Other examples of dipolar splittings which have been observed are ^{14}N splittings in ^{13}C spectra of glycine (*33*) and $K_2Pt(CN)_4Br_{0.3} \cdot 3H_2O$ (*34*), and ^{19}F splittings in ^1H spectra of KHF_2 (*35*). It is also possible to observe ^1H splittings in ^{13}C spectra and thus to determine C—H distances and directions, with an experiment which combines multiple pulse and dilute spin double resonance techniques. We discuss this hybrid experiment below.

Motion in Solids. One of the most exciting developments in high resolution NMR of liquids was the discovery that one could study rates and mechanisms of fast inter- and intramolecular chemical reactions in solution (*36*). High resolution solid state techniques permit examination of similar phenomena in solids. Specifically, they allow determinations of rates of anisotropic molecular motion, and they provide detailed information on the mechanisms of such motion. In early studies it was shown that benzene rings reoriented about their C_6 axis (*12*) and that $—CF_3$ groups rotated rapidly about their C_3 axis (*13*) in the solid. At that time it was assumed that this motion was continuous. More recent work has demonstrated the fact that molecules execute stepwise rather than continuous motion. For instance, P_4 tetrahedra jump by 109° steps (*37*), and benzene rings move by 60° steps (*38*). Similarly, water molecules execute 180° flips about the H—O—H bisector (*39*). Since motion in the solid state must reflect the symmetry of the lattice, one might, after a moment's thought, find these results not terribly surprising. Nevertheless, the NMR spectra provide rather convincing evidence of the discrete nature of the motions. Thus, observation of motionally averaged magnetic resonance tensors can provide detailed information on dynamic processes in solids.

How to recognize "Labelia Dementia" and what to do about it.

Labelia Dementia. A serious nervous disorder peculiar to laboratory workers who do a great deal of labeling. Especially in labs with makeshift labeling systems.

If you work in a laboratory and you label apparatus of any kind, chances are you suffer from this nervous disorder.

Danger signals to watch for:

Severe avoidance complex. Often appears in the form of charley horses in hand or going to important speeches by Orson Bean.

Five thumb syndrome. Usually the first indication of terminal dementia. Develops from working with separate tape, labels and dispensers.

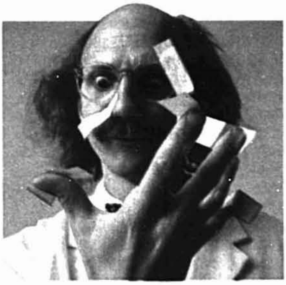

Rash outbursts of temper. Awkward labeling systems, combined with internal and external pressures, often cause violent reactions.

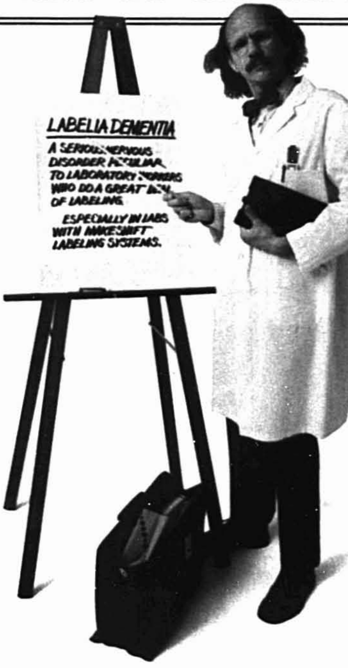
LABELIA DEMENTIA
A SERIOUS NERVOUS DISORDER PECULIAR TO LABORATORY WORKERS WHO DO A GREAT DEAL OF LABELING.
ESPECIALLY IN LABS WITH MAKESHIFT LABELING SYSTEMS.

Warning. Do not force Labelia Dementia sufferers to do labeling under any circumstances.

How to treat Labelia Dementia:

Treating the symptoms. Get a new job.

Treating the disease. Get a new labeling system, the most direct and successful treatment for Labelia Dementia.

Get a system with everything in one compact unit. Labels, protective tape, dispenser.

A system that works with one hand just as easily as two or three.

A system that's fast. And either portable or permanent.

A system that works. On all your apparatus. Under the worst conditions ever devised by science.

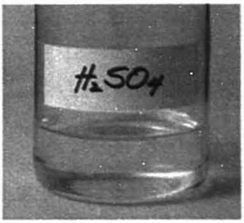

Get The System by 3M Laboratory Products. Circle our number on the return card for more information.

3M COMPANY

CIRCLE 201 ON READER SERVICE CARD

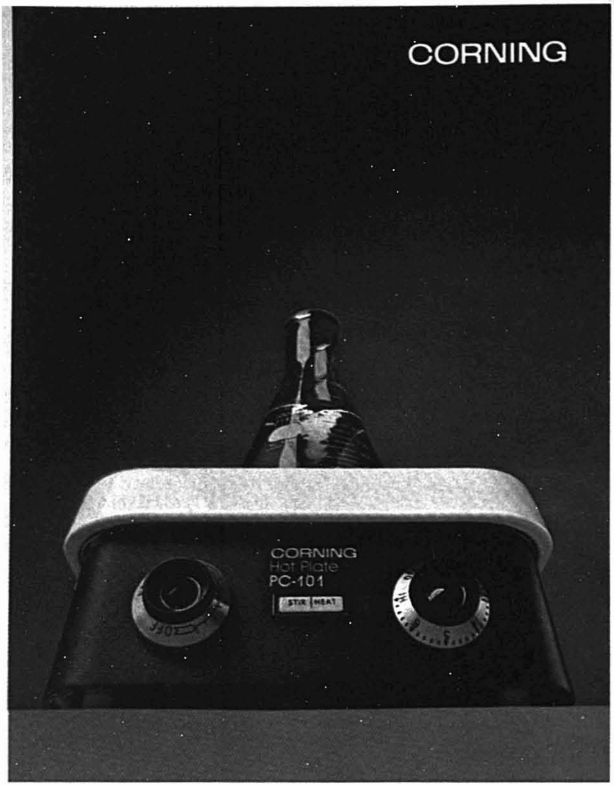

BIG TOP CREATES BIG STIR

- 100 SQUARE INCH TOP. NOW WITH STIRRER.
- Stirs 100 to 900 r.p.m. With or without heat.
- 10" x 10" surface. Holds big vessels.
- Fast, accurate heat. Fast heat-up. Fast cool-down.
- Overhang protects insides.
- PYROCERAM® glass-ceramic top. Inert. Impervious. Stays white.
- Nylon feet. Very quiet. Very smooth.
- Infinite variable control. LO to HI.
- Big, easy-to-read knobs.

NEW HOT PLATE/STIRRER, MODEL PC-101. Order from your distributor. Or call or write for the name of the distributor nearest you: 607-974-4126. Science Products Division, Corning Glass Works, Corning, New York 14830

CORNING®
hotware

CIRCLE 36 ON READER SERVICE CARD

III. Hybrid Experiments

In the last year or two, several experiments have been performed which combine multiple pulse, magnetic dilution, and MASS in very effective and interesting fashions. Recently, Hester et al. (*40*) and Stoll et al. (*41*) demonstrated that C—H dipolar couplings, and thus C—H distances and directions, can be obtained by combining multiple pulse and dilute spin double resonance. In this experiment one first cross polarizes and then performs a WAHUHA or MREV-8 (*2, 3*) multiple pulse experiment on the protons for some variable time τ. During this time the protons in the lattice are decoupled from one another but not from the ^{13}C's. Following this period is a second period, t, where the protons are decoupled from the ^{13}C and the free induction decay is recorded. Next, a double Fourier transform is performed as a function of t and τ to yield the dipolar split chemical shift spectrum. A typical two-dimensional spectrum of a single crystal of $Sr(CHO_2)_2 \cdot 2H_2O$ is shown in Figure 8; this spectrum can be analyzed to obtain C—H distances and directions (*42*). Thus far, this technique has been used to locate ^1H positions in Ca formate and Sr formate (*40, 42*), C_6H_6 (*41, 43*), ammonium hydrogen malonate (*42*), and, tetramethylcyclobuta-1,3-dione (*42*).

The second hybrid experiment, and possibly the most generally useful from an analytical point of view, combines MASS and dilute spin double resonance. This technique, first demonstrated by Schaefer and Stejskal (*44*), utilizes high power decoupling to remove proton dipolar interactions. At low fields and/or high spinning rates, MASS reduces shift anisotropy powder patterns to single "high resolution" lines. A spectrum that illustrates this for the polymer polysulfone is shown in Figure 9. At high fields where the shift anisotropy is large compared to the spinning rate, the lines still narrow but sidebands appear in the spectra (*45*). From a strict high resolution standpoint, these sidebands are annoying, and a clever technique involving synchronous sampling can be used to remove them (*46*). However, the intensity of the sidebands and their number contain information on the shift anisotropy and are thus potentially an important analytical tool (*45*). In summary, we see that with MASS and double resonance, one can potentially obtain a high resolution NMR spectrum of an arbitrary powder sample. Thus, this technique should be useful for studying a number of systems such as polymers which cannot be crystallized or otherwise

made to yield a "high resolution" NMR spectrum.

IV. Conclusions

One often hears the NMR spectroscopist use the phrase "everything is in Abragam" (*47*), but this is not quite true. The last decade has witnessed the development of high resolution NMR techniques for studying solids, and consequently, the opening of several new avenues of scientific research. The idea of averaging in "spin space" in the rotating frame permits observation of high resolution spectra of strongly coupled spin systems in solids, e.g., ^{1}H and ^{19}F. The simple approach of magnetic dilution, either isotopic or chemical dilution, together with decoupling, allows observation of spectra of many other nuclear species. The information such spectra provide on the anisotropy of magnetic interactions should form the basis for a better understanding of the quantum chemical aspects of magnetic shielding, and it should also be useful for examining structure and dynamics in the solid state. For example, knowledge of the molecular orientation of chemical shift and quadrupole coupling tensors can be used to interpret the NMR spectra of ordered and disordered systems to provide information on molecular structure. Data on bond distances and directions can be had rather easily from dipolar splittings, and we have seen such splittings are observable when dilute spin pairs are present and in hybrid multiple pulse–double resonance experiments. Dynamic processes in solids can be examined by observing motionally average magnetic resonance tensors. To date there has been only a handful of such experiments; nevertheless, they have demonstrated rather convincingly the discrete rather than continuous nature of molecular reorientation. Finally, by combining MASS with magnetic dilution, it is possible to obtain narrow line spectra of powdered samples. Although this hybrid approach to high resolution in solids is still being developed, it shows promise of becoming a powerful analytical tool for studying amorphous, sparingly soluble, or otherwise intractable solid samples.

References

(1) R. R. Ernst and W. A. Anderson, *Rev. Sci. Instrum.*, **37**, 93 (1966).
(2) U. Haeberlen, "Advances in Magnetic Resonance", Suppl. 1, Academic Press, New York, N.Y., 1976.
(3) M. Mehring, "NMR—Basic Principles and Progress", Vol 11, Springer, New York, N.Y., 1976.
(4) E. R. Andrew, *Prog. Nucl. Magn. Reson. Spectrosc.*, **8**, 1 (1971).
(5) I. J. Lowe, *Phys. Rev. Lett.*, **2**, 285 (1959).

THE TALL METERS
ORIGINATED BY CORNING

Tall to look you in the eye and save space.

A new generation of pH meters from a wedding of bioengineering and solid state of the art electronics. Digital display on top where your eyes are. Controls down the side where your hands are. Flexing sidearm to take electrodes where the work is. Mounts left side or right.

I-C chips. Single circuit board. Cool, energy-saving LED display. U/L and CSA listings.

Even the back is all up front. Everything orderly and easy to get at.

Tall and lean, including the price. Even with a general-purpose pH and a reference electrode thrown in, they cost less than comparable short meters.

At your Corning dealer.

2 and 3 decimal models.

THREE YEAR WARRANTY
THAT'S HOW RELIABLE THE TALL ONES ARE

Corning Glass Works warrants pH meters Model 125 and Model 130 to be free from defects in material and workmanship when used under normal laboratory conditions for a period of three (3) years.

CORNING™
pHware

CIRCLE 37 ON READER SERVICE CARD

Drug Metabolism Concepts

ACS Symposium Series No. 44

Donald M. Jerina, *Editor*
The National Institutes of Health

A symposium co-sponsored by the Division of Medicinal Chemistry and the Division of Analytical Chemistry of the American Chemical Society.

Eight chapters present in-depth research reports on the role of enzyme systems, especially cytochrome P-450, in drug activation and detoxification. This timely study on drug metabolic pathways is vital because of the possibilities of toxic or carcinogenic intermediates caused by the action of enzymes on drugs and anesthetics.

CONTENTS

Cytochrome P-450 in Oxygen Activation for Drug Metabolism • Synthetic Models for the Reaction Stages of Cytochrome P-450 • Isolation of Mutiple Forms of Liver Microsomal Cytochrome P-450 • Resolution of Multiple Forms of Rabbit Liver Cytochrome P-450 • Enantiomeric Selectivity and Perturbation of Product Ratios as Methods for Studying the Multiplicity of Microsomal Enzymes • Purified Cytochrome P-448 and Epoxide Hydrase in the Activation and Detoxification of Benzo[*a*]pyrene • In vitro Reactions of the Diastereomeric 9,10-Epoxides of (+) and (−)-*trans*-7,8-Dihydroxy-7,8-dihydrobenzo[*a*]pyrene with Polyguanylic Acid • Metabolic Activation in Chemical-Induced Tissue Injury

196 pages (1977) clothbound $15.50
LC 77-2279 ISBN 0-8412-0370-9

SIS/American Chemical Society
1155 16th St., N.W./Wash., D.C. 20036

Please send ________ copies of *SS 44 Drug Metabolism Concepts* at $15.50 per copy.

☐ Check enclosed for $ ________. ☐ Bill me. Postpaid in U.S. and Canada, plus 40 cents elsewhere.

Name ________

Address ________

City ________ State ________ Zip ________

(6) E. R. Andrew, A. Bradbury, and R. G. Eades, *Nature*, **183**, 1802 (1959).
(7) E. R. Andrew, L. F. Farnell, M. Firth, T. D. Gledhill, and I. Roberts, *J. Magn. Reson.*, **1**, 27 (1969).
(8) a) E. D. Osteroff and J. S. Waugh, *Phys. Rev. Lett.*, **16**, 1097 (1966); b) P. Mansfield and D. Ware, *Phys. Lett.*, **22**, 133 (1966).
(9) J. S. Waugh, L. M. Huber, and U. Haeberlen, *Phys. Rev. Lett.*, **20**, 180 (1968).
(10) A. Pines, M. Gibby, and J. S. Waugh, *J. Chem. Phys.*, **59**, 569 (1973).
(11) S. R. Hartmann and E. L. Hahn, *Phys. Rev.*, **128**, 2042 (1962).
(12) H. E. Bleich and A. Redfield, *J. Chem. Phys.*, **55**, 5405 (1971); P. K. Granell, P. Mansfield, and M.A.B. Whitaker, *Phys. Rev.*, **B8**, 4149 (1973).
(13) M. Mehring, R. G. Griffin, and J. S. Waugh, *J. Am. Chem. Soc.*, **92**, 7222 (1970); *J. Chem. Phys.*, **55**, 746 (1971).
(14) L. M. Stacey, R. W. Vaughan, and D. D. Elleman, *Phys. Rev. Lett.*, **26**, 1153 (1971).
(15) R. G. Griffin, J. D. Ellett, M. Mehring, and J. S. Waugh, *J. Chem. Phys.*, **57**, 2147 (1972).
(16) N. Bloembergen and T. J. Rowland, *Phys. Rev.*, **97**, 1679 (1955).
(17) R. G. Griffin and D. J. Ruben, *J. Chem. Phys.*, **63**, 1272 (1975).
(18) S. Pausak, A. Pines, and J. S. Waugh, *ibid.*, **59**, 591 (1973).
(19) S. Pausak, J. Tegenfeldt, and J. S. Waugh, *ibid.*, **61**, 1338 (1974).
(20) E. K. Wolff, R. G. Griffin, and J. S. Waugh, Proceedings XIXth Ampere Congress, Heidelberg, Germany, Sept. 1976.
(21) S. Kohler and M. P. Klein, *Biochemistry*, **15**, 967 (1976).
(22) J. Herzfeld, R. G. Griffin, and R. Haberkorn, *Biochemistry*, submitted for publication.
(23) A. Pines and J. J. Chang, *Phys. Rev. A*, **10**, 946 (1974); *J. Am. Chem. Soc.*, **96**, 3391 (1974); A. Pines, D. J. Ruben, and S. Allison, *Phys. Rev. Lett.*, **33**, 1002 (1974).
(24) D. L. Vander Hart, *J. Magn. Reson.*, **24**, 467 (1976).
(25) M. H. Cohen and F. Reif, "Solid State Physics, Quadrupole Effects in Nuclear Magnetic Resonance Studies in Solids", Vol 5, p 321, Academic Press, New York, N.Y., 1958.
(26) T. P. Das and E. L. Hahn, "Solid State Physics, Nuclear Quadrupole Resonance Spectroscopy", Suppl. 1, Academic Press, New York, N.Y., 1958.
(27) E. K. Wolff, R. G. Griffin, and C. Watson, *J. Chem. Phys.*, **66**, 5433 (1977).
(28) A. Pines, D. J. Ruben, S. Vega, and M. Mehring, *Phys. Rev. Lett.*, **36**, 110 (1976).
(29) S. Vega, T. W. Shattuck, and A. Pines, *ibid.*, **37**, 43 (1976).
(30) G. E. Pake, *J. Chem. Phys.*, **16**, 327 (1948).
(31) J. H. Robertson, *Acta Crystallogr.*, **18**, 410 (1965).
(32) H. van Willigen, R. Haberkorn, and R. G. Griffin, *J. Chem. Phys.*, to be published.
(33) R. G. Griffin, A. Pines, and J. S. Waugh, *ibid.*, **63**, 3676 (1975).
(34) M. E. Stoll, R. W. Vaughan, R. B. Saillant, and T. B. Cole, *ibid.*, **61**, 2896 (1974).
(35) P. Van Hecke, H. W. Spiess, U. Haeberlen, and S. Hannssühl, *J. Magn. Reson.*, **22**, 93 (1976).
(36) For a review of this subject, see C. S. Johnson, Jr., *Adv. Magn. Reson.*, **1**, (1965).
(37) H. W. Spiess, *Chem. Phys.*, **6**, 217 (1974); H. W. Spiess, R. Grosescu, and U. Haeberlen, *ibid.*, p 226.
(38) D. J. Ruben and A. Pines, to be published; see also Chap. 2 of ref. *3*.
(39) H. van Willigen, R. Haberkorn, and R. G. Griffin, *J. Chem. Phys.*, to be published; G. Soda and T. Chiba, *ibid.*, **50**, 434 (1969); J. W. McGrath and G. W. Ussman, *ibid.*, **46**, 1824 (1967).
(40) R. K. Hester, J. L. Ackerman, B. Neff, and J. S. Waugh, *Phys. Rev. Lett.*, **36**, 1081 (1976); J. S. Waugh, *Proc. Nat. Acad. Sci. USA*, **73**, 1394 (1976).
(41) M. E. Stoll, A. J. Vega, and R. W. Vaughan, *J. Chem. Phys.*, **65**, 4093 (1976).
(42) E. F. Rybaczewski, B. L. Neff, J. S. Waugh, and J. S. Sherfinski, *ibid.*, submitted for publication.
(43) R. K. Hester, V. R. Cross, J. L. Ackerman, and J. S. Waugh, *ibid.*, **63**, 3606 (1975).
(44) J. Schaefer and E. D. Stejskal, *J. Am. Chem. Soc.*, **98**, 1031 (1976).
(45) E. Lippma, M. Alla, and T. Tuhern, Proceedings XIXth Coll. Ampere, Heidelberg, Germany, Sept. 1976.
(46) M. Maricq and J. S. Waugh, *Chem. Phys. Lett.*, **47**, 327 (1977).
(47) A. Abragam, "Principles of Nuclear Magnetism", Oxford Univ. Press, Oxford, England, 1961.

The Francis Bitter National Magnet Laboratory is supported by the National Science Foundation.

R. G. Griffin

With all the spectrophotometers on the market, how do you choose your next one? **Ask yourself questions like these and draw your own conclusions.**

If you want to change from enzyme kinetics to thermal melts, from scanning wavelength to scanning gels, from sucrose gradient studies to column chromatography, etc, do you have to change spectrophotometers too? Maybe use your neighbor's instrument and (especially if it's a Gilford) stand in line? **Our Model 250 accommodates a variety of sample handling systems, and its unrestricted sample space even lets you design your own special-purpose devices. That tells you something about versatility.**

How important are the critical areas of measurement? The low UV, the dense sample, operation with flow-through or microcuvettes? **Model 250's throughput is exceptional; the proof lies in an absorbance range 50% greater than most (3*A* instead of 2*A*) and in sensitivity to 0.0001*A*. That also tells you something about routine performance.**

Which spectrophotometer is used to check questionable results from other instruments? **With Model 250's wavelength and absorbance standards directly traceable to NBS, verification of results is easy. That tells you something about accuracy.**

What's the oldest UV-VIS spectrophotometer still in use in your building? **There's every chance that it's a Gilford; and if so, there's also a good chance that it's using an accessory or two not listed on the original order. That tells you something about durability.**

Versatility, performance, accuracy, and durability: *that tells you something about Gilford.* As we see it, you have but two choices when it comes time to select your spectrophotometer:

you can shop for price
or you can shop for value.

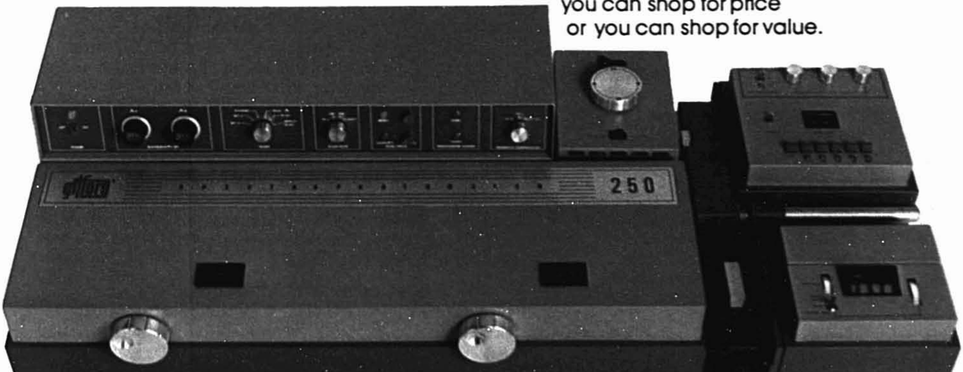

The Gilford Model 250: All the spectrophotometer you will ever need.

For information call or write
Gilford Instrument Laboratories Inc, Dept. 7-9-16
Oberlin OH 44074 (216) 774-1041.

CIRCLE 84 ON READER SERVICE CARD

gilford®
INSTRUMENT

Oberlin, Ohio 44074
Paris (Malakoff), France
Düsseldorf, W. Germany
Teddington, Middx., England
(216) 774-1041 Telex: 98-0456

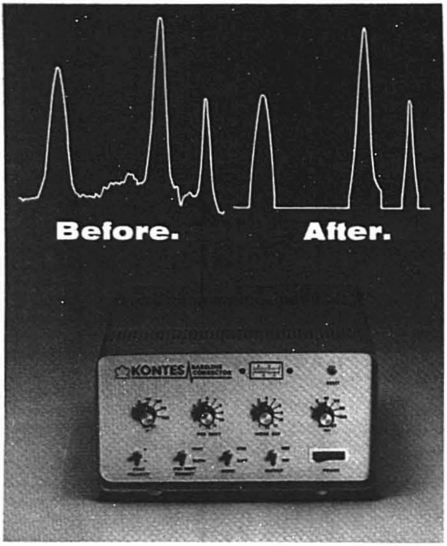

Dial out baseline drift and noise.

Our new and unique Kontes Baseline Corrector can modify the output signal from an analytical instrument and compensate for electronic drift, background noise, or other stray electronic signals.

The resultant clean, corrected baseline can then be reduced to significant data by means of a standard chart recorder, digital integrator, or other EDP hardware.

Specially designed solid-state circuitry in our Baseline Corrector permits a broad range of sensitivity adjustment and a high degree of baseline determination accuracy.

Dial out drift and noise and dial in accuracy and reproducibility. Baseline Corrector complete, ready for hook-up $925.

For more details or a demonstration, contact your Kontes representative or send for Bulletin K-21.

KONTES
Vineland, N.J. 08360

Exclusive Distributors: **KONTES OF ILLINOIS**, Evanston, Illinois
KONTES OF CALIFORNIA, San Leandro, California
KONTES (U.K.) LTD., Carnforth, England

CIRCLE 114 ON READER SERVICE CARD

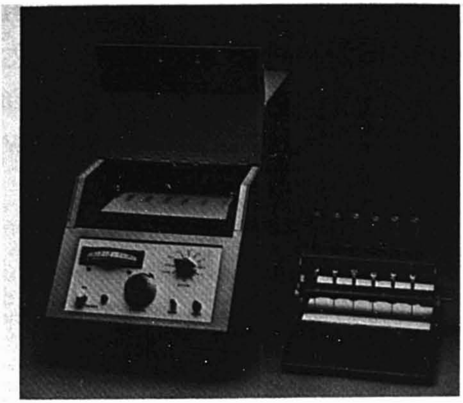

Patented and proven. The Kontes low-cost, quantitative TLC system.

Here is the proven Kontes system that offers high resolution, quantitative TLC analysis at low cost.

The brain of the system is the unique and patented Kontes Densitometer*[1]. It utilizes a rugged and highly reliable fiber optic scanner to create outputs compatible with all conventional data processing. It features single or double beam scanning in four modes—diffused reflectance, visible transmission, flourescence, and flourescence quenching. The densitometer sells for $2875 in U.S.

Our air-manifold Chromaflex® Spotter**[2] is the heart of the system. It consistently makes uniformly-sized spots on all standard TLC plates. Up to 2 ml of solvent extract can be spotted to a controlled diameter of 6mm or less with a reproducibility of ±2%. The Chromaflex Spotter sells for $150 in U.S.

In combination, our densitometer and spotter afford reproducible, quantitative analysis at a cost unmatched by other methods. The practicality of the Kontes system is documented by a bibliography of applications and a comprehensive manual.

For further information contact your Kontes representative or send for our detailed literature.

1. *U.S. Patents 3,562,539 and 3,924,948. "Determination of Reflectance of Pesticide Spots on Thin-Layer Chromatograms, Using Fiber Optics", Morton Beroza, K. R. Hill, Karl H. Norris, ANALYTICAL CHEMISTRY, September 1968.
2. "An automatic spotter for quantitative thin layer and paper chromatographic analysis by optical scanning", Melvin E. Getz, Journal of the AOAC, Volume 54, No. 4, 1971. **U.S. Patent 3,843,053

KONTES
Vineland, N.J. 08360

Exclusive Distributors: KONTES OF ILLINOIS, Evanston, Ill. • KONTES OF CALIFORNIA, San Leandro, Calif.
KONTES (U.K.) LTD., Carnforth, England

CIRCLE 113 ON READER SERVICE CARD

ANALYTICAL CHEMISTRY 1977

Enter your personal subscription to the foremost publication in the vital fields of chemical analysis. Treats both theoretical and applied aspects of analysis. Subscription includes "ANNUAL REVIEWS" and "LAB GUIDE" issue. Published monthly.

	U.S.	CANADA	PUAS	**OTHER NATIONS
*ACS Members	☐ $ 9.00	☐ $18.00	☐ $17.00	☐ $18.00
Nonmembers	☐ $12.00	☐ $21.00	☐ $23.00	☐ $24.00

☐ Payment enclosed *(Payable to American Chemical Society).* ☐ Bill me ☐ Bill company

Name ______________________ Position ______________

Your Employer ______________________________

Address ☐ Home

☐ Business ______________________________

City ______________ State __________ Zip ______

Employer's Business: ☐ Manufacturing ☐ Government ☐ Academic ☐ Other __________

If Manufacturer, Type of Products Produced ______________

Allow 60 days for your first copy to be put in the mail.
*NOTE: Subscriptions at ACS member rates are for personal use only. **Payment must be made in U.S. currency, by international money order, UNESCO coupons, U.S. bank draft; or order through your book dealer.

Formula
for a better tomorrow...

THE PUBLICATIONS
OF THE
AMERICAN CHEMICAL SOCIETY

FIRST CLASS
Permit No. 1411-R
Washington, D.C.

BUSINESS REPLY MAIL
No postage stamp necessary if mailed in the United States

Postage will be paid by

AMERICAN CHEMICAL SOCIETY
1155 Sixteenth Street, N.W.
Washington, D.C. 20036

ATTN: G. HEBRON

analytical
chemistry

Editor: **Herbert A. Laitinen**

EDITORIAL HEADQUARTERS
1155 Sixteenth St., N.W.
Washington, D.C. 20036
Phone: 202-872-4570 Teletype: 710-8220151

Managing Editor: Josephine M. Petruzzi
Associate Editor: Andrew A. Husovsky
Associate Editor, Easton: Elizabeth R. Rufe
Assistant Editors: Barbara Cassatt, Nancy J. Oddenino, Deborah C. Stewart
Production Manager: Leroy L. Corcoran
Art Director: John V. Sinnett
Designer: Alan Kahan
Artist: Diane Reich

Advisory Board: Donald H. Anderson, Richard P. Buck, Velmer Fassel, David Firestone, Robert A. Hofstader, Marjorie G. Horning, Philip F. Kane, Barry L. Karger, J. Jack Kirkland, Lynn L. Lewis, Harry B. Mark, Jr., Walter C. McCrone, Harry L. Pardue, Eugene A. Sawicki, W. D. Shults

Instrumentation Advisory Panel: Gary D. Christian, Nathan Gochman, Robert W. Hannah, Gary Horlick, Peter J. Kissinger, James N. Little, Sidney L. Phillips, R. K. Skogerboe, Donald E. Smith

Contributing Editor: Claude A. Lucchesi
Department of Chemistry, Northwestern University, Evanston, Ill. 60201

Published by the
AMERICAN CHEMICAL SOCIETY
1155 16th Street, N.W.
Washington, D.C. 20036

Books and Journals Division
Director: D. H. Michael Bowen
Editorial: Charles R. Bertsch
Magazine and Production: Bacil Guiley
Research and Development: Seldon W. Terrant
Circulation Development: Marion Gurfein

Manuscript requirements are published in the April 1977 issue, page 686. Manuscripts for publication (4 copies) should be submitted to ANALYTICAL CHEMISTRY at the ACS Washington address.

The American Chemical Society and its editors assume no responsibility for the statements and opinions advanced by contributors. Views expressed in the editorials are those of the editors and do not necessarily represent the official position of the American Chemical Society.

International Participation in Scientific Meetings

The typical European scientific meeting is international in character, whereas most meetings in the U.S.A. have few, if any, foreign participants. The reason does not lie in a lack of appreciation by Americans of the contributions of their foreign colleagues, but rather in the practical difficulties of meeting the costs of travel. Granting agencies in the U.S.A. have for years provided at least a modest level of support for Americans to attend meetings in foreign countries, but our own meetings often tend to lack the proper international perspective because corresponding support is not available in other countries.

This brings up the question of what would be the most economical and efficient means of sponsoring increased numbers of foreign visitors. From the viewpoint of economy and maximum benefit, what is needed is usually just one or two specialists at each of a number of conferences rather than a large number at one or two meetings. A peer review would be needed both on the conference and the suggested participants. Such a peer review system appears so administratively cumbersome as to explain why it has not happened. Yet it would seem possible to set up a single program within an agency such as the National Science Foundation, open to competitive requests by the organizers of symposia for participation by specific foreign specialists. Reviewers could be called upon for peer judgments to assure quality and equitable distribution of allocations.

Whatever the details of procedure, most of our scientific meetings would benefit from increased participation by our colleagues from overseas. Communication of current progress by personal contact represents a largely intangible but nevertheless important stimulus to creative work, and its effectiveness should not be severely limited by geographical barriers.

H. A. Laitinen

Spectroscopic System for the Study of Fluorescent Lanthanide Probe Ions in Solids

Marvin P. Miller, David R. Tallant,[1] Frederick J. Gustafson, and John C. Wright*

Department of Chemistry, University of Wisconsin, Madison, Wisconsin 53706

It has recently been shown that lanthanide ions can be used as fluorescent probes for the study of the defects in solids and for qualitative and quantitative determinations of trace concentrations of foreign ions included in the lattice. A spectroscopic system based on a tuneable dye laser excitation source is described which is capable of selectively exciting the probe ions present in different crystallographic sites. Facilities for measuring the fluorescent lifetimes using signal averaging have been developed, in addition to a computer controlled system for obtaining excitation and absorption spectra simultaneously, called EXABS. The use of this system allows the determination of radiative quantum efficiencies and the calculation of absolute site concentrations. A knowledge of these physical parameters is essential for the development and refinement of a new analytical procedure, based on the effect of foreign ions on the site distribution and fluorescence intensity of the lanthanide ion probe. Thus, the instrument has been constructed with the capability to undertake a wide variety of spectroscopic experiments of either a fundamental or an analytical character.

The crystal field splittings of lanthanide ions can be used as fluorescent probes of the short range structure in their immediate vicinity when placed in an ordered environment. Since in any real sample of analytical interest the lanthanide ions may encounter many local environments, a practical system must discriminate between the fluorescence transitions of the probe ions present in different crystallographic sites. The key idea for providing the necessary discrimination is the use of a narrow-band, tuneable dye laser which can selectively excite fluorescence from specific sites. This technique has been used to provide new insights into a number of fundamental problems in the understanding of solid materials and has recently been used to perform trace analysis by selectively exciting probe ion luminescence (SEPIL) with very high analytical sensitivity and selectivity (*1*, *2*). In the SEPIL method, lanthanide ions are incorporated into crystalline lattices as fluorescent probes by a variety of techniques. The inclusion of other ions into the lattice perturbs the crystal field levels of nearby lanthanide ions which produces a site with different optical transitions. The intensity and wavelength position of the transitions can be used for quantitative and qualitative measurements of the included ion. Alternatively, trace lanthanide ion concentrations can be measured directly. The continuing development of this new technique, however, requires more than the ability to measure intensity as a function of wavelength or concentration which by themselves do not provide any insight into the physical mechanisms behind these observed intensities. It is also necessary to know the radiative quantum efficiencies, radiative and nonradiative relaxation rates and mechanisms, absorption coefficients, and site concentrations for all sites present in a sample. Thus the selective laser excitation technique must be modified to permit the measurement of these important quantities while retaining the ability to discriminate between sites. For this reason, a system has been developed which allows both the fundamental studies of the physical processes and the analytical determination of trace concentrations of a dopant lanthanide ion or an ion coprecipitated into the lattice.

Studies of single crystals of the fluorite structure materials used for the ultra-trace analysis of lanthanide ions have been investigated with this system to understand the mechanisms behind the site distributions and the intensities observed. In these materials, the trivalent rare earth ion replaces a divalent cation, thus requiring a charge compensation. The different configurations of the rare earth ion and its charge-compensating ion produce a number of distinct crystallographic sites. The use of this system has led to an understanding of the dependence of the nonradiative relaxation rate on the energy gap between adjacent electronic levels. Measurement of fluorescent lifetimes and radiative quantum efficiencies allows the selection of efficient fluorescence transitions for development of an analytical method. By using the narrow-band dye laser excitation source, the individual charge compensated crystallographic sites present in CaF_2, SrF_2, and BaF_2 have been identified (*3–5*), permitting the identification of these same sites in powder samples formed for analytical determinations. A study of absolute site concentrations for each site as a function of total dopant concentration has led to an understanding of the necessity to convert all dopant ions to a single site symmetry for analytical work to eliminate the complex site distribution equilibria among sites (*6*, *7*).

The purpose of this paper is to describe the apparatus and procedure that have been developed and used in both the fundamental and applied aspects of this research. The apparatus is complex and for that reason has not been discussed in the previous papers. A detailed description of the apparatus is important, however, in understanding the SEPIL technique. A basic outline of the necessary theory will be presented, followed by a detailed description of the experimental apparatus used. Data will be presented to demonstrate the type of spectra obtained with selective excitation and to illustrate the physical measurements that are possible.

THEORY

The fluorescence intensity of a spectroscopic probe ion is determined by the radiative quantum efficiency, which in turn is a function of the radiative and nonradiative processes that can allow relaxation from an excited state back to the ground state. The measured fluorescent lifetime of the excited state, τ_T, is determined by the sum of the radiative rate, ω_R, the vibrational relaxation rate between successive levels, ω_N, and the rate of energy migration to a sink, ω_M.

$$\frac{1}{\tau_T} = \omega_T = \omega_R + \omega_N + \omega_M \tag{1}$$

If the nonradiative quantum efficiency for relaxation between adjacent levels, f, is defined as the ratio of ω_N/ω_T, the radiative quantum efficiency, η becomes:

$$\frac{\omega_R}{\omega_T} = \eta = 1 - f - \frac{\omega_M}{\omega_T} \tag{2}$$

---

[1] Present address, Sandia Laboratories, Albuquerque, N.M. 87115.

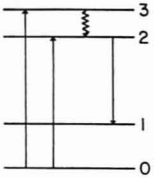

Figure 1. Diagram of the energy levels required for measurement of the efficiency of relaxation from level 3 → 2. The intensity of fluorescence from 2 → 1 is compared between direct excitation from 0 → 2 and indirect excitation from 0 → 3 followed by relaxation from 3 → 2

The quantity f can be measured directly by the EXABS system described later. A value for ω_M can be determined because it alone will show a dependence on the probe ion concentration. It therefore can be determined by measuring the total rate as a function of concentration and extrapolating to zero probe ion concentration.

For crystallographic sites consisting of a single ion, the relaxation rate between adjacent levels will result only from multiphonon relaxation because exciton migration and energy transfer can be neglected. If the site consists of two or more ions capable of nonradiative energy transfer steps which result in relaxation to a lower level and are competitive with the multiphonon relaxation, the determined rate will be a summation of the two nonradiative rates involved (*8*). Since the multiphonon rate is independent of site symmetry, the rate of energy transfer can be calculated by determining the total radiative rate and the nonradiative quantum efficiency for both single pair and dimer sites.

In order to understand the requirements for determining the nonradiative quantum efficiency, consider the example energy level diagram shown in Figure 1. If fluorescence is monitored from the 2 → 1 transition while exciting the 0 → 3 or 0 → 2 transitions, utilizing the ideas of Partlow and Moos (*9*), the fluorescence intensity for these two cases can be described by:

$$I_2(2) = \frac{P(2)}{h\nu_2}\alpha_2\eta_{21}\Omega \tag{3}$$

$$I_2(3) = \frac{P(3)}{h\nu_3}\alpha_3 f_{32}\eta_{21}\Omega \tag{4}$$

where $I_2(2)$ = observed fluorescence intensity from 2 → 1 exciting 0 → 2; $I_2(3)$ = observed fluorescence intensity from 2 → 1 exciting 0 → 3; $P(2)$, $P(3)$ = power of dye laser exciting 0 → 2, 0 → 3; ν_2, ν_3 = frequency of the 0 → 2, 0 → 3 transitions; α_2, α_3 = absorptivity of 0 → 2, 0 → 3 transitions; η_{21} = radiative quantum efficiency from 2 → 1; f_{32} = nonradiative quantum efficiency from 3 → 2; and Ω = instrumental constant.

Eliminating the common term from Equations 3 and 4 and solving for f_{32} yields:

$$f_{32} = \frac{\nu_3}{\nu_2}\cdot\frac{P(2)}{I_2(2)}\cdot\frac{I_2(3)}{P(3)}\cdot\frac{\alpha_2}{\alpha_3} \tag{5}$$

Thus in order to calculate f_{32}, one needs to measure the transition frequencies, the fluorescence intensities, absorptivities, and excitation beam powers for the two cases. Because of pulse to pulse variations in dye laser intensity and fluctuations in the dye laser bandwidth, it would prove difficult to measure the absorptivities and fluorescence intensities at different times. For these reasons, the EXABS system was developed to allow the simultaneous measurement of absorbance and fluorescence, thus eliminating any measurement error induced by different excitation bandwidths, with the capability to correct for source intensity fluctuations.

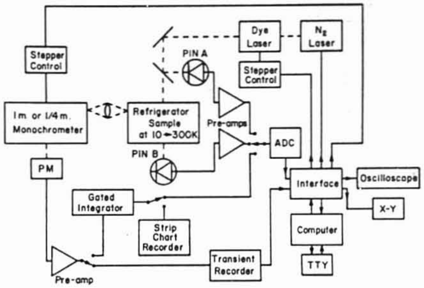

Figure 2. Block diagram of experimental apparatus. Dashed lines indicate light path

INSTRUMENTATION

Since the spectroscopic apparatus is called on to perform a variety of different measurements, each requiring a unique configuration of the available components, the basic system design was chosen to allow the frequent interchanges of all components. The foundation of the optical system was the rail and rider design of Walters (*10*) which enables optical components to be positioned on the optic axis quickly yet accurately with high long term reproducibility. The remainder of the system was built around this optical base. A block diagram of the entire apparatus is shown in Figure 2. The switches indicate variable connection schemes which permit the different measurements required. Each possible connection will be described in detail in subsequent sections. In this section, the components will be described individually, with further information given in Table I.

Excitation Sources. A nitrogen laser pumped tuneable dye laser is used as the primary excitation source. The high rf noise levels from the nitrogen laser discharge prevented the use of TTL level signals with the laser as purchased. In order to correct the problem, the power supply was disassembled and rebuilt as an integrated component within the laser head itself since shielding of the two separate units proved insufficient. A double walled, insulated copper mesh enclosure was constructed around the laser head with both shields anchored to a common ground. This procedure resulted in the suppression of the rf noise to negligible levels and permitted the operation of the laser in the presence of the sensitive electronic circuits described below. A procedure similar to this has recently been reported by Defreese and Malmstadt (*11*).

The nitrogen laser is normally operated at a repetition rate of 16 Hz. It is focused onto the dye cell by a two-lens system consisting of a 152-mm focal length bi-convex spherical lens and a 102-mm focal length cylindrical lens, producing a focused horizontal beam about 10 mm across. The dye laser cavity follows the design of Hänsch (*12*), utilizing an echelle grating, beam expanding telescope, dye cell and output mirror, giving a beam FWHM of 0.01–0.02 nm. The echelle grating (Model TF-R2, PTR Inc., Ann Arbor, Mich.) has a 63°35′ blaze angle with 316 grooves/mm and is used in 8th to 15th order. It is scanned linearly in wavelength by a conventional design sine bar mechanism driven by a stepper motor (Type SS50-1001, Superior Electric Co., Bristol, Conn.). The stepper motor can be driven manually by a controller or remotely under computer control. The beam expanding telescope is constructed from a 120-mm focal length achromatic doublet (LAU 117, Melles Groit, Irvine, Calif.) and a –5-mm focal length diverging lens. These inexpensive lenses allow tuning over the bandwidth of the dyes used without refocusing. The output mirror is a Hershel wedge (Edmund Scientific, Barrington, N.J.).

In order to facilitate dye interchange and to reduce the volume of dye required when expensive dye solutions are needed, a quartz cuvette is used in place of the conventional large volume flow cell design. The cuvette was constructed (ESCO Scientific, Oak Ridge, N.J.) with the opposing sides wedged at an angle of 1.5° to prevent amplification of broadband emission. It has a total volume of

Table I. Components of Instrumentation System

Component	Description and manufacturer
Minicomputer	Model PDP/8f computer (Digital Equipment Corp., Maynard, Mass.) 8K core, M1703 input interface, M1705 output interface, ASR-33 teletype.
Minicomputer interface system	Lab constructed, enables multiplexing of input and output lines, self-contained +5 V ± 15 V power supplies, plug in circuit card construction.
Transient recorder	Model 802 (Biomation, Cupertino, Calif.) dc to 500 KHz, 1000 channel, 500 ns to 20 ms per channel.
Monochromator/spectrometer	Model CT-103 one-meter spectrometer (Interactive Tech. Inc., Los Gatos, Calif.) 1200 grooves/mm grating blazed for 1 μm, straight adjustable slits. Model 82-410 $^{1}/_{4}$-meter monochromator, (Jarrell-Ash, Waltham, Mass.) high blaze grating; 1180 grooves/mm blazed for 600 nm. Low blaze grating; 590 grooves/mm blazed for 1 μm, interchangeable fixed slits.
Photomultipliers	For 1 meter: Type 9658R (EMI Gencom Division, Plainview, N.Y.) with extended S-20 photocathode. For $^{1}/_{4}$-meter: Type 1P28 (RCA, Harrison, N.J.) with S-5 photocathode.
PIN photodiodes	Model PIN-10 (United Detector Tech. Inc., Santa Monica, Calif.) Schottky barrier photodiode.
Cryogenic refrigerator	Model CSW-202 (Air Products and Chemicals, Inc., Allentown, Pa.). Two stage refrigerator capable of 10 K, with water cooled compressor.
Gated integrator	Lab constructed, variable gate width and delay, dual channel.
Stepping motor controllers	For 1-m monochromator: Model 103/210 (Interactive Tech. Inc., Los Gatos, Calif.) allows variable scan speeds in both manual and computer controlled operation. For dye laser: Lab constructed, either manual or computer controlled scanning of the dye laser.
Nitrogen laser	Model UV300 (Molectron Corp., Sunnyvale, Calif.) 300 kW pulsed with 30-kV power supply.
Dye laser	Shop constructed, all components mounted on rigid rail system (see text).
Strip chart recorder	Model 680 M (Hewlett-Packard, Pasadena, Calif.).
X-Y recorder	Series 2000 Omnigraphic (Houston Instrument, Belleair, Texas) with Type 3 and Type 6 signal modules.

about 3 mL. A Teflon-coated cell stirrer is placed inside the quartz dye cell and the cell is mounted above a magnetic stirrer. When the dye solution is placed in the cell it is constantly stirred, avoiding any local saturation of the dye and yet the total volume of dye needed is kept small. A single solution of dye can normally be used continuously for an 8-h period with only a minor degradation of output power. However, the dyes used in the near UV tend to deteriorate at a more rapid rate, requiring a new solution within 2 h. In addition to the tuneable dye laser excitation source, a high intensity air cooled tungsten–iodine lamp and a water cooled mercury capillary lamp (Model C-1-L, Illumination Industries, Inc., Sunnyvale, Calif.) are available for experiments requiring a conventional source.

Sample Holders and Temperature Control. A cryogenic refrigerator unit is used to provide sample temperatures between 10 K to 300 K. The sample is mounted in a holder (see Figure 3) appropriate for the experiment being run. The holder is mounted in thermal contact with the refrigerator copper cold finger through an indium washer and the refrigeration unit is then evacuated. For single crystal samples, thermal contact with the holder is maintained by a conductive grease (Cry-Con, Air Products and Chemicals Inc., Allentown, Pa.). Powder samples, such as precipitates, are packed into depressions in the holder shown in Figure 3a with an aluminum rod. The laser beam is directed onto the samples by a set of optics appropriate for the particular sample holder. For the powdered samples, a cylindrical and spherical lens combination is employed to focus the beam onto the sample in a vertical line. To introduce other samples into the fixed optic axis successively as required for multiple analyses or external standardization techniques, the cryogenic refrigerator is raised and a spacer inserted, aligning the next sample with the beam. The angle between the sample face and the laser beam in the horizontal plane is about 35°, with the sample fluorescence focused with an achromatic lens onto a mechanical chopper and then onto the entrance slit of the monochromator. The chopper is used to block the optical path to the monochromator for about 30 μs after the laser has fired preventing damage to the photomultiplier from broadband submicrosecond background fluorescence generated in the powder sample, arising possibly from parametric fluorescence processes induced by the laser pulse. The laser is triggered by a variable counter synchronized to the chopper to maintain proper timing. For most lanthanide fluorescence transitions, the lifetimes of fluorescent manifolds are in the range of 100 μs to 10 ms, allowing temporal discrimination between the analytical fluorescence and the broad background. Powder sample lifetimes can be measured in the same manner as single crystal lifetimes, as described later. The observed fluorescence intensity can be corrected for laser power fluctuations using the EXABS system. A similar system can be used for opaque single crystals.

When the maximum amount of fluorescence is required for single crystal samples, a holder is used (see Figure 3b) in which the beam is directed vertically through the crystal by reflection from a mirror mounted on the holder beneath the crystal. The resulting vertical line of fluorescence can be focused on the monochromator entrance slit. For experiments that require absorbance measurements, a sample holder is used (see Figure 3c) that allows the beam to pass through the crystal in the horizontal direction while the fluorescence is observed at right angles through the front surface. Since the fluorescent line in the crystal is orthogonal to the vertical slit height of the monochromator, the observed fluorescence intensity is correspondingly much lower than that observed with the holder shown in Figure 3b. This configuration is optimum however, for those experiments that require the fluorescence intensity to be insensitive to optical alignment.

Detectors and Wavelength Isolation. The fluorescence excited in the powdered samples or crystals by the dye laser is monitored by either the 1-meter or the $^{1}/_{4}$-meter monochromator. The $^{1}/_{4}$-meter instrument is used with sufficiently wide slits to provide a bandwidth of about 7 nm. For typical samples, this bandwidth is large enough to allow the detection of fluorescence from all crystallographic sites present. For measurements of individual fluorescence lines, the 1-meter monochromator is used in second order to provide a dispersion of 0.4 nm/mm. The photomultipliers described in Table I are used as detectors in the visible, with a PIN photodiode or PbS detector available for measurements in the near IR. The photomultiplier or photodiode output is amplified by a current to voltage converter (labeled as a preamp in Figure 2) with a variable gain of from 10^4 to 10^6 V/A. The preamplifier output is then either directed to the gated integrator or to the transient recorder. A stepping motor control unit allows either local or computer controlled scanning of the 1-meter monochromator.

For the measurement of absorbance, two PIN photodiodes are used. A portion of the laser beam is diverted into the channel

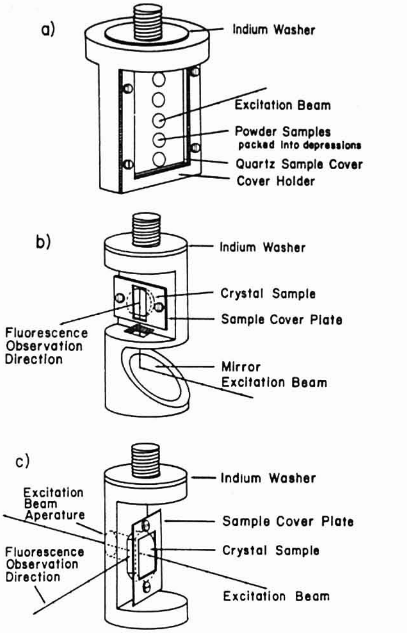

Figure 3. Sample holders. (a) For powder samples; fluorescence observed orthogonal to plane of page, analytical determinations. (b) For single crystals; time dependence and site classification studies. (c) For single crystals; EXABS holder, for quantum efficiency, site concentration and classification studies requiring absorption measurements

A photodiode holder by a beam splitter. The beam then passes through two pieces of frosted glass that minimize the highly directional character of the beam. A set of neutral density filters is used to reduce the intensity of the beam further so that it is within the linear response region of the photodiode. Thus, when the light strikes the photodiode, it is diffuse and the entire surface of the photodiode is illuminated. Any small wandering of the beam position will have a negligible effect on the intensity of the light actually striking the surface of the photodiode. A technique similar to this has been reported to eliminate a variation in detector response due to a nonuniform detector surface (*11*). Hence the signal detected by channel A is directly proportional to the intensity of the beam incident on the sample.

A second PIN photodiode, designated as channel B, senses the beam after it passes through the crystal. Before striking the detector surface, the beam is scattered by passing through frosted glass and attenuated with several neutral density filters. Since the intensity of the beam is measured before and after it passed through the sample, the absorbance of the crystal can be calculated. It should be noted that this absorbance measurement is possible only when the crystals are mounted in the sample holder shown in Figure 3c, but the channel A photodiode can be used to detect the incident beam intensity with any holder enabling the correction of the detected fluorescence for fluctuations in the nitrogen laser power from pulse to pulse, as described more fully below.

The current output of the photodiodes is amplified by a 3-stage preamplifier in the current-to-voltage converter configuration with gains of between 10^5 and 10^7 V/A. The preamplifier response has a rise time of ca. 5 µs and a decay of ca. 150 µs as required for the peak readers.

The peak readers are a modification of the design of Egbert, Selzer, and Yen (*13*) which allows use from 0–10 V. The circuit diagram is shown in Figure 4. The first two operational amplifiers (OA1 and OA2) are both in the feedback loop, with the third, OA3, wired as a unity gain inverter producing a positive output. The output of one channel of the preamplifier is connected to the noninverting input of OA1 which is essentially a voltage follower. Hence the output of OA1 will slew to follow the input, but will overshoot slightly, since direct feedback is inhibited by the 1N914 diode, until the voltage level at the output of OA2 tracks up to the signal level.

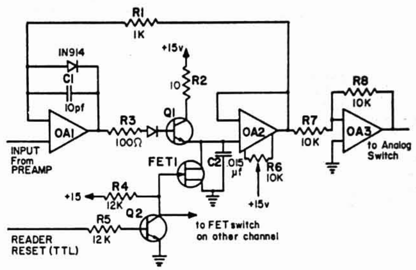

Figure 4. Peak reader circuit

The output of OA1 drives the base of Q1, controlling the collector-emitter current which charges the integrating capacitor C2 until it is at the voltage of the input signal. This capacitor will hold this charge as long as the gate of FET1 is maintained at +15 V, turning the FET off. As the input signal drops off from its peak value, the base-emitter junction of Q1 becomes reverse biased and the peak voltage level is held by C2, which maintains the output of OA2 at this voltage until the gate of FET1 is grounded, allowing C2 to discharge. This is accomplished by the TTL interface logic pulse READER RESET which occurs after the peak reader voltage has been transferred into the computer. Since the voltage range attainable by C2 is set to lie between 0–10 V, the READER RESET pulse must be boosted to +15 V to prevent leakage through the FET. This is done using Q2 as a switch controlled by the 5-V logic pulse.

Use of inexpensive 741 op-amps for OA1 and OA3 was found to be acceptable, but the offset current quickly caused C2 to charge to +15 V if used for OA2, even when using the offset null inputs. For this reason, an FET input op-amp (Signetics 536) was used for OA2, with a 10-K trimpot (R6) used to adjust the offset current. Since OA1 was found to slew very negative after the peak of the input signal, a diode was inserted between R3 and the base of Q1 to protect the base-emitter junction of Q1. This transistor provides the charging current for C2, as well as reducing the loading of OA1 and helping to decouple OA1 and OA2. The dynamic range of the peak readers is dependent upon the value of C2, a larger value increasing the dynamic range until other circuit properties come into effect. A discussion of the absorbance measurements obtained, their accuracy, and precision can be found below.

The output of the two channels of the peak reader were multiplexed to the analog-to-digital converter. An analog switch (IH 5010, Intersil Inc., Capertino, Calif.) is used for this function, with the two signals being sequentially gated through the switch into a sample and hold circuit and then latched into the ADC. Since the peak readers hold the signal until reset, the S/H circuit is not necessary. The control pulse train generated by a series of monostable multivibrators is shown in Figure 5 for the sequential switching of the two peak reader signals into the computer. The FIRE pulse is generated by a software command and causes the nitrogen laser to be triggered in addition to starting the peak reader sequence. The second pulse, RF DEL, establishes a delay of approximately 3 µs and then triggers the READER RESET monostable, which in turn brings the gate of FET1 in Figure 4, as well as the gate of the corresponding FET for the second channel, to +15 V enabling the integrating capacitor to begin to charge. This delay after the laser fires was found to be essential because of a small amount of rf noise present during this time. By leaving the integrating capacitors shorted, the peak readers do not detect this noise. Since the peak response for the preamps

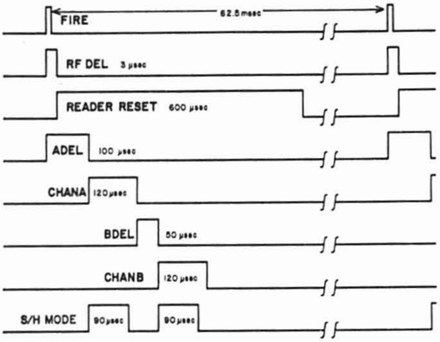

Figure 5. EXABS pulse train, sequence for reading in two peak reader values for one laser pulse (see text)

of the photodiodes occurs about 10 μs after the laser fires, this delay does not affect the ability of the peak readers to sense the maximum signal. The ADEL pulse establishes a delay of 100 μs before the channel A peak reader value is allowed to pass through the analog switch in order to allow the maximum intensity to be reached and the peak readers to become stable. The trailing edge of this pulse triggers the next one-shot, generating the CHANA pulse which turns the analog switch on, allowing the channel A signal to pass through. When the switch is first turned on, the S/H MODE pulse enables the S/H tracking mode which follows the output of the analog switch. About 30 μs before channel A is switched off, the tracking is halted. The trailing edge of S/H MODE is used to start the analog-to-digital conversion after a 1-μs delay to allow the S/H to settle and the conversion is completed in 30 μs. The ADC generates a pulse upon completion which is used to trigger the interrupt facility of the minicomputer, at which point the software takes over and reads the output of the ADC and stores it as the relative intensity of that laser pulse. As can be seen in Figure 5, a 50-μs delay occurs between the time CHANA is shut off and the time the CHANB pulse allows the channel B signal to pass through the analog switch. It is during this time that the conversion of the channel A signal takes place and is read by the computer. A similar sequence occurs to enable the conversion and recording of the channel B photodiode response maximum. Once both values have been obtained, the peak readers are reset by the READER RESET pulse, draining the integrating capacitors and preparing for the next laser pulse. The entire operation of obtaining the two values and calculating and storing the absorbance requires about 450 μs, leaving 62 ms before the next laser pulse. The photodiode responses are detected and recorded before the transient recorder completes its sweep, its fastest time base being 500 μs for 1000 points.

Signal Processing Devices. The output of the photomultiplier preamp can be processed with the gated integrator whose gate is synchronized with the laser pulse. The gated integrator has a variable gain of from ×1 to ×100 with a time constant of 1–30 ms. An external gate with a width of 10 μs to 10 ms and a delay of up to 5 ms is provided by a separate device. The combination of variable gate width and delay enables discrimination between fluorescence lines with differing relaxation rates. The output of the gated integrator is normally displayed on the strip chart recorder, although it is also possible to multiplex this signal into the ADC and the computer.

For the time dependence studies or for the EXABS system, the fluorescence detected by the photomultiplier is amplified and sensed by the transient recorder, a 1000-channel device with 8-bit resolution. The transient recorder is interfaced to the computer, allowing data transfer and computer control of arming and reading functions. One of the most useful functions of the transient recorder is the pretrigger record mode which allows storage of the input signal for a selected percentage of the total time base prior to the triggering of the nitrogen laser. This pretrigger region can be used to calculate the background signal level present in the photomultipler and preamplifier and, by summing a number of the transient recorder channels in this region, a correction can be made to the actual fluorescence signal recorded. This eliminates the need to detect the fluorescence decay curve until it decays to the zero level, enabling a greater freedom in the manner in which the decay is recorded. The stored signal may be output through D/A converters to an oscilloscope or an X–Y recorder.

DETERMINATION OF FLUORESCENT LIFETIMES

The fluorescence decay lifetime of the individual crystallographic sites is a spectroscopic parameter that characterizes the site and contains information about the radiative and nonradiative relaxation rates that determine analytical sensitivity and interference. In addition, the shape of the fluorescence transient contains information about energy transfer processes that may be taking place. The noise present in the fluorescence decay excited by a single laser pulse is high enough to require signal averaging, accomplished by using a transient recorder interfaced to a minicomputer.

The dye laser and monochromator are both tuned to lines characteristic of one site and the beam is focused through the crystal in a vertical line as shown in Figure 3b. The fluorescence is focused on the entrance slit of the monochromator, with the photomultiplier response being amplified and detected by the transient recorder. In this mode, the laser is fired from a pulse generator, with the transient recorder trigger synchronized to this pulse. The information stored in the 1000 channels of the transient recorder is read by the computer and summed to that from the previous pulses until the desired S/N is obtained. Normally, this requires the summation of approximately 4000 laser pulses.

Data processing routines have been developed to extract the lifetime values from the fluorescence decays and for simple data manipulations such as background correction and scaling routines. In the case of a single exponential decay, the lifetime is found directly by a weighted least-squares fit to the logarithm of a user selected portion of the decay curve. Fluorescence decays can be observed that are described by linear combinations of two or more simple exponentials if multiphonon relaxation or energy transfer processes are present. These phenomena have been treated in a previous paper (*8*). Computer generated decay curves of these combinations are used for comparison with experimentally obtained results to extract relaxation rates. Examples of these computer fits for multilevel decays can be found in Figures 5, 6, and 10 of Ref. 8.

OPERATION AND APPLICATION OF THE EXABS SYSTEM

The EXABS system was designed to enable the simultaneous recording of absorption and excitation (or fluorescence) spectra. This procedure is needed for the calculation of the nonradiative quantum efficiencies and for the measurement of the relative and absolute site concentrations where the fluorescence intensity must be corrected for absorbance of the excitation beam within the crystal. In addition, the EXABS system has proved especially valuable in classifying lines in the complex spectrum observed when many sites are present. In order to correct for the beam attenuation that occurs before the point where fluorescence is monitored, the distance from this point to the front crystal face is measured by backlighting the crystal with a tungsten lamp. The absorbance measured for the entire crystal thickness can then be used to correct the observed fluorescence intensity at all excitation wavelengths. Since both uncorrected fluorescence and absorption spectra are stored in the computer, the correction described is left as a user option, being implemented at the conclusion of the scan if desired. The fluorescence spectrum does not

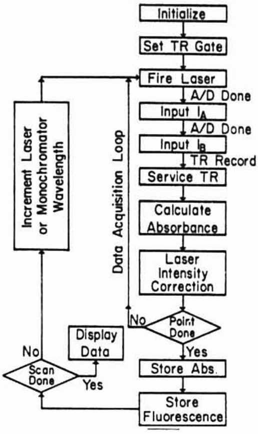

Figure 6. EXABS program flow chart. Sequence for taking excitation or fluorescence scan. TR = transient recorder

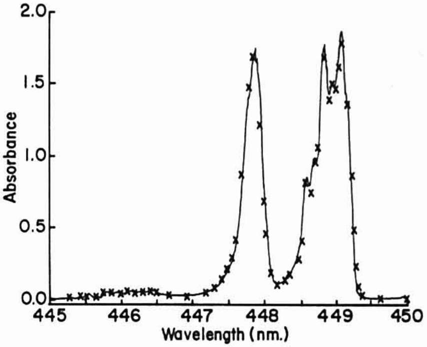

Figure 7. Comparison of EXABS and conventional absorption spectra. (——) Absorption spectrum of $CaF_2:Er^{3+}$ 2 mol % obtained using EXABS system. (X) Absorption values calculated from transmission spectrum of $CaF_2:Er^{3+}$ 2 mol % obtained using tungsten lamp and one-meter monochromator

usually require correction for self-absorption because the observed transitions are almost always nonresonant lines.

When using EXABS the crystal holder shown in Figure 3c is employed, with the laser beam passed through a $^3/_{16}$-in. diameter aperture to define the beam before it passes through the crystal and strikes the channel B photodiode. The aperture allows reproducible positioning of the laser beam to ensure a minimal error in positional stability.

The sequence of events which occurs when running the EXABS system is shown in block diagram form in Figure 6. The user must first initialize a number of control parameters which include the number of data points to be taken (maximum 1000), the number of laser pulses to be averaged for each data point, the wavelength interval between data points, and the time base and full scale voltage settings used on the transient recorder. (Required for normalization routines.) In addition, either the dye laser or the monochromator is selected to be scanned to take either excitation and absorption spectra or a fluorescence spectrum. Finally, the monochromator and dye laser are both tuned to the point of maximum fluorescence of the site being investigated, and the fluorescence is recorded by the transient recorder and displayed on the oscilloscope. Using this signal, that portion of the fluorescence transient that will be used to provide the fluorescence output intensity is selected by setting a gate width and position. When a scan is taken, the data points within this region will be summed to given an integrated intensity, while the pretrigger region is used for correction of background fluorescence. The transient recorder is thus used as a digital, computer-controlled gated integrator.

After initialization the computer enters the data acquisition loop by firing the nitrogen laser and triggering the acquisition electronics described previously. The computer then performs three measurements, reading the values of I_A (the incident laser intensity as measured by the channel A photodiode), I_B (the laser intensity transmitted through the crystal as sensed by the channel B photodiode), and F (the fluorescence decay stored in the transient recorder). The transient recorder data are read point by point and the signal data within the preselected gate are summed to a value that represents the integrated total of the gated portion of the fluorescence transient. The absorbance, A, is calculated and stored at this point. The laser intensity correction is applied to the value F using the relationship $F' = F(I_{ref}/I_A)$ where I_{ref} is a constant reference intensity equivalent to one-half of the full scale intensity and F and I_A are defined above. The entire data acquisition loop is repeated until the prescribed number of laser pulses per data point have been taken. The values of A and F' from each laser pulse are signal-averaged by summing values from sequential laser pulses and dividing by the number of pulses summed. Both absorption and excitation (or fluorescence) spectra can be scaled by a constant to maintain proper magnitude when displayed on the oscilloscope.

Upon completion of the data acquisition loop for one data point, the computer steps either the monochromator or dye laser the preselected interval and the acquisition loop is re-entered for the next point by firing the laser. Subsequent absorbance (A) and fluorescence (F') points are stored in sequential memory locations. Once all data points have been taken in this manner, the absorption spectrum resides in one continuous portion of the computer core memory while the excitation (or fluorescence) is in another. Either or both spectra can be displayed on the oscilloscope. The simultaneous display of the excitation and absorption spectra is a powerful way to analyze systems containing multiple sites as will become apparent in later discussion.

For very weak signals, as many as 100 laser pulses have been averaged for each of the 1000 data points, requiring about $1^3/_4$ h. Normally, 5–10 pulses per point is sufficient, requiring about 5 to 10 min. Hard copies of the spectra can be made on the X–Y recorder, normally superimposing absorption and excitation spectra for rapid wavelength correlation. A digital record of the spectra can be punched on paper tape for later data evaluation. Software routines have been written for integration of the entire spectrum or for specific transitions or regions.

The precision of the entire EXABS system was tested by periodically measuring the integrated excitation intensities of different sites in the $CaF_2:Er^{3+}$ 0.2 mol % crystal. The maximum range of measurements taken for one site over a period of several months is 10–15% (*6*). The accuracy of the EXABS absorbance measurement was compared with that taken by making a point by point measurement of the absorbance using the 1-m monochromator for wavelength isolation of the tungsten lamp (see Figure 7). The largest variation between the two methods appears at high absorbance values, where the intensity of the light reaching the channel B photodiode is very low, producing an output signal from the preamplifier-peak reader chain of only 50–100 mV. The accuracy of

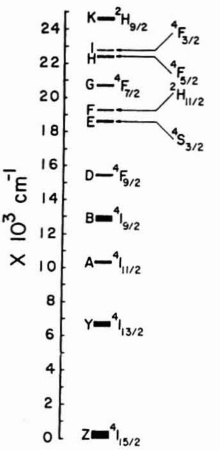

Figure 8. Free ion Er^{3+} manifolds of the 4f^n configuration

the absorbance measurement was further checked by inserting a series of neutral density filters between the two photodiodes and recording the decrease in the channel B response.

Since absorption and excitation spectra are obtained simultaneously with the EXABS system, a comparison of the two allows rapid site identification. By taking an absorption spectrum, one can quickly locate all possible laser wavelengths that can excite fluorescence. The dye laser is then tuned to each of these absorption lines sequentially and a fluorescence spectrum for each excitation frequency is taken. Each distinct site must give rise to a unique fluorescence spectrum, and by comparing these fluorescence spectra, the absorption lines can be classified as to their specific site origin. Confirmation can be obtained by setting the monochromator to a fluorescence transition characteristic of one site which does not overlap fluorescence lines from other sites and taking an excitation and absorption spectrum by scanning the dye laser. Each site will give rise to a unique excitation spectrum which must correspond to particular lines in the previously identified absorption spectrum. Any overlap of excitation lines in the absorption spectrum can be identified immediately, as demonstrated in Figure 9.

In Figure 9a, a portion of the absorption spectrum for the $^4I_{15/2}$ to $^2H_{11/2}$ transitions in a CaF$_2$:0.05 mol % Er^{+3} crystal is shown. (See Figure 8 for the positions of these energy levels (*14*).) Each line is identified as originating from the A, B, or C site, as designated in an earlier paper (*3*). This absorption spectrum is repeated in the upper traces of Figures 9b,c, d superimposed on the excitation spectra (the lower trace) of the A, B, and C sites respectively. This superposition represents the manner in which these data were obtained from the EXABS system and was acquired by monitoring a fluorescence transition characteristic of each site. The location of each excitation line is easily compared with those of the other sites because of the positional reference of the absorption spectrum. This method is superior to obtaining excitation spectra successively with a strip chart recorder or other device because of the elimination of the need for reproducibility and correlation of successive scans. Any nonlinearity in the scan rate will be apparent by a variation in the line position of the reference absorption spectrum, allowing a simple correction to be made to the excitation spectrum involved. This advantage is illustrated by the two absorption lines located at 516.26 nm and 516.35 nm in Figure 9b and 9d. The absorption line at 516.26 nm consists of two major transitions, one from the A site and one from the C site. A slight contribution from the B site, as shown by the shoulder in the excitation spectrum in Figure 9c, is also apparent. The absorption line at 516.35 nm is seen to be almost entirely the result of the B site absorbance in Figure 9c. Note even the relatively weak absorption lines at 516.43 nm and 516.45 nm can be matched

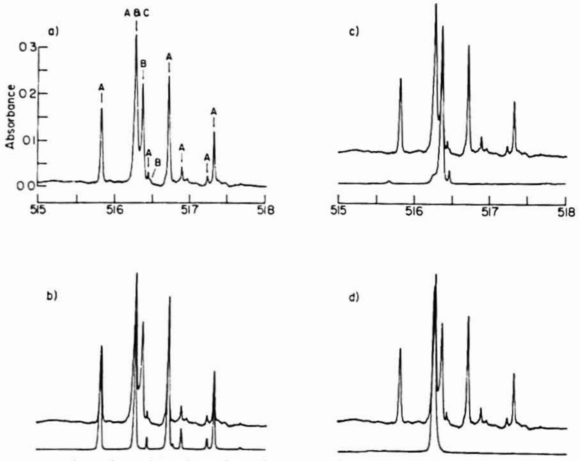

Figure 9. $^4I_{15/2} \rightarrow {}^2H_{11/2}$ absorption and excitation spectra of CaF$_2$:Er^{3+} 0.05 mol % using EXABS. (a) Absorption spectrum (reproduced as upper trace in b, c, and d). (b) Lower trace, A site excitation, monitoring 540.00 nm (E$_1$ → Z$_2$) (*3*). (c) Lower trace, B site excitation, monitoring 539.15 nm (E$_1$ → Z$_2$) (*3*). (d) Lower trace, C site excitation, monitoring 537.98 nm (E$_1$ → Z$_2$) (*3*)

Table II. Nonradiative Quantum Efficiencies

Site	f	$\tau(^4S_{3/2})$ μs (8)	$\omega_{\eta r}$ (s^{-1})[a]
A	0.012 ± 0.0015	1452 ± 5	8.3 ± 1
B	0.0074 ± 0.0015	848 ± 8	8.7 ± 1.8
C	0.082 ± 0.007	710 ± 6	115 ± 9
D(1)	0.13 ± 0.01	546 ± 9	238 ± 19
D(2)	0.11 ± 0.01	462 ± 7	238 ± 22

[a] Sum of all nonradiative rates.

to A and B site lines in parts b and c. The wavelength scale shown in Figure 9 results from the most rapid scan rate normally used for the dye laser. Scale expansions of 20 times this rate are possible, allowing resolution of even more nearly coincidence absorption lines originating from different sites. Absorbance scale expansions of ten times that shown are also possible, enabling the measurement of 0.005 absorbance unit.

The knowledge that an absorption line is composed of contributions from more than one site is vital when calculating quantum efficiencies, since it is necessary to know the absorbance of each site individually. Normally, it is possible to find a transition for each site which exhibits no overlap, allowing the unambiguous calculation of the quantum efficiencies. Methods for deconvoluting the absorption peaks are being developed.

Measurement of Quantum Efficiencies. The nonradiative quantum efficiencies can be calculated using Equation 5. The EXABS system directly measures the ratios $P(2)/I_2(2)$ and $P(3)/I_2(3)$ by correcting the observed fluorescence for the power of the laser pulse that generated it. These ratios are determined from the spectra by using the integration and normalization routines described above. In a similar manner, the absorptivities, α_2 and α_3, are taken from the absorption spectra stored by EXABS. In addition, the laser intensity measurement must be corrected slightly for the variation in response with wavelength of the photodiode for channel A and the neutral density filters used to attenuate the beam. These values were determined to an accuracy of 5% using a calibrated thermopile detector as a standard. The spectral response of the monochromator or photomultiplier is unimportant in this procedure because for a given quantum efficiency measurement, the same fluorescence transition is monitored for both excitation spectra. The gate width used by the computer for the fluorescence decay was set such that the entire decay curve was included. All excitation spectra are corrected for absorbance occurring within the crystal as described above.

The nonradiative quantum efficiencies for the A, B, C, D(1), and D(2) sites for the $^4S_{3/2}$ to $^4F_{9/2}$ case are given in Table II, along with the fluorescent lifetimes of the $^4S_{3/2}$ levels for these sites as determined with the time dependence system for a $CaF_2:Er^{3+}$ crystal. These values were used to calculate the nonradiative relaxation rate between the $^4S_{3/2}$ and $^4F_{9/2}$ manifolds from Equation 2. The 3050 cm^{-1} energy difference between the two manifolds must be dissipated by lattice phonons. It can be seen that the two single pair sites, A and B, which have only one Er^{3+} ion in the site, have essentially identical nonradiative relaxation rates. This nonradiative rate is determined by multiphonon relaxation which has no known dependence on site symmetry, but does depend on the energy gap and temperature (see, for example, (*9*, *15*)). The C, D(1), and D(2) sites have been shown previously to have at least two Er^{3+} ions clustered together in a configuration which allows a very efficient energy transfer step when relaxing from the $^4S_{3/2}$ to the $^4F_{9/2}$ manifold (*8*). The higher nonradiative rates caused by the additional energy transfer processes are quite evident for these sites in Table II. Additional work is continuing to determine these energy transfer rates. It should be noted that the D(1) and D(2) sites are each known to be made up of a number of nearly equivalent sites, exhibiting very similar excitation and absorption spectra. For the measurements presented in Table II, the assumption was made that all the D(1) sites and all the D(2) sites had the same quantum efficiency, allowing the fluorescence from all sites to be measured together. Data taken at a number of different fluorescence transitions were identical within experimental error, indicating this assumption is valid. The quantum efficiencies of several other nonradiative relaxations for the $CaF_2:Er^{3+}$ crystal system have been measured and those for $BaF_2:Er^{3+}$ and $SrF_2:Er^{3+}$ systems are currently being investigated.

Determination of Site Concentrations. The ability of the EXABS system to selectively excite the crystallographic sites and correct the measured fluorescence for source fluctuation and excitation beam absorbance is essential for the measurement of both relative and absolute site concentrations. By studying the absolute concentrations of individual sites as a function of total dopant concentrations, an understanding of the important defect equilibria involved in the site formation can be realized. Studies have been carried out on $CaF_2:Er^{3+}$ crystals with total dopant concentrations ranging from 10^{-4} to 1.0 mol %. The $^4I_{15/2}$ to $^4S_{3/2}$ excitation spectra for each site were obtained monitoring fluorescence from the $^4S_{3/2}$ to the $^4I_{13/2}$ manifold. The spectra were integrated, yielding a total relative excitation intensity for each site for each concentration crystal, corrected as described above. The intensity measurements are indicative of how a given site population varies with total dopant concentration, but comparison of populations of different sites requires a knowledge of the spectroscopic parameters for that site. These relative site concentrations can be calculated if the fluorescent lifetime, radiative quantum efficiency, fluorescent, and absorption branching ratios and integrated absorption intensity are known. The $^4S_{3/2}$ lifetimes were measured as described above and are reported in Table II. By studying the concentration dependence of these lifetimes, the rate of energy migration to a sink (also called the concentration quenching rate), ω_m, can be obtained. This value in turn allows the calculation of the radiative quantum efficiency from Equation 2, using the nonradiative quantum efficiencies from Table II and assuming the multiphonon relaxation rate is independent of site symmetry. Two fluorescent branching ratios are required; the ratio of fluorescence at the wavelength monitored to the total fluorescence intensity for a given site, and the ratio of fluorescence from the lowest crystal field level in the $^4S_{3/2}$ manifold to the lowest level in the $^4I_{15/2}$ manifold. One absorption branching ratio is needed, i.e. the ratio of absorbance (or excitation) for the transition between the lowest level in $^4S_{3/2}$ and the lowest level in $^4I_{15/2}$ to the total integrated absorption for all transitions between these two manifolds for that site. The quantities were determined by using EXABS to obtain fluorescence or absorption spectra for all transitions between the two manifolds, integrating all lines, and finding the ratio of the line of interest to the total making the necessary corrections for the spectral response characteristics of the instrument. To calculate absolute site concentrations, the integrated absorption intensity for the absorption line is required, which can also be obtained from the EXABS system.

Calculation of the absolute site concentrations of the different sites present in CaF_2 has led to some interesting results. The concentration of the single pair sites is found to go through a maximum and actually decrease in absolute value, while the dimer site concentrations continually increase. No equilibrium model to describe this behavior is possible, since the single pair site concentration will reach a maximum and level off in any such treatment. This behavior has been described by a quasi-equilibrium model, in which the idea of a solid state precipitate is used, along with the idea of "gettering" species first introduced by Yaney et al. (*16*). A complete description of the details of this experiment, the calculations, and the theoretical derivation of the model can be found elsewhere (*6, 7*).

ACKNOWLEDGMENT

The authors thank R. J. Lang, R. C. Riley, R. W. Schmelzer, K. G. Spielman, and T. J. Weight for design and construction of the dye laser and the optical system.

LITERATURE CITED

(1) F. J. Gustafson and J. C. Wright, *Anal. Chem.*, in press.
(2) J. C. Wright, *Anal. Chem.*, in press.
(3) D. R. Tallant and J. C. Wright, *J. Chem. Phys.*, **63**, 2074–2085 (1975).
(4) M. D. Kurz and J. C. Wright, *J. Luminescence*, in press.
(5) M. P. Miller and J. C. Wright, University of Wisconsin, Madison, Wis., unpublished work, 1976.
(6) D. R. Tallant, Thesis, University of Wisconsin, Madison, Wis., 1976, available at University Microfilms, Ann Arbor, Mich.
(7) D. R. Tallant, D. S. Moore, and J. C. Wright, *J. Chem. Phys.*, in press.
(8) D. R. Tallant, M. P. Miller, and J. C. Wright, *J. Chem. Phys.*, **65**, 510–521 (1976).
(9) W. D. Partlow and H. W. Moos, *Phys. Rev.*, **157**, 252–256 (1967).
(10) J. P. Walters, "A Synergic Approach to Research in Spectroscopy and in Spectrochemical Analysis" in "Contemporary Topics in Analytical and Clinical Chemistry", Vol. II, D. M. Hercules, G. M. Hieftje, L. R. Snyder, and M. A. Evenson, Ed., Plenum Press, New York, N.Y., in press.
(11) J. D. Defreese and H. V. Malmstadt, *Anal. Chem.*, **48**, 1530–1535 (1976).
(12) T. W. Hänsch, *Appl. Optics*, **11**, 895–898 (1972).
(13) W. C. Egbert, P. M. Selzer, and W. M. Yen, *Appl. Opt.*, **15**, 1158–1163 (1976).
(14) G. H. Dieke, "Spectra and Energy Levels of Rare Earth Ions in Crystals", Interscience Publishers, New York, N.Y., 1968, p. 142.
(15) L. A. Riseberg and H. W. Moos, *Phys. Rev.*, **174**, 429–438 (1968).
(16) P. P. Yaney, D. M. Schaeffer, and J. L. Wolf, *Phys. Rev. B*, **11**, 2460 (1975).

RECEIVED for review April 8, 1977. Accepted June 7, 1977. Acknowledgement is made to the donors of the Petroleum Research Fund, administered by the American Chemical Society, for partial support of this work and to the National Science Foundation under grant number MPS74-24394.

Determination of Porphyrins at Low Concentration Using Porphinatocopper(II) Phosphorescence

David K. Lavallee* and James Andrew

Department of Chemistry, Colorado State University, Fort Collins, Colorado 80523

We present a new technique utilizing phosphorescence which avoids interferences that are present in spectrophotometric and fluorometric procedures. This method, which determines concentration of free porphyrins by phosphorescence of the copper(II) complex, is intended for use in accurate biomedical studies rather than as a screening technique. Use of a synthetic internal standard of high stability, the copper(II) complex of tetraphenylporphyrin, is also described.

Analysis for porphyrins in body fluids is diagnostically useful in cases of lead poisoning, iron deficiency anemia, and a number of porphyrias. Present methods for the determination of the concentration of porphyrins in blood and urine utilize spectrophotometric and fluorometric techniques (*1–7*) which are subject to interferences. Many substances commonly found in body fluids absorb in the visible region of the spectrum used for the detection of porphyrins (near 400 nm). Particulate matter also interferes with spectrophotometric determinations. Bilirubin and other pigments fluoresce in the same region as the porphyrins. In urine samples, a nonspecific fluorescent interferent of varying intensity is found (*7*). No significant phosphorescence is commonly found, however, for body fluids under the experimental conditions that we report herein for the determination of porphyrins by a phosphorescence technique. This method involves complexation of copper(II) with the porphyrin and subsequent recording of the phosphorescence spectrum. Under the proper conditions, the reaction is relatively rapid and an internal standard (the synthetic porphyrin complex, tetraphenylporphinatocopper(II)) allows accurate determination of the porphyrin concentration.

EXPERIMENTAL

Free base protoporphyrin IX (Porphyrin Products, Logan, Utah-purity established from published visible absorption molar absorptivities (*8*)) was added to whole blood samples from healthy individuals, which was then diluted with $^1/_{10}$ its volume of 1.0 M Tris buffer (Sigma Chemical Co.) at pH 7.7 and incubated at 37 °C for 12 to 25 h. The samples were extracted with ethanol (the clinically preferred method of porphyrin extraction, showing consistent results and procedural simplicity (*1*)). The ratio of ethanol to blood was 3:1 by volume. The ethanol extract was then combined with one-tenth its volume 0.25 M $CuCl_2{\cdot}2H_2O$ in ethanol. The blood may be stabilized with normal amounts of EDTA (0.1%) since there is sufficient Cu(II) present for complexation with the porphyrin even though EDTA removes some. Blood stabilized with heparin was also used, with similar results.

After 2 to 3 min, the ethanol solution (e.g., 100 μL) was extracted by the addition of diethyl ether (e.g., 200 μL) and 1 mL of H_2O. The ether layer was removed and washed twice with additional 1-mL portions of water. It was then placed over about $^1/_2$ mL of 4 Å molecular sieves in a culture tube. After a few minutes (5 min is sufficient) 100 μL was withdrawn into a phosphorescence tube and frozen in liquid nitrogen. Spectra were then recorded within 2 h. The timing which is most important in this procedure is the time allowed for copper complexation—when the ethanol extract and the $CuCl_2{\cdot}2H_2O$ in buffered ethanol are mixed. For good reproducibility, the same time (2 to 4 min) must be allowed for each sample. Once the ether extract is frozen, it remains stable for over 2 h if protected from light. We use a short (25 cm) cylindrical Dewar with aluminum foil around the top for storing samples before taking phosphorescence spectra. The diethyl ether extract forms an excellent glass if it has been dried over the molecular sieves.

Blood from patients with conditions such as lead poisoning or iron deficiency anemia show very significant incorporation of zinc into non-heme protoporphyrin IX (*5*). It has been shown previously that HCl removes zinc readily from porphinatozinc complexes (*1*). The recombination of zinc(II) with free protoporphyrin is slow with the concentrations of zinc(II) which correspond to the concentration of protoporphinatozinc(II) in blood (*5, 9*). With these facts in mind, the following procedure has been used to convert protoporphinatozinc(II) (Porphyrin Products, Logan, Utah) in blood to the copper(II) complex. The blood with protoporphyrin IX added was extracted with ethanol (3:1 by volume). To the ethanol was added one-tenth of its volume of 1.0 M HCl. The acidified extract was shaken for 1 min and neutralized with 1.0 M Tris buffer. The procedure for reaction of copper(II) and the ether extract described above was then used.

To use the internal standard, tetraphenylporphinatocopper(II) (available from Strem Chemicals, Inc.), a stock solution containing the tetraphenylporphinatocopper(II) may be added either to the stock solution of $CuCl_2 \cdot 2H_2O$ in ethanol or to the ether extract. It is best to dissolve the tetraphenylporphinatocopper(II) in a small amount of diglyme (bis(2-methoxyethyl) ether) (Aldrich Chemical Co.) and dilute to the desired concentration with ethanol or ether. Use of the internal standard in the ethanol stock is recommended since the ethanol is less volatile and concentrations are, therefore, easier to maintain. If the internal standard is added to the ethanol extract, it is then not necessary to know the ether volume precisely since the porphyrin concentration is obtained with the *ratio* of the intensities of the phosphorescence of the copper complex of the natural porphyrins and the intensity due to tetraphenylporphinatocopper(II).

An Aminco-Bowman spectrophotofluorometer (SPF 125) with a Hamamatsu R818 photomultiplier tube and a phosphorescence accessory was used. The copper porphyrins have very short phosphorescence lifetimes (*10*), so the spinner was run near maximum velocity. The rotation rate was regulated by controlling the voltage to the motor using a digital voltmeter. The sensitivity of this unmodified commercial instrumentation is sufficient to detect normal porphyrin levels (*11*). Critical features of this procedure with respect to instrumentation are maintaining the same spinning rate for each sample and properly positioning the phosphorescence sample tube to obtain maximum emission intensity.

RESULTS AND DISCUSSION

Use of Copper Ion. The copper(II) ion was chosen as the reagent for porphyrin determination by phosphorescence because it is extremely efficient in causing phosphorescent emission from its complexes with porphyrins rather than the fluorescence normally encountered for metalloporphyrin complexes (*12*). The blood samples were buffered at pH 7.7 with Tris buffer because the reaction of copper(II) salts with porphyrins is much faster in slightly basic solutions than in acidic ones (*13*). In the procedure, the copper(II) concentrations are much greater than the highest known non-heme porphyrin levels in blood (*11*), giving pseudo-first-order conditions. Hence, the time it takes for the reaction (95% completion in 2 min at 25 °C) is dependent only on the copper(II) concentration, not the concentration of porphyrin in the sample. Kinetic runs for the incorporation of copper(II) ion into the principal free porphyrin found in blood, protoporphyrin IX, at 25 °C consistently gave pseudo-first-order behavior with a half life of less than 30 s for a copper(II) concentration of 2.5×10^{-3} M.

Phosphorescence Results. Since the most prevalent free porphyrin in blood is protoporphyrin IX, we report quantitative results for the copper(II) complex of this species. Experiments with the copper(II) complexes of coproporphyrins I and II and uroporphyrins I and III show similar results, with slight changes in emission wavelength (means of distinguishing these species from one another without tedious chemical separations are now being developed). The relationship between phosphorescence intensity and concentration of porphyrin, shown in Figure 1, refers to the diethyl ether extract of blood samples with protoporphyrin IX added. Dilution from the blood sample must be accounted for in determining the porphyrin concentration in the blood sample. The extraction efficiency for the procedure can be determined by the use of spiked samples and has been determined previously for the ethanol extraction procedure to be 56%, linear up to 4×10^{-6} M (*1*). A typical dilution (6.6) divided by extraction efficiency factor for this procedure is 12. The range of linearity illustrated in Figure 1 spans the range from non-heme porphyrin levels in the blood of healthy individuals to levels in the blood of those seriously ill from iron deficiency anemia, porphyrias, etc.

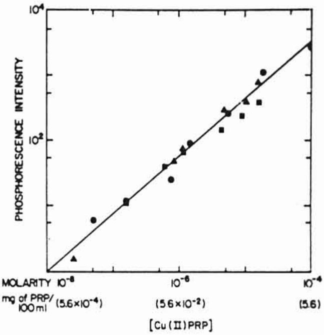

Figure 1. Variation of phosphorescence intensity as a function of protoporphinatocopper(II) concentration. Slope = 1.14, correlation coefficient = 0.987. SD of repetitive measurement on same sample <1%. SD of separate samples which were diluted to the same nominal concentration = ±5%

Internal Standard. The phosphorescence intensity of the synthetic porphyrin used as internal standard varied linearly with concentration from 10^{-8} to 10^{-5} M. Above a concentration of 10^{-5} M, the emission intensity no longer varies linearly with concentration, possibly because of the aggregation of the metalloporphyrin molecules at higher concentrations (*14*), or because of the high extinction coefficient of tetraphenylporphinatocopper(II) (*15*). The synthetic tetraphenylporphyrin complex is more stable toward decomposition than natural porphyrins and shows quite similar phosphorescence properties—similar regions of excitation and emission and similar phosphorescence decay lifetimes. Hence, it makes a very acceptable standard. The excitation wavelength for tetraphenylporphinatocopper(II) which gives maximum emission is sufficiently different from the copper(II) complexes of the natural porphyrins, however, that these complexes can be selectively excited. The spectra of separate solutions of protoporphinatocopper(II) and tetraphenylporphinatocopper(II) in diethylether are shown in Figure 2. A separate stock solution such as this can be used for instrument calibration.

Figure 3 shows the emission spectra of a solution containing both protoporphinatocopper(II) and the tetraphenylporphinatocopper(II) with excitation first at 420 nm and then at 405 nm. It is quite evident that the two complexes can be selectively excited without giving problematical interference. By knowing the relative intensities characteristic of the two complexes, the two measured intensities and the concentration of added CuTPP, the concentration of protoporphyrin is determined. Figure 4 shows the results of concentration determination by the internal standard method.

CONCLUSIONS

The procedure for protoporphinatocopper(II) analysis by phosphorescence is reasonably straightforward. After extraction with ethanol and complexation with copper(II), a second extraction with diethyl ether leads to a matrix which forms a good frozen glass for phosphorescence measurements. The emission intensity is proportional to concentration from 10^{-8} to 10^{-5} M.

In order to make quantitative determination by this method reliable, we have evaluated a stable internal standard which is commercially available. The copper(II) complex of the synthetic porphyrin, $\alpha,\beta,\gamma,\delta$-tetraphenylporphine, has many of the same characteristics as the copper(II) complexes of the natural porphyrins. It is however, more stable toward de-

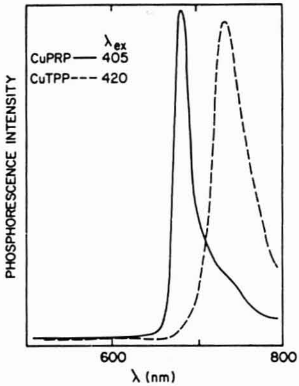

Figure 2. Spectra of protoporphinatocopper(II) (——) with 405 nm as excitation wavelength and of tetraphenylporphinatocopper(II) (- - -) with an excitation wavelength of 420 nm

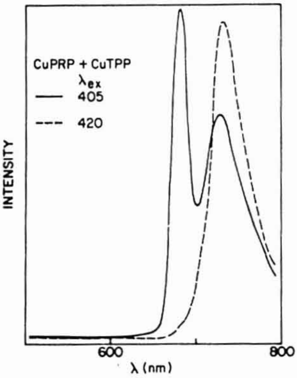

Figure 3. Spectra exhibited by a mixture of protoporphinatocopper(II) and tetraphenylporphinatocopper(II) using excitation wavelengths of 405 nm (——) and 420 nm (- - -)

composition by light, temperature, and chemical reactions. Identical spectra have been recorded after weeks of sample storage at room temperature (the solution was stored in the dark but no special care was required in handling the samples when spectra are taken). The position of the intense visible absorption band of tetraphenylporphinatocopper(II) is different from that of the protoporphyrin complex and allows the use of tetraphenylporphinatocopper(II) as an internal standard. One can selectively determine tetraphenylporphinatocopper(II) or protoporphinatocopper(II) by using their different absorption band wavelengths for excitation. The synthetic porphyrin also shows a linear dependence between emission intensity and concentration.

Our results demonstrate that the measurement of protoporphyrin IX in blood by phosphorescence of the copper(II) complex is sufficiently sensitive to detect levels found for healthy individuals (capability of this method is 5 μg of protoporphyrin per 100 mL of whole blood, while the normal adult range is 16 to 52 μg of protoporphyrin per 100 mL of whole blood (*16*)). This sensitivity is of the same order of magnitude reported for fluorescence methods of porphyrin determination (*1*). Reproducibility of ±5% for this method is also very similar to the reproducibility of the fluorescence methods (*1*). The phosphorescence method is not as simple as the use of the direct reading hematofluorometer (*5*), but is comparable to commonly used fluorescence techniques that involve extraction (*1*).

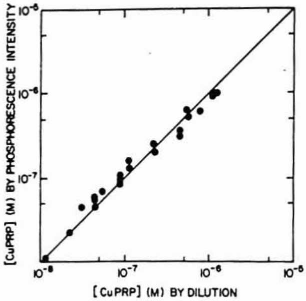

Figure 4. Use of CuTPP as an internal standard for determination of protoporphyrin concentration. The equation which relates [PRP] to [CuTPP] is: $[\mathrm{CuPRP}] = [(I_{\mathrm{CuPRP}}/I_{\mathrm{CuTPP}})\, I_0 \times 4.25 \times 10^{-7}]$. I_0 is $I_{\mathrm{CuPRP}}/I_{\mathrm{CuTPP}}$ for each porphyrin at 4.25×10^{-7} and is equal to 0.67

The phosphorescence method described herein measures total porphyrins in blood. Protoporphyrin IX is the most prevalent free porphyrin in blood with coproporphyrins generally constituting about 5% of total porphyrins and uroporphyrins even less. Given the reproducibility limitations, coproporphyrins and uroporphyrins in blood may prove not to be a problem in use of this technique. However, further work should be done to develop rapid separation of these porphyrins in blood, perhaps by an ion-exchange technique similar to that developed by Sobel et al. for urine samples (*7*). It will also be necessary to obtain samples from lead intoxicated and porphyric individuals to test this method against fluorescence methods currently in use. The potential for eliminating interference due to the fluorescence of bilirubin and other substances in blood will be evaluated further.

ACKNOWLEDGMENT

We appreciate the technical assistance of Anne Coleman and Marilyn Watkins.

LITERATURE CITED

(1) L. Hanna, D. N. Dietzler, C. H. Smith, and H. S. Zarkowsky, *Clin. Chem. (Winston-Salem, N.C.)*, **22**, 161 (1976) and references therein.
(2) S. Schwartz and M. H. Berg in, "Methods of Biochemical Analysis", Interscience, New York, N.Y., 1960, pp 253–255.
(3) S. Piomelli, *J. Lab. Clin. Med.*, **81**, 932 (1973).
(4) L. P. Kammholz, L. G. Thetcher, F. M. Blodgett, and T. A. Good, *Pediatrics*, **50**, 625 (1972).
(5) A. A. Lamola, M. Joselow, and T. Yamane, *Clin. Chem. (Winston-Salem, N.C.)*, **21**, 93 (1975).
(6) J. J. Chisholm, Jr., and D. H. Brown, *Clin. Chem. (Winston-Salem, N.C.)*, **21**, 1669 (1975).
(7) C. Sobel, C. Cano, and R. E. Theirs, *Clin. Chem. (Winston-Salem, N.C.)*, **20**, 1397 (1974).
(8) J. E. Falk, "Porphyrins and Metalloporphyrins", Elsevier, New York, N.Y., 1964.
(9) P. Hambright and P. B. Chock, *J. Am. Chem. Soc.*, **96**, 3122 (1974).
(10) P. Eastwood and M. Gouterman, *J. Mol. Spectrosc.*, **30**, 437 (1969).
(11) S. Granick, S. Sassa, and J. L. Granick, *Proc. Nat. Acad. Sci., USA*, **69**, 2381 (1972).
(12) R. Becker, "Theory and Interpretation of Fluorescence and Phosphorescence", Wiley, New York, N.Y., 1969.
(13) W. E. Scheider, *Struct. Bonding (Berlin)*, **23**, 123 (1975).
(14) W. I. White and R. A. Plane, *Bioinorg. Chem.*, **4**, 21 (1974).
(15) W. J. McCarthy and J. D. Winefordner in "Fluorescence Theory, Instrumentation and Practice", G. G. Guilbault, Ed., Marcel Dekker, New York, N.Y., 1976, pp 371–442.

RECEIVED for review February 18, 1977. Accepted June 6, 1977. Support of the National Institute of Environmental Health Sciences under Grant ES 00987-01 is gratefully acknowledged.

Multielement Trace Analysis of Geological Materials with Solvent Extraction and Flame Atomic Absorption Spectrometry

Philip Hannaker and T. C. Hughes*

Department of Geology, School of Earth Sciences, University of Melbourne, Parkville, Victoria 3052, Australia

The development of a precise analytical method is reported for the determination of the elements Cu, Ni, Co, Cr, Ag, Pb, Bi, Cd, Zn, Mn, Au, Tl, Sb, Ga, and Mo in geological materials. Results are quoted for USGS standard rocks and are compared with published values; practical limits of detection are generally better than 0.5 ppm. The method utilizes solvent extraction separation and preconcentration techniques (chloro complexes, diethyldithiocarbamate, and 8-hydroxyquinoline chelates are used with methyl isobutyl ketone and *n*-butyl acetate as solvents), with elemental determination by flame atomic absorption spectrometry. Analytical accuracy is achieved by the chemical elimination of chelate forming iron and manganese. The rock dissolution, chelation, extraction, and measurement procedures are reported, together with partition data, for a range of pH, Eh, and ionic strengths.

Atomic absorption spectrometry (AAS) has become a favored technique for elemental determinations in geochemical distribution and exploration studies. The technique is relatively simple and reliable in operation and the inherent micro (ppm) detection sensitivity for many elements of geochemical interest, together with the speed of analysis, has assisted in its acceptance.

AAS is subject to matrix interfering effects which can normally be more easily controlled with flame techniques rather than with the alternative furnace atomization methods. These interferences have been extensively investigated and methods now exist to minimize or correct for their effects (Amos et al. (*1*), Price (*2*), Slavin (*3*), Rubeska and Moldan (*4*)). A number of authors have reported specific elemental interferences. Govett and Whitehead (*5*) noted that for the elements Pb, Zn, Ni, and Co, which are used extensively in exploration geochemical studies, extreme caution must be used when employing the standard practice of varying sample weight and dilution of a sample solution to suit the expected elemental concentration. Foster (*6*) has tabulated the effect of high Ca content on trace Ni and Pb data, where Ni at 4 ppm showed an apparent 13 ppm and Pb at 20 ppm gave a 32 ppm result.

The main source of interference at low concentrations of trace elements (up to 5 ppm) and low concentrations of major elements (up to 5000 ppm total metal content) is considered to be enhancement due to background or nonatomic absorption. This effect can be corrected for using the hydrogen or deuterium continuum, or by the use of a nonabsorbing wavelength. Matrix matching and standard addition techniques can further improve the analytical precision. At higher concentrations of the matrix materials, suppression effects in the flame and a reduction of atomization efficiency in the nebulizer occur. When these conditions predominate, the use of the standard "background corrector" methods for total molecular absorption results in an overall negative error.

SAMPLE PREPARATION USING SOLVENT EXTRACTION METHODS

The use of solvent extraction techniques in AAS to eliminate undesirable matrix effects has been widely reported (Koirtyohann and Wen (*7*); Kinrade and Van Loon (*8*)). This relatively simple technique has the further advantage of significantly improving AA detection sensitivities by (a) allowing elemental preconcentration and separation, and (b) presenting the elements of interest to the flame in an aqueous free solvent which can possess excellent atomization and combustion characteristics (Lakanen (*9*); Culp et al. (*10*)). For AAS measurements at very low levels (below 1 to 5 ppm), some sample pre-treatment is required and the adoption of solvent extraction techniques has been shown to give accurate, reproducible results together with simple, rapid analytical processing and low chemical blanks.

This paper describes an investigation into the use of three solvent extraction systems for geological samples. The method has been developed for the determination of Cu, Ni, Co, Cr, Ag, Pb, Bi, Cd, Zn, Mn, Au, Tl, Sb, Ga, and Mo in a wide range of materials. Results are quoted for USGS standard rocks and are compared with published values.

A number of chelate and ion association solvent extraction systems were considered. Based on previously reported work (Morrison and Freiser (*11*), Stary (*12*), Zolotov (*13*)), cost availability and ease of handling, sodium diethyldithiocarbamate (NaDDC) and 8-hydroxyquinoline chelates and chloride ion association complex systems were adopted. Methyl isobutyl ketone (MIBK) (Kuwata et al. (*14*); Chau and Lum-Shue-Chan (*15*)), and *n*-butyl acetate were chosen as the nonaqueous solvents. NaDDC has been widely used for metal spectrometric determinations, particularly for river and seawater trace metal analysis (Welcher (*16*), Lacoste et al. (*17*), Kuwata et al. (*14*), Nix and Goodwin (*18*)). Mixed chelating agents such as ammonium pyrrolidine dithiocarbamate (APDC) and diethyl-ammonium diethyldithiocarbamate (DDDC) (*8*) were found to be unnecessary; the use of NaDDC with control of pH and general extraction conditions was adequate for the reproducible extraction of the chelate complexes from geological samples. 8-Hydroxyquinoline is known to readily form extractable complexes ((*11*), (*15*), Butler and Mathews (*19*)).

The use of nonspecific chelating agents for AAS preconcentration processes can be limited by the presence of relatively high concentrations of complex forming elements. In geological materials, Fe is often present at the 10–20% level and Mn occurs from minor amounts up to approximately 1%. Both of these elements form DDC complexes which have a saturation effect on the organic phase during solvent extraction. Their presence effectively reduces the partition of minor and trace elements into the MIBK, particularly for those chelates of lower stability. A light scattering process (Billings (*20*)) also becomes apparent at high complex concentrations when measuring organic phase constituents by AAS. The combination of poor extraction reproducibility and variable light scattering effects leads to a major loss of accuracy and detection capability. Dilution of the organic phase, although reducing the interfering effects, results in an unacceptable loss of sensitivity.

A quantitative chemical separation process was developed to eliminate Fe and Mn during the solvent extraction procedure. The Fe was removed in two stages, first using the chloride system with control of HCl concentration and second, using 8-hydroxyquinoline with control of pH. The Mn was held in the aqueous phase during the NaDDC extraction by the use of EDTA.

The importance of investigating extraction parameters, particularly pH and aqueous and organic phase compositions, to optimize elemental separations has been stated by Kinrade and Van Loon (*8*). Partition coefficients and extraction rates were therefore examined by the use of radiotracers. These were prepared by thermal neutron irradiation of pure elements in the HIFAR reactor at Lucas Heights, Sydney. The isotopes used were ^{51}Cr, ^{60}Co, ^{65}Zn, ^{99}Mo, ^{110}Ag, ^{113}Sn, ^{121}Sn, and ^{124}Sb. The radioactive tracers were added to crushed mineral samples and the dissolution and separation processes were followed by monitoring the associated γ activity after each step. The optimization of extraction times and the number of equilibration steps needed was readily assessed using the tracers. Further tracer work showed that some Hg and Ge was lost from geological materials during the dissolution step when $HF/HClO_4$ was used. The complete replacement of $HClO_4$ by H_2SO_4 eliminated the Hg loss (Ehmann and Lovering (*21*)) but the presence of insoluble sulfates resulted in the possibility of trace element occlusion by absorption into the precipitate and the determination of Hg was therefore omitted from the present scheme.

EXPERIMENTAL

Reagents. The reagents used were "analar" grade with the exception of *n*-butyl acetate which was reagent grade. All water used was distilled and deionized (DDI).

Solutions. *Buffer.* Dissolve 102 g potassium biphthalate in 500 mL water. Extract once with 15-mL MIBK.

8-Hydroxyquinoline. Dissolve 1 g 8-hydroxyquinoline in 100 mL MIBK.

NaDDC. Dissolve 6 g NaDDC in 100 mL water. Filter the resultant solution and extract three times with 15-mL portions of MIBK.

Standard Solutions. *Stock Standard Solutions.* Dissolve appropriate metal or stoichiometric salt ("analar" or 99.9% purity) to prepare stock standard solutions at a concentration of 1000 ppm.

Instrumentation. The AAS used was a Techtron Model AA-3 with a Varian Techtron 1M-6D Indicator Module. The pH measurements were made using a Radiometer Type TTT-1 Titrator–pH meter.

DISCUSSION

Elimination of Fe Interference. The extraction of Fe(III) as a chloro complex into an organic solvent is well known (McKaveney and Freiser (*22*)). The use of this process was investigated as a means of removing the majority of the Fe before adding the NaDDC complexing agent.

There are a number of elements which can be extracted with Fe from chloride solutions; they include Sb(V), As(III), Ga(III), Ge(IV), Au(III), Mo(VI) and Tl(III) (*11*). The partition coefficient and extraction efficiency of these ion association complexes depends essentially on HCl concentration and the organic solvent used. A number of systems were therefore examined to investigate the possibility of using the Fe removal step as an integral part of the preconcentration solvent extraction scheme. After removal of the Fe, it was found that Au, Tl, and Sb could be measured in the organic phase. Mo and Ga required a further solvent extraction step; they were found to closely follow Fe(III) in Cl-ion association systems and they required a chelate formation step before their separation could be achieved. Other elements which form extractable chloro ion association complexes were not considered in the present study.

The efficiency of extraction of metal–chloro ion association complexes into three solvents of suitable volatility and combustion characteristics, namely, ethyl acetate, methyl isobutyl ketone and *n*-butyl acetate, was examined. Morrison and Freiser (*11*) and Edwards and Voigt (*23*) reported a general increase in partition coefficients with increasing HCl concentration for these systems and this was observed with all of the solvents used. It was found that for acid concentrations greater than 4 M HCl, although the elemental extraction was essentially complete, the solubility of the organic solvents in the strongly acid aqueous solutions became a serious problem, except with *n*-butyl acetate. This ester was therefore used for the quantitative extraction of the elements

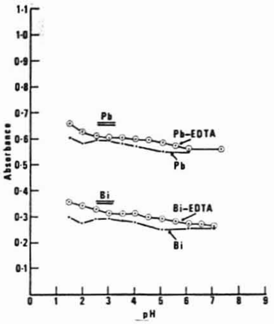

Figure 1. pH dependence of extractions with NaDDC showing the effect of EDTA–Pb and Bi

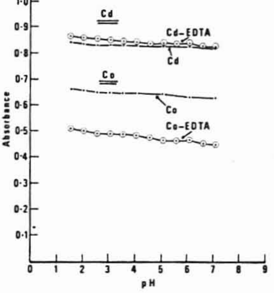

Figure 2. pH dependence of extractions with NaDDC showing the effect of EDTA–Cd and Co

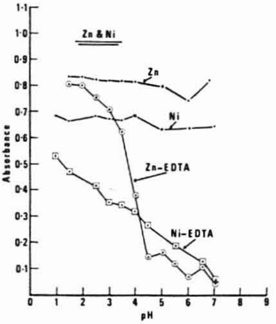

Figure 3. pH dependence of extractions with NaDDC showing the effect of EDTA–Zn and Ni

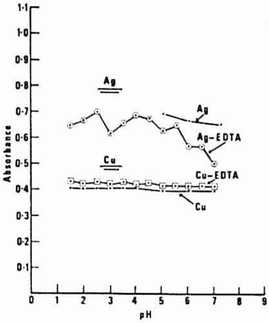

Figure 4. pH dependence of extractions with NaDDC showing the effect of EDTA–Ag and Cu

Fe(III), Au(III), Tl(III), Sb(V), Mo(VI), and Ga(III) from 8.0 M HCl solutions. Back extraction with 1 M HCl was found to completely remove the Fe, Mo, and Ga leaving the other extracted elements in the *n*-butyl acetate. Au, Tl, and Sb could then be measured directly by AAS.

Separation of Mo and Ga from Fe. Fe, Mo, and Ga are known to form extractable complexes with 8-hydroxyquinoline (Luke and Campbell (*24*), Welcher (*16*)). However, in acidic solutions (pH < 1.6) in the presence of ascorbic acid, Fe(II) does not react and Mo and Ga can be quantitatively extracted as 8-hydroxyquinoline chelates into MIBK, leaving the Fe in the aqueous fraction. The organic phase can then be analyzed directly by AAS for Mo and Ga.

Elimination of the Mn Interference. The use of metal DDC chelates as a means of preconcentrating a number of minor and trace elements in rocks is restricted by the ready formation of large amounts of the relatively unstable Mn-DDC chelate. The initial high Mn complex concentration and build up of decomposition products makes the general DDC extraction unreliable for accurate AAS measurement of other chelate forming elements (e.g., Cu, Ni, Co, Cr, Cd, Ag, Pb, Bi, and Zn).

Hague et al. (*25*) stated that Mn can be strongly masked with EDTA so as to restrict the formation of other extractable Mn complexes. This was found to be true even in the presence of concentrated NaDDC solutions (e.g., 2000 mg/L Mn was not precipitated from a 100-mL acidic solution containing EDTA in the presence of 10 ml of 6% w/v DDC solution).

The effect of EDTA on the formation and extraction of DDC complexes was investigated for the elements Mn, Cu, Ni, Co, Cr, Cd, Ag, Pb, Bi, and Zn. The atomic absorbance of solutions containing EDTA was compared with similar solutions which were EDTA free. The results are shown in Figures 1, 2, 3, and 4. It was observed: (1) That EDTA completely inhibited the formation of Mn-DDC chelates in acid solutions. (2) The presence of EDTA had little effect on the DDC complex partition coefficient of the elements Pb, Bi, Cd, Cu, Cr, and Ag over the pH range 1.5 to 7. (3) Zn and Ni showed very poor extraction characteristics above pH 2 but for lower pH solutions, EDTA had little effect. (4) Co showed a constant and reproducible (ca. 20%) reduction in absorption signal.

Stability of DDC Complexes at pH 2. The stability of DDC chelates of Cu, Ni, Co, Cr, Cd, Ag, Pb, Bi, and Zn with respect to time was fully investigated. The metal chelate stabilities were examined in aqueous solutions at pH 2 and also after extraction into MIBK with removal of the aqueous phase. In both experiments, the metals were prepared at approximately 300 ppb in 100 mL of solution in the presence of 10 mL 0.1M EDTA and 3 mL of phthalate at a pH 2.0 ±

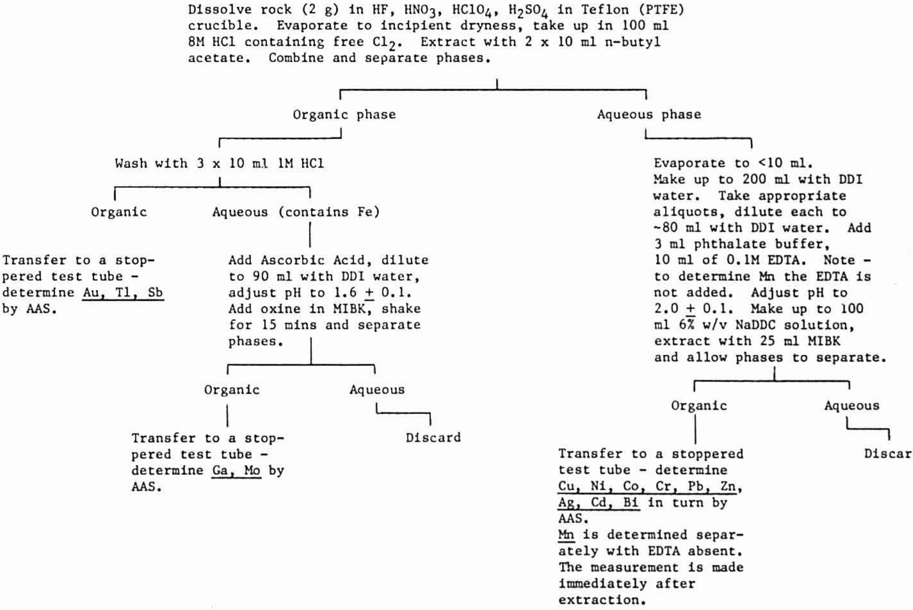

Dissolve rock (2 g) in HF, HNO_3, $HClO_4$, H_2SO_4 in Teflon (PTFE) crucible. Evaporate to incipient dryness, take up in 100 ml 8M HCl containing free Cl_2. Extract with 2 x 10 ml n-butyl acetate. Combine and separate phases.

Organic phase

Wash with 3 x 10 ml 1M HCl

Organic

Transfer to a stoppered test tube - determine Au, Tl, Sb by AAS.

Aqueous (contains Fe)

Add Ascorbic Acid, dilute to 90 ml with DDI water, adjust pH to 1.6 ± 0.1. Add oxine in MIBK, shake for 15 mins and separate phases.

Organic

Transfer to a stoppered test tube - determine Ga, Mo by AAS.

Aqueous

Discard

Aqueous phase

Evaporate to <10 ml. Make up to 200 ml with DDI water. Take appropriate aliquots, dilute each to ~80 ml with DDI water. Add 3 ml phthalate buffer, 10 ml of 0.1M EDTA. Note - to determine Mn the EDTA is not added. Adjust pH to 2.0 ± 0.1. Make up to 100 ml 6% w/v NaDDC solution, extract with 25 ml MIBK and allow phases to separate.

Organic

Transfer to a stoppered test tube - determine Cu, Ni, Co, Cr, Pb, Zn, Ag, Cd, Bi in turn by AAS. Mn is determined separately with EDTA absent. The measurement is made immediately after extraction.

Aqueous

Discard

Figure 5. Summary of analysis procedure

Table I. Elemental Concentrations in USGS Standard Rocks

Element	BCR-1, ppm		AGV-1, ppm		PCC-1, ppm	
	Measured concn	Quoted value^a	Measured concn	Quoted value^a	Measured concn	Quoted value^a
Sb	0.63	0.69	4.01	4.5	1.28	1.4
Tl	0.42	0.30	1.31	1.0	<0.2	0.8 ppb
Mo	3.63	1.1	3.35	2.3	BDL^b	0.2
Ga	20.0	20	24.1	20.5	BDL	0.4
Au	BDL^b	0.95 ppb	BDL^b	0.6 ppb	BDL	1.6 ppb
Ag	<0.2	0.036	<0.2	0.11	<0.1	5 ppb
Bi	<0.5	0.05	<0.5	0.057	<0.5	0.013
Cd	<0.2	0.12	<0.2	0.09	<0.2	0.1
Co	33.0	38	15.3	14.1	183	112
Cr	17.0	17.6	14.9	12.2	-	2730
Cu	22.4	18.4	65.0	59.7	10.0	11.3
Mn	1201	1406	693	763	815	959
Ni	18.1	15.8	18.7	18.5	2313	2339
Pb	20.1	17.6	37.4	35.1	17.0	13.3
Zn	146	120	118	84	40.0	36.0

[a] Flanagan (*26*), weighted average figure. [b] BDL, below detection limit.

0.1. The chelates were extracted into 15 mL of MIBK and the atomic absorbance measured at the appropriate time. It was observed that the presence of EDTA generally reduced the rate of decomposition of the metal-DDC complexes.

The stability of metal-DDC chelates in a separated MIBK phase was examined over a period of 8 h and no significant reduction of absorbance was observed for Cu, Ni, Co, Cr, Cd, Ag, Pb, Bi, and Zn. Nix and Goodwin (*18*) noted the stability of Cu, Fe, Mn, Co, Ni, Cr, Pb, and Zn chelates in MIBK and commented on the need to standardize the extraction and analysis times; this was particularly important in the case of Mn. With the Mn and Fe removed prior to DDC chelation, the time standardization was not critical over normal working periods. Mn was determined in an EDTA-free fraction and in this case the atomic absorption was carried out quickly after a fixed limited time interval.

PROCEDURE

The analytical procedure is shown diagrammatically in Figure 5. A more detailed account can be obtained from the authors.

RESULTS

Analytical results together with published values are shown in Table I for three USGS standard rocks. These results agree reasonably well with the recommended published values (Flanagan (*26*)) and demonstrate that the method can be successfully applied to geological samples. The procedure was tested extensively with mixed synthetic solutions and linearity of response for the elements being determined was established. Elements which are not measurable in the USGS rocks (listed as BDL in Table I) were shown to be readily determined when present at higher concentrations.

The solvent extraction separation and concentration of metal-DDC chelates was found to be quantitative if complex forming elements, when present in large excess (e.g. Fe and Mn), were removed. The presence of these elements in geological proportions interfered with the partition of trace element chelates particularly those of lower stability.

At very low levels (sub-ppm) the ultimate limit of detection of the AAS system was governed by the presence of other metal-DDC complexes at the 50–500 ppm level. A variable background due to a light scattering process was observed with mixtures of metal chelates covering the range of 0.1 to 100 ppm and this effect became particularly troublesome when attempting to measure concentrations below 0.5 ppm. To overcome this interference problem and to further extend the range of the present work, the use of a number of chelate separation techniques is under investigation.

LITERATURE CITED

(1) M. D. Amos, P. A. Bennett, J. P. Matoušek, C. R. Parker, E. Rothery, C. J. Rowe, and J. B. Sanders, "Basic Atomic Absorption Spectroscopy", Varian Techtron, Melbourne, 1975.
(2) W. J. Price, "Analytical Atomic Spectroscopy", Heyden, London, 1972.
(3) W. Slavin, "Atomic Absorption Spectroscopy", Wiley-Interscience, New York, 1968.
(4) I. Rubeska and B. Moldan, "Atomic Absorption Spectrophotometry", P. T. Woods, Trans. Ed., CRC Press, Cleveland, Ohio, 1969.
(5) G. J. S. Govett and R. E. Whitehead, *J. Geochem. Explor.*, **2**, 121 (1973).
(6) J. R. Foster, *Geochem. Explor., CIM Special Vol. No.* **11** (1971).
(7) S. R. Koirtyohann and J. W. Wen, *Anal. Chem.*, **45**, 1968 (1973).
(8) J. D. Kinrade and J. C. Van Loon, *Anal. Chem.*, **46**, 1894 (1974).
(9) E. Lakanen, *At. Absorpt. Newsl.*, **5**, 17 (1966).
(10) J. H. Culp, R. L. Windham, and R. D. Whealy, *Anal. Chem.*, **43**, 1321 (1971).
(11) G. H. Morrison and H. Freiser, "Solvent Extraction in Analytical Chemistry", J. Wiley and Sons, New York, 1957.
(12) J. Stary, "The Solvent Extraction of Metal Chelates", Macmillan, New York, 1964.
(13) Y. A. Zolotov, "Extraction of Chelate Compounds", Ann Arbor–Humphrey Science Publishers, Ann Arbor, Mich., 1970.
(14) K. K. Kuwata, K. Hisatomi, and T. Hasegawa, *At. Absorpt. Newsl.*, **10**, 111 (1971).
(15) Y. K. Chau and K. Lum-Shue-Chan, *Anal. Chim. Acta*, **48**, 205 (1971).
(16) F. J. Welcher, "Organic Analytical Reagents", Vol. 4, D. Van Nostrand Co., New York, 1948.
(17) R. J. Lacoste, M. H. Earing, and S. E. Wiberley, *Anal. Chem.*, **23**, 871 (1951).
(18) J. Nix and T. Goodwin, *At. Absorpt. Newsl.*, **9**, 119 (1970).
(19) L. R. P. Butler and P. M. Mathews, *Anal. Chim. Acta*, **36**, 319 (1966).
(20) G. K. Billings, *At. Absorpt. Newsl.*, **4**, 357 (1965).
(21) W. D. Ehmann and J. F. Lovering, *Geochim. Cosmochim. Acta*, **31**, 357 (1967).
(22) J. P. McKaveney and H. Freiser, *Anal. Chem.*, **29**, 290 (1957).
(23) F. C. Edwards and A. F. Voigt, *Anal. Chem.*, **21**, 1204 (1949).
(24) C. L. Luke and M. E. Campbell, *Anal. Chem.*, **26**, 1778 (1954).
(25) J. L. Hague, E. D. Brown, and H. A. Bright, *J. Res. Natl. Bur. Stand.*, **47**, 380 (1951).
(26) F. J. Flanagan, *Geochim. Cosmochim. Acta*, **33**, 1189 (1973).

RECEIVED for review January 18, 1977. Accepted May 20, 1977. Work supported by Department of Geology, University of Melbourne.

Enhancement of Emission by Potassium Chloride in the Low-Pressure Microwave-Induced Plasma Emission Spectrometer

Ikuo Atsuya,[1] Hiroshi Kawaguchi,[2] Claude Veillon, and Bert L. Vallee*

Biophysics Research Laboratory, Department of Biological Chemistry, Harvard Medical School, and the Division of Medical Biology, Peter Bent Brigham Hospital, Boston, Massachusetts 02115

The emission lines of many elements are greatly enhanced when potassium chloride is added to microvolume samples to be analyzed in the low-pressure, microwave-induced plasma emission spectrometer. This phenomenon is observed when hydrochloric acid is used in place of potassium chloride and is explained by considering the effect on the solute-volatilization process. An excitation mechanism in the helium plasma proposed earlier is confirmed.

In a low-pressure, microwave-induced plasma emission spectrometer employing tantalum filament volatilization (*1*), the addition of potassium chloride to sample solutions has been shown to enhance intensities of spectral emission lines of many elements. Zinc emission is enhanced by nearly one order, and copper and manganese by nearly three orders of magnitude. An appreciation of the mechanism of action of this additive requires evaluation of its effect on each of the processes of desolvation, volatilization, dissociation, and excitation.

In the previous paper (*2*), we have proposed a possible mechanism for the enhancement of excitation in this low-pressure helium plasma and have pointed out that potassium chloride enhances the spectral intensity largely by affecting the volatilization of metals from the filament. Metals are excited more effectively in the plasma when they are introduced as chlorides rather than as neutral atoms. The present paper examines the effect of hydrochloric acid on the intensities of manganese and copper lines and further confirms the proposed excitation mechanism.

EXPERIMENTAL

Apparatus. The experimental conditions and arrangements used in this work are described elsewhere (*2*). In addition to the conventional V-shaped tantalum filament, a 2-well, W-shaped tantalum filament of similar dimensions described in the previous paper (*2*) was employed which permitted the separate and simultaneous introduction of microvolume samples and matrix aliquots.

Reagents. All standard solutions were prepared from reagent grade salts or spectroscopically pure metals dissolved in metal-free acids and diluted to volume with metal-free water. Copper, manganese, and zinc were used as the nitrates.

Procedure. Sample solutions of 5 μL volume are placed on the tantalum filament (V- or W-shaped), and slowly desolvated by passing a current of 2–3 A through the filament. The plasma discharge is initiated, allowed to stabilize and the sample is then volatilized into the helium carrier gas by pulse-heating the filament via the discharge of a 0.22-F capacitor charged to 7.5 V. Pressure within the plasma tube is maintained at $\sim$4 Torr, and the sample vapor is carried into the discharge where it undergoes atomization and excitation. In the "automatic mode" of operation, all processes subsequent to deposition of the sample take place automatically and in sequence. Both the peak height and area of the emission line intensity are printed out digitally, and, in addition, the signal is displayed simultaneously on a dual-trace storage oscilloscope.

RESULTS AND DISCUSSION

Effect of Hydrochloric Acid on Spectral Intensity. Though the effect of anions present in sample solutions on the intensity of lines has not been described fully in the previous papers (*1*, *2*), their role is important from the viewpoint of solute-volatilization phenomena from the filament. The effect of chloride ions on the spectral intensity of copper and manganese was examined using hydrochloric acid with the results shown in Figure 1. The addition of hydrochloric acid to the samples increased the copper and manganese emission approximately 100-fold, and the enhancement occurred at lower HCl concentrations for manganese than it did for copper lines.

In the presence of hydrochloric acid, the manganese emission peak appeared at 14 ms after the initiation of heating of the filament (the duration was termed "delay time" (*2*)), while without the acid the delay time was 45 ms. These facts suggest that in the presence of hydrochloric acid, the nitrates of metals are converted to chlorides in the desolvation process on the filament, and the salts are volatilized at lower temperatures of the filament. In the absence of hydrochloric acid, the nitrates may be decomposed to oxides or free atoms in the volatilization process and necessitate higher filament temperature for complete volatilization to occur.

As expected, a log–log calibration curve for manganese in 0.05 M hydrochloric acid shifted toward a concentration range of manganese lower than that obtained without the acid, and the slope of the curve became steeper. When comparing these results with those obtained in the presence of potassium chloride in the sample solution (*2*), where 1000-fold enhancement and a calibration curve of unit slope were obtained, it seems that the hydrochloric acid is insufficient to retain the salts as chlorides on the filament during the volatilization process.

In the desolvation process, hydrochloric acid was also insufficient to stabilize the salts on the filament, as exemplified by copper emission (Figure 2). With increased desolvation current and in the absence of potassium chloride, the spectral line intensity of copper decreased rapidly, perhaps because of the partial loss of copper chloride from the filament.

Effect of Potassium Chloride in the Presence of Hydrochloric Acid. To examine the effect of hydrochloric acid on the potassium chloride enhanced manganese, line intensities were compared in the presence and absence of the acid. In the absence of hydrochloric acid, potassium chloride gradually increased the intensity of Mn 4030.75 Å to a maximal, constant intensity but in the presence of 0.05 M HCl the maximum was achieved at a lower KCl concentration (Figure 3). The effect on copper emission was quite similar: in the absence of HCl, constant emission was observed over

---

[1] Present address, Kitami Institute of Technology, Kitami, Japan.
[2] Present address, Nagoya University, Nagoya, Japan.

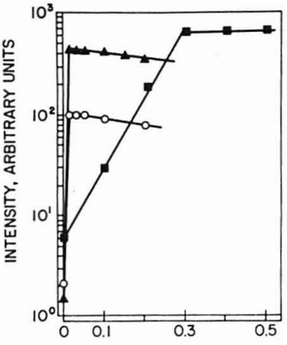

Figure 1. Effect of HCl on the emission intensities of Cu and Mn atomic and ion lines. (■) Cu I 3247.54 Å, 0.20 μg/mL. (O) Mn I 4030.75 Å, 0.32 μg/mL. (▲) Mn II 2576.10 Å, 2.0 μg/mL

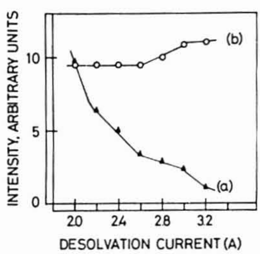

Figure 2. Effect of desolvation current on the line intensity of Cu I 3247.54 Å. (a) Cu 0.08 μg/mL in 0.4 M HCl solution. (b) Cu 0.08 μg/mL in 0.4 M HCl solution containing 0.75 mM KCl

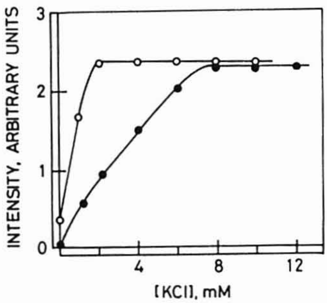

Figure 3. Effect of KCl on the line intensity of Mn I 4030.75Å with conventional V-shaped, single-well filament. (O) 0.20 μg Mn/mL in 0.05 M HCl. (●) 0.20 μg Mn/mL in water

a range of 4–12 mM KCl, but in the presence of 0.4 M HCl the range was 0.75–12 mM HCl. Hydrochloric acid apparently enhances the role of potassium chloride but cannot substitute for it.

The slope of a calibration curve for manganese (and copper), obtained with a solution containing solely 0.05 M hydrochloric acid, is steep (see above) and becomes unity on addition of potassium chloride; the slope of the curve obtained with the solution containing 1 mM KCl + 0.05 M HCl coincides with that for a solution of 10 mM KCl in the absence of HCl.

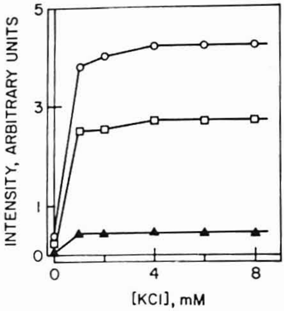

Figure 4. Effect of KCl on the emission intensities of Mn atomic and ion lines. Well 1: 5 μL of 0.10 μg Mn/mL in 0.05 M HCl. Well 2: 5 μL of various KCl concentrations. (O) Mn I 4030.75 Å. (□) Mn I 2794.82 A. (▲) Mn II 2576.10 A

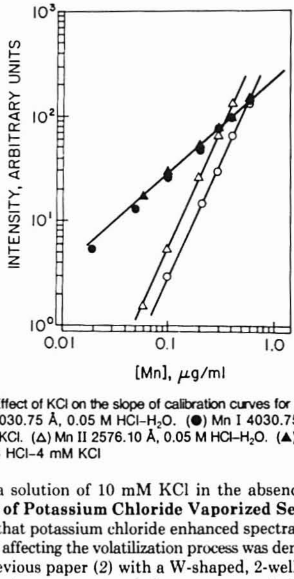

Figure 5. Effect of KCl on the slope of calibration curves for manganese. (O) Mn I 4030.75 Å, 0.05 M HCl–H_2O. (●) Mn I 4030.75 Å, 0.05 M HCl–4 mM KCl. (△) Mn II 2576.10 Å, 0.05 M HCl–H_2O. (▲) Mn II 2576 10 Å, 0.05 HCl–4 mM KCl

Effect of Potassium Chloride Vaporized Separately. The fact that potassium chloride enhanced spectral intensity largely by affecting the volatilization process was demonstrated in the previous paper (2) with a W-shaped, 2-well filament. This experiment was extended to manganese in 0.05 M hydrochloric acid. Five μL of 0.05 M hydrochloric acid solution containing 0.1 μg/mL manganese was placed in one of the wells, while the same volumes of various concentrations of potassium chloride solution were deposited in the other. Between 0 and 1 mM potassium chloride, the spectral intensities of the atom and ion lines of manganese increase rapidly, then rise very gradually to a constant level at 4 mM potassium chloride and beyond (Figure 4). At a manganese concentration of 0.1 μg/mL, potassium chloride when introduced separately enhances the atomic lines about 10-fold and the ion lines about 5-fold. These results can be explained by assuming that the decomposition of manganese salt in the vaporization process is suppressed or the recombination reaction is rapid because of the presence of the vapor of potassium chloride. Calibration curves for manganese in 0.05 M hydrochloric acid are shown in Figure 5 with or without separate introduction of 5 μL of 4 mM potassium chloride

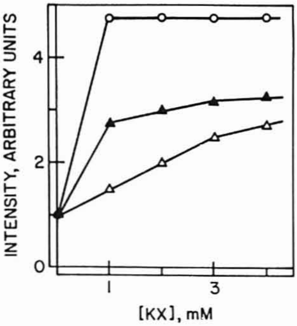

Figure 6. Effect of potassium halides on the emission line intensity of Zn 2138.56 Å. Well 1: 5 μL of 0.016 μg Zn/mL in water. Well 2: 5 μL of various concentrations of potassium halides (KX), where X = Cl (△), Br (▲), I (○)

solution. Although potassium chloride and manganese were volatilized into the plasma separately, the slope of the calibration curves for manganese altered to unity in support of the basis persumed to identify the steep calibration curves (see above) (*2*).

Effect of Recombination Reaction on the Intensities. To examine the effect of anions volatilized separately on the intensity of metals, the W-shaped, 2-well filament was used: 5 μL of a 0.016 μg Zn/mL solution was deposited in one of the wells and 5 μL of various concentrations of potassium chloride, bromide, or iodide solutions in the other. The spectral intensity of zinc depends on the particular halide introduced separately (Figure 6). This fact suggests that some interaction between zinc and potassium halides occurs in the vapor phase, since the zinc and potassium halide solutions placed on the filaments are desolvated and volatilized separately, but simultaneously. When the sample is volatilized from the heated filament, neutral atoms of metals are formed by dissociation of the compounds and can be observed by atomic absorption methods (*2*). This technique was applied to zinc halides under the same conditions described above, except that the microwave power was turned off. The axial distributions of neutral atoms of zinc along the discharge tube are shown in Figure 7. The population of zinc atoms decreases in the order chloride > bromide > iodide, an order opposite to that observed for the enhancement effect (Figure 6). From these results, recombination reaction after volatilization from the filament seems to have an important role in the enhancement of potassium halide when introduced separately. Apparently, the more rapid recombination of zinc and halogen atoms results in higher intensity of the zinc line.

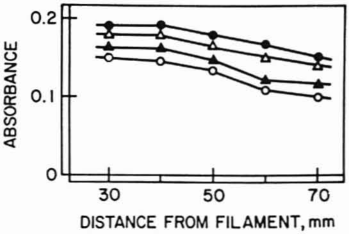

Figure 7. Axial distribution of the zinc atomic population along the discharge tube. Well 1: 0.3 μg Zn/mL in water. Well 2: (●) water. (△) 10 mM KCl. (▲) 10 mM KBr. (○) 10 mM KI

In summary, potassium chloride serves to prevent the decomposition of a sample salt in the process of volatilization and permits the volatilization of the sample from the filament as the chloride. The increase in spectral intensity of copper or manganese by the addition of hydrochloric acid is due to the same effect which is exercised by potassium chloride though HCl is less efficient. Even if neutral atoms of a metal are formed by dissociation when the sample is volatilized from the heated filament in the presence of potassium chloride, they largely recombine with chlorine atoms. An excitation mechanism in the low-pressure helium plasma has been proposed in an earlier paper (*2*): metal ions are produced directly from the metal chlorides by their collision with high energy electrons or metastable atoms of helium. This mechanism requires the sample to be introduced into the plasma as a vapor of metal chlorides and all evidence described above support the hypothesis.

LITERATURE CITED

(1) H. Kawaguchi and B. L. Vallee, *Anal. Chem.*, **47**, 1029 (1975).
(2) H. Kawaguchi, I. Atsuya, and B. L. Vallee, *Anal. Chem.*, **49**, 266 (1977).

RECEIVED for review November 3, 1976. Accepted June 13, 1977. This work was supported by Grant-in-Aid GM-15003 from the National Institutes of Health of the Department of Health Education and Welfare. One of the authors (C.V.) is recipient of Research Fellowship CA-01351 of the National Cancer Institute.

Determination of Phosphorus in Milk Powders by Optical Emission Spectrometry with a High Frequency Inductively-Coupled Argon Plasma Source

A. M. Gunn, G. F. Kirkbright,* and L. N. Ophelm

Department of Chemistry, Imperial College, London, SW7, U.K.

A rapid, direct method for the determination of phosphorus in milk powder solutions by optical emission spectrometry using an inductively-coupled argon plasma source operated at 27 MHz is presented. Optimum conditions for the determination have been established and a detection limit of 0.1 μg/mL P has been obtained at the phosphorus 213.62 nm line. A study of the precision of the technique has also been carried out and a relative standard deviation of 2% has been obtained for the complete analytical procedure.

The determination of phosphorus in aqueous solution by optical emission spectrometry using an inductively-coupled plasma source (ICP) has been reported by several groups of workers (*1–4*). The technique has been applied to the determination of phosphorus levels in blood by Greenfield and Smith (*5*) and Kniseley et al. (*6*); Kirkbright, Ward, and West (*7*) have reported its use for the determination of phosphorus in acetic acid extracts of soils. The results of the above studies indicated that the sensitivity attainable by the technique would allow the direct determination of total phosphorus in milk powders. There is a need for a rapid and precise direct method for the determination of phosphorus content of milk products without recourse to destruction of organic matter by wet ashing. As phosphorus is an essential nutritional component in milk, and is present at relatively high levels, it is necessary to achieve good precision in its determination. The molybdate colorimetric method (AOAC 7.095) is most commonly used for the determination. Inevitably, however, the necessity for wet ashing of samples before development of the absorbing species for solution spectrophotometry results in a lengthy and tedious procedure. In this paper we describe a rapid and convenient emission spectrometric method in which total phosphorus is determined by pneumatic nebulization of aqueous milk powder solutions into the inductively-coupled plasma source.

EXPERIMENTAL

Apparatus. The instrumental system employed utilized a 2-kW crystal-controlled radiofrequency generator operating at 27 MHz (International Plasma Corporation, Hayward, Calif.) and a 1-m plane grating scanning monochromator (Rank Hilger Ltd., Margate, Kent, U.K.). A demountable plasma torch assembly with tangential argon inlets and sample introduction from a central injector tube was used in this work. Specifications of the equipment employed are presented in Table I.

Reagents and Materials. All chemicals used were of reagent or analytical reagent grade. The phosphorus stock solution (1000 μg/mL) was prepared by dissolving potassium dihydrogen phosphate (Analar grade, Hopkin and Williams, Chadwell Heath, U.K.) in distilled water. Analyzed milk powder samples were kindly supplied by Cow and Gate Baby Foods, Trowbridge, Wiltshire, U.K.

Procedure. Approximately 0.5 g of the milk powder to be analyzed was weighed accurately and mixed with 10 mL of glacial acetic acid. This mixture was then diluted to 100 mL with distilled water to produce a stable solution.

Table I. Instrumentation

Plasma power supply	IPC model 120-27; operating frequency: 27.12 MHz; power output: 0–2 kW continuously variable. Work coil: $1\frac{1}{2}$ turns 6-mm o.d. copper tubing, internal diameter of coil 26 mm.
Spectrometer	Hilger Monospek 1000: Czerny-Turner scanning monochromator with plane grating (1200 lines mm^{-1}) blazed at 300 nm; reciprocal linear dispersion 0.8 nm mm^{-1}.
Optics	Plasma imaged in 1:1 ratio onto entrance slit with two fused silica lenses (7.5-cm focal length, 4-cm diameter).
Readout	Signal from EMI 6256 B photomultiplier tube displayed on Servoscribe chart recorder, model RE 511.
Plasma torch	Demountable fused silica torch with brass base. Coolant gas tubing: 18-mm i.d. Plasma gas tubing: 16-mm o.d. Injector tubing: 6-mm o.d., 1.5-mm orifice diameter.
Nebulizer	Concentric glass nebulizer and spray chamber (Plasma-Therm Inc., Kresson, N.J.). Uptake rate: 1.3 mL min^{-1} for water, 1.2 mL min^{-1} for 10% v/v acetic acid; at argon flow rate 1.3 mL min^{-1}. Efficiency for water, 3%. Efficiency for 10% v/v acetic acid, 4%.

Table II. Plasma Operating Conditions

Net forward RF power	1200 W
Spectrometer slits	20 μ entrance and exit slits
Argon coolant gas flow rate	11.0 L min^{-1}
Argon plasma gas flow rate	1.0 L min^{-1}
Argon sample transport gas flow rate	1.3 L min^{-1}
Viewing height	25 mm above work coil

Sample solutions prepared in this way contained between 5 and 40 μg/mL phosphorus. These were analyzed by measurement of the phosphorus emission intensity at 213.62 nm produced on nebulization of the sample solutions into the plasma and comparison with a calibration graph constructed by measurement of the intensity at 213.62 nm produced on nebulization of aqueous phosphate standard solutions prepared in 10% acetic acid solution. The plasma operating conditions employed are shown in Table II. These were chosen to optimize the signal-to-noise ratio observed at the phosphorus 213.62 nm line.

RESULTS AND DISCUSSION

Choice of Analytical Line for Phosphorus Determination. Although the principal resonance lines of the

Table III. Determination of Phosphorus Content of Milk Powders

Sample No.	Calcium content, %	Phosphorus content, %: By AOAC molybdate method[a]	Phosphorus content, %: By ICP-OES method	RSD, %
1	0.36	0.22	0.21	2.2
2	0.72	0.42	0.44	-
3	0.78	0.15	0.17	-
4	0.73	0.49	0.50	-
5	0.75	0.17	0.17	-
6	0.93	0.64	0.62	2.0
7	0.46	0.42	0.42	1.4

[a] Estimated precision, ± 3%.

phosphorus atom all lie below 200 nm, there are a number of atomic emission lines in the range 200–300 nm which are of sufficient intensity to be analytically useful. In order to establish the most suitable of these lines for determination of phosphorus, the relative intensities and detection limits for the 213.62, 214.91, 253.56, and 255.33 nm lines were measured; the 213.62 nm line exhibited the highest intensity and the lowest detection limit (0.1 μg mL^{-1}) and was therefore selected for use in all further work.

Effect of Calcium. The interference of phosphate in the determination of Ca is well known in flame atomic spectrometry and has been explained by the postulation that a relatively nonvolatile compound is formed between calcium and phosphorus in the flame (*8*). A number of studies of the effect of phosphate on calcium emission intensity in the ICP have been reported (*9–11*). These have indicated the absence of any significant interference in the plasma tail flame. This might be expected as a result of the large amount of thermal energy available in the ICP source combined with the relatively long residence times of the particles in the axial channel of the plasma.

The effect of the concomitant calcium ion on the intensity of phosphorus atom line emission observed in an early form of "tear drop" shaped ICP has been investigated by Kirkbright, Ward, and West (*7*); a 20% enhancement in the phosphorus emission intensity at 213.62 nm in the presence of a 50-fold excess of calcium was reported. As relatively high calcium levels are present in milk, it was decided to investigate the effect of calcium on the phosphorus determination with the source employed in this work. The results obtained at an observation height of 25 mm above the work coil demonstrated the absence of any significant interference in the presence of up to a 10-fold weight excess of calcium. A slight (4%) suppression was observed at a 50-fold excess but this is not important for the purposes of the present work, as calcium concentrations of this order are not encountered in milk powder samples as is evident from Table III. These results are in general agreement with the complementary observations (*10*) of the effect of phosphate on calcium emission in the ICP source.

Analysis of Milk Powders. The accuracy of the method was examined by determining the phosphorus content of seven milk powders which had been independently analyzed by the standard AOAC solution spectrophotometric method (7.095) after wet ashing.

Initial attempts to analyze the samples after their dissolution in hot or cold distilled water gave rise to low results for the majority of the samples. This was attributed to incomplete dissolution of phosphorus-containing protein components in the milk powders. This problem was overcome by the use of acetic acid in the procedure employed to prepare the sample solutions. Addition of glacial acetic acid to the milk powders resulted in the formation of a fine precipitate which could then be easily taken up by dilution with distilled water to form a homogeneous solution which did not settle out on centrifuging.

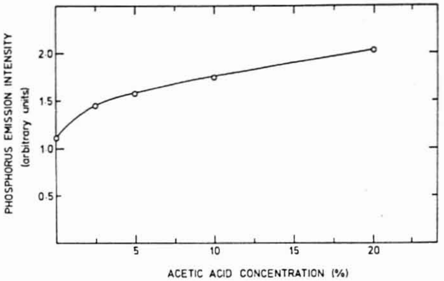

Figure 1. Effect of acetic acid on the emission intensity at 213.62 nm of a 10 μg mL^{-1} phosphorus solution

The presence of acetic acid in sample solutions was found to result in an enhancement of the phosphorus emission intensity at 213.62 nm as shown in Figure 1. This may be attributed in part to the effect of the changed physical properties of the solution (surface tension, density, and viscosity) on the nebulization efficiency as shown in Table I. Thus, in the determination of the phosphorus content of the milk samples, it was necessary to construct the calibration curve from aqueous phosphorus standards containing a concentration (10%) of acetic acid equivalent to that present in the sample solutions.

The results obtained for the phosphorus determinations using the recommended procedure are shown in Table III. These can be seen to be in good agreement with the results obtained by independent analysis.

Precision. The precision of the complete method was estimated by carrying out replicate analyses on three of the milk samples (sample numbers 1, 6, and 7 in Table III). Four separate solutions were prepared for each of the three samples and four replicate analyses were then made on each of these solutions. Intensity measurements were obtained for sample solutions by wavelength scans through the 213.62 nm line and these were compared with the emission intensity observed for a standard phosphorus solution measured in a similar manner. The relative standard deviations in the results of the 16 analyses for each sample were calculated and are shown in Table III.

An overall value for the precision of the complete method was also obtained by computing the pooled relative standard deviation for the three series of analyses (48 samples); a relative standard deviation of 2% was obtained in this way.

ACKNOWLEDGMENT

The authors thank J. V. Stevens, Cow and Gate Baby Foods, Trowbridge, Wiltshire, U.K., for the supply of the analyzed milk samples.

LITERATURE CITED

(1) G. W. Dickinson and V. A. Fassel, *Anal. Chem.*, **41**, 1021 (1969).
(2) V. A. Fassel and R. N. Kniseley, *Anal. Chem.*, **46**, 1110A (1974).
(3) P. W. J. M. Boumans and F. J. de Boer, *Spectrochim. Acta, Part B*, **30**, 309 (1975).
(4) M. H. Abdallah, R. Diemiaszonek, J. Japosy, J. M. Mermet, J. Robin, and C. Trassy, *Anal. Chim. Acta*, **84**, 271 (1976).
(5) S. Greenfield and P. B. Smith, *Anal. Chim. Acta*, **59**, 341 (1972).
(6) R. N. Kniseley, V. A. Fassel, and C. C. Butler, *Clin. Chem. (Winston-Salem, N.C.)*, **19**, 807 (1973).

(7) G. F. Kirkbright, A. F. Ward, and T. S. West, *Anal. Chim. Acta*, **62**, 241 (1971).
(8) G. F. Kirkbright and M. Sargent, "Atomic Absorption and Fluorescence Spectroscopy", Academic Press, London, 1974, p 516.
(9) S. Greenfield, I. L. Jones, and C. T. Berry, *Analyst (London)*, **89**, 713 (1964).
(10) G. F. Larson, V. A. Fassel, R. H. Scott, and R. N. Kniseley, *Anal. Chem.*, **47**, 238 (1975).
(11) M. H. Abdallah, J. M. Mermet, and C. Trassy, *Anal. Chim. Acta*, **87**, 329 (1976).

RECEIVED for review April 5, 1977. Accepted June 3, 1977. We thank the British Council for the award of a Postdoctoral Scholarship to one of us (L.N.O.).

Colorimetric Determination of Hippuric Acid in Urine and Liver Homogenate

Shinji Ohmori* and Mikiko Ikeda

Faculty of Pharmaceutical Sciences, Okayama University, Okayama 700, Tsushima-Naka-1, Japan

Shohei Kira and Masana Ogata

Department of Public Health, Okayama University Medical School, Okayama 700, Shikata 2-5, Japan

To a dried extract containing hippuric acid (HA), 1.0 mL of acetic anhydride and 2.0 mL of 0.5% *p*-dimethylaminobenzaldehyde (DAB) solution in pyridine were added, and the solution was kept at 40 °C for 1 h after thorough mixing. The absorbance was then determined at 458 nm against a blank containing acetic anhydride, DAB, and pyridine. This method was in good agreement with Beer's law within 1 to 100 μg and the mean ± SD absorbance for 20 μg HA was 0.939 ± 0.013 (n = 5). The apparent molar absorptivity of 2.5 × 10^4/mol/cm, and the relative standard deviation of 1.4% was calculated.

The determination of hippuric acid (HA) in urine is of great significance, mainly for testing of liver function (*1*), diagnosis (*2–4*), and estimation of the detoxication of alkylbenzenes and drugs (*5–7*).

In this paper a convenient and reproducible method based on colorimetry is presented. About 40 papers dealing with methods of determination of HA have been published. These methods depend on column chromatography (*8*), extraction (*9*), colorimetry (*10–13*), gas chromatography (*14–17*), thin-layer chromatography (*18*), paper chromatography (*19*), fluorimetry (*20*), titration (*21*), and determination of radioactivity (*22*). The method most widely used at present is based on gas chromatography. Applying this method to the determination of HA in liver homogenates of rat and eel (instead of urine), we had difficulties with overlapping peaks. The method to be described here is applicable to urine as well as liver homogenates.

Two colorimetric methods have been presented for the determination of HA. With the method of Umberger (*10*) which was later modified by Ogata, the color is produced in a mixture of the HA-containing sample with benzene–sulfonylchloride and pyridine. With the method reported by Gaffney et al. (*19*) and Ogata et al. (*23*), DAB is used. Gaffney et al. employed paper chromatography. They detected the HA spot by spraying a 4% solution of DAB in acetic anhydride which contained a few crystals of sodium acetate with subsequent heating of the chromatogram at 130–150 °C for 1–2 min. The absorbance of the color was determined after elution of the spot. Ogata et al. improved this method. Their reaction mixture additionally contained silica gel.

The colorimetric procedure reported in this paper is based on the DAB method.

EXPERIMENTAL

Chemicals and Instruments. Analytical grade chemicals from Wako Pure Chemical Industries Ltd (Osaka, Japan) were used. A Hitachi-139 Spectrophotometer was used for measuring the absorbance at 458 nm and a Hitachi-124 Spectrophotometer for recording the absorption spectra.

Determination of HA. *Extraction of HA from Urine.* Urine (0.1 mL), 10 μL 6 N HCl, ca. 20 mg NaCl, and 1 mL ethyl acetate in a 10-mL test tube were mixed for 30 s with a Vortex mixer (Thermonics Inc., Japan). After 5 min, a 0.1-mL aliquot of the ethyl acetate layer was transferred to a 20-mL test tube and evaporated to dryness under reduced pressure.

Extraction of HA from Liver Homogenates. Method A: for homogenates containing more than 20 μg HA per 0.5 mL. Rat liver (10 g) was homogenized in 90 mL of 1.15% KCl in a Potter–Elvejhem Teflon pestle homogenizer and then centrifuged at 1000 × g for 10 min.

To a 10-mL glass stoppered centrifuge tube, 0.5 mL of the supernatant and 20 μL 6 N HCl, 20 μL glacial acetic acid, ca. 150 mg NaCl, and 2.5 mL ethyl acetate were added. The mixture was agitated with a Vortex mixer for 30 s and centrifuged at 1500 × g for 5 min. The ethyl acetate layer was dried over anhydrous sodium sulfate. An aliquot (0.5 mL) was then evaporated under reduced pressure.

Method B: for homogenates containing less than 20 μg HA per 0.5 mL. To a 10-mL glass stoppered centrifuge tube 0.5 mL of the supernatant of the homogenate and 50 μL 6 N NaOH, ca. 150 mg NaCl, and 5 mL ethyl acetate were added. The mixture was agitated with a Vortex mixer. It was then centrifuged at 1500 × g for 10 min and the ethyl acetate layer was removed as thoroughly as possible. The aqueous layer was acidified with 0.1 mL 6 N HCl and extracted with 5 mL *n*-hexane by vortexing and centrifuging. After the hexane layer was removed as thoroughly as possible, the aqueous layer was extracted with 5 mL ethyl acetate by vortexing and centrifuging. The extract was dried with anhydrous sodium sulfate and an aliquot (3.5 mL) was evaporated under reduced pressure.

Development of the Color and Its Measurement. To the dried HA-containing residue, 1.0 mL of acetic anhydride and 2.0 mL of 0.5% DAB solution in pyridine were added in turn. After thorough mixing, the solution was kept at 40 °C for 1 h. The absorbance was then determined at 458 nm against a blank containing acetic anhydride, DAB, and pyridine.

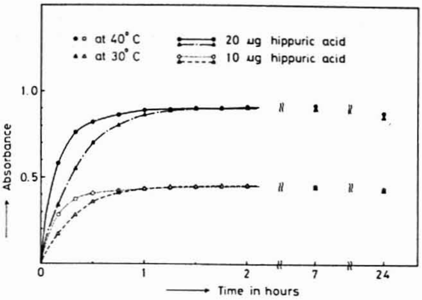

Figure 1. Time course of color development. HA (10 and 20 µg) was allowed to react with 1.0 mL of acetic anhydride and 2.0 mL of 0.5% DAB solution in pyridine at 30 or 40 °C

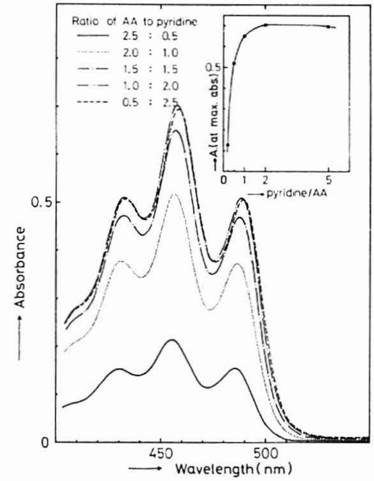

Figure 2. Absorption spectra under varying ratios of acetic anhydride and pyridine. HA (15 µg) was reacted in a final concentration of 0.33% DAB at 30 °C for 2 h

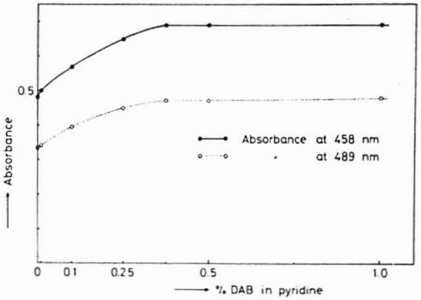

Figure 3. Influence of the concentration of DAB on color development. HA (15 µg) was allowed to react with 1.0 mL acetic anhydride and 2.0 mL of 0.5% DAB in pyridine at 40 °C for 1 h

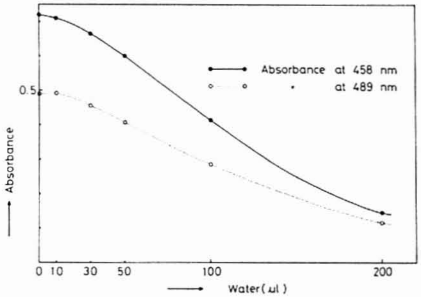

Figure 4. Influence of water on color development. HA (15 µg) was allowed to react with 1.0 mL acetic anhydride and 2.0 mL of 0.5% DAB in pyridine at 40 °C for 1 h, in the presence of different amounts of water

Table I. Reliability of Color Development under the Standard Condition[a]

HA, µg	N	Mean ± SD absorbance at 458 nm	Rel std dev, %
10	5	0.466 ± 0.015	3.2
20	5	0.939 ± 0.013	1.4
30	5	1.444 ± 0.017	1.2

[a] Using a standard ethyl acetate solution of HA, the color was developed according to the procedure in Experimental after ethyl acetate was evaporated.

RESULTS

Time Course of Color Development. As is shown in Figure 1, it takes about 1 h at 40 °C or up to 2 h at 30 °C to develop the maximum absorbance. The color is stable for at least one day.

Absorption Spectra under Varying Ratios of Acetic Anhydride and Pyridine. In a total volume of 3 mL with constant amounts of DAB and HA, the color was developed in the presence of different ratios of acetic anhydride and pyridine. As shown in Figure 2, there was a minute red shift with increasing pyridine concentration. The maximum absorbance at 458 nm was obtained with a pyridine/acetic anhydride ratio of 2.

Influence of Concentration of DAB on Color Development. HA (15 µg), 1.0 mL acetic anhydride and 2.0 mL of pyridine containing different concentrations of DAB were kept at 30 °C for 2 h. As shown in Figure 3, almost the same absorbance was found in the range of 0.375 to 1.0% DAB in pyridine. A final concentration of 0.33% DAB was, however, chosen as standard concentration to avoid HA-independent color development. Figure 3 also shows that the color is developed in the absence of DAB. It took, however, more than 3 h until the absorbance reached a constant value.

Influence of Water on Color Development. The color was developed under standard conditions except that varying amounts of water were added to the reaction mixture. As shown in Figure 4, up to 30 µL of water do not influence the color development significantly.

Calibration Curves. (*a*) *Calibration Curve without Extraction.* The calibration curves which were prepared using a standard ethyl acetate solution of HA showed fine linearity within 1 to 100 µg. Moreover as shown in Table I, this method is precise to 1.4% relative standard deviation for 20 µg HA. The apparent molar absorptivity was 2.5×10^4/mol/cm at 458 nm.

(*b*) *Calibration Curves with Extraction.* The calibration curves, which were prepared using an HA aqueous standard solution according to the extraction procedures for urine or

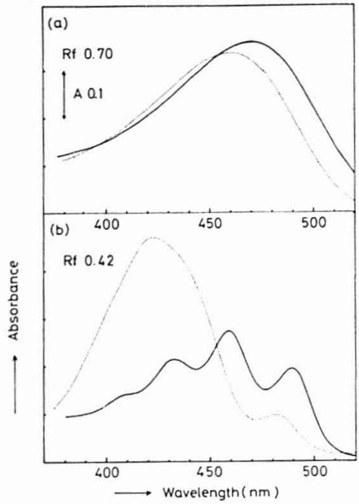

Figure 5. Absorption spectra of two yellow spots separated on a thin-layer chromatogram. The solid lines represent the absorption spectra in methanol and the dotted lines in the mixed solution of acetic anhydride and pyridine (1:2)

liver homogenate, also showed good agreement with Beer's law and about 94% of absorbance by comparing with (*a*).

Recovery Tests. As shown in Table II, recoveries of HA added to urine are 100.1 ± 3.4%, and in the case of liver homogenates, they are 73.8 ± 1.3% for Method B and 92.7 ± 2.3% for Method A. When Method A is applied to the sample containing less than 20 μg HA per 0.5 mL, an HA-independent color development attributable to the contents of liver homogenate prevents accurate determination. This is why two methods are applicable respectively.

DISCUSSION

The colorimetric method for determination of HA, presented in this paper, is simpler, more reproducible, and about 5 times more sensitive than the previous colorimetric methods.

With thin-layer chromatography of the colored substance on silica gel developing with toluene/acetic acid 9:1, three yellow spots (R_f 0.70, 0.48, and 0.42) could be separated. The absorption spectra of the eluted spots with methanol indicated that the colored compound with the R_f value of 0.42 mainly contributed to the absorbance at 458 nm (see Figure 5). This substance may be 2-phenyl-4-(1-hydroxyethylidene)oxazol-5-one which was synthesized by Attenburrow et al. (*24*). The substance with the R_f value of 0.70 may be 2-phenyl-4-(*p*-dimethylaminobenzal)oxazol-5-one, which was synthesized by Schueler et al. (*25*) and Gaffney et al. (*19*). The spot with the R_f value of 0.48 was paler than the other two. The color faded away after elution with methanol. Work is in progress to identify the colored substances.

Seventeen urine samples were used for comparing the present method with the gas chromatograph method by Buchet et al. (*14*), and from data a correlation coefficient of 0.977 and the regression line of $Y = 0.896X + 0.090$ was calculated (Y = the present method).

Table II. Recovery Studies of Hippuric Acid Added to Urine and Liver Homogenate by the Present Method

HA added, μg	HA(μg)/0.1 mL of urine (n = 3)	Recovery, %	HA added, μg	HA(μg)/0.5 mL of liver homogenate (n = 3)	Recovery, %
0	15.9 ± 0.2		0	N.D.	
10	25.4 ± 1.5	95.0	5	3.62 ± 0.08	72.4^a
15	30.5 ± 0.7	97.3	10	7.43 ± 0.28	74.3^a
20	35.9 ± 1.2	100.0	15	11.22 ± 0.39	74.8^a
50	65.3 ± 4.1	98.7	20	17.9 ± 1.2	89.5^b
100	121.2 ± 1.0	105.3	50	46.4 ± 3.0	92.8^b
150	169.8 ± 3.3	102.6	70	65.5 ± 4.6	93.6^b
200	218.9 ± 2.8	101.5	100	95.0 ± 7.2	95.0^b
Mean		100.1	Mean		73.8^a 92.7^b
SD		3.4	SD		1.3^a 2.3^b

[a] HA was extracted according to Method B. [b] HA was extracted according to Method A.

With the present method the absorbance can also be measured at 489 nm in good agreement with Lambert–Beer's law. Compared with measurements at 458 nm, the sensitivity is about 70%.

ACKNOWLEDGMENT

We are grateful to Y. Yoshida for help in the laboratory.

LITERATURE CITED

(1) A. J. Quick, *Am. J. Clin. Pathol.*, **10**, 222 (1940).
(2) A. Hill, G. N. Hoag, and W. A. Zaleski, *Clin. Chim. Acta*, **37**, 455 (1972).
(3) C. F. van Sumere, H.PE,R. Verbeke, and J. Bekaert, *Clin. Chim. Acta*, **26**, 85 (1969).
(4) T. D. Beardmore and W. N. Kelley, *Clin. Chem.* (*Winston-Salem, N.C*), **17**, 795 (1971).
(5) M. Ikeda and H. Ohtsuji, *Br. J. Ind. Med.*, **26**, 244 (1969).
(6) S. P. James and D. A. White, *Biochem. J.*, **104**, 914 (1967).
(7) Y. Kato, *Yakugaku Zasshi*, **92**, 1140 (1972).
(8) L. A. Barness, G. Morrow III, R. E. Nocho, and R. A. Maresca, *Clin. Chem.* (*Winston-Salem, N.C.*), **16**, 20 (1970).
(9) H. Chantrenne, *J. Biol. Chem.*, **189**, 227 (1951).
(10) C. J. Umberger and F. F. Fiorese, *Clin. Chem.* (*Winston-Salem, N.C.*), **9**, 91 (1963).
(11) K. Tomokuni and M. Ogata, *Clin. Chem.* (*Winston-Salem, N.C.*), **18**, 349 (1972).
(12) H. Kehl, *Clin. Chem.* (*Winston-Salem, N.C.*), **13**, 475 (1967).
(13) A. M. EL Masry, J. N. Smith, and R. T. Williams, *Biochem. J.*, **64**, 50 (1956).
(14) J. P. Buchet and R. R. Lauwerys, *Br. J. Ind. Med.*, **30**, 125 (1973).
(15) O. A. Mamer, J. C. Crawhall, and S. S. Tjoa, *Clin. Chim. Acta*, **32**, 171 (1971).
(16) U. Langenbeck and J. E. Seegmiller, *J. Chromatogr.*, **80**, 81 (1973).
(17) R. F. Coward and P. Smith, *J. Chromatogr.*, **45**, 230 (1969).
(18) H. Teuchy and C. F. van Sumere, *Clin. Chim. Acta*, **25**, 79 (1969).
(19) G. W. Gaffney, K. Schreier, N. Diferrante, and K. I. Altman, *J. Biol. Chem.*, **206**, 695 (1954).
(20) G. L. Ellman, A. Burkhalter, and J. La Don, *J. Lab. Clin. Med.*, **57**, 813 (1961).
(21) M. L. Verma and R. K. Srivastava, *Microchem. J.*, **14**, 396 (1969).
(22) J. W. Bridges, M. R. French, R. L. Smith, and R. T. Williams, *Biochem. J.*, **118**, 47 (1970).
(23) M. Ogata, K. Tomokuni, and Y. Takatsuka, *Br. J. Ind. Med.*, **26**, 330 (1969).
(24) J. Attenburrow, D. F. Elliot, and G. F. Penny, *J. Chem. Soc.*, 310 (1948).
(25) F. W. Schueler and S. C. Wang, *J. Am. Chem. Soc.*, **72**, 2220 (1950).

RECEIVED for review November 1, 1976. Accepted June 21, 1977. Work supported in part by a grant (No. 111315) from the Ministery of Education of Japan.

New Drift-Tube Source for Use in Chemical Ionization Mass Spectrometry

P. C. Price,[1] H. S. Swofford, Jr., and S. E. Buttrill, Jr.*[2]

Department of Chemistry, University of Minnesota, Minneapolis, Minnesota 55455

A new ion source incorporating an integral drift tube allows control over the extent of fragmentation of the quasi-molecular ions produced in chemical ionization mass spectrometry. Increasing the electric field strength in the drift-tube region causes fragmentation similar to that observed at higher source temperatures or with more energetic reagent gases. Effective *ion* temperatures in excess of 1000 K are available at the highest drift fields. Since a single drift voltage setting controls the extent of fragmentation, it is possible to obtain both molecular ion spectra and extensive fragmentation on successive scans of a single sample.

Chemical ionization mass spectrometry (CIMS) has gained very wide acceptance as an analytical tool in the decade since its initial development (*1*). One of the greatest advantages of CIMS over electron impact ionization is the great reduction or elimination of fragment ions, simplifying the spectrum and usually producing an intense quasi-molecular ion, i.e., either MH^+ or $(M - 1)^+$. CI conditions under which only quasi-molecular ions are present are ideal for quantitation of a compound, and they greatly facilitate the determination of the number of components or the purity of an unknown sample. However, the molecular weight alone is not sufficient to identify a compound; considerable additional information, such as is available from the masses and intensities of fragment ions, is almost always required.

The extent of fragmentation of the quasi-molecular ions in CIMS may be increased by increasing the source temperature (*2*), or by using a more energetic reagent gas (*3*). Both of these methods are relatively slow and experimentally inconvenient and would certainly require the introduction of additional samples with conventional instrumentation.

Early in the development of CIMS, it was recognized that increasing the electric field inside the ion source increased the relative intensities of fragment ions (*4–6*). This effect was attributed to unimolecular fragmentation of the MH^+ ions activated by energetic collisions with neutral reagent gas molecules in the source. This report describes a drift-tube chemical ionization source which uses this effect to provide a variable degree of fragmentation of the quasi-molecular ions in the CI spectrum.

A drift tube is a cylindrical chamber in which a uniform longitudinal electric field is maintained by a series of ring shaped electrodes. Ions introduced into one end of the tube by an ion source may be accelerated through a neutral buffer gas by applying a voltage gradient down the tube. The theory of ion motion in drift tubes has been reviewed by several authors (*7–11*). Briefly, ions entering a drift tube will acquire energy from the electric field. It has been shown that this energy is related to a parameter E/P, where E = electric field strength, and P = neutral gas pressure in the tube. E/P has the units V/cm Torr. This quantity may also be expressed as E/N or V cm^2 where N = molecules/mL, the conversion being $E/N = (E/P)(2.83 \times 10^{-17})$. Often E/N is expressed in Townsends, where Td = (V cm^2)(10^{17}).

The mean kinetic energy of the ion distribution may be approximated (*12*) by

$$KE = mv^2/2 + Mv^2/2 + 3kT/2 \tag{1}$$

where m = mass of the ion, M = mass of the neutral gas, v = drift velocity, and T = gas temperature. The additional ion kinetic energy from the electric field may be described in terms of an "effective ion temperature," which will be equal to T at very low E/P, but may be several thousand Kelvins as E/P enters the high field region (*13, 14*). This "effective temperature" is defined by Mason (*11*) as:

$$T_{eff} = T(1 + Mv^2/3kT) \tag{2}$$

Qualitatively, both the ion velocity and internal energy increase with E/P. The average translational energy of the ions is determined by the steady-state balance of the energy gained from the electric field and the energy lost to the neutrals as a result of collisions. These collisions with the reagent gas molecules also increase the internal energy of the ions, resulting in an effective "vibrational temperature" which is comparable to the "translational temperature." If ions are formed by the CI process at the rear of a drift tube, one should be able to raise the "effective temperature" of those ions by collisions with neutral gas molecules to very high values. This should simulate the operation of a conventional CIMS source at temperatures not normally attainable, and should result in increased fragmentation. Since the crucial parameter, E/P, may be rapidly changed by varying E, by merely changing the voltage of the drift electrodes, one should be able to rapidly change the "effective source temperature".

EXPERIMENTAL

The basic mass spectrometer used in this work is a DuPont 21-490B modified for CIMS as described previously (*15*). A cross-sectional view of the drift tube chemical ionization source is shown in Figure 1. The source is cylindrically symmetrical about the direction of ion motion.

The electron beam enters at the rear of the source at an angle of approximately 45° with respect to the axis. The filament and rear electrode of the Pierce style (*16*) electron gun are about 2.5 cm from the 0.79-mm electron beam entrance hole. Under the usual operating conditions, the filament and rear electrode are at zero potential, the front electrode is at 300–700 V, and the source is at accelerating potential (approximately 1300 V). From observation of the burned discoloration of the polished flat surface at the rear of the source housing, it appears that the image of the filament on the source is 100% to 125% of the actual filament area (0.75 × 7.5 mm). The filament is made of 0.75 mm × 0.025 mm rhenium ribbon and lasts at least 4 months in normal operation.

The metal parts of the source are machined entirely from stainless steel. The insulators are made of MACOR Machinable Glass-Ceramic (Corning Glass Works) and are shown shaded in Figure 1. Beginning at the left in Figure 1, part A is the ion source itself which may be biased by up to 45 V with respect to the drift tube base, part B. In addition to serving as the union between

---

[1] Present address, Union Carbide 770-120, P.O. Box 8361, South Charleston, W. Va. 25303.

[2] Present address, Stanford Research Institute, Menlo Park, Calif. 94025.

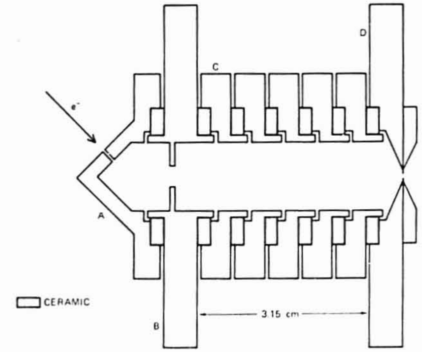

Figure 1. Drift tube ion source

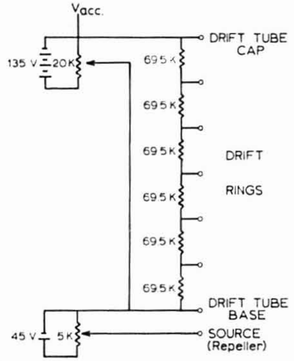

Figure 2. Drift tube CI source circuitry

the source and drift tube, the base plate, B, contains the gas inlets and a thermocouple well, which are not shown. Part C and the next four metal parts are the drift rings which are designed to completely shield the insulators from the ions moving through the drift tube. Part D is the drift tube cap and contains a second thermocouple well and mounting holes for an Einzel lens assembly (not shown). The ion exit aperture is a 1.0-mm hole in a 9.5-mm diameter disk 0.05 mm thick which is clamped to the cap.

To make the source relatively gas tight without the use of numerous gaskets, both the insulating rings and the mating surfaces on the metal parts were machined flat and highly polished. The entire stack is clamped tightly together with four 0-80 rods running through the eight metal parts.

The voltages for the drift tube source are provided by the circuit in Figure 2. The voltage divider, consisting of seven 69.5-kOhm 0.5% resistors, is mounted inside the source housing. The batteries and controls are enclosed in a box floated at accelerating potential. With this particular circuit, both the repeller field and the drift field may be varied independently over a wide range without appreciably changing the energy of the ions reaching the magnetic sector (but see below).

The electron gun could be biased at any potential up to 1000 V relative to the ion source. However, with the source pressure at 0.1 Torr, the ion current increased steadily with increasing electron energy. Thus, maximum sensitivity was obtained by running the filament at ground potential giving an electron energy of approximately 1300 eV. Using water as reagent gas, repeller settings of greater than 6 V gave less than 10% increase in sensitivity, even with low drift fields. Hence the repeller was usually run at 5 V or less. As in previous work with a more conventional CI source (*17–19*), maximum total ion current and stable operation were obtained by tuning the ion focusing and beam steering lenses to maximize the $H_9O_4^+$ ion from water reagent gas. Very detailed descriptions of the drift tube ion source (*20*) and the new source housing and ion optics (*21*) are available elsewhere.

Table I. Measurement of Approximate Effective Ion Temperature of MH^+ Ions from 1-Octene in Water Reagent Gas[a] as a Function of E/P

Drift voltage, V	E/P, V/cm Torr	ΔV_{acl}, V	T_{eff}, K
0	0	0	303
31.3	33.1	0.2	550
45.5	48.1	0.4	800
69.4	73.4	0.6	1040

[a] See text for experimental conditions.

The dynamic sensitivity of the drift-tube source was frequently measured with a standard sample as a check on tuning parameters and source conditions. With the source at 100 °C, 0.1 Torr, and E/P of 67 V/cm Torr (using water as a reagent gas), the detection limit for an injected aqueous solution of 1-octene was 5 to 10 ppm. While this present detection limit does not permit trace analyses, it is sufficient to demonstrate potential analytical utility.

RESULTS AND DISCUSSION

It was of immediate interest to demonstrate that, under CI conditions, large amounts of energy could be imparted to ions in the drift tube. This measurement was made by utilizing a basic property of a magnetic sector mass spectrometer; ions are focused at the detector according to the following formula:

$$m/e = kH^2r^2/V \tag{3}$$

where k is a constant, H is the strength of the magnetic field, and V is the voltage through which ions are accelerated. If a given ion is focused at the collector, it would be observed to shift position if the accelerating voltage was changed. Thus, at constant accelerating voltage, any changes in the energy (eV) of ions leaving the source will appear as a slight shift of V in Equation 3. There will then be a shift of the peak position as observed at the collector. If the accelerating voltage is changed an amount corresponding in voltage to the additional energy accumulated by the ion in the source, the peak should return to its previous position as observed at the collector.

First, to determine the accuracy of this method, an experiment was performed with the source operating in the electron impact mode. The source pressure was less than 1 μm, the temperature was 30 °C, and the repeller was set at 0 V; the only gas present was air. With the accelerating voltage set at 1270.6 V, m/e 28 was focused on the collector. An increase of the drift voltage from 0 to 3.3 V necessitated a decrease of 3.2 V of the accelerating voltage to 1267.4 V to refocus m/e 28. Thus, the application of 3.3-V drift voltage increased the ion energy by 3.2 eV. Similarly, 24.3 V applied to the drift tube contributed 24.5 eV to the ion energy, and 95.8 V contributed 95.4 eV of energy. From these data, it can be seen that by keeping an ion peak focused on the collector by varying the accelerating voltage, changes in energy of ions leaving the source can be measured. Slight errors are the result of the problems associated with measuring 0.1-V changes at the kilovolt level.

The experiment was repeated with the drift-tube source operated in the CI mode with water as the reagent gas and 1-octene as the sample. The source pressure was 0.217 Torr, the temperature was 30 °C, and the repeller voltage was 0. The MH^+ ion (m/e 113) was focused at the collector with the accelerating voltage at 1268.4 V. The results of increasing the drift voltage under these conditions are shown in Table I.

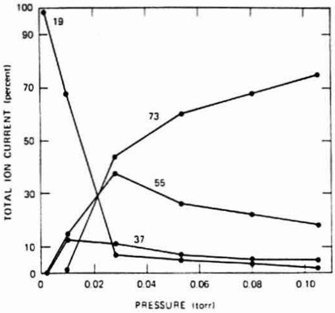

Figure 3. H_2O cluster ions vs. pressure: drift voltage = 15 V, 115 °C

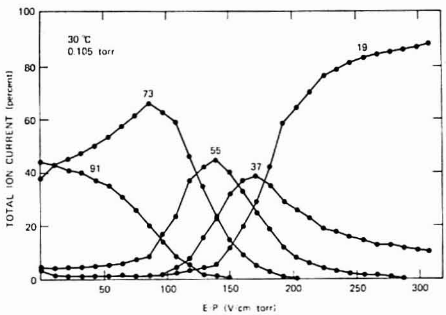

Figure 4. Water cluster ions: 30 °C, 0.105 Torr

As the drift voltage (or E/P value) was increased, the corresponding accelerating voltage necessary to center mass 113 at the collector decreased. At an E/P of 73.4 V/cm Torr, the ions exiting the source have accumulated an excess of 0.6 eV over their energy when the drift field is zero. This excess kinetic energy of motion along the axis of the drift tube ($e\Delta V$) is just the quantity represented by the first term (*11*) in Equation 1, so that we have a crude measure of the drift velocity. Combining this fact with Equation 2 yields an expression for the "effective temperature" which can be evaluated directly:

$$T_{\mathrm{eff}} = T[1 + (2Me\Delta V)/(3mkT)] \qquad (4)$$

As shown in Table I, the effective temperature of the ions estimated in this way exceeds 1000 K at E/P = 73.4 V/cm Torr.

It is of interest to compare the water reagent ion intensities obtained with this source with those observed in the more conventional CI source (*17*) and those expected under equilibrium conditions (*22*). Figure 3 shows the variation of water cluster ion intensities at 115 °C and constant 3.45 V/cm drift field. The larger clusters at m/e 55 and 73 begin to dominate the spectra at much lower pressures than in the modified DuPont source (*17*). This is undoubtedly due to the much longer distance which the ions must now travel within the source to reach the source exit aperture.

Figure 4 shows the variation of water cluster ion intensities with E/P at 0.105 Torr and 30 °C. The effects of increasing E/P are qualitatively very similar to those expected from raising the source temperature. Figure 5 is a plot of the relative equilibrium concentrations of the various ions in water calculated from Kebarle's thermochemical data for these ions (*22*). Comparing Figures 4 and 5 shows that at low values of E/P in water, the ion intensities are very close to those expected at equilibrium. The small signals at m/e 55 and 37 are possibly due to collisional dissociation of a small fraction of the ions as they leave the source. At higher values of E/P, the behavior of the relative intensities of the cluster ions deviates from that expected at any particular temperature. At any given E/P value between 100 and 200 V/cm Torr, three different ions are always present in significant (>15%) amounts, whereas under true thermal equilibrium, there is no temperature at which more than two ions are significant. This observation is totally consistent with the fact that *only* the *ion* "temperature" is increased by the drift field. Also, the ion speeds and vibrational energies are not accurately described by the Boltzmann distribution.

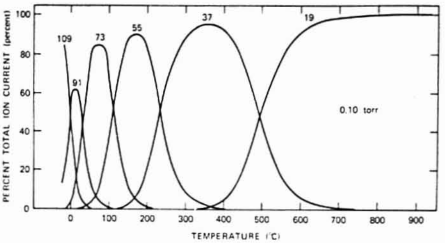

Figure 5. H_2O clusters vs. temperature at 0.10 Torr

Table II. Methane Reagent Gas Ions (Percent Total Ion Current) Observed in the Drift-Tube Source at 30 °C and 0.10 Torr

	E/P values, V/cm Torr					
m/e	0	33.3	66.7	133	200	267
15	6	0.3	0.3	1.9	6.3	12
17	28	15	26	26	18	14
19	11	32	22	6.4	1.9	0.6
27	0.9	0.3	3.2	22	28	29
29	45	37	34	19	27	30
39	0.0	0.1	0.4	10	12	9.8
41	9.3	15	14	15	7.0	3.9

Since methane was the first reagent gas used in CIMS and is probably still the most common, it was tried in the new source. Table II shows the intensities of the major peaks observed in methane with the drift-tube source at a variety of E/P values. At zero field, the spectrum is similar to that obtained by Field (*1*) and others under conventional CI conditions. As E/P is increased, there do appear to be increases in fragmentation; the m/e 15, 27, and 39 peaks increase, while m/e 17, 29, and 41 decrease. Plots of the intensity of ions in methane reagent gas vs. pressure were similar to Field's work (at low E/P), except it appeared that a "steady-state" population was reached at approximately 0.1 Torr. Notable exceptions were m/e 39 and 27, which continued to decrease in intensity up to 0.2 Torr. In terms of pressure behavior, methane is analogous to water reagent gas in that CI conditions are attained at 0.07 to 0.10 Torr in the drift-tube source (as compared to 0.7 to 1.0 Torr in many conventional CI sources). It should be noted that, in contrast to water, methane reagent gas is markedly affected by the repeller voltage. Above 10 V, the spectrum is "distorted", and m/e 41 becomes very intense. Because of the complex nature of the changes in the methane reagent ions with drift field, methane will probably be of limited value as a reagent gas in the drift tube CI source.

In contrast to methane, isobutane is almost ideal as a reagent gas for the drift tube CI source. Figure 6 shows the

Table III. Comparison of Decane CI Spectra (Percent Total Ion Current Above m/e 57)

	Methane CI (Ref. *23*) source temperature, °C			Methane CI at 110 °C E/P, V/cm Torr			Isobutane CI at 110 °C E/P, V/cm Torr			
m/e	35	100	200	0	100	200	0	100	200	m/e
71	12	15	25	23	46	43	10	32	42	71
85	10	15	25	23	36	36	8.4	35	33	85
99	4.2	6.1	12	12	7.6	13	5.3	7.4	12	99
113	1.2	1.2	1.2	2.9	1.0	–	2.4	3.2	–	113
127	2.8	2.1	0.6	0.3	–	–	2.4	–	–	127
141	70	60	36	39	9.4	8.7	71	22	14	141

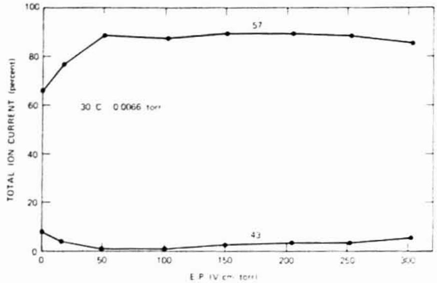

Figure 6. Major isobutane ions: 30 °C, 0.066 Torr

major ions in isobutane as a function of E/P at 0.066 Torr and 30 °C. Over most of the available range of E/P, the $C_4H_9^+$ ion at m/e 57 accounts for 90% of the total reagent ion current. At low values of E/P, there were some contributions from m/e 41 and 42 which are omitted from Figure 6 for clarity. The spectra obtained in the drift tube source at 0.06 to 0.09 Torr are similar to those obtained by Field (*4*) at somewhat higher pressures.

Both methane and isobutane CI spectra of decane were obtained at three different values of E/P in order to compare the variation in fragmentation available with the temperature effects reported by Hunt and McEwen (*23*). Since the $C_4H_9^+$ reagent ion from isobutane is identical with one of the decane fragment ions, only the peaks above m/e 57 are included in Table III. Hunt's data were obtained at 1.0 Torr methane pressure while the drift-tube source data were taken with 0.10 Torr of isobutane or methane. Using methane, it is obvious that, even at zero drift field, the drift-tube CI data show more fragmentation than Hunt found at 100 °C. This is probably the result of the lower source pressure, although, as noted above, the reagent ion distribution is also somewhat different. Increasing E/P causes fragmentation even more extensive than was observed by Hunt at 200 °C. The isobutane data show the extent of control over the degree of fragmentation available with the drift-tube CI source. With no drift field, the fragmentation of the $(M - 1)^+$ ion at m/e 141 is essentially the same as that found by Hunt at 1.0 Torr methane and 35 °C. With $E/P = 100$ V/cm Torr, the extent is substantially greater than that which can be obtained by heating the source to 200 °C.

The ability to control *and* rapidly change the extent of fragmentation under CI conditions has tremendous analytical utility. As an example, Figure 7 shows the isobutane CI spectrum of ethyl butyrate as a function of E/P. Below 50 V/cm Torr, the MH^+ ion at m/e 117 is 95% of the total sample ionization. At 200 V/cm Torr, the MH^+ is 70% fragmented. Furthermore, the fragments are just those which would be obtained from ethyl butyrate with methane CI reagent gas (*2*). Thus the additional information which could be obtained by switching from isobutane to methane reagent gas is available with the drift-tube CI source by simply changing a single voltage. This unique feature makes it possible to determine the molecular weight and purity of a material with one mass spectrometer scan and obtain structural information on the next scan of the same sample.

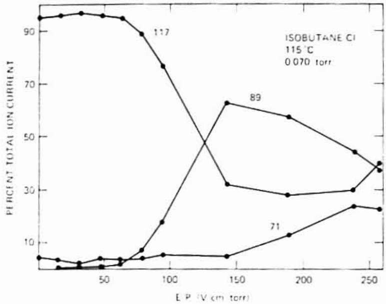

Figure 7. Isobutane CI spectrum of ethyl butyrate as a function of E/P. Isobutane pressure = 0.070 Torr; source temperature = 115 °C

LITERATURE CITED

(1) M. S. B. Munson and F. H. Field, *J. Am. Chem. Soc.*, **88**, 2621 (1966).
(2) M. S. B. Munson and F. H. Field, *J. Am. Chem. Soc.*, **88**, 4337 (1966).
(3) C. W. Tsang and A. G. Harrison, *J. Am. Chem. Soc.*, **98**, 1301 (1976).
(4) F. H. Field, *J. Am. Chem. Soc.*, **91**, 2827 (1969).
(5) J. Michnowicz and B. Munson, *Org. Mass Spectrom.*, **4**, 481 (1971).
(6) F. H. Field, in "Ion Molecule Reactions", J. L. Franklin, Ed., Plenum Press, New York, N.Y., 1972, pp 261–313.
(7) E. W. McDaniel et al., "Ion-Molecule Reactions", John Wiley, New York, N.Y., 1970, Chapter 2.
(8) E. W. McDaniel, "Collision Phenomena in Ionized Gasses", John Wiley, New York, N.Y., 1964, Chapter 9.
(9) I. R. Gatland, *Case Stud. At. Collision Phys.*, **4**, 369 (1974).
(10) D. R. James, E. Graham, G. R. Akridge, and E. W. McDaniel, *J. Chem. Phys.*, **62**, 1702 (1975).
(11) H. E. Revercomb and E. A. Mason, *Anal. Chem.*, **47**, 970 (1975).
(12) M. McFarland, D. L. Albritton, F. C. Fehsenfeld, E. E. Ferguson, and A. L. Schmeltekopf, *J. Chem. Phys.*, **59**, 6620 (1973).
(13) E. A. Mason, L. A. Viehland, H. W. Ellis, D. R. James, and E. W. McDaniel, *Phys. Fluids*, **18**, 1970 (1975).
(14) E. W. McDaniel, E. A. Mason, et al., *J. Chem. Phys.*, **63**, 2238 (1975).
(15) I. C. Wang, H. S. Swofford, Jr., P. C. Price, D. P. Martinsen, and S. E. Buttrill, Jr., *Anal. Chem.*, **48**, 491 (1976).
(16) J. R. Pierce, *J. Appl. Phys.*, **11**, 548 (1940).
(17) P. C. Price, H. S. Swofford, Jr., and S. E. Buttrill, Jr., *Anal. Chem.*, **48**, 494 (1976).
(18) P. C. Price, D. P. Martinsen, R. P. Upham, H. S. Swofford, Jr., and S. E. Buttrill, Jr., *Anal. Chem.*, **47**, 190 (1975).
(19) D. P. Martinsen and S. E. Buttrill, Jr., *Org. Mass Spectrom.*, **11**, 762 (1976).
(20) Philip C. Price, Ph.D. Thesis, University of Minnesota, Minneapolis, Minn., December 1976.
(21) David P. Martinsen, Ph.D. Thesis, University of Minnesota, Minneapolis, Minn., December 1976.
(22) P. Kebarle, in "Modern Aspects of Electrochemistry", G. Conway and J. O'M. Bockris, Ed., Plenum Press, New York, N.Y., 1974, Vol. 9, pp 1–46.
(23) D. F. Hunt and C. N. McEwen, *Org. Mass Spectrom.*, **7**, 441 (1973).

RECEIVED for review April 15, 1977. Accepted June 16, 1977. Presented in part at the 24th Annual Conference on Mass Spectrometry and Allied Topics, May 9–13, 1976, San Diego, Calif. This work was supported by NSF Grants GP-38764X, MPS-7510940, and CHE76-20096.

Negative Ion Chemical Ionization Mass Spectrometry of Volatile Metal Chelates

S. R. Prescott, J. E. Campana, and T. H. Risby*

Department of Chemistry, The Pennsylvania State University, University Park, Pennsylvania 16802

The negative ion chemical ionization mass spectra for 34 volatile metal chelates are reported. Also a sensitivity study using a gas chromatograph chemical ionization mass spectrometer computer system comparing detection limits for several Cr(β-diketonates)$_3$ in both negative and positive ion detection modes is described. This study illustrates the ability of negative ion chemical ionization mass spectrometry to provide two to three orders of magnitude increase in specific ion currents for compounds containing electronegative functional groups.

Chemical ionization mass spectrometry has been shown to be a potentially sensitive method of analysis for trace metals (*1–4*). Detection limits in the picogram range have been reported for several of the first, second, and third row transition metals (*4*). This earlier work used the more conventional positive ion detection mode in which ionization of the sample occurs by the transfer of a proton from a hydrocarbon reagent ion such as CH_5^+ or $C_4H_9^+$ to the sample molecule. In this paper the results of a companion study utilizing negative ion chemical ionization mass spectrometry are presented.

Recently it has been suggested that negative ion chemical ionization mass spectrometry is more sensitive than positive ion chemical ionization mass spectrometry for those compounds which contain heteroatoms that promote anion formation (*5–10*). In electron impact mass spectrometry, negative ions are formed by three generalized mechanisms which are dependent on the electron energies and pressure: (1) resonance capture; (2) dissociative resonance capture; and (3) ion-pair production (*11*). Historically, negative ion electron impact mass spectrometry has been limited by ion currents which are two or three orders of magnitude lower than the corresponding positive ion currents (*12*). The higher pressures available in a chemical ionization source produce larger numbers of low energy electrons, which are secondary and thermalized primary electrons. It has been found that at the normal chemical ionization source pressures (0.7–1.5 Torr) the secondary electron current is several times more intense than the primary electron current, which indicates that the primary electrons are undergoing multiple collisions with the reagent gas (*13*).

Under these conditions it is apparent that molecules which have large cross sections for electron capture (and/or large electron affinities) should form anions efficiently. Often these same molecules will have greater cross sections for electron capture than for proton transfer. This advantage has been exploited successfully in the electron capture gas chromatographic detector.

Although the formation of negative ions by chemical ionization mass spectrometry has been studied for several years, it has only recently been shown quantitatively that, for selected molecules, electron capture currents can exceed their corresponding positive ion currents by two or three orders of magnitude (*8*).

The purpose of this paper is to report on negative ion chemical ionization mass spectra for several transition metal β-diketonates together with a preliminary study on the use of various reagent gases. Also a relative sensitivity study will be discussed using time resolved scans to compare relative sensitivities in the positive and negative ion detection modes for several fluorinated and nonfluorinated chromium β-diketonates. Finally a quantitative determination of the detection limits for these same chelates using a gas chromatograph chemical ionization mass spectrometer system will be described.

EXPERIMENTAL

Chelate Preparation. The 2,4-pentanedionates (acac), the 1,1,1-trifluoro-2,4-pentanedionates (tfa), and the 2,2,6,6-tetramethyl-3,5-heptanedionates (thd) of VO(II), Mn(II), Ni(II),Cu(II), Zn(II), Pd(II), Pt(II), Cr(III), Mn(III), Fe(III), Co(III), Rh(III), and Ru(III) were prepared by methods reported previously (*14–16*). The chelates were purified by either recrystallization or reduced pressure sublimation. Chromium tris(1,1,1,5,5,5-hexafluoro-2,4-pentanedionate) [Cr(hfa)$_3$] and chromium tris-(1,1,1,2,2,2,3,3-heptofluoro-7,7-dimethyl-4,6-octanedionate) [Cr(fod)$_3$] were synthesized by modification of conventional methods and purified by sublimation at reduced pressures (*17, 18*).

Chemicals. 2,4-Pentanedione, H(acac), and 2,2,6,6-tetramethyl-3,5-heptanedione, H(thd) were obtained from Polysciences, Inc., Warrington, Pa.; 1,1,1,2,2,3,3-heptafluoro-7,7-dimethyl-4,6-octanedione, H(fod), 1,1,1,5,5,5-hexafluoro-2,4-pentanedione, H(hfa), and 1,1,1-trifluoro-2,4-pentanedione, H(tfa), from Pierce Chemical Co., Rockford, Ill.

Reagent Gases. Methane (99.0%) and isobutane (99.0%) were purchased from Air Products and Chemicals, Inc., Allentown, Pa.; nitrogen (99.99%) was obtained from Philip Wolf and Sons, Inc., Lewistown, Pa.; and argon-10% methane was purchased from Airco Industrial Gases, Rivertown, N.J.

Apparatus. The gas chromatograph–mass spectrometer–computer system consists of the following components: gas chromatograph with automatic injection system (Hewlett-Packard High Efficiency Gas Chromatograph 402B, Hewlett-Packard Automatic Injector 7171A); quartz capillary interface (General Electric Company); high temperature fine control bellows valve (Nupro B.M. Series); chemical ionization mass spectrometer (Scientific Research Instruments Corporation Biospect System); and computer system (Modcomp II/III, "Lab Box" system and graphics terminal Techtronix 4006-1).

Gas Chromatograph and GC/MS Interface. The column is connected so that the column eluent passes directly into the GC/MS interface without passing through a detector. In all the studies which used the gas chromatograph for sample introduction, the carrier gas was also the reagent gas. The column effluent was stream split so that most of it went to atmosphere and 10 mL/min passed into the CI source. This flow rate results in a source pressure of 1 Torr which produced the optimum signal. The GC/MS interface originally consisted of a length (50 cm) of silanized glass lined stainless steel tubing (Supelco Inc., 0.16-mm i.d.) but after a period of time the integrity of the glass lining was found to deteriorate. The inlet was then replaced by a quartz capillary tube (6-mm o.d., 0.25-mm i.d.). The interface was connected to the CI source through a fine control stainless steel needle valve which was adjusted so that the required flow rate of column effluent entered the CI source. The interface and needle

Table I. Instrumental Conditions

	$Cr(fod)_3$	$Cr(hfa)_3$	$Cr(tfa)_3$
Column temperature	170 °C	40 °C	140 °C
Interface temperature	190 °C	65 °C	165 °C
Source temperature	170 °C	70 °C	140 °C
Methane flow rate	40 mL/min	40 mL/min	40 mL/min
Retention time	1 min	3 min	6 min
Splitting ratio	7:1	7:1	6:1
Sample size	0.2 μL	0.2 μL	0.2 μL
Solvent	Hexane	Toluene	Toluene
Column	3% OV-101 on Gas Chrom Q 1 m, 4 mm (i.d.)	15% OV-101 on Chromsorb WHP 1 m, 4 mm (i.d.)	15% OV-101 on Chromsorb WHP 1 m, 4 mm (i.d.)

valve were wrapped with a heating tape and temperatures were measured at four different points with thermocouples. These temperatures were maintained at approximately 20 °C higher than the column temperature.

Mass Spectrometer Modifications. The chemical ionization mass spectrometer was modified so that the detection system could monitor either positive or negative ions in a manner similar to that which has been reported previously (*19*). In addition, a high voltage relay was used which enables the conversion from positive to negative ion detection systems to be made easily. Another modification was made which enables the quadrupole and detection systems to be computer controlled.

Computer Facilities. The GC/MS system is interfaced to The Pennsylvania State University Department of Chemistry's Modcomp II/III computer via the department's "Lab Box" system. The authors have developed a GC/MS software package, CAD, for data acquisition, mass spectrometer control, data manipulation, and display through a graphics terminal in their laboratory (*20*).

Procedure. Methane, isobutane, nitrogen, or argon–10% methane were used as reagent gases (*21*). Aliquots of known solutions of the metal chelates in toluene or hexane were evaporated onto a direct insertion probe, and the probe was inserted directly into the ionization source. The following are the source temperatures used to sublime the chelates into the mass spectrometer: 140–180 °C (acac), 100 °C (fod), 80 °C (hfa), 130–140 °C (tfa), and 140–160 °C (thd). All other conditions were identical with those previously reported (*1, 2*). The mass-to-charge ratios of the various peaks in the mass spectra were determined by the mass marker, which was calibrated with methyl stearate and $Lu(thd)_3$.

A study comparing the relative sensitivities for several Cr-(β-diketonates)$_3$ in the positive vs. the negative ion detection modes was carried out in the following manner: 1.0 μL solutions of $Cr(acac)_3$, $Cr(fod)_3$, $Cr(hfa)_3$, $Cr(tfa)_3$, and $Cr(thd)_3$ in toluene or hexane (10 ppm) were injected into sections (1 cm) of glass capillaries. The solvent was evaporated using an infrared lamp and the capillaries inserted into the CI source via the solids probe. The quadrupole controller was adjusted so that there was unit resolution at the region of the parent molecular ion and a 10-amu region encompassing the parent ion region was repetitively scanned (1 s/scan). The resulting time resolution spectra were integrated and relative sensitivities calculated.

Quantitative determinations of detection limits for $Cr(fod)_3$, $Cr(hfa)_3$, and $Cr(tfa)_3$ were made in a similar manner except that the sample was introduced from the gas chromatograph.

The gas chromatographic conditions are listed in Table I. Because of their lower volatility, the detection limits for $Cr(acac)_3$ and $Cr(thd)_3$ were obtained using a heated solids probe. Aliquots of the chelates in toluene or hexane were evaporated onto 1-cm capillary sections, placed on the probe, and inserted directly into the CI source. The probe was then heated while the quadrupole repeatedly scanned the parent ion region. This method proved to be reproducible and thus the decomposition problems associated with these chelates when injected into gas chromatographic columns were avoided. Stock solutions were prepared by dissolving a known amount of chelate in toluene or hexane to yield a 10-ppm solution (with respect to Cr). Subsequent dilutions yielded sample solutions ranging in concentration from 10^5 to 1 ppb.

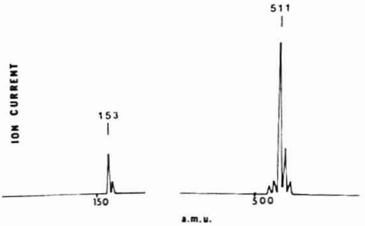

Figure 1. The methane negative ion chemical ionization mass spectrum of $Cr(tfa)_3$

RESULTS AND DISCUSSION

Reagent Gases 1. Methane. The methane used in our laboratory contains trace amounts of water (~1%) causing intense ions to be observed at 19, 37, and 55 amu, respectively, in the positive ion detection mode. These ions correspond to the protonated water monomer, dimer, and trimer. This observation is not surprising since methane is a stronger Bronsted acid than water and will upon collision transfer a proton.

$$CH_5^+ + H_2O \rightarrow CH_4 + H_3O^+$$
$$C_2H_5^+ + H_2O \rightarrow C_2H_4 + H_3O^+$$

In the negative ion mode a rather intense ion was observed at 32 amu which was determined to be the superoxide anion, $O_2^{\cdot-}$. This ion was due to the water present in the methane and was eliminated by passing the reagent gas through a drying tube containing activated molecular sieves.

2. Nitrogen, isobutane, argon/methane (10%). There was no evidence of reagent ions associated with any of these gases in the negative ion mode. Parent anions were observed for the chelates and there appeared to be no difference except that with nitrogen the maximum signal for the parent ion occurred at a slightly lower source pressure which suggests it is a more efficient moderator of the electron energy.

In all cases the major ion observed, disregarding the anion resulting from the ligand itself in a few cases, was the molecular parent ion formed by resonance capture of low energy electrons. An example of the negative ion chemical ionization mass spectrum for $Cr(tfa)_3$ using methane as the reagent gas is shown in Figure 1. It can be seen from this spectrum that, apart from the parent ion there is only one other ion of major importance (>5% parent ion intensity). This ion occurs at 153 amu and is attributed to the ligand H(tfa). The extreme simplicity of the $Cr(tfa)_3$ spectrum is not surprising since resonance capture involves electrons with energies near 0 eV. The chelates based on H(acac), H(fod), H(hfa), H(tfa), and H(thd) likewise exhibited little or no fragmentation. Prior to drying the methane, several of the chelate spectra showed another ion in the molecular parent ion region resulting from

Table II. Relative Sensitivities from Time Resolved Scans

Metal chelate	Mol wt, g	Relative sensitivity Positive mode $(M + 1)^+$	 Negative mode $(M)^-$
$Cr(hfa)_3$	673	1	5000
$Cr(tfa)_3$	511	1	100
$Cr(fod)_3$	937	1	10
$Cr(thd)_3$	601	10	1
$Cr(acac)_3$	349	10	1

an ion–molecule reaction between the superoxide ion (O_2^-) and the chelate to form an associated ion $[M + O_2]^-$. This ion–molecule reaction was observed with all the metal 1,1,1-trifluoro-2,4-pentanedionates, but only with a few of the divalent 2,4-pentanedionates or 2,2,6,6-tetramethyl-3,5-heptanedionates (VO, Zn, and Ni). Charge delocalization caused by the presence of many electronegative fluorine atoms contained by the metal 1,1,1-trifluoro-2,4-pentanedionates most certainly contributed to the stability of the ion–molecule product. In order to verify this assumption, another fluorinated β-diketonate $Cr(hfa)_3$ was studied. The $Cr(hfa)_3$ spectrum also contained an $[M + O_2]^-$ ion which disappeared when the methane was dried. The fact that the $[M + O_2]^-$ ion was observed with several of the divalent 2,4-pentanedionates and 2,2,6,6-tetramethyl-3,5-heptanedionates results from the divalent metal chelates containing two unoccupied coordination sites.

Several first row transition metal chelates of the ligands H(hfa) and H(tfa) have been analyzed by 70-eV negative ion mass spectrometry (*22, 23*). In most cases the spectra were simple with large ion currents located in the molecular parent ion region. However, in other cases the most dominant peaks observed were fragments resulting from fluorine migrations. Another interesting result was that during the analysis of $Co(hfa)_3$ the ratio of negative to positive ions in the ion source was (1:3). This observation indicates that the fluorinated β-diketonates have large electron capture cross sections, and if large low energy electron currents can be generated (i.e. the CI source), high sensitivities can be achieved.

A sensitivity study was undertaken using solutions of $Cr(tfa)_3$ (10 ppm) in toluene to determine the sensitivity difference between the positive and negative ion modes. The method of injecting solutions directly into the CI source was used which has been previously discussed (*3*). While the method of direct injection into the CI source is useful, it suffers from problems of perturbation of the CI source which are more acute in the negative ion mode. Unfortunately, together with the negative ions, electrons are also transmitted by the quadrupole mass filter and impinge on the ion multiplier causing a noise level of 100 mV to be observed when the ion multiplier and electrometer are maximized. This "system" noise is directly proportional to the electron density in the CI source and, when injections are made through the direct injection port, the "system" noise increases dramatically because of ionization of the solvent. It was for this reason that it became apparent that an alternative method of sample introduction would be needed to determine the sensitivity difference between the positive and negative ion modes.

Another routine method for determination of sensitivity was undertaken by the use of time resolved spectra (*24–28*). A series of Cr(β-diketonates) was analyzed by this method with the results summarized in Table II. (Figure 2 illustrates the structures of the ligands involved in this study.) The increased electron capture cross section of the $Cr(tfa)_3$ and $Cr(hfa)_3$ due to the presence of nine and 18 electronegative fluorine atoms on each metal chelate, respectively, is reflected in the increase in the sensitivity of these metal chelates in the negative ion mode. The expected decrease in the electron capture cross section of the $Cr(thd)_3$ and $Cr(acac)_3$, due to the presence of two electron donating *tert*-butyl groups on the H(thd) ligands and two-electrons donating methyl groups on the H(acac) ligands, is demonstrated by the increased sensitivities of $Cr(thd)_3$ and $Cr(acac)_3$ in the positive ion mode. $Cr(fod)_3$ which contains a ligand having an electron releasing *tert*-butyl group on one end and an electron capturing heptafluorinated propyl group on the other end is sensitive to both proton transfer and electron capture.

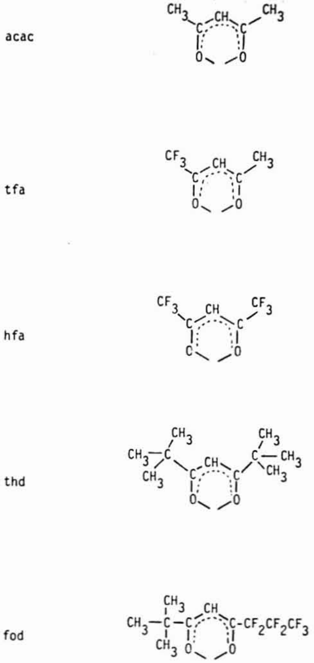

Figure 2. Structure of various β-diketonates

A quantitative sensitivity study was made using $Cr(acac)_3$, $Cr(fod)_3$, $Cr(hfa)_3$, $Cr(tfa)_3$, and $Cr(thd)_3$ in toluene or hexane (1 ppb–1 ppm by weight in terms of Cr). As discussed earlier, there were some problems associated with the direct injection port related to the amount and type of solvent injected into the mass spectrometer. Because of the difficulties associated with this sample introduction system, it was decided to couple a gas chromatograph to the mass spectrometer in order to separate the solvent and the chromium chelate. The resulting area of the mass chromatogram was measured and a calibration curve plotted. The relationship between the area of the mass chromatograms and the concentration of the Cr-$(\beta\text{-diketonate})_3$ was linear for three to four orders of magnitude in both the positive and negative ion modes. The minimum detectable limits, after taking into account the split ratio of the sample prior to entrance into the mass spectrometer for the chelates introduced through the gas chromatograph, are summarized in Table III. As expected, the minimum detectable limits in the negative ion mode for the fluorinated chromium chelates are greater than those for $Cr(acac)_3$ and $Cr(thd)_3$. This sensitivity increase is attributed to the large

Table III. Minimum Detectable Amounts

Metal chelate	Minimum detectable amount, g Cr Positive mode $(M + 1)^+$	 Negative mode $(M)^-$
$\mathrm{Cr(hfa)_3}$	1.3×10^{-9}	2.4×10^{-13}
$\mathrm{Cr(tfa)_3}$	1.2×10^{-11}	2.9×10^{-13}
$\mathrm{Cr(fod)_3}$	1.9×10^{-12}	1.9×10^{-13}
$\mathrm{Cr(thd)_3}$	8.6×10^{-12}	8.6×10^{-11}
$\mathrm{Cr(acac)_3}$	8.6×10^{-13}	8.6×10^{-12}

cross section for electron capture provided by the fluorine atoms on the H(fod), H(hfa), and H(tfa) ligands which promote anion formation. Increased sensitivity towards cation formation due to the electron releasing inductive effect of the methyl and *tert*-butyl groups associated with the chelates $\mathrm{Cr(acac)_3}$ and $\mathrm{Cr(thd)_3}$ is demonstrated by the higher sensitivities in the positive ion mode.

CONCLUSIONS

On the basis of this study, we feel that it is possible to postulate the mechanisms which account for the relative sensitivities (Table II). In the positive ion mode, the chelate is protonated either at the methylene carbon or at the oxygen atoms. The reason why the 2,4-pentanedionate or 2,2,6,6-tetramethyl-3,5-heptanedionate produces a larger ion current that the 1,1,1,2,2,3,3-heptafluoro-7,7-dimethyl-4,6-octanedionate, 1,1,1-trifluoro-2,4-pentanedionate, or 1,1,1,5,5,5-hexafluoro-2,4-pentanedionate is that the electron releasing inductive effect of the methyl or *tert*-butyl groups stabilize the cation whereas the trifluoromethyl or heptafluoropropyl groups have electron withdrawing inductive effects which destabilize the cation and decrease the probability of protonation. The presence of the *tert*-butyl group does not have the effect of increasing the stability of the cation as compared to the methyl group because of the reduced effect over an extra carbon atom and increased steric hindrance. Therefore the probability for proton transfer is as follows: acac > thd > fod > tfa > hfa.

In the negative ion mode, the chelate captures an electron which is stabilized either in the π electron system on the β-dienolate ring or on the oxygens. Once again the side groups affect the stability of the anion and the trifluoro methyl or heptafluoropropyl groups stabilize the ions through electron withdrawing inductive effects while the methyl or *tert*-butyl groups destablize the anion through an electron releasing inductive effect. As a result the probability for electron capture is as follows: hfa > tfa > fod > thd ~ acac.

ACKNOWLEDGMENT

We thank G. W. Gokel, P. C. Jurs, R. A. Olofson, and M. Shamma for their helpful discussions.

LITERATURE CITED

(1) T. H. Risby, P. C. Jurs, F. W. Lampe, and A. L. Yergey, *Anal. Chem.*, **46**, 161 (1974).
(2) T. H. Risby, P. C. Jurs, F. W. Lampe, and A. L. Yergey, *Anal. Chem.*, **46**, 726 (1974).
(3) S. R. Prescott, J. E. Campana, P. C. Jurs, T. H. Risby, and A. L. Yergey, *Anal. Chem.*, **48**, 829 (1976).
(4) J. J. Dulka and T. H. Risby, *Anal. Chem.*, **48**, 640A (1976).
(5) R. C. Dougherty, J. Dalton, and F. J. Biros, *Org. Mass Spectrom.*, **6**, 1171 (1972).
(6) H. P. Tannenbaum, J. D. Roberts, and R. C. Dougherty, *Anal. Chem.*, **47**, 49 (1975).
(7) R. C. Dougherty, J. D. Roberts, and F. J. Biros, *Anal. Chem.*, **47**, 54 (1975).
(8) D. F. Hunt, G. C. Stafford, Jr., F. H. Crow, and J. W. Russel, *Anal. Chem.*, **48**, 2098 (1976).
(9) D. F. Hunt, T. M. Harvey, and J. W. Russell, *J. Chem. Soc., Chem Commun.*, 151 (1975).
(10) D. F. Hunt, C. N. McEwen, and T. M. Harvey, *Anal. Chem.*, **47**, 1730 (1975).
(11) J. G. Dillard, *Chem. Rev.*, **73**, 589 (1973).
(12) C. E. Melton, "Principals of Mass Spectrometry and Negative Ions", Marcel Dekker Inc., New York, N.Y., 1970, Chapter 7.
(13) C. E. Klotz, "Fundamental Processes in Radiation Chemistry", P. Ausloos, Ed., John Wiley and Sons, New York, N.Y., 1968, Chapter 1.
(14) R. W. Moshier and R. E. Sievers, "Gas Chromatography of Metal Chelates", Pergammon Press, Elmsford, N.Y., 1965, references cited therein.
(15) G. Guiochan and C. Pommier, "Gas Chromatography in Inorganics and Organometallics", Ann Arbor Science Publishers, Ann Arbor, Mich., 1973, references cited therein.
(16) S. R. Prescott and T. H. Risby, in preparation.
(17) R. E. Sievers, R. W. Moshier, and M. L. Morris, *Inorg. Chem.*, **1**, 966 (1962).
(18) R. E. Sievers, J. W. Connolly, and W. D. Ross, *J. Gas Chromatogr.*, **5**, 241 (1967).
(19) A. L. C. Smith, M. A. J. Rossetto, and F. H. Field, *Anal. Chem.*, **48**, 2042 (1976).
(20) J. E. Campana, "CAEA Publication No. 456–76", pp 1–5.
(21) T. H. Risby, "CAES Publication No. 488–76", p 5.
(22) I. W. Fraser, J. L. Garnett, and Ian K. Greggor, *J. Chem. Soc., Chem. Commun.*, 365 (1974).
(23) I. W. Fraser, J. L. Garnett, and I. K. Greggor, *Inorg. Nucl. Chem. Lett.*, **10**, 925 (1974).
(24) A. E. Jenkins and J. R. Majer, *Talanta*, **14**, 777 (1967).
(25) A. E. Jenkins, J. R. Majer, and M. J. A. Reade, *Talanta*, **15**, 1213 (1968).
(26) J. R. Majer, M. J. A. Reade, and W. I. Stephen, *Talanta*, **15**, 373 (1968).
(27) R. Belcher, J. R. Majer, R. Perry, and W. I. Stephen, *Anal. Chim. Acta*, **43**, 451 (1968).
(28) B. R. Kowalski, T. L. Isenhour, and R. E. Sievers, *Anal. Chem.*, **41**, 998 (1969).

RECEIVED for review April 2, 1977. Accepted June 29, 1977. Work supported by the U.S. Environmental Protection Agency, Grant No. R803651-20.

Predicting Absolute Sensitivity and Limit of Detection for X-ray Analysis of Pollution Samples

L. S. Birks

Naval Research Laboratory, Washington, D.C. 20375

Tabulated parameters for x-ray emission, absorption, and scattering can be used to predict absolute line intensity and background scattering from pollution samples. Using only the simplest mathematics, an example calculation predicts 640 counts/s from 1 μg/cm^2 of Cd compared to an experimental value of 335 counts/s. Likewise the predicted detection limit for Cd was 0.7 ng/cm^2 in 100 s compared to an experimental value of 0.7 ng/cm^2.

With parameters already available in the literature, it is possible to calculate absolute values for both the characteristic x-ray emission lines and the scattered background for pollution samples. The characteristic emission divided by concentration is the sensitivity while the scattered background determines the limit of detection using the 3σ rule (*1*). As the example in the body of this paper will demonstrate, the predictions do not require elaborate mathematics or a computer but, in fact, may be done quite easily with only a slide rule. Thus the analyst may alter the parameters in the calculation at will, the better to judge what conditions would be required to measure any specified element and concentration. Such calculations also allow pencil-and-paper comparison of the x-ray method with any other analytical method whose capabilities are known or can be calculated. This should be helpful to management when selecting methods for new or untried applications.

SENSITIVITY

Sensitivity is defined (*1*) as the slope of the calibration curve, dI/dC. In x-ray fluorescence analysis of pollution samples, the units of I are usually counts per increment of time (viz. seconds or 100 seconds) and the units of C are μg/cm^2. To predict absolute sensitivity from first principles we must consider the parameters, Table I, which determine the generation and measurement of the element line of interest. We will assume a 1 μg/cm^2 sample of Cd to use as an illustration. The line of interest is the Cd Lα line and it is measured with a PET-crystal spectrometer. We will also assume a Cr target x-ray tube operated at 45 keV and 50 mA. (Similar predictions could be made for an energy dispersive spectrometer.)

First we will calculate the secondary x-ray intensity generated, i.e. the fluorescent line from the element of interest. We will follow the sequence of parameters shown in Table I.

Step 1. From the published spectra distribution for a Cr target x-ray tube (2) obtain the primary intensity, I_λ as a function of λ for that part of the spectrum which can be photoelectrically absorbed by the Cd L$_{\rm III}$ shell, see Figure 1. Multiply each I_λ by the $\Delta\lambda$ interval to get the increment of primary radiation. These values are listed in Table II.

Step 2. From Ref. 3, determine that part of the photoelectric absorption which represents the L$_{\rm III}$ shell. It is approximated by the difference between the extension of the L$_{\rm III}$ edge and the extension of the M edge in Figure 2. These τ_λ values are also listed in Table II.

Step 3. Recall that the incremental attenuation of x-ray intensity, ΔI, in a thin layer, Δz, can be expressed as

$$\Delta I/I = \mu_\lambda \rho \Delta z \qquad (1)$$

where μ_λ is the total mass-attenuation coefficient and ρ is the density of the layer. The photoelectric absorption part of μ_λ is τ_λ which is the part that excites fluorescence. For the thin layers of concern here ($\sim 10^{-6}$ g/cm^2) the increment $\rho\Delta z$ is the total mass thickness and commonly expressed as ρz. $\Delta I/I$ is the fractional attenuation in the layer. Therefore

$$\text{Fractional absorption} = \tau_\lambda \rho z \qquad (2)$$

Step 4. For each wavelength increment, $\Delta\lambda$, the number of incident photons/sr/s absorbed becomes $I_\lambda \Delta\lambda \times \tau_\lambda \rho$ and the total is just the sum over all the wavelength increments. As shown in Table II, the sum for the continuum spectrum plus the Cr target lines is 5.9×10^{10} ph/sr/s for the 1 μg/cm^2 Cd sample.

Step 5. X-ray fluorescent samples usually intercept between 1% and 3% of the total 4π solid angle around the x-ray tube, i.e. $\Omega = 0.120$ to 0.35 sr. We will use the 0.35-sr value in which case the absolute number of ph/s absorbed by the L$_{\rm III}$ shell of Cd becomes

$$0.35 \times 5.9 \times 10^{10} = 2.1 \times 10^{10}\ \text{ph/s}$$

Step 6. The total fluorescent yield (*4*) for the Cd L shell is about 0.1 and the Cd Lα line comprises about half of this. Therefore we use $\omega_{\rm io} = 0.05$ and multiply by the ph/s from Step 5 to obtain $I_{\rm p} = 10^9$ ph/s of Cd Lα emitted in the full 4π solid angle around the specimen. The secondary intensity per steradian is just $I_{\rm p}/4\pi$ or 8×10^7 ph/sr/s of Cd Lα emitted.

Step 7. Next we must introduce the efficiency of the crystal spectrometer. The efficiency depends on the R value integral reflection coefficient, R, of the analyzer crystal, the fanning angle, $\Delta\phi$, from the specimen to the detector window, and the detector efficiency $E_{\rm D}$. For PET, R is 1.6×10^{-4} rad for Cd Lα (*5*), and $\Delta\phi$ for the usual detector size and distance from the sample is about $^1/_8$ rad. The efficiency of a flow-proportional detector for Cd Lα is about $E_{\rm D} = 40\%$. The overall efficiency of the spectrometer is the product $R(\Delta\phi)E_{\rm D} = 8.2 \times 10^{-6}$. Using the emission from Step 6 and the spectrometer efficiency we obtain the absolute counting rate for 1 μg/cm^2 of Cd

$$8 \times 10^7 \times 8 \times 10^{-6} = 640\ \text{counts/s}$$

As a check on the calculations, we measured Cd samples with the Philips PW 1410 spectrometer and determined an experimental value for the sensitivity of 335 counts/s for 1 μg/cm^2 of Cd. This agreement between prediction and experiment is better than one might expect, considering the simple approximations used in the calculation.

LIMIT OF DETECTION

The minimum concentration which can be detected, $C_{\rm L}$, depends on the background parameters in Table I as well as the line intensity; so the next steps are to calculate the absolute background scattering from the 1 μg/cm^2 of Cd for the same operating conditions as above.

Table I. Factors in X-ray Sensitivity and Limit of Detection

Factor	Element line	Element background	Substrate background	Units
	Generation			
Primary intensity	$\Sigma_0^{\lambda_{abs}} I_\lambda \Delta\lambda$	$I_{\lambda i}\, \Delta\lambda_i$	$I_{\lambda i}\, \Delta\lambda_i$	ph/sr/s
Solid angle occupied	Ω	Ω	Ω	sr
Fraction absorbed	$\tau_{\lambda i}(\rho z)_i$	$\sigma_i(\rho z)_i$	$\sigma_s(\rho z)_s$	1
Fluorescent yield	ω_i	-	-	1
Total secondary radiation	I_P	I_{Bi}	I_{BS}	ph/s
	Measurement			
Secondary intensity per steradian	$I_P/4\pi$	$I_{Bi}/4\pi$	$I_{BS}/4\pi$	ph/sr/s
Spectrometer acceptance angle	$R_{\Delta\phi}$	$R_{\Delta\phi}$	$R_{\Delta\phi}$	sr
Detector efficiency	E_D	E_D	E_D	1
Counting interval	t	t	t	s
Total counts	N_P	N_{Bi}	N_{BS}	ph

Table II. Parameters for X-ray Emission and Scattering

(1 $\mu g/cm^2$ of Cd; Cr x-ray tube operated at 45 keV, 50 mA)

Emission

λ, A	keV	I_λ, ph/sr/s/A, all × 10^{12}	Δλ, A	τ_λ, cm² g	ρz, all 10^{-6}	$I_{absorbed}$, ph/sr/s, all × 10^6
0.32	39	25	0.04	1.2	1	1
0.36	34	35	0.04	1.6	1	2
0.40	31	42	0.04	2.4	1	4
0.45	28	47	0.05	3.2	1	7
0.50	25	49	0.05	4.8	1	12
0.60	21	48	0.1	6.7	1	32
0.80	15	43	0.2	18.7	1	161
1.0	12	37	0.5	40.2	1	744
1.5	8.3	22	0.5	76	1	836
2.0	6.2	13	0.5	171	1	1113
2.5	5.0	17	0.5	350	1	~3150
3.0	4.1	10	0.5	590	1	2950
3.5	3.6	6	0.5	750	1	2250
2.3	Cr Kα and Kβ – 200 × 10^{12}			240	1	48000
				Total		5.9 × 10^{10}

Scattering

λ_i	keV	I_i	$\Delta\lambda_i$	σ_i	ρz	$I_{scattered}$
3.96	3.1	3 × 10^{12}	9.4 × 10^{-3}	6	10^{-6} Cd	1.7 × 10^5
3.96	3.1	3 × 10^{12}	9.4 × 10^{-3}	0.6	5 × 10^{-4} C	8.7 × 10^6

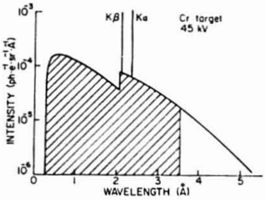

Figure 1. Excitation of Cd Lα is by the shaded portion of the primary spectrum

Step 8. The appropriate I_λ to be considered is I_i, that portion of the primary continuum at the element-line wavelength, because this is what will be diffracted at the same crystal setting. The Δλ increment is obtained from the differential form of Bragg's law

$$\Delta\lambda = 2d \cos\theta\, \Delta\theta \tag{3}$$

where Δθ is the divergence allowed by the collimator because there is some wavelength in the continuum appropriate to be diffracted anywhere within this Δθ range. Putting in the values of 2d and cos θ for PET and a Δθ of 0.0012 rad (a 0.005-inch spacing, 4 inches long), Δλ becomes

$$\Delta\lambda = 8.75 \times 0.89 \times 0.0012 = 9.4 \times 10^{-3}\ \text{Å}$$

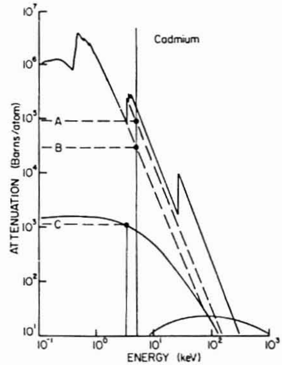

Figure 2. Photoelectric absorption by the L_{III} shell in Cd is the difference between the two dashed curves

Table II shows the appropriate $I_i\Delta\lambda$ for the background.

Step 9. The scattering coefficient σ_i is obtained from Ref. 3. The fraction of primary radiation attenuated by scattering (analogous to the photoelectrically absorbed fraction in Step

3) is $\sigma_i\ (\rho Z)$ which is 1.7×10^5 ph/sr/s for 1 μg/cm^2 of Cd as given in Table II.

Step 10. As with the characteristic line, we multiply by 0.35 for the sample area (Step 5), by $^1/_4\ \pi$ to get the scattered intensity per steradian (Step 6), and by 8×10^{-6} for the spectrometer efficiency (Step 7).

$$1.7 \times 10^5 \times 0.35 \times 8 \times 10^{-6}/4\pi = 3.8 \times 10^{-2}\ \text{counts/s}$$

The line/back ratio becomes

$$640/(3.8 \times 10^{-2}) = 1.7 \times 10^4$$

One must remember that this favorable line/background ratio is for 1 μg/cm^2 of Cd without any supporting substrate. If we include the scattering from, for example, 0.5 mg/cm^2 of carbonaceous substrate (like Mylar), Table II shows the scattering from it to be 8.7×10^6 ph/sr/s which is 51 times larger than the scattering from the Cd itself giving a total scattering of 2 counts/s. The practical line/background ratio becomes

$$640/2 = 320$$

Step 11. To estimate the limit of detection, C_L, we must use the total line and background counts, N_P and N_B, collected in a selected counting interval, t. For t = 100 s and the counting rates above, we get $N_P = 6.4 \times 10^4$ counts and $N_B = 2 \times 10^2$ counts. The definition for limit of detection (*1*) is that the line must exceed the background by 3 standard deviations of the background or $3\sqrt{200} = 42$ counts. Now we can form the ratio to determine C_L.

$$\frac{6.40 \times 10^4}{1\ \mu\text{g/cm}^2}\ \text{counts} = \frac{42}{C_L}\ \text{counts}$$

$$C_L = 42/6.4 \times 10^4 = 6.8 \times 10^{-4}\ \mu\text{g/cm}^2 \approx 0.7\ \text{ng/cm}^2$$

Again to compare with measured results, our experimental estimate of C_L was also 0.7 μg/cm^2 for Cd which happens to agree exactly with the prediction.

DISCUSSION

The prediction of absolute sensitivity and limit of detection for x-ray fluorescence analysis of pollution samples can be done with simple mathematics and parameters available in the literature. The expression for the measured total counts from a characteristic x-ray line is the product of the parameters in Table I.

$$N_P = [(\rho Z)\Omega\,\omega_i R(\Delta\phi)E_D\, t\Sigma_0{}^{\lambda_{abs}} I_\lambda \tau_{\lambda i}\Delta\lambda]/4\pi \tag{4}$$

Similarly the total background counts which interfere with the characteristic line come from the parameters in Table I and can be expressed as

$$N_B = N_{Bi} + N_{BS} = I_{\lambda i}\Delta\lambda R(\Delta\phi)E_D\, t[\sigma_i(\rho Z)_i + \sigma_S(\rho Z_{Si})]/4\pi \tag{5}$$

The calculated sensitivity and limit of detection for the example illustrated were in amazingly good agreement with the experimental values, but even disagreement by a factor of three to five times would have been completely satisfactory as a prediction method.

Although it was not demonstrated, the x-ray predictions can be made for energy dispersion as well as for crystal spectrometers. Perhaps advocates of other analytical techniques will be challenged to devise similar predictive capabilities for their methods so that various methods can be compared on paper and the most effective method selected scientifically rather than by intuition.

A word of warning should be noted about trying to predict absolute x-ray response for bulk specimens! In bulk specimens, absorption of both the incident and emerging radiation would alter the intensity so radically as to make the predictions impractical.

LITERATURE CITED

(1) IUPAC Report on Data Interpretation, *Pure Appl. Chem.*, **45**, 99 (1976); also *Anal. Chem.*, **48**, 273R (1976).
(2) D. B. Brown, J. V. Gilfrich, and M. C. Peckerar, *J. Appl. Phys.*, **46**, 4537 (1975).
(3) W. H. McMaster et al., Lawrence Radiation Laboratory, UCRL Rept. 50174 (revision 1), May 1969.
(4) R. W. Fink et al., *Rev. Mod. Phys.*, **38**, 513 (1966).
(5) J. V. Gilfrich, D. B. Brown, and P. G. Burkhalter, *Appl. Spectrosc.*, **29**, 322 (1975).

RECEIVED for review April 25, 1977. Accepted June 21, 1977.

Determination of Fluorine by Neutron Activation Analysis

H. Gene Knight,* A. Keith Furr, and T. F. Parkinson

Neutron Activation Analysis Laboratory, Virginia Polytechnic Institute and State University, Blacksburg, Virginia 24061

The analysis of fluorine by instrumental neutron activation analysis is hampered by the short half-life (11.41 s) of fluorine-20 and by frequent interference from chlorine. A procedure is described which mitigates these problems. Using this procedure, Teflon standards were analyzed and an estimated minimum detectable weight of 14 μg of fluorine was determined.

In recent years the fast and accurate determination of fluorine concentration has become increasingly important to researchers in many diverse fields. More work is now being done requiring fluorine determination over a wide range of concentrations. This range varies from the low concentrations of fluorine as it is found as an environmental pollutant to the high concentrations found when a fluorine compound is used as a solvent in coal liquefaction. The increased interest in determination of fluorine content emphasizes the importance of a single analytical technique which is suitable for use on a wide variety of materials and over a wide range of concentrations.

The conventional analysis methods include titration, x-ray spectrometric analysis, atomic absorption spectrometry, and neutron activation analysis (NAA). Other methods are available for fluorine determination in liquid media only; thus these methods are limited to specific types of samples. The advantages and problems associated with each major analytical method for fluorine determination are summarized below.

The chemical analysis for fluorine utilizes a thorium nitrate titration method. The titration end point is so poorly defined as to require computer refinement for determination. This ill-defined end point causes the analysis results to be questionable.

X-ray spectrometric analysis (or x-ray fluorescence) has a major handicap in that the absorption of the primary x-rays in the beryllium x-ray tube window becomes significant at the long wavelengths required to excite elements of atomic number less than 22 (*1*). With elements of low atomic number, the excited x-rays will be attenuated in the beryllium window and will not impinge on the Si(Li) detector; thus the fluorine content cannot be determined. Fluorine has an atomic number of 9 which precludes it from determination by the x-ray spectrometric method.

Any element may be determined by atomic absorption spectrometry (AA) if the resonance line is in the portion of the light spectrum which the AA instrument can utilize. Most instruments currently in use operate with wavelengths of greater than 1900 Å (*2*) which is in the upper portion of the ultraviolet and in the visible part of the spectrum. The fluorine resonance line has a wavelength of 955 Å and is thus below the operational limit of most atomic absorption instruments.

Fluorine has been a difficult element to determine by NAA because of interferences from other substances within a particular material, the very short half-life (11.41 s (*3*)) and the relatively high radiation levels associated with irradiated high density materials.

NAA utilizes the activation of stable fluorine-19 and the subsequent decay of fluorine-20 (*4*) to stable neon-20:

$$ {}_0n^1 + {}_9F^{19} \rightarrow ({}_9F^{20})^* \rightarrow {}_{10}Ne^{20} + \beta^-(5.41\ \mathrm{MeV}) + \gamma(1.6331\ \mathrm{MeV}) + Q \qquad (1) $$

The procedure discussed in this paper has been quite effective in overcoming the problems normally encountered and has proved to be a viable procedure for fluorine determination when used in conjunction with the soft-ware analysis program (*5, 6*) used at the VPI & SU Laboratory.

EXPERIMENTAL

The equipment used for this analysis consists of a 100 kW Argonaut type nuclear reactor used for sample irradiation in a thermal neutron flux of 1.2×10^{12} neutrons/cm^2-s, a γ radiation counting system featuring a high resolution Ge(Li) detector, a Nuclear Data Model 4420 Function Control Unit with a 100 MHz Analog-to-Digital Converter (ADC), an internal 32000 word computer central processing unit, a computer standard tape unit, an optional video-data terminal or teletype and the VPI & SU main computer system IBM 370-158. Two Ortec Model 775 scalers were added to the standard counting system to totalize counts for the dead-time correction. See Figure 1.

The observed weights of the standards are based on an absolute determination of fluorine content using the known composition of the standard materials, weights, half-lives, activation times, delay times, and neutron flux. The VPI & SU research reactor has an extremely stable neutron flux in the activation region over a long period of time. The initial determination of the absolute flux levels was made by absolute activation measurements of ^{60}Co and periodic rechecks affirm the stability of the flux.

An optimum activation time must be determined which will vary with the material composition. This time must be long enough to allow the fluorine-19 in the sample to become sufficiently activated while maintaining overall sample radiation levels low enough to allow data acquisition. Because of the short time interval (less than one half-life) between the end of activation and start of count, care must be exercised to avoid saturating the ADC or the Ge(Li) detector.

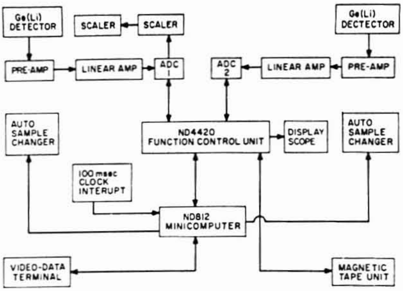

Figure 1. ND4420 counting system

To increase the activity at which a sample may be analyzed, a restricted region must be set up on the ADC to eliminate the effects of all other γ peaks not contained within the region of interest. The upper and lower level discriminators on the ADC must be adjusted to encompass the region immediately surrounding the fluorine-20 γ peak. This restricted region includes the fluorine peak at 1633.1 keV, a chlorine peak at 1642.4 keV and part of the Compton edge for aluminum. Since the ADC is affected only by the interactions occurring within the restricted region, the sample activity as sensed by the ADC will be quite low; thus the saturation of the ADC will no longer be a limiting factor.

The hard β particles (up to 5.41 MeV) emitted will cause an energy shift and broadening of the fluorine peak. It will also contribute to the overall radiation levels of the sample. To minimize the effects of this β particle and the associated bremsstrahlung, a sheet of lead 0.74 mm thick was installed between the sample and the Ge(Li) detector. Lead was selected because of sample and detector geometry considerations. Aluminum, with a lower atomic number, would have been the ideal shielding material but would have necessitated too great a change in the sample-to-detector geometry. This thickness of lead will not seriously attenuate the γ from fluorine-20 decay. The lead absorber decreases the energy shift, the peak broadening, and the radiation levels of the sample. Thus, a sample with a higher total activity may be analyzed with little peak distortion and without saturating the Ge(Li) detector, provided that the sample activity as sensed by the Ge(Li) detector is maintained at less than approximately 40% deadtime at which point the Ge(Li) detector will become too highly saturated. There is a deadtime correction factor incorporated into the analysis program (*7*) which will correct for error due to the percent deadtime.

A pile-up correction (*7, 8*) must be used to compensate for the loss of data due to the detector transmitting fluorine-20 photoelectric event pulses to the ADC which are not recognized as coming from fluorine-20. The time the detector requires to transmit a pulse from a single interaction to the ADC is called the resolving time (τ). During this period of time, two or more pulses may arrive at the detector and, since the detector cannot separate the multiple pulses, they will be summed together and transmitted as a single pulse of a higher energy. Their energies thus combined will be interpreted by the ADC as a γ photon of a higher energy than that for fluorine, resulting in an observed fluorine concentration which is lower than the true concentration. The resolving time has been determined to be 5.89 μs by the split-source method (*9*). The total number of interactions occurring within the Ge(Li) detector will determine the magnitude of the effect that pile-up will have upon a particular sample. The installed scalers will show the indicated count rate in the detector from the input signal to the ADC whether the ADC utilizes the signal or not; thus it is a measure of the total interactions occurring within the Ge(Li) detector.

Pulse pile-up affects the entire spectrum. However, the loss of counts from the photopeak area, and hence the amount of

Table I. Results of Analysis of $(C_2F_4)_n$ Standards

Sample	Calculated weight, μg[a]	Measured weight, μg[b]
1	76.0	65.9 ± 11.2
2	152	156 ± 4.8
3	380	381 ± 28.5
4	760	815 ± 45.9
5	1 520	1 770 ± 106
6	2 960	3 210 ± 257
7	5 930	6 230 ± 154
8	12 400	12 300 ± 447
9	23 800	21 800 ± 1 090
10	47 500	39 300 ± 1 260
11	95 000	71 900 ± 6 210
12	190 000	135 000 ± 5 960

[a] Calculated weight (micrograms) = (Molecular weight of fluorine × weight × 10^6)/(Molecular weight of C_2F_4) = micrograms (3). [4(18.9984) × 1 gram × 10^6]/[2(12.01115) + 4(18.9984)] = 759 815 μg ≃ 760 000 μg.

[b] Measured weight = mean ± standard deviation

fluorine present, can be computed by the method of Roscoe and Furr (*7*) using Equation 2.

$$\mu g/g_{\text{true}} = \frac{\mu g/g_{\text{obsd}}}{1 - \left[\dfrac{\text{total counts}}{\text{count time}}(\tau)\right]} \tag{2}$$

The overall effect of pile-up will be greater as the sample activity is increased.

Each sample analysis was replicated five times to minimize statistical variations and activation timing errors due to limitations of existing timing devices. The mean value and standard deviation of the mean were then calculated by the sum of squares method (*10*). A more complete discussion of errors due to the curve-fitting algorithm and to counting statistics is given in Ref. (*7*).

RESULTS AND DISCUSSION

In Figure 2 are shown typical γ spectra from samples containing fluorine. The fluorine content in the contaminated vegetation (Figure 2D) was found to be 106 ± 43 μg/g. This result demonstrates the capability of the analytical procedure for analyzing fluorine in the presence of chlorine.

The results of calibrating the system with Teflon standards, $(C_2F_4)_n$, are summarized in Table I and Figure 3.

As can be seen in Figure 3, a plot of experimental results for $(C_2F_4)_n$, the fluorine weight from NAA vs. the calculated weight correlates well until the higher mass samples begin to show an increasing systematic deviation. This deviation was tentatively attributed either to self-shielding effects or to double pulse pile-up. A self-shielding correction factor was calculated by the methods of Kruger (*11*) and Zweifel (*12*) and was found to be negligible. Samples exhibiting this deviation were then reactivated under the same conditions at approximately one-half the original activation times. The rationale for this procedure was that if this deviation were indeed caused by double pulse pile-up, then, by decreasing the activation time, the total activity and ultimately the effects of double pulse pile-up would be minimized. With less error contributed by the double pulse pile-up effect, the correlation between measured and calculated weights should be much improved. As can be seen in Table II, the double pulse pile-up effect was quite significant at very high fluorine concentrations. With the correction to decrease the effects of double pulse pile-up, the disparity between measured and calculated weights of fluorine was indeed decreased.

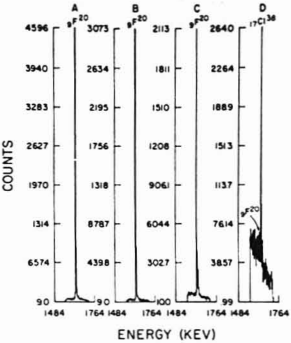

Figure 2. (A) Spectrum plot for MgF_2 standard. (B) Spectrum plot for C_2F_4 standard. (C) Spectrum plot for treated coal. (D) Spectrum plot for contaminated vegetation

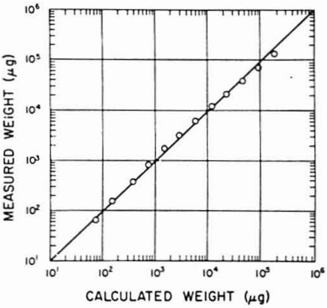

Figure 3. Comparison of measured and calculated weights in C_2F_4. The error bars are smaller than the symbols

Double pulse pile-up error may be minimized by decreasing the total activity of the sample while still maintaining sufficient activation for determination of the fluorine-19. This procedure, however, will not eliminate the error entirely. Hence a discrepancy will still exist between measured and calculated weights. A mathematical correction for double pulse pile-up, described by Cohen (*13*), may be used for the very high fluorine concentrations where this has been found to be a problem.

We have defined the minimum detectable weight for fluorine to be three times the background level. This corresponded to 14 μg for the Teflon, $(C_2F_4)_n$, standards analyzed.

Table II. Double Pulse Pile-up Effects

Sample No.	10	11	12
Calculated weight, μg	47 500	95 000	190 000
Measured weight, μg	39 300 ± 1 260	71 900 ± 6 210	135 000 ± 5 960
Activation time, s	30	15	9
Measured weight, μg	41 900 ± 3 180	85 400 ± 2 030	154 000 ± 3 850
Activation time, s	15	9	5

LITERATURE CITED

(1) E. P. Bertin, "Principles and Practice of X-ray Spectrometric Analysis", Plenum Press, New York–London, 1970.
(2) W. Slavin, "Atomic Absorption Spectroscopy", Interscience Publishers, New York, N.Y., 1968.
(3) G. Erdtman and W. Soyka, *Nucl. Instrum. Methods*, **121**, 197–201, (1974).
(4) C. M. Lederer, "Table of Isotopes", 6th ed., Wiley and Sons, New York, N.Y., 1967.
(5) B. A. Roscoe, "Acquisition and Analysis of Neutron Activation Data", Master of Science Thesis in Nuclear Science and Engineering, VPI & SU, 1976.
(6) B. A. Roscoe and A. K. Furr, *Nucl. Instrum. Methods*, **137**, 173–178 (1976).
(7) B. A. Roscoe and A. K. Furr, *Nucl. Instrum. Methods*, **140**, 401–404 (1977).
(8) Y. DeAisenberg, I. M. Cohen, R. O. Korob, and M. D. Rudelli, Nuclear Activation Techniques in the Life Sciences, IAEA-SM-157/72.
(9) G. H. Simmons, "A Training Manual for Nuclear Medicine Technologists", Public Health Service, BRH/DMRE 70-3.
(10) A. M. Selby, Standard Mathematical Tables, 21st ed., The Chemical Rubber Co., Cleveland, Ohio, 1973.
(11) P. Kruger, "Principles of Activation Analysis", Wiley-Interscience, New York, N.Y., 1971.
(12) P. F. Zweifel, *Nucleonics*, **18** (11), 174–175 (1960).
(13) E. J. Cohen, *Nucl. Instrum. Methods*, **121**, 25 (1974).

RECEIVED for review February 3, 1977. Accepted June 6, 1977.

Determination of 13 Elements with Atomic Numbers between 12 and 47 by 14-MeV Helium-3 Activation Analysis

C. S. Sastri, H. Petri,* and G. Erdtmann

Zentralabteilung für Chemische Analysen, Kernforschungsanlage Jülich GmbH, 5170 Jülich, West Germany

Nuclear reactions for the trace determination of the elements Mg, Al, Ti, V, Cr, Mn, Fe, Ni, Zn, Zr, Nb, Mo, and Ag by activation analysis with 14-MeV ^{3}He ions were investigated. For these reactions, thick target yields were measured and interference-free detection limits were calculated. For an irradiation of 1 h or 1 half-life, whichever is shorter depending on the product nuclide, at 2 μA, the detection limits are in the range 1–50 ppb for Al, Ti, V, Mn, Ni, Zn, and Nb; 50–100 ppb for Mo; and 100–500 ppb for Mg, Cr, Fe, Zr, and Ag.

Charged particle activation analysis has gained great importance in the detection of light elements at the sub-ppm level. The particles that are commonly used are protons, deuterons, tritons, helium-3 and helium-4 ions (*1–5*). Protons have been used (*6–8*) also to find heavy element impurities in high purity metals, minerals, etc. Sometimes other techniques like proton activation followed by x-ray counting and PIXE (particle induced x-ray emission) have been used (*9, 10*) for trace element study. Markowitz and Mahony (*11*) were the first to suggest ^{3}He ions for activation analysis of light elements. Following this, to a limited extent, this technique has been used for investigating heavy element impurities (*12, 13*). Ricci and Hahn (*14*) have calculated sensitivities for elements from Be to Ca for 18-MeV ^{3}He ions. Kormali and Schweikert (*15*) have measured thick target yields for elements from Zr to Cs with 40-MeV ^{3}He ions.

In our laboratory the light elements C and O in metals are being investigated by the 14-MeV helium-3 activation technique (*16, 17*). Concurrently systematic studies have been made to see if these irradiation conditions are useful also for the determination of heavy elements by nondestructive analysis. This energy corresponds to the Coulomb barrier of 14.2 MeV between ^{3}He nucleus and a target nucleus with $Z \approx 42$, assuming both the nuclei to be spheres with radii of $1.4 \times 10^{-13}\ A^{1/3}$ cm. This means that elements lighter than molybdenum will undergo nuclear reactions and therefore can be determined. With heavier elements, reactions take place to a very limited extent because of the tunnelling effect. Thus, metals and other elements with $Z > 42$ can be investigated for their low Z impurities.

In previous papers (*18, 19*), the determination of impurities in the matrices Nb, Ta, and W, by activation analysis with 14-MeV ^{3}He-particles was described. At this energy, the commonly observed nuclear reactions are (^{3}He, α), (^{3}He,2p), (^{3}He, p), (^{3}He,p2n), (^{3}He,n) and (^{3}He,2n).

In the present work, 13 elements between $Z = 12$ and $Z = 47$ were irradiated and from the γ-ray spectra of the irradiated targets, the optimum detection reactions having high specific activities and low nuclear interferences were found and the detection limits based on these reactions were calculated.

EXPERIMENTAL

High purity metal foils of natural isotopic composition (suppliers: Goodfellow Metals and Ventron) of the size 20 × 20 mm (approx.) were irradiated in the form of thick targets. The range of the 14-MeV ^{3}He ions was from 30 to 60 mg/cm^2 in the targets used; the target thickness varied from 100 to 150 mg/cm^2, in all cases being thicker than the range of the beam in the material. Most of the irradiations were made in the internal beam of the isochronous cyclotron JULIC at Kernforschungsanlage Jülich. The irradiations were made with 14-MeV ^{3}He ions at currents ranging from 50 to 500 nA and for times ranging from 10 to 30 min. It has been found that these irradiation conditions can be reproduced without difficulty.

As a check, the thick target yields for some of the standards were measured periodically. Short irradiation times of a minute or less were avoided to minimize the errors due to occasional fluctuations in currents, lasting a few seconds, that are likely to happen with the machine. If for some reason a large fluctuation in beam current had occured during an irradiation, such a measurement was discarded. A current integrator was not available for the present measurements.

Because of the high magnetic field in the cyclotron, Fe and Co targets could not be irradiated in the internal beam of JULIC. They were irradiated in the external beam of the Compact Cyclotron CV 28 of Kernforschungsanlage Jülich. Irradiations were made for 5 to 10 min at 400 nA to 1 μA current.

At the isochronous cyclotron JULIC, the internal beam ($\sim$2 mm diameter) strikes the rectangular target onto a side. In the compact cyclotron CV 28, the external beam ($\sim$10 mm diameter) strikes the rectangular target at the center. In both cases, the

Table I. Calculation of Detection Limits for 14-MeV ^{3}He Ions

Element	Nuclide	Half-life[a]	γ-Ray, MeV[a]	Net photopeak counting rate, P, counts/min[b]	Thick target γ-emission rate, A, γ/min[c]	Minimum detectable γ-emission rate, R, γ/min[d]	Detection limit, ppb[e]
Mg	^{27}Mg	9.48 m	0.843	2.3×10^6	2.9×10^8	65.0	220
			1.014	7.4×10^5	1.2×10^8	77.7	650
Al	^{28}Al	2.246 m	1.779	2.4×10^7	6.3×10^9	111.6	17
Ti	^{48}Cr	23.0 h	0.112	5.5×10^5	5.5×10^6	1.1	200
			0.308	2.1×10^5	6.4×10^6	0.90	140
	^{49}Cr	41.9 m	0.090	1.2×10^8	1.2×10^9	3.5	3
			0.153	6.7×10^7	7.8×10^8	3.6	5
V	^{52m}Mn	21.3 m	1.434	1.1×10^7	2.4×10^9	53.7	22
	^{52g}Mn	5.6 d	0.744	2.7×10^5	2.8×10^7	6.4	230
			0.935	2.2×10^5	3.1×10^7	8.3	270
			1.434	1.4×10^5	3.0×10^7	7.2	240
Cr	^{53g}Fe	8.51 m	0.378	6.6×10^6	2.7×10^8	33.3	120
Mn	^{56}Mn	2.576 h	0.846	4.3×10^6	5.4×10^8	20.9	40
			1.810	4.6×10^5	1.2×10^8	19.5	160
Fe	^{55}Co	17.9 h	0.931	2.1×10^5	2.9×10^7	8.0	280
	^{57}Co	270 d	0.122	2.5×10^5	2.7×10^6	1.2	440
	^{58}Co	71.3 d	0.810	2.2×10^4	2.6×10^6	0.71	270
Ni	^{61}Cu	3.41 h	0.283	3.7×10^6	1.0×10^8	4.2	40
			0.656	1.1×10^6	1.0×10^8	10.3	100
Zn	^{65}Ga	15.2 m	0.115	7.4×10^7	7.4×10^8	9.1	10
			0.153	1.2×10^7	1.4×10^8	8.3	60
	^{67}Ga	78.1 h	0.093	1.4×10^6	1.4×10^7	1.1	80
			0.184	5.6×10^5	9.0×10^6	1.8	200
			0.300	2.2×10^5	6.3×10^6	2.3	370
Zr	^{97}Nb	72.0 m	0.657	6.0×10^5	5.5×10^7	17.7	320
Nb	^{94g}Tc	4.88 h	0.703	2.7×10^6	2.7×10^8	9.3	30
			0.850	2.1×10^6	2.6×10^8	11.2	40
Mo	^{99m}Tc	6.02 h	0.140	2.1×10^6	2.6×10^7	1.9	70
	^{97}Ru	2.88 d	0.215	2.0×10^5	3.8×10^6	1.9	500
Ag	^{108g}In	58 m	0.876	3.7×10^5	4.9×10^7	21.8	440

[a] Half-lives and γ energies are taken from Ref. 20. [b] Photopeak counting rate (counts/min) at the end of an irradiation of 1 h or 1 half-life, whichever is shorter at 2 μA current and measured with a GETAC Ge(Li) detector which has 0.50% absolute efficiency (see text). Measurements done with another detector were normalized to this efficiency. [c] γ-emission rate $A = P/\epsilon$; P from column 5. ϵ = photopeak counting efficiency. [d] According to Equation 11. [e] According to Equation 1.

target-holders were water cooled.

After irradiation, the samples were measured with a γ-ray spectrometer consisting of a Ge(Li) detector and a Nuclear Data 4096 channel analyzer. Most of the measurements were made with a 50 cm^3 Ge(Li) detector (Getac, Mainz, Germany) and a few were made with a 30 cm^3 Ge(Li) detector (Canberra, Meriden, Conn.). Their characteristics were as follows; resolution 2.3 and 3.1 keV FWHM, respectively, for the 1332-keV γ line of ^{60}Co and absolute efficiencies 0.50% and 0.18%, respectively, for the 1332-keV γ line of ^{60}Co and for the geometries used. The peak area evaluation was done with the program ND 411007 developed by Nuclear Data Inc.

From the peak areas, the thick target yields at the end of irradiation were calculated by correcting for the decay between the end of irradiation and start of measurement and for the decay during measurement. As different irradiation times and fluxes were used for different targets, the thick target yields obtained were normalized to the conditions of 2 μA beam current and an irradiation of 1 h or 1 half-life, whichever was shorter, and for 100% detection efficiency.

RESULTS AND DISCUSSION

From the activation experiments, two values referring to the sensitivity of the method were calculated for each element and are given in Table I: the thick target yields and the detection limits. The thick target yields are the average values of 2 to 4 irradiations for each element and are expressed as gammas/min instead of disintegrations per min and therefore are named "thick target γ-emission rates". They were obtained by dividing the observed photopeak counting rates (counts/min) at the end of irradiation, by the efficiency of the Ge(Li) detector for the γ ray concerned of the given nuclide. While measuring the activated targets, their positioning was such that the irradiated side always faced the detector in order to minimize the absorption of, particularly low energy, γ rays in the target itself.

The detection limit is defined as follows:

$$\text{Detection limit (ppm)} = [\text{minimum detectable } \gamma\text{-emission rate } (R) \times 10^6]/[\text{thick target } \gamma\text{-emission rate } (A)] \quad (1)$$

The minimum detectable γ-emission rate is obtained from the minimum detectable net peak count rate which in turn is determined by a photopeak which is clearly contrasted from the background. In all practical cases the background under a photopeak is composed of three parts: (1) the "natural" background including all contributions from external sources, (2) the "intrinsic" background arising from the Compton, scattering, and bremsstrahlung continua of the radionuclides due to the element to be determined, and (3) the "matrix" background arising from all other radionuclides produced in the sample. The matrix contribution cannot be generally estimated since it strongly depends on the nature of the matrix and the purity of it. For this reason we have calculated "interference free" detection limits.

It can be shown by a simple mathematical treatment that, of the two remaining types of background, the natural background alone plays the major role in deciding the interference-free detection limits.

Assume that the minimum detectable peak area is given by

$$C = 3\sigma_B \quad (2)$$

where C is the number of net counts in the peak, σ_B is the standard deviation due to the statistical error of the total

Table II. Nuclear Interferences to the Applied Reactions with 14-MeV ^{3}He Ions

Element	Useful nuclear reaction	Q-value, MeV[a]	Interfering element	Interfering nuclear reaction	Q-value, MeV[a]	Interference level, %[b]
Mg	^{26}Mg(^{3}He,2p)^{27}Mg	−1.3	–	–	–	–
Al	^{27}Al(^{3}He,2p)^{28}Al	0.0	Mg	^{26}Mg(^{3}He,p)^{28}Al	+8.3	<10
Ti	^{46}Ti(^{3}He,n)^{48}Cr	+5.6	Cr	^{50}Cr(^{3}He,αn)^{48}Cr	−3.0	<0.1
	^{48}Ti(^{3}He,2n)^{49}Cr	−4.3	Cr	^{50}Cr(^{3}He,α)^{49}Cr	+7.6	<3
V	^{51}V(^{3}He,2n)^{52m}Mn	−2.7	Cr	^{52}Cr(^{3}He,p2n)^{52m}Mn	−13.2	<2
	^{51}V(^{3}He,2n)^{52g}Mn	−2.7	Cr	^{52}Cr(^{3}He,p2n)^{52g}Mn	−13.2	<0.1
Cr	^{52}Cr(^{3}He,2n)^{53g}Fe	−5.7	Fe	^{54}Fe(^{3}He,α)^{53g}Fe	+7.2	<2
Mn	^{55}Mn(^{3}He,2p)^{56}Mn	−0.4	Cr	^{54}Cr(^{3}He,p)^{56}Mn	+7.6	<1
Fe	^{54}Fe(^{3}He,pn)^{55}Co	−2.7	–	–	–	–
	^{56}Fe(^{3}He,pn)^{57}Co	−1.7	Mn	^{55}Mn(^{3}He,n)^{57}Co	+8.5	<1
			Co	^{59}Co(^{3}He,αn)^{57}Co	+1.5	<10
	^{56}Fe(^{3}He,p)^{58}Co	+6.9	Co	^{59}Co(^{3}He,α)^{58}Co	+10.1	15
Ni	^{60}Ni(^{3}He,pn)^{61}Cu	−2.9	Co	^{59}Co(^{3}He,n)^{61}Cu	+6.6	12
			Cu	^{63}Cu(^{3}He,αn)^{61}Cu	+1.5	12
Zn	^{64}Zn(^{3}He,pn)^{65}Ga	−3.8	Cu	^{63}Cu(^{3}He,n)^{65}Ga	+3.9	<5
	^{66}Zn(^{3}He,pn)^{67}Ga	−2.4	Cu	^{65}Cu(^{3}He,n)^{67}Ga	+6.5	<5
				^{69}Ga(^{3}He,αn)^{67}Ga	+2.0	<8
Zr	^{96}Zr(^{3}He,pn)^{97}Nb	−0.2	–	–	–	–
Nb	^{93}Nb(^{3}He,2n)^{94g}Tc	−4.3	Mo	^{92}Mo(^{3}He,p)^{94g}Tc	+5.0	<2
Mo	^{95}Mo(^{3}He,n)^{97}Ru	+5.1	Ru	^{96}Ru(^{3}He,α)^{97}Ru	+10.3	1
	^{98}Mo(^{3}He,pn)^{99m}Tc	−1.2	–	–	–	–
Ag	^{107}Ag(^{3}He,2n)^{108m}In	−5.5	Cd	^{108}Cd(^{3}He,p2n)^{108m}In	−13.6	<1

[a] From Keller et al. (Ref. 21). [b] Interference level (%): (γ-emission rate per ppm of interfering element)/(γ-emission rate per ppm of element to be determined) × 100.

background, B in the energy window of interest.

The natural background, B_n, is obtained from a separate measurement for t_B min.

$$B_n = \frac{I_B t_s}{t_B} \tag{3}$$

where I_B = number of counts in the energy window of interest during the measuring period t_B. t_s = measuring period for the sample; this period is taken as 1.8 × half-life or 20 h whichever is less.

The intrinsic contribution to the background is obtained from the peak to background ratio Q for a given photopeak in the γ spectrum of a sample of pure element.

$$Q = \frac{P}{B - B_n} \tag{4}$$

where P is the net peak area expressed in counts obtained during the measurement of the standard. With high counting rates which are typical for a standard $B \gg B_n$ so that B only consists of the intrinsic contribution B_i. When a γ spectrum is measured at the detection limit, the P is substituted by C, and B_i becomes

$$B_i = \frac{C}{Q} \tag{5}$$

Thus,

$$B = B_n + B_i \tag{6}$$

$$\sigma_B = \sqrt{B_n + B_i} \tag{7}$$

and

$$C = 3\sigma_B = 3\sqrt{(B_n + \frac{C}{Q})} \tag{8}$$

$$= \frac{9}{2Q} + \sqrt{(\frac{9}{2Q})^2 + 9B_n} \tag{9}$$

From Equation 9, it becomes obvious that for large values of Q,

$$C \approx 3\sqrt{B_n} \tag{10}$$

This means the intrinsic contribution becomes negligible. It can be shown that Equation 10 even becomes true for $Q > 3$, which, in general, is valid for all peaks selected for instrumental analysis. Therefore the natural background is the only one to be considered in the estimation of detection limits.

Hence, for the calculation of detection limits, the minimum detectable γ-emission rate R is given by

$$R = \frac{3\sqrt{B_n}}{\epsilon t_s} \tag{11}$$

where ϵ = counting efficiency of the detector for the given γ ray.

In Table I, thick target yields and detection limits for 13 elements with $12 > Z > 47$ are listed. The study has been limited to those elements which could be obtained as thick foils. From the many radionuclides produced from each element, usually 1 or 2 of them are found suitable for trace analysis and are listed in Table I. The criteria for the selection of these nuclides are that their half-lives must be >2 min and they must not, or only to a low percentage level, be affected by nuclear interference.

Many nuclides emit more than one prominent γ line. If, in an analysis, one of them is interfered by γ rays from other components of the matrix, one of the other lines may be chosen for an assay of the element. Therefore, the calculation of detection limits was made for up to three γ lines, if found suitable, for each nuclide. The 511-keV positron annihilation line is not considered for any of the nuclides since most of the radionuclides formed with ^{3}He ions are positron emitters.

γ-Ray interferences from radionuclides produced from the element itself have been observed in four cases; vanadium, chromium, manganese, and iron. With vanadium, the nuclides ^{52m}Mn and ^{52g}Mn are useful for trace analysis and both emit 1434-keV γ rays. In applying ^{52m}Mn for analysis, the influence of the latter nuclide, calculated from its other γ lines 744 keV and 935 keV, on the former is found to be <1% for short irradiation periods. With chromium, ^{53g}Fe and ^{52m}Mn are produced and both nuclides emit 378-keV γ rays. The contribution of ^{52m}Mn on ^{53g}Fe, found from the 1434-keV γ line of ^{52m}Mn, is <1%. For manganese, the useful γ lines of the nuclide ^{56}Mn are 846 keV and 1810 keV and both are interfered by γ lines of ^{56}Co. The contributions, found from the 1238-keV γ line of ^{56}Co, are <1% and <0.05% for 846 keV and 1810 keV, respectively, and for short irradiation periods. For iron, the interference is observed if ^{58}Co (half-life = 71.3 d) is used as the identifying nuclide. The interference caused by the 812-keV γ line of ^{56}Ni (half-life = 6.1 d), found from its 158-keV γ line, is 3% but this can be brought to <1%, after an appropriate waiting period for the matrix, because of the large difference in the half-lives of the two nuclides.

Besides the list of elements presented in Table I, we have irradiated Co and Cu foils but we could not find any useful reactions with low levels of nuclear interference to identify them. The thick target yield from Co via ^{59}Co(^{3}He,2n)^{60}Cu is of the same magnitude as that from Ni via ^{58}Ni(^{3}He,p)^{60}Cu. It is but natural that the actual detection limits will be much higher than those "interference-free" limits reported in column 8. The true limits for a given matrix will depend on the activity induced in it and the purity of it. This limit is influenced also by the ranges of the 14-MeV ^{3}He ions in the given matrix and the element of interest. If the matrix is highly activated, it may be difficult to measure short lived nuclides formed from Mg, Al, Cr, and V when they are present at very low concentrations. Even if the matrix activity is not high, the determination of some of the elements may not be possible if the product nuclides from the matrix emit γ rays with the same energy as those expected from the element under study. For example, because of the tunnelling effect, the matrix tantalum gets activated with 14-MeV ^{3}He ions and the γ-ray interference caused by the product nuclides of this matrix makes the determination of Ni, Zn, and Mo in Ta not possible.

In Table II, the useful nuclear reactions for the identification of the elements and the reactions causing nuclear interference along with the level of interference are listed. The level of interference in each case was found by irradiating the interfering element (excepting Ga and Ru) under identical conditions and assuming an equal concentration of the element of interest and the interfering element. For Ga and Ru, the level was theoretically calculated (*21*).

From all these limitations, it becomes clear that the matrix is the ultimate deciding factor in knowing whether a given element can be detected at all, and what its detection limit is. Nevertheless, these "interference-free" detection limits will help to decide if it is useful to take into consideration the application of this method to a given analytical problem.

ACKNOWLEDGMENT

The authors thank J. Reich, J. Hemmerich, and the operation personnel of the cyclotrons JULIC and CV 28 for their kind cooperation.

LITERATURE CITED

(1) J. L. Debrun, J. N. Barrandon, and Ph. Albert, in "Use of cyclotrons in chemistry, metallurgy and biology", Butterworth, London 1970.
(2) T. Nozaki, Y. Yatsurugi, N. Akiyama, Y. Endo, and Y. Makide, *J. Radioanal. Chem.*, **19**, 109 (1974).
(3) M. Peisach, *J. Radioanal. Chem.*, **12**, 251 (1972).
(4) Ch. Engelmann, *J. Radioanal. Chem.*, **7**, 89 (1971).
(5) C. Vandecasteele, F. Adams, and J. Hoste, *Anal. Chim. Acta*, **72**, 269 (1974).
(6) D. L. Swindle, L. R. Novak, and E. A. Schweikert, *Anal. Chem.*, **46**, 655 (1974).
(7) J. L. Debrun, J. N. Barrandon, and P. Benaben, *Anal. Chem.*, **48**, 167 (1976).
(8) I. O. Konstantinov, B. V. Zatolokin, N. N. Krasnov, Yu. G. Sevastyanov, and L. S. Volkova, *J. Radioanal. Chem.*, **31**, 487 (1976).
(9) J. R. McGinley and E. A. Schweikert, *Anal. Chem.*, **48**, 429 (1976).
(10) T. B. Johansson, R. E. Van Grieken, J. W. Nelson, and J. W. Winchester, *Anal. Chem.*, **47**, 855 (1975).
(11) S. S. Markowitz and J. D. Mahony, *Anal. Chem.*, **34**, 329 (1962).
(12) B. Parsa and S. S. Markowitz, *Anal. Chem.*, **46**, 186 (1974).
(13) D. C. Riddle and E. A. Schweikert, *Anal. Chem.*, **46**, 395 (1974).
(14) E. Ricci and R. L. Hahn, *Anal. Chem.*, **39**, 794 (1967).
(15) S. M. Kormali and E. A. Schweikert, *J. Radioanal. Chem.*, **31**, 413 (1976).
(16) H. Petri and C. S. Sastri, *Fresenius' Z. Anal. Chem.*, **277**, 25 (1975).
(17) H. Petri and C. S. Sastri, *Radiochem. Radioanal. Lett.*, **21**, 225 (1975).
(18) C. S. Sastri, H. Petri, and G. Erdtmann, in "Modern Trends in Activation Analysis", München 1976, pp 842–849.
(19) C. S. Sastri, H. Petri, and G. Erdtmann, *Anal. Chim. Acta*, **89**, 141 (1977).
(20) G. Erdtmann and W. Soyka "Die γ-Linien der Radionuklide", Jül-1003-AC, Jülich, 1973.
(21) K. A. Keller, J. Lange, and H. Münzel "Q-values and excitation functions of nuclear reactions", Landolt Börnstein, New series, Vol. 5, Springer Verlag, Berlin, 1973.

RECEIVED for review February 7, 1977. Accepted May 16, 1977.

Determination of the Surface Predominance of Toxic Elements in Airborne Particles by Ion Microprobe Mass Spectrometry and Auger Electron Spectrometry

R. W. Linton,[1] **Peter Williams, and C. A. Evans, Jr.***

School of Chemical Sciences and Materials Research Laboratory, University of Illinois at Urbana-Champaign, Urbana, Illinois 61801

D. F. S. Natusch

Department of Chemistry, Colorado State University, Fort Collins, Colorado 80523

Surface analytical techniques including ion microprobe mass spectrometry and Auger electron spectrometry have been used to demonstrate elemental surface predominance in coal fly ash particles. Substantiation and quantitation of the ion microprobe data were achieved by using a multitechnique approach including solvent leaching and bulk multielemental analysis using spark source mass spectrometry. Elemental surface predominance in coal fly ash is explained in terms of a volatilization–condensation mechanism. The substantial leachabilities and strongly enhanced surface region concentrations of numerous elements, including potentially toxic ones such as Pb, Tl, Mn, and Cr, indicate that coal fly ash may have a more deleterious environmental impact than is apparent solely on the basis of conventional bulk analysis.

The surface predominance of potentially toxic elements has been demonstrated recently in coal fly ash particles emitted to the atmosphere (*1*). Preliminary studies also indicate that elemental surface predominance may be a general phenomenon occurring in airborne particles derived from high temperature combustion operations (*1, 2*).

These findings are of significance in part because they provide direct confirmation of previous predictions (*3, 4*) that surface predominance should occur. The phenomenon is attributed to the condensation of species previously volatilized in the high temperature combustion zone of a particulate emission source (*3, 4*).

The existence of elemental surface predominance is also important in demonstrating that bulk analysis techniques, which give only average concentration values, provide little insight into the actual chemical nature of the particles. For example, results obtained solely on the basis of bulk analysis markedly underestimate the potential environmental impact of airborne particles derived from high temperature combustion operations in that (1) surface regions of the particles have enhanced concentrations of elements, including some which are potentially toxic, and (2) the smallest particles will have much higher bulk (μg/g) concentrations of such elements because of larger surface area to volume ratios (*3*). The first factor is of environmental significance because it is the particle surface which comes in contact with, and is extracted by, body fluids upon ingestion or inhalation; which is subjected to aqueous extraction in the natural environment; and which takes part in the catalysis of heterogeneous atmospheric reactions such as the oxidation of SO_2 to sulfate (*5, 6*). Enhanced bulk elemental concentrations in the smallest particles are also highly undesirable from an environmental standpoint because it is the small particles (less than about 5 μm in aerodynamic diameter) which most readily elude particle collection devices (*7*), which have long atmospheric lifetimes (*8*), and which penetrate the innermost regions of the lung when inhaled (*9*).

On the basis of the above discussion, it is apparent that there is a need for analytical techniques capable of surface and in-depth elemental characterization of individual particles. Several approaches to obtain this analytical information comprise the subject matter of this paper. Principal methods employed include the surface analytical techniques of secondary ion mass spectrometry (SIMS) and Auger electron spectrometry (AES) as practiced for microanalysis, i.e., ion microprobe mass spectrometry and scanning Auger microscopy.

This paper also illustrates the benefits of a multitechnique approach, not only by the application of several complementary surface microanalytical techniques, but also by the use of solvent leaching in conjunction with both surface and bulk (spark source mass spectrometry) analyses. Specifically, the combination of leaching, bulk, and surface techniques demonstrates that the observed elemental surface predominance is not the consequence of artifacts, especially those which may result from the use of ion sputtering to obtain depth profiles. It also permits semi-quantitation of elemental concentrations in the surface region.

In the case of coal fly ash, the information obtained by this approach provides substantial insight into the physicochemical characteristics of fly ash surfaces and permits assessment of its potential environmental impact.

EXPERIMENTAL

Sample Selection. The fly ashes studied were emitted by coal fired power generating plants, one utilizing chain grate stoking and the other pulverized coal feed, and both burning midwestern U.S. bituminous coal. Samples were collected in the stack systems at temperatures in the range of 200–300 °C. Ash from the chain grate stoked plant was studied most extensively because it had generally higher trace element bulk concentrations, facilitating detection by the various analytical techniques. Large particles (45–180 μm physical diameter) were analyzed to facilitate both particle handling and the characterization of individual particles using surface microanalytical techniques.

Analytical Procedures and Instrumentation. *Solvent Leaching and Bulk Analysis.* Solvent leaching of the fly ash was performed using Fisher reagent grade dimethyl sulfoxide (DMSO) and triply distilled water. DMSO was chosen after inorganic species were found in DMSO extracts during studies investigating the extraction of trace organics, while H_2O was employed to simulate leaching in the natural environment. Leaching with DMSO was carried out for 48 h in a Soxhlet extractor at a temperature of 40 °C and a pressure of $\sim$0.1 mm Hg. A DMSO blank was prepared by leaching of an empty Soxhlet thimble using identical experimental conditions. Leaching with H_2O was performed by placing fly ash in a glass jar containing triply-distilled water for a 12-h period. The jar was also placed in a DISONtegrator Model 320 and sonicated for 1 h in a water bath in order to maximize interaction of the solvent with fly ash surfaces. The leachate solution was then filtered twice through Whatman No. 41 filter paper, as was an H_2O solution serving as the blank. The aqueous leaching procedure was used primarily to indicate relative elemental leachabilities under the conditions employed, and thus it may not solubilize the entire available fraction of most elements (*10*).

---

[1] Present address, Department of Chemistry, University of North Carolina, Chapel Hill, N.C. 27514.

To assess the extent of elemental leachability from fly ash, bulk analyses of particles and solution leachates were performed with an AEI MS-7 spark source mass spectrometer (SSMS) employing photographic detection. Unleached and leached particles were crushed to increase homogeneity, and 50 mg of the crushed fly ash was then mixed with 200 mg of spectroscopic graphite containing 5 mg of MG-1 Spex Spikes. Leachate solutions were prepared for analysis by doping 250 mg of spectroscopic graphite containing 5 mg of the Spex Spikes with 1–2 mL of leachate using 2 mL acetone-free methanol as a wetting agent. Complete evaporation of the solvents was carried out at a low temperature (50 °C). The leachate and particle samples were homogenized by use of a mechanical shaker and subsequently pressed into electrodes. All electrodes were sparked using a 25-μs spark duration and a repetition rate of 300 s^{-1}.

Of the six possible internal standards in the Spex Spikes, ^{95}Mo and ^{153}Eu were least subject to natural abundance interferences from the fly ash and thus were chosen as the internal standards. A series of graded photographic exposures was obtained for each sample. Subsequently, ion intensities for the internal standards and elements of interest were determined by densitometry and expressed as Seidel numbers (*11*). Elemental concentrations in the electrode material were calculated by use of the following equation:

$$\frac{C_u}{C_s} = \frac{S_u}{S_s} \cdot \left[\frac{\dfrac{60}{m_s}}{\dfrac{60}{m_u}}\right]^{3/2} \cdot \frac{\phi_s}{\phi_u} \qquad (1)$$

where u, s = analyte and internal standard quantities, respectively; S = Seidel number; m = atomic mass; ϕ = isotopic abundance; and C = concentration. The terms containing m are empirical corrections for the variation in photoplate sensitivity with atomic mass. C_u in the above equation was also multiplied by the appropriate factor to convert from concentration in the electrode to concentration in the original particle or solution sample.

Elemental Depth Profiles. The variation of elemental concentrations as a function of depth for both leached and unleached fly ash particles was determined by ion microprobe mass spectrometry and Auger electron spectrometry combined with ion etching. The procedure for particle mounting involved placing large particles (45–180 μm) in a folded strip of indium foil and hand pressing to imbed them into the foil. This mounting technique has the advantages that indium is electrically conducting, presents few spectral interferences, is soft and malleable allowing imbedding of particles without physical alteration, has a low vapor pressure for ultra high vacuum compatibility and is inexpensive (*12*).

An AEI Model IM-20 ion microprobe was used to obtain elemental depth profiles. Basic features of the instrumentation have been described previously (*13*). A 25-keV negative oxygen primary beam of 40 nA and 20-μm diameter was rastered rapidly over an area of 100 μm by 100 μm. The rastering procedure was important primarily because it enabled fairly uniform current densities to be maintained over the entire area of the particle being analyzed. Mass spectrometer resolving powers used ranged from 250 to 1800 (10% valley definition) as required to resolve molecular ion interferences. Depth profiles were acquired by two methods: (1) continuously monitoring the positive secondary ion intensity of one element vs. time using electrical detection, and (2) use of photographic detection of the positive secondary ions as dispersed by the double-focusing Mattuch–Herzog analyzer. Results reported herein were obtained only by electrical detection since the use of photographic detection was limited by a lack of sensitivity.

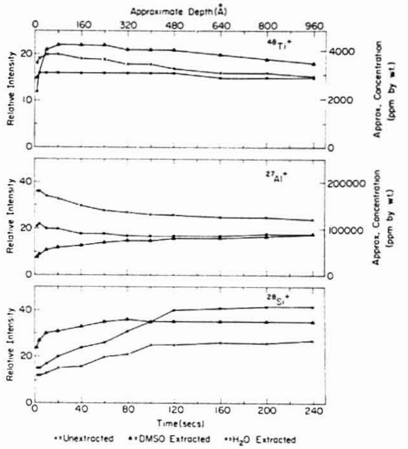

Figure 1. Ion microprobe depth profiles of the Group A elements (Ti, Al, Si) obtained for unleached and leached fly ash samples. All secondary ion intensities were normalized to Si ($^{28}Si^+$ or $^{30}Si^+$) measured at a depth of ~1000 Å

In order to convert sputtering time to depth, sputtering rates for SiO_2 were measured under identical primary ion beam conditions as those used for the analysis of fly ash. The time required to sputter a 3000 Å SiO_2 layer on Si was determined by monitoring the Si intensity and corresponded to a sputtering rate of 4 Å (±0.5 Å) per second.

Elemental depth profiles were also obtained using a Physical Electronics Industries Model 545 Scanning Auger Microprobe. The indium foil containing the imbedded particles was mounted on the standard carrousel at 30° grazing incidence to a 5-keV, 50-μm primary electron beam. Elemental depth profiles were obtained by recording entire Auger spectra after incremental periods of sputtering with 2-keV Ar^+. Sputtering rate calibrations were achieved in an analagous manner to those for the ion microprobe depth profiles.

RESULTS AND DISCUSSION

Ion Microprobe Analysis. On the basis of its inherently high sensitivity, good depth resolution, and ability to perform microanalysis of samples (including those which are insulators), ion microprobe mass spectrometry was a priori one of the most useful surface analytical techniques for the in-depth characterization of airborne particles. Specific analytical concerns or objectives involved in the application of the ion microprobe to obtain elemental depth profiles of individual fly ash particles were the following: (1) to establish which elements of environmental interest could be characterized, (2) to analyze particles before and after solvent leaching to reduce concerns about possible sputtering artifacts, (3) to use solvent leaching and bulk analysis to substantiate and to quantitate the ion microprobe results, i.e., to estimate surface region elemental concentrations, and (4) to examine general constraints on the analysis such as limits to depth resolution or possible effects due to charging. Experimental results with regard to the above objectives will be summarized in the following paragraphs.

Ion microprobe depth profiles for 15 elements in fly ash are shown in Figures 1–6. These elements include all of the major and minor elements in fly ash (greater than about 1% by weight) as well as six trace elements with concentrations below 1000 ppm as determined by bulk analysis. Other elements

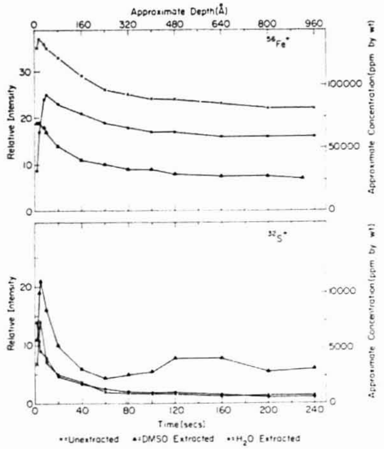

Figure 2. Ion microprobe depth profiles of the Group B elements (Fe, S) obtained for unleached and leached fly ash samples. All secondary ion intensities were normalized to Si ($^{28}Si^+$ or $^{30}Si^+$) measured at a depth of ~1000 Å

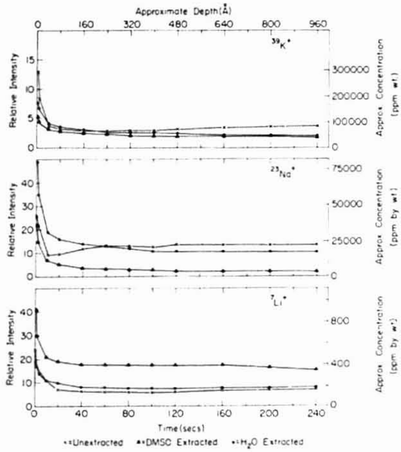

Figure 3. Ion microprobe depth profiles of the Group B elements (K, Na, Li) obtained for unleached and leached fly ash samples. All secondary ion intensities were normalized to Si ($^{28}Si^+$ or $^{30}Si^+$) measured at a depth of ~1000 Å

of possible surface predominance and toxicity (*3, 14*) which could not be characterized were Co, As, Ni, Zn, Se, Cd, Hg, and Sb. These elements were present at low bulk concentrations ranging from approximately 10–1000 ppm by weight. Secondary ion mass spectral interferences from species such as molecular ions, hydrocarbons, and isotopes of major elements were common in the fly ash mass spectra and generally required the use of high mass resolution (*13, 15*) with an accompanying loss in sensitivity. The above eight elements were not of sufficient intensity to be characterized. Elemental identifications were made only when multi-isotopic species exhibited correct isotope ratios or when monoisotopic species could be mass-resolved from interferences and identified by mass difference measurements. Most of the elements listed above also have intrinsically poor detection limits since they have relatively low positive secondary ion yields (*16*).

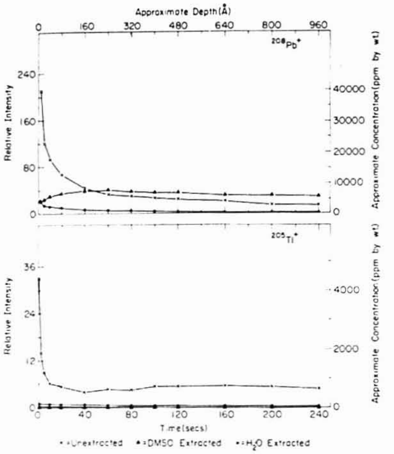

Figure 4. Ion microprobe depth profiles of the Group C elements (Pb, Tl) obtained for unleached and leached fly ash samples. All secondary ion intensities were normalized to Si ($^{28}Si^+$ or $^{30}Si^+$) measured at a depth of ~1000 Å

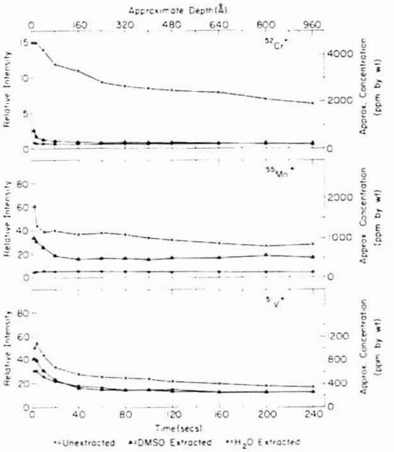

Figure 5. Ion microprobe depth profiles of the Group C elements (Cr, Mn, V) obtained for unleached and leached fly ash samples. All secondary ion intensities were normalized to Si ($^{28}Si^+$ or $^{30}Si^+$) measured at a depth of ~1000 Å

The major potential constraints on the depth resolution of the ion microprobe elemental depth profiles of fly ash (Figures 1–6) are variations in the sputtering rate over the area of the particle being analyzed (*16*), crater edge effects (*17, 18*), escape depths of secondary ions (*19*), and cascade mixing of subsurface layers resulting from penetration of the primary ion beam into the sample (*20, 21*). For purposes of sputtering rate calibration, an SiO_2 standard was used to approximate the composition of the glassy aluminosilicate fly ash matrix. The major limitation in applying this calibrated rate to fly ash was

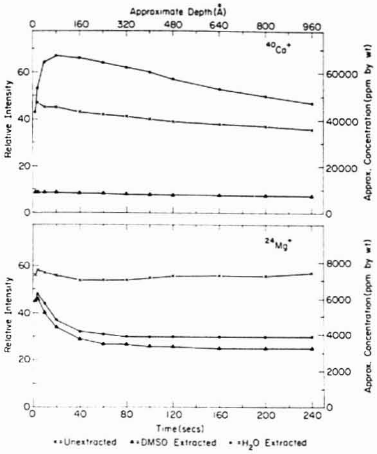

Figure 6. Ion microprobe depth profiles of the Group D elements (Ca, Mg) obtained for unleached and leached fly ash samples. All secondary ion intensities were normalized to Si ($^{28}Si+$ or $^{30}Si^+$) measured at a depth of ~1000 Å

that the irregular surface of a fly ash particle may cause substantial variations in sputtering rate over the region sampled. That is, microtopographical features approaching grazing incidence with respect to the primary beam (e.g., the edges of a particle) will sputter faster (up to about a factor of 3) than those at normal incidence (*16*). Therefore, the calibrated sputtering rate was considered to be a minimum rate for fly ash, with secondary ions actually being produced from a range of depths approximately 1–3 times greater than the calibrated depth. Thus, the remaining factors mentioned above affecting depth resolution are considered insignificant relative to the effects of sputtering rate variation and would in any case tend to diminish and broaden, rather than enhance, surface peaks.

One of the most important analytical requirements was to establish that the observed elemental surface predominance was not the consequence of sputtering or analysis artifacts. Conventional methods to assure that variations in secondary ion intensities reflect relative differences in element concentrations are to (1) perform the profile under conditions which ensure a high oxygen concentration in the sample surface, (2) reference the profiled element intensity to a uniformly distributed element, and (3) apply quantitation procedures to the data (*20*). All of these methods have been utilized and will be discussed as follows.

First a high oxygen concentration in the sample surface was ensured by using an oxygen primary beam. Specifically, the purpose of using a negative oxygen primary beam was twofold: (1) oxygen promotes the production of stable, high intensity yields of positive secondary ions (*22*) and (2) a negative primary beam has been shown to maintain charge neutrality on insulating surfaces (*23*). The absence of large variations in the secondary ion intensities of matrix elements (Si, Al, Ti in Figure 1) beyond the initial rise in the first 100 Å did indicate that secondary ion yields are relatively constant over the greater part of the depth profile.

All secondary ion intensities (Figures 1–6) were referenced to Si in order to permit a direct comparison of depth profiles for different elements and also for comparison of the same element in the leached vs. the unleached sample. Use of Si as the internal standard allowed compensation for variations in the amount of sample within the rastered area and for variable ion extraction efficiency. Silicon was felt to be the most appropriate element since (1) it was homogenously distributed in all particles at depths greater than several hundred angstroms, (2) the Si profiles showed minor variations for different particles in the same sample, and (3) Si was negligibly leached by either DMSO or H_2O. The use of Si as an internal standard was also necessary in the quantitation procedures to be discussed.

Table I. Leaching of Fly Ash

Element	Concentration (ppm by wt) in unleached particles	% Leached (wt%)	
		DMSO	H_2O
Ti	4 700	1.5	0.5
Al[a]	>6 600		
Si	120 000	0.1	0.3
Fe	92 000	0.7	5.8
S	7 100	27	36
K	39 000	0.2	6.0
Na[a]	>5 300	<5.2	
Li	200	17	14
Pb	620	3.4	0.4
Tl	30	25	11
Cr	380	2.4	4.5
Mn	310	7.1	35
V	380	1.5	3.9
Ca[a]	>12 000	<1.3	<5.8
Mg	12 000	0.6	2.7

[a] Could not be quantitated because of interferences, or analytical lines were too intense to fall within the working range for the internal standards.

Quantitation of the Ion Microprobe Results—Use of Solvent Leaching and Bulk Analysis. In order to quantitate the ion microprobe results (i.e., determine surface region elemental concentrations), it was first necessary to obtain additional experimental confirmation that elemental surface predominance was not the consequence of analysis artifacts. This was accomplished by the use of the following: (1) complementary surface analytical techniques such as AES (to be discussed later), and (2) solvent leaching of the fly ash particles.

Semiquantitative values for bulk elemental leachabilities were obtained by ratioing the total mass of an element in a solution leachate to its total mass in the original fly ash sample as was determined using spark source mass spectrometry (SSMS). Analytical precisions for the solution or ash samples were about ±20%. The percent leached values (Table I) were accurate to within about a factor of two of the true value. This can be attributed to the small variations in the sensitivity of the same element in different matrices (*24*) (i.e., the sensitivity of an element in the leachate solution doped onto graphite differs somewhat from its sensitivity in the fly ash–graphite mixtures).

High elemental leachability should in part reflect high surface accessibility. Results indicated that the extent of leachability (Table I) did correlate with the extent of surface predominance (depth profiles of unextracted particles in Figures 1–6). Specifically, the elements which were not surface predominant (e.g., Si, Mg, Ca, Ti) generally had the lowest leachabilities.

Of the instrumental methods presented in this paper, the ion microprobe was the only one that detected trace level elements including Pb, Tl, Cr, Mn, and V. Solvent leaching was used to substantiate the surface predominance of these elements by comparison of their depth profiles before and after solvent leaching (Figures 4 and 5). Normalized secondary ion intensities for a given element were reproducible to about a factor of two for different particles in either the leached or unleached samples. Following leaching, secondary ion intensities of Pb, Tl, Cr, and Mn near the surface were reduced by more than a factor of four (Figures 4 and 5). Thus, the depletions in the surface region concentrations of these elements following leaching were indeed significant.

The factor of two irreproducibility in the depth profiles was largely the result of variations in the chemical composition of individual particles. Because of this imprecision, solvent leaching cannot be considered to have a significant effect on the depth profiles of the other elements (Figures 1–3, 6). As was anticipated, depth profiles of elements (Al, Si, Ti, Ca, Mg) with negligible surface peaks and only low to moderate leachability generally showed no significant change following leaching (Figures 1 and 6). However, the highly leachable and surface predominant elements (Na, K, Li, S, Fe) surprisingly showed no significant reduction in peak secondary ion intensity after leaching (Figures 2 and 3). These elements (with the exception of Li and S) are present at high concentrations in less soluble forms as part of the bulk matrix composition of fly ash. Such high "interior" concentrations may obscure the effect of the surface leaching of Fe, K, and Na on the shape of the depth profiles within the limits of reproducibility for different particles. These elements also may be present to some extent in insoluble species near the particle surface. Thus, dissolution of such elements may be limited in part by solubility product considerations. Secondary ion intensities observed for the alkali metals in the unleached and leached particles also may be influenced by alkali ion migration to the surface sometimes observed for insulators during negative ion bombardment (*21*, *25*).

With regard to methods for quantitation of surface region concentrations, it is well known that secondary ion yields are highly variable from element to element and exhibit strong matrix effects. For fly ash, the surface elemental composition apparently is very different from the interior and standards suitable for surface analysis are not available. To obtain the estimates of elemental concentrations shown in Figures 1–6, the essentially constant secondary ion intensities observed for all elements at depths greater than about 500 to 1000 Å were taken to approximate bulk concentration levels. As summarized below, this assumption was verified using calculated relative elemental sensitivity factors, the bulk concentration of Si in fly ash as an internal standard, and the results of bulk analysis using SSMS.

Our quantitation procedure was based upon the empirical observation that a simplified form of the Saha–Eggert equation can be used in reducing secondary ion yields to elemental concentrations (*26*):

$$\frac{N_i^+}{N_i^0} = \frac{AT^{3/2}w}{N_e}[\exp^{-I_i/kT}] \tag{2}$$

where N_i^+ and N_i^0 are the number densities of singly charged and neutral atoms of element i, A is a numerical constant, w is the ratio of ground state statistical weights of the ion and neutral, I_i is the first ionization potential and N_e (electron density) and T (temperature) are fitting parameters. An empirical relationship between the parameters N_e and T in the Saha–Eggert equation has also been established giving an equation with only one dependent variable (T) (*26*). In the absence of several internal standards for the fly ash samples, sets of relative elemental sensitivity factors were calculated using the one-parameter equation for various values of the fitting parameter T. Relative atomic concentrations (C_i^{rel}) were then obtained from relative sensitivity factors and ion count rates corrected for isotopic abundance (I_i^+) according to the relation:

$$C_i^{\text{rel}} = I_i^+ \left[1 + \left(\frac{N_i^+}{N_i^0}\right)^{-1}\right] \tag{3}$$

Absolute concentration values were established by assuming that the Si intensity measured at the end of each elemental profile resulted from 12% by weight Si (SSMS bulk value).

The bulk analysis values were used to guide the choice of the best value of T at which to calculate relative sensitivity factors as follows. All elements exhibited nearly constant secondary ion intensities at depths greater than 500 Å to 1000 Å. In addition, the region of surface predominance can be shown to have a negligible contribution to the bulk concentration determined by SSMS for the large particles studied. Therefore, at a depth of 1000 Å, where comparisons to Si were made, the concentrations of surface predominant elements should approach their bulk analysis values. For the ten elements for which complete SSMS data were available (Pb, Tl, Cr, Mn, V, K, Li, Fe, Ti, Mg), a value of T of 12 000 K satisfied these conditions best. In fact, for the fitting parameter chosen, all ten elements for all samples at the 1000-Å depth were within approximately a factor of 3 of the SSMS concentration. The only exceptions were Pb, Tl, and Cr in the unleached sample for which elemental concentrations were more than 5 times above the bulk value. By comparison of the secondary ion intensity at 1000-Å depth for the unleached sample to the maximum secondary ion intensity observed for the leached sample, it is apparent that sputtering to 1000 Å did not completely remove the surface predominant region for the elements Tl and Cr.

An alternative approach to the quantitation of surface region concentrations was to ratio the mass of a given element leached from the particles to the total mass removed from the particles during leaching. This procedure was deemed unsatisfactory for the following reasons: (1) it integrates the elemental concentration over the entire surface region that is leached, and (2) it is not known how uniformly, or to precisely what depth, the particles are leached.

Auger Electron Spectrometry. The application of Auger electron spectrometry (AES) for in-depth characterization was of interest since Auger depth resolutions are roughly comparable to those obtainable with the ion microprobe and microfocusing of the primary electron beam also permits the analysis of individual particles. Unfortunately, the application of AES was severely limited by electron beam charging effects (*27*) and the inability to detect elements at concentrations less than about 0.1–1% atomic in the analytical volume.

The charging problem was the result of the insulating nature of fly ash. Charging effects are normally minimized by use of grazing or glancing incidence to increase secondary electron emission coefficients. However, for irregular surfaces such as those of fly ash particles, grazing incidence cannot be readily maintained over the entire area being analyzed. The resultant charging caused occasional loss of particles during analysis, instabilities and/or shifts in the positions of Auger peaks (especially those having energies below a few hundred eV), and shifts in the position of the electron beam.

Because of the basic limitations discussed, Auger electron spectrometry was used only to obtain qualitative elemental depth profiles of Al, Ca, Fe, K, Na, S, and Si contained in fly ash particles. For unleached particles, Auger depth profiles showed agreement with the ion microprobe results in that only K, Na, and S exhibited major surface enhancement. Examples of Auger elemental depth profiles are shown in Figure 7. The qualitative agreement between the Auger and ion microprobe data obtained using different sputtering conditions offers additional evidence that both techniques yield depth profiles which reflect the actual elemental composition of the surface region.

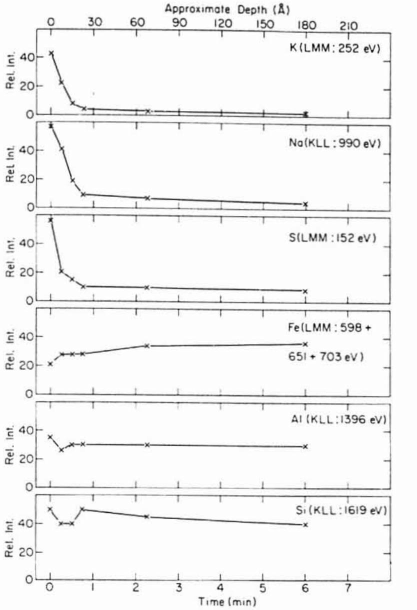

Figure 7. Examples of AES elemental depth profiles for unleached fly ash

The solvent leaching experiments were of minor value in substantiating the Auger results for two reasons: (1) the highly leachable, surface predominant trace elements could not be detected and (2) the leached particles were more susceptible to charging. No pronounced changes in the Auger depth profiles were observed following leaching with the exception of Na and K. The stronger surface enhancement shown by Na and K following leaching may have resulted from charge-induced migration of alkalies to the particle surface (*25*). Leached particles were generally observed to be more susceptible to charging as the consequence of the apparent removal of a more conducting surface layer by solvent leaching.

Despite the limitations discussed, scanning Auger microscopy does exhibit several advantages relative to the ion microprobe for particle characterization: (1) The initial surface spectrum is obtained without sputtering and thus is not subject to the effects of sputtering artifacts. (2) Multielement depth profiles of the same particle are more readily obtained (the IM20 ion microprobe does not have rapid magnetic peak switching or multiple electrical detection capabilities). (3) Spectral interferences may be less severe for a few elements. For example, sulfur was routinely determined by Auger, but the ion microprobe mass spectrometric analysis required high mass resolution.

Other Techniques—Scanning Electron Microscopy, Electron Spectroscopy for Chemical Analysis. The major disadvantage of scanning electron microscope or electron microprobe methods for in-depth characterization is the lack of depth resolution, i.e., x-ray escape depths are on the order of a micron relative to the 10–50 Å analytical escape depths for the ion microprobe or Auger techniques.

Qualitative differences between surface and interior composition can be discerned, however, by comparison of x-ray spectra before and after the removal of material in the surface region by ion sputtering (*1, 28, 29*). X-ray intensities can also be measured from the sputtered and unsputtered sides of the same particle (*1, 28*). Experimental results using Ar^+ sputtering of fly ash were previously reported using scanning electron microscopy–energy dispersive x-ray spectrometry (SEM/EDS) (*1, 28*). Results indicated enhanced surface region concentrations of Pb, Zn, K, Na, P, and S with no detectable surface predominance of Ca, Si, Al, and Fe. Thus, the SEM/EDS technique is significant in providing a qualitative corroboration of the results obtained with the true surface microanalytical techniques for the mutually detectable elements.

Other possible approaches to the surface characterization of particles using the electron microprobe include the following: (1) varying the primary electron beam energy to produce a variation in the analysis depth (*30*) or (2) ratioing x-ray intensities of elements to matrix elements as a function of particle size (*31*). Both methods suffer from the poor depth resolutions obtainable using electron probe techniques. To make use of the first technique above also requires a very stable electron beam current and extensive x-ray quantitation methods including corrections for particle shape (*30, 32*). Elemental detection limits also increase at lower electron beam energies, thus limiting the extent to which beam energies may be reduced. The second approach assumes that the smaller the particle, the greater is the relative surface area being sampled by the electron beam (*31*). However, this approach oversimplifies the mechanisms of x-ray production and really requires detailed corrections for the effects of particle shape on the emission of x-rays.

Electron spectroscopy for chemical analysis (ESCA) is another technique used for the surface characterization of environmental particles (*33, 34*). ESCA not only has depth resolution and detection limits generally comparable to AES, but has advantages over AES for surface characterization in that (1) chemical information is more available since ESCA chemical shifts are usually more readily related to oxidation states (*35*) and (2) charging of insulating particles is minimized since x-rays rather than electrons serve as the source of ionization. However, ESCA is not favored over AES for in-depth characterization because (1) chemical information is potentially lost since destructive ion sputtering may alter the forms of the elements present (*35*) and (2) individual particles cannot be depth profiled since ESCA microanalysis is not yet feasible. Thus, heterogeneity and variations in sputtering rate within the field of particles being analyzed are major difficulties in obtaining meaningful ESCA depth profiles.

Interpretation of Surface Chemistry. It is evident that the combination of solvent leaching with bulk multielemental analysis and with surface microanalysis provides the information necessary to construct a composite picture of the physicochemical characteristics of the surface regions of fly ash particles. Based upon the leachability, the extent of surface predominance, and the effect of leaching on the extent of surface predominance, the elements studied can be categorized into four general groups (Table II).

The Group A elements (Si and Al) are major constituents of the glassy fly ash particle matrix (*36*). The refractory nature and low solubility expected for Al and Si coalesced as oxides in the fly ash matrix account for the lack of surface predominance and low leachabilities observed for these elements. Similar analytical results for Ti and its close association with complex silicates in the original coal (*37*) indicate that Ti is also incorporated as a minor component in the fused fly ash matrix.

The Group D elements (Ca, Mg) exhibit behavior similar to the Group A elements. The alkaline earths are often

Table II. Summary of Analytical Results-Surface Characterization of Fly Ash Particles

Group	Elements	Significant surface peak observed?	Effect of leaching on concentration in the immediate surface region	Leachability
A	Al, Ti, Si	no	insignificant	low
B	S, Fe, K, Na, Li	yes	insignificant	moderate to high
C	Pb, Tl, Mn, Cr, V	yes	depletions observed following leaching	moderate to high
D	Ca, Mg	no	generally not significant	moderate

present largely as carbonates in coal and subsequently decompose to form refractory oxides during combustion (*38*). The refractory nature of the alkaline earth oxides apparently explains their lack of surface predominance in fly ash. The oxides are potentially quite soluble, as are alkaline earth sulfates which form by reaction with sulfur oxides in the flue gas (*37, 39, 40*).

The surface predominance observed for the Group B and C elements (Table II) apparently results from the volatilization of these species in the high temperature combustion zone and their subsequent deposition on the surfaces of refractory particles as the temperature falls inside the stack (*1, 3*). It has been established that certain trace metals, for example Hg and Se, are so volatile that a large percentage of their total emission from coal-burning power plants is in the vapor phase (*4, 41*). Enrichments of elemental concentrations observed in fly ash relative to the residual slag or bottom ash are in excellent agreement with the results of the depth profiles. Specifically, elements which were not surface predominant (Groups A and D) have shown negligible concentration enhancements in fly ash relative to the slag (*41*). However, elements which exhibited significant surface predominance in this study (Groups B and C) also have been observed to show minor to major enrichments in fly ash relative to the slag (*41*). In summary, the results of the ion microprobe and AES depth profiles, the enrichment of elements in fly ash relative to the slag (*41*), and the inverse dependence of bulk elemental concentrations on particle size (*3*) strongly suggest that a volatilization–condensation process occurs for the Group B and C elements.

Environmental Significance. Potentially toxic elements including Pb, Tl, Cr, and Mn have been shown to have surface concentrations much higher than hitherto supposed on the basis of conventional bulk analytical data. For example, Pb and Tl were present at concentrations of only 620 and 30 ppm on the basis of bulk analysis (Table I), but reached respective concentrations of 4% and 4500 ppm near the particle surfaces (Figure 4). In addition, the surface predominant region for such elements was highly leachable. The region of surface predominance is thus very likely to be accessible to the environment either by washout processes in the atmosphere or ground waters, or by solubilization in lung and digestive fluids of higher organisms. Undoubtedly, the high surface concentrations and substantial solubilities of many elements must be considered in assessing the overall environmental impact of fly ash emitted from coal-burning power plants. They must also be recognized in the design of bioassay or inhalation studies using simulated particles.

Knowledge of the chemical nature of fly ash surfaces is also of potential use in suggesting or understanding control procedures used to minimize emissions via physicochemical modification of the particles (*7, 42*). Previous studies have indicated that the higher the bulk concentration of the alkalies, Fe, and S in fly ash, the greater its electrical conductivity and efficiency of collection by electrostatic precipitation (*7, 43*). Our results indicate that higher concentrations of these elements may increase conductivity in part by promoting the formation of condensed alkali-iron sulfates which may render the points of contact between particles more conducting.

Results of this study also suggest the possibility that elemental surface predominance may be a general phenomenon in particles derived from high temperature processes for which volatilization and subsequent condensation of elements is likely to occur. Preliminary studies have already established the surface predominance of Br, Cl, S, P, Pb, Tl, K, and Na in automobile exhaust particles and of Mn and Zn in incinerator fly ash (*2*).

LITERATURE CITED

(1) R. W. Linton, A. Loh, D. F. S. Natusch, C. A. Evans, Jr., and P. Williams, *Science*, **191**, 852 (1976).
(2) R. W. Linton, P. Williams, C. A. Evans, Jr., and D. F. S. Natusch, unpublished results, 1976.
(3) R. L. Davison, D. F. S. Natusch, J. R. Wallace, and C. A. Evans, Jr., *Environ. Sci. Technol.*, **8**, 1107 (1974).
(4) J. W. Kaakinen, R. M. Jorden, M. H. Lawasani, and R. E. West, *Environ. Sci. Technol.*, **9**, 862 (1975).
(5) T. Novakov, S. G. Chang, and A. B. Harker, *Science*, **186**, 259 (1974).
(6) H. S. Judeikis and S. Siegel, *Atmos. Environ.*, **7**, 619 (1973).
(7) W. Strauss, "Industrial Gas Cleaning", 2nd ed., Pergamon Press, Elmsford, N.Y., 1975.
(8) S. S. Butcher and R. J. Charlson, "An Introduction to Air Chemistry", Academic Press, New York, N.Y., 1972.
(9) D. F. S. Natusch and J. R. Wallace, *Science*, **186**, 695 (1974).
(10) D. F. S. Natusch and H. Matusiewicz, unpublished results, 1976.
(11) H. Farrar, in "Trace Analysis by Mass Spectrometry", A. J. Ahearn, Ed., Academic Press, New York, N.Y., 1972.
(12) G. Theriault, T. Barry, and M. Thomas, *Anal. Chem.*, **47**, 1492 (1975).
(13) D. K. Bakale, B. N. Colby, and C. A. Evans, Jr., *Anal. Chem.*, **47**, 1532 (1975).
(14) D. F. S. Natusch, J. R. Wallace, and C. A. Evans, Jr., *Science*, **183**, 202 (1974).
(15) P. Williams and C. A. Evans, Jr., in "Secondary Ion Mass Spectrometry", *Natl. Bur. Stand.* (*U.S.*), *Spec. Publ.*, **427**, 63–68 (1975).
(16) P. D. Townsend, J. C. Kelly, and N. E. W. Hartley, "Ion Implantation, Sputtering and Their Applications", Academic Press, New York, N.Y., 1976, pp 125, 233.
(17) C. A. Evans, Jr., *Anal. Chem.*, **44**, (13), 67A (1972).
(18) P. Williams and C. A. Evans, Jr., "A Simple Electronic Aperture for Rastered-Beam Depth Profiles", *Int. J. Mass Spectrom. Ion Phys.*, in press, 1976.
(19) J. A. McHugh, ref. 15, pp 179–189.
(20) J. M. Morabito, ref. 15, pp 191–221.
(21) J. W. Coburn, *J. Vac. Sci. Technol.*, **13**, 1037 (1976).
(22) J. F. Lovering, ref. 15, pp 135–178.
(23) C. A. Andersen, H. J. Roden, and C. F. Robinson, *J. Appl. Phys.*, **40**, 3419 (1969).
(24) A. J. Ahearn, in "Trace Characterization-Chemical and Physical", *Natl. Bur. Stand.* (*U.S.*), *Monogr.* **100**, 347–376 (1967).
(25) D. V. McCaughan and R. A. Kushner, in "Characterization of Solid Surfaces", P. F. Kane and G. B. Larrabee, Ed., Plenum Press, New York, N.Y., 1974, pp 627–640.
(26) D. S. Simons, J. E. Baker, and C. A. Evans, Jr., *Anal. Chem.*, **48**, 1341 (1976).
(27) C. C. Chang, ref. 25, pp 509–576.
(28) A. Loh, Ph.D. Thesis, University of Illinois, Urbana, Ill., 1975.
(29) L. D. Hulett, Progress Report—Oak Ridge National Laboratories, Oak Ridge, Tenn., 1973.
(30) J. T. Armstrong, and P. R. Buseck, Abstracts of the First Chemical Congress of the North American Continent, Envir. Paper 48, 1975.
(31) R. F. Peuschel, C. C. Van Valin, and F. P. Parungo, *Geophys., Res. Lett.*, **1**, 51 (1974).
(32) J. T. Armstrong and P. R. Buseck, *Anal. Chem.*, **47**, 2178 (1975).
(33) N. L. Craig, A. B. Harker, and T. Novakov, *Atmos. Environ.*, **8**, 15 (1974).
(34) G. E. Gordon, "Atmospheric Impact of Major Sources and Consumers of Energy", NSF-RANN Progress Report, University of Maryland, College Park, Md., Oct. 1974–Aug. 1975.
(35) C. A. Evans, Jr., *Anal. Chem.*, **47**, 818A (1975).
(36) D. F. S. Natusch, C. F. Bauer, H. Matusiewicz, J. Baker, C. A. Evans, Jr., A. Loh, R. W. Linton, and P. K. Hopke, Proceedings of International Conference on Heavy Metals in the Environment, Toronto, Oct. 1975.
(37) R. R. Ruch, H. J. Gluskoter, and N. F. Shimp, Illinois State Geological Survey Report 72, Urbana, Ill., August 1974.

(38) W. T. Reid, "External Corrosion and Deposits", Elsevier, New York, N.Y., 1971.
(39) A. H. Miguel, Ph.D. Thesis, University of Illinois, Urbana, Ill., 1976.
(40) G. L. Fisher, D. P. Y. Chang, and M. Brummer, *Science*, **192**, 553 (1976).
(41) D. H. Klein, A. W. Andren, J. A. Carter, J. F. Emergy, C. Feldman, W. Fulkerson, W. S. Lyon, J. C. Ogle, Y. Talmi, R. I. Van Hook, and N. Bolton, *Environ. Sci. Technol.*, **9**, 973 (1975).
(42) P. Ditl and R. W. Coughlin, *A.I.Ch.E. J.*, **22**, 730 (1976).
(43) R. E. Bickelhaupt, *Environ. Sci. Technol.*, **9**, 336 (1975).

RECEIVED for review January 12, 1977. Accepted May 31, 1977. This research was supported in part by the National Science Foundation Grants DMR-76-01058, CHE-74-05745, and ERT-74-24276.

X-ray Photoelectron Spectroscopic Studies of Iron Oxides

N. S. McIntyre* and **D. G. Zetaruk**

Analytical Science Branch, Whiteshell Nuclear Research Establishment, Pinawa, Manitoba, Canada

Core line x-ray photoelectron spectra are reported for the iron compounds αFe_2O_3, γFe_2O_3, $\alpha FeOOH$, $NiFe_2O_4$, $CoFe_2O_4$, Fe_3O_4, and FeO. Such XP spectra are of particular value in characterizing surface films containing iron corrosion products. For the oxides and hydroxides FeOOH, FeO and Fe_3O_4, the observed chemical shift is sufficiently large to permit these species to be uniquely distinguished from other iron oxides. In Fe_3O_4, both ferrous and ferric oxidation states are observed and their relative concentrations can be determined using spectral line fitting procedures. The oxides αFe_2O_3, γFe_2O_3, $NiFe_2O_4$, and $CoFe_2O_4$ have almost identical core binding energies, but the multiplet splitting patterns observed in their Fe(2p) core levels are sufficiently different to permit their use for characterization. The Fe(2p) multiplet pattern observed for αFe_2O_3 agrees well with splitting previously calculated for the free Fe^{3+} ion. Valence band spectra for γFe_2O_3, αFe_2O_3, Fe_3O_4 and FeO are reported and band assignments are made. The effect of ion bombardment of iron oxide surfaces has been studied and evidence for the reduction of ferric oxides to FeO is presented.

The formation of a variety of ferrous and ferric oxides and hydroxides is possible during the aqueous corrosion of iron metal surfaces under alkaline conditions. At low temperatures (<100 °C) in high-oxygen environments, a number of forms of ferric hydroxide result, which, on further heating gradually transform to $\alpha FeOOH$ (geothite) and αFe_2O_3 (hematite) (*1*). At similar temperatures but under reducing conditions, Fe_3O_4 (magnetite) is a major corrosion product. (*1*). At high temperatures (300 °C), ion exchange occurs rapidly between Fe_3O_4 surfaces and other ions such as Ni^{2+} or Co^{2+} leading to the formation of the mixed spinels $NiFe_2O_4$ and $CoFe_2O_4$ (*2*). Electrochemical studies of magnetite oxidation show that γFe_2O_3 (maghemite) is formed by hydrolysis as a passivating layer on the Fe_3O_4 surface (*3*). In corrosion studies in this laboratory, it is of interest to identify these and other oxide species in thin films grown on iron and iron alloy surfaces. X-ray Photoelectron Spectroscopy (XPS or ESCA) is being used as a surface analytical tool to determine such chemical structures.

This paper reports a study of the XPS spectra of the simple and mixed iron oxides αFe_2O_3, γFe_2O_3, Fe_3O_4, FeO, $NiFe_2O_4$ and $CoFe_2O_4$ and the oxyhydroxide $\alpha FeOOH$. The details of core line spectra (Fe(2p), Fe(3s), Fe(3p), and O(1s)), valence band spectra, and Auger line spectra ($L_3M_{4,5}M_{4,5}$) are discussed with the particular view to identifying features which allow identification of each species in corrosion systems. In addition, the effect of ion bombardment on a number of iron oxide systems has been studied to determine the chemical effects of depth profiling in an iron oxide film.

One other comparative study of iron oxide XP spectra has been made by Allen et al. (*4*) who obtained Fe(2p) and O(1s) spectra of αFe_2O_3, Fe_3O_4, FeO, $\alpha FeOOH$, and several ferrates. They found that the Fe(2p) spectra were particularly difficult to analyze, because of a steeply rising background and broadened line widths. They attributed such broadening to multiplet splitting and shape-up phenomena. In this work, the spectra of some of these and other oxides have been obtained under higher resolution and distinct structure within the peak envelopes can be identified in most cases. The resolved structure is found generally to agree with multiplet splitting parameters calculated for free ferric and ferrous ions, but the structure of the surrounding environment also has some effect on the splitting of the Fe(2p) line. The resultant shape of the Fe(2p) line is useful for characterizing some of the ferric oxides where chemical shifts are minimal. Using both chemical shift and multiplet splitting effects, distinct spectral characteristics can be described for each oxide studied.

Several previous XPS studies have been concerned with the analysis of Fe_3O_4 (*4–9*). This inverse spinel oxide is of particular interest because it contains both ferric and ferrous ions in a 2:1 ratio and these should be distinguishable by their differing chemical shifts. Previous XPS investigations of Fe_3O_4 have shown that the core line shapes are skewed on their low binding energy side, compared to spectra of pure ferric oxides, particularly after ion bombardment of the Fe_3O_4 surface (*6*). This suggests the presence of a ferrous ion component of low binding energy under the envelope. Asami et al. (*9*) have recently attempted to isolate such a ferrous iron component by subtraction of the Fe(2p $^3/_2$) spectrum of Fe_2O_3 from that for Fe_3O_4. In this work the Fe_3O_4 spectra are analyzed by a novel process of least squares spectral line fitting in which the line shape contribution from ferric ion is restrained during the computer assisted resolution of the envelope. This method can be used to estimate Fe^{2+}/Fe^{3+} ratios on magnetite surfaces. A major problem confronting XPS investigations of Fe_3O_4, FeO, and $NiFe_2O_4$ is the tendency of these surfaces to react rapidly with oxygen to yield an overlayer of Fe_2O_3 (*10*). In this present work, spectral characterization of these oxides has been improved considerably by taking account of this during sample handling.

EXPERIMENTAL

Spectroscopic Procedure. The photoelectron spectrometer used was a McPherson ESCA-36 with a cryogenically pumped sample chamber whose operating pressure is 5×10^{-7} Pa. Calibration of the energy dispersion of the spectrometer was done using the known energy difference of 1253.6 eV between the Mg(2p) and Mg(1s) lines for evaporated magnesium metal. The instrumental work function was set to give a value of 84.00 eV for Au(4f $^7/_2$) line for metallic gold. Appropriate relativistic corrections were made to the energy values (*11*). During operation, copper metal was used as a secondary energy standard in the spectrometer. The values of Cu(2p) $^3/_2$) and Cu(3p $^3/_2$) lines used were 932.45 eV ± 0.1 and 75.10 ± 0.1 eV respectively. Al Kα exciting radiation was used, except where the higher resolution Mg Kα radiation was required for improved definition of a complex peak shape.

Surface charging was not detected on any sample except αFeOOH. This observation is based on the invariance of the background hydrocarbon C(1s) binding energy (285.0 ± 0.15 eV) as well as the reproducibility of sample binding energies to better than ±0.2 eV for at least three independently prepared specimens. The surface charging of αFeOOH was measured using the C(1s) line and ranged from 0.9–2.3 eV.

Ion bombardment of sample surfaces was carried out with a Varian ion gun. With this gun, it is possible to raster the ion beam evenly over an area 7 × 7 mm. Argon ions of 3-KeV energy were used with a flux density of 20 mA/m^2. The beam intersected the surface at a glancing angle of 50°.

Sample Preparation. All powder specimens were mounted by smearing them onto a grooved copper flat. αFe_2O_3 (hematite) was examined as a powder (Fisher Reagent) and as a thin film grown on iron metal in oxygenated water. They gave identical spectra. γFe_2O_3 (maghemite) was prepared by reaction of iron(II) sulfate and iron(III) ammonium sulfate in boiling 1 M NaOH, followed by autoclaving under oxygen in 1 M NaOH at 130 °C for 4 days. X-ray diffraction showed that the tetragonal phase of γFe_2O_3 was the only form present. The powder was crushed under argon immediately before examination to reveal surfaces not previously exposed to air. XPS spectra were identical to those for uncrushed powder showing that no decomposition product such as hematite formed on the outside surface. $CoFe_2O_4$ was obtained from Cerac Inc., Butler, Wis. and its structure was confirmed by x-ray diffraction. $NiFe_2O_4$ was made by coprecipitation of the oxalates of nickel and iron followed by heating at 600 °C for several days. Although the bulk composition was confirmed to be $NiFe_2O_4$ by x-ray diffraction, changes in the Ni(3p)/Fe(3p) intensity ratio with time showed that the surface of $NiFe_2O_4$ was air sensitive, often forming iron rich oxide phases on the surface. Samples were considered acceptable only where the corrected intensity ratio (*12*) approached that expected from stoichiometry.

High purity Fe_3O_4 was prepared in a quartz tube furnace by reacting αFe_2O_3 at 700–1000 °C under a mixture of CO and CO_2, calculated (*13*) to give stoichiometric Fe_3O_4 at that temperature. The sintered product was rapidly quenched to room temperature and immediately transferred to the spectrometer sample chamber, always under a nitrogen atmosphere. X-ray diffraction analysis showed only lines attributable to Fe_3O_4. The Fe^{2+}/Fe^{3+} concentration ratio was determined to be 0.50 ± 0.02 by redox titration of a sample immediately following its dissolution in dilute sulfuric acid. Fe_3O_4 spectra with ferrous/ferric ion concentrations lower than normal were obtained from samples prepared using iron metal as a starting material rather than Fe_2O_3 (*14*). *Ferrous oxide* (Wustite) was also prepared by reducing Fe_2O_3 at 600 °C in a CO/CO_2 mixture whose ratio was adjusted (*13*) to give $FeO_{0.95}$. This sample was also handled completely under nitrogen. $\alpha FeOOH$ (Goethite) was prepared by dehydration of gelatinous $Fe(OH)_3$, which was precipitated from a 1 M $Fe(NO_3)_3$ solution by 0.1 N NH_4OH (*15*). The precipitate was dried in a vacuum furnace for four days and was confirmed to be pure $\alpha FeO(OH)$ by x-ray diffraction.

Spectrum Analysis. To reduce distortion caused by the sharply rising backgrounds in the Fe(2p) and Fe(3p) spectra, a baseline correction function of the type suggested by Barrie and Street (*16*) was subtracted. The form of this function is shown in Figure 1(*a*). The magnitude of the correction at any point is proportional to the integrated spectra intensity on the low binding energy side of the point. Fitting of the low binding energy onset region with Gauss–Lorenzian peak shapes is found to be substantially better when using this function, instead of the more common linear approximation which overestimates the background contribution in this region.

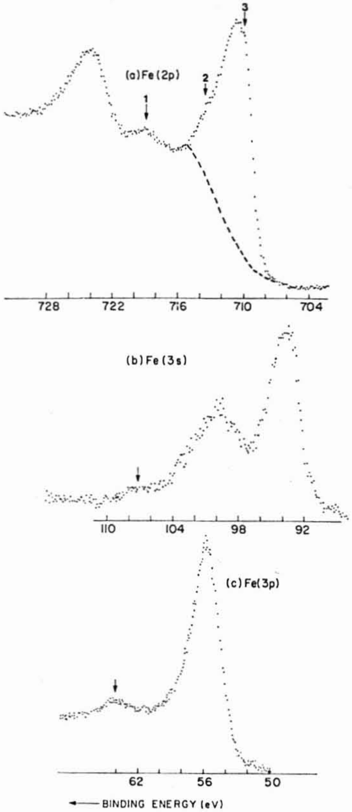

Figure 1. Major core line photoelectron spectra of αFe_2O_3. (*a*) Fe(2p) spectrum, (*b*) Fe(3s) spectrum, (*c*) Fe(3p) spectrum. The dashed line in the Fe(2p) spectrum represents the form of background function subtracted during peak fitting procedures. Arrows indicate spectral features discussed in text

The peak fitting routine used in this work has been described previously by Bancroft et al. (*17*). The bands used in fitting a peak envelope are defined according to their centroid position, half-width, shape (usually an equal combination of Gaussian and Lorenzian distributions), and intensity. These parameters are then varied to obtain a minimum error sum of squares between the values for the experimental curve and the trial combination of bands. A quantitative measure of the "goodness" of the final fit is provided. An important feature of this program is its ability to constrain certain parameters of selected bands within set limits, while allowing others to vary freely. This permits known contributions to the band envelope to be fixed, while a best fit is established for the remaining portion of the envelope.

RESULTS

Core Line Spectra. *αFe_2O_3, γFe_2O_3, and $\alpha FeOOH$.* These compounds are grouped together because of certain basic similarities in their Fe(2p) spectra which will be discussed below. The iron core line spectra of αFe_2O_3 are shown in Figure 1, while high resolution Fe(2p $^3/_2$) spectra of α and γ forms of Fe_2O_3 are compared in Figure 2. Although the main Fe(2p $^3/_2$) line is broad (FWHM ≃ 3 eV), considerable

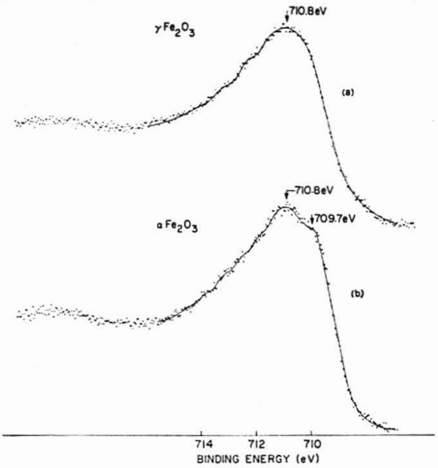

Figure 2. Detailed Fe(2p $^3/_2$) spectra of (*a*) γFe_2O_3, (*b*) αFe_2O_3

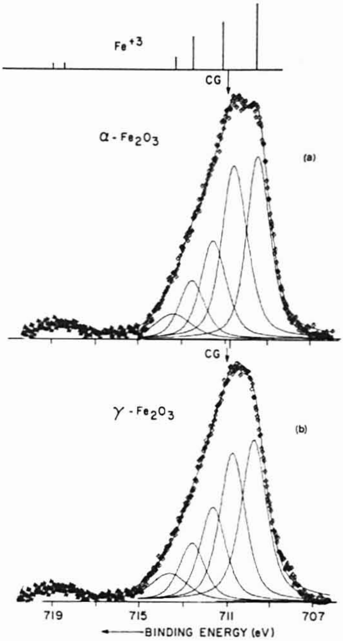

Figure 3. Spectral line fit of (*a*) αFe_2O_3, (*b*) γFe_2O_3. Calculated splitting and relative intensities for a free Fe^{3+} ion are shown by the solid bars. CG denotes peak center of gravity. The solid line drawn through the points is the sum of the individual bands in the envelope. The different point symbols indicate regions subjected to separate background subtraction procedures

structure, which is quite reproducible, is seen as part of the asymmetric peak envelope (see arrows 2 and 3 in Figure 1(*a*)). Prominent also in the αFe_2O_3 Fe(2p) spectrum is a satellite band about 8 eV above the Fe(2p $^3/_2$) line (see arrow 1 in Figure 1(*a*)). For γFe_2O_3, the shape of the main Fe(2p $^3/_2$) line is clearly narrower. The spectrum of the α form has two distinct peaks separated by ~1 eV while that for the γ form has only slightly broadened maximum. Further peak structure is found on the high binding energy side of both peaks, which are asymmetric on the high binding energy side.

The structure in the Fe(2p) spectra was fitted by least squares routine following subtraction of the background. The steep leading edge and double maximum in the αFe_2O_3 Fe(2p $^3/_2$) spectrum was found to be well fitted by two narrow (FWHM = 1.4 eV) peaks of approximately equal intensity, separated by 1.2 eV. The remainder of the envelope was fitted by a series of peaks of decreasing intensity constrained to similar width and shape (see Figure 3). Any other attempted combination of fewer peaks and greater half-width could not reproduce the structure in the envelope.

The intensity distribution of these peaks can be rationalized on the basis of multiplet splitting of the Fe(2p) core line. Gupta and Sen (GS) (*18*) have calculated the multiplet structure expected for core p levels of the free Fe^{3+} ion, taking account of electrostatic and spin–orbit interactions and using the Hartree–Fock approximation of the free ion. The model is considered appropriate for highly ionic solids. The energy–intensity distribution calculated for the Fe(2p) spectrum of Fe^{3+} is plotted in Figure 3 for comparison with the experimental distribution determined for the α and γ Fe_2O_3 spectra. The energy–intensity distributions of the experimental spectra clearly resemble that predicted for Fe(2p) multiplet splitting of the Fe^{3+} ion. The weak satellite 8 eV above the main Fe(2p $^3/_2$) line (see arrow 1 in Figure 1(*a*)) is predicted at this energy as a component of the Fe(2p $^1/_2$) line multiplet splitting by the level 2 model of GS. The major peaks fitted within the Fe(2p $^3/_2$) envelope correspond well to the predicted four-line distribution for Fe(2p $^3/_2$).

The measured splitting of the two most intense components of the αFe_2O_3 Fe(2p $^3/_2$) line is 1.2 eV, as compared with 1.6 eV calculated for Fe^{3+}. An analysis of the same Fe(2p $^3/_2$) envelope for γFe_2O_3 yields an intensity distribution almost identical to that in αFe_2O_3, but splitting is reduced by 0.2 eV resulting in the observed narrowing of the peak maximum. The mean binding energy of 711.0 ± 0.15 eV (weighted average of all components) is the same for α and γ Fe_2O_3. The only change is in the multiplet splitting distribution within each peak.

The oxyhydroxide αFeOOH has a Fe(2p) spectrum similar, in many respects, to that for Fe_2O_3 (see Figure 4(*a*)). Evidence of several components under the Fe(2p $^3/_2$) envelope is seen. The main core line is again asymmetric to the high energy side and a weak satellite is observed 8 eV above it. A least-squares fit of the envelope (see Figure 4(*b*)) yields components similar to αFe_2O_3 in energy distribution, but with a somewhat altered intensity distribution. The mean binding energy of the line (711.85 ± 0.2 eV) has shifted 0.85 ± 0.1 eV above that for Fe_2O_3 (see Table I). Metal(2p) chemical shifts of a similar magnitude and direction have been previously found between the equivalent oxides and hydroxides of copper, cobalt (*19*), zinc and chromium (*20*). A shift of 0.9 eV is sufficiently large to permit FeOOH to be distinguished from Fe_2O_3.

The Fe(3p) spectra of α and γFe_2O_3 are identical, both in terms of intensity distribution and the measured binding energy of the main peak. The Fe(3p) spectrum of αFeOOH has an intensity distribution similar to Fe_2O_3, but is chemically shifted 0.6 ± 0.2 eV to higher binding energy (see Table I). A low intensity satellite is observed 7.0 eV above the main 3p for all these compounds (see arrow 1 in Figure 1(*c*)). Neither this peak nor the shape of the main line can be explained by the Fe(3p) multiplet splitting predicted for Fe^{3+} by GS (*18*). However, electron correlation effects in the Fe(3p)

Table I. Binding Energies of Major Core Lines in the Iron Oxides[a]

Compound	Fe(2p $^3/_2$)[b]	Fe(3p $^3/_2$, $^1/_2$)[c]	Fe(3s)[c]	O(1s)[c]
Fe metal	706.9 ± 0.10	53.0 ± 0.15	90.9 ± 0.3	
FeO	709.5 ± 0.2	54.9 ± 0.3	92.5 ± 0.2	530.0 ± 0.2
Fe_3O_4 Fe^{2+}	708.3 ± 0.15	53.9 ± 0.2		530.2 ± 0.2
Fe_3O_4 Fe^{3+}	d	d	d	
$NiFe_2O_4$	710.6 ± 0.2	55.9 ± 0.2	93.5 ± 0.2	530.1 ± 0.2
$CoFe_2O_4$	710.6 ± 0.2	55.9 ± 0.2	93.5 ± 0.2	
αFe_2O_3	711.0 ± 0.15	55.7 ± 0.15	93.6 ± 0.2	529.8 ± 0.10
γFe_2O_3	711.0 ± 0.15	55.7 ± 0.15	93.6 ± 0.2	530.0 ± 0.10
αFeOOH	711.9 ± 0.2	56.6 ± 0.2	94.2 ± 0.2	530.3 ± 0.2 531.4 ± 0.2

[a] Errors quoted are one standard deviation. [b] Refers to mean binding energy taken as the weighted average of all discernible components of the line. [c] Refers to peak maximum binding energy. [d] Inferred from binding energies of $NiFe_2O_4$ and $CoFe_2O_4$ (see text).

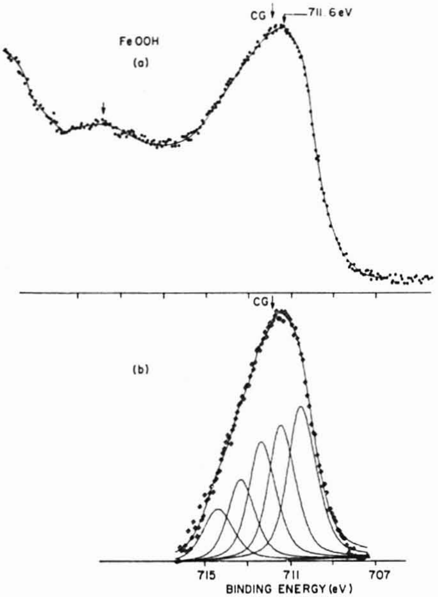

Figure 4. (*a*) Fe(2p) spectrum of αFeOOH, (*b*) Spectral line fit of Fe(2p $^3/_2$) envelope using peaks of identical width to those in Figure 3(*b*). CG denotes peak center of gravity

level are expected to be more important than in deeper core lines and would be expected to affect strongly the observed Fe(3p) intensity distribution (*21*).

The Fe(3s) peak for αFe_2O_3 (see Figure 1(*b*)) is split into two major components as expected for a high spin d^5 ferric ion (*22*). The relative intensity of the components, 6:5, is in reasonable agreement with the 7:5 ratio expected from the 3s multiplet splitting of an ion with a ^6S ground state. In addition to the two main components separated by 6.2 ± 0.2 eV, an additional weak line appears 13.2 eV above the main line (see arrow 1) which again may be due to correlation effects, similar to those seen in the Mn(3s) spectrum of MnF_2 (*23*). The 3s spectrum for γF_2O_3 shows identical splitting of the components.

The O(1s) spectra for α and γFe_2O_3 and αFeOOH are shown in Figure 5(*a*)–(*c*). The lattice oxygen binding energy in αFe_2O_3 is shifted 0.2 ± 0.05 eV lower than for γFe_2O_3 (see Table I). For relatively clean α and γFe_2O_3 surfaces (Figures 5(*a*) and (*b*)), two additional low intensity bands are observed with quite similar binding energies. These are likely due to chemisorbed hydroxyl or carbonyl species. The very low intensity of these bands in the reference spectra of α and γFe_2O_3, indicates that surface hydroxides of iron do not complicate the spectra of these oxides. Such hydroxides can form on some metal and oxide surfaces because of reaction with moisture in the air.

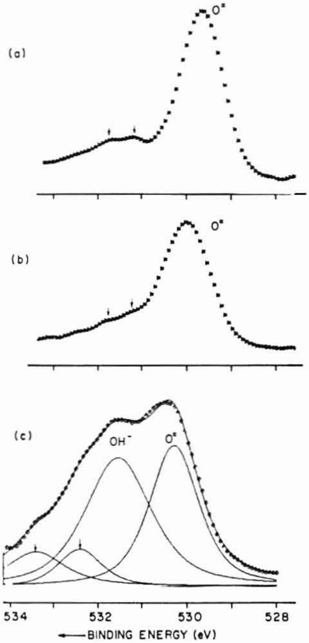

Figure 5. O(1s) spectra for (*a*) αFe_2O_3, (*b*) γFe_2O_3, (*c*) FeOOH. The ratio of hydroxide to oxide peak areas is 0.9. The presence of some adsorbed species appears likely at binding energies above 532 eV

The spectrum for αFeOOH (see Figure 5(*c*)) contains approximately equal contributions from hydroxyl and oxide oxygen, as expected from stoichiometry (0.9:1.0 ratio in Figure 5). Allen et al. (*4*) previously observed the broadened O(1s) band for FeOOH under lower resolution. The lattice oxygen (O^{2-}) O(1s) line in FeOOH is shifted significantly higher (0.5 ± 0.1 eV) than that for the structurally similar αFe_2O_3. This suggests that the proton on the hydroxyl oxygen has some

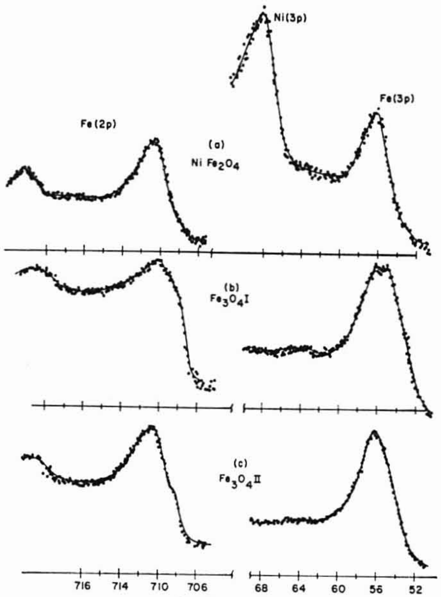

Figure 6. Fe(2p) and Fe(3p) spectra of (*a*) $NiFe_2O_4$, (*b*) pure Fe_3O_4, (*c*) partly oxidized Fe_3O_4

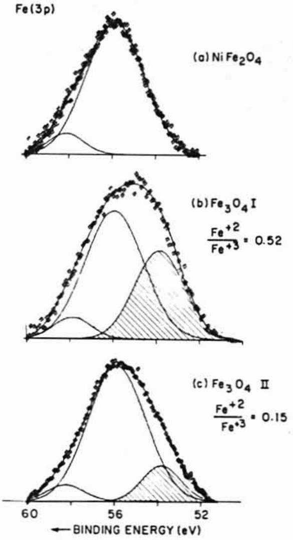

Figure 7. Spectral line fits of the Fe(3p) line for (*a*) $NiFe_2O_4$, (*b*) pure Fe_3O_4, (*c*) partly oxidized Fe_3O_4. The peak parameters obtained for the $NiFe_2O_4$ spectrum in (*a*) were constrained to these values in spectra (*b*) and (*c*). Cross-hatched areas are ascribed to the ferrous iron contribution

interaction with the O^{2-} oxygen. The binding energy for the hydroxyl oxygen is very similar to that in $Ni(OH)_2$ and $Co(OH)_2$ (*19*).

$NiFe_2O_4$, $CoFe_2O_4$ and Fe_3O_4. The Fe(2p) and Fe(3p) spectra of mixed oxide $NiFe_2O_4$ are shown in Figure 6(*a*). In the 3p spectrum the Ni(3p)/Fe(3p) intensity ratio, corrected with the appropriate photoelectron cross-sections (*12*), gives a Ni/Fe atom ratio of 1:2. The overall intensity distribution under the Fe(2p) spectral envelope differs from that for γ or αFe_2O_3. In $NiFe_2O_4$, the core line shape is almost symmetric and appears to contain none of the fine structure seen for the oxides discussed above. The satellite peak 8 eV above the Fe(2p) line, which is particularly characteristic of the Fe(2p) spectra of Fe_2O_3 and FeOOH, is not observed in the Fe(2p) spectrum of $NiFe_2O_4$. Spectra of similar shape are obtained for $CoFe_2O_4$. Using such characteristics of the Fe(2p) spectrum, it is possible to determine if iron oxide in a mixture with nickel or cobalt oxides is present mainly as a separate single oxide phase, i.e., Fe_2O_3, or if it has reacted with nickel or cobalt oxide to form a mixed inverse spinel oxide.

Table I lists binding energies of the major core line positions for $CoFe_2O_4$ and $NiFe_2O_4$. No differences in binding energy were found between these ferrites. Core line chemical shifts between the ferrites and Fe_2O_3 are also quite small and are not very useful for analytical purposes.

The Fe(2p) and Fe(3p) spectra for pure and partially oxidized Fe_3O_4 are shown in Figures 6(*b*) and 6(*c*). The iron core line spectra of Fe_3O_4 can be compared with those for $NiFe_2O_4$—an iron oxide of identical structure but containing only ferric ions. Both Fe_3O_4 and $NiFe_2O_4$ have inverse spinel structures with similar cell constants ($a_0(Fe_3O_4) = 0.8396$ nm. $a_0(NiFe_2O_4) = 0.8339$ nm). It is assumed that ferric iron binding energies are not affected by the exchange of Ni^{2+} ions in the lattice for Fe^{2+}. This is supported by the fact that the ferric iron binding energies and peak shapes are identical for the inverse spinels $CoFe_2O_4$ and $NiFe_2O_4$. From inspection, the Fe_3O_4 Fe(3p) spectra are clearly broadened on the low binding energy side compared with the $NiFe_2O_4$ spectrum. In the equivalent Fe(2p) spectra, the presence of an additional component is also apparent from the sharp shoulder around 708 eV. In both spectra the low binding energy components are ascribed to the presence of ferrous iron.

These Fe_3O_4 spectra were analyzed in detail using the least-squares peak fitting program, allowing the ferric iron contribution under each Fe_3O_4 envelope to be represented by the equivalent iron core line spectrum of $NiFe_2O_4$. In Figure 7(*a*), the Fe(3p) spectrum of $NiFe_2O_4$ was fitted using two peaks whose energy centroids, half-widths, and relative intensities define its characteristic shape. These parameters were constrained within the limits of experimental reproducibility and the entire shape was fitted under the Fe_3O_4 Fe(3p) envelope, allowing only the overall intensity of the entire ferric contribution to vary. The remaining portion of the Fe_3O_4 spectrum was attributed to the ferrous iron contribution and the peak(s) representing this contribution did not have their parameters constrained.

In Figure 7(*b*), the Fe(3p) spectrum of pure Fe_3O_4 is analyzed using this procedure. The two peaks at higher binding energy represent the ferric iron contribution derived from the shape of the Fe(3p) spectrum of $NiFe_2O_4$. The lower binding energy peak (cross-hatched in Figure 7(*b*)) represents the ferrous iron contribution under the Fe_3O_4 envelope. The resultant "best fit" from the least squares analysis indicates that the ferrous contribution can be represented by a single, symmetric, relatively narrow peak (FWHM = 2.4 eV). Its energy centroid is 2.1 eV below the center of gravity of the ferric component of the Fe_3O_4 spectrum. In the pure Fe_3O_4 Fe(3p) spectrum, the ferrous/ferric intensity ratio of the resolved components was found to be 0.52. This is in excellent

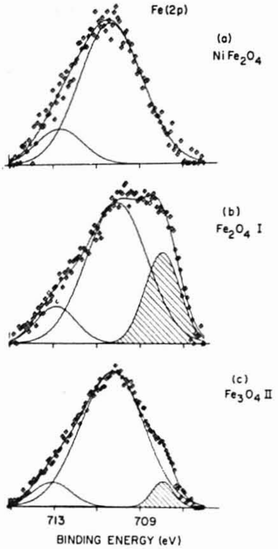

Figure 8. Spectral line fits of the Fe(2p $^3/_2$) line for (*a*) NiFe$_2$O$_4$, (*b*) pure Fe$_3$O$_4$, (*c*) partly oxidized Fe$_3$O$_4$. Cross-hatched areas are ascribed to the ferrous ion contribution

agreement with the ferrous/ferric stoichiometry of 0.50 in Fe$_3$O$_4$ and is good evidence that proper discrimination of the ferrous and ferric components in the Fe(3p) spectrum has been achieved.

The above procedure has been applied to the analysis of Fe$_3$O$_4$ surfaces containing lower concentrations of ferrous ion (Sample II). In Figure 7(*c*) the Fe(3p) spectrum from Figure 6(*c*) has been analyzed. The resulting peak representing ferrous iron had the same shape, width, and energy as in the analysis of pure Fe$_3$O$_4$, but its intensity, relative to the ferric component, was reduced to 0.15.

The Fe(2p) spectra of these Fe$_3$O$_4$ samples were analyzed using the same spectral line fitting procedure as outlined above. The Fe(2p $^3/_2$) spectrum of NiFe$_2$O$_4$ (see Figure 8(*a*)) is used as a model for the ferric iron contribution. The ferrous iron contribution which is derived from the Fe$_3$O$_4$ envelope using this procedure is a symmetric narrow peak (FWHM =1.8 eV) centered at 708.3 eV (see Figure 8(*b*)). The Fe^{2+}/Fe^{3+} peak intensity ratio is 0.32, which is low compared to the "correct" value of 0.5 obtained from Fe(3p) line analysis. This discrepancy could arise from the presence of additional weak Fe^{2+} line components on the high binding energy side of the peak. Such components would be included as part of the ferric contribution using the present method of analysis.

The Fe(2p) spectrum for Fe$_3$O$_4$ with a lower Fe^{2+} concentration is shown in Figure 8(*c*). The Fe^{2+}/Fe^{3+} ratio of 0.07 measured from this spectrum is 22% of the measured ratio for pure Fe$_3$O$_4$ in Figure 8(*b*). This corresponds well with a factor of 27% obtained from the Fe(3p) spectrum analysis. Thus, although the absolute ratio measured from the Fe(2p) spectrum analysis does not reflect the actual stoichiometry of the Fe$_3$O$_4$ surface, the change in this ratio appears to reflect changes in the ferrous/ferric ratio.

FeO. The Fe(2p) spectrum of the divalent oxide is shown in Figure 9. As in the spectra of the ferric oxides, the Fe(2p $^3/_2$) peak is quite broad and some evidence of structure is seen. A broad satellite band extends for ~6 eV above the main peak (see arrow).

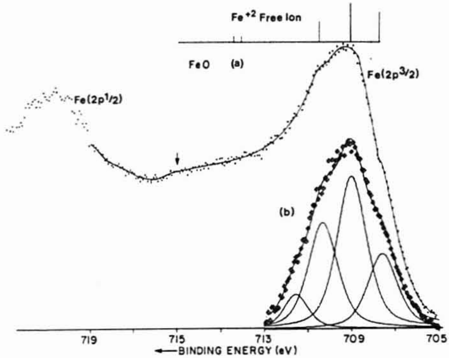

Figure 9. (*a*) Fe(2p $^3/_2$) spectrum for FeO, (*b*) spectral line fit of a portion of the FeO Fe(2p $^3/_2$) spectrum. Calculated splitting and relative intensities for the free Fe^{2+} ion are shown by the solid bars

The structure under the subtracted background Fe(2p $^3/_2$) line was fitted, using components of the same shape and width as in the analyses of the Fe$_2$O$_3$ spectra. Three major bands were required to fit the Fe(2p $^3/_2$) line. The energy splitting of these bands, and their approximate intensity distribution, were in reasonably good agreement with the multiplet splitting pattern calculated for the Fe^{2+} free ion by Gupta and Sen (*24*). This is seen from Figure 9, where the experimental line fit is compared with the calculated Fe^{2+} splitting.

Table I lists core line binding energies for FeO. The mean binding energy of the Fe(2p $^3/_2$) line (709.5 ± 0.2 eV) is shifted 1.5 ± 0.3 eV below that for Fe$_2$O$_3$ and chemical shifts of 1.0 eV and 1.1 eV are found for Fe(3p) and Fe(3s) lines, respectively. Shifts of this magnitude are clearly useful for discriminating ferrous and ferric oxides.

The ferrous iron binding energies in Fe$_3$O$_4$ are substantially lower than those for ferrous iron in FeO. Moreover, the Fe(2p) line shape for Fe^{2+} in Fe$_3$O$_4$ is considerably narrower and less complex than that in FeO. This could possibly result from different multiplet splittings of Fe^{2+} in the FeO and Fe$_3$O$_4$ structures.

Valence Band Spectra. Figure 10 shows XPS valence band spectra for FeO, αFe$_2$O$_3$, γFe$_2$O$_3$, and Fe$_3$O$_4$ samples. Valence orbitals in iron oxides are formed from Fe(3d) and O(2p) atomic orbitals. Valence states with high p character have low cross-sections when excited by x-ray energies, so that the bands observed in the present spectra provide a measure of the partial densities of localized d states. The XPS spectrum of FeO (Figure 10(*a*)) has two maxima—a strong one at 4.0 eV and a shoulder at 1.5 eV. These spectral features agree with the partial densities of Fe(3d) states in FeO derived from a frequency dependent photoelectron study made recently by Eastman and Freeouf (*25*). The peaks at 1.5 eV and 4.0 probably represent excitations from e$_g$ and t$_{2g}$ levels, respectively.

In the valence spectra of both α and γFe$_2$O$_3$ (Figures 10(*b*) and 10(*c*)), three distinct peaks are observed. Following background subtraction, these spectra were subjected to a least-squares fit using three bands of identical shape. The band positions and intensities resolved from the spectra (see Figure 11), are clearly different in the spectra for γ and αFe$_2$O$_3$. The two bands of lowest energy are assigned to excitations from 3e$_g$ and 2t$_{2g}$ orbitals, respectively. A recent SCF X$_\alpha$ calculation for αFe$_2$O$_3$ (*26*) has determined a splitting

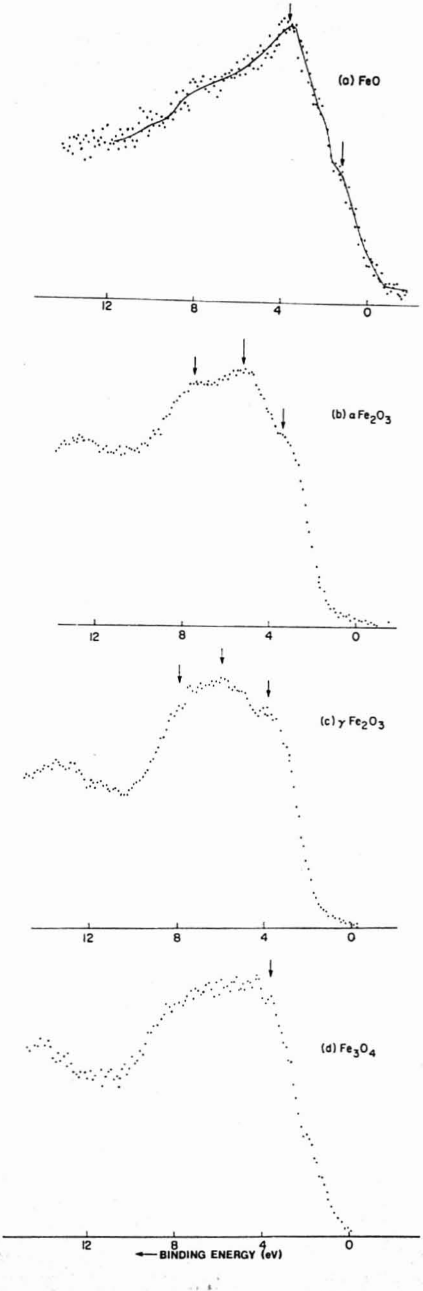

Figure 10. Valence band photoelectron spectra for (*a*) FeO, (*b*) αFe_2O_3, (*c*) γFe_2O_3, (*d*) Fe_3O_4. Exciting radiation used was Mg Kα (1253.6 eV)

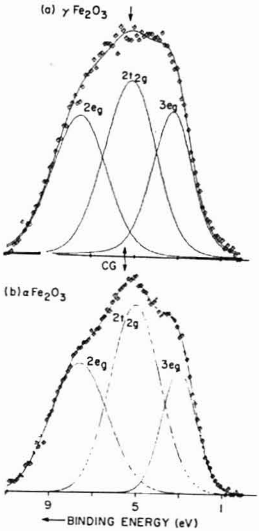

Figure 11. Spectral line fits of the valence band spectra for (*a*) γFe_2O_3, (*b*) αFe_2O_3. CG denotes envelope center of gravity

energy of 2.5 eV between the $3e_g$ and $2t_{2g}$ orbitals, in good agreement with our experimental value of 2.3 eV. The splitting found in γFe_2O_3 is also 2.3 eV, but the absolute position of both bands has shifted 0.4 eV closer to the Fermi level and the relative emission intensities of the two bands has altered considerably. The third band in the αFe_2O_3 envelope located 2.4 eV above the $2t_{2g}$ band is identified with the $2e_g$ orbital, which also has strong 3d character. In the X_α calculations (*26*), this orbital was determined to lie approximately 2.5 eV below the $2t_{2g}$ level in the energy level diagram. The center of gravity of the valence band system is 5.5 ± 0.1 eV for both γ and αFe_2O_3. This suggests that all bands result from orbitals with strong 3d character, since each band system is split about a common energy.

The valence band spectrum of pure Fe_3O_4 (Figure 10(*d*)) is too complex for detailed treatment, but it appears to contain features seen in both ferric and ferrous oxide spectra. Lower ferrous ion concentration in the Fe_3O_4 matrix results in a diminution of the peak around 4 eV.

Auger Spectra. Wagner (*27*) has shown that the Auger line chemical shifts observed for many compounds of the nontransition elements, are, in fact, larger than the equivalent photoelectron core line shifts. Changes in the Fe $M_{2,3}$ VV line shape with chemical structure have been observed by Seo et al. (*28*), using electron excited Auger spectroscopy. Analysis using this particular line is not practical in XPS, but the more intense $L_3M_{4,5}M_{4,5}$ and $L_3M_{2,3}M_{4,5}$ lines were investigated for several oxides to determine if they could provide further characterizable spectra. The $L_3M_{4,5}M_{4,5}$ lines for FeO, αFe_2O_3, γFe_2O_3, and Fe_3O_4 were quite broad (6–9 eV (FWHM)), because of the many overlapping Auger lines. Only slight alterations in the shape of the envelope were found and these were of little use for analytical purposes. No changes in the $L_3M_{2,3}M_{4,5}$ line shape were observed.

Ion Bombardment Effects. Analysis of iron oxide corrosion films by XPS frequently involves ion bombardment of the oxide, in order to obtain a concentration profile through the film. If characterization of the iron oxide within the film

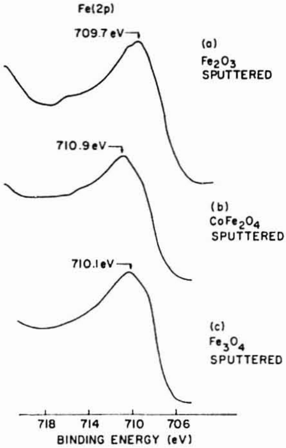

Figure 12. Fe(2p $^3/_2$) spectra of (*a*) Fe_2O_3, (*b*) $CoFe_2O_4$, (*c*) Fe_3O_4 following 2 min of bombardment with 3-KeV argon ions with a flux of 20 mA/m^2

is to be made, the effects of ion bombardment on the chemical integrity of each possible oxide species must be known. Consequently, the oxides αFe_2O_3, $NiFe_2O_4$, Fe_3O_4, and FeO were subjected to a 3-keV argon ion beam flux of 20 mA/m^2 for periods up to 10 min. This is equivalent to removal of ~40 nm of oxide film (*12*).

Bombardment of an αFe_2O_3 surface resulted in almost complete reduction to FeO during the first few minutes of ion sputtering. This can be seen from the Fe(2p) spectrum of sputtered Fe_2O_3 in Figure 12(*a*) which has the same structural features and mean binding energy as the spectrum of FeO in Figure 9.

Ion bombardment of the spinels Fe_3O_4 and $CoFe_2O_4$ also resulted in the appearance of a new low binding energy component in the Fe(2p $^3/_2$) and Fe(3p) spectra that indicates their partial conversion to ferrous oxide. This is particularly clear in the Fe(2p) spectrum of $CoFe_2O_4$ (Figure 12(*b*)), where only a single ferric component was visible before ion bombardment. The low binding energy component produced by sputtering was derived using the previously described procedure and was tentatively identified as FeO. For the more complex Fe_3O_4 spectra, (Figure 12(*c*)) the partial reduction to FeO was inferred from the spectral broadening observed and the analagous behavior of $CoFe_2O_4$. No effect of ion bombardment on FeO was found.

Ion bombardment of ferric oxides under our conditions thus results in the conversion of at least a portion of the top several atomic layers to FeO. XPS identification of a specific iron oxide phase thus becomes difficult following ion bombardment. However, in all cases studied, ion bombardment of iron oxides caused no reduction of oxide to metal. Thus, an oxide phase can be differentiated from iron metal by XPS following sputtering, even though its specific chemical structure cannot be readily identified.

DISCUSSION

Some of the iron oxide structures studied are identifiable on the basis of their chemical shift. A chemical shift results from a change in the *average* electrostatic potential field about an atom. This occurs, for example, in Fe_3O_4 where ferrous and ferric ions in the same lattice can be readily distinguished by the 2.0-eV difference in their core line binding energies. Similarly, in FeOOH, introduction of the more electronegative hydroxyl groups into the oxide lattice results in a decrease in the average charge on the ferric ion and this change is reflected in the increased binding energies for all core lines. The presence of FeOOH, precipitated from alkaline solution, has been detected on actively corroding iron surfaces, using the distinctly higher Fe(2p) and Fe(3p) core binding energies for this species (*29*). The chemical shift between Fe_2O_3 and FeO is useful for characterizing the initial oxide species formed during oxidation of a clean iron metal surface. Kishi and Ikeda (*30*) report a mean Fe(2p) binding energy difference of 0.8 eV between that for the initial oxide and the Fe_2O_3 which predominates after increased oxygen exposure. The initial oxide phase which nucleates during exposure of an iron surface to oxygen has been identified as FeO in earlier LEED studies (*31*).

Among the simple and mixed ferric oxides, very little change in mean core line binding energy is evident, and characterization by means of binding energy is not possible. However, differences in the Fe(2p) core line spectra due to multiplet interaction are clearly present and these can be used to provide "fingerprint" identification of the particular oxide species present. For example, the product of the oxidation of an Fe_3O_4 surface in air could be identified as α or γFe_2O_3 on the basis of the Fe(2p) peak shape provided this product layer were sufficiently thick (3 nm) to obscure any contribution from the original Fe_3O_4.

In their treatment of multiplet interaction in free transition metal ions, Gupta and Sen (*24*) point out that the crystal field could be important in determining the final terms of the ion, particularly if the degeneracy of the ground state is removed by this field, resulting in a redistribution of the intensities of the predicted lines. However, even without crystal field and other effects being taken into account, remarkably good agreement has been achieved between the predicted energy–intensity distributions and those observed experimentally for a number of transition metal compounds with high spin. In addition to the reasonably good accord shown here between the Fe^{2+} and Fe^{3+} free ion models and their respective oxides, Kowalczyk et al. (*23*) have found even better correspondence between Gupta and Sen's predicted Mn(2p) structure for high spin Mn^{2+} and their experimentally observed structure for MnF_2. The exceptionally good agreement probably results from the highly ionic nature of the compound used. Signorelli (*32*) has also compared multiplet structure in the Fe(2p) spectra of high spin ferric organometallic complexes with the Fe^{3+} results of Gupta and Sen.

A study of the XP spectra of both structures of Fe_2O_3 is useful in isolating some of the factors affecting chemical shifts and multiplet splitting in different core levels. In both γ and αFe_2O_3, the metal core line binding energies are identical, within experimental error, suggesting that the average potential about the metal ion is the same. This is also suggested by the identical Fe(3s) multiplet structure observed for both α and γFe_2O_3. Because this multiplet results from ^7S and ^5S final spin states, it is affected only by the average charge about the metal ion. The two iron oxide structures do differ in the symmetry of the crystal field about the metal ion, and it is this difference that likely affects the observed change in multiplet splitting of the Fe(2p) levels. The energy splitting of the two main multiplets is 0.20 eV larger for αFe_2O_3 than for γFe_2O_3. In the hexagonal close packed αFe_2O_3 structure, the octahedrally situated oxygens create a symmetric field about each ferric iron, while in the distorted spinel structure of γFe_2O_3, an axial field component is present. It is possible for such an axial field to result in reordering of final states and change of the splitting. This could arise from the interaction of an axial field with a low-lying P or D initial state to result in a final state which was more stable than the ^7P or ^5P states calculated for Fe^{3+} (*18*).

The multiplet structure in the Fe(2p) spectrum of FeOOH is similar to that observed in Fe_2O_3, except that some alteration in the relative intensity of the components appears likely. As in αFe_2O_3, the ferric ions are octahedrally surrounded by oxygen, but three of these are hydroxyl ions which create a slightly asymmetric field on the metal ion. No component structure is observed in the Fe(2p) spectra of the iron spinels, $NiFe_2O_4$ and $CoFe_2O_4$. The absence of structure comparable to that calculated for the Fe^{3+} free ion may be at least partly associated with the high axial field component present in these oxides.

Since satellite structure observed in the oxides can at least be qualitatively accounted for by multiplet interaction, shake-up interaction does not appear to make a major contribution to the spectra. However, Carlson (*33*) has shown that the shake-up process is responsible for strong satellites in the Fe(2p) spectra of a number of ferric and ferrous salts. In the case of the oxides, the probability of the (O(2p) $\rightarrow$ M(3d)) charge transfer transition, thought responsible for shake-up in these compounds (*34*), is apparently very low.

ACKNOWLEDGMENT

The authors acknowledge helpful discussions with S. K. Sen, R. P. Gupta, and C. R. Brundle. They also thank P. R. Tremaine, J. LeBlanc, and T. E. Rummery for supplying several of the iron oxides, M. Duclos for x-ray characterization, and L. Coatsworth for assistance with the peak fitting program.

LITERATURE CITED

(1) U. R. Evans, "The Corrosion and Oxidation of Metals", Edward Arnold Ltd., London, 1968.
(2) T. E. Rummery and B. Montford, Atomic Energy of Canada Limited, Report AECL-4444 (1975).
(3) C. D. Stockbridge, P. B. Sewell, and M. Cohen, *J. Electrochem. Soc.*, **108**, 928 (1961).
(4) G. C. Allen, M. T. Curtis, A. J. Hooper, and P. M. Tucker, *J. Chem. Soc., Dalton Trans.*, **14**, 1525 (1974).
(5) T. P. Hoar, M. Talerman, and P. M. A. Sherwood, *Nature (London), Phys. Sci.*, **240**, 116 (1972).
(6) J. P. Coad and J. G. Cunningham, *J. Electron Spectrosc. Relat. Phenom.*, **3**, 435 (1974).
(7) G. Okamoto, K. Tachibana, T. Shibata, and K. Hoshino, *J. Jpn Inst. Met.*, **38**, 117 (1974).
(8) I. Olefjord, *Met. Sci.*, **9**, 263 (1975).
(9) K. Asami, K. Hashimoto, and S. Shimodaira, *Corros. Sci.*, **16**, 35 (1976).
(10) G. Hagg, *Z. Phys. Chem.*, *Abt. B*, **29**, 95 (1935).
(11) G. Johansson, J. Hedman, A. Berndtsson, M. Klasson, and R. Nilsson, *J. Electron Spectrosc. Relat. Phenom.*, **2**, 295 (1973).
(12) N. S. McIntyre and D. G. Zetaruk, *J. Vac. Sci. Technol.*, **14**, 181 (1977).
(13) J. Smiltens, *J. Chem. Phys.*, **20**, 990, (1952).
(14) P. R. Tremaine and N. S. McIntyre, unpublished results.
(15) A. Noerlund Christensen, *Acta Chim. Scand.*, **22**, 1487 (1975).
(16) A. Barrie and F. J. Street, *J. Electron Spectrosc. Relat. Phenom.*, **7**, 1 (1975).
(17) G. M. Bancroft, I. Adams, L. L. Coatsworth, C. D. Bennewitz, J. D. Brown, and W. D. Westwood, *Anal. Chem.*, **47**, 586 (1975).
(18) R. P. Gupta and S. K. Sen, *Phys. Rev. B*, **10**, 71 (1974).
(19) N. S. McIntyre and M. G. Cook, *Anal. Chem.*, **47**, 2208 (1975).
(20) N. S. McIntyre and P. H. Tewari, *J. Colloid Interfac. Sci.*, **59**, 195 (1977).
(21) S. P. Kowalczyk, L. Ley, F. R. McFeely, and D. A. Shirley, *Phys. Rev. B*, **11**, 1721 (1975).
(22) C. S. Fadley in "Electron Spectroscopy", D. A. Shirley, Ed., American Elsevier Company, New York, 1972, p 781.
(23) S. P. Kowalczyk, L. Ley, R. A. Pollak, F. R. McFeely, and D. A. Shirley, *Phys. Rev. B*, **7**, 4009 (1973).
(24) R. P. Gupta and S. K. Sen, *Phys. Rev. B*, **12**, 15 (1975).
(25) D. E. Eastman and J. L. Freeouf, *Phys. Rev. Lett.*, **34**, 395 (1975).
(26) J. A. Tossell, D. J. Vaughan, and K. H. Johnson, *Nature (London), Phys. Sci.*, **244**, 42 (1973).
(27) C. D. Wagner, *Discuss. Faraday Soc.*, **60**, 291 (1975).
(28) M. Seo, J. B. Lumsden, and R. W. Staehle, *Surf. Sci.*, **50**, 541 (1975).
(29) N. S. McIntyre, unpublished results.
(30) K. Kishi and S. Ikeda, *Bull. Chem. Soc. Jpn*, **46**, 341 (1973).
(31) C. Leygraf and S. Ekelund, *Surf. Sci.*, **40**, 609 (1973).
(32) A. Signorelli, Ph.D. Thesis, University of Notre Dame (1975) University Microfilms 75-1860.
(33) T. A. Carlson, *Discuss. Faraday Soc.*, **60**, 30 (1975).
(34) K. S. Kim, *Chem. Phys. Lett.*, **26**, 234 (1974).

RECEIVED for review March 30, 1977. Accepted May 23, 1977.

Sampling Error in Ion Microprobe Analysis

G. J. Scilla[1] **and G. H. Morrison***

Department of Chemistry, Cornell University, Ithaca, New York, 14853

The sampling constant concept is applied to the in-situ microsampling of solids by the ion microprobe. Equations are provided which estimate the degree of heterogeneity present, and procedures are recommended for establishing the practical number of replicate analyses required to achieve a desired precision. The approach, which is experimentally verified using NBS SRM low alloy steels, can be used to minimize sampling error and to evaluate the applicability of specific standards for microprobe analysis.

Ion microprobe techniques have found wide application in such diverse fields as metallurgy, geology, solid state materials characterization, and biology (*1–4*). The main objective is to provide in-situ microchemical information on small features in solid samples and thus establish their chemical identity and possible compositional variations that might exist between different features.

It is common practice to calibrate the microprobe signals with standard samples that have been certified for bulk concentrations using more conventional analytical techniques not sensitive to concentration gradients on a microscale. This situation often gives rise to large errors mainly due to improper sampling. Attempts to evaluate quantitative methods of ion microprobe analysis have been limited by this fact, since empirical (*5, 6*) and semi-theoretical (*7, 8*) calibration approaches have shown marked discrepancies for some species from the known concentration in the standard samples used. Consequently, an understanding of the sampling problem as it applies to microprobe analysis is a prerequisite to any complete evaluation of quantitation attempts in secondary ion mass spectrometry (SIMS).

Normal procedures for reducing sampling error in analysis include choosing as large a sample as practical, followed by grinding, mixing, and/or dissolution to ensure homogeneity of the subsequent laboratory subsamples used for analysis. Many studies of the theory of bulk sampling can be found in the literature (*9–11*). Also, a fair amount has been done to characterize the theory of sampling and homogenization techniques for laboratory subsamples (*12–15*).

---

[1] Present address, The Procter and Gamble Company, Winton Hill Technical Center, 6110 Center Hill Rd., Cincinnati, Ohio 45224.

Table I. Approximate Analytical Sample Sizes for Microprobe Techniques

Technique	Volume sampled, μm^3	Mass sampled, g
Electron microprobe	1-10	10^{-11}-10^{-10}
Ion microprobe	0.1-50	10^{-12}-10^{-9}
Laser microprobe	10-1000	10^{-10}-10^{-8}

In microprobe analysis, however, the analyst is presented with two unique sampling problems. Unlike most analytical techniques, no homogenization treatments to reduce sampling error are employed since the primary advantage of a microprobe lies in its ability to perform in-situ analysis. A second problem that exists is the extremely small volume sampled. Table I lists the analytical sample sizes common to the various microprobe techniques. In view of these two constraints, sampling of heterogeneous materials with a microprobe is a serious problem and often the major contribution to the total analysis error.

The only viable approach to the microprobe analysis of a heterogeneous material, therefore, is one which allows for the a priori estimation of sampling error to be expected if the experiment is to be carried out in a certain way. Ingamells and Switzer (*12*) have used the sampling constant concept of Gy (*10*) and Visman (*16*) to establish criteria for proper sampling of bulk geological materials. The present study develops such an approach applicable to the in-situ microsampling situation encountered in ion microprobe analysis. Equations are provided which estimate the degree of heterogeneity present, and procedures are recommended for establishing the practical number of replicate analyses required to achieve a desired precision. The approach is experimentally verified using NBS SRM-662 and 664 low alloy steels. The method can also be used to evaluate the applicability of specific standard reference materials to ion microprobe analysis. The concepts developed here should be directly applicable to other microprobe techniques with little or no modification.

EXPERIMENTAL

Samples. Samples of 99.999% polycrystalline iron and copper and NBS SRM-660 low alloy steels were polished using a series of silicon carbide abrasive papers to 600 grit, followed by fine polishing using 1 μm, 0.3 μm, and 0.05 μm alumina. Samples of ⟨100⟩ single crystal gallium arsenide were polished using a chemical-mechanical polishing scheme (*3*).

Instrumental. A CAMECA IMS-300 Ion Microprobe/Ion Microscope previously described in the literature (*17*) was used in this study. In the analysis of all of the samples, the primary ion beam was $^{16}O_2^+$ at an energy of 5.5 KeV. The ion current was 0.5 μA rastered over a 300-μm × 300-μm area. Sputtering rates were measured using a Rank Precision Industries Talystep depth measuring device, and were determined to be less than 25Å per second in all cases. All materials were pre-sputtered for at least 5 min prior to analysis to remove contamination caused by polishing and handling. Ambient pressure in the vacuum system was approximately 10^{-7} Torr in all cases.

Data were collected in the pulse counting mode using a DEC PDP-11/20 computer interfaced directly to the ion probe. The computer was equipped with a DEC GT-40 graphics display unit as a peripheral device for real time monitoring of the data. Mechanical apertures located at the exit of the mass spectrometer were used in the ion probe to vary the analytical area viewed by the detector.

RESULTS AND DISCUSSION

In order to properly evaluate the sampling problem it is helpful to consider the different types of information usually desired from microprobe analysis. These may be classified as (1) chemical identification of microfeatures in the bulk of the sample, (2) distribution of these microfeatures in the bulk, and (3) bulk analysis of volumes too small for other techniques. Implicit in all of these is the need to calibrate signal with standards. For the complete characterization of a heterogeneously distributed constituent in a microfeature, evaluation of the degree of heterogeneity is a prerequisite to the characterization of the microfeature. Thus, the analysis of any one microfeature may entail separate analyses of smaller microfeatures within the larger host.

If the information required is related to the distribution of microfeatures in the bulk, then the sampling problem is identical to that encountered in particulate analysis (*18, 19*), metallurgical studies (*20*), and image analysis (*21, 22*).

If the analyst is concerned with information from a particular homogeneous microfeature large enough so that the only signal collected originates from within the boundaries of the microfeature, then there will be no sampling error. If the microfeature, either homogeneous or heterogeneous, is so small that it is smaller than the minimum collection area of the instrument used, then assuming that the entire microfeature can be sampled, the sampling error should be minimal provided the background area contains none of the constituent of interest, or if a simple correction for background contribution is applied.

Finally, if the analyst is concerned with information from a heterogeneous microfeature so large that collection of signal from the entire microfeature is impractical, or if bulk analysis of a microvolume is required, the sampling situation is more complex. This situation is commonly encountered in ion probe analysis with the use of standards either for empirical methods of quantitation, or for comparison of results from theoretical or semi-theoretical calculations to known bulk concentrations. As previously stated, sampling error in this case may become the major contribution to the total analysis error. It is in this final situation that the concept of a sampling constant will be most useful. The sampling constant can be used as a quantitative measure of heterogeneity, to estimate sampling error and to determine the number of replicate analyses required for a desired precision.

Precision of Measurement of Signal Arising from a Homogeneous Material. Before embarking on a study of the effect of sample heterogeneity on precision and accuracy in ion microprobe analysis, a full understanding of the precision of measurement which is associated with the analysis of a homogeneous material is required. For these purposes, samples of polycrystalline Fe, polycrystalline Cu, and single crystal ⟨100⟩ GaAs were highly polished as described above, to avoid the possibility of topographical effects. Each material was studied using varying pulse count times and mechanical aperture sizes, so that the effects on precision of volume, area, and time sampled could be determined. Twenty sets of five data points were taken for each case, from the same area on the sample in order to avoid effects of polycrystallinity or any possible heterogeneities. The relative standard deviation (RSD) for each set of five was calculated and the mean value of RSD for the twenty sets was determined, the RSD values being taken as a direct measure of precision. The approach of choosing sets of five data points was adopted since in practice few analysts use more than five replicates. Data were collected using peak heights, after adjusting the magnet to the maximum signal for the mass being monitored.

It was experimentally determined that RSD is inversely proportional to the square root of pulse count time, analysis area, and analysis volume, the proportionality constant being a function of the element. By combining the data, and plotting RSD vs. mean number of counts, the plot displayed in Figure 1 is obtained. This plot defines the equation:

$$\mathrm{RSD} = 100(N)^{-1/2} \tag{1}$$

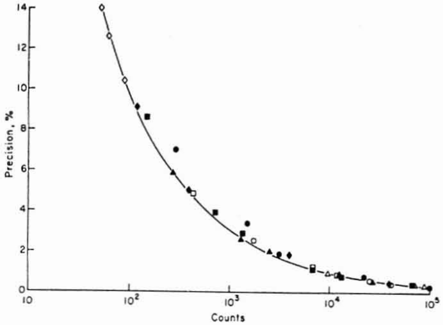

Figure 1. Precision of measurement vs. mean number of counts collected. Data collected using varying collection times: (●) $^{63}Cu^+$. (■) $^{56}Fe^+$. (▲) $^{69}Ga^+$. Data collected using varying aperture sizes: (○) $^{63}Cu^+$. (□) $^{56}Fe^+$. (△) $^{69}Ga^+$. Data collected with varying collection time and aperture: (◊) Cu. Data collected at photomultiplier by opening converter to light leak: (◆) No secondary ion current

where N is the mean number of counts collected. Equation 1 may be reduced to the form:

$$s^2 = \text{Variance} = N \tag{2}$$

where s is the standard deviation. Data which follow Equation 2 are distributed with Poisson Statistics (*23*). Therefore, the experimentally determined precision in ion microprobe analysis is the reciprocal square root of the mean number of counts independent of how the data were collected and follows the Poisson distribution.

A similar situation exists in electron microprobe analysis where precision is theoretically estimated by the Poisson Statistics associated with x-ray photo emission (*24*). However, Ziebold (*25*) has shown that the actual experimental precision with the electron probe does not generally follow the reciprocal square root of the number of counts, which is an overestimate of precision. This is due to the fact that with the electron probe, the excitation step is governed by Poisson statistical fluctuations, thus allowing for propagation of error throughout the spectrometer. On the other hand, with the ion microprobe, the reciprocal square root relationship is experimentally determined at the detector and is the actual precision of measurement from a homogeneous material. The response of the detector itself is governed by the Poisson distribution (see Figure 1); therefore other sources of error, if they exist, must be small relative to the reciprocal square root of the number of counts.

However, the analyst must exercise caution, even when calibrating signals with a homogeneous standard with the ion probe. This is due to the effect of crystallographic orientation on secondary ion yield. The effect is most serious when bombarding with inert gas ions, is somewhat better when bombarding with oxygen ions, and is least serious when bombarding with oxygen ions in the presence of a pressure of oxygen gas (approximately 10^{-4} Torr) (*26*, *27*). If a polycrystalline standard is employed and the crystal phases are large, erroneous results may be obtained.

The effect is illustrated for 99.999% polycrystalline Fe in Figure 2. Figure 2a is the $^{56}Fe^+$ ion image arising from bombardment of the sample with 5.5-keV $^{16}O_2^+$ primary ions. The varying secondary ion yields from the different crystal faces are evident in this picture. Figure 2b shows a light micrograph of the same region after sputtering, the crystal faces clearly visible due to the etching effect of the primary beam. Finally, Figure 2c is a line scan across the sample surface using a 10-μm aperture to limit the area on the surface of the sample viewed by the detector. The changing $^{56}Fe^+$ signal is apparent in this figure.

Sampling Constants. *Mathematical Derivations.* A rigorous statistical treatment of sampling error, encompassing all of the possible cases encountered in three-dimensional microanalysis, would be tedious at best. However, with some simplifying assumptions, equations can be derived which give an estimate of the sampling error to be expected in an analysis.

If, in the analysis of a heterogeneous constituent, it is assumed that the constituent of interest is located mainly in inclusions and it is also assumed that the total volume of the inclusions is small relative to the overall sample volume, then the inclusions may be approximated as point masses in space. In this case, the Poisson probability function can be used to model the distribution of the inclusions (*23*). Let $\bar{n}$ = the average number of inclusions per unit volume and v_0 = volume sampled. It is assumed that each inclusion contributes more or less equally to the total signal. Taking a set of volumes of size v_0, and counting the number of inclusions in each volume yields a mean value which estimates the population or true mean, $\bar{n}v_0$. According to the properties of the Poisson distribution, the population variance, σ^2, is equal to the mean, therefore

$$\sigma^2 = \bar{n}v_0 \tag{3}$$

and

$$\sigma_r = (\bar{n}v_0)^{-1/2} \tag{4}$$

where σ_r is the true or population relative standard deviation. The value of σ_r is then used to represent E_s, the error associated with sampling alone. If reasonable care is taken to minimize systematic errors caused by instrumental, sample preparation, matrix effects, etc., then these sources of error are small relative to E_s, so that E_s approximates the total analysis error. It has been shown that appropriate calibration standards can be used to correct for many of the above types of error except heterogeneity (*5*). The assumption that the constituent of interest is located mainly in inclusions can be dropped simply by multiplying the expression for E_s by a correction term, $|I_1 - I_2|/I$ where I_1 and I_2 are the signals arising from the inclusions and matrix, respectively, and I is the overall signal. The expression for sampling error then becomes:

$$E_s = (\bar{n}v_0)^{-1/2}\,\frac{|I_1 - I_2|}{I} = K(v_0)^{-1/2} \tag{5}$$

where

$$K = (\bar{n})^{-1/2}\,\frac{|I_1 - I_2|}{I} \tag{6}$$

and K is the sampling constant for in-situ analysis, dependent only on inherent properties of the sample being analyzed. If v_0 is expressed in μm^3 and $\bar{n}$ in inclusions/μm^3, K has the units of $\mu m^{3/2}$.

A more complete expression for the sampling constant can be derived by dropping the assumption of point masses, and considering the volume of the inclusions. Letting $\bar{v}_p$ = the average volume of the inclusions, the entire specimen is imagined to be divided into units of size $\bar{v}_p$. The effect of distribution of volume, shape of inclusion, and density, have been neglected. Certain of these units are the actual inclusions. The probability of selecting a unit which is an inclusion is:

$$p = \frac{\text{Total \# inclusions}}{\text{Total \# units}} = \frac{\bar{n}v_T}{v_T/\bar{v}_p} = \bar{n}\bar{v}_p \tag{7}$$

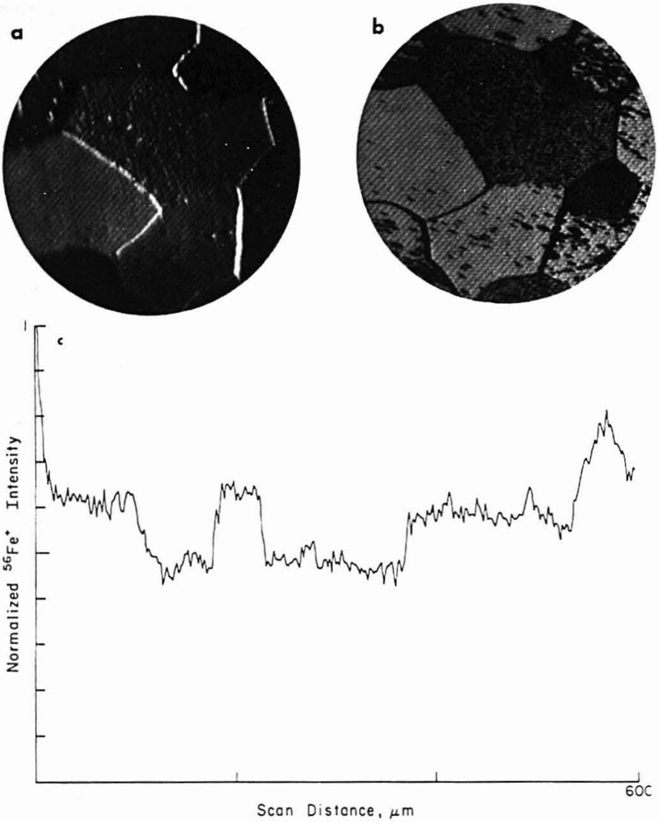

Figure 2. 99.999% Polycrystalline Fe sample: (a) $^{56}Fe^{+}$ ion image; (b) light micrograph of same region; (c) line scan across the surface of the sample

where $\bar{n}$ is the number of inclusions per unit volume and v_T is the total volume of the specimen. The total number of units sampled in an analysis volume v_0 is:

$$n = v_0/\bar{v}_p \tag{8}$$

Using the properties of the binomial distribution (*23*) the expression for σ_r can be derived as

$$\sigma_r = (1-p)^{1/2}(np)^{-1/2} \tag{9}$$

Substituting for p and n, and dropping the assumption of constituent of interest located mainly in the inclusions, we have for sampling error:

$$E_s = (1 - \bar{n}\bar{v}_p)^{1/2} \; (|I_1 - I_2|/I)/(\bar{n}v_0)^{1/2} \tag{10}$$

Equation 10 is identical to Equation 5 if the sampling constant is written as:

$$K = (1 - \bar{n}\bar{v}_p)^{1/2}(|I_1 - I_2|/I)/(\bar{n})^{1/2} \tag{11}$$

where again K is dependent only on inherent properties of the sample and has the same dimensions as the K defined by Equation 6. The expression for the sampling constant given by Equation 11 reduces to that given by Equation 6 as the volume of inclusions, v_p, approaches zero (assumption of point masses). Also, it should be noted that the quantity $\bar{n}\bar{v}_p$ is equivalent to the fraction of the material which is occupied by inclusions. As this fraction approaches unity, the entire sample is comprised of inclusion material, and is therefore homogeneous. In this case, Equation 10 correctly predicts a sampling error of zero.

It is possible that the constituent of interest may be located in heterogeneities with different distributions superimposed on each other (dropping the assumption that each inclusion contributes more or less equally to the total signal). In this case a sampling constant for each distribution, or a range of distributions, could be determined. The "total" sampling constant would then be calculated by taking each distribution constant, weighted for its contribution to the total signal, and doing a square root of the sum of squares calculation. This approach will be especially useful when calculating sampling constants with computerized image analysis techniques.

One final approximation is made in this study, that being the consideration of sampled area as opposed to sampled volume. We are justified in making the approximation since the area sampled in SIMS is so much greater than the depth sampled, the heterogeneity of the area under analysis should not change significantly during the time of analysis. The derivations of the sampling equations above are also valid for

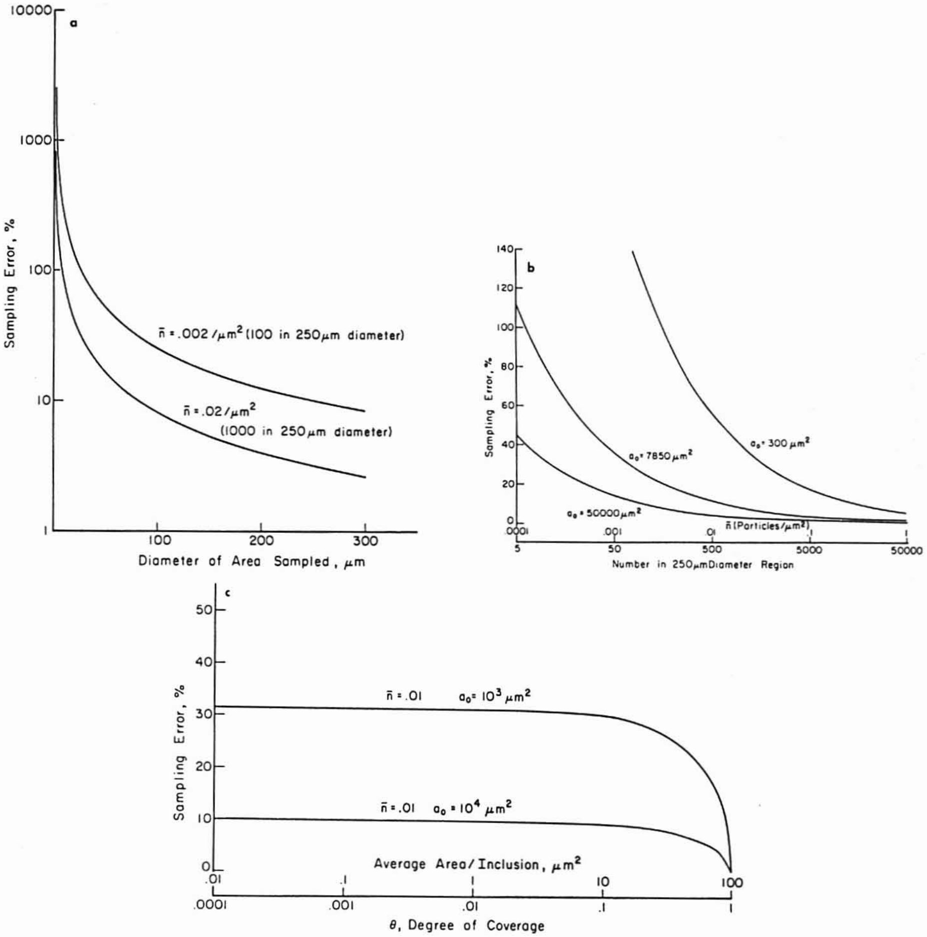

Figure 3. Sampling error vs. (a) area sampled; (b) number of heterogeneities; (c) area of inclusions (coverage)

areal analysis, the equations now being expressed in terms of number of inclusions/unit area, $\bar{n}$, area analyzed, a_0 and average area of inclusions, $\bar{a}_p$. Sampling constants are now expressed in units of microns. This approximation is made merely to aid in the visualization of the concepts of sampling and heterogeneity, as applied to the ion probe.

Plots of the various parameters associated with Equations 5 and 10 are displayed in Figure 3. In Figure 3a, E_s is plotted vs. area sampled for various heterogeneity distributions using the point mass approximation. Figure 3b displays the behavior of E_s as a function of heterogeneity for various sampled areas, again using the point mass approximation. These plots illustrate the potential severity of the sampling problem, the sampling error becoming excessive as area sampled decreases. Finally, Figure 3c is a plot of the effect of area of inclusions, a_p, on the sampling error. Here, the effect of the size of the inclusions can be seen to be minimal for a total coverage of less than 10%.

Equations 5 and 10 above were derived to be used as a tool to enable the analyst to estimate the sampling error associated with the material under study. The equations utilize the true or population standard deviation and mean to estimate the sample or experimental standard deviation and mean. The larger the number of replicate analyses, the more exactly the experimental statistical parameters approach the population parameters. Even if only a few replicates are taken, an estimate of sampling error will be available.

One of the more powerful applications of these equations is that once a sampling constant is calculated for a particular element in a sample, guidelines are available which suggest the number of replicates required for a particular confidence limit, assuming sampling is the major source of error. The confidence interval can be expressed in terms of percent of the mean as:

$$\Delta(\%) = 100\ ts_r/(N)^{1/2} \tag{12}$$

Table II. Sampling Constant from Ion Images for Ti-NBS SRM-662

Image	Blocks counted[a]	Inclusions counted	Inclusions per block	$\bar{n}$($\times 10^{-2}$) (Inclusions/μm^2)	K(μm)
1	210	80	0.381	0.273	19.1
2	200	91	0.455	0.327	17.5
3	184	73	0.399	0.287	18.7
4	203	86	0.424	0.305	18.1
5	203	82	0.404	0.291	18.5
	Total = 1000	Total = 412	mean = 0.413	mean = 0.297	mean = 18.4[b]

[a] 1 block = 139 μm^2. [b] mean K = 18.4 ± 0.8 at 95% confidence level.

where $\Delta\%$ is the percent confidence interval, N is the number of replicate measurements, t is a statistical factor dependent on N, and s_r is the relative standard deviation.

Again, if other sources of error are small relative to sampling, the relative standard deviation is equivalent to sampling error, E_s. Rearranging terms in Equation 12 and substituting for E_s, the expression for the number of replicate analyses required for a confidence interval of $\Delta(\%)$ where sampling is the major source of error, is given as:

$$N = (100\, tK/\Delta(\%)\sqrt{a_0})^2 \qquad (13)$$

where K is the sampling constant and a_0 is the area sampled. This equation can also be used to estimate $\Delta(\%)$ for an analysis using N replicates of area a_0. If other sources of error are of significant magnitude relative to sampling error, an estimate of the total analysis error may be obtained through the laws of propagation of error if a good estimate of the other sources of error is available. The total analysis error could then be used in Equation 12 to predict either $\Delta(\%)$ or the number of replicates required for a particular $\Delta(\%)$. Also, it should be noted that the value for the statistical factor t in the above equations can be obtained from the Student t tables which are calculated for normally distributed data, since for our purposes, the Poisson and Binomial distribution can be approximated by the normal distribution (*28*). As an example of the applicability of the above equations, assume that the desired results of a particular analysis are required ±10% at the 95% confidence level. Assume also that a good estimate of K for a particular element is 20 and that the analysis area is 20 000 μm^2. Using Equation 13 and a value of 1.96 for t, we have: $N = [(100)(1.96)(20)/(10)(20\,000)]^2 = 7.7$. The results of eight replicate analyses, therefore, should have a precision of ±10% at the 95% confidence level, assuming other sources of error are small relative to sampling.

The value of t used when calculating $\Delta(\%)$ or N will depend on the accuracy with which the value of K has been determined. For example, if K has been determined with one set of 20 replicate analyses, the t value corresponding to 19 degrees of freedom should be used. If K has been obtained from a large number of measurements, and a good estimate of K is available, the value of t used can be that calculated for an infinite number of degrees of freedom.

As a final consideration, it should be noted that in this study we have used precision as a measure of sampling error. This approach is justified only for large sample areas and becomes erroneous when the area sampled is small. This approach is necessary, however, since SIMS is not quantitative at this time and precision presents the most convenient means of measuring sampling error.

Calculation and Application. Sampling constants may be calculated either from ion images or indirectly by equating experimental RSD with sampling error. The first method is difficult to accomplish without the aid of a high speed image analyzing computer, except for relatively simple heterogeneity distributions. The latter method has the disadvantage that a large number of replicate analyses, typically 20, are required to obtain a reasonable estimate of K. Also, a quantitative estimate of other sources of error is required to determine the contribution due to sampling alone to the total analysis error.

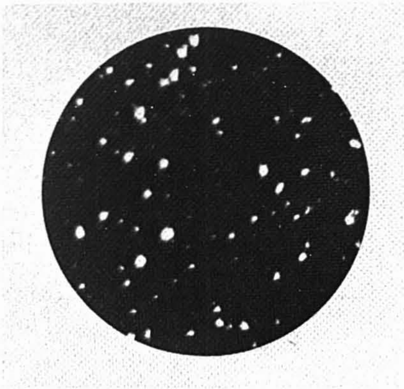

Figure 4. ^{48}Ti$^+$ ion image from NBS SRM-662

Table III. ^{48}Ti$^+$/^{56}Fe$^+$ Ratios from Twenty Random Spots of 49000 μm^2-NBS SRM-662

Area	^{48}Ti$^+$/^{56}Fe$^+$	Area	^{48}Ti$^+$/^{56}Fe$^+$	Area	^{48}Ti$^+$/^{56}Fe
1	0.383	8	0.444	15	0.362
2	0.470	9	0.396	16	0.412
3	0.400	10	0.423	17	0.407
4	0.346	11	0.366	18	0.354
5	0.410	12	0.408	19	0.385
6	0.380	13	0.417	20	0.429
7	0.369	14	0.448		

s = 0.033. $\bar{x}$ = 0.401. s_r = 8.2%. K = 18.2 μm.

Each of the methods above was used to calculate K for Ti in NBS SRM-662. Figure 4 is the ^{48}Ti$^+$ image from this steel. A grid dividing the sample surface into 139 μm^2 regions was superimposed on the image during the photographic printing process to simplify counting. The number of inclusions contained in a total of 1000 such grid spacings were counted on a series of ion images taken randomly on the sample. From these date $\bar{n}$ was calculated and used to determine K neglecting the effect of signal arising from the matrix. The results are displayed in Table II. The resultant K from five ion images is 18.4 ± 0.8 μm at the 95% confidence level. This result was compared to the K calculated from the relative standard deviation of replicate analysis of 20 random areas on the sample. The ratio of ^{48}Ti$^+$/^{56}Fe$^+$ signals were used to avoid the effect of changes in the primary beam intensity during analysis. The data for this determination are displayed in Table III. Here the value of K, assuming sampling error is large relative to the other sources of error, is 18.2 μm, well

Table IV. Predicted Sampling Error vs. Experimental RSD for Ti-NBS SRM-662

a_0, μm²	E_s, predicted[a]	Exptl RSD%
49000	8.3%	9.0
49000	8.3%	7.7
49000	8.3%	9.0
3420	31.3%	34.9
3420	31.3%	30.6
3420	31.3%	31.1

[a] $K = 18.3$ μm.

Table V. Sampling Constants from RSD of Twenty Replicates-NBS SRM-664[a]

	Ni	Co	V	Ti	Cr	Mn
Set 1	40.0	5.1	9.8	38.0	6.3	7.2
Set 2	33.5	4.9	12.9	42.0	10.3	9.3
Average	36.8	5.0	11.4	40.0	8.3	8.3

[a] K's in microns.

Table VI. Predicted E_s vs. Experimental RSD of Ten Replicate Analyses at 49 000 μm²-NBS SRM-664

	Ni	Co	V	Ti	Cr	Mn
Predicted E_s, %	17	2	5	18	4	4
Experimental RSD, %	17	2	4	11	5	7
	17	2	6	15	3	3
	15	2	5	18	4	5
	23	2	5	20	4	

Table VII. Predicted E_s vs. Experimental RSD of Ten Replicate Analyses of 3420 μm²-NBS SRM-664

	Ni	Co	V	Ti	Cr	Mn
Predicted E_s, %	63	8	19	68	14	14
Experimental RSD, %	51	4	12	79	12	11
	53	6	10	80	9	12
	61	7	10	55	9	6
	62	8	11	83	12	11

within experimental error of K determined by imaging.

The data in Table III can be used to illustrate the use of K to predict the required number of replicates for a particular confidence limit. For example, using $K = 18.3$ μm, and a t factor for $N = 20$ of 2.09, Equation 13 predicts the number of replicates required for a 10% of the mean confidence limit at the 95% level is three. Choosing the worst possible case of the three highest and three lowest data points, a percent deviation from the mean of 13% for the high values and 12% for the low values is obtained. Therefore, the % deviation from the mean of three replicates would be better than 10% except for the unlikely case of obtaining the three highest or lowest values in a row.

Finally, K was used to estimate the experimental RSD associated with ten replicate analyses for Ti using areas of 49 000 μm² and 3420 μm². The results are displayed in Table IV. The predicted sampling error is 8.3% and 31.5% for the larger and smaller areas, respectively. The counting error in both cases was less than 0.5%. Three independent sets of data were taken for each area. As can be seen in Table IV, the experimental RSD is close to that predicted by the sampling equation.

Sampling constants for a number of elements in NBS SRM-664 were determined by the method of equating experimental RSD to sampling error. Again, the ratio arising from the constituent of interest to the $^{56}Fe^+$ signal was used to avoid the effects of changes in the bombarding beam during the analysis. Two sets of 20 replicate analyses each were obtained on a highly polished sample after presputtering for 5 min to remove surface contamination. The sampling constants obtained for Ni, Co, V, Ti, Cr, and Mn are displayed in Table V. In each case, except for cobalt, the experimental RSD was much greater than that which would be expected from counting error alone, so that the major source of error was assumed to be sampling error. With cobalt the magnitude of the experimental RSD was approximately the same as that expected from counting error. However, when sampling constants are determined by equating experimental RSD to sampling error, the contribution of the analytical error is incorporated into the sampling constant since the counting error also follows a reciprocal square root law. The K values displayed in Table V were used to estimate the sampling error expected for analysis areas of 49 000 μm² and 3420 μm². The estimated sampling error for each case and the actual experimental RSD are displayed in Tables VI and VII. Each experimental RSD represents 10 replicate analyses. In each case the experimental RSD is closely estimated by the sampling error calculated using the sampling constant.

Significance. The in-situ sampling constant concept provides a link between bulk and microscale analysis; i.e., guidelines are established for the extension of standards characterized by bulk techniques to the microsampling situation. It is now possible to evaluate the usefulness of a given standard reference material for microprobe analysis. These constants also provide a convenient means of condensing and storing information from prior analyses regarding the precision of measurement of unknown materials. Sampling constants are also useful as a quantitative measure of the heterogeneity of a material, as well as a means of predicting sampling error and required number of replicates for a desired precision.

Although the sampling constants presented here have been determined in a manner which lends itself to the SIMS instrument available in this laboratory, it is possible to determine constants applicable to any in-situ measurement technique. The correctness of the constants determined by one technique to analyses using other techniques or instrumental conditions may vary, but since the purpose of these constants is to estimate expected sampling error this should not diminish their usefulness. For example, in ion probe analysis, cognizance must be taken of both spatial and phase heterogeneity. This is due to the varying effect on secondary ion yield of chemical speciation, crystal orientation, vacuum conditions, matrix, etc. To a certain extent, phase heterogeneity can be compensated for by backfilling the source chamber with a partial pressure of oxygen (oxygen leak). The apparent homogeneity may then improve somewhat for certain elements. However, if the sampling constant has been determined at residual vacuum (no oxygen leak), an estimate of the upper limit of sampling error is obtained and thus the most serious case defined.

Finally, it should be noted that analysis of heterogeneous samples with an ultra small probe (a few microns in diameter) may yield both unrealistically high precision and erroneously low concentrations. This is because with a constituent located both in inclusions and in the matrix, the probability of the probe striking an inclusion may be quite small, especially if the number of inclusions per unit volume is small. This will result in a set of replicates which reflect the concentration of the constituent in the matrix, with the possibility of an occasional "anomalous" result which in reality arises from the probe striking an inclusion. If the occasional "anomalous" result is neglected, precision may be quite good. The above situation arising during calibration with a standard will cause subsequent analysis of unknowns to yield erroneously high results. Use of a sampling constant here would define how many replicates will be required for each constituent to obtain results within a certain confidence limit of the true concentration, and also eliminate the rejection of valid data.

LITERATURE CITED

(1) E. Berkey, G. G. Sweeney, and W. M. Hickam, *Nucl. Technol.*, **16**, 263 (1972).
(2) C. A. Andersen and J. R. Hinthorne, *Geochim. Cosmochim. Acta*, **37**, 745 (1973).
(3) J. J. Berenz, G. J. Scilla, V. L. Wrick, L. F. Eastman, and G. H. Morrison, *J. Vac. Sci. Technol.*, **13**, 1152 (1976).
(4) L. G. Petersson, G. Frostell, and A. Lodding, *Z. Naturforsch.*, *C*, **29**, 417 (1974).
(5) J. A. McHUgh, "Secondary Ion Mass Spectrometry," in "Methods of Surface Analysis", S. P. Wolsky and A. W. Czanderna, Ed., Elsevier Publishing Co., New York, N.Y., 1976.
(6) D. E. Newbury, K. F. Heinrich, and R. L. Myklebust, "Errors Observed in Quantitative Ion Microprobe Analysis", in "Surface Analysis Techniques for Metallurgical Applications", ASTM STP 596, American Society for Testing and Materials, Philadelphia, Pa., 1976.
(7) C. A. Andersen and J. R. Hinthorne, *Anal. Chem.*, **45**, 1421 (1973).
(8) T. Ishitani, H. Tamura, and T. Kondo, *Anal. Chem.*, **47**, 1294 (1975).
(9) P. D. LaFleur, Ed., "NBS Special Publication 422—Accuracy in Trace Analysis: Sampling, Sample Handling, Analysis", Vol. 1 and 2, U.S. Govt. Printing Office, Washington, D.C., 1976.
(10) P. Gy, "Sampling of Materials in Bulk-Theory and Practice", Societé de l'Industrie Minèrale, Saint Étienne, France, 1971.
(11) A. J. Duncan, *Technometrics*, **4**, 319 (1962).
(12) C. O. Inganıells and P. Switzer, *Talanta*, **20**, 6c, 547 (1963).
(13) A. A. Benedetti-Pichler, "Theory and Principles of Sampling for Chemical Analysis", in "Physical Methods of Chemical Analysis", Vol. 3, W. M. Berl, Ed., Academic Press, New York, N.Y., 1956, pp 183–217.
(14) W. E. Harris and Byron Kratochvil, *Anal. Chem.*, **46**, 313 (1974).
(15) G. H. Morrison and A. M. Rothenberg, *Anal. Chem.*, **44**, 515 (1972).
(16) J. Visman, *Mater. Res. Stand.*, **9** (11), 8 (1969).
(17) G. H. Morrison and G. Slodzian, *Anal. Chem.*, **47**, 932A (1975).
(18) G. Herdan, "Small Particle Statistics", 2nd ed., Academic Press, New York, N.Y., 1960.
(19) E. M. Chamot and C. W. Mason, "Handbook of Chemical Microscopy", 3rd ed., Vol. 1, John Wiley and Sons, New York, N.Y., 1958.
(20) R. M. Greaves and H. Wrighton, "Practical Microscopical Metallography", 4th ed., Chapman and Hill, Ltd., London, 1966.
(21) M. L. Mendelsohn, B. H. Mayall, J. M. S. Prewitt, R. C. Bostrom, and W. G. Holcomb, "Digital Transformation and Computer Analysis of Microscope Images", in "Advances in Optical and Electron Microscopy", Academic Press, New York, N.Y., 1968.
(22) H. Malissa, J. K. Kaltenbrunner, and M. Grasserbauer, *Microchim. Acta*, *Suppl.* **5**, 453 (1974).
(23) A. M. Mood, F. A. Graybill, and D. C. Boes, "Introduction to the Theory of Statistics", 3rd ed., McGraw-Hill, New York, N.Y., 1974, pp 93–99, 538–539.
(24) S. J. B. Reed, "Principles of X-Ray Generation and Quantitative Analysis with the Electron Microprobe", in "Microprobe Analysis", C. A. Andersen, Ed., John Wiley & Sons, New York, N.Y., 1973, p 76.
(25) T. O. Ziebold, *Anal. Chem.*, **39**, 858 (1967).
(26) M. Bernheim and G. Slodzian, *Int. J. Mass Spectrom. Ion Phys.*, **12**, 93 (1973).
(27) M. Bernheim and G. Slodzian, *Surf. Sci.*, **40**, 169 (1973).
(28) A. M. Mood, F. A. Graybill and A. C. Boes, "Introduction to the Theory of Statistics", 3rd ed., McGraw-Hill, New York, N.Y., 1974, p 120.

RECEIVED for review April 29, 1977. Accepted June 13, 1977. Financial support was provided by the National Science Foundation under Grant No. CHE-7608531 and through the Cornell Materials Science Center.

Qualitative Analysis of Thin Gallium Nitride Films with Secondary Ion Mass Spectrometry

J. Edward Andrews,*[1] **A. P. Duhamel,**[2] **and Michael A. Littlejohn**

Department of Electrical Engineering, North Carolina State University, Raleigh, North Carolina 27607

Gallium nitride (GaN) thin films grown from the vapor phase by pyrolyzing $Ga(C_2H_5)_3{\cdot}NH_3$, were analyzed using Secondary Ion Mass Spectroscopy (SIMS). Comparative mass spectra were obtained from GaN grown by two other laboratories using two different techniques and were found to be similar. The SIMS technique identified the presence of Ga, N, and O, in all the GaN films. C was detected in the GaN film prepared by pyrolysis. Evidence of H as part of the ionic structure was in the higher mass spectra of all the samples; however, it could not be determined with certainty if the source of H originated in the SIMS instrument, the samples, or both.

Thin gallium nitride (GaN) films grown on α-Al_2O_3 substrates by pyrolytic decomposition of $Ga(C_2H_5)_3{\cdot}NH_3$ in a chemical vapor deposition system have been described in an earlier publication (*1*). The as-grown films were typically yellowish brown in color instead of transparent as would be expected for a material with a 3.5-eV energy band gap (*2*). This yellowish color was characteristic of the films grown throughout the temperature range from 500 to 1000 °C. Since this was the first time that this growth process and system had been used to grow GaN, it was not at all certain that the deposits obtained were GaN, especially in view of the coloring noted above. Therefore effort during the early part of the research was directed toward obtaining a qualitative analysis of the deposits. Several analytical techniques were eventually used (electron microprobe, x-ray diffraction, electron diffraction, secondary ion mass spectrometry) with each providing some useful but not complete information concerning the nature of the deposits. The analytical technique reported here is worthy of note because of its ability to detect nitrogen as well as the lighter elements, including hydrogen, and was particularly valuable in analyzing deposits that were too amorphous to give useful diffraction data.

This paper reports the results of the qualitative analysis of the GaN thin films using the technique of Secondary Ion Mass Spectrometry (SIMS). The combination of sputter etching and mass spectrometry used in the SIMS technique permits a convenient and rapid qualitative analysis of thin films and surfaces. In depth discussions of the SIMS technique and available instrumentation have recently been presented (*3–5*). A comparison of the performance of the SIMS technique with Auger Electron Spectroscopy (AES) and x-ray photoelectron spectroscopy (XPS) given in Ref. 6 in-

---

[1] Present address, Research Triangle Institute, P.O. Box 12194, Research Triangle Park, N.C. 27709.

[2] Present address, U.S. Energy Research and Development Administration, Washington, D.C. 20545.

Table I. Experimental Conditions Used for Sample Analysis

(1) Primary ion beam gas: argon[a]
(2) Argon gas pressure: 3×10^{-5} Torr
(3) Accelerating voltage for argon ions: 6 KeV
(4) Ion-beam current at sample surface: 150 μA

[a] Oxygen was substituted for argon and mass spectrum retaken on the GaAs sample after the various samples had been analyzed.

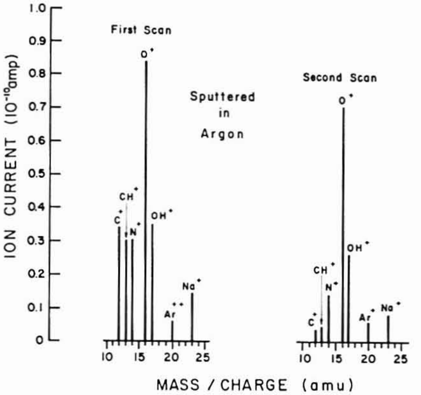

Figure 1. Two consecutive mass scans of sample 55S

dicates that the SIMS technique is capable of a much lower detection threshold.

For purposes of comparison, GaN samples furnished by courtesy of IBM and RCA were also analyzed. The IBM GaN was prepared by sputtering Ga in the presence of N_2 (*7*, *8*). The RCA GaN was prepared by the ammonolysis of GaCl (*9*).

EXPERIMENTAL

The analysis of the GaN films (plus a sample of single crystal undoped GaAs) was performed using an Ion Beam Surface Mass Analyzer (ISMA). This instrument and its operation have been described in detail in (*5*). The analysis of the undoped GaAs was performed in order to eliminate possible background effects obtained from the instrument and to assist in the interpretation of the spectral data obtained from the GaN films.

The analysis of the GaN films and pure GaAs were performed under constant experimental conditions listed in Table I.

Sample chamber pressures prior to sample analysis were oridinarily of the order of 8×10^{-8} Torr. The mass resolution of the ISMA was typically 0.4 amu.

Mass spectra for the GaN and GaAs were obtained over the mass ranges 10–25, 62–77, and 80–95. Each range was scanned in a 2-min period at a rate of 0.125 amu/s with several scans performed consecutively to obtain data on the variation of various peak intensities as a function of time.

Species of potential interest in the mass ranges 10–25, 62–77, and 80–95 were ^{12}C, ^{14}N, ^{16}O; ^{69}Ga, ^{71}Ga; $^{69}Ga^{12}C$, $^{69}Ga^{14}N$, $^{69}Ga^{16}O$, $^{71}Ga^{12}C$, $^{71}Ga^{14}N$, and $^{71}Ga^{16}O$, respectively.

RESULTS AND DISCUSSION

Figure 1 shows spectra resulting from the first two mass scans of GaN sample 55-S grown at 600 °C by the process described in Ref. 1. (The ordinate gives a measure of the ion beam current, in A, produced by the secondary ions sputtered from the surface of the sample.) Figure 1 indicates hydrocarbon fragments being detected only in the first few minutes of analysis. Normally, hydrocarbon fragments detected with this technique and exhibiting this behavior (disappearing after a few minutes of etching) are usually attributed to vacuum system pump oil that has accumulated on the surface. However, GaAs spectra obtained under identical experimental conditions (see Figure 2) showed no indication of hydrocarbon fragments. This would strongly suggest that the hydrocarbon fragments observed in the GaN spectra were not an instrument artifact.

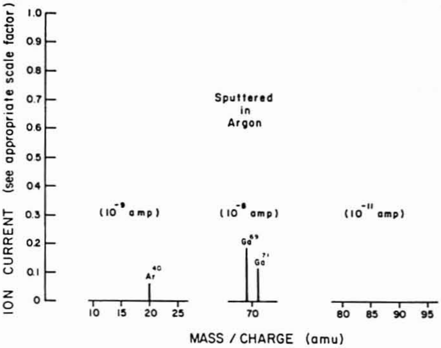

Figure 2. Mass spectrum of GaAs

The sample 55-S mass peaks observed at 14 and 16 amu persisted with continued etching while those at 12 and 13 amu gradually disappeared. The peaks at 12, 13, and 16 amu were interpreted as $[^{12}C]^+$, $[CH]^+$, and $[^{16}O]^+$, respectively.

The interpretation of the peak at 14 amu, however, is more complicated since it could be due to $[CH_2]^+$, $[^{14}N]$ or both. The gradual disappearance of the $[^{12}C]^+$ and $[CH]^+$ peaks suggests that the related $[CH_2]^+$ peak should similarly disappear. Since the peak at 14 amu persisted, it could eventually be interpreted as being primarily $[^{14}N]^+$ as indicated in the second scan in Figure 1. The peak at 14 amu was seen to still be very evident in Figure 3 which is the spectrum after 8 to 10 min of etching. The absence of similar peaks in the GaAs spectra (Figure 2) indicates that background interferences were not responsible for the observed peaks in the GaN spectra.

It was noted (compare Figures 2 and 3) incidentally that the Ga ion yield for sample 55S was more than 1 order of magnitude larger than that of the GaAs sample. Sample 55S was determined previously to be nearly amorphous in nature and might therefore be expected to yield Ga ions much more easily than the single crystal GaAs used for the reference.

Figure 3 shows the mass spectra obtained for sample 55S through the mass range 80–95 amu. No significant mass peaks were observed for the GaAs in this mass range. The 55S spectra, however, show distinct peaks at 85, 86, 87, 88, and 89 amu. Weak peaks were also observed at 83 and 84.

It is interesting here to compare these data with the GaAs mass spectrum obtained in the 80–95 amu range using an O_2^+ primary ion beam (see Figure 4). As was seen in Figure 2, the GaAs spectrum (sputtered with Ar) gave no observable peaks in the 80–90 amu range whereas Figure 4 shows peaks that were similar to the GaN spectra (the oxygen-containing fragments were formed as a result of ion–molecule reactions between the sample and O_2^+ ions from the beam). This comparison would strongly indicate that the GaN films contained oxygen.

Figure 4 also indicates the existence of hydrogen in some of the fragments detected. Both $[AsO]^+$ and $[AsOH]^+$ fragments were believed to be responsible for the peaks observed at 91 and 92 amu, respectively. The Ga from the GaAs apparently gave rise to $[GaO]^+$, $[GaOH]^+$, and $[GaOH_2]^+$ at (85, 87), (86, 88), and (87, 89) amu, respectively, with $[GaOH]^+$ corresponding to the prominent peak.

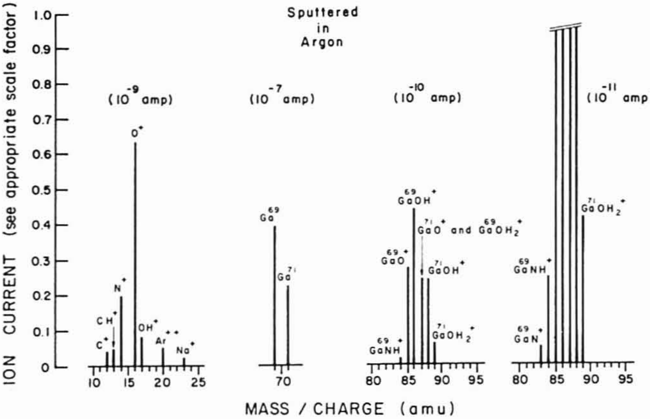

Figure 3. Mass spectrum of sample 55S (GaN) with the mass range 80–95 amu shown at two different sensitivities (this spectrum persisted throughout the remainder of the analysis of this work)

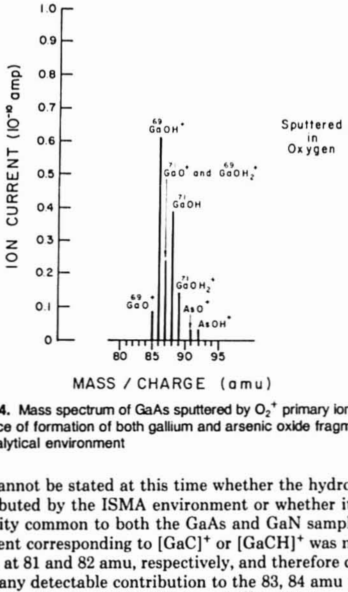

Figure 4. Mass spectrum of GaAs sputtered by O_2^+ primary ion beam. Evidence of formation of both gallium and arsenic oxide fragments in the analytical environment

It cannot be stated at this time whether the hydrogen is contributed by the ISMA environment or whether it is an impurity common to both the GaAs and GaN samples. A fragment corresponding to $[GaC]^+$ or $[GaCH]^+$ was not detected at 81 and 82 amu, respectively, and therefore cannot make any detectable contribution to the 83, 84 amu peaks.

The likelihood of $[^{69}GaCH_2]^+$ and $[^{69}GaCH_3]^+$ was considered in the interpretation of the peaks considered at 83 and 84 amu since it is here that $[^{69}GaN]^+$, and $[^{69}GaNH]^+$ would be detected if they exist and could result in an ambiguity in interpretation. The identification of the fragment ions at 83 and 84 amu as $[^{69}GaN]^+$ and $[^{69}GaNH]^+$, respectively, is supported by comparing the mass spectra of GaN samples grown by the two other processes referenced earlier.

Comparison of Mass Spectra for GaN Grown by Other Techniques. Two other samples of GaN grown by the two techniques referenced earlier (identified as the IBM and RCA samples) were analyzed while still using the GaAs for a reference. The spectra for the IBM sample are shown in Figure 5 while the spectra for the RCA sample are shown in Figure 6.

These GaN samples resulted in spectra similar to 55S throughout the 83–89 amu range. In addition, these spectra were also similar to the one shown in Figure 4 (GaAs sputtered with oxygen) in the 85–89 amu range. The RCA sample was small and thus exposed the edge of the sapphire (α-AlO_3) substrate to the primary ion beam; thus the oxygen indicated by the spectra for the RCA sample (i.e., through $[GaO]^+$ fragments) could easily have resulted from the ion–molecule reaction between substrate furnished oxygen and sample supplied Ga atoms. The RCA sample contributed rather definite peaks at 83 and 84 amu which were interpreted at $[^{69}GaN]^+$ and $[^{69}GaNH]^+$, respectively, which supports a similar interpretation in the 55S spectra.

Sample 55S and the IBM sample did not experience any substrate interference; therefore oxygen indicated in their spectra was interpreted as originating from the samples.

As stated earlier, hydrogen is also very much in evidence in these spectra, but cannot be identified as originating from the sample or the ISMA.

CONCLUSIONS

The qualitative analysis of deposits obtained from the pyrolysis of $Ga(C_2H_5)_3{\cdot}NH_3$ has shown that the sample contains gallium, nitrogen, oxygen, and carbon, the latter being concentrated near the surface of the sample. While x-ray diffraction was relied on for the verification of the deposits to be GaN, it is significant that SIMS provided a means of directly detecting the presence of nitrogen in the deposits. Hydrocarbons from the vacuum system oil were ruled out as a source of carbon because of the absence of hydrocarbons in the GaAs spectra. Hydrocarbons detected in the S-55S film would be significant since this was suspected to be the reason for the yellow-brown color that has been characteristic of the films grown from $Ga(C_2H_5)_3{\cdot}NH_3$. It was interesting to note that sample 55S has changed color (in the region being analyzed) from yellowish brown to gray. No explanation can be offered for this change in color at the present time.

The GaAs sample permitted establishing a background baseline against which the GaN spectra could be compared. The mass spectra obtained from the GaN grown by two other laboratories added confidence to the interpretation of the mass peaks as did the spectra obtained by using the oxygen primary

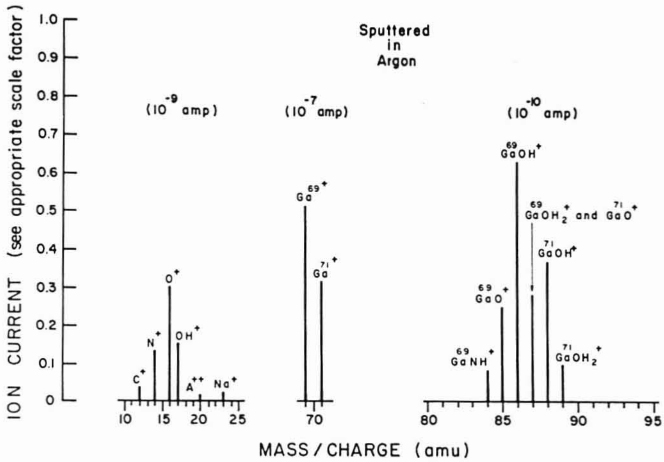

Figure 5. Mass spectrum of IBM GaN

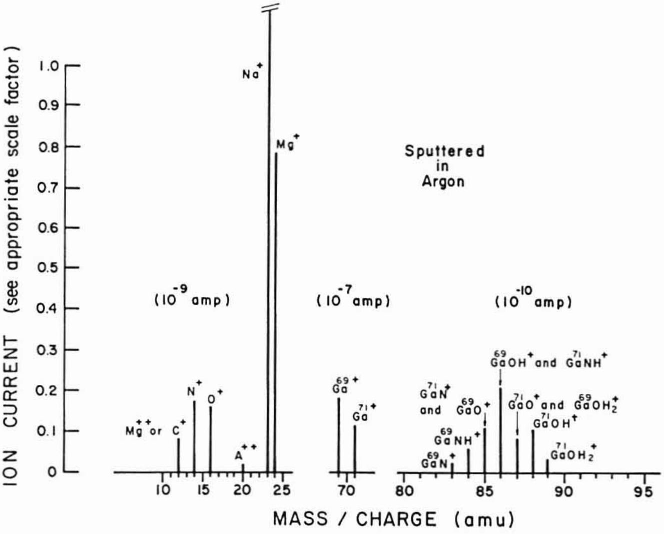

Figure 6. Mass spectrum of RCA GaN

ion beam on the GaAs sample at the end of the analysis.

Some of the fragment ions occurred at an m/e that could be explained only through the addition of one or two hydrogen atoms (or ions). Although the analytical environment of the ISMA could itself be a source of hydrogen, one cannot rule out the actual growth process and systems as a source, especially where reactants such as NH_3 or $Ga(C_2H_5)_3{\cdot}NH_3$ are involved. It was in fact the hydrogen question that motivated the analysis of the IBM sample which did not intentionally use any hydrogen-containing reactants. Only extremely careful experimental procedure can hope to pinpoint the source(s) of the hydrogen. It is emphasized here that the evidence for hydrogen persisted even after extended lengths of sputter etching.

Upon reviewing these spectra, it appears unnecessary to seek $[GaN]^+$ ions directly as evidence of the N in GaN for the experimental conditions described here. Nitrogen ions detected at 14 amu are attributed to the sample and not to the instrument background for the conditions of our analysis.

ACKNOWLEDGMENT

The authors are especially grateful for the courtesy and generosity extended by the Commonwealth Scientific Co., which provided the ISMA used for the analyses reported. Special thanks are due to J. I. Pankove, RCA, Princeton, N.J., and P. J. Burkhardt, IBM, Hopewell Junction, N.Y., who donated their samples for comparison, and for their permission to publish the results of the analyses related to these samples.

LITERATURE CITED

(1) J. E. Andrews and M. A. Littlejohn, *J. Electrochem. Soc.*, **122**, 1273 (1975).
(2) M. Ilegems, R. Dingle, and R. A. Logan, *J. Appl. Phys.*, **43**, 3797–3800 (1972).
(3) C. A. Evans, Jr., *Anal. Chem.*, **44**, (13), 67A (1972).
(4) C. A. Evans, Jr., *Thin Solid Films*, **19**, 11–19 (1973).
(5) F. W. Karasek, *Res./Dev.*, **24**, 40–46 (1973).
(6) M. Gettings and J. P. Coad, *Surf. Sci.*, **53**, 636–648 (1975).
(7) H. J. Hovel and J. J. Cuomo, *Appl. Phys. Lett.*, **20**, 71–73 (1972).
(8) J. C. Veseley, M. Shatzkes, and P. J. Burkhardt, *Phys. Rev. B*, **10**, 582 (1974).
(9) R. E. Enstrom, E. A. Miller, and A. G. Sigai, Final Report for NASA–Langley Research Center, Contract NAS 12-538 (1971).

RECEIVED for review August 9, 1976. Accepted June 6, 1977. This work was partially supported by the Office of Naval Research.

Characterization of Lignites by Pyrolysis–Gas Chromatography

C. S. Giam,* T. E. Goodwin, P. Y. Giam, K. F. Rion, and S. G. Smith

Department of Chemistry, Texas A&M University, College Station, Texas 77843

A technique has been developed for the rapid characterization and "screening" of lignite samples by pyrolysis–gas chromatography. The application of this technique to a series of Texas lignites is described. The production of *n*-paraffins and 1-olefins with 1–5 carbons is monitored.

Pyrolysis is probably the oldest operation to be carried out on coal (*1, 2*) and is the foundation for many coal liquefaction (*3, 4*) and gasification (*5–7*) procedures. Recent innovations in this area include vacuum pyrolysis in a mass spectrometer (*8–13*), laser irradiation (*14, 15*), "flash heating" (*16, 17*) and the use of arc plasmas (*18*).

While this manuscript was in preparation, Hanson, Vanderborgh, and Brookins (*14*) reported their applications of laser pyrolysis–gas chromatography to study the influence of coal composition on the distribution of gaseous products. Correlations between experimental results and elemental compositions were presented.

Romováček and Kubát (*19*) developed a technique for rapid pyrolysis whereby the coal sample is dropped into a bath of molten tin. The product gases were swept by an inert carrier gas into a gas chromatograph, whereby the production of selected low molecular weight hydrocarbons was monitored at several pyrolysis temperatures.

Coates, Chen, and Pope (*20*) studied the amount and composition of gases evolved during rapid pyrolysis (1350 °C in <0.3 s) of a bituminous coal. A number of other pyrolysis–gas chromatography procedures have been reported (*21–25*).

Recently Gray, Cogoli, and Essenhigh (*26*) reviewed the literature regarding coal pyrolysis and came to the following conclusions, inter alia: (a) Rapid heating can raise coal samples to high temperatures without significant decomposition, and they can then pyrolyze at a constant temperature with a yield of volatiles that is higher than can be obtained under any other experimental conditions. (b) Pyrolysis at lower heating rates may cause part of the coal substance to cross-link during the period of temperature rise to the final, constant pyrolysis temperature. This cross-linking binds material that would otherwise be able to escape as volatiles, thus reducing the volatile yield.

This manuscript describes a simple procedure for the rapid pyrolysis of lignite samples. The use of gas chromatography for determination of the C_1–C_5 pyrolysis products is reported.

EXPERIMENTAL

Apparatus. At our request Chemical Data Systems, Inc. (Oxford, Pa.) designed a "Controlled Atmosphere Pyrolysis System". It consists of a "Pyroprobe" pyrolyzer with a coiled platinum wire as the heating element, an interface to a gas chromatograph, and three detectors (electron capture, thermal conductivity and flame ionization). Only the flame ionization detector was used for the analyses described herein.

The gas chromatograph was fitted with a 10-ft × $^1/_8$-in. stainless steel column packed with Poropak Q (80–100 mesh) (*27*). The air, hydrogen, and nitrogen (carrier gas) flow rates were 200, 40, and 40 mL/min, respectively. The column was held at 60 °C for 3 min after injection, temperature-programmed at 12.5 °C/min up to 150 °C, and held at that temperature for the duration of the run. The injector, detector, interface (between pyrolyzer and GC), and final pyrolysis temperatures were 150, 360, 250, and 850 °C, respectively. A ramp speed of 1 °C/ms was used to arrive at the final pyrolysis temperature. The total pyrolysis time was 20 s.

Procedure. The lignite samples were air-dried, crushed, sieved to <200 mesh, dried at least 12 h at 160 °C and allowed to cool to room temperature. It was necessary to allow the samples to achieve "moisture-equilibration" with laboratory air in order to get consistent pyrolysis results. Attempts to keep the lignite anhydrous led to weighing difficulties due to its "molecular sieve-type" properties.

Open-ended, quartz pyrolysis tubes (2.4 o.d. × 27.7 mm) were cleaned before each run by soaking overnight in chromic acid cleaning solution and rinsing with distilled water, ammonium hydroxide, distilled water, acetone, and distilled water. The tubes were dried at least 12 h at 350 °C. A small plug of quartz wool was inserted halfway into a clean quartz tube and this was heated twice for 20 s at 850 °C in the pyrolysis apparatus. Subsequently, the tubes were manipulated with tweezers and "Micro-wipes". It is quite easy to obtain pyrograms of "skin oils" if the tubes come in contact with the skin.

Small portions (<1 mg) of the lignites were precisely weighed into a clean quartz tube using a Mettler Microbalance Model M5 (accuracy approximately ± 0.002 mg). Some conventional analyses of the lignite samples are given in Table I.

The heights of the peaks (corresponding to C_1–C_5 *n*-paraffins and C_2–C_5 1-olefins) in the pyrograms and their elution times were compared with those obtained from GC analyses of pure gases and of calibration mixtures containing known amounts of the constituents under investigation. Figure 1 portrays a typical pyrogram.

Peak heights were found to be acceptable indicators of product yields. In the latter stages of this work when an automatic, area integration system (Varian CDS-111) was acquired, peak areas were used for quantitative purposes.

Table I. Analyses of the Lignite Samples Used for Pyrolysis-Gas Chromatography

Sample No.	Origin	Moisture, %	Ash, % (dry basis)	VM,[a] d.a.f., %	FC,[b] d.a.f., %	% C, d.a.f.	% H, d.a.f.	% N, d.a.f.	% Sulfur (dry basis)	BTU/lb (dry basis)
1	Brazos Co.[c]	8.1	35.0	62.9	37.1	69.8	4.8	1.3	3.6	7158
2	Brazos Co.	10.0	26.1	57.5	42.5	68.0	4.8	1.4	3.6	4791
3	Brazos Co.	9.2	28.0	57.6	42.4	83.1	4.9	1.2	3.3	5356
4	Madison Co.	10.2	30.0	57.1	42.9	59.7	3.2	1.3	3.4	7005
5	Marion Co.	10.6	34.3	56.0	44.0	76.0	4.2	1.9	1.6	8070
6	Marion Co.	15.1	23.6	51.7	48.3	60.6	4.2	1.3	1.0	9890
7	Grimes Co.	24.0	20.2	58.0	42.0	73.9	5.1	1.3	2.8	8439
8	Grimes Co.	30.8	20.2	52.1	47.9	76.5	4.9	1.7	2.1	8161
9	Grimes Co.	16.2	20.7	61.2	38.8	66.0	5.3	1.3	2.7	10130
10	"East Texas"	39.4	20.9	51.3	48.7	67.9	5.2	1.1	1.5	10330
11	N. Dakota	38.9	6.2	42.7	51.1	66.8	4.4	1.0	0.4	11060
12	W. Virginia	23.8	8.6	43.9	47.5	64.7	4.4	1.0	0.5	10750

[a] Volatile matter; dry, ash-free basis. [b] Fixed carbon. [c] Texas (samples 1-10).

Table II. Peak Heights[a] (mm) from Pyrolysis Experiments

Sample No.	CH_4	C_2H_4	C_2H_6	C_3H_6	C_3H_8	C_4H_8	C_4H_{10}	C_5H_{10}	C_5H_{12}
1. Peak height	239.7	189.7	127.4	179.1	60.5	99.7	48.5	22.6	34.7
% std dev	9.6	16.3	11.9	15.2	6.3	15.8	12.0	25.2	23.1
2. Peak height	234.4	108.9	87.4	98.7	43.3	59.0	31.0	15.8	20.5
% std dev	3.9	13.0	5.3	11.4	10.9	17.5	11.9	11.4	20.5
3. Peak height	233.1	116.7	93.0	110.5	47.8	61.1	31.2	14.1	20.4
% std dev	22.5	7.4	13.9	8.7	13.8	9.0	11.5	27.0	10.3
4. Peak height	129.5	55.5	43.1	55.2	27.8	35.5	20.7	11.3	14.3
% std dev	20.5	16.0	11.8	14.1	9.0	10.4	33.3	40.7	23.1
5. Peak height	141.8	91.0	67.0	93.5	33.9	49.9	23.0	11.8	17.1
% std dev	22.1	7.6	9.0	10.3	12.4	12.0	11.3	3.4	4.7
6. Peak height	202.9	85.7	66.9	83.7	37.1	50.2	25.4	12.0	17.4
% std dev	4.9	6.7	2.4	5.1	5.7	5.4	2.4	12.5	8.6
7. Peak height	332.1	173.0	145.4	155.9	73.5	102.5	49.6	24.8	33.2
% std dev	4.2	5.2	9.6	5.4	8.4	6.9	10.3	13.7	10.5
8. Peak height	313.3	143.9	125.3	140.0	61.0	81.3	40.7	17.6	26.0
% std dev	10.7	12.7	9.1	4.5	7.2	4.2	6.6	5.7	1.9
9. Peak height	414.4	247.8	196.7	234.6	97.8	140.8	68.3	31.6	43.2
% std dev	16.5	9.1	12.3	12.1	14.7	7.7	15.5	21.8	12.7
10. Peak height	275.3	137.7	107.2	131.1	54.4	77.6	37.3	15.7	26.5
% std dev	9.8	10.3	6.3	10.3	5.1	9.8	1.3	7.0	10.6
11. Peak height	262.5	90.4	68.6	82.6	32.8	46.6	22.2	9.8	16.9
% std dev	33.9	9.2	19.2	4.2	11.9	8.4	15.8	31.6	16.0
12. Peak height	245.6	95.4	74.9	84.8	36.5	47.0	21.9	8.7	16.3
% std dev	0.7	3.9	7.5	8.7	4.9	6.8	8.2	9.2	9.2

[a] mm; arithmetic mean of 3 runs normalized to a 1-mg sample.

For accuracy determinations, quartz tubes containing precisely-weighed amounts (approximately 0.5 mg) of *n*-hexatriacontane ("Quant Grade", Polyscience Corp.) or picolinic acid (pyridine-2-carboxylic acid) were prepared as described above. Eastman practical grade picolinic acid was recrystallized from 95% ethanol, mp 137–138 °C (reported (28) 136–137 °C), dried under vacuum, and finely-powdered before weighing. Pyrolysis products from *n*-hexatriacontane (*n*-C_{36} alkane) were chromatographed on a Poropak Q column using the conditions described above. For picolinic acid pyrolyses, the gas chromatograph was fitted with a 10-ft × $^1/_8$-in. stainless steel column packed with 10% SP-2100 on 100/120 Supelcoport. The flow rates were as previously described. The column was held at 125 °C for 3 min after injection, temperature-programmed at 30 °C/min up to 250 °C, and held at that temperature for 6 min. The injector, detector, interface, and pyrolysis conditions were as listed above. Toluene injections were also made on the SP-2100 column using the conditions outlined previously.

RESULTS AND DISCUSSION

Precision. Three precisely-weighed samples (of approximately equal weight) of each lignite were pyrolyzed (Figure 1). The peak heights (mm) representing the major components, i.e., C_1–C_5 *n*-paraffins and 1-olefins, were normalized for a 1-mg sample. It is noteworthy that acetylene was never observed as a pyrolysis product.

Table III. 1200 °C Pyrolysis of Lignite Sample No. 8

Product	% std dev (pk. ht.)[a]	Product	% std dev (pk. ht.)[a]
CH_4	6.2	C_4H_8	1.3
C_2H_4	8.6	C_4H_{10}	3.0
C_2H_6	2.7	C_5H_{10}	25.4
C_3H_6	5.6	C_5H_{12}	12.7
C_3H_8	7.3		

[a] Three replicates.

The data were processed to obtain the arithmetic mean peak height and the percent standard deviation. These results are listed in Table II. For some lignite samples, the percent standard deviations were quite low (e.g., samples 6 and 12) while for others, the values were quite high (e.g., samples 1 and 9).

Since pyrolytic studies of pure standards revealed better reproducibility for pyrolysis at 1200 °C (vide infra), this temperature was applied to a lignite sample. Three portions of sample number 8 (Table I) were pyrolyzed as before, except that the final temperature was 1200 °C. Except for the two higher hydrocarbons (C_5), the standard deviation values were below 10% (Table III). This level, although not thoroughly

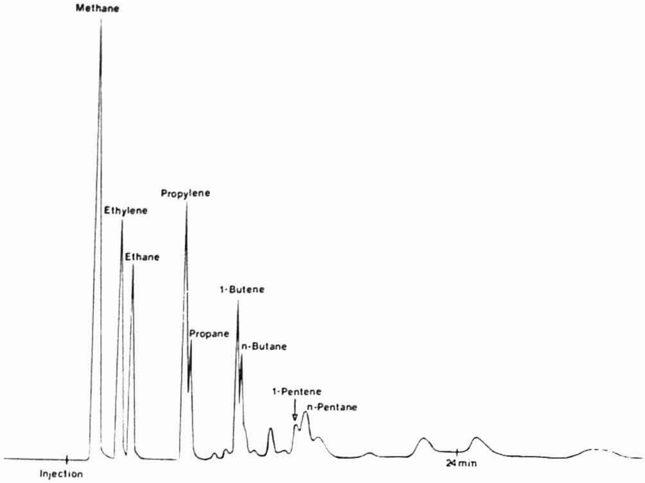

Figure 1. Gas chromatogram from lignite pyrolysis

Table IV. Pyrolysis–Gas Chromatography Data from *n*-Hexatriacontane

	850 °C		1200 °C	
Product	% S.D.[a] (area)	% S.D. (pk. ht.)	% S.D. (area)	% S.D. (pk. ht.)
CH_4	16.3	11.1	4.3	8.1
C_2H_4	13.2	14.2	2.7	6.5
C_2H_6	13.7	13.6	13.0	11.9
C_3H_6	15.8	12.6	3.3	10.1
C_3H_8	10.0	10.3	3.3	5.2
C_4H_{10}	14.3	14.0	8.9	9.2
C_5H_{12}	10.1	10.5	15.3	14.8
Average	13.3	12.3	6.8	9.4

[a] Standard deviation, 3 replicates.

satisfying, is in accord with similar work. Hanson and coworkers (*29*) recently reported deviations of about 10% in the product yields from laser pyrolysis–gas chromatography of oil shales.

It is desirable to know how much of this variation can be attributed to either the instrument or our technique, and how much (if any) is attributable to the heterogeneous nature of the various lignite samples. The experiments designed to answer these questions are described below.

Tests of Reproducibility of Procedure and Instrument. The pyrolytic decomposition of *n*-hexatriacontane (n-C_{36} alkane) was studied to assess the reproducibility of our pyrolysis procedure using a pure, homogenous substrate (which lignite is not!). The C_1–C_5 *n*-alkanes and 1-alkenes produced thereby were monitored by peak height measurements from the chromatograms, and by area determinations.

Three precisely-weighed samples (of approximately equal weight) were pyrolyzed at 850 °C under the conditions used for lignite pyrolysis. Three similar pyrolyses were carried out at 1200 °C. The product peak heights and areas were normalized to a 1-mg sample, and the percent standard deviations of the normalized data are shown in Table IV. The results were more reproducible at 1200 °C, reaching a maximum reproducibility for ethylene (percent standard deviation = 2.7, from area measurements).

Table V. Reproducibility of Toluene Injections

Sample No.	Peak ht. (mm)	Arithmetic mean	% std dev
1	89.50	89.50	3.9
2	86.00		
3	93.00		

Table VI. Picolinic Acid Pyrolysis Data

Sample No.	Wt. (mg)	Pyridine peak ht. (mm), 1 mg	Arithmetic mean	% std dev[a]
1	0.485	275.3	260.10	10.6
2	0.459	289.8		
3	0.585	246.2		

[a] Three replicates.

Three 1.1-μL injections of toluene were made through the gas chromatograph under the same conditions as above (but without pyrolysis). The reproducibility of the toluene peak heights was taken as a measure of the maximum error (since syringe error is included) in reproducibility of the GC detector. These data are in Table V.

In cases where the percent standard deviation for *n*-hexatriacontane pyrolysis products exceeds 3.9% (Table IV), the excess may be taken as a measure of the instrumental/operational error. In cases where the standard deviation values for lignite pyrolysis products (Table II) exceed corresponding values for *n*-hexatriacontane pyrolysis, the excess may be attributed to the heterogeneous nature (at the molecular level) of the particular lignite sample under investigation, or to variable amounts of adsorbed atmospheric moisture.

As an additional check of the reproducibility of our procedure, picolinic acid (pyridine-2-carboxylic acid) was pyrolyzed. Picolinic acid is known (*30*) to undergo thermal degradation to pyridine and carbon dioxide. Three samples of approximately equal weight were pyrolyzed at 850 °C and the peak heights corresponding to pyridine were measured and normalized to 1 mg. The arithmetic mean and percent

Table VII. Yields of Pyrolysis Products (850 °C for 20 s) from Lignite Sample No. 8

Product	% yields[a]	Product	% yields[a]
CH_4	4.4	C_4H_8	1.4
C_2H_4	1.8	C_4H_{10}	2.6
C_2H_6	1.5	C_5H_{10}	0.3
C_3H_6	1.5	C_5H_{12}	0.6
C_3H_8	0.8		

[a] Average of three replicates; not corrected for adsorbed moisture.

Table VIII. Weight Loss upon Pyrolysis (850 °C for 20 s)

Sample No.	% weight loss	% std dev
1	31.1	0.5
2	47.0	7.2
3	38.1[a]	7.1
4	39.7	19.9
5	28.2	4.3
6	29.9	13.9
7	36.1[a]	14.9
8	47.3	4.9
9	46.9[a]	8.4
10	41.6	15.1
11	40.7[a]	8.4
12	36.9[a]	3.8

[a] Arithmetic mean of two runs (others were three replicates).

standard deviation of the normalized peak heights are shown in Table VI. These results compare favorably with the percent standard deviation data from the 850 °C *n*-hexatriacontane pyrolysis.

Yields of Pyrolysis Products. Using known amounts of pure gas standards, the yields of pyrolysis products were determined. The yield averages, which must be regarded as approximate, are listed in Table VII. Repyrolysis of the samples gave more of the same products; therefore it is recognized that the yields expressed in Table VII are not maximized. The data in Table VII have not been corrected to allow for the presence of adsorbed moisture in the lignite samples; thus the actual yields are somewhat higher.

Weight Loss upon Pyrolysis. The tared samples were weighed before and after pyrolysis and the percent weight loss is shown in Table VIII as the arithmetic mean of three runs. A large portion of the weight lost was due to adsorbed water. Investigations are in progress to identify all the major pyrolysis products.

CONCLUSION

We have developed a rapid pyrolysis–gas chromatography technique for the characterization and "screening" of lignites. Only about 0.5 h (excluding weighing time) and 0.5 mg of lignite are required for each analysis, and the production of a number of important products can be monitored. Significant differences in hydrocarbon ratios and yields can be discerned among the various lignite samples (Table II). Such data may be useful in evaluating lignites for commercial coal projects. Work is in progress to extend this technique to coals of all ranks. In addition, these procedures are being extended to monitor the production of higher molecular weight products.

The pyrolysis–gas chromatography system described herein should be quite versatile in application. The reproducibility is good for a multicomponent system of this sort, as evidenced by the pyrolyses of *n*-hexatriacontane and picolinic acid. As we have shown, the reproducibility is acceptable even when pyrolyzing lignite, a complex, irregular polymer of indefinite structure. Preliminary data indicate the utility of this technique for pyrolytically "screening" various organic wastes (e.g., cotton gin wastes, bovine manure) as potential sources of hydrocarbons for fuel and chemical usage.

ACKNOWLEDGMENT

We are grateful to the Texas Municipal Power Pool, C. Matthewson, R. Anthony, and W. Sackett for furnishing lignite samples.

LITERATURE CITED

(1) J. B. Robertson, "Chemistry of Coal", Van Nostrand, New York, 1919, Chapter V.

(2) H. C. Howard in "Chemistry of Coal Utilization", Vol. 1 (1945) and Suppl. Vol. (1963), H. H. Lowry, Ed., Wiley, New York.

(3) G. A. Mills, *Ind. Eng. Chem.*, **61**, 6 (1969).

(4) "Project Western Coal: Conversion of Coal into Liquids", Report No. OCR/R&D, 18/Final, from the Department of Mineral Engineering, University of Utah, to the Office of Coal Research, Washington, D.C., May 1970.

(5) "Coal Gasification", L. G. Massey, Ed., *Adv. Chem. Ser.*, **131**, 1974.

(6) A. J. Forvey et al., "The Synthane Coal-to-Gas Process", from the IGT Symposium on Clean Fuels from Coal, Sept. 10–14, 1973, Chicago, Ill.

(7) G. A. Mills, *Environ. Sci. Technol.*, **5**, 88 (1971).

(8) H. W. Holden and J. C. Robb, *Nature (London)*, **182**, 340 (1958).

(9) H. W. Holden and J. C. Robb, *Fuel*, **39**, 385 (1960).

(10) A. G. Sharkey, Jr., J. L. Shultz, and R. A. Friedel, *Fuel*, **40**, 423 (1961).

(11) A. G. Sharkey, Jr., J. L. Shultz, and R. A. Friedel, *Carbon*, **4**, 365 (1966).

(12) H. Jüntgen and K. H. van Heek, *Fuel*, **47**, 103 (1968).

(13) M. Vahrman and R. H. Watts, *Fuel*, **51**, 130 (1972).

(14) R. L. Hanson, N. E. Vanderborgh, and D. G. Brookins, *Anal. Chem.*, **49**, 390 (1977).

(15) W. K. Joy, W. R. Ladner, and E. Pritchard, *Fuel*, **49**, 26 (1970).

(16) A. F. Granger and L. R. Ladner, *Fuel*, **49**, 17 (1970).

(17) R. A. Graff, S. Dobner, and A. M. Squires, *Fuel*, **55**, 109, 113 (1976).

(18) S. C. Chakravartty, D. Dutta, and A. Lahiri, *Fuel*, **55**, 43 (1976).

(19) J. Romováček and J. Kubát, *Anal. Chem.*, **40**, 1119 (1968).

(20) R. L. Coates, C. L. Chen, and B. J. Pope, *Adv. Chem. Ser.*, **131**, 92 (1974).

(21) P. S. Groom, *Fuel*, **48**, 161 (1969).

(22) C. Barker, *Am. Assoc. Petrol. Geol. Bull.*, **58**, 2349 (1974).

(23) C. Barker, *Fuel*, **53**, 176 (1974).

(24) H. S. Rao et al., *Fuel*, **52**, 168 (1973).

(25) A. F. Gaines and Y. Yurum, *Fuel*, **55**, 129 (1976).

(26) D. Gray, J. G. Cogoli, and R. Essenhigh, *Adv. Chem. Ser.*, **131**, 72 (1974).

(27) M. Papic, *J. Gas Chromatogr.*, **6**, 493 (1968).

(28) I. Heilbron and H. M. Bunbury, Ed., "Dictionary of Organic Compounds", Vol. 4, Oxford University Press, New York, N.Y., 1953.

(29) R. L. Hanson, D. Brookins, and N. E. Vanderborgh, *Anal. Chem.*, **48**, 2210 (1976).

(30) *cf.*, E. V. Brown and R. J. Moser, *J. Org. Chem.*, **36**, 454 (1971).

RECEIVED for review April 25, 1977. Accepted May 27, 1977. We are indebted to the Center for Energy and Mineral Resources, Texas A&M University, for the financial support of this work.

Generation of Nitrosamines for Gas Chromatographic Analysis via Direct Injection

D. J. Freed* and A. M. Mujsce

Bell Laboratories, 600 Mountain Avenue, Murray Hill, New Jersey 07974

Techniques for in situ generation of nitrosamines for chromatographic analysis are described. Using amine salt precursors, reaction on potassium nitrite precolumns affords high (greater than 95%) and reproducible yields of the corresponding nitrosamines in the 10- to 100-ng range.

Although the estimation of nitrosamines is an extremely important subject, in which much interest has been generated, the extraordinary toxicity of these compounds renders the preparation of standards extremely hazardous (*1–3*). Recently, we have demonstrated that it is possible to generate precisely controlled amounts of toxic or hazardous materials directly in the injection port of a gas chromatograph (*4*). Application of this in situ method circumvents the necessity for storage and manipulation of these potent carcinogens and facilitates the preparation of accurate (±3%) trace level comparison standards (in the 10- to 100-ng range). This report describes techniques and methods for generating submicrogram amounts of nitrosamines for gas chromatographic analysis.

EXPERIMENTAL

Instrumentation. A Varian MAT 112 Gas Chromatograph–Mass Spectrometer was used for all investigations. Chromatograms were recorded by use of a second ionizer operated at 20 eV with detection by means of a Faraday cup and dc amplifier. The column used for this work was 2 m by 3.2 mm (stainless steel) packed with Chromosorb 103 (100–120 mesh). Injections were made with Hamilton 7101 syringes which had been gravimetrically calibrated with mercury. These were found to be reproducible to ±1.8% for a 0.5-μL injection.

Materials. Morpholine, pyrrolidine, piperidine, and diethylamine were purchased from Aldrich, Inc., and redistilled before use. Dimethylamine (gaseous) was purchased from Linde, Inc., and used directly. Standard solutions of the above (in the range 0.1 to 1.0 mg/mL) were prepared by dissolution in water and titration with 0.1 M HCl. Diethyl nitrosamine was prepared in small amounts (ca. 5 mg) using glove box techniques (*5*). Standards were prepared from the above material using a sealed ampoule technique (*6*). Precolumns were constructed from Teflon tubing (8 cm by 6 mm o.d.), packed with 1 g of ACS Reagent Grade KNO_2, plugged with glass wool at each end, and preconditioned at 200 °C for 12 h before use.

RESULTS AND DISCUSSION

The generation of nitrosamines is easily accomplished by direct injection of the corresponding amine salt onto a suitably prepared precolumn of KNO_2. Solutions of the desired amine were prepared by dilution of a freshly prepared and standardized master solution with 1 *M* sulfuric acid. These solutions gradually decreased in strength (after two weeks 90% of the original amine was still present) and therefore, for highest accuracy, periodic restandardization by titration was employed. Attempts to use the amines as their hydrochloride salts led to poor reproducibility. We attribute this to the volatilization of the amine hydrochloride which results in incomplete reaction with the KNO_2. Table I lists nitrosamines prepared by this technique together with absolute yields obtained for diethyl nitrosamine generation. These latter were obtained as follows. Aqueous solutions of chromatographically pure diethyl nitrosamine were prepared in the range 10 to 100 μg/mL by gravimetry and suitable dilution. A calibration plot of total integrated ion current in the nitrosamine peak was obtained for amounts from 10 to 100 ng. Aliquots of the diluted diethylamine sulfate solution were then injected and the integrated total ion currents under the generated nitrosamine peak were also plotted on the same graph after correction by the gravimetric factor for the reaction stoichiometry (for the case of diethyl nitrosamine this is 0.716 for the reaction $Et_2NH + HONO \rightarrow Et_2NNO + H_2O$). These curves are shown in Figure 1a. In order to ensure that the nitrosamine did not react with KNO_2, amounts from 5 to 50 ng were injected onto both packed and empty precolumns. No differences greater than 2% in the measured peak areas could be seen (cf. Figure 1a). The yields exhibited little dependence on either injector temperature (in the range 180 to 250 °C) or on flow rates (in the range 10 to 30 mL/min). Therefore these parameters were chosen so as to optimize column efficiencies.

Table I. Yields and Conditions for Generation of Nitrosoamines[a]

Compound	Amount generated, nmol	Yield	t'_R, min
N-Nitrosodiethylamine	0.86	95 ± 3%	3.7
	0.66	94 ± 3%	
	0.44	94 ± 3%	
	0.22	94 ± 3%	
N-Nitrosodimethylamine		*b*	1.5
N-Nitrosopyrrolidine		*b*	11
N-Nitrosopiperidine		*b*	12.6
N-Nitrosomorpholine		*b*	10.6

[a] The column was operated at 220 °C with a helium flow rate of 20 mL/min. The injector port temperature was 200 °C. [b] See text.

The efficiency of nitrosamine generation depends strongly on the acid concentration of the precursor amine solution. A plot of relative yields as a function of sulfuric acid concentration is shown in Figure 1b. As expected, increasing acid concentrations favor increased yields (i.e., by ensuring an adequate generation of nitrous acid); however, too strong an acid concentration actually lowers the yields. This is due to the reverse reaction of the nitrosamine with acid to regenerate the original amine salt. For this work, an optimum acid concentration was found to be 1 M. At this concentration the absolute yield of diethyl nitrosamine was high and reproducible (95 ± 3% in the range from 10 to 100 ng). Precolumns were found to be stable for approximately 30 injections and, as also expected, lifetimes decreased drastically at higher acid concentrations.

Although a mass spectrometer was used as a detector, it was not feasible to use single ion monitoring at the parent peak for high sensitivity detection of the nitrosamines. A previous

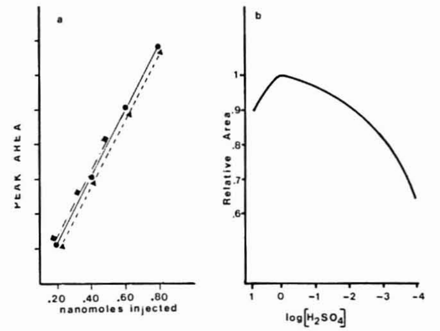

Figure 1. (a) Calibration curve for generation of diethyl nitrosamine. Gravimetrically prepared standard (—). Generated standard (- - -). Gravimetric standard on unpacked precolumn (-·-). (b) Yield vs. solution pH for 50 ng of generated diethyl nitrosamine

report (*7*) demonstrates, and we have confirmed, that at ion source temperatures much above 100 °C thermal decomposition is evident, resulting in loss of NO and much variability in the parent peak intensity. During our work, it was possible to ensure that the method results in nitrosamine production by operating the source at 60 °C. However, because of the low volatility of the nitrosamines, condensation in the source quickly resulted in high backgrounds at this temperature. Therefore measurements were made at a source temperature of 200 °C. The resulting mass spectra were those of the amine portion of the nitrosamine, although they appeared at the GC retention time of the authentic nitrosamine.

In this work, other nitrosamines have not been synthesized directly for absolute yield studies. However, comparison of the measured ion currents from the respective nitrosamines generated in situ with that of diethylamine (for which the sensitivities should be similar) suggests that the efficiency of generation for all amines tested should be well over 90%.

LITERATURE CITED

(1) G. Hawksworth and M. J. Hill, *Biochem. J.*, **122**, 28 (1970).
(2) N. P. Sen, *J. Chromatogr.*, **51**, 301 (1970).
(3) D. H. Fine, D. Lieb, and F. Rufeh, *J. Chromatogr.*, **82**, 291 (1973).
(4) D. J. Freed and A. M. Mujsce, *Anal. Chem.*, **49**, 139 (1977).
(5) A. I. Vogel, "A Textbook of Practical Organic Chemistry", 3rd ed. John Wiley & Sons, New York, N.Y., 1966, p 426.
(6) S. Siggia, "Quantitative Organic Analysis via Functional Groups", John Wiley and Sons, New York, N.Y., 1963, Chap. 26.
(7) G. Schroll, R. G. Cooks, P. Klemmenses, and S.-O. Lawesson, *Ark. Kemi*, **28**, 413 (1967).

RECEIVED for review April 18, 1977. Accepted June 13, 1977.

Determination of Intact Oxazepam by Electron Capture Gas Chromatography after an Extractive Alkylation Reaction

Jörgen Vessman,*[1] Margareta Johansson, Per Magnusson, and Signhild Strömberg

AB KABI, Research Department, Analytical Chemistry, Fack, S-112 87 Stockholm, Sweden

Oxazepam was converted to an N_1,O_3-dimethyl derivative in an extractive alkylation reaction. The derivative was quantitated by electron capture gas chromatography using lorazepam as an internal standard. Concentrations down to 1 ng/mL could be determined. At the 25 ng/mL level 98.4 ± 3.2 % were recovered. Serum samples taken after administration of diazepam or clorazepate contained measurable concentrations of oxazepam after 2 to 4 h. The dialkyl derivatives of the two benzodiazepines, especially that of lorazepam, are converted to isomeric derivatives with high concentrations of the quaternary ammonium hydroxide in the organic phase. The conditions which give quantitative formation without isomerization are discussed.

The 1,4-benzodiazepines are a widely used class of drugs. The compounds have been assayed in biological fluids by various techniques, but gas chromatography (*1*) and polarography (*2*) are the principal ones. The bioanalytical field has been reviewed (*3*).

The gas chromatographic techniques used in the early sixties were based on the product of hydrolysis, e.g. aminochlorobenzophenone (*4*). The sensitivity of electron capture detection was good, but the selectivity could be doubtful in some cases because of the interferences of metabolites yielding the same hydrolysis product. Direct determinations for diazepam and medazepam were introduced by de Silva (*5*).

Oxazepam cannot be determined directly as it undergoes ring contraction when injected into the gas chromatographic column. The product of the rearrangement, a quinazoline derivative, has a shorter retention time than that of the unchanged benzodiazepine, but the gas chromatographic properties of the compound make analysis difficult below about 50 ng/mL. The structure of oxazepam favors ring contraction. However, alkylation at the N_1 position or absence of the 3-hydroxy group or derivatization of this group will give thermally stable derivatives (*6*).

The present paper describes a procedure for dialkylation of oxazepam by an extractive alkylation procedure and its subsequent determination by electron capture gas chromatography.

EXPERIMENTAL

Apparatus. A Varian Model 1400 gas chromatograph with a scandium type electron capture detector was used with a 1.5 m × 1.8 mm glass column, filled with 3 % OV-225 on Chromosorb G (100–120 mesh, acid washed and silanized). The column temperature was kept at 265 °C after conditioning with gas flow for 2 h at 290 °C. The detector temperature was 300 °C. The nitrogen flow rate was 30 mL/min. The mass spectra with electron impact ionization were run in an LKB 9000 gas chromatograph mass spectrometer with an ionization energy of 70 eV. The gas chromatographic column was as indicated above, but used with a helium flow of 20 mL/min at 250 °C. The mass spectra with chemical ionization were run in an LKB 2091 instrument with

---

[1] Present address AB HAESSLE, Fack, S-431 20 Mölndal, Sweden.

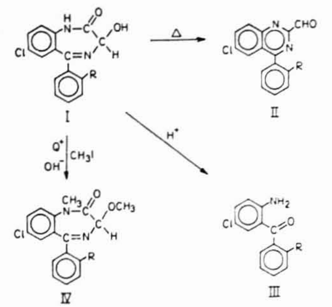

Figure 1. Structures of the compounds involved. R = H oxazepam, R = Cl lorazepam. (I) Benzodiazepine, (II) quinazoline-carboxaldehyde obtained after thermal rearrangement, (III) benzophenone obtained after hydrolysis, (IV) N_1,O_3-dimethylated benzodiazepine

isobutane at 0.5 mm Hg and an ionization energy of 300 eV.

Reagents. Methylene chloride and toluene, both of analytical quality, Merck, Darmstadt, German Federal Republic, were used. Methyl iodide was analytical quality, redistilled. Oxazepam was obtained from AB KABI, Stockholm, Sweden. Lorazepam was obtained from Wyeth Laboratories Inc., Radnor, Philadelphia, Pa. Tetrahexylammonium hydrogen sulfate (THA) was obtained from AB HAESSLE, Mölndal, Sweden.

Standard Solution: A solution containing 500 ng/mL of oxazepam in methylene chloride was prepared.

Internal Standard Solution. A solution containing 500 ng/mL of lorazepam in methylene chloride was used.

Tetrahexylammonium Hydrogen Sulfate. THA, 0.1 M; 4.51 g are dissolved in and diluted to 1 L with 0.1 M sodium hydroxide.

Methyl Iodide. 4 M; 14.2 g (6.2 mL) of methyl iodide are diluted to 25 mL with methylene chloride.

Saturated Silver Sulfate Solution. A small amount of Ag_2SO_4 ($\sim$25 mg) is shaken with $\sim$20 mL of water and heated on a boiling water bath. Prepared fresh each time it is used.

All centrifuge tubes were washed with chromium trioxide in acetic acid containing 6% (w/v) sulfuric acid (7) and then rinsed with ethanol.

Procedure for Determination of Intact Oxazepam in Serum. (1) A dilution of serum ($\leq$2 mL) corresponding to 5 to 50 ng of oxazepam is diluted with 4 mL of a phosphate buffer, pH 7.4. Then 50 μL of internal standard solution are added and the compounds are extracted into 8 mL of methylene chloride for 15 min.

(2) After centrifugation the organic layer is filtered through silanized glass wool in a Pasteur pipet into a 12-mL centrifuge tube and then evaporated to dryness.

(3) The tubes are cooled and 1.5 mL of 4 M methyl iodide and 0.5 mL of 0.01 M THA (pH 13) are added. The mixture is shaken for 5 min.

(4) The organic layer is filtered through silanized glass wool into a centrifuge tube (10 mL) with a tapered bottom section with a volume of about 200 μL. The solvents are evaporated.

(5) One mL of hot, saturated silver sulfate solution is added to the residue which is dissolved by vortexing for 10 s on a Vibromixer.

(6) One-tenth mL of toluene is added and vibrated in a Vibromixer for 10 s.

(7) One to two μL of the toluene layer are injected into the gas chromatograph.

A standard curve is prepared from the peak area ratio vs. the weight ratio obtained from the analysis of known amounts of oxazepam and lorazepam. 0, 15, 30, and 60 μL of the oxazepam standard solution, (i.e., 7, 5, 15, and 30 ng) and 50 μL of the lorazepam standard solution (= 25 ng) are added to four centrifuge tubes together with 0.2 to 0.5 mL of a blank serum.

RESULTS AND DISCUSSION

The aim of this study was to make possible the gas chromatographic determination of oxazepam without ring contraction or hydrolysis. The structure of oxazepam favors ring contraction, which has also been shown to occur with the analogue lorazepam and with 3-hydroxynitrazepam (*8*). For structures see Figure 1. Substitution at the N_1 position will prevent this reaction, cf. 3-hydroxydiazepam.

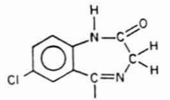

N_1-Desmethyldiazepam

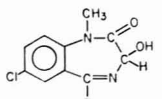

3-Hydroxydiazepam

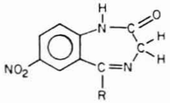

Nitrazepam

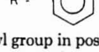

Absence of the hydroxyl group in position 3 also excludes ring contraction, cf. *N*-desmethyl diazepam (nordiazepam) and nitrazepam. Simple silylation of the 3-hydroxy group giving thermally stable derivatives has recently been described by de Silva (*6*). The introduction of alkyl groups on the N_1 nitrogen can be effected easily by extractive alkylation as shown by Ehrsson and Tilly for nitrazepam (*9*) and by de Silva et al. for clonazepam (*10*). One alkyl group was introduced into these benzodiazepines. The presence of the hydroxyl group in position 3 of oxazepam may, however, also give rise to O-alkylation. This would indeed be favorable as compounds like, for instance, 3-hydroxydiazepam have rather poor gas chromatographic properties. By extractive alkylation, more than one alkyl group can be introduced as has been clearly demonstrated by Ervik and Gustavii (*11*) by the introduction of four alkyl groups into chlorothalidon.

Initial experiments in extractive alkylation with oxazepam and lorazepam in particular showed that the formation of single derivatives was not readily accomplished. Instead, a mixture of two derivatives in varying proportions was obtained with each of the benzodiazepines.

The yields in the studies of effects of pH, quaternary ammonium ion, and alkyl iodide concentration were determined with microgram amounts of the two benzodiazepines using a hydrocarbon, hexatriacontane, as reference substance and flame ionization detection.

Identification of the Alkylated Derivatives. Two products were obtained from each benzodiazepine. The derivative formed first (derivative 1) had the longer retention time (See Table I). It was identified as a dimethylated derivative by gas chromatography and mass spectrometry. By comparison with *O*-methylated 3-hydroxydiazepam, available as a reference substance, it was established that both N_1- and O_3-methylation had occurred with oxazepam.

The second derivative appearing in the reaction mixture (derivative 2) and having a shorter retention time (See Table I), was shown by gas chromatography–mass spectrometry (electron ionization and chemical ionization) to have the same molecular weight as derivative 1.

The electron ionization mass spectra of derivatives 1 and 2 were almost identical. All derivative 1 compounds exhibited the expected molecular ion M^+. The dimethyl derivatives of oxazepam showed *m*/*e* 271 as the base peak which is the same as reported for *N*-methyloxazepam (or 3-hydroxydiazepam) (*8*). The corresponding base peak in the dimethyl lorazepam derivative was *m*/*e* 305.

Table I. Relative Retention of Oxazepam and Lorazepam Alkyl Derivatives

	Oxazepam	Lorazepam
Rearrangement product	0.66	0.85
Methyl derivative 1[a]	2.02	2.76
Methyl derivative 2	0.98	1.20
Ethyl derivative 1	1.62	2.47
Ethyl derivative 2	0.84	1.13
Hexatriacontane	1.02	
Diazepam[b]	1.00	
Temazepam (3-hydroxydiazepam)	3.73	

[a] For structure see Figure 1, IV. [b] Diazepam has a retention time of 4.5 min on a column of 1% OV-225 on Chromosorb G at 265 °C.

Extractive Alkylation. The extractive alkylation process can be described as a two-step reaction, in which the anion, X^- of an acid HX (e.g., oxazepam), is first extracted as an ion pair with a suitable quaternary ammonium compound, Q^+, into an organic phase where the alkylation then takes place.

$$X^- + Q^+ \rightleftarrows QX_{org} \qquad \text{Step 1, extraction (1)}$$

$$QX_{org} + RI_{org} \rightarrow RX_{org} + QI_{org} \qquad \text{Step 2, alkylation (2)}$$

The concentration of QX in the organic phase, QX_{org} is governed by the partition ratio expressed as

$$D_{QX} = E_{QX}[Q^+] \qquad (3)$$

where E_{QX} is the extraction constant for the ion pair (*12*). It is seen from this equation that the partition of the ion pair into the organic phase can be regulated by both the concentration of the quaternary ammonium compound in the aqueous phase, $[Q^+]$, and its chemical nature. The more lipophilic the counter ion, Q^+, the easier the ion pair will partition into the organic layer and the more rapidly will the alkylation reaction proceed (*13*). In this study it was necessary to use tetrahexylammonium (THA) as the counterion, as tetrabutylammonium required too long a reaction time.

If the ion pair and the undissociated acid simultaneously are partitioned to the organic phase, this will decrease the reaction rate as the ion pair is a considerably more reactive species in solvents like methylene chloride (*13, 14*). In ion pair extraction this coextraction of the acid can be treated as a side reaction with the use of α coefficients as discussed in detail by Modin and Schill (*12*).

The conditional extraction constant, $E_{QX}{}^x$, is related to the true extraction constant, E_{QX}, in the following way if the undissociated acid is extracted simultaneously.

$$E_{QX}{}^x = E_{QX} \times \frac{1}{1 + \dfrac{a_H + (1 + k_{dHX})}{K'_{HX}}} \qquad (4)$$

where k_{dHX} is the partition coefficient for the acid HX with the apparent dissociation constant K_{HX}'.

The pK_a values of oxazepam have been reported to be 1.7 and 11.6 and those of lorazepam 1.3 and 11.5 (*15*). The site of deprotonation has been discussed by Hagel and Debesis (*16*). After comparisons with structurally related compounds, these authors concluded that the slightly acidic hydrogen on the amide function (N_1) is responsible for the value around 11.5 and the azomethine nitrogen for the value around 1.5. The amide anion is thus the ion pair forming form.

From distribution data in a previous study (*17*), k_d for oxazepam (CH_2Cl_2) was calculated to be 100. This means that at pH = pk = 11.5, $E_{QX}{}^x$ is only $^1/_{100}$ of E_{QX}.

A pH of pk + 2 would, however, give negligible influence from the acid. It was found in practice that the yields of the dialkylated benzodiazepines increased up to about pH 13. Higher pH values favored the formation of derivative 2 from derivative 1, especially for lorazepam.

The tendency to form the rearranged dimethylated product was most apparent with lorazepam, the more lipophilic compound, and was clearly influenced by the THA concentration and the pH of the aqueous phase. The isomerization was negligible when pH was 13 and the concentration of THA 0.01 M. This indicates that the formation of derivative 2, the isomer, is dependent on the amount of THA hydroxide present in the organic phase.

$$(THA^+)_{aq} + (OH^-)_{aq} \rightleftarrows (THA^+ \, OH^-)_{org} \qquad (5)$$

The extraction constant for this ion pair has been determined by Nordgren and Modin (*18*) to be ~10, which gives a concentration of 5×10^{-3} or more in the organic phase in a typical experiment.

In experiments with the dimethyl derivative 1 of lorazepam (prepared by the analytical procedure) in methylene chloride *without* any alkylating agent present and with an aqueous phase of 0.05 M THA at pH 13, it was found that derivative 1 completely disappeared in 10 min with the simultaneous appearance of derivative 2. With oxazepam this isomerization process was considerably slower. After 3 h more than 75% of the dimethyl derivative 2 had formed.

These findings verified that the isomerization was dependent on the presence of the hydroxide ion pair in the organic phase.

Isomerization could also occur when the reaction mixture was evaporated to dryness, as during this operation the concentration of the THA hydroxide increased as well as the temperature, resulting in unreliable yields. This could be prevented by shaking the reaction mixture before evaporation with an acidic aqueous phase. However, under the conditions used in the method, this acid washing step could be omitted.

Methyl iodide was used as alkylating agent. To obtain constant yield from lorazepam and oxazepam, the concentration of the iodide in methylene chloride had to be 1 and 4 M, respectively. The reaction was complete in less than 5 min at room temperature. Ethyl iodide required 15 min with otherwise equal conditions.

The dimethyl derivatives 1 were very rapidly formed. None of the N_1-monoalkylated derivatives (e.g., 3-hydroxydiazepam) were observed under the experimental conditions employed. It was also found that 3-hydroxydiazepam did not react at all under the experimental conditions. 3-Hydroxydiazepam (N_1-methylated oxazepam) does not form an ion pair and is therefore not a probable intermediate during the course of the reaction from oxazepam to the dialkylated derivative. Both alkyl groups are therefore most probably introduced into oxazepam simultaneously.

Of the two benzodiazepines it was always possible to convert lorazepam derivative 1 into 2, whereas oxazepam was most easily retained as derivative 1. Conditions which yielded only derivative 1 were therefore chosen in the procedure.

Gas Chromatographic Properties. The gas chromatographic properties of the alkylated products were excellent. Compared with the rearrangement product, the adsorption phenomena are eliminated. The high column temperature used is a drawback, however, as the stationary phase is depleted from the support, which shows up in the form of tailing and, finally, adsorption effects. The life time of the column was two to three weeks. A gas chromatogram is shown in Figure 2.

The relative retention times for the various derivatives, including the rearrangement products, are given in Table I. It can be seen that the ethyl derivatives have shorter retention times than the corresponding methyl compounds. 3-Hydroxydiazepam does not undergo alkylation and will not interfere as such.

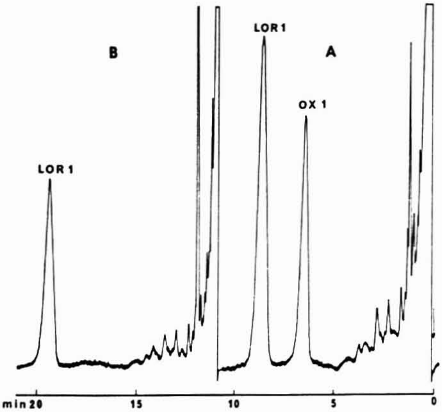

Figure 2. Gas chromatogram of derivatives from a serum extract. (A) Dimethyloxazepam (=OX 1) from a sample containing 197 ng/mL of oxazepam. (B) Serum blank. (LOR 1 = dimethyllorazepam)

The detectability of the dimethyl derivative 1 of oxazepam expressed as MDQ (Minimum Detectable Quantity) was 7×10^{-15} mol/s in the electron capture detector used (*17*). This corresponds to $\sim$60 pg injected onto the column (retention time 7 min).

Elimination of Interference from THA. The presence of residual amounts of the quaternary ammonium iodide caused interferences such as broad solvent peaks already noticeable with the flame ionization detector. Ehrsson removed these by treating the mixture with silver sulfate (*19*). This approach was utilized here with the modification of heating the silver sulfate solution on a boiling water bath. This decreased the influence of the tailing solvent front considerably.

Interferences. When oxazepam is assayed in samples obtained after the administration of diazepam, the metabolites *N*-desmethyldiazepam and 3-hydroxydiazepam are present in addition to oxazepam. Under the experimental conditions the *N*-demethylated compound yielded diazepam, whereas the hydroxylated one was found to be unaffected. This metabolite has a longer retention time (Table I). No interference is therefore involved.

Under the present conditions the method cannot measure diazepam and *N*-desmethyldiazepam simultaneously with oxazepam. By the use of another alkyl halide, preferably *n*-butyl iodide (cf. *20*), it would be possible to determine diazepam, *N*-desmethyldiazepam, and oxazepam in the same sample.

Quantitative Applications to Serum Samples, Recovery and Precision. The alkylation procedure was applied to methylene chloride extracts from human serum samples.

The conditions for the extraction of oxazepam from serum were as outlined in the hydrolysis procedure for oxazepam (*17*). Under the present conditions quantitative analysis was possible down to about 1 ng/mL. The relative recovery at 25 ng/mL was $98.4 \pm 3.2\%$.

It was found that standard curves from plain aqueous solution and from serum were linear but did not coincide. The standard curves were therefore always prepared with the addition of 0.2 to 0.5 mL of blank serum. Experiments with ^{14}C oxazepam showed that the difference was due to a slight loss (about 5% for 2 mL of serum) of oxazepam in the extraction step when serum was present. The decrease in recovery depended on the amount of serum. Most probably this loss was due to incomplete recovery of the organic phase from the interface formed in the presence of the serum sample, an effect that the internal standard apparently did not fully compensate for.

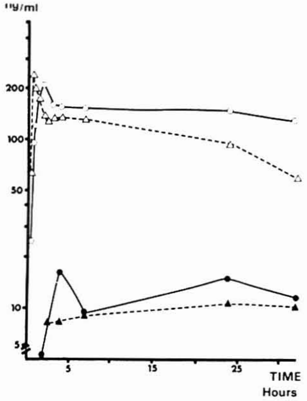

Figure 3. Serum levels of oxazepam after single dose administration of diazepam and clorazepate. ○ = Diazepam (5 mg p.o.). △ = *N*-desmethyldiazepam (after clorazepate 10 mg p.o.). ● = Oxazepam after diazepam dose. ▲ = Oxazepam after clorazepate dose. Diazepam and *N*-desmethyldiazepam analyzed according to Wretlind et al. (*20*)

The alkylation reaction was found to be more than 99% complete with reference to the standard compound, N_1,O_3-dimethyloxazepam. The alkylation reaction was complete within 2 min for extracts, both from water and serum.

Twenty-one samples analyzed with the hydrolytic procedure (*17*) one month before were analyzed with the present method. A plot of the oxazepam concentrations obtained with the two methods gave a regression line with a slope of 0.90 and a regression coefficient of 0.97. The good agreement between the two methods is not surprising as oxazepam in samples after administration of oxazepam does not give rise to interfering metabolites in the hydrolysis procedure (*17*). It was therefore more interesting to see if the method was sensitive enough to detect oxazepam in serum after the administration of diazepam or clorazepate. These two drugs have oxazepam as the major metabolite. The hydrolytic procedure cannot be applied to samples containing these compounds as the same benzophenone is formed from *N*-desmethyldiazepam (clorazepate) and oxazepam.

Serum samples taken in comparative studies of diazepam and clorazepate with oxazepam (*20*) were analyzed for the presence of oxazepam. As can be seen in Figure 3, the administration of 10 mg of clorazepate (*N*-desmethyldiazepam precursor) rapidly produced measurable concentrations of oxazepam with a peak value after about 4 h. The administration of 5 mg of diazepam produced a slower increase in the concentration of oxazepam, probably due to the fact that in this case two metabolic steps are necessary for the formation of oxazepam.

In monitoring drug levels after administration of oxazepam, the hydrolysis procedure is somewhat easier to handle in practice. However, the alkylation procedure is more rapid and can be used where the hydrolysis method gives rise to interferences. The present method can also be useful for the determination of lorazepam.

ACKNOWLEDGMENT

We thank Ragnar Ryhage for the chemical ionization mass spectra. The gift of Temazepam and Nordiazepam from J. A. F. de Silva, Hoffmann La Roche Inc., as well as ^{14}C oxazepam and N_1,O_3-dimethyloxazepam from Hans W. Ruelius and H. P. K. Agersborg, Jr., Wyeth Laboratories, are gratefully acknowledged.

LITERATURE CITED

(1) D. M. Hailey, *J. Chromatogr.*, **98**, 527 (1974).
(2) M. A. Brooks and J. A. F. de Silva, *Talanta*, **22**, 849 (1975).
(3) J. M. Clifford and W. Franklin Smyth, *Analyst* (*London*), **99**, 241 (1974).
(4) J. A. F. de Silva, M. A. Schwarz, V. Stefanovic, J. Kaplan, and L. D'Arconte, *Anal. Chem.*, **36**, 2099 (1964).
(5) J. A. F. de Silva and C. V. Puglisi, *Anal. Chem.*, **42**, 1725 (1975).
(6) J. A. F. de Silva, I. Behersky, C. V. Puglisi, M. A. Brooks, and R. E. Weinfeld, *Anal. Chem.*, **48**, 10 (1976).
(7) J. Vessman, S. Strömberg, and G. Rietz, *Acta Pharm. Suec.* **7**, 363 (1970).
(8) A. Frigerio, K. M. Baker, and G. Belvedere, *Anal. Chem.*, **45**, 1846 (1973).
(9) H. Ehrsson and A. Tilly, *Anal. Lett.*, **6**, 197 (1973).
(10) J. A. F. de Silva, C. V. Puglisi, and N. Munno, *J. Pharm. Sci.*, **63**, 520 (1974).
(11) M. Ervik and K. Gustavii, *Anal. Chem.*, **46**, 39 (1974).
(12) R. Modin and G. Schill, *Acta Pharm. Suec.*, **4**, 301 (1967).
(13) H. Ehrsson, *Acta Pharm. Suec.*, **8**, 113 (1971).
(14) A. Brändström, "Preparative Ion Pair Extraction", Apotekarsocieteten and Hässle Läkemedel, Stockholm, 1974, p 93.
(15) J. Benett, W. Franklin Smyth, and I. E. Davidson, *J. Pharm. Pharmacol.*, **25**, 387 (1973).
(16) R. B. Hagel and E. M. Debesis, *Anal. Chim. Acta*, **78**, 439 (1975).
(17) J. Vessman, G. Freij, and S. Strömberg, *Acta Pharm. Suec.*, **9**, 447 (1972).
(18) T. Nordgren and R. Modin, *Acta Pharm. Suec.*, **12**, 407 (1975).
(19) H. Ehrsson, *Anal. Chem.*, **46**, 922 (1974).
(20) M. Wretlind, Å. Pilbrant, A. Sundwall, and J. Vessman, "The Pharmacokinetic Profile of Oxazepam", *Acta Pharmacol. Toxicol. Suppl.*, 28 (1977).

RECEIVED for review February 11, 1977. Accepted June 13, 1977.

Ion-Exchangers for Gas–Solid Chromatography

Roland F. Hirsch*[1]

Chemistry Department, Seton Hall University, South Orange, New Jersey 07079

Courtenay S. G. Phillips

Merton College, Oxford, England

Lightly-sulfonated porous polymers are efficient and selective packings for gas–solid chromatography. They are easy to prepare and do not show the tailed peaks observed when conventional macroreticular ion-exchange resins are used in GSC. The degree of sulfonation can be varied, and with it the extent of specificity for compounds forming complexes with the metal counterion on the packing. Reactions catalyzed by the packings were also observed.

Ion-exchange materials are finding increased use in gas chromatography because they offer a great range of potential selectivity through variation of the ionic form of material (*1–5*). Two difficulties have prevented more widespread use of ion exchangers in GC: their chromatographic separation efficiencies are poor, and they are such strong adsorbants that many substances cannot be eluted without raising the temperature above the decompostion point of the ion exchanger or of the sample.

One solution to these problems has been to prepare bound-monolayer cation exchangers, in which the ion-exchange group is covalently bound to a porous silica support (*5*). Impressive separations of cis-trans isomers of olefins were obtained with these packings. However, their synthesis is time-consuming and requires special handling techniques for some of the reagents, and the matrix must be deactivated by silanization after the ion exchanger has been prepared.

We wish to report on the use of lightly-sulfonated porous polymers as ion exchangers for gas–solid chromatography. These materials, which have previously found application in liquid chromatography (*6–8*), allow efficient separations at moderate temperatures. They are easy to prepare and require no special treatment prior to use. The extent of sulfonation of the polymer determines the degree of enhancement of retention of specifically-adsorbed substances; hence it is possible to tailor the packing to the needs of a particular separation problem by choosing the proper synthesis conditions.

EXPERIMENTAL

All chromatographic experiments were carried out in Pye-Unicam Series 104 gas chromatographs with flame ionization detectors. Nitrogen was the carrier gas. Glass columns ($^1/_4$-inch o.d.) contained the packing materials.

Commercial ion-exchange resins were washed with 2-propanol, water, 1 M NaOH, 1 M HCl, and water, dried at 110 °C for at least 4 h, and sized into the 40–60 mesh range using standard screens. The resins were converted into the silver form by washing with 1 M $AgNO_3$, to the sodium form by washing with 1 M NaOH, to the nickel form by washing with 0.2 M $Ni(NO_3)_2$, and to the cadmium form by washing with 0.5 M $CdCl_2$, followed in all cases by washes with water, and drying at 110 °C for at least 4 h.

Porapak Q (80–100 mesh) was sulfonated by suspending a 10-g portion of the porous polymer in about 50 mL of concentrated sulfuric acid (*6, 9*). The mixture was swirled vigorously for the prescribed time, and then about 50 mL of 50% aqueous sulfuric acid was added to quench the reaction. The resin was washed with dilute sulfuric acid and water. It was then converted to the desired metal ion forms in the same way as already described for the commercial ion exchangers. The degree of sulfonation was determined by controlling the temperature and duration of the sulfonation step, as discussed below. It was measured by titration of a portion of the washed resin with sodium hydroxide solution. The silver ion content of the silver form was determined by atomic absorption spectrometry of an acid-digested portion of the resin.

RESULTS AND DISCUSSION

For use in gas chromatography, an ion-exchange resin must have a permanent pore structure, as there is nothing present

---

[1] On sabbatical leave at the Inorganic Chemistry Laboratory, Oxford, 1975–76.

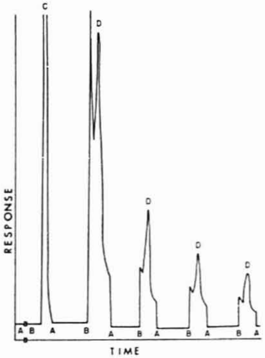

Figure 1. Stopped-flow gas chromatography on a commercial ion-exchange resin. Ni^{2+} form of Amberlyst 15: 2,2-dimethylbutane, 180 °C, 10 mL/min N_2 carrier: (*A*) flow of carrier gas stopped, (B) flow restarted, (*C*) main peak, (*D*) stopped-flow peak

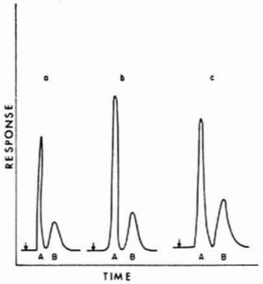

Figure 2. Separations of 2-pentene isomers on short columns of sulfonated Porapak Q. (*a*) Resin I, 13-cm column, 230 °C. (*b*) Resin II, 13-cm column, 230 °C. (*c*) Resin III, 11-cm column, 170 °C. (A) *trans*-2-Pentene. (B) *cis*-2-Pentene. Ag^+ form of resins

(as in liquid chromatography using polar solvents) to swell the resin to allow the sample access to the ionic groups inside the beads of resin. The macroporous (or macroreticular) type of resin is therefore necessary for gas chromatography (*2*).

Rohm and Haas Amberlyst 15 macroreticular cation-exchange resin, which was used in a previous study (*2*), gives a satisfactory range of retention for many samples, but the efficiency (in terms of the height per theoretical plate) is not adequate. On further study of this resin as a GSC packing, it was discovered that a small but distinct tailing is present, regardless of the type of hydrocarbon being tested or the metal ion form of the resin. Other macroporous cation-exchange resins were obtained and tested in their sodium and silver ion forms. Among the resins studied were Rohm and Haas Amberlite 200 and Amberlite 252, Permutit Zerolit 625, and Dow Chemical Dowex MSC-1. All were unsatisfactory in their poor efficiency and lack of freedom from tailing.

This tailing was present regardless of the sample size used (over a range from 1 ng to greater than 1 μg) and the retention time of the peak did not change until the largest sample sizes were reached. The tailing therefore is not of thermodynamic origin. To prove that it is a kinetic phenomenon, several samples were chromatographed using flow stops before and after elution of the main portion of the sample (*10*). In all cases, new peaks appeared after each flow stop period on the trailing edge of the main peak, indicating that a slow process had proceeded during the stop, releasing some of the sample for elution. An example is shown in Figure 1.

Since this behavior occurred with all samples on all of the resin forms, it was concluded that a chemical reaction was not responsible for the peak after each flow stop. In other words, the stopped-flow peaks correspond to the same chemical substance which was originally injected. Rather, a slow mass transfer process within the stationary phase must be the source of these observations. Although the resins are all of the macroporous type, their internal volume contains small ("micro") as well as large ("macro") pores (*11*). Slow diffusion of sample molecules within the small pores would explain the results obtained with the resin packings.

Elimination of the small pores should eliminate this kinetic tailing. Several unsuccessful attempts were made to do so. A sample of Amberlyst 15 was heated in concentrated sulfuric acid at 110 °C for 1 week in the hope that sulfonation of the relatively small number of unsulfonated aromatic rings would occur under these extreme conditions, making the material more homogeneous and enlarging the small pores. The peak shapes were not significantly improved compared with the original resin. Several experiments were carried out using carrier gas saturated with water or a high-boiling organic liquid (such as *n*-butyl benzene) in the hope that the resin would become swollen, opening up the small pores. These experiments were interesting in their own right as they represent a controlled case of competition of two species for an adsorption site, and this work is being pursued. However, the tailing was not entirely eliminated, and the conditions are somewhat awkward for routine use in gas chromatography.

It was then decided to take a copolymer of styrene and divinylbenzene (the basis of most ion exchangers) and to sulfonate it lightly. By selecting a porous polymer which gave efficient separations in gas chromatography and modifying it only on the surface of the large pores, it was expected that the efficiency would be retained and tailing prevented, since no small pores would be produced. This has proved to be the case in liquid chromatography on similar materials; such ion exchangers allowed more rapid chromatographic separations than conventional, fully-sulfonated resins (*6–8*).

Three sulfonations were carried out on the porous polymer, Porapak Q. The first (designated I) was carried out for 5 min at 75 °C, and resulted in a resin with an exchange capacity of about 1.5 mmol H^+/g dry resin, and 15.5% silver content (1.4 mmol Ag^+/g) for the silver ion form. The second (II) was carried out for 2 min at 25 °C, with the product having 0.9 mmol H^+/g exchange capacity, and 9.0% silver content (0.8 mmol Ag^+/g) after conversion to the silver form. The third (III) was carried out for about 1 min at 5 °C, with the product having 0.6 mmol H^+/g exchange capacity, and 5.5% silver content (0.5 mmol Ag^+/g) after conversion to the silver ion form.

These resins gave sharp, symmetrical peaks for a wide variety of saturated and unsaturated hydrocarbons. Efficiencies were good; plate heights were 1 mm, with a value of 0.7 mm achieved for *cis*-2-butene on the silver form of resin I. Typical plate heights on the commercial exchangers, in contrast, were 2–6 mm (*2*). Tailing was not observed on the new resins, except in situations where the sample was reacting on the column, as described below. Short columns (10–15 cm) could be used to obtain good and rapid separations of isomeric compounds (see Figure 2; each chromatogram required less than 4 min).

The retention times for saturated hydrocarbons were comparable on all three resins. The unsaturated compounds gave retention times which depended directly on the silver ion content of the resin. The retention indices for these compounds therefore increase with increasing sulfonation, as

Table I. Retention of Unsaturated Compounds on Sulfonated Porapak Q

	Kovats Retention Index on			
	Resin I (15.5% Ag)	Resin II (9% Ag)		Resin III (5.5% Ag)
	225 °C	230 °C	140 °C	140 °C
trans-2-Butene	...	620	680	570
cis-2-Butene	...	720	750	650
1-Pentene	900	800	...	730
trans-2-Pentene	830	720	780	680
cis-2-Pentene	930	830	860	750
Benzene	920	830	810	700
Toluene	1070	960	...	830

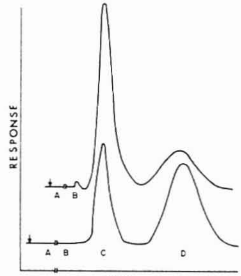

Figure 3. Stopped-flow studies of the 2-butenes. Cd^{2+} form of resin II; 140 °C; 45 mL/min carrier gas flow; (A) flow stopped, (B) flow restarted, (*C*) *trans*-2-butene, (*D*) *cis*-2-butene. Top chromatogram is for pure *trans*-2-butene, bottom for pure *cis*-2-butene injected into column

is shown in Table I. In all cases they are fully resolved from the saturated hydrocarbons, but the enhancement of retention is different for each resin.

The cadmium form of resin II gave quite different results for the olefins. While *trans*-2-butene and *cis*-2-butene gave separate peaks with retention indices of 620 and 725, respectively (at 140 °C), 1-pentene and the 2-pentenes produced a single peak with a retention index of 700 and considerable tailing and 1-hexene provided a peak with a retention index of only 760, also with substantial tailing. It appeared that the samples were undergoing a reaction catalyzed by the packing material. Stopped-flow experiments with the 2-butenes, shown in Figure 3, confirmed this. The chromatograms show that the initially pure isomers have isomerized to a significant extent while they were stopped in contact with the resin. The larger olefins may well isomerize to the most readily eluted form, providing a single peak with a tail caused by further reaction of the more strongly retained isomers taking place gradually on the column. Cadmium ion is known to catalyze these reactions (*12*).

The partially-sulfonated porous polymer packings are easy to prepare and retain the high separating efficiency of the parent material. They would appear to offer a great deal of flexibility in meeting the selectivity requirements of a specific sample. Further work is under way to determine more completely the advantages and limitations of these packings in gas chromatography.

LITERATURE CITED

(1) K. Ohzeki and T. Kambara, *J. Chromatogr.*, **55**, 319 (1971).
(2) R. F. Hirsch et al., *Anal. Chem.*, **45**, 2100 (1973).
(3) K. Fujimura and T. Ando, *J. Chromatogr.*, **114**, 15 (1975).
(4) S. Allulli et al., *Anal. Chem.*, **48**, 1259 (1976).
(5) P. Magidman et al., *Anal. Chem.*, **48**, 44 (1976).
(6) J. S. Fritz and J. N. Stary, *Anal. Chem.*, **46**, 825 (1974).
(7) L. C. Hansen and T. W. Gilbert, *J. Chromatogr. Sci.*, **12**, 458, 464 (1974).
(8) T. S. Stevens and H. Small (Dow Chemical Company), U.S. Patent 3,966,596 (1976).
(9) H. Small, *J. Inorg. Nucl. Chem.*, **18**, 232 (1961).
(10) R. Lane, B. Lane, and C. S. G. Phillips, *J. Catal.*, **18**, 281 (1970).
(11) D. G. Howery and S. Tada, *J. Macromol. Sci., Chem.*, **3**, 297 (1969).
(12) I. Hadzistelios, F. Lawton, and C. S. G. Phillips, *J. Chem. Soc., Dalton Trans.*, 2159 (1973).

RECEIVED for review March 18, 1977. Accepted June 27, 1977. Acknowledgement is made to the donors of the Petroleum Research Fund, administered by the American Chemical Society, for support of this research.

Determination of Ethyl and Methyl Parathion in Runoff Water with High Performance Liquid Chromatography

Daniel C. Paschal,* Richard Bicknell, and David Dresbach

Department of Chemistry, Illinois State University, Normal, Illinois 61761

High performance liquid chromatography with variable wavelength detection is described for the determination of methyl and ethyl parathion at the part per billion level in runoff water. The macroreticular resin XAD-2 was used as an adsorption medium for preconcentration of trace organics in water by a factor of 100. Linear relationships between peak height or area and concentration were obtained in the range 0 to 120 ppb of methyl and ethyl parathion, with a lower detection limit of 2 to 3 ppb ($S/N = 2$). Relative standard deviations in this range were 1 to 6%, with an average recovery of 99%. Only 30 min is required for the complete determination, and as little as 2 ng of methyl or ethyl parathion can be quantified with a 10-μL injection.

Organophosphorous insecticides enjoy wide use due to their relatively rapid decomposition and low accumulation in biological food chains. For these reasons, the organophosphorous insecticides are rapidly replacing the more persistent organochlorine agents. In fact, recent EPA restrictions have curtailed the use of several of the once widely used organochlorine pesticides such as DDT, aldrin, dieldrin, and heptachlor (*1*). Among the more popular replacements for these organochlorine compounds are ethyl and methyl parathion.

Ethyl parathion (diethyl *p*-nitrophenyl phosphorothionate) and methyl parathion (dimethyl *p*-nitrophenyl phosphorothionate) were introduced in the 1940s. Their high, wide-spectrum insecticidal activity makes them useful in a number of applications. Both methyl and ethyl parathion are subject to hydrolysis, with a strong dependence on pH and temperature. In general, half life decreases at elevated temperature and pH. For example, at pH 7.4 and 20 °C, ethyl parathion has a half life of 2594 h, while at the same temperature and pH 5.0, the half life is 3670 h. At pH 5.0 and 70 °C, the half life decreases to 19.5 h (*2*). Under field application conditions, about 1–10 lb (0.45 to 4.5 kg)/acre are normally applied (*3*), which could lead to entry of the parathion into runoff water. The presence of ethyl or methyl parathion in runoff water presents a potential hazard due to the high mammalian toxicity of ethyl and methyl parathion as well as that of their major hydrolysis product, *p*-nitrophenol. Under environmental conditions both ethyl and methyl parathion could persist at the sub-ppm level in water for a number of days or weeks, depending on temperature and pH (*4*).

Most methods for the determination of methyl or ethyl parathion involve an extraction followed by chromatographic separation and quantification. Thin-layer chromatography methods are generally slow and difficult to quantify; while gas chromatographic methods can give unreliable results due to the thermal lability of ethyl and methyl parathion. High performance liquid chromatography offers a nearly ideal system for determination of parathions due in part to the gentleness of the technique in which separations are accomplished at ambient temperature. A recent review article (*5*) described the usefulness of liquid chromatography for ethyl parathion and other thermally labile compounds such as the carbamates. Variable wavelength detectors offer much in the way of increased selectivity, a factor particularly important in environmental samples in which a large number of potentially interfering compounds are often present. As has been suggested in recent articles (*6, 7*) the variable wavelength spectrophotometer also permits the optimization of sensitivity, a function of source intensity and detector response as well as the absorption maximum of the species determined. With the use of such a detector, even such weak UV absorbers as lindane can be determined at the microgram level.

Extraction procedures have been developed recently which involve the use of macroreticular resins which offer much in the way of pre-concentration (*8*). The XAD materials (Rohm and Haas) are particularly useful in this regard. Organics in water can be sorbed on a small column of macroreticular resin, and the sorbed organics then eluted by diethyl ether. After evaporation of the eluate, the concentrated organics can be determined by chromatography. In addition to the obvious benefit of 100- to 1000-fold concentration, this method offers the possibility for on-site sampling, avoiding the necessity to transport, store, and preserve large volumes of water (*9, 10*).

A procedure has been developed for the determination of ethyl and methyl parathion using an XAD resin for sampling and preconcentration, followed by chromatographic separation and quantification by high performance liquid chromatography on a reverse phase microparticle column, with detection by variable wavelength UV-vis detector. The method is simple, rapid, and free from most interferences.

EXPERIMENTAL

Apparatus. A modular chromatographic system was used consisting of a Spectra-Physics Model 740B pump, a Glenco 7000 PSI six-port valve injector, a Whatman (Reeve Angel) prepacked microparticle reverse phase column (Partisil ODS), and a Perkin-Elmer Model LC-55 variable wavelength detector. The pump was used in the analytical range (0–4 mL/min) at a flow rate of 2.4 mL/min. Injections were 10 μL and were accomplished with fixed volume sampling loop for maximum precision. The detector was operated at 270 nm for the determination of methyl and ethyl parathion, or at an absorption maximum of potentially interfering compounds in the interference study. A 10-mV recorder was used in the 5-mV range with scale expansion of 5X from the detector, which provides a sensitivity of 0.02 aufs.

Reagents and Materials. The macroreticular resin XAD-2 was obtained from Rohm and Haas and was purified by soxhlet extraction as described by Junk et al. (*8*), and stored under AR methanol. Pesticide grade acetonitrile was used as received; diethyl ether was glass distilled before use. Glass distilled water was used throughout. Parathions were "analytical standard" grade (99+% by GC analysis) obtained from Monsanto Agricultural Products (ethyl) or Research Triangle Health Effects Research Lab (methyl). Both parathions were stored in the dark at 4 °C, and fresh 100-ppm methanolic stock solutions were made from the standard materials at least once a week. The methanolic standards were also stored at 4 °C in the dark. Interference studies were conducted using analytical reference standards obtained from Research Triangle Health Effects Research Lab, used as received. Precautions similar to the above were taken with organophosphorous and carbamate pesticides.

Procedure. *Preparation of Standards.* Microliter amounts of 100-ppm stock solutions of organophosphorous insecticides made up in methanol were diluted volumetrically with glass distilled water to 100 mL. The diluted standards were then passed through a 10-cm column of purified XAD-2 resin, prepared according to the method of Junk et al. (*8*), at a rate of 4–6 mL/min. After the last of the dilute aqueous standards were passed through the column, most of the water clinging to the resin was removed by gentle vacuum aspiration. Thirty mL of glass distilled diethyl ether was then passed through the column at 2–3 mL/min, after which the last of the ether was removed by passing dry purified nitrogen through the column. The ether was dried by shaking with 2 g of anhydrous sodium sulfate, and evaporated to dryness using a rotary evaporator at temperatures not exceeding 35 °C. The residue was then dissolved in 1.00 mL of nanograde acetonitrile, and the resulting solution chromatographed on a Partisil-ODS reverse phase column at 2.40 mL/min with 50% acetonitrile–water mobile phase.

Recovery Studies. Standards made as described were compared with volumetric dilutions of methanolic stock solutions in nanograde acetonitrile to evaluate the recoveries obtained by the described method. Comparison of the peak areas and heights of the extracted and volumetrically diluted standards showed a 98–101% recovery of methyl and ethyl parathion, with an average value of 99% recovery.

Extraction of Runoff Water. Grab samples of 2-L volume were obtained from a nearby drainage stream which removes runoff water from a large agricultural area. Samples were either analyzed immediately or stored for no more than 24 h at 4 °C in the dark. Since ethyl and methyl parathion were not found in the samples at levels above the limit of detection of the procedure (2 ppb), microliter amounts of the methanolic parathion standards were diluted with runoff water to evaluate the chromatographic behavior of extracts of these spiked samples and to evaluate recoverability of the parathions in this matrix. Extracts were prepared as in the above procedure, and chromatograms were evaluated to establish calibration curves for the parathions.

RESULTS AND DISCUSSION

In order to evaluate the efficiency of extraction of XAD-2 for trace organics in natural water samples, several different types of water were analyzed. Well water, spring water, and runoff water were all examined by the described procedure. A large number of peaks were present in the 0–2 min region of the chromatogram in all three water samples. An increase in the number of peaks and peak areas was observed in runoff water as compared to either spring or well water. This result suggests a greater variety and larger number of dissolved organics in the runoff water. This is consistent with previous work (*11*), in which similar observations were made. The chromatograph of runoff water used in this study is shown in Figure 1. A number of relatively polar compounds elute early in the chromatogram, with relatively few peaks in the 3–10 min region of the chromatogram. On changing from 50% acetonitrile to 100% acetonitrile to regenerate the column,

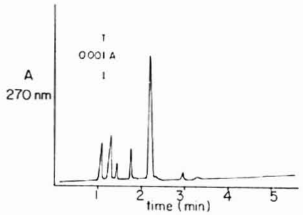

Figure 1. Chromatogram of runoff water extract. Separation of organics in runoff water. Eluent; 50:50 (v/v) acetonitrile water, Partisil ODS 4.6 mm × 25 cm; detector at 270 nm, 0.02 aufs

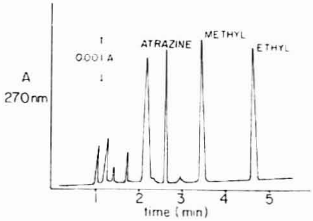

Figure 2. Chromatogram of spiked runoff water extract. Conditions as in Figure 1

several more peaks were eluted, apparently consisting of less polar materials strongly adsorbed under the conditions of the procedure. No interference was obtained from these strongly adsorbed compounds, although it was found to be useful to regenerate the ODS column with 100% acetonitrile after every five to six runs to insure reproducibility.

The retention times for methyl and ethyl parathion, obtained from volumetric dilutions of methanolic standards with acetonitrile, were 3.45 and 4.65 min, indicating no interference from naturally occurring organics in the runoff water. Spiked samples of runoff water were prepared containing ethyl and methyl parathion. A typical chromatogram for such a spiked sample is shown in Figure 2. The parathions are well-separated, with no observed interference from organics already present in the water. Retention times obtained for the parathions were in agreement with those of standards.

Preparation of Calibration Curves. Calibration curves were prepared from a set of standards made up by volumetric dilution of methanolic stock solutions in runoff water. The concentration range of parathions in the resulting solutions was from 10 to 120 ppb. Atrazine was added as an internal standard to the concentrated extracts, on the basis of examination of the chromatogram of the runoff water for the absence of any eluted material with retention time identical to atrazine. Since no material naturally occurring in the water samples determined was found that behaved like atrazine chromatographically under the conditions described, it was determined to be a suitable internal standard. Ratios of peak heights or areas of parathions to those of atrazine were plotted vs. concentration. Good linearity was obtained over the range of concentration examined for both parathions. In order to evaluate the accuracy and reproducibility of the method, a series of solutions was prepared in runoff water with concentrations of parathions in the range of the calibration curve. The results of this study are given in Table I. The lower limit of detection, defined as that amount giving a reproducible signal at least twice that of noise, was calculated from these data to be 3.1 and 2.9 ng for methyl and ethyl parathion, respectively.

Table I. Reproducibility of Method

Taken μg/L	Found μg/L[a]	SD	RSD, %
Methyl Parathion			
15.0	14.8	0.45	3.0
37.5	37.1	1.07	2.8
75.0	75.9	0.73	1.0
112.5	112.7	2.56	2.3
Ethyl Parathion			
Taken μg/L	Found μg/L[a]	SD	RSD, %
10.0	9.9	0.37	3.7
25.0	24.6	1.40	5.6
50.0	49.3	0.97	1.9
75.0	75.0	2.40	3.2

[a] Average of six determinations.

Table II. Interference Study

Compound	Relative retention (Methyl Parathion = 1.00)	Wave-length measured, nm
Aroclor 1260	3.94–5.88 multiple peaks	225
Atrazine	0.75	265
Azinphos Ethyl	1.14	285
Alachlor	0.89	235
Carbaryl (Sevin)	0.69	280
Carbofuran	0.61	270
Chloramben	0.26	240
Chlorpyrifos	2.01	290
p,p'-DDT	2.78	235
DEHP	1.59	235
Dialifor	1.61	290
Diazinon	1.30	245
Dyfonate (Fonofos)	1.36	240
Fenitrothion	1.08	265
Methoxychlor	1.72	225
p-Nitrophenol	0.72	310
Phosmet	0.93	230
Phorate	1.30	220
Propachlor	0.67	260
2,3,5-T	0.28	250
Trifluralin	0.58	270

Interference Studies. Potential interference by other agricultural chemicals and organics commonly occurring in natural water were examined, the results of which are given in Table II. All compounds were examined under the conditions described for analysis, and relative retention times were calculated in comparison with methyl parathion. Wavelengths chosen for measurement were at or near the absorbance maxima for the compounds as determined by UV scans from 350–200 nm. If a potentially interfering compound showed a retention time near one of the parathions, then chromatography was performed with detection at 270 nm. Many of the pesticides and herbicides are in common use in Central Illinois (*12*), a somewhat representative agricultural area. Of the compounds investigated, only Fonofos (Ethyl *S*-phenyl ethyl phosphonothiolothionate) interferes. All others are either separated chromatographically or only weakly absorb at 270 nm. A 10-ppm solution of Fonofos elutes at 4.7 min and absorbs at 270 nm to the same extent as 2 ppm ethyl parathion. However, if the wavelength of detection is changed to 280 nm, the interference is overcome. Only a slight loss of sensitivity is observed for the parathions at this wavelength, so that if Fonofos (Dyfonate) is known to be present, then analysis can be performed at this wavelength.

LITERATURE CITED

(1) *Chem. Eng. News*, **53** (30), 19–21 (1975).
(2) S. D. Faust and H. M. Gomaa, *Environ. Lett.*, **3** (3), 171–201 (1972).
(3) M. Eto, "Organophosphorous Insecticides, Organic and Biological Chemistry", CRC Press, Cleveland, Ohio, 1974, p 241.
(4) S. D. Faust and H. M. Gomaa, *Environ. Lett.*, **3** (3) 171–201 (1972).
(5) H. A. Moye, *J. Chromatogr. Sci.*, **13**, 268–279 (1975).
(6) D. H. Rodgers, *Am. Lab.*, **9** (2), 133–138 (1977).
(7) C. M. Sparacino and J. W. Gines, *J. Chromatogr. Sci.*, **14**, 546–556 (1976).
(8) G. A. Junk et al., *J. Chromatogr.*, **99**, 745–762 (1974).
(9) A. K. Burnham et al., *Anal. Chem.*, **44**, 139–142 (1972).
(10) *Chem. Eng. News*, **54** (16), 35–36 (1976).
(11) C. G. Creed, *Res./Dev.*, **27** (9), 40–44 (1976).
(12) Eugene Mossbacker, extension advisor for agriculture, McLean County Cooperative Extension Service, Private Communication.

RECEIVED for review April 11, 1977. Accepted June 23, 1977. Work supported in part by an institutional grant from Illinois State University (No. 75-32).

Laser Two-Photon Excited Fluorescence Detection for High Pressure Liquid Chromatography

Michael J. Sepaniak and Edward S. Yeung*

Ames Laboratory-ERDA and Department of Chemistry, Iowa State University, Ames, Iowa 50011

A laser two-photon excited fluorometric detector for high pressure liquid chromatography is described and characterized for the separation of the oxadiazoles PPD, PBD, and BBD. Excitation is provided by the absorption of two photons of radiation at 5145 Å from an argon ion laser. The detection limits, linearity of response, precision, and selectivity are reported and are found to compare favorably with other UV detection methods.

While the fluorometric high pressure liquid chromatography (HPLC) detector is not as commonly used as the UV absorbance detector (*1, 2*), it does possess some definite advantages, namely higher sensitivity for those compounds with an appreciable fluorescence quantum efficiency and greater selectivity since relatively few of the molecules that absorb UV radiation actually fluorescence. Selectivity is also enhanced by the fact that fluorescent molecules have both an excitation and emission spectrum that can be scanned (*3, 4*). The present paper describes a fluorometric detection method that has two unique features. First, excitation is provided by an argon ion laser capable of 4 W of radiation at 5145 Å. Second, the excitation process is the result of the absorption of two photons of the 5145-Å light.

In 1931 Maria Göppert-Mayer realized that a molecule could absorb two photons simultaneously to achieve a change in its quantum level (*5*). The process involves some distinctive selection rules and represents a way for spectroscopists to find and describe new molecular states (*6*). The value of the two-photon process in fluorometric HPLC detection lies in its improved selectivity. The fact that two-photon absorption involves different selection rules than one-photon absorption results in different one-photon and two-photon absorption spectra, and this produces an additional variant in the selective detection of fluorescent molecules. Two-photon fluorescence detection is somewhat limited by the small size of the two-photon absorption strength (δ) and it is only with the high output power of a laser that measurable fluorescence signals can be obtained.

The two-photon absorption strength is defined by the relationship

$$\Delta P = P^2 C L A^{-1} \delta \tag{1}$$

where ΔP is the absorbed optical power, P is the optical power, C is the solute concentration, L is the path length, and A is the optical beam cross-sectional area (*6*). Typical values for δ are $\leq 10^{-48}$ cm^4 s photon^{-1} molecule^{-1}. The fraction of the absorbed optical power that is actually detected as fluorescence (R) can be calculated from Equation 2

$$R = Qkq \tag{2}$$

where Q is the solute fluorescence quantum efficiency, k is the optical collection efficiency, and q is the detector quantum efficiency.

This report characterizes a laser two-photon excited fluorometric (LTPEF) detector used in the two-photon detection of PPD, PBD, and BBD. These oxadiazoles have the general structure

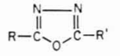

where R and R′ are either phenyl or biphenyl groups. A UV absorbance detector is used for the comparison of detection limits, linearity of response, and selectivity.

EXPERIMENTAL

Chromatographic System. The liquid chromatographic system was composed of a LDC, Riviera Beach, Fla., minipump capable of delivering 16–160 mL/h of eluent at pressures up to 5000 psi, Rheodyne, Berkeley, Calif., injection valve with a 100-μL sample loop, and a Waters Associates, Milford, Mass., μ-Bondapak C_{18} column (30 cm long × 3.9 mm i.d.). The eluent used for all separations was 60/40 UV grade tetrahydrofuran/water. The oxadiazoles were from Pfaltz and Bauer, Inc. Separations were all at ambient temperature with a flow rate of 2.0 mL/min and an injection volume of 100 μL.

UV Absorbance Detector. The UV detector used for comparison purposes was a Chromatronixs, Berkeley, Calif., Model 230 mixed wavelength detector. The detector was operated at 280 nm where background noise was smallest and oxadiazole absorptivities greatest.

LTPEF Detector. The fluorometric detector (see Figure 1) is composed of a light-tight cubic metal box containing a 1-mm i.d. × 3-mm o.d. quartz flow cell. The 5145-Å laser radiation of a Control Laser model 553 argon ion laser passes through a 0.5-inch aperture, then two Corning 3-71 sharp cut-off filters, and one Corning 4-96 wide bandpass filter, before being focused on the center of the flow cell by a 50-mm focal length × 25-mm diameter

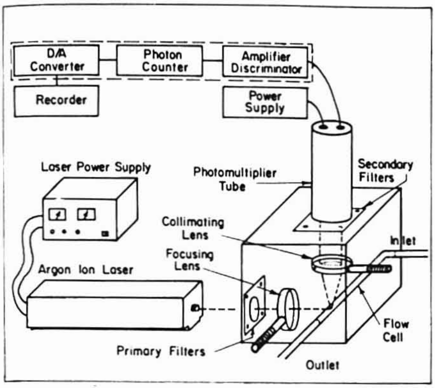

Figure 1. Schematic diagram of laser two-photon excited fluorometric detector. The Ortec photon counting system is outlined by the dashed line

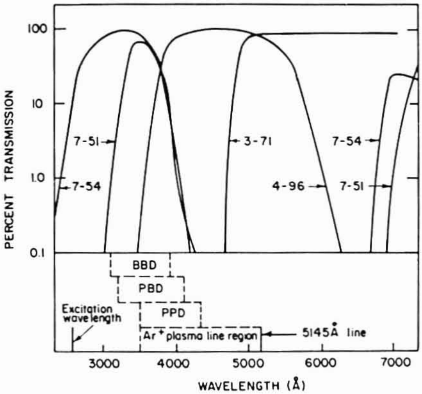

Figure 2. Spectral considerations for the fluorometric detector. Upper graph: Transmission curves for primary filters (3-71 and 4-96) and secondary filters (7-51 and 7-54). Lower graph: Fluorescence emission regions for PPD, PBD, and BBD. The super radiance of the argon ion laser contains Ar$^+$ plasma line emission in the region from 3500 to 5145 Å

quartz focusing lens. The fluorescence emanating from the flow cell is collected and collimated by a 38-mm diameter quartz lens with a *f*-number of 1. The collimated fluorescence is passed through three UV bandpass filters (two Corning 7-51 filters and one Corning 7-54 filter), then onto the photocathode of an Amperex, Hicksville, L.I., N.Y., 56-DVP photomultiplier tube. The purpose of the Corning 3-71s is to eliminate laser plasma lines present in the laser super radiance (*7*), and the Corning 4-96 is used to block orange fluorescence, from the Corning 3-71s, which is passed by the secondary filters. This and other spectral considerations are illustrated in Figure 2.

Signal Processing. The fluorescence signal was counted in 0.5-s intervals with an Ortec, Oak Ridge, Tenn., photon counting system (see Figure 1). A latching circuit and Ortec D/A converter were used to convert the digital signal to an analog readout on an Omini-scribe stripchart recorder. The D/A converter time constant was set at 0.1 s, since it was found that longer time constants decreased detector precision.

Detector Optimization. Prior to chromatographic operation, the detector optics were optimized and standardized by placing a stagnant solution of 10^{-3} M PPD in the flow cell, then adjusting the optics (the lens holders shown in Figure 1 provide slight adjustment of the optics) to give a photon count of 20000 counts/s at a laser power of 1 W. The focusing lens adjustment was critical but, once set, the system remained stable until other experimental operations required moving the laser.

Table I. Detection Limits[a]

	UV absorbance detector, ng	LTPEF detector, ng
PPD	13	150
PBD	10	9
BBD	76	31

[a] Detection limit taken as amount of solute that gives $S/N = 3$ where S is peak height and N is peak to peak background noise.

RESULTS AND DISCUSSION

Detection Limits. The concentration necessary to detect a particular solute with a given response can be calculated using Equations 1 and 2. For the present detection system, R is approximately 10^{-3}; L, the diameter of the flow cell, is 0.1 cm; and A, the cross-sectional area of the focused laser beam, is roughly 10^{-4} cm^2. Using these quantities the concentration necessary to register a photon count of 100 counts/s, at a power of 4 watts (5145 Å) for a solute with an absorption strength of 10^{-48} cm^4 s photon^{-1} molecule^{-1}, is 1.5×10^{-9} M. As seen from this calculation, sub parts-per-million concentrations can, in principle, be detected even for solutes with moderate two-photon absorption strengths, providing high laser output power can be obtained at the proper absorbing frequency.

In the previous calculation a relatively small photon count of 100 counts/s was chosen as an easily detectable signal. This is mainly due to the ease with which optical filters can be used to reduce background signals. The laser light is better separated, spectrally, from the fluorescence (see Figure 2) than in normal one-photon excitation fluorescence (*8*).

The favorable detection limits of the LTPEF detector are shown in Table I where detection limits for two of three oxadiazoles are better for the LTPEF detector. The peak-to-peak background noise, and therefore the detection limits, of the UV absorbance detector could be, in principle, improved by effective eluent pulse dampening, but the improvement is limited by detector drift and fluctuations other than the regular pumping noise of the system. And, in fact, the elimination of pumping noise, solvent peaks, detector drift, and problems with gradient elution are some of the distinct advantages of the LTPEF detector.

There are a few LTPEF detector improvements that should in theory improve sensitivity. The first is to replace the primary filters by a good quality dispersive prism, which would remove plasma lines from the laser super radiance with approximately 40% less beam attenuation than with the filters. The second is to use a focusing lens with a shorter focal length. The theoretical limit of the cross-sectional area of the focused laser beam (A in Equation 1) is dependent on the focal length of the focusing lens (*9*). With a shorter focal length lens, higher power densities, and therefore larger two-photon absorption, could be obtained. The quadratic dependence of two-photon signals on laser power is shown in Equation 1. A third improvement would therefore be increasing the laser output power by means of a mode locker. The reader is referred to Ref. 7, p 199, for a good description of mode locking. When mode locked, the continuous output of the argon ion laser is converted to a series of high energy pulses. Sensitivity could then be greatly enhanced by properly gating the detection sytem so that signals are counted only during and directly after a laser pulse. Even without gating the

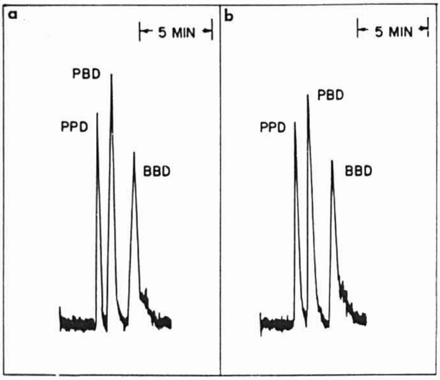

Figure 3. Chromatograms for laser two-photon excitation fluorometric detection of PPD, PBD, and BBD, 100-μL injection volume, sensitivity 100 counts per inch. (a) 2.4 × 10^{-5} M PPD, 1.5 × 10^{-6} M PBD, 4.0 × 10^{-6} M BBD; (b) same oxadiazole concentrations but with approximately 10^{-5} M phenol, fluorene, chrysene, and anthracene

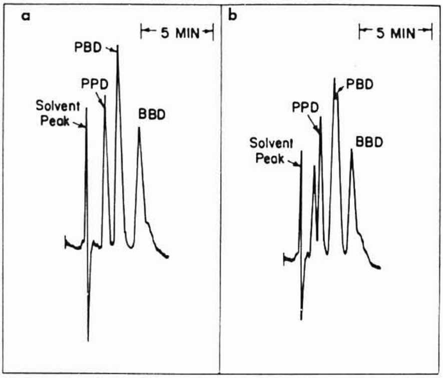

Figure 4. Chromatograms for UV absorbance detection of PPD, PBD, and BBD, 100-μL injection volume, sensitivity 0.008 absorbance unit per inch. (a) 4.0 × 10^{-6} M PPD, 7.0 × 10^{-6} PBD, 1.0 × 10^{-5} M BBD; (b) same oxadiazole concentrations but with approximately 10^{-5} M phenol, fluorene, chrysene, and anthracene

detection system, the mode locker could theoretically produce approximately a two-fold increase in signal.

Linearity of Response. Calibration plots for 100-μL injections of 3.0 × 10^{-7} M to 1.0 × 10^{-3} M PBD were drawn for both detectors. The inner-cell effect oftentimes causes nonlinearity in fluorometric detection (*10*), but the small active cell-length (about 1 mm) and large incident radiation of the LTPEF detector result in a linear calibration curve for PBD, even at solubility limited concentrations. The linear regression constants for the calibration plots were 0.984 for the UV absorbance detector and 0.987 for the LTPEF detector, showing equally good linearity.

Precision. The precision of the detection system was evaluated by making five injections of the three oxadiazoles at the concentrations listed in Figure 3. The peak heights were measured and the BBD peaks were used as internal standards. This was done so that only inconsistencies resulting from detector response would be considered. The relative standard deviation for the five PPD and PBD peaks were 6.7% and 10.1%, respectively. The LTPEF detector reproducibility compares favorably with that reported by Perchalski, Winefordner, and Wilder for a fluorometric HPLC detector (*11*), but is not as good as the reproducibility of a fluorometric detector reported by Cassidy and Frei (*12*). Inconsistencies in LTPEF detector response can be attributed, in part, to the nonlinear dependence of two-photon signals on laser power density, which makes beam and power stability critical to reproducibility. Better reproducibility could be attained if fluorescence signals were normalized to laser power output using Equation 1.

Selectivity. The selective detection of the oxadiazoles PPD, PBD, and BBD is illustrated in Figure 3. Chromatograms 3a and 3b are essentially identical despite the fact that the sample injected in Figure 3b contains several Polyaromatic Hydrocarbons (PAH) at concentrations of approximately 10^{-5} M. The same separations in Figure 4 show appreciable interference effects for the UV absorbance detector. In Figure 4b the PBD peak is almost totally obscured by the PAH and the PPD peak is unresolved as well. The PAH were chosen so that the BBD peak was not interfered and could be used as an internal standard.

At this point the selectivity of the LTPEF detector is limited by the availability of laser output frequencies. The present detector employs an argon ion laser which has several visible plasma lines between 4579 and 5145 Å. To take full advantage of the uniqueness of two-photon spectra, lasing action must be attained at two-photon frequencies covering most of the near UV region of the spectrum. This could possibly be done with high output power tunable dye lasers.

While two-photon absorption strengths are very small, molecular two-photon states are as common as one-photon states. This means that LTPEF detection can be applied to most fluorescent compounds provided a laser can be found with the proper output frequency and power. Of course many compounds would require laser output frequencies and powers which are not available at this point but, with the steady advancement of laser technology and two-photon absorption research, more applications of LTPEF detection are possible.

LITERATURE CITED

(1) J. N. Done, J. H. Knox, and J. Loheac, "Applications of High Speed Liquid Chromatography", J. Wiley and Sons, New York, N.Y., 1974, p 10.
(2) M. Krejci and N. J. Pospisilova, *J. Chromatogr.*, **73**, 105 (1972).
(3) S. G. Perry, R. Amos, and P. I. Brewer, "Practical Liquid Chromatography", Plenum Press, New York-London, 1972, p 194.
(4) E. D. Pellizzari and C. M. Sparachino, *Anal. Chem.*, **45**, 378 (1973).
(5) M. Göppert-Mayer, *Ann. Phys.*, **9**, 273 (1931).
(6) W. M. McClain, *Acc. Chem. Res.*, **7**, 199 (1974).
(7) B. A. Lengyel, "Lasers", J. Wiley and Sons, New York, N.Y., 1971, Chapter 9.
(8) G. G. Guilbault, "Practical Fluorescence", Marcel Dekker, New York, N.Y., 1973, p 138.
(9) A. E. Siegman, "An Introduction to Lasers and Masers", McGraw-Hill Book Co., New York, N.Y., 1971, p 317.
(10) D. R. Baker, R. C. Williams, and J. C. Steichen, *J. Chromatogr. Sci.*, **12**, 505 (1974).
(11) R. J. Perchalski, J. D. Winefordner, and B. J. Wilder, *Anal. Chem.*, **47**, 1993 (1975).
(12) M. Cassidy and R. W. Frei, *J. Chromatogr.*, **72**, 293 (1972).

RECEIVED for review March 30, 1977. Accepted June 6, 1977. Work performed for the U.S. Energy Research and Development Administration under Contract No. W-7405-eng-82.

Trace Chloride Determination by Rate Controlled Coulometric Titration

Michael J. Zetlmeisl* and David F. Laurence

Tretolite Division, Petrolite Corporation, 369 Marshall Avenue, St. Louis, Missouri 63119

A new type of coulometric instrument which uses feedback from the sensor to the generator in such a way that the current is a decaying exponential function of the concentration of chloride is described in detail. Mathematically, it is shown that for this instrument dE/dt is a constant at a good distance from the equivalence point and equal to one half the initial constant value in the vicinity of the equivalence point. Using conventional cell components with the instrument, trace chloride determinations are performed automatically on samples with concentrations as low as 2.8×10^{-5} M. A technique requiring some manual control is described for samples down to 5.6×10^{-6} M. The precision of the data is within a few percent of the relative standard deviation. The deviations from the known values are no worse than 5% for the samples down to 2.8×10^{-5} M. The relative accuracy gets worse for the more dilute samples. Common interferences to argentimetric analysis are obviated by means of preoxidation with $KMnO_4$.

Since the time of Lingane's (*1*, *2*) original work on coulometric determination of chloride in the early fifties, determination of chloride by coulometric procedures has become widely accepted. The lower sensitivity level for Cl^- has been extended into the nanoequivalent region by the use of special instrumentation and cells. The use of feedback circuits, such that silver ions are produced only as needed, dates back to at least 1960 (*3*). The method involved use of 70% acetic acid as electrolyte to suppress K_{sp} levels. Work at the nanoequivalent level was reported by Lädrach et al. (*4*), but success of the method depended on precise knowledge of the end-point potential which changed appreciably with small amounts of water added to the acetic acid electrolyte. Bishop aad Dhaneshwar employed differential electrolytic potentiometry to determine Cl^- at the subnanogram level at about 20% accuracy and with special manipulation of the sample and the use of a 0.5-mL microcell (*5*). The use of organic solvents as electrolyte has been widely investigated, and seems to be gaining universal acceptance (*6*, *7*). Cedergren also has reported data in the nanoequivalent range, but his method at these lower levels entails making a curve each day to obtain a correction for the drift at the electrodes (*7*). The lowest concentration of chloride in the samples analyzed by Bishop and Cedergren was 5×10^{-6} M. McCracken has developed an instrument in which a feedback signal which is proportional to the first time derivative of the indicator electrode potential continuously varies the electrolysis current. Data in the 1–100 μequiv range are reported (*8*).

In this paper, we would like to report Cl^- analysis with a new type of instrument which uses feedback from the sensor to the generator in such a way that the generator current decays exponentially as needed. As pointed out by the other authors, the benefits of this type of instrumentation arise from a better approximation of equilibrium at the end point, avoidance of overshoot, and ease of performing cumulative titrations in the same solvent.

The range of data that we have investigated extends down to a lower sensitivity of 0.2 ppm Cl^- in water or about 6×10^{-6} M. The method is fully automatic for concentrations down to 1 ppm, and requires a minimum of manual control for samples more dilute than this. No standardization or blank correction is made and macro titration cells with conventional components are employed. Minor drift of the electrodes is no problem. Moreover, multiple titrations can be performed in the same electrolyte, each titration taking only a few minutes to perform. In short, this technique is a rapid, simple, and automatic method of routinely analyzing for Cl^- at trace levels.

PRINCIPLE OF THE INSTRUMENT

Whereas other coulometric instruments have worked on either a constant current or a constant potential principle, this instrument works on the principle of constant rate of change of potential with time. The instrument supplies a current which is proportional to the antilog of the voltage difference between the cell potential and some bias voltage which is selected to be near the equivalence point. When a large amount of Cl^- is present, the cell potential is far removed from the bias voltage, and a large current passes. As the Cl^- is titrated and its concentration is reduced, the cell potential increases and the titration current level exponentially decreases. Consequently, the titrator approaches the equivalence point slowly near the end of a titration, thereby reducing the possibility of overshoot. Moreover, since current levels are low near the end of a titration, only very slight errors are encountered when E_{bias} is set considerably different from the equivalence point potential.

A block diagram of the apparatus is given in Figure 1. A differential input amplifier receives the voltage signals from the reference, E^r, and indicator, E^s, electrodes respectively and provides an output voltage equal to the difference between the two, $E^s - E^r = E$. This potential difference will be directly proportional at all times to the logarithm of the Cl^- concentration through the Nernst equation as follows: $E = E^\circ - (RT/nF) \ln [Cl^-]$. A comparator receives the voltage output from the amplifier and subtracts from it some arbitrary reference voltage, E_{bias}. This output of the comparator, $E - E_{bias}$, is applied to an antilogarithm converter in such a way that the output of the antilogarithm converter is proportional to the comparator output, $i = i_c \exp \{(-nF/RT)(E - E_{bias})\}$ where i_c is a small preset current of a few microamps. The current output is passed through the generator section of the cell. The total amount of current passed during a determination is registered in the integrator of the instrument.

The experimental relationship between current at the working electrode and cell potential brings about a situation in which silver ions are generated according to the demand for them by the presence of excess chloride ions. Moreover, the chloride is titrated at a constant rate as reflected in the derivation presented in the following paragraphs.

In these determinations, we are concerned with the coulometric generation of silver ions which then titrate the chloride ions according to the following equation: $Ag^+ + Cl^- \rightarrow AgCl$. In order to explain how the instrument can process the chloride at a constant rate, it is convenient to consider first the situation that exists at a good distance from the equivalence point; i.e., chloride decreasing in concentration

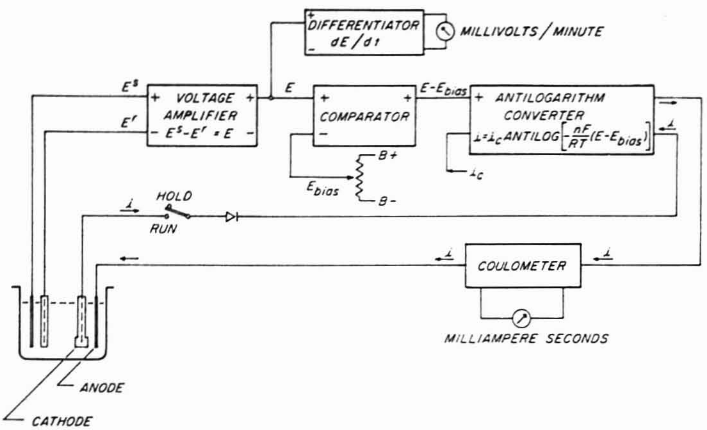

Figure 1. Block diagram of instrument

on a 1:1 basis with the silver ion being produced. For this situation, we can write the following Nernst equation:

$$E = E^\circ - \frac{RT}{nf}\ln\left([\mathrm{Cl^-}]_o - \left[\frac{Q}{FV}\right]\right) \tag{1}$$

where $[\mathrm{Cl^-}]_0$ = initial chloride ion concentration, $[Q/FV]$ = amount of charge that has passed, F = Faraday constant, and V = volume.

$$[\mathrm{Cl^-}]_o - \frac{Q}{FV} = \exp\left[\frac{-nf}{RT}(E - E^\circ)\right] \tag{2}$$

Equation 1 can be differentiated with respect to time:

$$\frac{\mathrm{d}E}{\mathrm{d}t} = -\left(\frac{RT}{nf}\right)\left(\frac{1}{FV}\right)\left(\frac{-\mathrm{d}Q}{\mathrm{d}t}\right)\left[\frac{1}{[\mathrm{Cl^-}]_o - [Q/FV]}\right] \tag{3}$$

But, $\mathrm{d}Q/\mathrm{d}t = i$, and, substituting Equation 2 into 3

$$\frac{\mathrm{d}E}{\mathrm{d}t} = \left(\frac{RT}{nf}\right)\left(\frac{1}{FV}\right)\left[\frac{\mathrm{i}}{\exp\left[\frac{-nf}{RT}(E - E^\circ)\right]}\right] \tag{4}$$

Let $(RT/nf)\ 1/FV = K$. Built into the instrument is Equation 5:

$$i = i_c \exp\left[\frac{-nf}{RT}(E - E_{\mathrm{bias}})\right] \tag{5}$$

So:

$$\frac{\mathrm{d}E}{\mathrm{d}t} = K\left[\frac{i_c \exp\left[\frac{-nF}{RT}(E - E_{\mathrm{bias}})\right]}{\exp\left[\frac{-nF}{RT}(E - E_{\mathrm{bias}})\right]}\right] \tag{6}$$

$$\frac{\mathrm{d}E}{\mathrm{d}t} = K\left[i_c \exp\left[\frac{nF}{RT}(E_{\mathrm{bias}} - E^\circ)\right]\right] \tag{7}$$

Equation 7 says that, at a considerable distance from the end point, $\mathrm{d}E/\mathrm{d}t$ is constant for any given value of E_{bias}. Moreover, the value of $\mathrm{d}E/\mathrm{d}t$ can be made greater or smaller by changing the value of E_{bias}. This value, however, should be chosen as close to the equivalence point as possible.

As described by MacInnes (*9*), a more complicated expression is needed to describe adequately the concentrations of silver and chloride in the vicinity of the equivalence point of this type of titration. Exactly at the equivalence point, of course, the following holds: $[\mathrm{Ag^+}] = [\mathrm{Cl^-}]$ and $[\mathrm{Ag^+}][\mathrm{Cl^-}] = K_{\mathrm{sp}}$.

Because silver ion is the generated species, it is convenient in describing the situation near equivalence to discuss a point infinitesimally past equivalence, and look at the cell potential as a function of silver ion concentration. At this hypothetical point infinitesimally past equivalence, the chloride ion concentration will be infinitesimally less than $\sqrt{K_{\mathrm{sp}}}$ and the silver infinitesimally greater than $\sqrt{K_{\mathrm{sp}}}$.

$$(\sqrt{K_{\mathrm{sp}}} - \Delta[\mathrm{Cl^-}])(\sqrt{K_{\mathrm{sp}}} + \Delta[\mathrm{Ag^+}]) = K_{\mathrm{sp}} \tag{8}$$

The situation of being slightly past equivalence is brought about by adding silver ions coulometrically. Some of these silver ions stay in solution as excess and some cause more chloride to precipitate. Consequently, the increment in the equivalents of charge, $\Delta Q/96500$, can be described as the sum of the silver that stays in solution as excess and that which precipitates more AgCl. The part of the silver that precipitates will, of course, precipitate $\mathrm{Cl^-}$ in the same amount and consequently that part of the silver can be equated to the amount of $\mathrm{Cl^-}$ that precipitates, $\Delta[\mathrm{Cl^-}]$, $[\Delta Q/F = \Delta(\text{equivalents Ag}^+)] + [\Delta(\text{equivalents Cl}^-)]$.

But, $[\Delta(\text{equivalents Ag}^+)]/V = \Delta[\mathrm{Ag^+}]$ and $[\Delta(\text{equivalents Cl}^-)]/V = \Delta[\mathrm{Cl^-}]$ where V = volume.

Therefore, $\Delta Q/F = V(\Delta[\mathrm{Ag^+}] + \Delta[\mathrm{Cl^-}])$ and

$$\Delta[\mathrm{Cl^-}] = \frac{\Delta Q}{FV} - \Delta[\mathrm{Ag^+}] \tag{9}$$

Substituting Equation 9 into 8

$$(\sqrt{K_{\mathrm{sp}}} + \Delta[\mathrm{Ag^+}])(\sqrt{K_{\mathrm{sp}}} - \frac{\Delta Q}{FV} + \Delta[\mathrm{Ag^+}]) = K_{\mathrm{sp}} \tag{10}$$

Solving the quadratic equation:

$$\Delta[\mathrm{Ag^+}] = -\sqrt{K_{\mathrm{sp}}} + \Delta Q/(2FV) + \sqrt{K_{\mathrm{sp}} + (\Delta Q)^2/(4F^2V^2)} \tag{11}$$

Taking the first derivative of Equation 11 with respect to time, and rearranging:

$$\frac{\mathrm{d}[\mathrm{Ag}^+]}{\mathrm{d}t} = \frac{1}{FV}\cdot\frac{\mathrm{d}Q}{\mathrm{d}t}\cdot\frac{1}{2}\left(1 + \frac{\dfrac{\Delta Q}{2FV}}{\sqrt{K_{\mathrm{sp}} + (\Delta Q)^2/(4F^2V^2)}}\right) \tag{12}$$

In the vicinity of the equivalence point ΔQ has become very small, and the second term in the parentheses of Equation 12 approaches zero.

Consequently,

$$\frac{\mathrm{d}[\mathrm{Ag}^+]}{\mathrm{d}t} = \frac{1}{2}\left[\frac{1}{FV}\cdot\frac{\mathrm{d}Q}{\mathrm{d}t}\right] \tag{13}$$

or

$$\frac{\mathrm{d}[\mathrm{Ag}^+]}{\mathrm{d}t} = \frac{1}{2}\left[\frac{i}{FV}\right] \tag{14}$$

We can now write a Nernst equation describing the cell potential as a function of $[\mathrm{Ag}^+]$.

$$E = E^{\circ\prime} + \frac{RT}{nF}\ln\,[\mathrm{Ag}^+] \tag{15}$$

$$\frac{\mathrm{d}E}{\mathrm{d}t} = \left(\frac{RT}{nf}\right)\left(\frac{\mathrm{d}[\mathrm{Ag}^+]}{\mathrm{d}t}\right)\left(\frac{1}{[\mathrm{Ag}^+]}\right) \tag{16}$$

Since $[\mathrm{Ag}^+] = [\mathrm{Cl}^-]$ at equivalence, we can write

$$[\mathrm{Ag}^+] = \exp\left[\frac{-nF}{RT}(E - E^\circ)\right] \tag{17}$$

Substituting Equations 14 and 17 into 16:

$$\frac{\mathrm{d}E}{\mathrm{d}t} = \frac{1}{2}(K)\left[\frac{i_{\mathrm{c}}\exp\left[\dfrac{-nF}{RT}(E - E_{\mathrm{bias}})\right]}{\exp\left[\dfrac{-nF}{RT}(E - E^\circ)\right]}\right] \tag{18}$$

and finally,

$$\frac{\mathrm{d}E}{\mathrm{d}t} = \frac{1}{2}(K)i_{\mathrm{c}}\exp\left[\frac{nF}{RT}(E_{\mathrm{bias}} - E^\circ)\right] \tag{19}$$

Comparing, Equation 19 with Equation 7, we see that $\mathrm{d}E/\mathrm{d}t$, the rate of change of potential with time at equivalence, is $^1/_2$ the value of $\mathrm{d}E/\mathrm{d}t$ at a good distance away from equivalence. Consequently, we can begin a titration and determine $\mathrm{d}E/\mathrm{d}t$ at the start of a titration. When the starting value of $\mathrm{d}E/\mathrm{d}t$ has decayed to half the original value, the determination is complete.

There is no need for a description of the situation much beyond the equivalence point since the generation of silver ions essentially stops at equivalence owing to the fact that $E - E_{\mathrm{bias}}$ is zero at this point and $i = i_{\mathrm{c}}$.

Proving that the potential changes at a constant rate with time is also proof, of course, that the chloride is disappearing at a constant rate with time. Considering the first derivative of the Nernst equation for $[\mathrm{Cl}^-]$

$$\frac{\mathrm{d}E}{\mathrm{d}t} = -\frac{RT}{nF}\,\frac{\mathrm{d}\ln\,[\mathrm{Cl}^-]}{\mathrm{d}t} \tag{20}$$

at 25 °C and for a 1-electron change

$$\frac{\mathrm{d}E}{\mathrm{d}t} = -0.026\,\frac{\mathrm{d}\ln\,[\mathrm{Cl}^-]}{\mathrm{d}t} = -0.059\,\frac{\mathrm{d}\log\,[\mathrm{Cl}^-]}{\mathrm{d}t} \tag{21}$$

This says that for each 26-mV change in potential per unit time, the $[\mathrm{Cl}^-]$ ion correspondingly decreases by a factor of "e" (59 mV per factor of 10) in the same period of time. A plot of actual experimental data for E vs. t and $\ln i$ vs. t is given in Figure 2. The consequent decrease in $[\mathrm{Cl}^-]$ is calculated in the same figure.

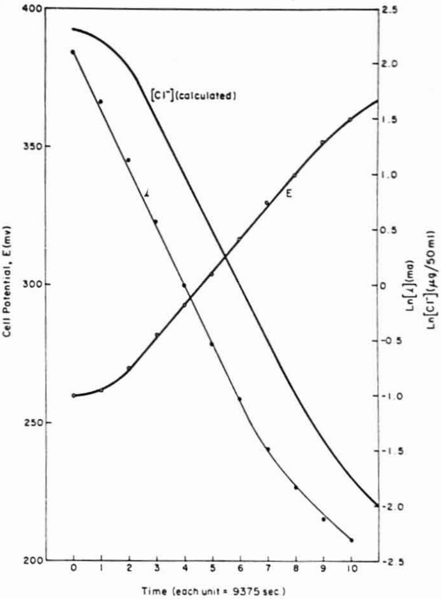

Figure 2. Plots of E, $\ln(i)$, $\ln[\mathrm{Cl}^-]$ vs. time

As we can see from Figure 2, E is a linear function of time except at the beginning and end of the titration. The former deviation is due to time lag at the sensor electrode which prevents the sensor from instantaneously seeing the change in Cl^- due to the current that has passed. The latter deviation is due, of course, to the fact that the current becomes very small when $E > E_{\mathrm{bias}}$. In other words, there is no longer any significant demand for current. The deviation from linearity in the beginning of the Cl^- curve is due, of course, to the deviation in the potential curve. The important point to note from these curves is that the current line is parallel to the Cl^- line. This parallelism is reflected in the following equations describing the $\ln\,(i)$ and $\ln\,[\mathrm{Cl}^-]$ functions with potential:

$$\ln\,(i) = \ln\,(i_{\mathrm{c}}) - \frac{nF}{RT}(E - E_{\mathrm{bias}}) \tag{22}$$

$$\ln\,[\mathrm{Cl}^-] = -\frac{nF}{RT}(E - E^\circ) \tag{23}$$

Since E is a linear function of time and $\ln\,(i)$ and $\ln\,[\mathrm{Cl}^-]$ are inverse linear functions of time, $\ln\,(i)$ and $\ln\,[\mathrm{Cl}^-]$ are inverse linear functions of E. This is reflected in Figure 3 where actual data for $\ln\,(i)$ vs. E is plotted and $\ln\,[\mathrm{Cl}^-]$ vs. E is calculated. The failure of the two lines to superimpose is explained by the difference in the constants of the two equations. Also, the deviation from linearity in the current line is explained once again by time lag in the sensor electrodes. If there were no time lag, the $\ln\,(i)$ and $\ln\,[\mathrm{Cl}^-]$ lines would be parallel from the beginning.

In performing a titration, an E_{bias} is set and current begins to pass according to Equation 5. The passage of current causes decay in the Cl^- ion concentration, causing an increase in cell potential. When the cell potential has reached the value of E_{bias}, the current is equal to i_{c}, and at this point the current automatically and very rapidly decays to a value approaching

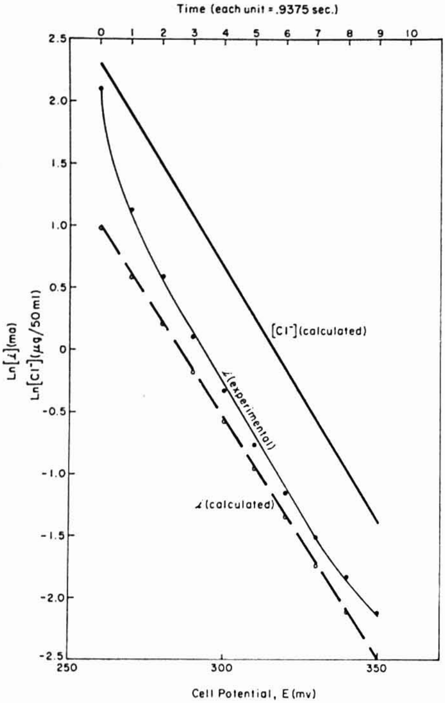

Figure 3. Plots of ln(I), ln[Cl$^-$] vs. cell potential and time

zero. An E_{bias} setting of 350 was used for the data generated in Figures 2 and 3. To get an idea of how closely these curves approach ideality, as shown in Figure 3, we can calculate the current line using the i_c value which is set in the instrument. The lack of correspondence is explained by the approximately half second time lag between what the sensor sees and what the working electrode is doing. This lag causes an insignificant error at the minute current levels at the end of a titration. Moreover, this error could be made even less by slowing the titration down by choosing a smaller E_{bias} or lowering the value of i_c. Using the approximate calculated concentration of Cl$^-$ at the end of the titration, a K_{sp} of about 10^{-14} would be calculated, in close agreement with published values of K_{sp} for AgCl in 90% acetone (*10*) which was the approximate composition of this electrolyte.

In short, the advantage of this method is that relatively large currents pass at a good distance away from the equivalence point, and decrease to very small values as the equivalence point is reached. The error due to time lag at the electrodes and the resulting end-point overshoot is minimized. Consequently, titrations in nonaqueous media can be performed without worrying about poor transport properties and end-point overshoot. Moreover, since the titrations essentially stop at the endpoint, cumulative titrations can be performed.

In using a nonaqueous electrolyte and adding aqueous samples, the end-point potential will change slightly from sample to sample due to changes in the K_{sp}. It should be clear to the reader that the ideal E_{bias} setting is at, or a little before, the equivalence point potential. Slight anticipation of the equivalence point in the setting helps compensate for time lag at the electrode. Some knowledge of the standard S-shaped curve is helpful in deciding this setting. If the break is very sharp, a setting anywhere along the sharp portion, and preferably below the midpoint of the break can be used. If the nature of the standard curve is not known, one can set a very high E_{bias}, let the machine pass current until the potential levels out, then back off E_{bias} until the current nulls to i_c. One or two quick pre-titrations of this type can determine E_{bias}. Because of the decaying nature of the current, relatively large errors in the end-point setting will lead to very small errors in the Cl$^-$ determination as long as a value on the steep portion of the S-shaped curve is chosen.

EXPERIMENTAL

Apparatus. The instrument used in these determinations is the Petrolite "Iontrak Analyzer", available from Petrolite Instruments, 4411 Bluebonnet, Suite C, Stafford, Texas 77477.

The data reported in this paper were determined using two basic cells, designated cell A and cell B. Cell A consisted of a 100-mL Berzelius beaker with the electrodes mounted in a Teflon cap, Part No. 180751, available from Beckman Instruments. The generator cathode was a platinum wire in a glass sleeve with fine frit, and a planar spiral of silver wire about 1 cm in diameter was the anode. The anode spiral was placed about 2 mm from the frit. A silver wire was the indicator electrode and the Orion Model 90-02-000 electrode, or a low impedance custom-made glass electrode from Markson was the reference. Cell B consisted of the Brinkmann cell cap, EA874, and the titration reservoir No. EA875-50 or EA875-20. A glass sleeve with fine frit was mounted in a plastic sleeve No. 20-21-570-4, available from Brinkmann. A hole was drilled into the side of the sleeve to accommodate the silver anode of the same type as used in cell A. Platinum was once again the cathode. Brinkmann No. EA242 silver electrode was the indicator and the Brinkmann double junction electrode was the reference. Alternatively, the Beckman glass electrode in a porous Vycor test tube, filled with water and a few drops of 35% $HClO_4$ was used as a reference. The internal portion of the Brinkmann double junction reference was filled with a saturated solution of LiCl in methanol or KCl in water. The external chamber was filled with titration electrolyte.

It was our experience that a few simple cell maintenance procedures should be followed at least daily. The anode should be cleaned by dipping in concentrated nitric acid solution for a few seconds and then rinsing thoroughly in distilled or deionized water. The isolation frit should be soaked in nitric acid overnight, and rinsed thoroughly before use. The indicator should be wiped with a soft tissue when precipitate begins to flocculate at its surface. The solvent should be titrated with standard solution twice after any such manipulation of cell components.

Reagents. The electrolyte was acetone plus 5 drops of 35% $HClO_4$. Cell A used 50 mL of solvent whereas cell B used 20 mL. The isolation sleeve was filled about half way with acetone and one drop of 35% $HClO_4$ was added. Other organic solvents could doubtlessly be used as long as the K_{sp} of AgCl in them is low (*5–7*). The same electrolyte can be used for up to 20 titrations, or until the acetone becomes appreciably wet. Standard Cl$^-$ solution, prepared by accurately weighing 0.0850 g dry, reagent grade NaCl into 100 mL deionized water, was pre-titrated several times in fresh electrolyte before samples were titrated. Standard Cl$^-$ solution was added to the titration vessel with a Hamilton microsyringe, CB-700-200.

Preoxidation of Interferences. Common interferences such as S^{2-}, SH^-, CN^-, and SCN^- were conveniently handled by means of preoxidation with $KMnO_4^-$ under acidic conditions. The sample with interferences was added to the cell, and 7–10 additional drops of acid were added. With the electrodes out of the solution, 1% $KMnO_4$ was added until a pink color persisted. The excess MnO_4^- was discharged by adding 1% ascorbic acid until the color disappeared. Ascorbic acid was used instead of the more conventional oxalic acid because the latter reacted with Ag^+ in acetone. One precaution with the preoxidation procedure is that the acetone must have a few percent water for good results. The addition of extra aqueous acid takes care of this problem.

Instrumental Procedures. For samples with 1 ppm Cl$^-$ or more, the analyst can leave the machine unattended during a

Table I. Determinations of Cl^- in Aqueous Samples Using Cell A

Cl^- taken, μg	No. of determinations	Mean, μg	SD, μg[a]	RSD, %[b]	Reference electrode
50.4	7	52	1.71	3.3	Double junction Ag/AgCl
50.4	9	52	1.52	2.9	Double junction Ag/AgCl
50.4	10	49.7	0.75	1.5	Double junction Ag/AgCl
50.4	10	48.3	1.49	3.1	Double junction Ag/AgCl
25.2	60	25.95	0.57	2.2	Glass electrode
25.2	6	26	1.14	4.4	Glass electrode
25.2	29	25.2	0.25	1.0	Glass electrode

[a] SD = Standard Deviation. [b] RSD = Relative Standard Deviation.

Table II. Determination of Cl^- in Aqueous Samples Using Cell B

Cl^- taken, μg	No. of determinations	Mean, μg	SD, μg	RSD, %	Reference electrode
53	15	54.3	0.75	1.3	Double junction SCE
53	6	52.4	0.38	0.7	Double junction SCE
53	6	55.25	0.94	1.7	Double junction SCE
53	9	53.37	1.05	2	Double junction SCE
53	12	54.63	0.13	0.24	Double junction SCE
10.3	5	10.1	0.48	4.9	Double junction SCE
10.3	5	10.09	0.25	2.4	Double junction SCE
5.15	6	5.4	0.25	5.7	Double junction SCE
10.3	6	10.2	0.43	4.2	Glass electrode in porous Vycor test tube
10.3	10	9.8	0.52	5.3	Glass electrode in porous Vycor test tube
10.3	11	10.26	0.68	5.7	Glass electrode in porous Vycor test tube
5.15	9	5.10	0.14	2.7	Glass electrode in porous Vycor test tube

titration. The only setting to be determined is E_{bias}, which, for concentrated samples, can vary over the range, 100–200 mV. E_{bias} can be determined by running a few trial auto-titrations of Cl^- standard and finding the setting for E_{bias} where the current nulls to zero at the end point. A potential close to the equivalence point potential can also be chosen for E_{bias}, if that potential is known. Using the Orion reference electrode, E_{bias} settings in the 270–350 mV range were found optimum. With the Brinkmann electrode, using nonaqueous filling solutions, potentials of 375–425 mV were found optimum. With the glass electrode, a setting of −125 to −150 mV was used.

For samples with much less than 1 ppm, observation of the change in dE/dt was used to indicate the end point. Dilute solutions require addition of such large samples that we end up with high K_{sp} values and small potential displacements. Consequently, we are fairly close to equivalence even at the beginning of a titration, and we must titrate very slowly or we will overshoot. After adding sample and letting the electrodes equilibrate, the titration is run with a bias voltage sufficient to give an initial rate of 10–20 mV per minute. This initial rate of change, dE/dt, is the maximum, constant rate at which the instrument settles. When the rate has decayed to half the initial value, the titration is complete. Several pretitrations were performed before data collection began.

RESULTS AND DISCUSSION

Representative data of Cl^- analyses using cell A are given in Table I. To put these data in the context of a field sample, it is possible to use up to a 10-mL aqueous sample in 50 mL of electrolyte. Consequently, the data presented here represent about 5 ppm Cl^- (1.4×10^{-4} M) in the sample. For samples where greater sensitivity is required, a smaller cell such as the one discussed below with Table II, or the rate end-point method can be used. The data in Table I were generated using either a double junction Ag/AgCl reference electrode filled with aqueous KCl interior, and aqueous NH_4NO_3 exterior solutions or a glass electrode. Whereas the glass electrode was noisier than the double junction Ag/AgCl electrode, it had the advantage of absolutely eliminating the possibility of Cl^- leak.

Table III. Determination of Cl^- in Aqueous Samples Using Cell B and Various E_{bias} Settings

Cl^- taken, μg	No. of determinations	Mean, μg	SD	RSD, %	E_{bias}
53	5	55.4	1.82	3.2	350
53	2	54.8	3.3	6	400
53	4	55.5	0.7	1.2	450
53	4	55.5	1.58	2.8	500

In Table II, data are reported from cell B and two different reference electrodes. Comparing the deviations from the known values and the precision of the data from the two cells for Cl^- values of about 50 μg, it is concluded that this cell is slightly better than the 50-mL cell. Moreover, because of the smaller volume and consequent higher Cl^- concentration for a given Cl^- assay, it was possible to analyze samples down to 5 μg Cl^-. When the series at 5 μg Cl^- was performed, a total of 5 mL of water had been added to the cell. Therefore, these results would represent aqueous samples with about 1 ppm Cl^- (2.8×10^{-5} M), about a factor of 5 more sensitive than the data in Table I. The deviations from the known values are no worse than 5% for any of the data in Tables I and II, even the less concentrated samples.

Tables I and II contain many sets of multiple determinations under identical conditions. The reason for this repetition was to convince ourselves of the reproducibility of our methods. A period of at least a day, and in some cases several months, elapsed between the data gathering represented in each line of Tables I and II.

Both the double junction SCE and a glass electrode were used with cell B with comparable results. A 17-mm porous Vycor test tube filled half way with water and then two drops of 35% $HClO_4$ offered an aqueous bridging solution between the glass electrode and the electrolyte. This configuration

Table IV. Determination of Cl^- Using dE/dt Mode on Aqueous Samples Such That Titration Cell Contains 33.3% H_2O–66.6% Acetone

μgCl^-/mL taken	Sample size, mL	No. of determinations	Mean, μgCl^-/mL	SD	RSD, %
1.04	50	14	1.08	0.02	1.54
0.207	50	8	0.204	0.036	17.57
0.202	25	12	0.25	0.008	6.51
0.207	25	15	0.232	0.009	3.85

Table V. Determination of Cl^- in Presence of S^{2-}, SH^-, CN^-, and SCN^-

Cl^- taken, μg	No. of determinations	Mean, μg	SD	RSD, %	Interferences present, μg			
					S^{2-}	SH^-	CN^-	SCN^-
50.1	35	50.8	1.25	2.47	0	0	0	0
25.2	60	26	0.57	2.20	0	0	0	0
50.2	8	53.65	3.85	7.18	106.2	0	52	0
50.2	8	51.43	3.12	6.07	106.2	0	52	51
50.2	13	51.43	1.97	3.83	106.2	297	52	51

removed some of the electrical noise from the glass electrode, and prevented dehydration of the membrane. The porous Vycor junction offered very low impedance and low leak rate.

As pointed out above, the leeway in setting E_{bias} is a function of the total potential displacement. From Equation 5, it is obvious that E_{bias} must be greater than the cell potential at the start of a titration and less than, or equal to, the cell potential at the end in order for the current to approach zero. Consequently, the range of possible choices for E_{bias} is greater for a larger potential break than for a smaller one. To illustrate the invariance of the results when the break is large, the data in Table III were generated. The potential break for this determination is 250 mV. As we can see, the results were the same for E_{bias} settings over a 150-mV range. The only caution is that the first titration after changing E_{bias} should not be used, because this titration sets the finishing point of a determination. Whether that point is exactly the same as the equivalence point is not important after the first titration because it will take exactly the amount of Cl^- in the next sample to bring us back to the finishing point.

The end-point can also be located by observing a decrease in dE/dt. This method depends on the fact that potential is a linear function of time as described above. As the end point of a titration approaches, the change of potential with time approaches one half the original value, and we can use this point as an indication of the end point of a determination. The way that we actually monitor the linear E vs. t region is by observing the region where dE/dt is constant, and then continuing to pass current until dE/dt decays to one half of its initial value.

Data generated using this mode of operation are summarized in Table IV. The enhanced sensitivity comes from the fact that we can analyze samples that cause a very small potential displacement, 10–20 mV. Note that the sample size used in Table IV was 25–50 mL. A 100-mL Berzelius beaker was used for the smaller samples and a 200-mL beaker for the larger. Such large aqueous samples give us an appreciable amount of Cl^- ($\simeq$5 μg) even for samples of very low concentration such as 0.2 ppm. These data demonstrate another order of magnitude sensitivity over the data in Tables I and II, and concentrations comparable to those reported by Bishop and Cedergren (*5, 7*). The precision and accuracy of these determinations is not as good as for the more concentrated samples in the auto-mode of operation.

Interferences common to argentimetric analysis such as S^{2-}, SH^-, CN^-, and SCN^- have been successfully handled by means of preoxidation with $KMnO_4$. Data from these analyses are reported in Table V.

ACKNOWLEDGMENT

The authors acknowledge the many enlightening discussions with R. R. Annand of Tretolite Division, Petrolite Corporation, and J. M. Victor of Petrolite Instruments.

LITERATURE CITED

(1) J. J. Lingane and L. A. Small, *Anal. Chem.*, **21**, 119 (1949).
(2) J. J. Lingane, *Anal. Chem.*, **26**, 630 (1954).
(3) D. M. Coulson and L. A. Cavanaugh, *Anal. Chem.* **32**, 1245 (1960).
(4) W. Lädrach, F. Van de Craats, and P. Gouverneur, *Anal. Chim. Acta*, **50**, 219 (1970).
(5) E. Bishop and G. Dhaneshwar, *Anal. Chem.*, **36**, 726 (1964).
(6) T. S. Propokov, *Mikrochim Acta*, 401 (1968).
(7) A. Cedergren and G. Johansson, *Talanta*, **18**, 917 (1971).
(8) J. E. McCracken and J. C. Guyon, *Chem. Instrum.*, **3**, 311 (1972).
(9) D. A. MacInnes, "The Principles of Electrochemistry", Dover Publications, New York, N.Y., 1961, p 314.
(10) G. J. Janz and R. P. T. Tomkins, "Nonaqueous Electrolytes Handbook", Vol. 2, Academic Press, New York, N.Y., 1973, p 123.

RECEIVED for review April 21, 1977. Accepted June 13, 1977.

Study of the Steady-State Current at Tubular Electrodes in the Micromolar Concentration Region

W. J. Blaedel* and D. G. Iverson

Department of Chemistry, University of Wisconsin, Madison, Wisconsin 53706

The steady-state current at tubular electrodes was found to consist of a flow rate independent (I_{ind}) and a flow rate dependent (I_{dep}) component. In micromolar ferricyanide solutions containing phosphate buffer, the effects of electrode pretreatment, ferricyanide concentration, pH, ionic strength, applied potential, and electrode material on the steady state current components are reported. The component I_{dep} varies with the cube root of the flow rate, whereas I_{ind} is independent of flow rate. Both components depend linearly on ferricyanide concentration. A pulsed flow and an alternate solution method of measurement for low concentrations of electroactive material are investigated. The pulsed flow mode of voltammetry shows considerable analytical promise for the measurement of low concentrations of electroactive materials.

Steady-state voltammetry at solid convective electrodes has been found to have advantages compared to scanning voltammetry for the measurement of low concentrations of electroactive materials (*1*). Ideally, in the steady-state mode, charging currents and transient currents due to electrode surface reactions are permitted to die away, and the remaining steady-state current reflects only the presence of electroactive material which is convectively brought to the electrode surface.

It is generally well established, theoretically and experimentally, that the steady-state current at tubular electrodes depends on the cube-root of the flow rate. However, work at micromolar concentrations in our laboratory over the past few years indicates that the steady-state current at small tubular flowthrough electrodes (2 mm long, 1–2 mm diameter) consists of two components:

$$i_{ss} = i_{ind} + i_{dep} \tag{1}$$

The component i_{ind} is independent of flow rate, and the component i_{dep} shows the cube-root dependence on flow rate.

The existence of a flow-rate independent current component has not been recognized by some workers including ourselves. Recently, however, several investigators have reported currents deviating from those expected in simple hydrodynamic regimes. Current components similar to i_{ind} have been described at tubular and flow-through electrodes (*2–5*) and have been ascribed by most workers to an axial diffusion mode of transport. Also, the role of a diffusional component along with a convective component has been established at rotated disk electrodes (*6*).

The main purpose of the following work is to study how the two steady-state current components of Equation 1 depend on the physical and chemical characteristics of the system. As a result of this study, a pulsed-flow voltammetric procedure is indicated to have definite advantages for the measurement of low concentrations of electroactive materials with tubular electrodes. The advantage of measuring very low concentrations of electroactive material by a differential current measurement between zero and high flow rates has been described (*7*). An analogous procedure has been described by Miller and Bruckenstein (*8*) with a rotated disk electrode driven at sinusoidally modulated speeds, with limits of detection approaching the nanomolar level.

THEORY

The character of i_{dep} for tubular electrodes is well defined (*9*):

$$i_{dep} = 2{:}01\ nFC_bD^{2/3}R^{2/3}X^{2/3}V_f^{1/3} \tag{2}$$

In Equation 2, n is the number of electrons per molecule of electroactive species transformed, F is the value for the Faraday, C_b is the bulk concentration, and D is the diffusion coefficient of the electroactive material. R and X are the radius and length of the tubular electrode respectively, and V_f is the volume flow rate of solution.

According to Equations 1 and 2, a plot of i_{ss} vs. $V_f^{1/3}$ should be linear with an intercept (i_{ind}) and a slope S ($S = 2.01\ nFD^{2/3}R^{2/3}X^{2/3}C_b$), so that

$$i_{ss} = i_{ind} + SV_f^{1/3} \tag{3}$$

Almost all of the data presented in this paper are condensed into the slopes and intercepts of straight line plots of Equation 3.

In practice, the steady-state current may sometimes have to be measured on top of a residual or drifting background current that is significant at low concentrations of electroactive material. Such residual currents may be troublesome when i_{ss} is used as a measure of concentration of electroactive species. These complications may be circumvented with a pulsed flow technique in which the difference of two steady-state currents is measured—one at a high flow rate and one at a low flow rate:

$$\Delta i = i_{ss,hi} - i_{ss,lo} = S(V_{hi}^{1/3} - V_{lo}^{1/3}) \tag{4}$$

Since S is proportional to the bulk concentration of the electroactive material, the steady-state current difference (Δi) is also proportional to C_b for a fixed set of high and low flow rates:

$$\Delta i \propto C_b \tag{5}$$

Equation 5 is the basis for the pulsed flow method of measuring concentrations.

EXPERIMENTAL

Instrumentation. Potentials were applied to the two electrode cell with a simple battery powered potentiometer. Current was measured with a picoammeter (Model 414S, Keithley Instruments, Cleveland, Ohio) and recorded on a strip chart recorder (Omniscribe, Series 5000, Single Channel; Houston Instruments, Bellaire, Texas). Cell resistances were measured with a conductance bridge (Model RCM 15B1, A. H. Thomas Co., Philadelphia, Pa.) Measurement of the cell voltage was performed with a vacuum tube voltmeter (Model 850, Triplett Electrical Instrument Co., Bluffton, Ohio), during times when current measurements were not being made, mainly to simplify circuitry and to avoid interference with the reading of low currents.

Cell and Electrodes. The cell (Figure 1) consisted of two cylindrical Lucite blocks held together with 4 stainless steel bolts

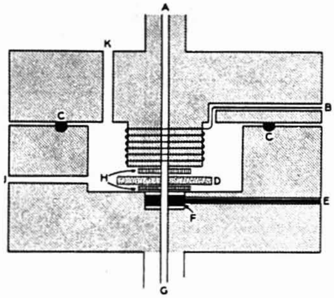

Figure 1. Flowthrough cell with tubular electrode and silver–silver chloride reference electrode. A. Sample solution outlet. B. Lead to reference electrode. C. O-ring. D. Fritted disk, agar impregnated. E. Lead to tubular electrode. F. Tubular electrode (platinum or gold). G. Sample solution inlet. H. Silicone rubber washers. J. Reference electrode solution inlet (0.01 M KCl). K. Reference electrode solution outlet

(not shown). The upper block held the silver–silver chloride reference electrode (15 cm of 24 gauge silver wire), wound around a post which fitted into the cavity of the lower block. The tubular electrode was potted into the lower block with epoxy (Epotek 349, Epoxy Technology, Watertown, Mass.). Two interchangeable lower block assemblies were made: one with a platinum electrode (0.055-in. diameter, 0.099 in. long), and one with a gold electrode (0.055-in. diameter, 0.102 in. long). Bridging between the sample channel and the reference electrode solution cavity was made with an agar impregnated fritted disk (20F, Corning Glass Works, Corning, N.Y.) sandwiched between two silicone rubber washers. When the lower and upper blocks were bolted together, compression of the washers gave a leak-proof seal between the sample solution and the reference electrode solution. The separation between the tubular electrode and the bridging frit was about 2 mm.

The solution inlet tube was made of glass rather than Lucite, on which there appeared to be a high tendency for bubbles to form and adhere, which in turn interfered with sample washout and rinsing.

The electrode leads were made of heavy gauge copper wire, inserted into holes which had been bored into the block and slightly into the electrode material, and then joined with conducting epoxy (Epotek 410E).

After the cell was assembled, and before use, the silver wire electrode was converted to a silver–silver chloride electrode (SSCE) by anodization (*10*).

The Solution Train. The sample solution was contained in a beaker fitted with a parafilm cap containing two holes: one for the sample solution inlet of the cell (Figure 1), and another for a deaeration tube that delivered a stream of nitrogen. After exit from the cell, the sample solution was passed via Tygon tubing through a calibrated rotameter (No. 9143 Fischer and Porter, Warminster, Pa.) and a Teflon needle valve to control flow rate. The drainage end of the tubing was well below the sample solution beaker, to provide siphoning that produced a steady flow of solution.

To provide the high and low flow rates needed for pulsed flow voltammetry, a manual flow pulser was inserted between the rotameter and the Teflon needle valve. The pulser consisted of two parallel branches: one containing a Teflon stopcock and one containing a length of Tygon tubing with a screw clamp. The low flow rate (about 0.5 mL/min) was achieved with the stopcock closed, by adjusting the pinch clamp. The high flow rate (5 or 9 mL/min) was achieved with the stopcock open, by adjusting the needle valve.

The reference solution was also deaerated, siphoned through glass tubing to the reference electrode cavity, and drained through Tygon tubing below the reservoir. Reference solution flow was controlled at about 0.1 mL/min by a screw clamp.

Preparation of Solutions. Tap distilled water was redistilled once from a basic permanganate solution. All chemicals were analytical reagent grade. Phosphate buffer solutions were made from 0.1 M stock solutions of $K_2HPO_4{\cdot}3H_2O$ and KH_2PO_4. Buffer solution at pH 7.4 was prepared from a 1:4 mixture of the dihydrogen and monohydrogen phosphate stock solutions; and pH 6.4 solution was prepared from a 4:1 mixture.

A 1 mM stock solution of ferricyanide was prepared every 10 days from $K_3Fe(CN)_6$ in the phosphate buffer of the desired pH and stored in the dark. The working standards were prepared by diluting the stock solution with the desired buffer as needed each day.

The reference electrode solution was 0.01 M KCl saturated with AgCl. All potentials in this work were measured against the Ag–AgCl electrode in 0.01 M KCl.

Measurement Procedures. The electrodes were polished with 600-mesh carborundum on a wetted, wooden match stick. A 0.01 M buffer solution (pH 7.4) was purged continuously and vigorously in the parafilm covered beaker with dry, purified tank nitrogen. After 10–15 min of deaeration, the buffer was allowed to flow slowly through the cell for 1–2 min. Electrical pretreatment of the electrode was changed through the course of the work. Most data were taken with pretreatment of the electrode at +0.9 V, −0.9 V and +0.9 V for 1 min at each potential. Following pretreatment, the desired working potential was applied and transient currents were allowed to decay until steady state was reached. Decay times were about an hour, although longer times up to two hours were allowed when very low background currents were sought. Typical background currents in the potential region from −0.3 V to −0.6 V were less than 3 nA with noise levels around ±0.3 nA.

Current vs. flow rate data for various conditions were obtained over flow rates ranging up to about 10 mL/min by adjusting the Teflon needle valve and reading the recorded current. Current response for the platinum electrode and 4 μM ferricyanide solution at pH 7.4 ranged from about 55 to 110 nA over the stated flow rate range. Blank buffer solutions gave only about 1 nA of current at an applied potential of −0.3 V.

To delineate i_{∞} vs. $V_f^{1/3}$ plots, currents were measured for about seven flow rates. A least squares calculator program gave the intercept, slope, and their 90% confidence limits (*11*). Pulsed flow analysis was performed by switching between low and high flow rates of 0.95 and 9.5 mL/min early in the work, and between 0.5 and 5 mL/min for later experiments. This was done by turning the stopcock on the pulser on and off. Estimates of the current differences (Δi) were obtained by averaging over five cycles of low to high flow rates. Ferricyanide solutions ranging up to 4μM were measured at an applied potential of −0.3 V. After a change in flow rate, only 2–3 s were needed to reachieve steady currents.

An alternate solution procedure was devised that consisted of exchanging the sample solution and the blank periodically, and measuring the current difference between them. Here, beakers containing deaerated blank solution and sample solution were exchanged manually at the sample tube inlet. Except for a 1-s shut-off time during the exchange, the solution flow rate was maintained at 3 mL/min. After an exchange of beakers, about 3 min were needed to reachieve steady currents. Estimates of the current differences were obtained by averaging over three cycles of solution exchange.

RESULTS AND DISCUSSION

Effect of Electrode Pretreatment on Current-Flow Rate Data. In general, plots of steady-state current vs. the cube root of flow rate were highly linear (see Figure 2). Because the electrode surface was not polished reproducibly, and because the surface aged slowly over several days after polishing, day-to-day data showed greater variation than within-day data. Within-day variations of the slopes and intercepts were around 5% relative. It is well known that platinum and gold electrode surfaces are subject to oxidation at around +0.4 V and +0.9 V vs. SCE respectively (*12*). A procedure was therefore adopted for electrochemical pretreatment of the platinum electrode by applying +0.9 V and −0.9 V for 1 min at each potential followed by a 10-min application of +0.4 V where slight oxidation occurs, and then 5 min at −0.6 V to remove any oxide coating. A 5-min ap-

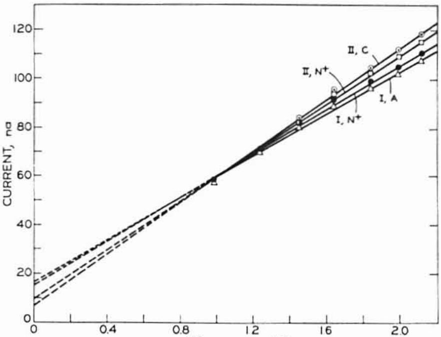

Figure 2. Current–flow rate plots for different electrode pretreatments. These plots give some of the slopes and intercepts summarized in Table I. Curve identification is made with a Roman numeral (day) and a letter to indicate mode of pretreatment (*N* is normal) according to Table I. Conditions: As in Table I

Table I. Effect of Electrode Pretreatment on Current-Flow Rate Parameters[a]

Pretreatment[b]	Slope,[c] nA/(mL/min)$^{1/3}$	Intercept,[c] nA
DAY I		
Normal[d]	45.4 ± 1.7	15.3 ± 2.8
Modification A	54.5 ± 1.0	8.7 ± 1.8
Modification B	52.2 ± 1.9	7.6 ± 3.1
Modification A[d]	43.5 ± 2.6	16.0 ± 4.3
DAY II		
Modification A[d]	45.9 ± 1.6	11.7 ± 2.6
Normal[d]	50.1 ± 1.6	9.7 ± 2.7
Modification C	52.8 ± 1.7	7.1 ± 2.8
2-day Av. (std dev)	49.2 (4.2)	10.9 (3.6)

[a] Conditions: 4 μM $K_3Fe(CN)_6$ in 0.01 M phosphate buffer (pH 7.4) at platinum electrode, with applied potentail of −0.3 V vs SSCE (0.01 M KCl). [b] Normal pretreatment is described in text. Modification A: −0.9 V (1 min), +0.9 V (1 min), +0.05 V (5 min). Modification B: +0.4 V (10 min), −0.6 V (5 min), +0.05 V (5 min). Modification C: −0.9 V (1 min), +0.9 V (1 min), −0.9 V (1 min). [c] Tabled values include 90% confidence limits. [d] Preceded by electrode polishing.

plication of an intermediate potential (+0.05 V) preceded the application of the −0.3 V working potential. The effect of various modes of electrode pretreatment on the current-flow rate plot parameters is summarized in Table I. It appears that there is little difference among the electrochemical pretreatments, which is the basis for choosing the simple 3-min treatment (Modification C) in most of the following work. However, there does appear to be a definite effect of polishing in reducing the slope and perhaps in increasing the intercept.

Effect of Ferricyanide Concentration on the Steady-State Current Components. The slopes and intercepts of current-flow rate plots were measured for 10 ferricyanide concentrations over the range 0–40 μM. As expected from Equation 2, the slope (related to the flow rate dependent component, i_{dep}) was linearly dependent on the ferricyanide concentration. In addition, the flow rate independent current component (i_{ind}, as measured by the intercept) was also linearly dependent on ferricyanide concentration, as shown in Figure 3. This suggests that i_{ind} is due entirely to transport of the electroactive material, but by a mechanism different from the radial transport of the laminar flow regime that gives rise to i_{dep}. Axial transport (*3*), particularly at the ends of the tubular electrode, would explain the observed behavior of i_{nd}.

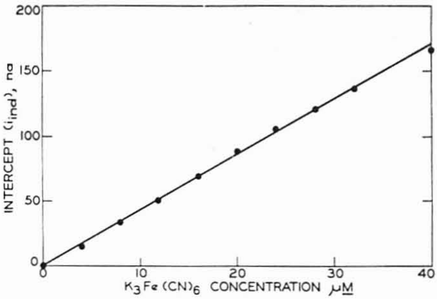

Figure 3. Concentration dependence of the flow rate independent current component (i_{ind}). Conditions: Various concentrations of $K_3Fe(CN)_6$ in 0.01 M phosphate buffer (pH 7.4) at platinum electrode with applied potential of −0.3 V vs. SSCE (0.01 M KCl)

Table II. Effect of Ionic Strength on Current-Flow Rate Plot Parameters[a]

Total phosphate molarity	Slope,[b] nA/(mL/min)$^{1/3}$	Intercept,[b] nA
0.01	54.8 ± 1.2	4.6 ± 1.9
0.05	62.9 ± 1.1	−1.1 ± 1.8
0.10	65.1 ± 0.9	−2.5 ± 1.5
0.05	60.7 ± 1.1	−0.8 ± 1.8
0.01	50.8 ± 1.6	7.8 ± 2.6

[a] Conditions: As in Table I, except variable phosphate buffer concentration (pH 7.4). [b] Tabled values include 90% confidence limits.

Examination of the original data and calculations leading to Figure 3 shows that i_{ind} is obtained by extrapolation, and that it is only a component of the larger experimentally measured steady-state current, i_{ss}. (The 90% confidence limits of the data points in Figure 3 are around ±15%, relative). Consequently i_{ind} is not very precisely measurable by the simple procedure of this paper. However, if an equally simple but more precise way could be found, it might prove to be an easy and rapid way to obtain information on the diffusional properties of electroactive substances, because the axial component appears to be diffusion-controlled rather than convection-controlled.

Effect of pH and Ionic Strength on the Steady-State Current Components. Measurements in $K_3Fe(CN)_6$–phosphate buffer systems indicated little effect due to pH in the range 6.4 to 7.4 on the steady-state current components. Table II shows small but significant effects on the slope and intercept caused by several-fold changes in ionic strength. For example, even though small, i_{ind} appears to change from cathodic to anodic as the buffer concentration increases. Since this effect could be associated with impurities in the phosphate salts, it was not investigated further. Also, the slope appears to increase significantly with the ionic strength, perhaps because of its effect on the diffusion coefficient or kinematic solution viscosity.

The Gold Electrode. After the −0.3 V working potential was applied, less time was required for the gold electrode to reach steady state than for the platinum electrode. The steady-state background currents (about 0.9 ± 0.4 nA) were also more reproducible. However, the day-to-day response to ferricyanide was less reliable and more dependent on

Table III. Current-Flow Rate Plot Parameters for the Gold Electrode[a]

Day	Slope,[b] nA/(mL/min)$^{1/3}$	Intercept,[b] nA
1[c]	42.3 ± 1.8	7.4 ± 3.0
2[c]	48.4 ± 1.8	1.1 ± 3.0
3	40.0 ± 2.4	9.2 ± 4.0
4[c]	46.5 ± 1.3	4.0 ± 2.1
5	42.5 ± 2.0	6.6 ± 3.2
Average (std dev)	43.9 (3.4)	5.7 (3.2)

[a] Conditions: As in Table I. [b] Tabled values include 90% confidence limits. [c] Preceded by electrode polishing.

Table IV. Comparison of Pulsed Flow and Alternate Solution Procedures[a]

$K_3Fe(CN)_6$ concn, μM	Pulsed flow Δi, nA	Alt. soln Δi, nA
4	39.8	53.5
2	20.5	30
1	10.6	14
0.4	4.5	5.7

[a] Conditions: Various concentrations of $K_3Fe(CN)_6$ in 0.01 M phosphate buffer (pH 7.4) at platinum electrode with applied potential of −0.3 V vs. SSCE (0.01 M KCl). Pulsed flow rates: 0.95 and 9.5 mL/min. Alternate solution flow rate: 3.0 mL/min. Characteristics of plots of the above data (Δi vs. $K_3Fe(CN)_6$ concentration) are, for pulsed flow and for alternate solution procedures, respectively: slopes (nA/μM), 9.8 ± 0.2 and 13.3 ± 1.9; intercepts (nA), 0.74 ± 0.47 and 1.2 ± 4.4; S_Y (nA), 0.19 and 1.8.

polishing. The gold electrode also responded more slowly to changes from blank to ferricyanide solution. Table III gives daily measurements on the current-flow rate plot parameters under conditions similar to those for the platinum in Table I. Comparison of the average slopes and intercepts in Table I and III indicates slightly smaller values for the gold electrode than for the platinum electrode. However, the differences are not significant enough to warrant the statement that ferricyanide reduction is inherently easier at the platinum electrode than at the gold electrode, even though the geometries and surface finishing of the two electrodes are virtually identical.

Comparison of the Pulsed Flow and Alternate Solution Procedures for the Measurements of Low Concentrations. A comparison of the two procedures is given in Table IV. It is clear that the precision of the alternate solution procedure is much poorer than that for the pulsed flow method. The chief reason for the poorer precision of the alternate flow procedure was postulated to be that much more manipulation and a longer time are involved in determining Δi, which is a difference in current between two different solutions.

Table V gives the results of a quantitative study of the dependence of pulsed flow current (Δi) on ferricyanide concentration in the submicromolar region. The plot of Δi vs. concentration is highly linear up to 4 μM, which was the highest concentration studied. If the limit of detection is taken to be equal to the background level, or to be the standard deviation of the individual data points from the straight line, a value around 0.05 μM is obtained.

Table V. Dependence of Pulsed Flow Current upon Ferricyanide Concentration[a]

$K_3Fe(CN)_6$ concn, μM	ΔI, nA
4	40.9
2	21.0
1	11.5
0.5	6.5
0.2	3.5
0.1	2.1
0	0.76

[a] Conditions: As in Table IV, except that pulsed flow rates are 0.5 and 5.2 mL/min. Characteristics (with 90% confidence limits) of plots of Δi vs. $K_3Fe(CN)_6$ concentration are: slope, 9.9 ± 0.18 nA/μM; intercept, 1.3 ± 0.32 nA; S_Y, 0.32 nA.

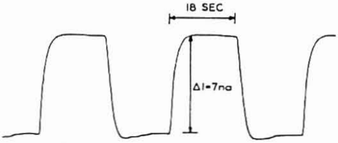

Figure 4. Pulsed flow response for 1 μM $K_3Fe(CN)_6$. Conditions: 1 μM $K_3Fe(CN)_6$ in 0.01 M phosphate buffer (pH 7.4) at platinum electrode with applied potential of −0.3 V. Flow rates: 0.5 and 5.2 mL/min. A 1500-mf capacitor was used across the recorder input to reduce noise when the flow rate was pulsed

Figure 4 is a reproduction of a pulsed flow chart record for 1 μM ferricyanide in 0.01 M phosphate buffer (pH 7.4). The low blank value and also the reproducibility with which Δi is measurable indicate considerable promise for pulsed flow as a method of measuring low concentrations of electroactive materials.

LITERATURE CITED

(1) W. J. Blaedel and R. A. Jenkins, *Anal. Chem.*, **46**, 1952 (1974).
(2) T. O. Osterling and C. L. Olson, *Anal. Chem.*, **39**, 1546 (1967).
(3) J. B. Flanagan and L. Marcoux, *J. Phys. Chem.*, **78**, 718 (1974).
(4) R. C. Alkire and A. A. Mirarefi, *J. Electrochem. Soc.*, in press.
(5) G. Razumney, H. S. Wroblowa, and G. L. Schrenk, *J. Electrochem. Soc.*, **69**, 299 (1976).
(6) D. J. Myers and R. A. Osteryoung, *Anal. Chem.*, **46**, 2089 (1974).
(7) W. J. Blaedel and S. L. Boyer, *Anal. Chem.*, **43**, 1538 (1971).
(8) B. Miller and S. Bruckenstein, *Anal. Chem.*, **46**, 2026 (1974).
(9) W. J. Blaedel and L. N. Klatt, *Anal. Chem.*, **38**, 879 (1966).
(10) D. T. Sawyer and J. L. Roberts, "Experimental Electrochemistry for Chemists", Wiley, New York, N.Y., 1974.
(11) W. J. Blaedel and D. G. Iverson, *Anal. Chem.*, **48**, 2027 (1976).
(12) R. N. Adams, "Electrochemistry at Solid Electrodes", Marcel Dekker, New York, N.Y., 1969.

RECEIVED for review October 29, 1976. Accepted June 13, 1977. Work supported by funds from the National Science Foundation (Grant No. CHE76-15128 A02).

Mechanism of Neutral Carrier Mediated Ion Transport through Ion-Selective Bulk Membranes

A. P. Thoma, A. Viviani-Nauer, S. Arvanitis, W. E. Morf, and W. Simon*

Department of Organic Chemistry, Swiss Federal Institute of Technology, Universitätstrasse 16, CH-8092 Zurich, Switzerland

Analytically relevant neutral carrier membranes selective for K^+, Ca^{2+}, Na^+, Li^+, and organic cations respectively were studied. By applying an electrical potential gradient, a cation transference number of nearly 1 was found. To elucidate the mechanism of this cation permselectivity, electrodialysis experiments as well as interdiffusion studies were carried out on 0.02-cm valinomycin-based solvent polymeric membranes, using ^{14}C-labeled valinomycin and millimolar aqueous solutions of $^{42}K^+$ and $^{36}Cl^-$. The carrier concentration profile thus obtained agrees with theoretical predictions. The ion concentration levels in the membrane (potassium: ~0.5 mM; chloride: ~0.006 mM) indicate the presence of additional anionic species. Further experiments were performed to study the nature of these charged sites. They originate from the aqueous system and offer an explanation for the cation permselectivity observed, the extraction behavior described by other authors, as well as for the electric characteristics of neutral carrier membranes at extreme voltages.

Of the different types of ion-selective membrane electrodes known so far, liquid-membrane sensors offer a wide range of accessible ion selectivities. In these electrodes, mobile ion-selective sites, e.g. ion-selective ligands, dissolved in an appropriate solvent, are interposed between the sample solution and a reference system. Extremely high selectivities can be achieved by using neutral ion-specific ligands as membrane components (*1–3*). These ion carriers or ionophores have the property to complex certain ions (usually cations) of the sample solution and to transport these across lipophilic membranes by carrier translocation.

In spite of the wide use of carrier membrane electrodes in analytical chemistry, some facts as to their mode of function remain obscure. This point was emphasized by Buck (*4, 5*) who therefore styled these systems as "apparent neutral carrier membranes" (*4*). There is no doubt, however, that electrically neutral complexing agents such as valinomycin, macrotetrolides, and related compounds exhibit real carrier properties for cations in membranes. This is underscored by evidence from thin lipid bilayer membranes (*6, 7*) as well as from thick solvent polymeric membranes (*6, 8*) (see also below).

The predominant problem is then to explain permselectivity of carrier membranes for cations, as is observable in both potentiometric measurements and electrodialysis experiments. This means that a carrier membrane tends to be permeable for cations only and, accordingly, its electrical properties are scarcely influenced by sample anions such as chloride. For an ideal system, the integral transference number of anions, t_x, comes out to be zero and the general relationship for the zero-current membrane potential (*9–11*):

$$E = (1 - t_x)\frac{RT}{z_iF} \ln \frac{\Sigma K_i a_i'}{\Sigma K_i a_i''} + t_x \frac{RT}{z_xF} \ln \frac{\Sigma k_x a_x'}{\Sigma k_x a_x''} \quad (1)$$

reduces to a pure cation-response function of the Nicolsky type:

$$E = \frac{RT}{z_iF} \ln \frac{\Sigma K_i a_i'}{\Sigma K_i a_i''} = \text{const} + \frac{RT}{z_iF} \ln \left[a_i' + \Sigma_{j\neq i} K_{ij} a_j'\right] \quad (2)$$

In addition to the parameter t_x, the potential-determining factors in Equations 1 and 2 are: a', a'' = activities of cations (index i, j), respectively, anions (index x) in the aqueous solutions contacting the membrane. K_i, K_j, k_x = partition coefficients of permeating ionic forms. $K_{ij} = K_j/K_i$ = selectivity factor for cations of the same charge. z_i, z_x = charge of permeating cations and anions respectively; in units of the proton charge. RT/F = Nernst factor.

Different theories and views are called upon to explain the origin of cation permselectivity of neutral-carrier-based liquid membranes.

(a) The fundamental thin membrane model by Ciani, Eisenman, and Szabo (*12–14*) does not stipulate electroneutrality, and cationic carrier complexes therefore may be the only charged species existing within the membrane. Hence, permselectivity for cations may be explained by a complete exclusion of hydrophilic anions from the lipid membrane. This theory was extended to thick membranes by Boles and Buck (*15*) who still assume large deviations from electroneutrality to occur within the membrane interior (see also (*5*)).

(b) A recent suggestion made informally by Buck (*5*) is that slow anion interfacial kinetics permit near-Nernstian response to cations.

The remaining theories (c) to (e) of thick neutral carrier membranes may be summarized under the general assumption that the anions present within the membrane are rather immobile. The reasons for such a behavior may be as follows.

(c) The membrane contains permanent anions that are chemically bound to the supporting material, as was suggested by Kedem, Perry, and Bloch (*16*) (see also (*15*)).

(d) The membrane contains permanent anions that are immobilized because of their poor water-solubility (*11, 17, 18*).

(e) The membrane extracts anions from the sample solution but the integral mobility of these species across the membrane is low as compared to the cationic complexes (*11, 19–22*).

We present here experimental evidence that reveals an actual mechanism for permselectivity in neutral-carrier-based solvent polymeric membranes. These results are at variance with most of the theories mentioned above.

EXPERIMENTAL

Cell Assembly. In electrodialysis experiments the cell consisted of two electrolyte compartments separated by the membrane or membrane stack studied. The cell shown in Figure 1 was used for all experiments involving radioactively labeled species. All other experiments were performed in a similar cell (electrolyte compartment volume: 10 mL) described earlier (*20*).

Procedures. Permselective liquid membranes consisting typically of 1 wt % ligand, 33 wt % poly(vinylchloride) and 66

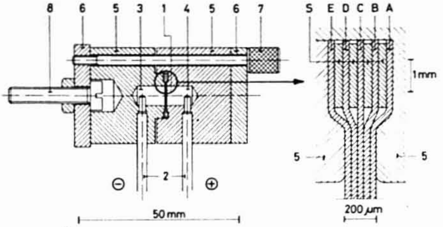

Figure 1. Cell used for electrodialysis. (1) Membrane stack or compact membrane. (2) Ag/AgCl electrodes; in the presence of $^{36}Cl^-$ platinum electrodes were used. (3) Cathode compartment (volume 230 μL) containing ~200 μL electrolyte solution. (4) Anode compartment (volume 230 μL) containing ~200 μL electrolyte solution. (5) Cell body (Teflon). (6) Cell support (brass). (7) 4 tightening screws. (8) Connecting-screw to wristshaker (the continuous mixing of the half-cell contents was achieved by shaking the cell with a frequency of about 5 Hz); (A, B, C, D, E) membrane segments (thickness: 40 μm, diameter: 13 mm). (S) Spacer rings (Teflon, thickness: 50 μm; inner diameter: 9 mm; outer diameter: 13 mm)

wt % plasticizer were used throughout the experiments. For the preparation technique, see (*23*). For preparation and composition of silicone rubber membranes, see (*24*). Compact membranes were 40- to 200-μm thick. Composite membranes (stacks) consisted of 5 identical segments each 40-μm thick. In order to facilitate a swift unstacking at the end of electrodialysis, four 50-μm thick Teflon spacer rings were mounted as a skeleton between the membrane segments sticking together (see Figure 1). For the determination of transference numbers, the time-current integral was measured by means of an integrator and the quantity of the ion of interest transported to the cathode and anode compartment respectively was evaluated either by radioactivity counters (Geiger-Muller and liquid scintillation counters) or by an atomic absorption spectrophotometer. The transference number of an ion was obtained as the ratio of the charge equivalent of the transferred species to the time-current integral.

For ion profile studies the membrane segments were mounted on steel sample holders and forwarded to the Geiger-Muller counting tube. For ^{14}C-labeled ligand profile studies, the membrane segments were dissolved in a mixture of 0.5 mL dimethylsulfoxide and 0.5 mL toluene before adding 15 mL of butyl-PBD-scintillator cocktail. For determination of the current-voltage curve of a permselective membrane, the two compartments of the electrodialysis cell were filled with identical electrolyte solutions. A stepwise decreasing voltage was applied and the respective current, constant in time, was reached after 10 to 60 min.

In ion-exchange experiments, 200-μm thick membranes mounted in liquid-membrane electrode bodies (Philips IS 560; diameter of exposed membrane surface: 4 mm) were conditioned in a 2×10^{-3} M KCl solution for 48 h (internal filling solution: 2×10^{-3} M KCl). Then the inactive sample solution was replaced by 2×10^{-3} M $^{42}K^{36}Cl$ and the uptake of the labeled ions was measured as a function of time.

Changes in pH of previously de-gassed electrolytes in quartz test tubes where carrier membranes had been introduced were recorded by means of a mini-pH-electrode (Philips type C71/02) dipped in the argon-flushed sample. For further details see (*25*).

Reagents. Synthetic carriers: for preparation see (*26*); poly(vinylchloride): PVC SDP hochmolekular, Lonza AG, Basle, Switzerland. Tris(2-ethylhexyl)phosphate (purity: 98%): Merck AG, Darmstadt, Germany. Dibutyl sebacate (purum), dioctyl adipate (purum), and tetrahydrofuran (puriss., p.a., 0.025%, 2,6-di-*tert*-butyl-4-methyl-phenol): Fluka AG, Buchs, Switzerland. Valinomycin: Calbiochem, Los Angeles, Calif. 90054; ^{14}C-labeled valinomycin: graciously offered by Yu. A. Ovchinnikov, USSR Academy of Sciences, Shemyakin Institute for Chemistry of Natural Products, Moscow, USSR. ^{42}K as anhydrous K_2CO_3: obtained by neutron activation (2×10^{13} n cm^{-2} s^{-1} at the Eidgenössisches Institut für Reaktorforschung, Würenlingen, Switzerland) of K_2CO_3 suprapur, Merck AG, Darmstadt, Germany.

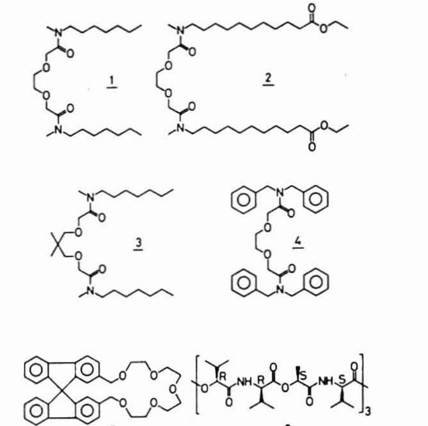

Figure 2. Ion-selective ligands used. A racemic mixture of the enantiomers R and S of carrier **5** was used. Carrier **6** is the natural enantiomer of valinomycin

^{36}Cl as a 0.2 M HCl solution: code CIS.1, The Radiochemical Centre, Amersham, Great Britain. Butyl-PBD-scintillator cocktail: Ciba-Geigy AG, Basle, Switzerland.

Apparatus. Digital voltmeter: type LM 1440, The Solartron Electronic Group Limited, Farnborough, Hampshire, Great Britain. Microammeter: type 150 B, Keithley Instruments, Cleveland, Ohio 44139. Integrator: recorder model SRG/disc integrator, Sargent & Co., Chicago, Ill. Geiger-Muller anticoincidence counting unit: detector: Isotope Development Laboratories, Edinburgh, Great Britain; low-background anticoincidence unit: type PW 4092, Philips; high voltage power supply: type PW 4022 and PW 4023, Philips; counting unit: type ELD 5 and ELB 5, Landis & Gyr, Switzerland; printer: type ERH 1, Landis & Gyr, Switzerland. Liquid scintillation counting unit: Mark I, Nuclear Chicago. Atomic absorption spectrophotometer: type 300 (graphite cell HGA 72), Perkin-Elmer, Ueberlingen, Germany.

RESULTS AND DISCUSSION

Evidence for Permselectivity. As a rule all the analytically relevant cation-selective neutral-carrier-based liquid-membrane electrodes studied in detail so far exhibit cation permselectivity in electrodialysis experiments (*10, 20, 27–30*). A summary of the presently available information is given in Table I. It includes data published earlier as well as new results obtained on membranes containing the carriers 1–6 (see Figure 2). Throughout, a cation transference number of nearly 1 ($t_x \approx 0$; Equation 1) is found which is in perfect agreement with the slope of the electrode response observed for the same membranes (see Equation 1 and last column of Table I). In one case (valinomycin in dioctyl adipate) the transference number for $^{42}K^+$ of 1.02 ± 0.04 is corroborated by the simultaneous radiochemical determination of the transference number of the sample anion $^{36}Cl^-$ of 0.0004 ± 0.0002. It can therefore be concluded that the integral transference number t_x for anions (Equation 1) is practically zero for the systems studied.

Ion and Ligand Profiles in Neutral Carrier Membranes. In order to reveal the mechanism of permselectivity of neutral carrier membranes, the concentration profiles of cations, anions, as well as ionophores within the membrane phase were studied. To this end radioactively labeled carriers, cations, and anions were used in electrodialysis experiments with stacked solvent polymeric membranes (see Figure 1). The

Table I. Transport Numbers and Slopes of the Electrode Response of Cation Permselective Neutral Carrier Membrane

	Membrane composition			Electrolytes			
Cation studied	Ligand; wt %	Solvent;[d] wt %	Matrix; wt %	Anode compartment	Cathode compartment	Transference number for cations studied[a]	Slope of electrode response in percent of theoretical slope
Ca^{2+}	2; 3	*o*-NPOE; 65	PVC; 32	10^{-3} M $CaCl_2$	10^{-3} M KCl	0.99 ± 0.08 (*27*)	94 (*31*)
Ca^{2+}	2; 3	DBS; 65	PVC; 32	10^{-3} M $CaCl_2$	10^{-3} M KCl	1.00 ± 0.105 (*27*)	...
Ca^{2+}	2; 3	*o*-NPOE; 65	PVC; 32	5×10^{-4} M $CaCl_2$ 5×10^{-4} M $MgCl_2$	10^{-3} M KCl	0.99 ± 0.08 (*27*)	94 (*31*)
Ca^{2+}	2; 3	*o*-NPOE; 65	PVC; 32	5×10^{-4} M $CaCl_2$ 5×10^{-4} M NaCl	10^{-3} M KCl	0.99 ± 0.02 (*27*)	94 (*31*)
Ca^{2+}	2; 3	*o*-NPOE; 65	PVC; 32	10^{-4} M $CaCl_2$	10^{-4} M KSCN	0.995 ± 0.025 (*20*)	94 (*31*)
Ca^{2+}	1; 3	*o*-NPOE; 65	PVC; 32	10^{-3} M $CaCl_2$	10^{-3} M KCl	1.01 ± 0.08 (*28*)	95 (*32*)
Na^+	4; 3	DBS; 65	PVC; 32	10^{-3} M NaCl	10^{-3} M KCl	0.92 ± 0.08 (*27, 29*)	...
Na^+	4; 3	DMK; 65	PVC; 32	10^{-3} M NaCl	10^{-3} M KCl	0.92 ± 0.061 (*27*)	...
Na^+	4; 3	*o*-NPOE; 65	PVC; 32	10^{-3} M NaCl	10^{-3} M KCl	0.90 ± 0.075 (*27*)	96 (*33*)
Li^+	3; 5.8	TEHP; 62.8	PVC; 31.4	10^{-2} M LiCl	10^{-2} M KCl	0.97 ± 0.11	97 (*34*)
Li^+	3; 5.8	TEHP; 62.8	PVC; 31.4	10^{-3} M LiCl	10^{-3} M KCl	1.02 ± 0.21	97 (*34*)
Li^+	3; 5.8	TEHP; 62.8	PVC; 31.4	10^{-4} M LiCl	10^{-4} M KCl	0.98 ± 0.10	97 (*34*)
K^+	6; 3	DPP; 67	PVC; 30	10^{-2} M KCl	10^{-2} M HCl	1.08 ± 0.07 (*27, 30*)	...
K^+	6; 5	...	Silicone rubber; 95	10^{-2} M KCl	10^{-2} M HCl	1.1 ± 0.15 (*27, 30*)	...
K^+	6; 5	...	Silicone rubber; 95	10^{-2} M KCl	10^{-2} M $HClO_4$	1.1 ± 0.15 (*27, 30*)	...
K^+	6; 1	DOA; 66	PVC; 33	9×10^{-4} M KCl	9×10^{-4} M KCl	1.02 ± 0.04	100 (*35*)
$PEAH^+$ [b]	5; 1	DOA; 65	PVC; 34	4×10^{-3} M PEAHCl	4×10^{-3} M PEAHCl	0.95 ± 0.04	(120)[c] (*25*)

[a] Measured on the membrane specified in the region of ohmic behavior of the current-voltage curve (at low voltage) (*20*); 95% confidence limits. [b] $PEAH^+$: ^{14}C-α-phenylethylammonium cation. [c] From electrode response in buffered 10^{-1} M and 10^{-2} M solutions of the ammonium salt; activity coefficients unknown. [d] *o*-NPOE: *o*-nitrophenyloctyl ether; DBS: dibutyl sebacate; DMK: decylmethyl ketone; TEHP: tris-(2-ethyl-hexyl)-phosphate; DPP: dipentyl phthalate; DOA: dioctyl adipate.

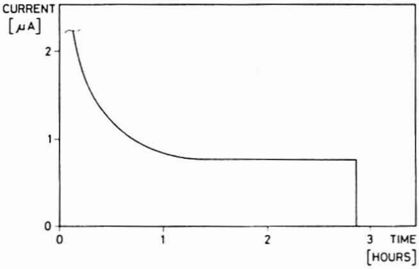

Figure 3. Current-time characteristics of neutral carrier membrane. A potential gradient of 20 V was applied to a 200-μm thick valinomycin-based liquid membrane in contact with KCl solutions; the cell is shown in Figure 1

current-time characteristics obtained on a stack of membranes containing ^{14}C-labeled valinomycin (0.99 wt %) in dioctyl adipate (66.2 wt %)/PVC (32.8 wt %) in contact with 4×10^{-3} M KCl is given in Figure 3. One hour after reaching the steady state, the electrodialytic transport was stopped and the membranes were unstacked within 3 min. Identical experiments were carried out by bringing the membrane stack (not labeled) in contact with 9×10^{-4} M ^{42}KCl in the anode and 9×10^{-4} M $K^{36}Cl$ in the cathode compartment. The measurements of the radioactivities in the different membrane sections led to the profiles displayed in Figure 4. As indicated earlier for a different carrier system (*8, 36*), an ionophore concentration gradient builds up which is in agreement with theoretical predictions (*20*). This is an unambiguous proof for carrier translocation accompanying the cation transport and it is a requirement for the back-diffusion of free carriers to end up in a steady state (*20*). This back-diffusion is substantiated by results presented earlier (*36*). There the complete decay of the ionophore concentration gradient within the membrane after reestablishing a zero-current state was experimentally confirmed for the valinomycin-induced transport of α-phenylethylammonium ions. These experiments led to a diffusion coefficient for valinomycin of (1.8 ± 0.3) × 10^{-8} cm^2 s^{-1} (*25*).

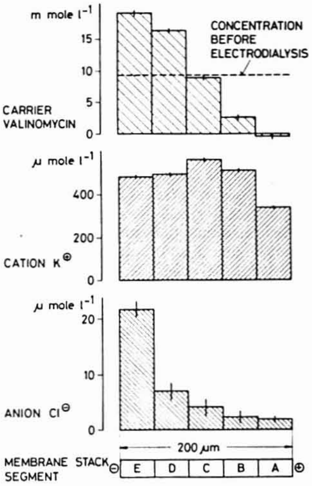

Figure 4. Ionophore and ion concentration profiles within a valinomycin-based liquid membrane (stack). Results represent the ion profiles 3 min after interrupting a steady-state electrodialysis. The 95% confidence limits are given by vertical bars

In a similar experiment of the valinomycin-induced transport of α-phenylethylammonium ions (*8*), only the carrier in the membrane section contacting the anode compartment (section A, Figure 1; entry for cations) was labeled. After the transport experiment, only about 20% of the labeled ligand drained off section A reached section E (*8*). This proves an exchange of ligands during the transport process so that a carrier-relay mechanism must be operative (*25, 37*).

According to Figure 4, cations as well as anions enter the membrane phase. Although this was expected, it is most remarkable that the overall concentration of cations K^+ exceeds by far (factor 85) the one of the sample anions Cl^-. This fact can be explained only when assuming either dramatic deviations from electroneutrality or the presence of anionic species other than Cl^- within the membrane phase. The rather high cation concentration level (see Figure 4) as well as the relatively low electrical resistance of only about 10^6 ohm cm^2 (*25*) found for the valinomycin-based membranes studied here are at variance with the space-charge theory (a) mentioned above. If anions were completely excluded from the membrane phase, the limiting resistance for a thick membrane would be (*10, 15, 38*):

$$R_m = \frac{d^3}{4\pi^2\epsilon_0\epsilon D} \tag{3}$$

and the theoretical concentration of cationic charges in the center of the membrane would be (*8, 38*):

$$c_m(d/2) = \frac{2\pi^2\epsilon_0\epsilon RT}{d^2F^2} \tag{4}$$

Inserting the experimental values $d = 0.02$ cm for the membrane thickness, $D = 1.8 \times 10^{-8}$ cm^2 s^{-1} for the diffusion coefficient of carrier complexes in the membrane, $\epsilon = 4$ for the dielectric constant of the membrane, and the fundamental constants $\epsilon_0 = 8.85 \times 10^{-14}$ C/V cm, $RT/F = 0.0257$ V at 25 °C, and $F = 96500$ C/mol, the following values are calculated:

$$R_m = 3.18 \times 10^{13}\ \Omega\ \text{cm}^2$$

$$c_m(d/2) = 4.65 \times 10^{-15}\ \text{mol/cm}^3$$

Obviously, these values are far from reality and therefore a space-charge model (hypothesis (a)) appears to be untenable for thick carrier membranes. The sample anion deficiency in the membrane phase of around 99 mol % presented in Figure 4 must be due to anions different from Cl^-.

To differentiate between the other models suggested, diffusion experiments were carried out. A valinomycin-based solvent polymeric membrane previously conditioned with 2×10^{-3} M KCl was brought in contact with 2×10^{-3} M $^{42}K^{36}Cl$. Results of the uptake of labeled ions by the membrane are given in Figure 5. The number of moles of cations exchanged is higher by a factor of 35 to 70 than that of the exchanged anions. The ratio of the slopes of the curves in Figure 5, which is a measure for the ion-exchange flux ratio, varies from 25 to 80.

If the interdiffusion of isotopes within the membrane is the rate-controling step, i.e. if there is no kinetic limitation at the phase boundary, the initial tracer uptake can be described by (*39*):

$$M_\nu = 2Ac_\nu\sqrt{D_\nu t/\pi} \tag{5}$$

where M_ν = amount of labeled ion ν in membrane at time $t \geq 0$ (mol). A = phase boundary area (cm^2). c_ν = concentration of unlabeled ion ν in the membrane in equilibrium with the aqueous phase at $t \leq 0$ (mol cm^{-3}). D = diffusion coefficient of ion ν in the membrane (cm^2 s^{-1}).

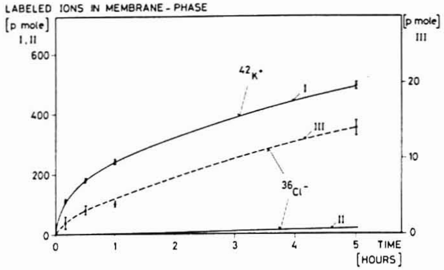

Figure 5. Time-dependent uptake of labeled ions from aqueous solution by a neutral carrier membrane. A valinomycin-based liquid membrane was equilibrated with an electrolyte solution containing unlabeled ions. Curves I and II refer to the left-hand scale; curve III refers to the blown up scale on the right-hand side. Vertical bars indicate 95% confidence limits

On the other hand, when the tracer transfer from the aqueous phase into the membrane is rate-determining (hypothesis (b)), the initial flux J_ν across the phase boundary is given by (*20*):

$$J_\nu = k_\nu a_\nu \tag{6}$$

and therefore

$$M_\nu = Ak_\nu a_\nu t \tag{7}$$

where k_ν = rate constant (cm s^{-1}) for the transfer of the ion ν into the membrane (including a phase boundary potential contribution (*20*)). a_ν = activity of the tracer in the aqueous solution at $t \geq 0$ (mol cm^{-3}).

Equation 7 predicts a linear increase of M_ν with time (at least in the initial stage of the diffusion experiment) which clearly contradicts the curves in Figure 5. According to Equation 5 we should expect the uptakes of labeled ions ν to be linear functions of $\sqrt{t}$ having a slope proportional to $c_\nu \sqrt{D_\nu}$. Such a time-dependence has indeed been found in our experiment (see Figure 6) as well as in similar studies on glass membranes made earlier by Eisenman (*39*). The ratio of the slopes of the straight lines in Figure 6 is $(c_K\sqrt{D_K})/(c_{Cl}\sqrt{D_{Cl}}) \approx 40$ and compares favorably with the ratio c_K/c_{Cl} found previously in Figure 4. Correspondingly, the diffusion coefficients D_K and D_{Cl} must be of the same order of magnitude and we therefore have no kinetic control of the preference of K^+ over Cl^-. We then have to conclude that hypothesis (b) is not a likely explanation for the cation permselectivity.

Since the different sections of the stacked membranes were prepared under identical conditions from the same batch of raw material, the chemically bound anions suggested in (*16*) (hypothesis (c)) should be homogeneously distributed throughout the membrane. This is in contrast to the situation presented in Figure 4. There the difference between the K^+ and Cl^- concentrations, which represents the apparently missing anions, varies significantly from section A to E. This, as well as the indication of cation permselectivity for liquid membranes prepared only from *n*-heptane and valinomycin (*40*), clearly rules out the fixed-site theory (c). The latter argument also contradicts hypothesis (d) because lipophilic anions permanently in the membrane phase can be introduced only through impurities or additives (*17*). The anion deficiency documented in Figure 4 is around 1.0×10^{-4} mol L^{-1}. Such high levels of impurities are excluded by select methods of preparation of cation permselective solvent polymeric membranes. Therefore, the apparently missing anions in the membrane phase must originate from the aqueous system.

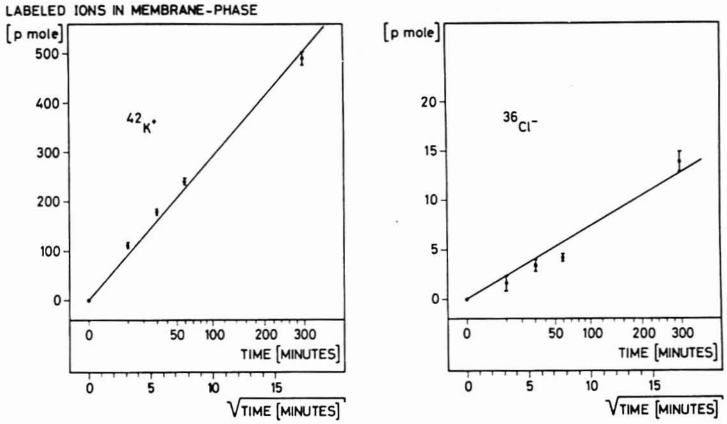

Figure 6. Uptake of labeled ions by a valinomycin-based liquid membrane as a function of the square root of time. See legend to Figure 5. Vertical bars indicate the 95% confidence limits

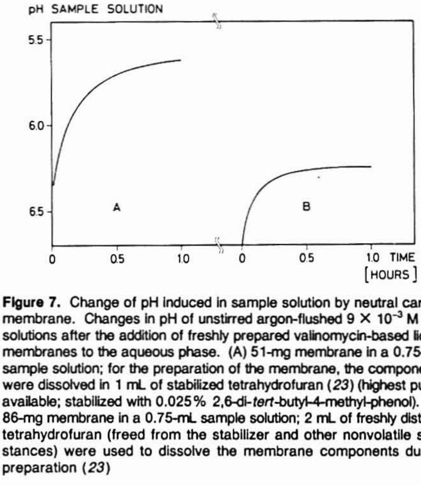

Figure 7. Change of pH induced in sample solution by neutral carrier membrane. Changes in pH of unstirred argon-flushed 9 × 10^{-3} M KCl solutions after the addition of freshly prepared valinomycin-based liquid membranes to the aqueous phase. (A) 51-mg membrane in a 0.75-mL sample solution; for the preparation of the membrane, the components were dissolved in 1 mL of stabilized tetrahydrofuran (*23*) (highest purity available; stabilized with 0.025% 2,6-di-*tert*-butyl-4-methyl-phenol). (B) 86-mg membrane in a 0.75-mL sample solution; 2 mL of freshly distilled tetrahydrofuran (freed from the stabilizer and other nonvolatile substances) were used to dissolve the membrane components during preparation (*23*)

Mechanism of Cation Permselectivity. Since in addition to theory (e) there is no clear-cut explanation for the cation permselectivity left, one has to rationalize the nature of the dominant anions in the membrane phase as well as their apparently poor mobility. In agreement with earlier observations (*41*), solvent polymeric membranes of the type discussed are susceptible to water uptake and water permeability. A 200-μm thick membrane prepared from valinomycin (1.0 wt %), dioctyl adipate (66.2 wt %) and PVC (32.8 wt %) equilibrated with a 9 × 10^{-4} M aqueous KCl solution on each side shows a water concentration of about 0.15 mol L^{-1} and a water flux of about 1.7 × 10^{-8} mol cm^{-2} s^{-1}. These values were obtained by labeling the water with ^3H. Even membranes prepared from *n*-heptane and valinomycin have a water uptake of around 0.003 mol L^{-1} (25 °C) (*42*). It is therefore reasonable to assume that the dominant anions in the membrane originate from proton exchange reactions involving water. If a freshly prepared membrane is brought into contact with an aqueous KCl solution, there is indeed a flux of protons out of the membrane phase (Figure 7) according to the formal exchange reaction:

$$K^+(\text{aqueous}) + H_2O(\text{membrane}) \rightleftharpoons K^+(\text{membrane}) + OH^-(\text{membrane}) + H^+(\text{aqueous}) \quad (8)$$

Because of a possible formation of water clusters involving the OH^- formed by reaction 8, the mobility of these anionic sites is likely to be low. It may, however, be expected that a direct electric transference of such sites occurs under extreme conditions. In Figure 8 a current/voltage diagram including transference information covering the range from 10 to 70 V is given. Whereas up to about 30 V the theoretically predicted behavior of an ideal cation permselective carrier membrane is observed, the transference number for K^+ drops well below 1.0 at extreme voltages. The contribution to the electric current by Cl^- with a value of 0.0007 at 70 V is still negligible (see Figure 8). The remaining 23% contribution to the current in the electrodialysis experiment at 70 V must then be due to the transport of charged forms of water.

The mechanism suggested here gives a plausible explanation for the unusual extraction behavior reported by Lev et al. (*40*). For a valinomycin-modified heptane membrane and KCl (as

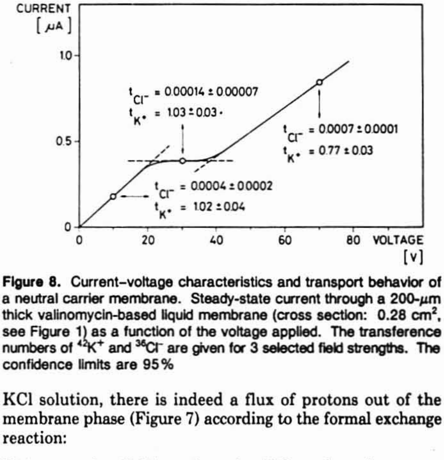

Figure 8. Current–voltage characteristics and transport behavior of a neutral carrier membrane. Steady-state current through a 200-μm thick valinomycin-based liquid membrane (cross section: 0.28 cm^2, see Figure 1) as a function of the voltage applied. The transference numbers of $^{42}K^+$ and $^{36}Cl^-$ are given for 3 selected field strengths. The confidence limits are 95%

well as other alkali metal chlorides) in the aqueous sample solutions, these authors found that the concentration c_K of the extracted cations is a function of the square root of the sample concentration $c_K{}^{aq}$. This may be explained by assuming the existence of an equilibrium 8 described by

$$c_K \times c_{OH} \times c_H{}^{aq} = \text{const} \times c_K{}^{aq} \times c_{H_2O} \tag{9}$$

and

$$c_K = c_{OH} \tag{10}$$

If the concentration of water c_{H_2O} in the membrane phase as well as the pH of the sample solution remain constant, we indeed obtain:

$$c_K \text{ prop. } \sqrt{c_K{}^{aq}} \tag{11}$$

The facts presented here lead to the conclusion that the neutral carrier membrane model developed earlier (*20*) (hypothesis (e)) gives the most adequate description of the observed electromotive and transport behavior. Accordingly, the origin of permselectivity is the presence of anions of low mobility in the membrane which can be considered as "fixed" charges (*20*). The crucial difference between this theory and the pioneering model suggested by Kedem, Perry, and Bloch (*16*) (hypothesis (c)) rests in the nature of the immobile sites, which we show as originating from the aqueous system.

ACKNOWLEDGMENT

We thank Yu. A. Ovchinnikov for the generous supply of ^{14}C-labeled valinomycin and V. Prelog for ligand 5. We gratefully acknowledge the stimulating discussions and the experimental support of P. Jordan and K. May (Radiochemical Laboratory, ETHZ).

LITERATURE CITED

(1) J. Koryta, "Ion-Selective Electrodes", Cambridge University Press, Cambridge, London, New York, and Melbourne, 1975.
(2) E. Pretsch, D. Ammann, and W. Simon, *Res./Dev.*, **25** (3), 20 (1974).
(3) D. Ammann, R. Bissig, Z. Cimerman, U. Fiedler, M. Güggi, W. E. Morf, M. Oehme, H. Osswald, E. Pretsch, and W. Simon, in "Ion and Enzyme Electrodes in Biology and Medicine", M. Kessler, L. C. Clark, Jr., D. W. Lübbers, I. A. Silver, and W. Simon, Ed., Proceedings of a International Workshop at Schloss Reisensburg, Germany, September 15–18, 1974, Urban & Schwarzenberg, Munich, Berlin, Vienna, 1976, p 22.
(4) R. P. Buck, *Anal. Chem.*, **46**, 28R (1974).
(5) R. P. Buck, *Anal. Chem.*, **48**, 23R (1976).
(6) G. Eisenman, Ed., "Membranes", Vol. 2, Marcel Dekker, New York, N.Y., 1973.
(7) P. Läuger, *Science*, **178**, 24 (1972).
(8) W. Simon, W. E. Morf, and A. P. Thoma, Proceedings of the Symposium on Ion Selective Electrodes, Mátrafüred, Hungary, 18–21 October 1976.
(9) W. E. Morf, *Anal. Chem.*, **49**, (1977), in press.
(10) W. E. Morf and W. Simon, Proceedings of the Symposium on Ion Selective Electrodes, Mátrafüred, Hungary, 18–21 October 1976.
(11) W. E. Morf and W. Simon, in "Ion-Selective Electrodes", H. Freiser, Ed., in press.
(12) S. M. Ciani, G. Eisenman, and G. Szabo, *J. Membr. Biol.*, **1**, 1 (1969).
(13) S. M. Ciani, G. Eisenman, R. Laprade, and G. Szabo, Ref. 6, Chap. 2.
(14) G. Eisenman, in "Ion-Selective Electrodes", R. A. Durst, Ed., *Nat. Bur. Stand.* (*U.S.*), *Spec. Publ.*, **314**, Washington, D.C., 1969.
(15) J. H. Boles and R. P. Buck, *Anal. Chem.*, **45**, 2057 (1973).
(16) O. Kedem, M. Perry, and R. Bloch, IUPAC International Symposium on Selective Ion-Sensitive Electrodes, paper 44, Cardiff, 1973.
(17) W. E. Morf, G. Kahr, and W. Simon, *Anal. Lett.*, **7**, 9 (1974).
(18) H. Seto, A. Jyo, and N. Ishibashi, *Chem. Lett.* (*Jpn.*), 483 (1975).
(19) H.-R. Wuhrmann, W. E. Morf, and W. Simon, *Helv. Chim. Acta*, **56**, 1011 (1973).
(20) W. E. Morf, P. Wuhrmann, and W. Simon, *Anal. Chem.*, **48**, 1031 (1976).
(21) O. Ryba and J. Petránek, *J. Electroanal. Chem.*, **67**, 321 (1976).
(22) R. Büchi, E. Pretsch, W. E. Morf, and W. Simon, *Helv. Chim. Acta*, **59**, 2407 (1976).
(23) G. J. Moody, R. B. Oke, and J. D. R. Thomas, *Analyst* (*London*), **95**, 910 (1970).
(24) J. Pick, K. Tóth, E. Pungor, M. Vašák, and W. Simon, *Anal. Chim. Acta*, **64**, 477 (1973).
(25) A. P. Thoma, Diss. ETHZ (1977).
(26) D. Ammann, R. Bissig, M. Güggi, E. Pretsch, W. Simon, I. J. Borowitz, and L. Weiss, *Helv. Chim. Acta*, **58**, 1535 (1975).
(27) P. Wuhrmann, Diss. ETHZ 5606 (1976).
(28) P. Wuhrmann, A. P. Thoma, and W. Simon, *Chimia*, **27** (12), 637 (1973).
(29) U. Fiedler, *Anal. Chim. Acta*, **89**, 101 (1977).
(30) E. Lindner, P. Wuhrmann, W. Simon, and E. Pungor, Proceedings of the Symposium on Ion-Selective Electrodes, Matráfüred, Hungary, 18–21 October 1976.
(31) D. Ammann, E. Pretsch, and W. Simon, *Anal. Lett.*, **5**, 843 (1972).
(32) R. Bissig, private communication.
(33) D. Ammann, E. Pretsch, and W. Simon, *Anal. Lett.*, **7**, 23 (1974).
(34) M. Güggi, U. Fiedler, E. Pretsch, and W. Simon, *Anal. Lett.*, **8**, 857 (1975).
(35) H. Osswald, private communication.
(36) A. P. Thoma, E. Pretsch, G. Horvai, and W. Simon, in "Biochemistry of Membrane Transport", G. Semenza and E. Carafoli, Ed., Proceedings in Life Sciences, FEBS-Symposium No. 42 at the Swiss Federal Institute of Technology, Zurich, 1976, Springer-Verlag, Berlin, Heidelberg, New York, 1977, p 116.
(37) H.-K. Wipf, A. Olivier, and W. Simon, *Helv. Chim. Acta*, **53**, 1605 (1970).
(38) P. Läuger and B. Neumcke, Ref. 6, Chap. 1.
(39) G. Eisenman, "Glass Electrodes for Hydrogen and Other Cations", Marcel Dekker, New York, N.Y., 1967, Chap. 5.
(40) A. A. Lev, V. V. Malev, and V. V. Osipov, Ref. 6, Chap. 7.
(41) H.-K. Wipf, Diss. ETHZ 4492 (1970).
(42) R. Schatzberg, *J. Phys. Chem.*, **67**, 776 (1963).

RECEIVED for review May 6, 1977. Accepted June 20, 1977. Work partly supported by the Swiss National Science Foundation and by Ciba-Geigy AG, F. Hoffmann-La Roche & Co. AG, Sandoz AG, Lonza AG.

Redox Thermodynamics and Electron Transfer Reactivity of Heme by Enthalpimetry and Voltammetry

Raymond Bury[1] **and Joseph Jordan***

Department of Chemistry, The Pennsylvania State University, 152 Davey Laboratory, University Park, Pennsylvania 16802

The first extensive investigation of the redox thermochemistry of protoheme is described. A wealth of thermodynamic information was obtained by judiciously combining results of potentiometric and thermometric titrations. Heats, Gibbs free energies, and entropies of the reduction of ferriheme to ferroheme have been determined in dimethylformamide (DMF), in dimethylacetamide (DMA), and in mixtures of DMF or DMA and water. The reducing agent was chromous acetate. In order to segregate solvent effects attributable to the ferro–ferriheme half-reaction, the ΔH, ΔG, and ΔS assignments have been referred to the ferrocene/ferricinium couple whose energetics are known to be virtually independent of solvent. The thermodynamic parameters of the ferroheme–ferriheme redox process exhibited remarkable nonmonotonic trends as function of solvent composition. The results were generally consistent with concomitantly observed effects of solvent–solute interactions on electrode kinetics. Relevant electrochemical rate constants were evaluated by polarography and cyclic voltammetry.

Oxidation-reduction properties of octahedral complexes of iron with the equatorial ligand protoporphyrin IX are of evident biological interest because the prosthetic groups of hemoproteins ("heme") are moieties of this type. They are implicated in crucial physiological functions (*1*) including oxygen transport (by hemoglobin), oxygen storage (by myoglobin), and cellular respiration (via cytochrome *c*). Extensive information is available in classical monographs (*2, 3*) on the standard and formal potentials of metalloporphyrin redox couples. Because heme tends to dimerize and polymerize in aqueous solutions (*1, 4–7*) many recent electrochemical studies have been carried out in the presence of nonaqueous solvents (*1, 4, 8–11*) where the situation is not complicated by aggregation.

Surprisingly, data on the thermochemistry of oxidation–reduction reactions of heme are conspicuous by their absence. In fact, only one study on the redox thermochemistry of *any* iron porphyrin (viz., of hematoporphyrin) has been reported in the literature (*12*). In the present paper, calorimetric results are presented and discussed involving the heat of reduction of ferriheme to ferroheme with chromous acetate in the aprotic solvents *N,N′*-dimethylformamide (DMF) and *N,N′*-dimethyl acetamide (DMA), and in mixtures of these with water. Concomitantly, Gibbs free energies were estimated by electrochemical methods and corresponding entropies were computed. These thermodynamic findings were complemented by evaluation of electrode kinetics via cyclic voltammetry yielding illuminating insights on mechanistically significant solvent effects.

EXPERIMENTAL

General Conditions. Very dilute solutions of ferriheme, ferroheme, and chromous acetate (in a range between 0.0001 M and 0.001 M) were prepared in purified solvents (DMF, DMA, and mixtures of these with water). Since ferroheme and chromous acetate were prone to air-oxidation, oxygen was eliminated by storing all chemicals in an inert atmosphere (nitrogen or argon), by deaerating solvents and solutions, and by maintaining a supernate of nitrogen or argon in all experiments. Traces of oxygen were removed from the inert gases by bubbling through a solution of vanadous sulfate. Likewise the purging gases and supernates were equilibrated by bubbling through wash bottles containing solvents of compositions identical with those used in the thermochemical and electrochemical experiments.

Two types of studies were performed, viz., (I) Investigations of chemical oxidation–reduction reactions between ferriheme and chromous acetate. (II) Voltammetric studies of the ferro–ferriheme redox couple. All experiments of type I were carried out in the presence of a 0.01 M sodium salicylate–0.01 M salicylic acid buffer whose pH is known to be 7.94 in DMF (*13*). Chromous acetate proved stable under these experimental conditions, while it decomposed rapidly (e.g., by reducing water contained in the solvent) in unbuffered solutions. In experiments of type II, 0.1 M tetraethylammonium perchlorate (TEAP) or 0.1 M perchloric acid was used as supporting electrolyte. All results reported in this paper were obtained in a temperature range of (25.00 ± 0.02) °C.

Thermometric Enthalpy Titrations. Heats of reaction were determined by a titration calorimetric method, viz., thermometric enthalpy titrations (TET). Titration curves were obtained by monitoring the change in temperature, ΔT, in an adiabatic cell, concomitantly with the addition of chromous acetate to ferriheme. Because solutions were extremely dilute, ΔT was on the order of a few millidegrees. A typical "normalized curve" is illustrated in Figure 1. Temperature increments shown on the ordinate are values corrected for changes of heat capacity due to the inevitable changes (e.g., volume increments) occurring during the titration. ΔT was normalized to an average heat capacity, k, effective at the mid-point of the titration. Actual heat capacities were determined by appropriate joule heating calibrations carried out in situ. Heats of reaction were computed from the ordinate increment, using Equation 1

$$\overline{Q} = k\Delta T = -n\Delta H_{\mathrm{F}}^{0} \qquad (1)$$

where Q denotes the number of calories evolved, n the number of moles reacted at the stoichiometric end point, $\Delta H_{\mathrm{F}}^{0}$ denotes a *formal* heat of reaction which corresponded to infinite dilution [identified by the superscript "0" (zero)] of the redox reactants in a specific solvent in the presence of buffer. The crucial temperature increment, ΔT, (and the corresponding integral heat, Q) were assigned with the aid of the self-explanatory extrapolation shown in Figure 1, which corrects satisfactorily for extraneous effects. The most important of these were the heats of mixing as is apparent from the excess reagent line (between the "end point" and the stop of titrant addition).

Actual titration curves were recorded automatically by delivering solutions of titrants at a constant rate from a motor-driven syringe–buret. Temperature was monitored with the aid of a thermistor bridge which had the effective sensitivity of a thousand-junction thermocouple. The bridge unbalance potential (proportional to ΔT) was displayed on the Y-axis of a strip-chart dc millivoltmeter whose time (X)-axis was driven by a synchronous motor. Taking into account the likewise synchronous titrant delivery (and the concentration of the titrant), the abscissa was calibrated in terms of moles of titrant added. Detailed procedures and instrumentation have been described previously (*14*).

Entropy and Gibbs Free Energy Assignments. Equilibrium constants were evaluated from potentiometric titration curves

---

[1] Postdoctoral Scholar (1974–75) on leave from Université Pierre et Marie Curie; present address, Laboratoire d'Electrochimie, 4 place Jussieu, 75230 Paris Cedex 05, France.

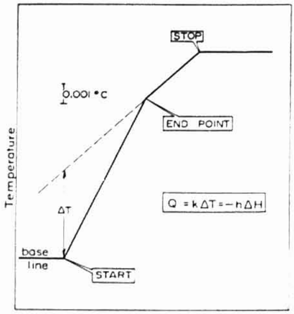

Figure 1. Typical normalized thermometric enthalpy titration curve in DMF. Appreciable slope of excess reagent line is due to the relatively large heats of dilution in nonaqeuous solvents of low dielectric constant ($\epsilon = 37$)

of ferriheme with chromous acetate, which were carried out under the same conditions as the corresponding thermometric enthalpy titrations. A conventional platinum indicator electrode was used. Conditional "formal" Gibbs free energy and entropy values were computed from the well-known thermodynamic relationships:

$$\Delta G_F{}^0 = -RT \ln K \qquad (2)$$

$$\Delta H_F{}^0 = \Delta G_F{}^0 + T\Delta S_F{}^0 \qquad (3)$$

Voltammetry. Current–voltage curves of ferriheme and ferroheme were recorded with the aid of a Model 170 Electrochemical System, supplied by Princeton Applied Research Co., Princeton, N.J. The indicator electrodes used were the dropping mercury electrode (DME) or Kemula's hanging drop mercury electrode (HDME) for classical polarographic measurements and cyclic voltammetry, respectively. The counter electrode was a platinum wire of relatively large area. Special care was taken to minimize uncertainties due to liquid junction potentials. With this purpose in mind, all electrochemical experiments were duplicated using two different reference electrodes, viz., (1) A conventional aqueous saturated calomel electrode (SCE) with an agar bridge saturated with aqueous KCl. (2) Pantony's silver–silver chloride half-cell (*15*) in DMF saturated in potassium chloride and containing 0.8 M potassium perchlorate with a salt bridge consisting of a methyl–methyl cellulose gel impregnated with a saturated solution of tetraethylammonium perchlorate (TEAP) in DMF.

Experimental potentials of the indicator electrodes DME and HDME measured against each of the two reference half cells were intercompared and found to be consistent with directly measured potential differences (60–80 mV) between the SCE and Patony's Electrode (PE), when the two reference half cells were connected via a solvent (pure DMF and/or DMF plus water) containing 0.1 M TEAP. The potential of Pantony's electrode vs. a normal hydrogen electrode (NHE) in DMF is known to be +0.279 V (*15*). Accordingly all potential assignments reported in this paper have been referred to the NHE in DMF. This must—naturally—be taken into account when comparing numerical assignments in the present communication with our preliminary data reported earlier in Ref. 8, where we referred potentials to the conventional aqueous SCE. The two sets of data are in satisfactory substantive agreement: where minor differences transpire, the values in the present communication represent the definitive assignments.

Heterogeneous electron transfer rate constants ($k_{Ox} = k_{Red} = k_0$), effective at relevant formal potentials, were evaluated (*16*) from anodic-cathodic potential peak separations, ΔE_p, observed on cyclic voltammograms, using the equation

$$\psi = \left[\frac{D_{Ox}}{D_{Red}}\right]^{\alpha} \frac{k_0}{\left[\frac{\pi D_{Ox} nF}{RT}\right]^{1/2} v^{1/2}} \qquad (4)$$

where ψ denotes a function of ΔE_p which has been tabulated by Nicholson (*17*), v is the potential scan rate in volt per second, D denotes diffusion coefficients and the subscripts Ox and Red refer to ferri- and ferro-heme respectively. The transfer coefficient α was assumed equal to 0.5.

In order to specify the formal potential at which our various k assignments were effective, the following procedure was used:

(a) Polarographic half-wave potentials ($E_{1/2}{}^{exp}$) in the various solvents were determined experimentally at the dropping mercury electrode.

(b) Corresponding reversible half-wave potentials ($E_{1/2}{}^{rev}$) were evaluated from the relationships (*18, 19*)

$$E_{1/2}{}^{exp} = E_{1/2}{}^{rev} + \frac{RT}{\alpha nF} \ln 0.886\, k_0 \sqrt{\frac{t}{D}} \qquad (5)$$

(c) Formal potentials, $E_F{}^0$, were estimated using the equation:

$$E_{1/2}{}^{rev} = E_F{}^0 + \frac{RT}{nF} \ln \frac{D_{Red}}{D_{Ox}} \qquad (6)$$

Density and Viscosity Measurements and Heats of Mixing. A Cannon pycnometer (volume = 25.4842 mL at 25 °C) and an Ubbelhode viscometer were used. These devices were calibrated with triply distilled water, utilizing the following "reference values" (*20*)

$$d_4{}^{25} = 0.99707$$

$$\eta^{25} = 0.8903 \text{ cp}$$

Heats of mixing of water and DMF (and water plus DMA) were determined by an unconventional procedure, viz., by titrating pure water into pure DMF, using the same titration calorimeter as in the thermometric enthalpy titrations described previously.

Chemicals. Triply re-crystallized hemin chloride (FW 651.59), supplied by Nutritional Biochemical Corporation, Cleveland, Ohio, served as the source of ferriheme. Ferroheme was prepared from hemin chloride by controlled potential electrolysis using a vigorous stirred mercury pool cathode and a Model 61-TR Wenking Potensiostat. Chromous acetate was prepared from 0.2 M aqueous chromic chloride which contained 0.05 M sulfuric acid. That solution was percolated through a Jones reductor column (amalgamed zinc, 5% mercury) into aqueous sodium acetate, yielding a red brick chromous acetate precipitate whose composition was $[Cr(OAc)_2]_2H_2O$. This hydrated dimer was washed successively with water, ethanol, and ether, pulverized, dried, and stored under argon. The presence of the water of crystallization in the compound precluded, naturally, the preparation of completely anhydrous solutions of chromous acetate in DMF or DMA. However, since the chromous solutions used in this investigation were invariably very dilute ($\leq$0.001 M) the contamination amounted to 20 ppm or less. This proved tolerable and results could readily be extrapolated to the pure anhydrous solvents (see section on Results below).

Solvents consisted of mixtures of *N,N'*-dimethylformamide (DMA, dielectric constant = 36.7) or *N,N'*-dimethylacetamide (DMA, dielectric constant = 37.8) and water. The aprotic solvents DMF and DMA were painstakingly purified by appropriate distillation procedures (*21, 22*).

RESULTS

Thermodynamic Assignments. Experimental findings actually obtained by potentiometric and thermometric enthalpy titrations of ferriheme with chromous acetate yielded readily ΔH, ΔG, and ΔS assignments for the reaction:

$$\text{Fe(III) heme} + \text{Cr(II)} = \text{Fe(II) heme} + \text{Cr(III)} \qquad (7)$$

Any interpretation regarding solvent effects on the ferri–ferro heme couple require, naturally, their segregation from effects due to the chromic-chromous half reaction, which is, in principle, impossible without extrathermodynamic assumptions. The following procedure was used to circumvent this difficulty.

(a) Ferricinium was titrated with Cr(II) under the same conditions (solvent, etc.) as prevailed in Reaction 7. In this

Table I. Thermodynamic Assignments[a] in Mixed DMF-Water Solvents

Concentration of water in DMF, C_W(mol L^{-1})	$-\Delta G_F°$(kcal mol^{-1})			$-\Delta H_F°$(kcal mol^{-1})			$-\Delta S_F°$(cal mol^{-1} deg^{-1}
	Reaction			Reaction			
	7	8	9	7	8	9	Reaction 9
0	2.49	0.15	2.34	15.50	3.15	12.35	33.6
1	3.25	0.25	3.00	23.00	3.60	19.40	55.0
2	3.57	0.32	3.20	24.20	3.95	20.25	57.2
3	3.70	0.41	3.29	24.65	4.40	20.25	56.9
4	3.87	0.50	3.37	24.95	4.95	20.00	55.8
5	3.94	0.65	3.29	25.00	5.50	19.50	54.4
6	3.99	0.72	3.27	24.80	5.80	19.00	52.8
8	4.06	0.94	3.12	23.65	7.00	16.65	45.4
10	4.13	1.05	3.08	20.90	8.45	12.45	31.4
12	4.17	1.18	2.99	17.40	10.40	7.00	13.4

[a] The absolute precision of the data (expressed as the standard deviation of the mean of 5 replicates) was ± 2 units of the last significant figure tabulated above. Estimation of the absolute accuracy is not feasible, because comparable independent assignments are not available in the literature. The data tabulated here are the first known relevant assignments.

Table II. Thermodynamic Assignments[a] in Mixed DMA-Water Solvents

Concentration of water in DMA, C_W(mol L^{-1})	$-\Delta G_F°$(kcal mol^{-1})			$-\Delta H_F°$(kcal mol^{-1})			$-S_F°$(cal mol^{-1} deg^{-1})
	Reaction			Reaction			
	7	8	9	7	8	9	Reaction 9
0	2.80	0.18	2.62	17.70	4.25	13.45	36.3
1	2.90	0.27	2.63	24.90	4.70	20.20	58.9
2	3.05	0.35	2.70	25.80	5.05	20.75	60.5
4	3.20	0.50	2.70	26.85	6.20	20.65	60.2
6	3.35	0.85	2.50	26.00	18.65	7.35	54.1
8	3.50	1.09	2.41	25.05	15.60	9.45	44.2
10	3.75	1.42	2.33	21.90	10.70	11.20	28.0
12	3.95	1.80	2.15	18.20	3.80	14.40	5.5

[a] See footnote *a*, Table I.

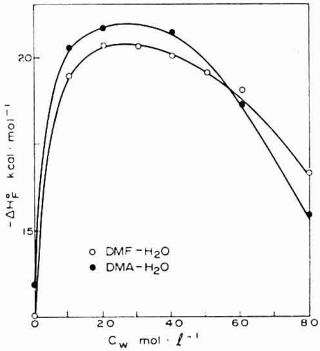

Figure 2. Heat of Reaction 9 as function of water present (C_w) in DMF and DMA solvents

manner, effective ΔH, ΔG, and ΔS assignments were obtained for the process:

$$\text{ferricinium} + \text{Cr(II)} = \text{ferrocene} + \text{Cr(III)} \quad (8)$$

(b) By appropriately substracting the relevant heats, Gibbs free energies and entropies of Reactions 7 and 8, thermodynamic assignments were obtained for the hypothetical redox process:

$$\text{Fe(III) heme} + \text{ferrocene} = \text{Fe(II) heme} + \text{ferricinium} \quad (9)$$

Thermodynamic parameters of Reaction 9 are not amenable to direct experimental determination because of the closeness of the standard potentials of the two couples and to slow kinetics, which, however, presented no difficulty in the case of Reactions 7 and 8.

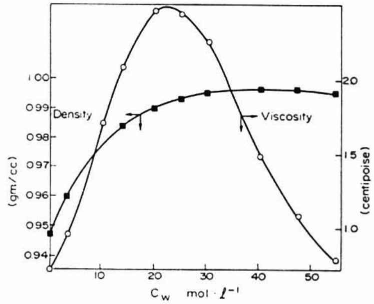

Figure 3. Physical properties of DMF-water solvents as function of water content (C_w)

(c) Using Strehlow's hypothesis (*23*), viz., that the thermodynamic parameters of the ferrocene–ferricinium couple are virtually independent of solvent composition, it was assumed that any solvent effects observed in Reaction 9 reflected exclusively solvent–solute interactions affecting the ferriheme–ferroheme couple.

Data obtained in mixtures of water with DMF and DMA are summarized in Tables I and II. Results in DMA and DMF exhibited similar trends which are apparent from Figure 2. Figures 3 and 4 show results of corresponding measurements of physical properties of the solvent mixtures.

Table III. Polarographic Diffusion Coefficients of Ferriheme (D_{Ox}) and Ferroheme (D_{Red}) in Various Solvents[a]

Concentration of water in solvent mixtures, C_W(mol L^{-1})	DMF			DMA		
	10^6 D_{Ox} cm^2/s	10^6 D_{Red} cm^2/s	D_{Ox}/D_{Red}	10^6 D_{Ox} cm^2/s	10^6 D_{Red} cm^2/s	D_{Ox}/D_{Red}
0	4.9	5.1	1.05	...	...	...
1	5.2	5.2	1.00	5.2	5.3	0.98
2	4.8	5.2	1.08	5.0	5.1	0.98
3	5.0	5.2	1.04	5.0	5.3	0.94
4	4.9	4.8	0.97	5.1	5.0	1.02
5	4.9	5.1	1.05	5.0	5.2	0.96
6	4.7	4.9	1.05	5.0	5.2	0.96
8	5.0	5.5	1.10	5.3	5.4	0.98
10	5.1	5.2	1.02	5.3	5.5	0.96
12	4.9	4.7	0.95	5.5	5.5	1.00
15	5.2	4.9	0.95	5.7	5.9	0.97
18	4.9	5.0	1.02	5.8	6.2	0.94

[a] Supporting electrolyte 0.1 M TEAP.

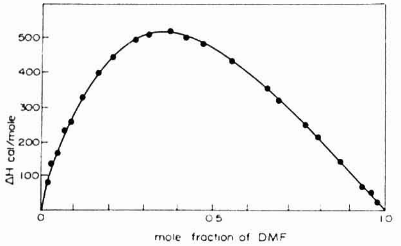

Figure 4. Heat of mixing of DMF and water as function of mole fraction of DMF

Electrode Kinetics. Specific ("standard") rate constants k_0 for the electrode reaction:

$$\text{Fe(III) heme} + e = \text{Fe(II) heme} \tag{10}$$

determined in the present study are plotted in Figure 5 as function of solvent composition. The same results were obtained in DMF and DMA solvents in the presence of comparable amounts of water. Our DMA data agree satisfactorily with earlier work by Davis and Bynum (*24*). The corresponding standard potentials (where $k_{Ox} = k_{Red} = k_0$) are also shown in the figure. In order to evaluate E^0 and k_0 in the various solvent mixtures via Equations 4, 5, and 6, the diffusion coefficients of ferriheme and of ferroheme were required. These were calculated from polarographic diffusion currents with the aid of Koutecky's expanded Ilkovic Equation (*25*). The assignments which transpired are shown in Table III.

DISCUSSION

The experimental findings are accounted for as follows.

(a) The electroreactive Fe(III) heme and Fe(II) heme species had the axial coordination illustrated in Figure 6. The divergence of the E^0 and k_0 plots in Figure 5 when $C_{H_2O} < 5$ M was due to the chloride abstraction process:

$$\text{X} + \text{H}^+ + \text{X(Fe heme)}\overline{\text{Cl}} = \text{HCl} + \text{X(Fe heme)X}$$

(where X denotes DMF or DMA) occurring in the presence of $HClO_4$, which is a strong acid in DMF and DMA, while HCl is known to be a weak acid in these solvents (*26*). In contradistinction, chloride remained axially coordinated (as in crystalline hemin chloride) in the presence of TEAP. When $C_{H_2O} > 10$ M, both *X(Fe heme)Cl* and *X(Fe heme)X* were converted to *H_2O(Fe heme)X*. This was in complete accordance with previous reports in the literature (*8*).

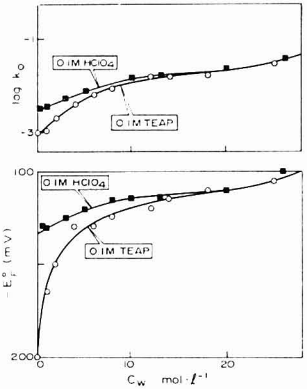

Figure 5. Specific (formal) electrochemical rate constants and corresponding formal potentials of the ferri-ferroheme couple in DMF in the presence of water. Supporting electrolytes are specified on each curve. C_w = concentration of water present

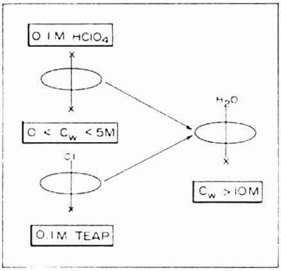

Figure 6. Axial coordination of electroreactive species in solutions prepared from hemin chloride. C_w = molarity of water. X = DMF or DMA. Supporting electrolyte (0.1 M $HClO_4$ or 0.1 M TEAP) as specified

(b) The convergence of the k_0 values in Figure 5 (top curves) is paralleled by striking effects in the entropies of Reaction 9, as is apparent from the minimum in Figure 7. Concomitantly the solvent properties (heat of mixing viscosity and density) also exhibit corresponding maxima or leveling features (see Figures 3 and 4). However, it is worth emphasizing that specific analytic geometry features in Figures 2, 3, 4, 5, 7 (e.g., maxima in plots of physical properties vs. leveling off of rate

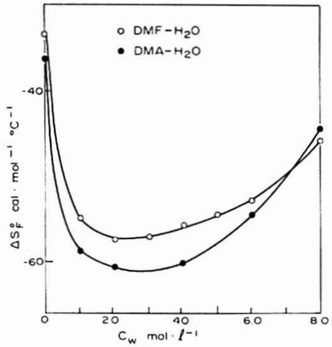

Figure 7. Variation of the entropies of Reaction 9 as function of solvent composition

constants or formal potentials) are not necessarily the same. The point we wish to make is merely the qualitative observation that changes in physical solvent properties appeared to be most drastic in certain domains of solvent composition where electrochemical thermodynamic and kinetic parameters also changed a great deal. The observed solvent property effects are indicative of changes in liquid structure which are known to be due to *solvent–solvent* interactions (*27–29*). Our findings suggest that they were matched by corresponding *solvent–solute* interactions reflected in electrochemical behavior.

Indeed, the trends in the electrode kinetics on the one hand (Figure 5, top), and in redox thermodynamics on the other hand (Figure 5, bottom, and Figure 7), both appear to point to the involvement of the solvent–solute interactions. The kinetic effects are entirely consistent with an electron transfer path via the porphyrin ring while the entropy effects can reasonably be accounted for by the solvation of the periphery of the equatorial porphyrin ligands (*8*). It should be noted, however, that the findings reported in the present paper (per se!) do *not necessarily* preclude supplementary effects due to the involvement of axial coordination orbitals of heme-iron. Work is in progress to clarify this interesting question.

LITERATURE CITED

(1) A. L. Underwood and R. W. Burnett, "Electrochemistry of Biological Compounds", *Electroanal. Chem.*, **6**, 1–85 (1973).
(2) J. E. Falk, "Porphyrin and Metalloporphyrins", Elsevier, Amsterdam, 1964; 2nd ed., K. M. Smith, Ed., Elsevier, Amsterdam, 1975.
(3) W. M. Clark, "Oxidation-Reduction Potentials of Organic Systems", William and Wilkins, Baltimore, Md., 1960.
(4) D. G. Davis and D. J. Orleron, *Anal. Chem.*, **38**, 179 (1966); D. G. Davis and R. F. Martin, *J. Am. Chem. Soc.*, **88**, 1365 (1966).
(5) T. M. Bednarski and J. Jordan, *J. Am. Chem. Soc.*, **86**, 5690 (1964); **89**, 1552 (1967).
(6) S. B. Brown and I. R. Lanske, *Biochem. J.*, 115, 279 (1969).
(7) K. M. Kadish and J. Jordan, *Anal. Lett.*, **3**, 113 (1970).
(8) B. A. Feinberg, M. Gross, K. M. Kadish, R. S. Marano, S. J. Pace, and J. Jordan, *Bioelectrochem. Bioenerg.*, **1**, 73 (1974).
(9) H. R. Gygax and J. Jordan, *Discuss. Faraday Soc.*, **45**, 227 (1968).
(10) D. W. Clark and N. S. Hush, *J. Am. Chem. Soc.*, **87**, 4238 (1965).
(11) G. Peychal-Heiling and G. W. Wilson, *Anal. Chem.*, **43**, 545 (1971).
(12) A. C. Censullo, J. A. Lynch, D. H. Waugh, J. Jordan, "Biochemical and Clinical Applications of Titration Calorimetry and Enthalpimetric Analysis" in "Analytical Calorimetry", R. S. Porter and J. F. Johnson, Eds., Plenum Press, New York, N.Y., Vol. III, 1974, pp 217–235.
(13) J. Juillard and R. Loubinoux, *C. R. Acad. Sci. Paris*, **264**, 1680 (1964).
(14) J. Jordan, J. K. Grime, D. H. Waugh, C. D. Miller, H. M. Collis, and D. Lohr, *Anal. Chem.*, **48**, 427A (1976).
(15) G. P. Kumar and D. A. Pantony in "Polarography 1964, Proceedings of the Third International Congress", Macmillan, London, 1966, p 1061.
(16) R. S. Nicholson, *Anal. Chem.*, **37**, 1351 (1965).
(17) R. S. Nicholson and I. Shain, *Anal. Chem.*, **36**, 706 (1964).
(18) J. Koutecky, *Chem. Listy*, **47**, 323 (1953).
(19) J. Weber and J. Koutecky, *Chem. Listy*, **49**, 562 (1955).
(20) J. F. Swindells, C. F. Snyder, R. C. Hardy, and P. E. Golden, *Natl. Bur. Stand. (U.S.), Circ. Suppl.*, **440**, 700 (1958).
(21) H. Kojima and A. J. Bard, *J. Electroanal. Chem.*, **63**, 117 (1975).
(22) J. E. Prue and P. J. Sherington, *Trans. Faraday Soc.*, **57**, 1795 (1961).
(23) H. Strehlow, *Z. Elektrochem.*, **56**, 827 (1952).
(24) D. G. Davis and L. M. Bynum, *Bioelectrochem. Bioenerg.*, **2**, 184 (1975).
(25) M. Olsztajn, P. Turq, and M. Chemla, *J. Chim. Phys.*, **67**, 217 (1970).
(26) P. G. Sears, R. W. Wolford, and L. R. Dawson, *J. Electrochem. Soc.*, **103**, 633 (1956).
(27) R. Paul, P. S. Guraya, and B. R. Sreenathan, *Ind. J. Chem.*, **1**, 335 (1963); **3**, 300 (1965).
(28) B. G. Cox, A. J. Parker, and W. E. Waghorne, *J. Phys. Chem.*, **78**, 1731 (1974).
(29) O. D. Bonner and U. S. Choi, *J. Phys. Chem.*, **78**, 1723 (1974).

RECEIVED for review June 7, 1977. Accepted June 29, 1977. Presented in part before the 4th International Conference on Chemical Thermodynamics, Montpellier, France, August 26–30, 1975. Supported by the National Science Foundation (Research Grant CHE 76-21666), the National Institutes of Health (Research Grant 5R01 HL 02342 from the National Heart, Lung, and Blood Institute), and the North Atlantic Treaty Organization (NATO Research Grant RG 794).

Assay of Phenobarbital with an Ion-Selective Electrode

Gary D. Carmack and Henry Freiser*

Department of Chemistry, University of Arizona, Tucson, Arizona 85721

A rapid and reliable phenobarbital tablet assay method was developed based on the potentiometric sensing of the phenobarbital anion using a coated-wire electrode. The results obtained are in agreement with the standard USP method.

Phenobarbital (5-ethyl-5-phenylbarbituric acid) is conventionally assayed in pharmaceutical preparations using the extractive-spectrophotometric procedure specified in the U.S. Pharmacopeia (*1*). A number of other analytical methods are also available including fluorimetry (*2*), coulometry (*3*), and liquid chromatography (*4*). However, these methods generally involve the use of more sophisticated instrumentation or more complex procedures and are perhaps best suited to the analysis of complex mixtures, e.g., human sera.

The development of ion-selective electrodes based on ion association systems in this laboratory (*5–7*) and other (*8*) have demonstrated that a wide variety of simple and economical analyses are possible with these sensors.

This study deals with the application of a coated-wire phenobarbital electrode based on the ion-pair complex between phenobarbital anion and the quaternary ammonium cation, tricaprylylmethylammonium, for the analyses of phenobarbital solutions. The advantages of using this electrode instead of previously mentioned methods are simplicity, speed of analysis, and economy.

EXPERIMENTAL

Materials. ACS Reagent grade chemicals were used except as noted. Aliquat 336S (tricaprylylmethylammonium chloride) was obtained from General Mills Chemicals, Inc. Chromatographic grade poly(vinyl chloride) powder, epoxy resin (Epon 826), and curing agent (diethylenetriamine) were from Polysciences, Inc. Mallinckrodt sodium phenobarbital was used for preparation of standard solutions. Decyl alcohol, melting point 5.5–6.5 °C, was from Eastman Kodak. Chloroform, spectrophotometric grade, was obtained from Aldrich Chemical Co. Platinum wire (0.07-cm diameter) was used without special preparation of the metal surface.

Conversion of Aliquat 336S to the Phenobarbital Form. Five milliliters of Aliquat 336S were dissolved in approximately an equal volume of decyl alcohol and equilibrated with four separate 10-mL aliquots of 0.5 M sodium phenobarbital raised to pH 9.0 by addition of 0.01 M NaOH. After each shaking, the aqueous phase was separated and tested for the presence of chloride with acidified $AgNO_3$. The absence of chloride indicated complete exchange. The organic phase was washed twice with deionized water and then centrifuged until a clear liquid was obtained.

Construction of Electrodes. Coated-wire electrodes were constructed using the technique as reported previously (*5–7*). Weighed amounts of the electroactive material were dissolved either in a 5% (w/w) solution of PVC in tetrahydrofuran or mixed with the epoxy mixture (containing equal weights of resin and curing agent) and the end of a platinum wire repeatedly dipped into the mixtures until a uniform coating was obtained. This usually required about three dippings. A greater number could be tolerated as long as the electrode impedance does not exceed 10^7 Ω. The electrodes were cured or air-dried overnight. The exposed portion of the wire was wrapped tightly with Parafilm (American Can Co.).

All electrodes were subjected to initial conditioning by soaking for an hour in a 10^{-1} M sodium phenobarbital solution. Immediately before use, the electrodes were soaked in a dilute (ca. 10^{-4} M) phenobarbital solution for approximately 15 min. When not in use, they were stored in air.

An Orion Model 701 digital pH meter was used for all measurements and a Beckman Fiber Junction calomel electrode served as reference electrode. Calibration curves were obtained using sodium phenobarbital solutions; the pH was adjusted to 9.6 by the addition of 0.01 M sodium hydroxide. All potentiometric measurements were made at 25.0 °C.

Interference Studies. These were carried out by the mixed solution procedure described previously (*5–7*). The concentration of sodium phenobarbital was fixed at 5×10^{-3} M while the concentration of interfering anions was varied between 10^{-3} to 10^{-1} M. A pH of 9.6, chosen to retain the phenobarbital quantitatively in the anionic form without unduly raising the concentration of the interfering hydroxide ion, was maintained for all solutions.

Electrode Analysis of Phenobarbital Tablets. Phenobarbital tablets (Eli Lilly and Co.) were analyzed by finely powdering a batch of not less than 20 tablets. A portion of the powder, equivalent to about 50 mg of phenobarbital, was transferred to a 100-mL volumetric flask and diluted to volume with water. The pH was adjusted to 9.6 with 0.01 M NaOH. Potentiometric measurements were alternately made on this solution and a standard solution having approximately the same phenobarbital concentration, until a reproducible difference in readings was obtained (±0.1 mV).

USP Procedure. The USP procedure (*1*) for the assay of phenobarbital tablets involves successive chloroform extractions from an acidic phenobarbital solution. Following evaporation of the chloroform solution, the residue was taken up in an alcoholic-borate solution and the UV absorbance determined at 240 nm.

Table I. Selectivity Ratios for Various Anions with Coated-Wire Phenobarbital Electrodes

Foreign ion	Selectivity ratio, $K_{A/i}$[a]
Nitrate	0.2
Chloride	0.1
Acetate	0.02
Salicylate	0.7
Sulfate	See text
Phosphate	See text

[a] As defined by the equation: $E_A = E_A^\circ + 59.2 \log(a_A + K_{A/i}a_i^{1/n_i})$ where E_A is the potential of the phenobarbital electrode, a_A its ionic activity, and a_i the activity of an anion *i* of charge *n*.

RESULTS AND DISCUSSION

The response characteristics of the electrodes were tested using solutions of from 0.1 M to 10^{-5} M sodium phenobarbital, pH 9.6. The optimal membrane composition was 70 wt % Aliquat salt in the PVC films and 50 wt % for the epoxy films. The PVC coated-wire electrodes gave a linear response (slope = 55 ± 2 mV/log *a*) from 0.1 M to approximately 10^{-4} M. Coated-wire electrodes using the epoxy films gave slightly greater sensitivity (slope = 57 mV/log *a*) and were therefore used for the tablet analyses. In both types, the sensitivity of the electrodes rapidly decreases beyond a concentration of ca. 10^{-4} M phenobarbital because of hydroxide ion interference.

The response time of the coated-wire electrodes was fast, being nearly instantaneous at higher concentrations and requiring less than 1 min with a 10^{-4} M phenobarbital solution. The potential readings could be reproduced to better than ±1 mV over the entire concentration range, but the absolute potential varied daily from 5 to 15 mV necessitating a one-point restandardization before each run. The useful lifetime of these electrodes is at least three months.

The interference by other anions was determined from selectivity studies in which the calculated selectivity ratio, *K* (*9*), is used in evaluating the degree of interference. The results, summarized in Table I, show that most of the ions interfered moderately. Sulfate and phosphate gave negligible interference when present in approximately the same concentration as that of phenobarbital but, unexplicably, the electrode response became unstable when large excesses (>10-fold) of either ion was present.

The ions listed in Table I were chosen as representative of potentially low level contaminants in the phenobarbital tablet preparations. The bulk of the excipient, usually consisting of a lactose diluent and maize starch or gelatin binders (*10*), should not show any interference.

High precision (relative standard deviation of ±1.3%) quality control-type analyses are made possible with these electrodes because the approximate phenobarbital content of a tablet is known beforehand. A standard solution containing this concentration can be prepared and measurements can be performed repeatedly on it and the sample solution until a reproducible (±0.1 mV) potential difference is obtained between the two solutions. Usually, the difference in potential was within 1–2 mV. So despite an electrode drift of approximately 1 mV during the course of several determinations, the relative potential difference remained constant. Samples exhibiting readings differing from the standard by more than 2 mV can either be rejected or redetermined by preparing a more closely matched standard.

The results of the potentiometric analyses of phenobarbital tablets using an epoxy coated-wire electrode are reported in Table II. In contrast to the 4 h required for assay by the USP

Table II. Comparison of Conventional and Electrode Method for the Analysis of Phenobarbital Tablets

Tablet[a]	Electrode method, mg/tablet	USP method, mg/tablet
16 mg	15.7 ± 0.2[b]	15.8 ± 0.2
32.5 mg	31.9 ± 0.4	32.1 ± 0.2

[a] Concentration as stated by manufacturer. [b] Standard deviation (at least 4 determinations with electrode and 2 with USP method).

method (*2*), an electrode assay can be accomplished within 20 min. The rapidity with which the assay can be carried out using the coated-wire electrode makes it practical to perform the procedure on single tablets, so that tablet-to-tablet variation could be followed if desirable.

These results clearly show that ion-selective potentiometry using a coated-wire electrode sensitive to sodium phenobarbital is a useful and accurate method of analysis.

LITERATURE CITED

(1) United States Pharmacopeia, XVIII Ed., American Pharmaceutical Association, Washington, D.C., 1970, p 490.
(2) C. I. Miles and G. H. Schenk, *Anal. Lett.*, **4**, 61 (1971).
(3) J. R. Monforte and W. C. Purdy, *Anal. Chim. Acta*, **52**, 25 (1970).
(4) P. Menyharth, A. L. Levy, and D. P. Lehane, *Chromatogr. Newsl.*, **4**, 15 (1976).
(5) R. W. Cattrall and H. Freiser, *Anal. Chem.*, **43**, 1905 (1971).
(6) H. J. James, G. D. Carmack, and H. Freiser, *Anal. Chem.*, **44**, 856 (1972).
(7) B. M. Kneebone and H. Freiser, *Anal. Chem.*, **45**, 449 (1973).
(8) N. Ishibashi, K. Kina, and N. Mackawa, *Acta. Pharm. Suec.*, **9**, 641 (1972).
(9) A. K. Covington, *Crit. Rev. Anal. Chem.*, **3**, 355 (1974).
(10) H. Burlinson, "Tablets and Tabletting", Heinemann, London, 1968.

RECEIVED for review May 12, 1977. Accepted June 16, 1977. Work supported by a grant from the Office of Naval Research.

Silver-110 Microgram Sulfate Analysis for the Short Time Resolution of Ambient Levels of Sulfur Aerosol

Joseph Forrest* and Leonard Newman

Atmospheric Sciences Division, Department of Applied Science, Brookhaven National Laboratory, Upton, New York 11973

Atmospheric particulate samples collected on glass fiber or quartz filters have been routinely analyzed for total sulfur at the milligram level with ^{110}Ag tracer. The method has been refined to permit sulfate analyses of <10 μg SO_4^{2-}. Samples are reduced with a mixture of HI, H_3PO_3, and HCl, converting SO_4^{2-} to H_2S, which is adsorbed as CdS. Metathesis of CdS with $AgNO_3$ containing tracer ^{110}Ag is followed by collection of Ag_2S on a membrane filter and gamma counting in a NaI(Tl) well counter. Recoveries of ~97% with a std dev of ±7% were obtained with standard sulfate solutions, and recoveries were comparable in the presence of quartz or glass-fiber particulate filters. Comparisons were made between total and soluble particulate sulfate in ambient air samples collected at urban and rural locations, utilizing the ^{110}Ag technique. The technique was also compared with a soluble sulfate turbidimetric method of analysis.

With the recent awareness that atmospheric particulate sulfate may be a serious health hazard (*1*, *2*), increased emphasis is being placed upon control strategies for this pollutant. An important aspect to the identification of the significance of this concern is the accurate determination of the ambient concentration of aerosol sulfur. Critical reviews on the current state of analytical methodology for sulfate in airborne particles (*3*, *4*) discuss the limitations of existing technology. Although real time instrumental sensing of aerosol sulfate would be the most desirable means for monitoring atmospheric concentrations, existing techniques are not yet practical. Consequently, filter collection of airborne particulates followed by any one of numerous procedures for sulfate analysis remains the popular recourse. Determination of total aerosol sulfur is presently limited to direct determination on a filter by x-ray fluorescence techniques (*5*). Remaining procedures require preliminary extraction by water prior to analysis. Errors may arise from incomplete extraction of insoluble sulfates or formation of insoluble sulfates with certain cations after dissolution (*6*).

The origin of aerosol sulfate and conversion of atmospheric sulfur dioxide to particulate sulfur are problems undergoing extensive scrutiny (*7*). Aircraft tracking of power plant plumes (*8*) and urban and rural air masses (*9*) over extended distances from their origin is a popular experimental mode of investigation. As an example, our participation in the Multistate Atmospheric Power Production Pollution Study (MAP3S) (*10*) requires short-time resolution of atmospheric pollutants for adequate modeling input. This requirement results in obtaining samples for analysis with only a few micrograms of aerosol sulfate.

Among the many current procedures for measuring ambient sulfate, the most widely used are probably turbidimetry, thorin, methyl thymol blue, and x-ray fluorescence. An exhaustive study (*6*) of 24-h high-volume samples taken at three geographical locations and analyzed by the first three of the above methods indicated acceptable agreement among procedures. In all cases, the glass fiber filter extracts were diluted to provide optimum concentrations for each technique. Additional comparisons were made between thorin, methyl thymol blue, and x-ray fluorescence on 24-h samples taken with low-volume (12 L/min) filters. Results revealed differences of up to a factor of 2 for individual samples and 1.6 when pooled by sampling site, contrasting markedly with the high-volume samples. X-ray fluorescence results by two different laboratories differed by nearly a factor of two. The need for improvement at these levels seems evident.

A recently-developed technique, ion chromatography (*11*, *12*), has shown promising capabilities for measuring sulfate with good precision and sensitivity. The method has not been extensively tested with real samples; in addition, specialized equipment is needed. Total time for analysis would not be significantly less than for the method proposed in this publication.

In this paper we describe a technique for direct determination of low-level (microgram) amounts of total, both soluble and insoluble, particulate sulfur collected on glass or quartz fiber filters with a time resolution for ambient levels of less than a half hour. Quartz fiber filters were demonstrated to retain particulates at ≥ 99.9% efficiency, similar to glass fiber filters, at varying air velocities and particle sizes (*13*).

Routine analyses have been performed at Brookhaven on field samples using a turbidimetric procedure with a Technicon AutoAnalyzer. The results obtained therein were used as a basis for comparison with the newly devised ^{110}Ag technique.

PRINCIPLE

Reduction of sulfate to hydrogen sulfide followed by detection of H_2S by any one of the many sensitive available reagents offers an attractive basis for the determination of total sulfate. Reduction was first proposed by St. Lorant (*14*) who employed hydriodic acid for this purpose. He measured the evolved sulfide colorimetrically as methylene blue. Luke (*15, 16*) used a mixture of hydriodic, hydrochloric, and hypophosphorous acids to convert sulfate, followed by iodimetry. He later increased sensitivity by photometrically determining sulfur as a suspension of lead sulfide (*17*). Pepkowitz and Shirley (*18*) using Luke's reducing solution, detected microgram quantities with ammonium molybdate–potassium thiocyanate solution. Johnson and Nishita (*19*) analyzed plant material sulfate as methylene blue with a hydriodic acid, formic acid, red phosphorous mixture. An extensive study of hydriodic acid reduction was made by Gustafsson (*20*) who applied a medium of hydriodic and hypophosphorous acids in acetic acid solution followed by methylene blue detection. Davis and Lindstrom (*21*) replaced acetic acid with acetic anhydride to overcome water interference and measured sulfide with ferric ion and 1,10-phenanthroline.

Thode et al. (*22*) described a procedure for processing seawater, minerals, and meteorites to produce highly purified SO_2 for $^{34}S/^{32}S$ isotope ratio mass spectrometry. Yields of over 99% were obtained in all steps as a prerequisite to avoid the possibility of isotope fractionation. Seawater sulfate was precipitated as $BaSO_4$ which was subsequently reduced with a mixture of hydriodic, hypophosphorous, and hydrochloric acids. Hydrogen sulfide was swept out with a stream of nitrogen, washed in distilled water, and collected in a cadmium acetate solution. Because silver sulfide was easier to filter than cadmium sulfide, the latter was converted to Ag_2S by adding 0.1 N $AgNO_3$. The Ag_2S was then filtered, dried, and further processed by combustion to SO_2 for mass spectrometry.

Adaptation of Thode's procedure plus miniaturization of equipment enabled us to analyze milligram quantities of atmospheric SO_2 and particulate sulfur for $^{34}S/^{32}S$ isotope ratios (*23*). Simultaneously, a modification of the reduction step which took advantage of the normal preparation scheme and required little additional time was developed to provide accurate estimations of sulfur levels. This involves the addition of ^{110}Ag tracer to the standard $AgNO_3$. The sulfide precipitate filtered on a quartz wool plug was introduced into a counting tube and counted in a NaI(Tl) well counter. An aliquot of the $^{110}AgNO_3$ standard was counted for reference. From the ratio of sample counts to reference, the weight of silver, and therefore of sulfur, was calculated. Particulates collected on glass filters were reduced directly by digesting the filter plus contents. In this fashion, prior extraction was eliminated and total sulfate, rather than soluble sulfate, can be measured.

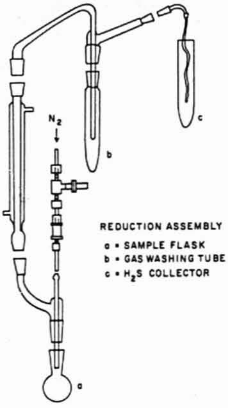

Figure 1. Reduction assembly

The above technique required hundreds of micrograms of material for an accurate analysis. Following, we describe the extension and testing of the technique for the determination of <10 μg of sulfate.

EXPERIMENTAL

Reagents. *Reducing Solution.* Place 816 mL of concentrated hydrochloric acid, 500 mL of hydriodic acid (48% Baker Analyzed Reagent) and 245 mL of hypophosphorous acid (50% J. T. Baker Purified) into a 4-L beaker. Add several boiling chips, cover with a watch glass, and boil gently for 1.5 h to volatilize any sulfur contaminants. Cool and store in stoppered bottles.

Cadmium Acetate, 0.1 M (Dihydrate, Baker Analyzed Reagents). Allow the solution to age for at least 2 days. Filter through a glass frit filter.

Silver Nitrate, 0.01 M (Baker Analyzed Reagent, 99.9%). Dry reagent grade $AgNO_3$ at 110 °C. Weigh 1.6987 g, dissolve and dilute to 1 L with doubly distilled water. The solution may be assayed gravimetrically for highest accuracy. A mL is equivalent to 160.3 μg S. Several drops of a concentrated ^{110}Ag solution (New England Nuclear Corp.) are added to give about 80 000 counts min^{-1} mL^{-1}. Counting 1 mL for 1 min is sufficient to standardize this solution. With a half-life of 252 days, the solution will maintain its activity for relatively long periods of time, but may be renewed with several drops of ^{110}Ag concentrate.

Nitrogen. Prepurified cylinder nitrogen.

Filters. Cellulose membrane filters 0.22 μm porosity, 25-mm diameter (Millipore Corp. GSWP 025 00).

Filter Holder. Pyrex microanalysis frit support consisting of Pyrex funnel and base, fritted glass filter support, aluminum spring clamp, neoprene stopper (Millipore Corp. XX10 025 00)). The length of the funnel may be shortened by removing a section from the center and re-attaching the base to the funnel.

Apparatus. The reduction train, shown in Figure 1, is fabricated from borosilicate glass. Sample and acid are placed in a 50-mL round-bottom flask with standard taper 24/40 joint and heated by a micro burner. The stopper assembly contains a side arm leading to a water-cooled condenser and also a capillary gas inlet tube, 7-mm o.d. and 1-mm i.d., extending to 2 mm from the bottom of the flask. Standard taper 19/38 joints are fitted to both ends of the condenser. Gas is led from the condenser to the gas washing tube via an assembly with two standard taper 19/38 joints and a side arm ending in a 12/30 joint. The gas washing tube is made from a 50-mL centrifuge tube fitted with a standard taper 19/35 joint. Gas is introduced to the collector tube by a short piece of glass tubing beginning with a standard taper 12/30 joint and terminating with a 5-mm inner Luer glass ground joint to which is attached a Teflon needle with Kel-F Luer hub (Hamilton Co. KF28TF, 1 ft). A 50-mL centrifuge tube, lengthened by 4 cm, serves as the H_2S collector. Tapered joints are lubricated with silicone grease and fastened with springs.

Nitrogen is supplied to a bank of reduction assemblies from a 1A cylinder leading to a $^1/_4$-in. copper tubing manifold. The Tygon line from the cylinder regulator to the manifold is "teed" to a fritted disk-gas washing bottle filled with mercury to provide a constant head pressure. Flow of nitrogen to the individual sample flasks is controlled by a fine metering valve (Nupro. Co. B-2MA) followed by a check valve (Nupro Co. SS4C-1/3) to prevent acid back-up. Tygon tubing connects the check valve to the gas capillary inlet tube.

$^{110}Ag_2S$ is gamma counted in a 3 in. × 3 in. NaI (Tl) well counter with preamplifier, amplifier, scaler, and timer (Ridl Corp.).

Sample Collection. A conventional (*23*) 8 × 10 in. high volume filter assembly has been replaced with 5-in. diameter circular filters. This permits a higher sample to blank ratio, but at a sacrifice of absolute quantity of material collected per unit time. It has been found that the particulates can be collected on Pallflex tissuquartz 2500QA0 filters (Pallflex Production Corp.), pretreated with phosphoric acid to neutralize alkaline sites (*24*). A portion of the sampled filter is devoted to sulfate speciation. The remaining sample available for total sulfate analysis contains 3–50 μg S on 10 in.^{2} of quartz fiber filter.

Procedure. As with any trace analysis, care should be taken to avoid extraneous contamination. Assemble the cleaned apparatus as illustrated in Figure 1, greasing joints with silicone grease. Thirty mL of distilled water and cadmium acetate solution are placed in the gas washing tube and collection tube, respectively.

Cut sample filter into small sections, place into flask ($\leq$10 in.^{2}, 50-mL flask; 20–40 in.^{2}, 100-mL flask). Add 25 mL reducing acid for 10 in.^{2}; 50 mL for 20–40 in.^{2}. With water flowing through condensers, commence N_2 flow at ~2.5 bubbles s^{-1} through washing tube (17 mL min^{-1}).

Using a small flame, heat flask gently until boiling begins and continue for 20 min. Increase N_2 flow to ~40 mL min^{-1} for an additional 15 min. Again increase flow rate to a vigorous flow of about 75 mL min^{-1} and shut flame. Purge system for 15 min without heat.

Remove the collector tube and add $^{110}AgNO_3$ solution: 0.5 mL for $\leq$25 μg S, 1 mL for 25–50 μg S, 2 mL for 50–150 μg S. Place in a darkened area for 0.5–1 h.

Filter the Ag_2S through a cellulose membrane filter. Rinse tube and wash the filter eight times with water. Wash the Ag_2S with minimal amounts of ammonium hydroxide followed by five washings with water.

Remove the filter, fold, and insert into a small sample test tube precounted for background. Wipe the filtering funnel and collection tube free of adhering particles with a small piece of paper tissue and insert tissue into the counting tube.

Count 1.00 mL of $^{110}AgNO_3$ reagent, equivalent to 160.3 μg S, in the well counter, and calculate counts min^{-1} μg^{-1} S. Then count the sample and calculate the μg S.

Adherence of Ag_2S to collection tube walls could be minimized by filling the tubes with chromic acid cleaning solution between use. With a bank of 10 distillation trains, total working time per sample, including sample preparation and clean-up is ~40 min.

RESULTS

Sample handling and transfer, not solubility, are the potential limitations to the utilization of this ^{110}Ag–Ag_2S method. In order to evaluate the sampling transfer aspects, we added $^{110}AgNO_3$ to standard sulfide solutions.

Reagent grade $Na_2S \cdot 9H_2O$ (Mallinckrodt Analytical Reagent, crystal) was washed, dried and weighed directly. Based upon the experience of Axelrod et al. (*25*), this reagent yields solutions accurately containing 97% of the stated value and further standardization for our purposes was unnecessary. One-half mL of $^{110}AgNO_3$ was added to varying amounts of "standard" S^{2-} in 25 mL water. After 0.5 h the resultant colloid was filtered through a 0.22-μm membrane filter. The walls of the tube and funnel were wiped, and the combined filters and wipings counted in a small test tube for ^{110}Ag. Table I indicates that recoveries were quite complete even for samples containing significantly less than the equivalent of 10 μg of sulate.

Table I. Recovery of Sulfide with Silver-110

μg S^{2-}	
Added	Found
1.95	1.87
2.91	2.78
4.88	4.87
9.75	9.36
48.8	46.9

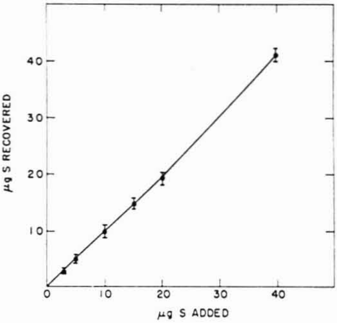

Figure 2. Recovery of SO_4^{2-}

Microgram amounts of sulfate were next reduced and distilled to confirm this step of the procedure. Anhydrous sodium sulfate (Baker Analyzed Reagent, anhydrous powder, 99.9%) dried at 100 °C, was weighed as a standard to prepare a 5 mg mL^{-1} solution of S. This working standard was further diluted and aliquots were reduced with the hydriodic, hypophosphorous, hydrochloric acids mixture. Evolved sulfide was scrubbed with water and collected directly in a $^{110}AgNO_3$ solution. Erratically high yields were attributed to the reduction of Ag^+ to Ag^0 probably by volatile products of the combined acids. It was found necessary to employ 0.1 M cadmium acetate solution as the absorbant followed then by the addition of $^{110}AgNO_3$ to metathesize the CdS to $^{110}Ag_2S$.

Recoveries of sulfate were now checked by reducing 3 to 40 μg S for 1 h. Yields averaged 97% ± 7.2% rel std dev over this range (Figure 2).

Corrections for reagent blanks of 0.5 μg S were employed. These experiments were then repeated by analyzing sections of quartz fiber filters (6–10 in.^{2}) to which standard sulfate solution had been added. Filter plus reagent blank corrections of 0.2 μg S in.$^{-2}$ are required. The results averaged 101% ± 5.6% rel std dev. Subsequent experiments indicated that sample heating time could safely be reduced from 1 h to 35 min with no loss in yields, and this modification was adopted.

In spite of the substitution of cadmium acetate for silver nitrate as absorbant for H_2S, occasional spuriously high results were still encountered. They were usually accompanied by the appearance of a silver mirror on the walls of the collector tube, suggesting that reduction of Ag^+ to Ag^0 could still occur. Davis and Lindstrom (*21*) mention that phosphorous acid could decompose when heated with the evolution of phosphine. The transferred phosphine could then cause reduction of the Ag^+. Consequently, after precipitation of the CdS and prior to addition of $AgNO_3$, the system was flushed for 15 min with N_2. The burner was off during the flushing. Evidence of reduced silver was now absent and the precision of subsequent analyses was markedly improved, to ~±3% rel std dev.

Among the more abundant and common constituents of atmospheric particulates, the nitrate ion would be most likely

Table II. Interference of Nitrate

μg S added as SO_4^{2-}	Added μg NO_3	Found μg S (corrected for blank)
20	50	19.6
20	50	19.2
20	100	19.1
20	100	20.1

Table III. Response to Sulfite

μg S added as SO_4^{2-}	μg S added as SO_3^{2-}	μg S found (corrected for blank)
20	~20	37.9
20	~20	38.3
20	~20	39.8[a]
20	~20	39.1[a]

[a] In presence of 6 in.^{2} of quartz filter.

Table IV. Comparison of Ambient Particulate Sulfate

Total (^{110}Ag) μg m^{-3} SO_4^{2-}	Soluble (^{110}Ag) μg m^{-3} SO_4^{2-}	Turbidimetric (AutoAnalyzer) μg m^{-3} SO_4^{2-}
	New York City	
17.2	15.9	26.5
17.1	18.4	19.9
2.42	3.14	23.8[a]
16.5	17.8	17.6
24.2	26.5	24.7
24.1	24.1	26.5
	High Point	
9.44	9.17	7.39
23.6	20.3	16.4
20.3	20.3	17.8
27.9	27.3	20.4
22.2	25.2	20.0

[a] Taken during hurricane weather; high atmospheric sea spray.

Table V. Comparison of Particulate Sulfate Measurement Techniques for Samples Taken at Elevated Altitudes

Total (^{110}Ag) μg m^{-3} SO_4^{2-}	Turbidimetric (AutoAnalyzer) μg m^{-3} SO_4^{2-}
5.48	4.64
4.11	7.11
2.84	6.75
3.48	3.70
9.30	8.13
11.8	11.3
12.6	17.8
12.7	16.7
7.84	8.22
12.1	11.9
11.4	13.8
13.2	14.4
1.36	0.98
1.39	0.81
2.25	1.55
4.41	4.70

to act as an interferent. Accordingly, 20 μg S as sulfate added to 6 in.^{2} of quartz filter was analyzed in the presence of 50 and 100 μg NO_3^-. The results presented in Table II show no interference from this source.

Another source of potential interference could arise from metal cations forming insoluble sulfides which could go undetected. However, Davis and Lindstrom (*21*) obtained complete recovery of sulfate with a similar reducing medium in the presence of Pb^{2+}, Sn^{2+}, and As^{3+}.

Sulfite might be present in ambient aerosols (*26, 27*) and, since this technique measures total sulfur, its presence should be determinable. Approximately 20 μg S from an unassayed Na_2SO_3 (Baker Analyzed Reagent, anhydrous powder, 99.3%) solution was added to 20 μg S as SO_4^{2-}. Results of the analyses, both in the absence and presence of quartz filters, are presented in Table III. As anticipated, sulfite responded equally with sulfate.

AMBIENT SAMPLES

Virtually all methods for the measurement of aerosol sulfate in atmospheric particulates depend upon prior dissolution of soluble sulfate from the collection media. Inasmuch as the present procedure yields total sulfur by the direct digestion of the particulates collected on the filter, it is of interest to discern if differences exist between the soluble and total sulfur. Atmospheric particulates were collected at BNL for 165 min with a 8 × 10 in. high-volume sampler on a quartz fiber filter. Quadruplicate 2 × 3 in. strips were cut from the center of the filter and reduced directly to obtain total sulfur. Similar quadruplicate sections were heated with 15.0 mL of water to extract SO_4^{2-} and then 5.0-mL aliquots from each were placed into 50-mL flasks. After addition of several mg of K_2CO_3 to neutralize any acid, the extracts were evaporated to dryness and analyzed by the present technique. Total sulfur averaged 93.9 μg S ± 7.3% rel std dev as compared to 88.0 μg S ± 7.3% rel std dev for soluble sulfur. Based upon the Student "t" test, the difference between total and water soluble SO_4^{2-} is not significant in this instance. A substantial portion of the analytical scatter unfortunately is attributable to the variation of particulate loading (±5%) across the face of the filter (*28*).

Further comparison was explored with selected ambient particulate samples obtained at urban (New York City) and rural (High Point, N.J.) locations. One-quarter sections of 4-in. diameter quartz filters were available from the New York City series. A 1-in. diameter circle was punched out from each filter for total reduction; the balance of the filter was extracted with 15.0 mL water; a portion of the solution was analyzed for sulfur by a turbidimetric method (*29*). A 5.0-mL aliquot was evaporated for soluble sulfur. The High Point samples were taken on 8 × 10 in. glass filters. Total sulfur was again obtained from 1-in. diameter circles and 3-in.^{2} sections extracted with 20.0 mL water. Again a portion was analyzed for SO_4^{2-} by a turbidimetric method and 5.0-mL aliquots were analyzed for soluble sulfur. Results are given in Table IV.

Comparison of the two ^{110}Ag methods, one measuring total S, the other soluble S, by the Student "t" test, indicated no significant difference at the 95% confidence level. Turbidimetric measurements occasionally yielded results which appear to be obviously in error. Sometimes the differences were explainable, e.g., the New York City sample taken during hurricane weather could have unusual interferences introduced by the high sea spray content. However, comparison of the turbidimetric sulfate values with either of the two ^{110}Ag results by the Student "t" test (omitting the sea spray sample) showed no significant difference.

The Milwaukee urban plume was sampled with an airplane as it traversed downwind of the city across Lake Michigan. These samples were taken on 4-in. diameter filters. Results of analyses of total sulfur by ^{110}Ag and turbidimetric soluble sulfur for some typical samples are presented in Table V. Comparison of the two methods by the Student "t" test did not permit a conclusive statement of correspondence at the 95% level.

Plume samples of the Long Island Lighting Co. power plant at Northport, N.Y., were taken on 5-in. diameter filters and analyzed by both procedures. Comparison of both sets of data in Table VI by the "t" test indicates a significant difference

Table VI. Comparison of Particulate Sulfate Measurement Techniques for Samples from Northport Power Plant Plume

Distance	Total (^{110}Ag) μg m^{-3} SO$_4^{2-}$	Turbidimetric (AutoAnalyzer) μg m^{-3} SO$_4^{2-}$
	Series 1	
Bkgd	1.85	3.80
0.5	5.22	5.33
1	2.13	1.96
3	2.84	3.33
18	0.70	1.61
	Series 2	
Bkgd	7.06	7.05
0.5	22.8	23.0
1	9.78	16.5
3	11.5	14.1
10	9.20	10.2
	Series 3	
Bkgd	3.81	5.97
0.5	25.5	28.0
1	19.5	25.4
3	34.8	37.8
10	24.1	27.7
	Series 4	
Bkgd	8.38	9.08
0.25	69.8	85.8
3	16.3	18.4
10	10.1	11.5

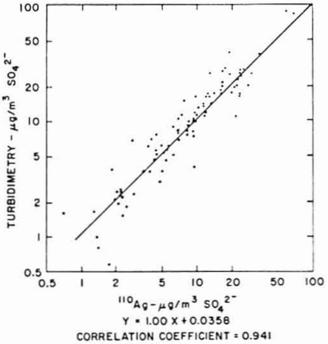

Figure 3. Composite plot comparing soluble sulfur by turbidimetry and total sulfur by silver-110

at the 95% confidence level, with turbidimetry showing an apparent bias toward higher concentrations.

A series of 2-h samples taken atop the 410-ft Brookhaven meteorological tower with 4-in. diameter filters were subjected to both methods of analysis, as presented in Table VII. A significant difference at the 95% level is again indicated, with turbidimetric results once more being biased toward greater values.

In Figure 3, turbidimetric soluble sulfur was plotted against total sulfur by ^{110}Ag for 91 samples, including some not listed in the tables, but omitting the sea spray sample. A best fit least-squares regression line was drawn, using logarithmic coordinates to give equal weight to all points. A slope of 1.00 was obtained, with a correlation coefficient of 0.941.

Table VII. Comparison of Particulate Sulfate Measurement Techniques for Samples Taken on Brookhaven Tower

Total (^{110}Ag) μg m^{-3} SO$_4^{2-}$	Turbidimetric (AutoAnalyzer) μg m^{-3} SO$_4^{2-}$
2.18	2.44
2.20	2.60
2.25	2.33
2.04	2.46
6.44	5.17
5.20	5.48
4.53	5.64
5.60	5.82
5.57	5.96
5.04	6.16
7.02	8.25
6.31	8.87
8.31	7.65
8.64	9.84
6.91	8.16
6.85	8.12
9.58	10.1
9.48	10.2
6.86	10.5
9.62	12.0
14.3	17.5
16.6	21.6
8.21	8.38
7.43	11.3

The lack of agreement at times between the ^{110}Ag and turbidimetric procedures by the "t" test may be attributed to the propensity of the latter to errors introduced by a variety of interferences. These results suggest that any uncritical routine use of turbidimetry for particulate sulfate analyses may be accompanied by a compromise in accuracy.

DISCUSSION

The capability of the ^{110}Ag method to accurately measure microgram quantities of atmospheric particulate sulfur has been demonstrated. The direct treatment of samples collected on glass or quartz fiber particulate filters eliminates the necessity for prior extraction. All aerosol sulfur species are completely converted to H_2S by the mixture of hydriodic, hypophosphorous, and hydrochloric acids; H_2S is efficiently absorbed by cadmium acetate. The metathesis of CdS by $AgNO_3$ is stoichiometric and quantitative and the employment of the specific activity of a $^{110}AgNO_3$ solution is all that is necessary to calculate the μg S in the sample.

If the threshold for sulfate detection is taken as a signal equal to the blank value, it will correspond to a detection limit of 1.1 ± 0.3 and 1.7 ± 0.6 μg S for 6 in.^{2} and 10 in.^{2} of filter, respectively. The BNL airborne 5-in. diameter filter pack can sample 10 m^3 air in 20 min (*30*). Analyzing half the filter (10 in.^{2}), we can detect 1 μg m^3 SO$_4^{2-}$ with this time resolution. Analytical precision for pure sulfate solution at this level is ~±10%. However, a value for actual filter samples would be ~±40% at this level because of the variability in filter blanks. At 3 μg m^{-3} SO$_4^{2-}$ and 20-min time resolution, the precision would improve to ±10%. Additional accuracy may be achieved by longer sampling times or increased flow rates. Further optimization can only be obtained by finding a method to reduce the filter blank variability.

Utilizing the ^{110}Ag method, the data obtained to date indicate no major differences between total and soluble sulfur. However, when comparing ^{110}Ag to turbidimetry, discrepancies do arise, which we attribute to errors in the latter measurements. Although somewhat slower than automated methods, we feel the ^{110}Ag technique is less subject to error and should find a roll in routine use and in addition could be used as a referee method for the determination of total aerosol sulfur.

ACKNOWLEDGMENT

We thank Mary Kinsley of Brookhaven for her assistance and informative conversations. We also acknowledge A. J. Alkezweeney and J. Hales of Battelle Pacific Northwest Laboratories for operating our sampler during their Milwaukee plume experiments, and P. O. Lioy of the Interstate Sanitation Commission for supplying the High Point, N.J., samples. We are further grateful to Roger Tanner and Mary Phillips of BNL for the turbidimetric sulfate analyses.

LITERATURE CITED

(1) "Health Consequences of Sulfur Oxides: A Report from CHESS 1970-1971", U.S. Environmental Protection Agency, Publication No. EPA-650/1-74-001, Research Triangle Park, N.C. (May 1974).
(2) M. O. Amdur, T. R. Lewis, M. P. Fitzhand, and K. I. Campbell, U.S. Environmental Protection Agency Publication No. AP-111, Research Triangle Park, N.C. (July 1972).
(3) R. L. Tanner and L. Newman, *J. Air Pollut. Control Assoc.*, **26**, 737 (1976).
(4) J. Forrest and L. Newman, *J. Air Pollut. Control Assoc.*, **23**, 761 (1973).
(5) T. G. Dzubay and R. K. Stevens, *Environ. Sci. Technol.*, **7**, 663 (1975).
(6) "Comparison of Wet Chemical and Instrumental Methods for Measuring Airborne Sulfate", U.S. Environmental Protection Agency, Publication No. EPA-600/2-76-059, Research Triangle Park, N.C. (March 1976), p 57.
(7) A. P. Altshuller, *J. Air Pollut. Control Assoc.*, **26**, 318 (1976).
(8) L. Newman, J. Forrest, and B. Manowitz, *Atmos. Environ.*, **9**, 959, 969 (1975).
(9) W. E. Wilson, R. J. Charlson, R. B. Husar, K. T. Whitby, and D. Blumenthal, 69th Ann. Meeting of the Air Pollution Control Assoc., Portland, Ore. (June 1976).
(10) Division of Biomedical and Environmental Research, U.S. Energy Research and Development Administration, Washington, D.C. (1975).
(11) H. Small, T. S. Stevens, and W. C. Bauman, *Anal. Chem.*, **47**, 1801 (1975).
(12) J. Mulik, R. Puckett, D. Williams, and E. Sawicki, *Anal. Lett.*, **9**, 653 (1976).
(13) D. A. Lundgren and T. C. Gunderson, *J. Am. Ind. Hyg. Assoc.*, **36**, 866, (1975).
(14) I. St. Lorant, *Z. Physiol. Chem.*, **185**, 252 (1929).
(15) C. L. Luke, *Ind. Eng. Chem., Anal. Ed.*, **15**, 602 (1943).
(16) C. L. Luke, *Ind. Eng. Chem., Anal. Ed.*, **17**, 298 (1945).
(17) C. L. Luke, *Anal. Chem.*, **21**, 1369 (1949).
(18) L. P. Pepkowitz and E. L. Shirley, *Anal. Chem.*, **23**, 1709 (1951).
(19) C. M. Johnson and H. Nishita, *Anal. Chem.*, **24**, 736 (1952).
(20) L. Gustafsson, *Talanta*, **4**, 236 (1960).
(21) J. B. Davis and F. Lindstrom, *Anal. Chem.*, **44**, 524 (1972).
(22) H. G. Thode, J. Monster, and H. B. Dunford, *Geochim. Cosmochim. Acta*, **25**, 159 (1961).
(23) J. Forrest and L. Newman, *Atmos. Environ.*, **7**, 561 (1973).
(24) R. L. Tanner, R. Cederwall, R. Garber, D. Leahy, W. Marlow, R. Meyers, M. Phillips, and L. Newman, *Atmos. Environ.*, in press.
(25) H. D. Axelrod, J. H. Cary, J. E. Bonelli, and J. P. Lodge, Jr., *Anal. Chem.*, **41**, 1856 (1969).
(26) N. L. Craig, A. B. Harker, and T. Novakov, *Atmos. Environ.*, **8**, 15 (1974).
(27) L. D. Hansen, L. Whiting, D. E. Eatough, T. E. Jensen, and R. M. Izatt, *Anal. Chem.*, **48**, 634 (1976).
(28) R. B. King, J. S. Fordyce, A. C. Antoine, H. F. Leibecki, H. E. Neustadter, and S. M. Sidik, *NASA Tech. Note*, **TN D-8110** (1976).
(29) "Sulfate Method VIb Via Turbidimetry", Technicon Corp., Tarrytown, N.Y. (1959).
(30) D. Leahy and R. Garber, Brookhaven National Laboratory, Upton, N.Y., personal communication, 1977.

RECEIVED for review April 14, 1977. Accepted June 27, 1977.

Determination of Acid POH Groups of Hydrolysis-Susceptible Esters of Phosphorous Acid

Robert Siegfried

Federal Research Centre for Nutrition, D-75 Karlsruhe, West Germany

Quantitative determination of acid POH groups of hydrolysis-susceptible compounds of phosphorous acid, based on the conductivity in water-free medium is described. Water-free methanol (*1*) serves as solvent. It is very similar to water and particularly well suited because of its good dissolving property, low conducting power, and ionizing power. Phosphorous acid is applied as indicator. The limit of detection for POH groups is 0.01 mmol.

As was demonstrated by more than 200 publications during the years of 1974 and 1975 (*2*), titration in nonaqueous solutions is a method widely used to solve, in an elegant way, individual problems such as the determination of acid groups in samples sensitive to hydrolysis, for instance. Our problem was to determine the acid groups during the polycondensation of ethyl-(β-hydroxethyl)phosphite (I).

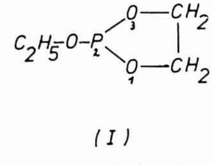

(I)

Acid POH-groups are present only as free phosphorous acid or as end groups ROPH($\rightarrow$O)OH, since the two-proton phosphorous acid cannot contain any more acid POH groups within a diester chain. Titration using lyes in aqueous solutions, however, leads more or less rapidly to the formation of another acid POH group and is therefore not applicable. In a titration using alcoholates (for instance, sodium methylate) in a water-free medium (for instance, methanol), the following reactions are supposed to take place in the presence of free phosphorous acid and its monoesters (diesters do not react).

$$H_3PO_3 + NaOR = NaH_2PO_3 + HOR \tag{1}$$

$$NaH_2PO_3 + NaOR = Na_2HPO_3 + HOR \tag{2}$$

$$[R_1OPH(\rightarrow O)O]^- + H^+ + R_2ONa = [R_1OPH(\rightarrow O)O]^- + Na^+ + R_2OH \tag{3}$$

The reactions can be followed by means of a conductometer. If the conductivity (Ω^{-1}) is plotted vs. the quantity (mL) of alcoholate added, a bend can be expected at the point where acid H^+ is completely exchanged by Na^+. Partly hydrolyzed dialkyl phosphite, however, results in a continuous increase of the conductivity, and it can therefore be assumed that in methanol all participating electrolytes of Equation 3 have about the same ionic mobility. Determination is possible, however, by means of an indicator (in our case: phosphorous acid), as will be shown below under the paragraph Results and Discussion.

EXPERIMENTAL

Apparatus. The conductivity was measured at 3 KHz using a conductometer by F. Bauer, Frankfurt/Main, FRG. A glass

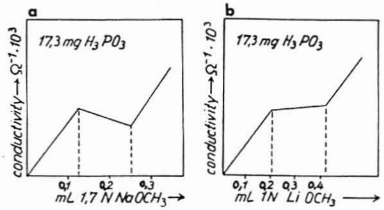

Figure 1. (a) Conductometric titration curve of H_3PO_3 in water-free methanol. Titration with sodium methylate. (b) Conductometric titration curve of H_3PO_3 in water-free methanol. Titrated with lithium-methylate

cell with 2 platinum electrodes of about 0.5 cm^2 each at a distance of about 0.7 cm from each other served as measuring cell. The microtitration apparatus Metrohm that we used consisted of: (a) a stand, (b) a microburet (accuracy 0.001 mL), (c) a receptacle of 5 mL with heat regulator and cover (the latter with 5 openings for thermometer, measuring cell, nitrogen inlet, nitrogen outlet, and one opening to fill in samples, and (d) a stirring motor.

Reagents. Methanol of the highest quality (Merck) was dried over molecular sieves and distilled. Its water content after this procedure was less than 10^{-5}% (Karl Fischer titration). The alcoholates were made out of this methanol and oxide-free metals. The titration solutions were: $NaOCH_3$ 1.7 N, $LiOCH_3$ 1.0 N. Diethyl phosphite (Fluka) of the highest quality was distilled twice over Vigreux columns under nitrogen. Phosphorous acid (Fluka) of the highest quality was found to have a purity degree higher than 99% after aqueous neutralization titration.

Procedures. The samples (oligomeric compounds of the phosphorous acid esters) 0.5–1.2 g were weighed into the titration receptacle under nitrogen and 5 mL of methanol were added. The receptacle temperature was kept constant at 25 ± 0.1 °C. The platinum measuring cell, the thermometer, and the nitrogen supply lead were connected. By using the nitrogen stream, an access of atmospheric moisture to the apparatus was avoided. Then 17.3 mg of phosphorous acid were added (1-mL solution: made of 1.730 g phosphorous acid filled up with methanol to 100 mL). The content was vigorously stirred using a Teflon-coated stirring rod. For the titration, the above alcoholates were used.

RESULTS AND DISCUSSION

Whether or not a titration of the acid protons of phosphorous acid in water-free medium is generally feasible, was tested by titration of water-free H_3PO_3 in methanol. This titration yielded a curve with 2 bends, shown in Figures 1a and 1b.

The consumption of methylate until the first bend corresponds precisely to the molar quantity of H_3PO_3 applied (neutralization of the first acid POH group). The methylate consumption recorded from the first to the second bend corresponds as well to the applied molar quantity (neutralization of the second acid POH group). The different gradients of the curve sections facilitate the determination of intersection points. When lithium methylate is used as titrating solution, Li_2HPO_3 precipitates after the neutralization of the first acid POH group and after further addition of lithium methylate. Frequently, however, a supersaturation occurs in the solution, and in these cases the bend is not sharp or delayed particularly when the phosphorous acid concentration is very low. Sodium methylate is preferable in this case.

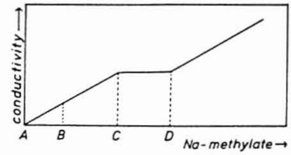

Figure 2. Conductometric titration curve of a monoalkyl phosphite in water-free methanol with $NaOCH_3$ after addition of H_3PO_3

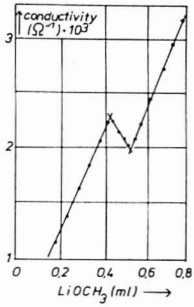

Figure 3. Conductometric titration curve of a distillate residue of 2-ethoxy-1,2,3-dioxaphospholane. Indicator H_3PO_3. Titer solution $LiOCH_3$

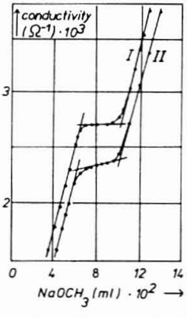

Figure 4. Conductometric titration curve of a distillate of 2-ethoxy-1,2,3-dioxaphospholane. Curve I = 0.5361 g weighed portion, curve II = 0.5011 g weighed portion. Indicator H_3PO_3. Titer solution $NaOCH_3$

It is possible therefore to obtain, by addition of H_3PO_3 to a monoalkyl phosphite, a titration curve with two bends, which can be interpreted in the following way. The distance A–C (until the first bend) corresponds to the sum of the acid POH groups of the monoalkyl phosphite and the first neutralization phase of the added phosphorous acid. The distance C–D corresponds to the second neutralization phase of the added phosphorous acid. When C–D is subtracted from A–C, one obtains A–B which indicates the share of POH groups (monoalkyl phosphite) in the partly hydrolyzed dialkyl phosphite.

The accuracy of the method is demonstrated by the following examples. Five determinations using 17.3 mg of H_3PO_3 were made. The deviations were 0.1 mg H_3PO_3 at the maximum per determination, i.e., less than 1%. Also, multiple determinations of the products obtained by means of polycondensation resulted in deviations of less than 1% in samples of about 500 mg. A sample of monomethyl phosphite (for which we thank Pflüger) was found to be 99.5% pure. This finding could be verified by gas-chromatography. 2-Ethoxy-1,3,2-dioxyphospholane (I) was prepared according to Lucas (*3*). This compound hydrolyzes rapidly and quantitatively with H_2O. Increasing (up to molar) quantities of H_2O were added, and the POH groups formed were determined. The POH groups formed out of the added water corresponded to the quantity calculated theoretically. The accuracy was better than 1% also in this case. If an excess amount of H_2O

is added to hydrolysis-susceptible esters, complete hydrolysis takes place. In this case no water-free titration is necessary since all POH-groups in aqueous solution can be titrated with lye. The described method is also suitable to determine hydrolysis-susceptible samples with a high degree of accuracy. Figures 3 and 4 show conductometric titration curves.

The method allows one to examine, besides phosphorous acid and its monoesters, other acids and esters also for the presence of POH groups.

LITERATURE CITED

(1) J. Jander-Ch. Lafrenz, "Wasserähnliche Lösungsmittel", Verlag Chemie GmbH, Weinheim/Bergstr., 1968.
(2) B. Kratochvil, *Anal. Chem.*, **48**, 355R (1976).
(3) H. J. Lucas, F. W. Mitchell, Jr., and C. N. Scully, *J. Am. Chem. Soc.*, **72**, 5491 (1950).

RECEIVED for review January 10, 1977. Accepted June 6, 1977. Part of the author's thesis submitted for his diploma, D.-65 Mainz, West Germany, 1970.

Reaction-Rate Method for the Determination of Hydrocortisone

R. M. Oteiza, D. L. Krottinger, M. S. McCracken, and H. V. Malmstadt*

School of Chemical Sciences, University of Illinois at Urbana-Champaign, Urbana, Illinois 61801

A reaction-rate method for the determination of hydrocortisone is described. The method is based upon a modification of the widely accepted blue tetrazolium reaction. An analysis time of only 30 s is required. Relative standard deviations of about 1% or less are obtained, and the analytical working curves are linear. Analysis of pharmaceutical skin preparations by the new rate method gave results which correlate well with the time-consuming standard equilibrium method.

The quantitative determination of corticosteroids by various spectrophotometric methods has been previously discussed (*1*). One of these is based on the reduction of blue tetrazolium in an alcoholic solution of a strong base by the α-ketol group on the C_{17} side chain of the corticosteroid to form a chromagen which has an absorbance maximum at 525 nm. This absorbance, measured 90 min after mixing the sample with blue tetrazolium and the base, is then compared to that of a standard and blank solution to obtain quantitative information concerning the steroid concentration in the sample (*2, 3*). This is the basis for the official method of the National Formulary (*4*) and the United States Pharmacopeia (*5*).

Graham et al. have studied the blue tetrazolium procedure and have noted a first-order dependence of the corticosteroid concentration on the rate of the reaction (*6*). By employing the time-saving advantage of reaction-rate methods (*7*), we have developed a new procedure which decreases the analysis time considerably. Results obtained by the reaction-rate procedure are compared with the official method of the USP for pharmaceutical skin preparations.

EXPERIMENTAL

Apparatus. The apparatus used for the reaction-rate method was the automated system described by Malmstadt et al. (*8*). This system provides for automatic aliquoting and mixing of sample and reagent and delivery of the mixed solution into the measurement cuvet (2-cm pathlength, 60-μL volume) by means of a stopped-flow unit incorporated in a modular spectrophotometer. A ratio-recording spectrophotometer (Model 721, GCA/McPherson, Acton, Mass. 01720) was used for the equilibrium measurements.

Reagents. A single 10 mg/dL hydrocortisone stock solution was prepared weekly by dissolving 10 mg of hydrocortisone (Sigma Chemical Co., St. Louis, Mo. 63178) in 100 mL of 95% ethanol. A 0.5% blue tetrazolium (Sigma Chemical Company) solution was prepared by dissolving 0.5 g of blue tetrazolium in 100 mL of absolute methanol. A 5% solution of tetramethylammonium hydroxide was prepared by dissolving 5 g of tetramethylammonium hydroxide pentahydrate (Sigma Chemical Company) in 50 mL of USP, reagent quality, absolute ethanol (U.S. Industrial Chemicals Company, Tuscola, Ill. 61953). Different base concentrations were prepared from the 5% solution by appropriate dilution with absolute ethanol. The standard hydrocortisone solutions were prepared daily by adding 2 mL of the blue tetrazolium solution to an appropriate volume of the stock hydrocortisone solution and diluting to 10 mL with 95% ethanol.

Table I. Reaction-Rate Result for Different Measurement Times^a

Measurement time, s	Rate, ΔmA/s^b	RSD, %
1.0	26.5	3.7
5.0	25.6	1.0
10.0	25.2	0.8
15.0	24.8	0.4
30.0	23.7	0.5
45.0	23.8	1.0

^{a} Analysis of 2.5 mg/dL standard with 15-s delay time.
^{b} Average of 5 determinations on a single sample.

Sample Preparation. Samples were prepared from the pharmaceutical preparations—creams, gels, and ointments—by the column chromatographic procedure of Graham et al. (*9*) in which the corticosteroid is trapped in the column while interferences are removed by *n*-heptane. The corticosteroid is then removed from the column with chloroform. The eluate obtained from the column is carefully evaporated to dryness. The residue from the chloroform eluate is then dissolved in 95% ethanol and diluted to 25 mL. A 5-mL aliquot is then added to 2 mL of the blue tetrazolium solution and diluted to 10 mL with 95% ethanol. This 10-mL solution will be referred to in subsequent discussions as the sample. Approximately 30 minutes are routinely required for the sample preparation which provides an interference-free sample for analysis.

Equilibrium Procedure. The equilibrium procedure was the official procedure given in the USP XIX (*5*) with the absorbance measured 90 min after mixing the standard with the two reagents.

Reaction-Rate Procedure. One hundred μL each of a tetramethylammonium hydroxide solution and the appropriate standard or sample are sampled by the automatic syringes of the stopped-flow module (*8*). The syringes in the module then drive the solutions through the mixer and transfer the mixed solution to the observation cell. The change in absorbance is automatically monitored at 525 nm during the measurement time and used to construct a rate curve, working curve, or provide quantitative concentration information for the pharmaceutical skin preparations.

For the results presented, the solutions and spectrophotometer were at ambient temperature in a temperature-controlled lab-

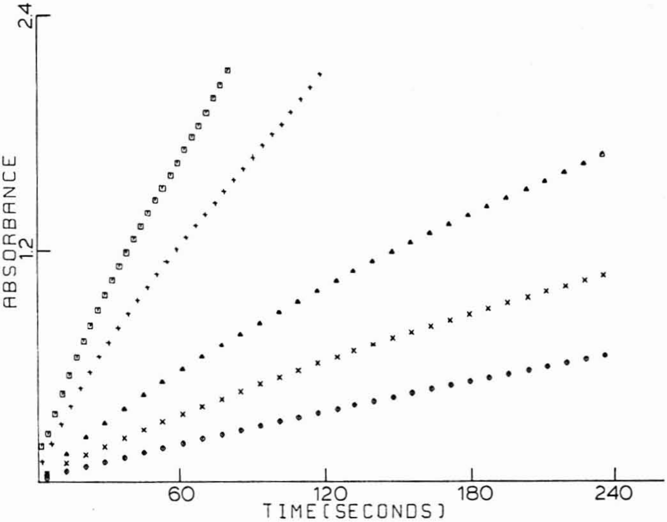

Figure 1. Effect of tetramethylammonium hydroxide concentration [(□) 5%, (+) 3%, (Δ) 1%, (X) 0.5%, (◊) 0.25%] on the rate of reaction for hydrocortisone concentration of 3 mg/dL

Table II. Results Used for Hydrocortisone Reaction-Rate Working Curve[a]

Hydrocortisone concn, mg/dL	Rate, ΔmA/s[b]	RSD, %
1.06	9.5	1.2
1.59	13.8	0.4
2.12	18.3	0.4
2.65	23.1	0.5
3.18	27.7	0.4

[a] Working curve: Slope = 8.62, intercept = 0.2, r = 0.9998. [b] Average of 5 determinations on a single sample.

oratory maintained at a nominal temperature of 25 °C.

RESULTS AND DISCUSSION

As shown in Figure 1, the rate of the reaction is dependent on the base strength. The appropriate base strength can be chosen to provide the degree of sensitivity needed at a minimum cost per analysis. For our system, good sensitivity and precision could be obtained in a short measurement time with the 5% base.

The reaction-rate curves for the five standards with 5% base over a period of 90 s are shown in Figure 2. A delay of 15 s after mixing was employed before the measurement period began. This allows for any nonreproducible behavior near the beginning of the reaction to terminate as shown in the insert of Figure 2. The optimum measurement time was determined by using the 15-s delay and varying the measurement of rate data over various periods from 1 to 45 s. The results are shown in Table I. It can be seen that the best reproducibility, about 0.4%, is obtained with a 15-s measurement time. Thus, a 15-s delay and a 15-s measurement time are used for the determinations.

The results obtained for the working curve are shown in Table II and give a correlation coefficient of 0.9998 and a relative standard deviation of 0.4 to 1.2%. The working curve can be generated in about 8 min for triplicate analyses on each standard. This is more than a factor of 10 less than the time required to prepare a working curve for the equilibrium method where a single determination on a standard, sample, and blank are generally performed (5). Thus, the total analysis time including sample preparation can be reduced from over 2 h using the equilibrium procedure to slightly over 30 min

Table III. Hydrocortisone Assay Results of Commercial Skin Preparations

Preparation	Concentration, %	Product type	Assay, % of Declared		Difference[c]
			Reaction rate[a]	Equilibrium[b]	
1	0.5	cream	70.0	71.0	−1.0
2	0.5	cream	58.8	59.3	−0.5
3	1.0	gel	95.6	94.9	+0.7
4	1.0	gel	94.4	95.4	−1.0
5	1.0	cream	93.6	95.3	−1.7
6	1.0	cream	94.3	93.0	+1.3
7	1.0	cream	95.5	95.1	+0.4
8	1.0	cream	95.5	93.8	+1.7
9	1.0	ointment	91.6	91.5	+0.1
10	1.0	ointment	95.5	94.9	+0.6

[a] Average of 3 determinations on a single sample. [b] Average of 2 determinations on a single sample. [c] % of reaction-rate − % by equilibrium.

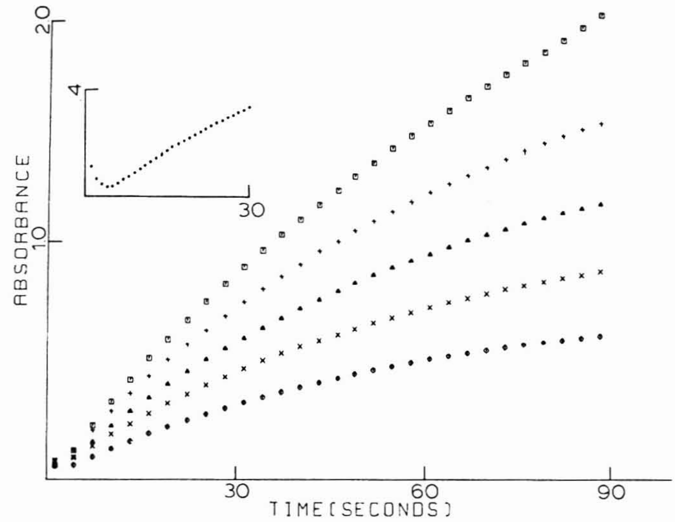

Figure 2. Reaction-rate curves for hydrocortisone concentrations of 3.18 (□), 2.65 (+), 2.12 (Δ), 1.59 (X), and 1.06 (◊) mg/dL using 5% tetramethylammonium hydroxide

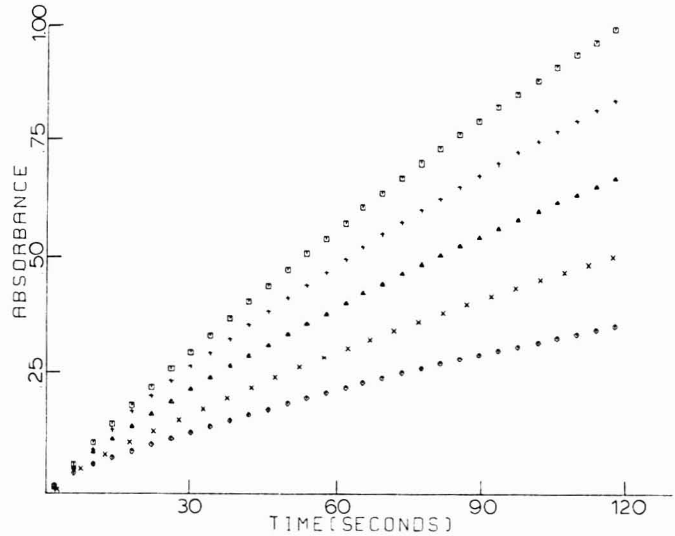

Figure 3. Reaction-rate curves for hydrocortisone concentrations of 3.18 (□), 2.65 (+), 2.12 (Δ), 1.59 (X), and 1.06 (◊) mg/dL using 1% tetramethylammonium hydroxide

with the reaction-rate procedure. Table III shows the results obtained on a series of commercial creams, gels, and ointments by the new reaction-rate method and the official method for steroid analysis. Good agreement exists between the two methods.

Successive serial dilutions on one of the commercial creams were analyzed by both the reaction-rate and the equilibrium methods. A direct comparison between the two methods yielded a correlation coefficient of 0.9995 and a slope of 1.053.

The stopped-flow module used in this study allowed observation of the absorbance of the reaction mixture in less than 1 s after mixing. For many laboratories this speed of mixing and transfer of the solution to the measurement cuvette is not possible, but by varying the base concentration this short time is not necessary. Shown in Figure 3 are the reaction-rate curves for the five standards over 2 min with the 1% base.

Table IV. Reaction-Rate Working Curve[a] for 1% Base[b]

Hydrocortisone concn, mg/dL	Rate, ΔmA/s[c]	RSD, %
1.06	3.38	0.8
1.59	4.92	0.2
2.12	6.78	2.5
2.65	8.53	2.7
3.18	10.01	0.4

[a] Working curve: Slope = 3.17, intercept = -0.01, r = 0.9993. [b] Analysis using 30-s delay time and 30-s measurement time. [c] Average of 4 determinations on a single sample.

By decreasing the base strength, we were able to slow the reaction so that the reaction-rate curve is linear over a longer period of time. For the case where a manual mixing operation must be performed, it may take 30 s or longer to mix the two solutions and place the cuvette in the spectrophotometer. We show in Table IV the results obtained for a 30-s delay time and a 30-s measurement time for the series of standards analyzed previously. Good precision and a linear working curve were still obtained, but at twice the previous analysis time. However, this is still a vast improvement over the 90-min equilibrium procedure.

It should be emphasized that these results were obtained on an automated spectrophotometric system which incorporates several features to ensure high reliability in its measurements. A beam splitter and reference detector are employed to correct for light source fluctuations which may occur during the measurement time (*10*). The stopped-flow module provides precisions better than 0.2% RSD for the aliquoting, mixing, and transfer of solutions to the 2-cm long observation cell. Finally, control of the spectrophotometer, acquisition of data, and reduction of these data to provide quantitative information are all reproducibly performed by a minicomputer and associated interface electronics. It also should be noted that the sample and standards were run in rapid succession, thus precluding the necessity of thermostating the solutions. If standard and sample information are to be obtained at significantly different times, precise temperature control of the stopped-flow module can be maintained (*8*) over long periods. These factors should be considered when comparing results obtained with other instruments.

ACKNOWLEDGMENT

The authors thank McKinley Health Center, University of Illinois, and R. D. O'Keefe, Champaign, Ill., for the pharmaceutical skin preparations used in this study.

LITERATURE CITED

(1) R. E. Graham, P. A. Williams, and C. T. Kenner, *J. Pharm. Sci.*, **59**, 1152 (1970).
(2) W. Madder and R. Buck, *Anal. Chem.*, **24**, 666 (1952).
(3) C. Chen, J. Wheeler, and H. Tewell, *J. Lab. Clin. Med.*, **42**, 463 (1956).
(4) "The National Formulary", XIV, Mack Publishing Company, Easton, Pa., 1975, p 976.
(5) "The United States Pharmacopeia", XIX, Mack Publishing Company, Easton, Pa., 1975, p 622.
(6) R. E. Graham, E. R. Biehl, C. T. Kenner, G. H. Luttrel, and D. L. Middleton, *J. Pharm. Sci.*, **64**, 226 (1975).
(7) H. V. Malmstadt, E. A. Cordos, and C. J. Delaney, *Anal. Chem.*, **44**, (12), 26A (1972).
(8) D. L. Krottinger, M. S. McCracken, and H. V. Malmstadt, *Am. Lab.*, **9** (3), 51 (1977).
(9) R. E. Graham, P. A. Williams, and C. T. Kenner, *J. Pharm. Sci.*, **59**, 1472 (1970).
(10) K. R. O'Keefe and H. V. Malmstadt, *Anal. Chem.*, **47**, 707 (1975).

RECEIVED for review May 6, 1977. Accepted June 13, 1977. Research partially supported by the NIH through Grant HEW PHS GM 21984-02.

Cyclic and Differential Pulse Voltammetric Behavior of Reactants Confined to the Electrode Surface

Alan P. Brown and Fred C. Anson*

A. A. Noyes Laboratory, California Institute of Technology, Pasadena, California 91125

Experimental and theoretical cyclic and differential pulse voltammograms are compared for reactants irreversibly attached to the surface of graphite electrodes. Quantitative agreement between experiment and theory can be obtained only if account is taken of possible nonideal behavior in applying the Nernst equation to the attached reactants. The intentional addition of external uncompensated resistance when recording differential pulse voltammograms leads to significant increases in the sensitivity of this technique for monitoring small quantities of attached reactants. An approximate method is described which allows the surface concentrations of attached reactants to be estimated when the quantities present are too small to yield discernible cyclic voltammograms.

Electrochemistry with electroactive reactants attached to electrode surfaces is under active study in a number of laboratories (*1–5*). In a recent publication (*6*), we described the electrochemical behavior of several reactants that were bound to the surface of graphite electrodes by strong, spontaneous adsorption. The experimental data indicated that differential pulse voltammetry could prove to be a more sensitive technique than cyclic voltammetry for examining the electrochemical behavior of such systems. The advantages of the former technique are particularly noteworthy when the quantity of bound reactant is small.

In this paper, more detailed experimental results are presented and are compared with theoretical analyses of the expected cyclic and differential pulse voltammetric behavior of reactants irreversibly attached to electrode surfaces. To account for the observed peak heights and wave shapes (e.g., half-peak widths), it was necessary to include activity coefficients which depend on the surface concentrations in the Nernst equation as written for the surface-bound reactants.

One unique virtue of the differential pulse voltammetric technique is that enhanced sensitivity can be obtained by the intentional addition of uncompensated resistance to the cell circuit. In addition, the dependence of peak currents on the amount of uncompensated resistance added provides an approximate method for determining the surface concentration of the attached reactant.

EXPERIMENTAL

Materials. Electrodes were constructed from both pyrolytic graphite and vitreous carbon. All of the electrodes used were cylindrical rods which were sealed onto glass tubing by means of heat-shrinkable polyolefin tubing (Alpha Wire Co., style FIT 300). With pyrolytic graphite (Union Carbide Corporation, Parma, Ohio), the electrodes were mounted so as to expose either the basal-plane surface or the plane edges to the solution. The vitreous carbon electrodes (Grade GC-A, Tokai, Ltd., Tokyo, Japan) and the exposed-edge pyrolytic graphite electrodes were polished with an aqueous slurry of 0.5 μ alumina before use, producing smooth, shiny surfaces. The basal-plane pyrolytic graphite electrodes were freshly cleaved with a razor blade just prior to being used. The exposed electrode areas were 0.2 cm^2 for the vitreous carbon and basal-plane pyrolytic graphite and 0.08 cm^2 for the exposed-edge pyrolytic graphite.

9,10-Phenanthrenequinone and benzo[*c*]cinnoline were recrystallized twice from benzene and 9,10-anthraquinone-2-monosulfonate was recrystallized from ethanol. 1,4-Naphthaquinone was sublimed just prior to use. Iron protoporphyrin IX chloride (Aldrich Chemical Company) was used as received. Iron tris(dibenzyldithiocarbamate) was prepared according to reference (*7*). Its electrochemical behavior matched that described in reference (*8*). Supporting electrolyte salts and buffers were reagent grade materials used without further purification.

Apparatus. A conventional two-compartment electrochemical cell was employed. In perchlorate electrolytes, potentials were measured vs. a sodium chloride-saturated calomel electrode which has a potential 5 mV more negative than the conventional SCE.

Cyclic and differential pulse voltammograms were recorded with a Model 174 Polarographic Analyzer (Princeton Applied Research, Princeton, N.J.). For some experiments, a modified version of this instrument was used in which the pulse width, sampling time, and memory time constant could be varied (*9*).

Methodology. In early experiments it was observed that the differential pulse voltammetric peak currents obtained with moderate to high concentrations of attached reactants exhibited strong and unexpected dependences on the rate at which the dc potential of the electrode was scanned. This was traced to the relatively large memory time constant employed in the standard PAR 174 instrument (*10, 11*). To obtain differential pulse voltammetric responses that accurately reflected the true *instantaneous* currents for which the equations in this paper were derived, it proved necessary either to restrict the rate of the dc potential scan to values no greater than 1 mV s^{-1} or to utilize a modified version of the PAR 174 (*9*) in which shorter memory time constants could be selected. Acceptable values of scan rate or memory time constant were established by determining the point at which no significant changes in the peak current resulted from further decreases in scan rate or memory time constant.

The other experimental settings employed during the recording of differential pulse polarograms were: Pulse amplitude: 5 mV; "Drop time": 0.5 s (i.e. pulse repetition rate: 2 s^{-1}). The effective time at which the current is measured in the unmodified PAR 174 is 48.5 ms.

Most experiments were conducted in solutions containing 0.5–1.0 μM concentration of the adsorbate. At these concentrations about 30 min were required for the adsorption to reach a stable value. If the equilibrated electrodes were washed and transferred to solutions free of adsorbate, their initial behavior was identical to that observed in the solution of low adsorbate concentration. However, with no adsorbate in solution, slow desorption gradually lowered the surface concentration. To avoid this desorptive loss, the very dilute solutions of the adsorbates were usually employed.

Numerical calculations were carried out with a PDP 11/40 computer.

RESULTS AND DISCUSSION

Cyclic Voltammetry. The solid curve in Figure 1 is a cyclic voltammogram recorded for 9,10-phenanthrenequinone irreversibly adsorbed on a basal-plane pyrolytic graphite electrode. The area under the curve corresponds to about 1.9 × 10^{-10} mol cm^{-2} of the quinone (Q) on the electrode surface. If the electrode reaction, Equation 1,

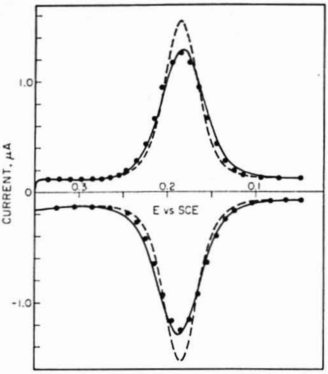

Figure 1. Experimental and theoretical cyclic voltammograms for 1.9 × 10^{-10} mol cm^{-2} of 9,10-phenanthrenequinone irreversibly adsorbed on a basal-plane pyrolytic graphite electrode. Potential scan rate: 50 mV s^{-1}. Supporting electrolyte 1 M HClO$_4$. (—) experimental voltammogram. (----) theoretical voltammogram calculated from Equation 2. (●) points calculated from Equations 7 and 8 with a nonideality parameter, *r*, of −2.7 × 10^9 mol^{-1} cm^2

$$Q + 2e^- + 2H^+ \rightleftharpoons H_2Q \tag{1}$$

is assumed to obey the Nernst equation (written in terms of the concentrations of Q and H$_2$Q on the electrode surface), the expected current–potential behavior in cyclic-voltammetric experiments is given by Equation 2 (*12, 13*)

$$i = -\frac{n^2F^2\Gamma_T\nu}{RT}\,\frac{\xi}{(1+\xi)^2} \tag{2}$$

where Γ_T is the total amount of Q initially present on the electrode surface, ν is the potential scan rate, $\xi = \exp[(nF/RT)(E - E°)]$, and the other symbols have their customary significance. It follows that the cathodic and anodic current peaks will both appear at $E°$, the standard potential for the Q/H$_2$Q couple, and will have equal magnitudes given by Equation 3.

$$i_p = \frac{n^2F^2\Gamma_T\nu}{4RT} \tag{3}$$

The dashed curve in Figure 1 is the cyclic voltammogram calculated on the basis of Equation 2 using the value of Γ_T obtained from the area under the experimental voltammogram (corrected for the background current). The calculated and experimental voltammograms are quite similar in shape but the use of Equation 2 does not produce a good quantitative match. Although the smaller experimental peak currents could be the result of slow electron transfer kinetics, the lack of any significant separation of the anodic and cathodic peak potentials and the lack of asymmetry in the wave shapes [both of which are also predicted consequences of slow charge transfer kinetics (*14*)] do not support such an interpretation.

Another possible explanation for the differences between the calculated and observed curves in Figure 1 is that the surface activities of the attached reactants differ from their surface concentrations. To account for such nonideal behavior, surface activities must be used in place of surface concen-

Table I. Nonideality Parameters and Peak Potentials for 9,10-Anthraquinone-2-monosulfonate Attached to Various Carbon Electrodes[a]

Electrode[b]	Total attached reactant, mol cm^{-2}[c]	$10^{-9}r$, mol^{-1} cm^{2}[d]	Peak potential,[e] mV vs. Na SCE
BPG	1.4×10^{-10}	−5.86	−208
EPG	1.3×10^{-10}	−4.44	−209
VC	1.1×10^{-10}	−6.05	−209

[a] Supporting electrolyte was 1 M $NaClO_4$–0.01 M $HClO_4$. [b] BPG = basal-plane pyrolytic graphite. EPG = polished exposed-edge pyrolytic graphite. VC = polished vitreous carbon. [c] Determined by measuring the area under a cyclic voltammogram. [d] Evaluated by fitting the cyclic voltammograms to Equation 8. [e] Average of the cathodic and anodic peak potentials; peak separations were smaller than 10 mV.

trations in writing the Nernst equation for the attached reactant couple:

$$\xi = \frac{a_O}{a_R} = \frac{\gamma_O \Gamma_O}{\gamma_R \Gamma_R} \tag{4}$$

where a, γ, and Γ are the surface activities, activity coefficients, and concentrations, respectively; the subscripts indicate the oxidized (O) and reduced (R) forms of the adsorbate. The existence of nonideal behavior in reversibly adsorbed molecules is well recognized (*15*) and it is not surprising that it should also occur with irreversibly adsorbed species. Reversibly adsorbing organic species often exhibit activity coefficients which are exponentially dependent on their surface concentrations (*15, 16*). The activity coefficients for the two species on the electrode surface in the present case were therefore represented as in Equations 5 and 6:

$$\gamma_O = \exp -(r_{OO}\Gamma_O + r_{OR}\Gamma_R) \tag{5}$$

$$\gamma_R = \exp -(r_{RR}\Gamma_R + r_{RO}\Gamma_O) \tag{6}$$

r_{OO} and r_{OR} are parameters which describe the perturbing influence experienced by a given molecule of attached oxidant due to the presence of the other attached oxidant and reductant molecules, respectively. r_{RR} and r_{RO} are the analogous parameters for a given reductant molecule. A very similar treatment of the nonidealities encountered in the reversible adsorption of molecules on electrode surfaces has been utilized by Laviron (*17*). As did she, we will neglect the possibility that the interaction parameters depend upon potential.

Substituting Equations 5 and 6 in Equation 4 and designating the fraction of the molecules on the surface in their oxidized form as f, leads to Equation 7:

$$\xi = \frac{f}{1-f} \exp -\left\{\Gamma_T\left[f(r_O + r_R) - r_R\right]\right\} \tag{7}$$

where $r_O = r_{OO} - r_{OR}$ and $r_R = r_{RR} - r_{RO}$.

The use of Equation 7 in place of the Nernst equation in deriving the expected cyclic voltammetric behavior gives Equation 8 from which the current–potential behavior can be calculated, using Equation 7 to relate the potential and the parameter f.

$$i = -\frac{n^2F^2\Gamma_T\nu f(1-f)}{RT[1 - f\Gamma_T(r_O + r_R)(1-f)]} \tag{8}$$

(As expected, Equation 8 reduces to Equation 2 if $r_O = r_R = 0$). Important predictions of Equation 8 are that the cathodic and anodic peak currents have equal magnitudes given by Equation 9.

$$i_p = \frac{n^2F^2\Gamma_T\nu}{RT[4 - \Gamma_T(r_O + r_R)]} \tag{9}$$

and the two peak potentials are given by Equation 10

$$E_{p_a} = E_{p_c} = E'_{O,R} - \frac{RT\Gamma_T(r_O - r_R)}{2nF} \tag{10}$$

where $E'_{O,R}$ is the formal potential for the attached couple.

Equation 10 predicts that the two peak potentials, while remaining equal, will shift along the potential axis as a function of the total concentration of attached reactant unless $r_O = r_R$. We observed constant peak potentials (±2 mV) for all of the reactants examined even though Γ_T was varied by more than an order of magnitude. For this reason the two nonideality parameters, r_O and r_R, were equated in fitting the experimental current–potential data to Equation 8.

The current–potential data calculated with a value of $r = r_O = r_R = -2.7 \times 10^9$ mol^{-1} cm^2 in Equation 8 are shown by the points plotted in Figure 1. The agreement with the experimental curve is very good. Comparably good fits also resulted with the other reactants examined (see Experimental section) independent of the particular type of electrode employed. For example, Table I lists the nonideality parameter evaluated from cyclic voltammograms for the strongly adsorbing 9,10-anthraquinone-2-monosulfonate molecule on three types of electrode. Note that while the value of r depends on the type of carbon used, the peak potentials are invariant. This observation adds support to the approximation made in equating r_O and r_R in Equation 8.

Table II summarizes nonideality parameters evaluated for a variety of reactants that are very strongly adsorbed on basal-plane pyrolytic graphite electrodes. In every case we have examined thus far, the current-potential behavior could be accounted for quantitatively only if a nonideality parameter was introduced, i.e., no system yielded an r value of zero. The fact that the values of r in Table II are negative indicates that the processes responsible for the nonideality act to destabilize the attached reactants.

Although the origins of nonideal behavior of reactants on surfaces have been discussed in a variety of contexts (*16–20*),

Table II. Nonideality Parameters for Several Reactants Attached to Basal-Plane Pyrolytic Graphite Electrodes

Attached reactant	Supporting electrolyte	Quantity attached,[a] mol cm^{-2} × 10^{10}	$10^{-9}r$, mol^{-1} cm^{2}[b]
1,4-Naphthaquinone	1 M $HClO_4$	5.1	−1.6
9,10-Phenanthrenequinone	1 M $HClO_4$	1.9	−2.7
9,10-Anthraquinone-2-monosulfonate	1 M $NaClO_4$–0.01 M $HClO_4$	1.4	−5.9
Iron protoporphyrin IX	0.1 M $Na_2B_4O_7$ adjusted to pH 10	1.1	−4.0
Iron tris(dibenzyldithiocarbamate)	1 M $HClO_4$	0.5	−3.4
Benzo[*c*]cinnoline	1 M HCl	1.2	−3.1

[a] Determined by measuring the area under a cyclic voltammogram. [b] Evaluated by fitting the cyclic voltammogram to Equation 8.

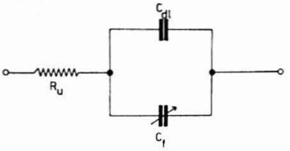

Figure 2. Simple equivalent circuit for an irreversibly attached reactant. R_u is the total uncompensated resistance in the cell and measuring circuit, C_{dl} is the double layer capacitance, and C_f is the faradaic pseudo-capacitance

none of the previous treatments seems directly applicable to the cases at hand. We wish to complete additional experiments involving kinetic measurements and temperature variations before speculating further on the physical basis for the observed nonideal behavior of the attached reactants.

Differential Pulse Voltammetry. The differential pulse voltammetric response to be expected with attached reactants can be usefully discussed in terms of the simple equivalent circuit given in Figure 2. The parallel combination of the electrode double layer capacitance, C_{dl}, and the faradaic pseudocapacitance, C_f, arising from the attached reactant is in series with the uncompensated cell resistance, R_u. The potential-dependent, faradaic pseudocapacitance can be expressed as in Equation 11:

$$C_f = nF\frac{d\Gamma_O}{dE} = nF\,\frac{d\Gamma_O}{d\xi}\cdot\frac{d\xi}{dE} \tag{11}$$

Γ_O can be calculated from Equation 7 which leads to Equation 12 when $r = r_O = r_R$:

$$\Gamma_O = \frac{\Gamma_T\xi}{\exp[r(\Gamma_T - 2\Gamma_O)] + \xi} \tag{12}$$

Differentiation of Equation 12 and substitution in Equation 11 produces the following expression for C_f:

$$C_f = \frac{n^2F^2\Gamma_T}{RT}\,\frac{f(1-f)}{1 - 2\Gamma_T rf(1-f)} \tag{13}$$

If the amplitude of the potential steps employed in recording the differential pulse voltammogram is sufficiently small to allow the change in surface concentrations of the oxidant and reductant to be ignored, the faradaic pseudocapacitance can be regarded as constant during the life-time of each pulse. Making this assumption, and neglecting the much smaller potential dependence of C_{dl}, the current flowing in the circuit of Figure 2 following each potential pulse can be shown to obey Equation 14.

$$i = \frac{\Delta E}{R_u}\exp - \left[\frac{t}{R_u(C_{dl} + C_f)}\right] \tag{14}$$

where ΔE is the magnitude of each potential pluse and t is the time since its application.

Equation 14 predicts that at any fixed t the largest currents will result when C_f is largest and according to Equations 7 and 13 C_f will reach its maximum value at the standard potential. In fact, although experiment differential pulse voltammograms for irreversibly attached reactants exhibit current peaks at the standard potential, the magnitudes of the peak currents are typically several orders of magnitude greater than those calculated from Equation 14. The source of this discrepancy was traced to the approximation that C_f remains constant for the duration of each potential pulse. Even with pulse amplitudes as small as a few millivolts, the value of C_f can undergo significant changes during the life-time of each pulse, especially when the dc potential is near the standard potential. Allowing C_f to vary during the duration of the pulse leads to Equation 15 which cannot be solved analytically.

$$\frac{\Delta E - \epsilon}{R_u} = \left[C_{dl} + C_f\right]\frac{d\epsilon}{dt} \tag{15}$$

where ϵ is the true potential difference across the parallel combination of C_{dl} and C_f with the potential dependence of the latter being implicitly expressed in Equation 13. Equation 15 was solved numerically by means of a standard fourth-order Runga-Kutta method (*21*) as part of a complete numerical evaluation of the expected differential pulse voltammetric response.

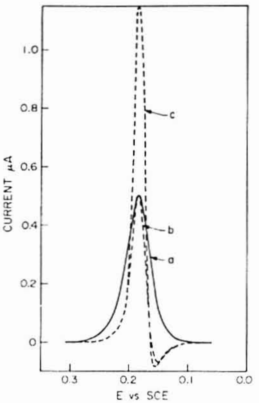

Figure 3. Experimental and theoretical differential pulse voltammograms for 1.9×10^{-10} mol cm^{-2} of 9,10-phenanthrenequinone irreversibly adsorbed on a basal-plane pyrolytic graphite electrode. Potential scan rate: 5 mV s^{-1}; memory time constant of the modified PAR 174 polarograph: 14.0 ms. (*a*) Experimental voltammogram; supporting electrolyte: 1 M $HClO_4$. (*b*) Theoretical voltammogram calculated as described in the text using a nonideality parameter, r, of -2.7×10^9 mol^{-1} cm^2. (*c*) Theoretical voltammogram calculated for $r = 0$

Figure 3 shows a comparison of such a theoretical voltammogram (curve *b*) with the experimental voltammogram (curve *a*) for attached 9,10-phenanthrenequinone. The values of r, Γ_T, and C_{dl} employed in the calculation were evaluated from a cyclic voltammogram recorded just prior to the differential pulse voltammogram. The value of R_u used to obtain the best fit shown in the figure compares favorably with independent measurements of the uncompensated resistance (50–100 Ω)

Curve *c* in Figure 3 is the differential pulse voltammogram calculated by neglecting any nonideality in writing the Nernst equation, i.e., setting $r = 0$. Comparing curves *b* and *c* in Figure 3 with their cyclic voltammetric counterparts in Figure 1 shows that the differential pulse response is much more sensitive to the nonideal behavior of the attached reactants. The fact that the half-peak widths of the experimental and simulated voltammograms in Figure 3 do not match as well as do the peak currents is probably a reflection of uncertainties in accounting for the background currents. The circuit in Figure 2 is not a good model for the background current observed in the absence of attached reactants. These currents appear to contain appreciable contributions from faradaic processes associated with the graphite electrode surface. Accurate correction for this current is not straightforward because of its uncertain origin and because its magnitude is affected by the attachment of reactants to the surface.

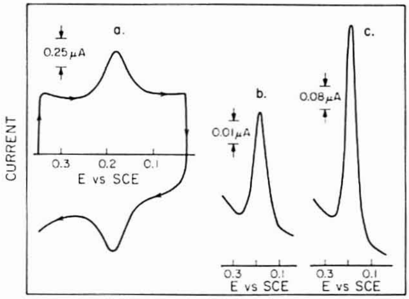

Figure 4. Experimental cyclic and differential pulse voltammograms for 1.2×10^{-11} mol cm^{-2} of 9,10-phenanthrenequinone irreversibly adsorbed on a basal-plane pyrolytic graphite electrode. Supporting electrolyte: 1 M $HClO_4$. (*a*) cyclic voltammogram recorded with potential scan rate of 50 mV s^{-1}. (*b*) Differential pulse voltammogram recorded with a potential scan rate of 2 mV s^{-1}; modified PAR 174 memory time constant: 22.3 ms; uncompensated resistance ~75 Ω. (*c*) As in *b* except that 2 kΩ of additional uncompensated resistance was placed in the measuring circuit

The most important point to note in comparing the differential pulse voltammograms in Figure 3, and the cyclic voltammograms in Figure 1, is that they both yield current peaks at the same potential, i.e., the formal potential for the attached reactant couple. This observation coupled with the ability of the numerical calculation to match the peak currents and potentials of the differential pulse voltammograms is good evidence that this technique can be used confidently to identify quantities of attached reactants too small to be found with cyclic voltammetry alone. However, it should be emphasized that discrepancies between the peak potentials obtained with the two techniques can result unless the differential pulse voltammograms are recorded at scan rates no greater than 1 mV s^{-1} with the standard PAR 174 instrument or with an instrument modified to provide a shorter memory time constant (*9*).

The small over-shoot at the foot of the calculated differential pulse voltammograms in Figure 3 arises because the numerical calculation is approaching a true derivative of the cyclic voltammogram. Indeed, under certain conditions (small pulse amplitude, scan rate, and uncompensated resistance), experimental differential pulse voltammograms having negative components on one side of the peak have been recorded by employing the modified version of the PAR 174 instrument (*9*) with a memory time constant of a few milliseconds (*22*). The fact that such behavior is not obtained under most experimental conditions results primarily from the slow effective response time of the unmodified PAR 174 instrument and the larger uncompensated resistance usually encountered.

Effect of Uncompensated Resistance. The rate of decay of the current following the application of each potential pulse decreases as R_u increases. So long as R_u is not too large (see below), the magnitude of the current sampled near the end of each pulse is correspondingly greater and the more so the larger the value of C_f. Thus, adding external resistance in series with the working electrode can lead to larger differential pulse voltammetric peak currents and enhanced sensitivity in the detection of small quantities of attached reactants. For example, Figure 4 shows a cyclic voltammogram for an electrode with only 1.2×10^{-11} mol cm^{-2} of 9,10-phenanthrenequinone on its surface. The faradaic peaks are now almost dominated by the background currents. By contrast, the differential pulse voltammogram for the same electrode (curve *b*, Figure 4) leaves no doubt about the presence of the attached reactant and when 2 kΩ of additional uncompensated resistance is added (curve *c*), the response is very large and easy to measure.

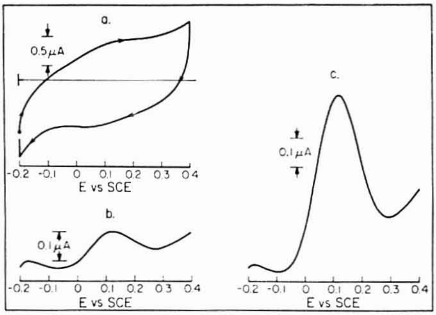

Figure 5. Cyclic and differential pulse voltammograms for an edge-on pyrolytic graphite electrode to which approximately 4.2×10^{-11} mol of a ruthenium(II) pentammine complex is covalently attached (*23*). Supporting electrolyte: 1 M CF_3COOH. (*a*) Cyclic voltammogram. Potential scan rate: 50 mV s^{-1}. (*b*) Differential pulse voltammogram. Potential scan rate: 5 mV s^{-1}; memory time constant: 114 ms; uncompensated resistance: ~100 Ω. (*c*) as in (*b*) but with 1000 Ω of additional uncompensated resistance placed in the measuring circuit

An even more persuasive example of the enhanced sensitivity obtainable by the intentional addition of extra uncompensated resistance to the cell is evident in Figure 5 which shows the behavior of a ruthenium(II) pentammine complex covalently bonded to an exposed-edge pyrolytic graphite electrode (*23*). The faradaic peaks in the cyclic voltammogram (curve *a*, Figure 5) are almost imperceptible. The differential pulse voltammetric response for the same electrode (curve *b*, Figure 5) shows a small, but clearly evident peak and when an additional 1000 Ω of uncompensated resistance is added to the circuit (curve *c*, Figure 5), the peak is enhanced significantly and provides excellent evidence for the presence of the attached reactant. The implications for the study of electrodes to which only very small quantities of reactants are attached seem clear.

Differentiating Equation 14 with respect to R_u leads to the prediction that the current at any fixed sampling time will reach a maximum at the value of R_u given in Equation 16:

$$\left[R_u\right]_m = t(C_{dl} + C_f)^{-1} \tag{16}$$

The plotted points in Figure 6 show the variation in peak current produced by increasing R_u with an electrode to which 9,10-phenanthrenequinone was attached. The predicted peak current maximum is evident. The solid curve in Figure 6 represents the peak currents of voltammograms calculated for each value of R_u by means of the same numerical procedure used to obtain voltammogram *b* in Figure 3. The good agreement between the experimental and calculated peak currents is apparent.

When R_u is selected to produce the maximum peak current, the rate of change of Γ_O (and Γ_R) is much smaller than when no uncompensated resistance is intentionally added. The approximation involved in regarding C_f as a constant throughout the duration of the potential pulse is more justified under these conditions and the evaluation of C_f can then be used to estimate Γ_T. The maximum predicted peak current, $(i_p)_m$, in plots such as Figure 6 is given by Equation 17.

$$(i_p)_m = \frac{\Delta E(C_{dl} + (C_f)_p)}{\tau e} \tag{17}$$

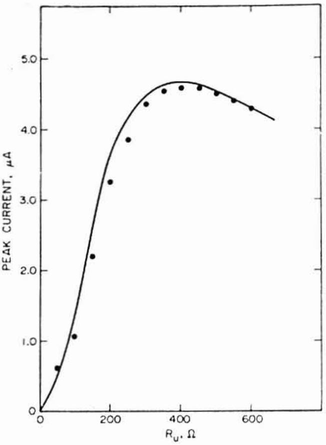

Figure 6. Differential pulse voltammetric peak current vs. the total uncompensated resistance in the measuring circuit for 1.9 × 10^{-10} mol cm^{-2} of 9,10-phenanthrenequinone irreversibly adsorbed on a basal-plane pyrolytic graphite electrode. Supporting electrolyte: 1 M $HClO_4$. Potential scan rate: 5 mV s^{-1}. (●) experimental points; modified PAR 174 memory time constant was 14 ms. (—) peak currents of differential pulse voltammograms evaluated numerically as described in the text

Where ΔE is the magnitude of the potential pulse, $(C_f)_p$ is the faradaic pseudocapacitance at the peak potential, τ is the time after the pulse application when the current is measured, and $e = 2.718$. Since $(C_f)_p$ corresponds to $f = 0.5$ in Equation 13, its magnitude is given by

$$(C_f)_p = \frac{n^2F^2\Gamma_T}{2RT(2 - r\Gamma_T)} \tag{18}$$

With systems such as 9,10-phenanthrenequinone, which yield values of $(C_f)_p$ much larger than C_{dl}, the contribution of the latter to the peak current given by Equation 17 is virtually negligible. In such instances the peak current may justifiably be measured with respect to the extrapolation of the background current flowing on either side of the peak in the voltammogram. (This current presumably results from faradaic processes associated with the oxidation and reduction of the graphite electrode surface.) Making this approximation and combining Equations 17 and 18 yields Equation 19

$$\Gamma_T = \frac{2RT(i_p)_m}{r(i_p)_m + \dfrac{n^2F^2\Delta E}{2RT\tau e}} \tag{19}$$

from which Γ_T can be calculated if r is known. The value of $(i_p)_m$ shown in Figure 6 and the r parameter obtained from the cyclic voltammogram ($r = -2.7 \times 10^9$ mol^{-1} cm^2) were substituted in Equation 19 with the other known experimental parameters to obtain a value of Γ_T of 1.9×10^{-10} mol cm^{-2}. The value obtained from integration of the area under the cyclic voltammogram obtained with the same electrode was $1.9 \pm 0.2 \times 10^{-10}$ mol cm^{-2}. Thus, Equation 19 can provide a reliable estimate of Γ_T when $(C_f)_p \gg C_{dl}$.

Figure 7 shows a differential pulse voltammogram for attached 9,10-phenanthrenequinone recorded with the value of R_u required to produce the maximum peak current. The plotted points were calculated numerically as described above. The excellent agreement shows that the shapes of differential pulse voltammograms can be understood quantitatively under conditions where background currents are negligible compared to the faradaic current resulting from the attached reactant. Even when the attached reactant is present in quantities too small to yield discernible cyclic voltammograms from which the nonideality parameter, r, would be evaluated, Equations 16, 17, and 18 may still prove useful: At sufficiently low surface concentrations, the second term in the denominator of Equation 18 will become negligible compared to the first, concentration-independent term so that a knowledge of r is not required.

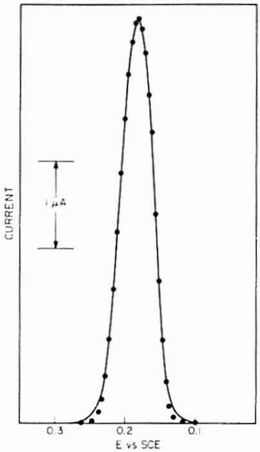

Figure 7. A comparison of experimental and theoretical differential pulse voltammograms recorded with a value of total uncompensated resistance (400 Ω) corresponding to the maximum peak current in Figure 6. (—) experimental voltammogram; (●) calculated currents. Experimental parameters as in Figure 6

In cases where the double layer and faradaic capacitances are more nearly commensurate, the peak current measured with respect to an extrapolation of the background current will not correspond to the current calculated from Equation 19 because the faradaic and background currents cannot be separated reliably in this way. A simple, approximate procedure for obtaining a rough estimate of the surface concentrations in such cases is to evaluate C_f via Equation 16 using the value of R_u corresponding to the maximum peak current in a plot such as Figure 6 and the effective value of C_{dl} estimated from the background current in a cyclic voltammogram. The value of Γ_T is then calculated from Equation 14 by assuming that the surface concentration is low enough to allow the nonideality parameter to be neglected. For example, the differential pulse voltammogram shown in Figure 4 corresponds to $1.2 \pm 0.2 \times 10^{-11}$ mol cm^{-2} of 9,10-phenanthrenequinone (determined from the area of a cyclic voltammogram). The value of C_{dl} estimated from the cyclic voltammogram was 10 μF and the maximum peak current resulted when R_u was 2.5 kΩ. These data and Equations 16 and 18 (with r set equal to zero) lead to 1.2×10^{-11} mol cm^{-2} for Γ_T. This good agreement is somewhat fortuitous and is critically dependent upon having an accurate value for the effective double layer capacitance. On freshly cleaved, basal-plane pyrolytic graphite electrodes, C_{dl} can be determined with reasonable accuracy. The same cannot be said for roughened, edge-on pyrolytic graphite, vitreous carbon, or heavily oxidized graphite electrodes, at least in our hands (*23*). However, even in these cases, the differential pulse voltammograms obtained with added uncompensated resistance produced readily detectable waves where no cyclic voltammetric responses were noted. The use of Equation 16 in estimating attached reactant concentrations for such waves, while exceedingly approximate, is not likely to produce errors greater than a factor of five to ten in the calculated values of Γ_T.

CONCLUSIONS

The primary objective of this study was to demonstrate the properties of differential pulse voltammetry as applied to reactants attached to electrode surfaces in order to allow this highly sensitive technique to be utilized in examinations of sub-monolayer quantities of attached reactants. The results have shown that it is possible to provide a semiquantitative account of the observed differential pulse and cyclic voltammetric responses by introducing concentration-dependent activity coefficients for the attached reactant molecules. Having done so, the magnitude of differential pulse peak currents can be correlated with the quantity of adsorbed reactant and the peak potentials with the standard potentials of the reactant couples. Tests of the equations and suggestions presented here are under way with a wider variety of attached reactants in order to verify more precisely the ranges of their validity.

ACKNOWLEDGMENT

Helpful suggestions and comments from Carl Koval and James Flanagan are a pleasure to acknowledge.

LITERATURE CITED

(1) R. F. Lane and A. T. Hubbard, *J. Phys. Chem.*, **77**, 1401, 1444 (1973).
(2) C. M. Elliott and R. W. Murray, *Anal. Chem.*, **48**, 1247 (1976).
(3) P. R. Moses and R. W. Murray, *J. Am. Chem. Soc.*, **98**, 7435 (1976).
(4) D. G. Davis and R. W. Murray, *Anal. Chem.*, **49**, 194 (1977).
(5) T. Kuwana and co-workers, private communication (1977).
(6) A. P. Brown, C. Koval, and F. C. Anson, *J. Electroanal. Chem.*, **72**, 379 (1976).
(7) A. H. White, E. Kokot, R. Roper, H. Waterman, and R. L. Martin, *Aust. J. Chem.*, **17**, 294 (1964).
(8) R. Chant, A. R. Hendrickson, R. L. Martin, and N. M. Rohde, *Inorg. Chem.*, **14**, 1894 (1975).
(9) R. H. Abel, J. H. Christie, L. L. Jackson, J. G. Osteryoung, and R. A. Osteryoung, *Chem. Instrum.*, **7**, 123 (1976).
(10) PAR 174 Manual, Princeton Applied Research Corp., Princeton, N.J.
(11) J. H. Christie, J. G. Osteryoung, and R. A. Osteryoung, *Anal. Chem.*, **45**, 210 (1973).
(12) E. Laviron, *Bull. Soc. Chim. Fr.*, 3717 (1967).
(13) H. A. Laitinen, C. A. Vincent, and J. J. Bednarski, *J. Electrochem. Soc.*, **115**, 1024 (1968).
(14) A. T. Hubbard and F. C. Anson in "Electroanalytical Chemistry", Vol. **4**, A. J. Bard, Ed., Marcel Dekker, New York, N.Y., 1970.
(15) B. B. Damaskin, O. A. Petri, and V. V. Batrakov, "Adsorption of Organic Compounds on Electrodes", Plenum Press, New York, N.Y., 1971.
(16) A. N. Frumkin, *Z. Phys. Chem.*, **116**, 466 (1925).
(17) E. Laviron, *J. Electroanal. Chem.*, **52**, 395 (1974).
(18) B. E. Conway and E. Gileadi, *Trans. Fararaday Soc.*, **58**, 2493 (1962).
(19) M. Boudart, *J. Am. Chem. Soc.*, **74**, 3556 (1952).
(20) G. Halsey and H. S. Taylor, *J. Chem. Phys.*, **15**, 624 (1947).
(21) M. Abramowitz and I. A. Segun, Ed., "Handbook of Mathematical Functions", Dover Publications, New York, N.Y., 1964.
(22) K. Takahashi and F. C. Anson, unpublished results, 1976.
(23) C. A. Koval and F. C. Anson, to be submitted.

RECEIVED for review May 16, 1977. Accepted June 22, 1977. This work was supported by a grant from NSF-RANN.

Ion-Exchange Separation and Determination of Calcium and Magnesium

Michael D. Arguello and James S. Fritz*

Ames Laboratory-ERDA and Department of Chemistry, Iowa State University, Ames, Iowa 50011

Magnesium(II) and calcium(II) are separated from each other and from several other metal ions by ion-exchange chromatography on a sulfonated macroporous resin of 1.8 to 2.0 mequiv/g capacity. The eluent is 1 M ammonium chloride or 0.03 M ethylenediammonium chloride. The separated metal ions are detected automatically with a color-forming reagent and are quantitated with the aid of a calibration plot.

The separation and determination of calcium and magnesium has been a problem of continuing analytical interest because of the many kinds of materials in which significant amounts of these two elements occur together. Cation-exchange procedures for separation of calcium and magnesium have included elution with hydrochloric acid (*1–3*), ammonium chloride (*4*), ammonium acetate (*5*), ammonium acetylacetonate (*6*), EDTA (*7*), ammonium lactate (*8*), and pH-5 α-hydroxybutyric acid (*9*). These procedures are rather slow and are not readily adaptable to automatic detection of the eluted metal ions. Ion exchange with forced eluent flow and automatic detection of eluted species has been successfully used for separation of a number of metal ions. Fritz and Story (*10*) used spectrophotometric detection after addition of a color-forming reagent. Small, Stevens, and Bauman (*11*) employed conductance detection after removal of eluent ions on a "stripper" column. Freed (*12*) used flame emission for detection of calcium, strontium, and barium separated on a Zipax SCX cation exchanger.

A method is now given for rapid separation of calcium and magnesium from each other and from other metal ions. The separation is done on a column containing a sulfonated macroporous resin of low capacity. The elution curves are recorded using a unique color-forming system and spectrophotometric detection.

EXPERIMENTAL

Apparatus. The liquid chromatograph has been described previously (*13*) and is shown schematically in Figure 1. A Milton Roy minipump (Model 396) and a Chromatrix CMP-2 metering pump were used for solvent delivery as well as for delivery of buffered color-forming reagent.

Columns were constructed from lengths of 4-mm i.d. Pyrex tubing onto which Altex 200-28 glass connectors had been fused. The use of Viton O rings between the polypropylene bushings and caps of the glass connectors resulted in columns that were both leak-tight and chemically inert. All plumbing components (tubing, tube-end fittings, couplings, plugs, tees, valves, sample loops, etc.) used were either purchased from Laboratory Data

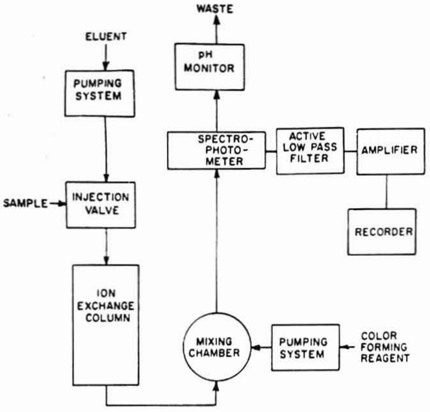

Figure 1. Block diagram of forced-flow chromatograph

Control or Altex or were constructed in the Ames Laboratory shops.

Reagents. Stock solutions (0.01 M) of metal ions were prepared from the best available grade of metal salts. In most cases reagent grade chloride salts were used but in a few cases it was necessary to use metal oxides or other salts. Sufficient hydrochloric acid was added to each stock solution to prevent hydrolysis.

Ethylenediammonium chloride (en·2HCl) was prepared by dissolving 100 g of ethylenediamine (J. T. Baker) in 1 L of distilled water. The solution was cooled in an ice bath and 330 mL of concentrated hydrochloric acid (Dupont reagent grade) was added slowly with stirring. The en·2HCl was crystallized by the addition of 2-propanol, filtered with suction, washed with acetone, and air dried.

Resin. Partially sulfonated XAD-2 was prepared by a procedure similar to that described by Fritz and Story (*10*).

A 5- to 10-g portion of the 250–325 mesh fraction was suspended in concentrated sulfuric acid (Dupont Reagent grade) and stirred for 30 min at 102–103 °C. Close control of temperature was maintained by means of a well regulated, electrically heated oil bath. The capacity of resin was 1.8 to 2.0 mequiv/g.

Color-Forming Reagents. To prepare Arsenazo I reagent, 121.1 g of THAM (Tris(hydroxymethyl)aminomethane) was dissolved in approximately 750 mL of distilled water. Sufficient concentrated hydrochloric acid was added to adjust the pH of the solution to 9.0 and the volume was made up to 1 L using distilled water. Then 0.100 g of Arsenazo I was added with stirring. The resulting solution could be used immediately and was stable at room temperature for a month or longer.

PAR reagent was prepared by dissolving 0.100 g of PAR (Eastman No. 7714) in 1 L of THAM-HCl buffer (pH 9.0).

A stock solution of Zn(EDTA) was prepared by reacting stoichiometric amounts of zinc and EDTA stock solutions. The correct ratio was determined by prior titration of the zinc stock solution with the EDTA stock solution using xylenol orange as indicator at pH 5. Several NaOH pellets were added to each liter of freshly prepared solution to raise the pH sufficiently to prevent the precipitation of the free acid form of EDTA. The Zn(EDTA) concentration of the final solution was 7.65×10^{-3} M.

Fifty mL of this solution was added to each liter of PAR reagent and the final solution was made 0.200 M in sodium hydroxide. The resulting solution of PAR-Zn(EDTA) reagent was 4.43×10^{-4} M in PAR and $3.64 \times 3.64 \times 10^{-4}$ M in Zn(EDTA) and the pH was approximately 12.

Detection Wavelength. A wavelength setting of 590 nm was chosen for use in conjunction with Arsenazo I and a setting of 495 nm for use with PAR-ZnEDTA.

Column Parameters. In general a column 7 cm × 0.4 cm was filled with 250–325 mesh sulfonated XAD-2 resin, 1.8 to 2.0 mequiv/g. An eluent flow rate of 2 mL/min was usually employed.

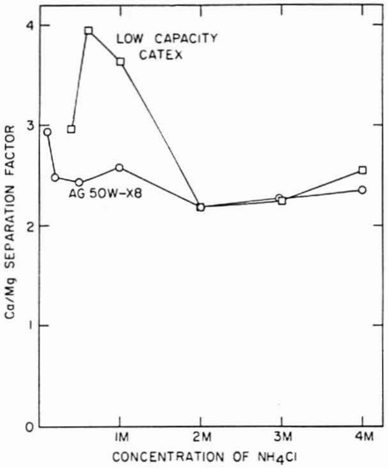

Figure 2. Calcium/magnesium separation factors on AG 50W-X8 and 1.9 mequiv/g low capacity catex as a function of ammonium chloride concentration

The flow rate of color-forming reagent was usually 0.5 mL/min.

RESULTS AND DISCUSSION

Resin. A highly cross-linked resin that does not swell or shrink appreciably is best for column separations where the eluent is under pressure. The resin used here (XAD-2) is a highly cross-linked macroporous polystyrene which has been sulfonated under mild conditions. This results in a resin with excellent exchange kinetics and with lower capacity than conventional resins. The lower capacity (1.8 to 2.0 mequiv/g of air-dried resin) permits use of more dilute eluents than would be needed with conventional resins. With commonly used eluents, the separation factor for calcium/magnesium is also more favorable with the sulfonated XAD-2 resin.

Eluent. Hydrochloric acid and several ammonium salts were tested as eluents for separation of calcium and magnesium on sulfonated XAD-2 resin. Of these, ammonium chloride is the best with a separation factor for calcium/magnesium of approximately 4.0 with 0.6 M ammonium chloride (Figure 2). Several column separations of calcium and magnesium were achieved using 0.8- to 1.0 M ammonium chloride as the eluent.

Ethylenediammonium chloride, first proposed as an eluent by Fritz and Karraker (*14, 15*), is a 2+ cation and is more effective in eluting metal cations than the usual eluents containing 1+ cations. Thus a 0.035 M solution of ethylenediammonium chloride is roughly as effective for eluting calcium and magnesium as a 1.0 M solution of ammonium chloride. The lower concentration of ethylenediammonium chloride eluent also permits a more sensitive detection of calcium and magnesium with color-forming reagents than the ammonium chloride eluents. Distribution coefficients of several metal ions are plotted as a function of ethylenediammonium chloride concentration in Figure 3.

Color-Forming Reagents. Solutions of the following indicators were checked for sensitivity of color-forming reaction with calcium and magnesium at 9 different pH values from pH 4.2 to 12.0: Arsenazo I and III, Sulfonazo III, Methylthymol Blue, Titan Yellow, Murexide, sodium rhodizonate, Eriochrome Black T, Chlorophosphonazo, and TAR. Of these, Arsenazo I appeared best suited for use in the

Table I. Effective Molar Absorptivities, M^{-1} cm^{-1}

Metal ions	Arsenazo I (0.8 M NH_4Cl)[a]	Arsenazo I (0.03 M en · 2HCl)[a]	Arsenazo I	PAR-Zn(EDTA)
Mg	1 900	4 600	8 300	17 000
Ca	870	1 700	6 800	22 000
Sr	---	---	2 500	19 000
Ba	---	---	1 400	18 000

Color-Forming Reagents

[a] Values in parentheses refer to background electrolyte.

Table II. Chromatographic Separation and Determination of Calcium and Magnesium

Other ion	Ratio of other ion: Ca or Mg	Mg, μg Taken	Mg, μg Found	Ca, μg Taken	Ca, μg Found
Li^+	50	25.0	24.0	41	41
Na^+	50	25.0	27.2	41	39
K^+	50	25.0	22.6	41	40
NH_4^+	50	25.0	24.6	41	38
Sr^{2+}	0.1	25.0	24.6	41	42
Ba^{2+}	1	25.0	23.8	41	41
Be^{2+}, Al^{3+}	1	23.8	23.8	41	41
Cd^{2+}, Co^{2+}, Cu^{2+}, Zn^{2+}	1 each	25.0		41	40
UO_2^{2+}, Fe^{3+}, Mn^{2+}	1 each	25.0		41	44
Ni^{2+}	1	25.0		41	42
Er^{3+}, Yb^{3+}, Nd^{3+}	0.75 each	25.0	25.6	41	41
$H_2PO_4^-$	25	25.0	24.0	41	39
$H_2PO_4^-$	2.5	25.0	25.5	41	41

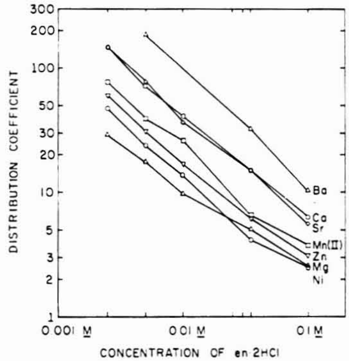

Figure 3. Distribution coefficients of several divalent metal ions on 2.0 mequiv/g low capacity catex as a function of ethylenediammonium chloride concentration

continuous spectrophotometric detection of calcium and magnesium in column effluents. The sensitivity of Arsenazo I for metal ions is reduced by the eluent salt, especially in the case of calcium (Table I). However, Arsenazo I was used for most of the results reported.

Towards the end of the work a much superior color-forming reagent, PAR–ZnEDTA, was developed. Equal-molar concentrations of PAR and zinc(II)–EDTA are mixed together and buffered at pH 9.0 with THAM and hydrochloric acid. The reaction with calcium(II) or magnesium(II) is as follows:

$$Ca^{2+} + ZnEDTA + PAR \rightarrow CaEDTA + ZnPAR$$

The molar absorptivity of the resulting color (ZnPAR) is 17 000 for magnesium and 22 000 for calcium, vs. a reagent blank (Table I). The kinetics for this reaction are favorable and no delay loop is needed in the detection system. As seen in Table I, this color-forming system is also effective for strontium and barium.

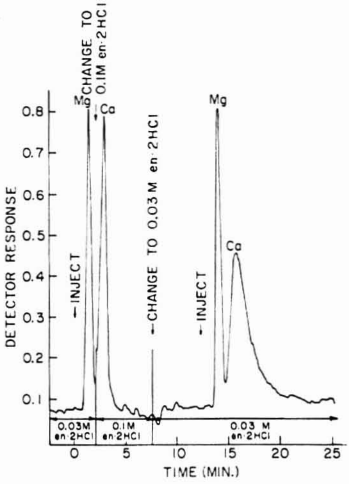

Figure 4. Comparison of stepwise and single stage elution of calcium and magnesium. Column: 2.0 mequiv/g low capacity catex; 7 cm × 0.4 cm. Eluents: 0.03 M en-2HCl; 2 mL/min; 0.1 M en-2HCl; 2 mL/min. Detection: Arsenazo I color-forming reageant; 0.5 mL/min; 590 nm. Sample: 38.1 μL; 4.63 μg Mg and 30.5 μg Ca

Separations. Elution with 0.03 M ethylenediammonium chloride is compared with stepwise elution in Figure 4. The stepwise elution is clearly better but requires careful timing in the change of eluent. For this reason, a constant 0.03 M ethylenediammonium chloride or 0.8 to 1.0 M ammonium chloride was used for all calcium/magnesium separations reported.

The effect of several other metal ions on the separation of calcium and magnesium was studied. Beryllium(II) and aluminum(III) can be eluted from the cation-exchange column

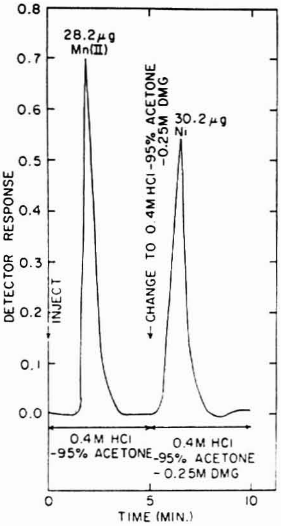

Figure 5. Separation of manganese(II) and nickel. Column: 1.9 mequiv/g low capacity catex; 7 cm × 0.4 cm. Eluents: 0.4 M HCl-95% acetone; 1.5 mL/min; 0.4 M HCl-95% acetone-0.25 M DMG; 1.5 mL/min. Detection: Methanolic solution of PAR saturated with THAM; 4 mL/min; 490 nm. Sample: 51.4 μL

Table III. Analysis of Hard Water Samples

Sample No.	Metal detnd	Our analysis, ppm	AA, ppm	EDTA tit., ppm	Plasma emission, ppm
1	Mg^{2+}	33.5	34.0	38.8	34.0
	Ca^{2+}	99.5	106	98.8	104
2	Mg^{2+}	10.5	10.1	10.5	10.5
	Ca^{2+}	38.0	36.9	35.9	36.0

with 0.1 M sulfosalicylate (pH 3.6). After 2.5 min, the eluent is switched to 0.8 M ammonium chloride or 0.03 M ethylenediammonium chloride and the calcium and magnesium are separated from each other.

Divalent metal ions that readily form anionic chloride complexes can also be eluted prior to a calcium/magnesium separation. Cadmium(II), cobalt(II), copper(II), iron(III), manganese(II), uranium(VI), and zinc(II) are eluted with 0.4 M hydrochloric acid in 95% acetone. After 7.5 to 15 min, the recorder trace returns to baseline and calcium and magnesium can be separated. Although the distribution coefficients of both magnesium(II) and calcium(II) are high in 0.4 M hydrochloric acid-95% acetone, the magnesium recovery was always low in actual separations. However, results for calcium were always quantitative.

Nickel(II) was found to be completely eluted with 0.25 M dimethylglyoxime in 0.4 M hydrochloric acid-95% acetone. By this method, nickel(II) can be separated quantitatively from manganese and other metal ions (Figure 5).

Rare earths are more tightly held than calcium and magnesium on the cation-exchange column. Following a calcium/magnesium separation, rare earths can be eluted with 4 M ammonium chloride.

Separations can be quantitated by measuring the peak height and reading the amount of metal from a calibration plot, which is nearly linear, of peak height vs. amount of metal ion. Data for quantitative calcium/magnesium separations in various samples are summarized in Table II.

The column chromatographic method can be used to determine separately calcium and magnesium in hard water samples. This procedure should be advantageous when more detailed information than just "total hardness" is required. Results for the chromatographic method are compared with other common analytical methods in Table III.

ACKNOWLEDGMENT

The authors thank Walter Sutherland for performing several plasma emission analyses. They also thank Rohm and Haas for providing the XAD-2 resin used in this work.

LITERATURE CITED

(1) O. Samuelson, "Ion Exchange Separations in Analytical Chemistry", John Wiley and Sons, New York, N.Y., 1963.
(2) F. W. E. Strelow, C. J. Liebenberg, and A. H. Victor, *Anal. Chem.*, **46**, 1409 (1974).
(3) F. W. E. Strelow and C. R. van Zyl, *Anal. Chim. Acta*, **41**, 529 (1968).
(4) M. L. Abdullah and J. P. Riley, *Anal. Chim. Acta*, **33**, 391 (1965).
(5) A. K. De and A. K. Sen, *Talanta*, **13**, 1313 (1966).
(6) G. R. Greenhalgh, J. P. Riley, and M. Tongudai, *Anal. Chim. Acta*, **36**, 439 (1966).
(7) M. Marhol and K. L. Cheng, *Anal. Chem.*, **42**, 652 (1970).
(8) G. M. Milton and W. E. Grummitt, *Can. J. Chem.*, **35**, 541 (1957).
(9) F. H. Pollard, G. Nickless, and D. Spincer, *J. Chromatogr.* **13**, 224 (1964).
(10) J. S. Fritz and J. N. Story, *Anal. Chem.*, **46**, 825 (1974).
(11) H. Small, T. S. Stevens, and W. C. Bauman, *Anal. Chem.*, **47**, 1801 (1975).
(12) D. J. Freed, *Anal. Chem.*, **47**, 186 (1975).
(13) Mark D. Seymour, Ph.D. Thesis, Iowa State University, Ames, Iowa, 1972.
(14) J. S. Fritz and S. K. Karraker, *Anal. Chem.*, **31**, 921 (1959).
(15) J. S. Fritz and S. K. Karraker, *Anal. Chem.*, **32**, 957 (1960).

RECEIVED for review May 16, 1977. Accepted June 27, 1977. Work supported by the U.S. Energy Research and Development Administration, Division of Physical Research.

Automated Atomic Absorption Spectrometric Determination of Total Arsenic in Water and Streambed Materials

Marvin Fishman* and Roberto Spencer

U.S. Geological Survey, Mail Stop 407, Box 25046, Denver Federal Center, Denver, Colorado 80225

An automated method to determine both inorganic and organic forms of arsenic in water, water-suspended mixtures, and streambed materials is described. Organic arsenic-containing compounds are decomposed by either ultraviolet radiation or by sulfuric acid–potassium persulfate digestion. The arsenic liberated, with inorganic arsenic originally present, is reduced to arsine with sodium borohydride. The arsine is stripped from the solution with the aid of nitrogen and is then decomposed in a tube furnace heated to 800 °C which is placed in the optical path of an atomic absorption spectrometer. Thirty samples per hour can be analyzed to levels of 1 μg arsenic per liter.

Automated methods for the determination of inorganic arsenic at the microgram level in water by atomic absorption spectrometry using hydride generation have been reported. Goulden and Brooksbank (*1*) determined arsenic, antimony, and selenium using stannous chloride, potassium iodide, and aluminum for the hydride generation. The hydrides produced in the automated system are then passed to a tube furnace mounted in the light path of an atomic absorption spectrometer. The use of a tube furnace gives an increase in sensitivity over the conventional hydrogen–argon–entrained flame. The system will measure any inorganic arsenic present in the sample. To determine arsenic in organo arsenic compounds, they first used a manual hydrochloric acid–persulfate pretreatment to decompose any organic compounds present. Pierce et al. (*2*) employed sodium borohydride to convert selenium and arsenic to their respective hydrides. They used the stripping column suggested by Goulden and the tube furnace combustion concept. Again, only inorganic arsenic was determined.

It has been reported in the literature that some alkylated arsenicals can be determined without digestion. Braman and Foreback (*3*) separated and determined arsenic(III), arsenic(V), monoethylarsonic acid and dimethylarsonic acid based on sodium borohydride reduction of the arsenicals to their corresponding arsines. They used a specialized electrical discharge apparatus for the measurement of the arsines. Talmi and Bostick (*4*) used a similar technique followed by gas chromatography. More recently Edmonds and Francesconi (*5*) reported that the time consuming and possible error inducing digestion stage could be omitted from atomic absorption spectrometric procedures for estimating some alkylated arsenicals. When using the method of Pierce et al. (*2*), we were unable to obtain 100% recovery of some alkylated arsenicals (see Table I) and felt that a digestion step was necessary with their procedure.

We have been unable to find any mention in the literature of an automated method that incorporates a procedure to first decompose organo arsenic compounds prior to the hydride formation. Automated methods for determining other complex organically bound substances have been reported. El-Awady, Miller, and Carter (*6*) described an automated method to determine organomercury in water and wastewater using either acid persulfate–dichromate or acid–permanganate digestions. An automated method to determine cyanide was reported by Goulden, Afghan, and Brooksbank (*7*). To determine complex cyanides, they passed the solutions first through an ultraviolet digestor. The purpose of our study was to incorporate a digestion procedure into the automated arsenic procedure of Pierce et al. (*2*). Two automated digestion procedures are described: (1) ultraviolet radiation and (2) acid–persulfate digestion. The arsenic liberated by digestion, with inorganic arsenic originally present, is reduced to arsine with sodium borohydride. The arsine is stripped from the solution with the aid of nitrogen and is then converted to arsine ground state atoms in a tube furnace placed in the optical path of an atomic absorption spectrometer. The stripping column and tube furnace used by Pierce were incorporated into this method. Thirty samples per hour can be analyzed.

The method may be used to analyze waters and water-suspended sediment mixtures containing at least 1 μg arsenic per liter. Samples containing more than 15 μg/L, must be diluted. The method may also be used to analyze bottom materials containing at least 1 μg arsenic per gram. For samples containing more than 15 μg/g, less sediment is used. Both inorganic and organic forms of arsenic are determined.

EXPERIMENTAL

Apparatus. A P-E 603 atomic absorption spectrometer with arsenic electrodeless discharge lamp and P-E Model 056 stripchart recorder for data readout were used.

The automated equipment consists of a Technicon sampler with stirrer, proportioning pump, ultraviolet digestor and/or heating bath. The ultraviolet digestor is used only for dissolved arsenic and cannot be used when analyzing water-suspended sediment mixtures or bed materials. The heating bath is used only in the acid–persulfate digestion procedure.

The stripping column is identical to that used by Pierce et al. (*2*) and is packed with glass helices or beads. Because the stripping column is not heated, it is not necessary to cool the condensing column. Nitrogen is introduced into the stripping column and is used to carry the arsine to the tube furnace. The flow rate is adjusted for maximum sensitivity by analyzing a series of identical standards. A flow rate of approximately 100 mL/min has been found satisfactory.

The tube furnace is made from quartz tubing, 10 mm i.d. × 100 mm, with an eyelet at each end of the tube to anchor the nickel-chrome wire. The tube is fused at the center with a 2-mm i.d. quartz tube for the gas entry port. A ball and socket joint may be fused at the end of the condensing column and gas entry tube to facilitate in joining the two units together. The tube furnace is wrapped with 18 ft of 26-gauge nickel-chrome wire, covered with asbestos cloth and mounted in the optical path of the atomic absorption spectrometer.

Reagents. The concentration of the reagents used in this method are as follows: hydrochloric acid (6 M), potassium iodide (100 g/L), potassium persulfate (50 g/L), sodium hydroxide (10 M), and sulfuric acid (3 M). The sodium borohydride solution is prepared by dissolving 5 g $NaBH_4$ and 40 g NaOH in water and diluting to 1 L. Demineralized water is used to prepare these reagents.

Procedure. Determine arsenic at 193.7 nm. Apply a voltage of 47 V or more (voltage regulator) as necessary to the tube furnace

Table I. Recovery of Arsenic from Organic Arsenic Compounds by Automated and Manual Procedures (All results in $\mu g/L$)

		Amount found[a]			
		Automated methods			Manual method
Compound	Amount added	No digestion	Ultraviolet radiation	Acid-persulfate digestion	Nitric-sulfuric acid digestion
Phenylarsonic acid	10	3.9	9.8	9.8	2
Phenylarsonic acid	5	2.8	4.8	5.0	1
Thorin (*o*-(2-hydroxy-3,6-disulfo-1-naphthylazo)benzene arsonic acid)	10	1.8	5.6	7.0	5
DSMA (Disodium methane arsonate)	15	7.9	14.9	14.4	10
Cacodylic acid (Dimethylarsonic acid)	10	6.3	10.4	10.2	7.5

[a] Based on several replicates.

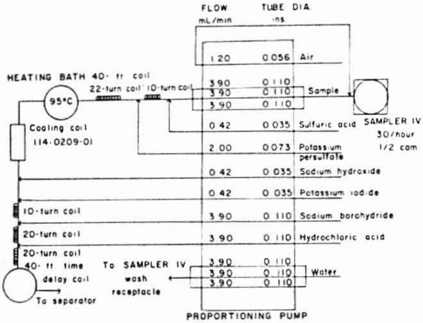
FLOW
mL/min
TUBE DIA
ins
1 20
0 056
Air
HEATING BATH 40- ft coil
22-turn coil
10-turn coil
95°C
3 90
0 110
3 90
0 110
Sample
3 90
0 110
Cooling coil
114-0209-01
0 42
0 035
Sulfuric acid
SAMPLER IV
30/hour
1/2 cam
2 00
0 073
Potassium persulfate
0 42
0 035
Sodium hydroxide
0 42
0 035
Potassium iodide
10-turn coil
3 90
0 110
Sodium borohydride
20-turn coil
3 90
0 110
Hydrochloric acid
20-turn coil
40- ft time delay coil
To SAMPLER IV wash receptacle
3 90
0 110
3 90
0 110
Water
3 90
0 110
To separator
PROPORTIONING PUMP

Figure 1. Acid persulfate digestion manifold. If only dissolved arsenic is to be determined, add air just prior to the sulfuric acid

Table II. Comparison of the Automated and Manual Determination of Arsenic on Filtered Water Samples (All results in $\mu g/L$)

	Automated methods		Manual method
Sample No.	Acid-persulfate digestion	Ultraviolet radiation	Nitric-sulfuric acid digestion
1	0.4	0.4	0.0
2	0.7	1.4	0.3
3	1.0	0.7	0.4
4	1.1	1.0	0.8
5	1.2	0.8	0.8
6	1.6	1.1	1.2
7	1.6	0.4	0.0
8	1.9	1.6	1.7
9	3.2	3.2	3.0
10	5.1	4.7	1.0
11	5.3	4.8	6.0
12	6.4	6.0	4.9
13	8.3	7.6	6.0
14	8.7	7.5	9.0
15	10.0	9.9	9.0
16	18.2	18.1	17.0

Table III. Arsenic Working Curves for Automated Methods

	Recorder peak heights in absorbance mode	
Arsenic standards, $\mu g/L$	Ultraviolet radiation	Acid persulfate digestion
15.0	58	58
12.5	51	49
10.0	40	39
5.0	21	21
2.0	9	9
1.0	5	5

to obtain a constant temperature of 800 °C. Use a portable pyrometer to check the temperature of the tube furnace. Place the tip of the thermocouple just inside the end of the tube. Remove the thermocouple when the furnace temperature becomes constant. Set up the manifold as described in Figure 1 (acid–persulfate) or Figure 2 (ultraviolet radiation) (use only for dissolved arsenic samples that have been filtered). Feed all reagents through the system using demineralized water in the sample line and allow the heating bath to warm to 95 °C. Beginning with the highest standard, place a complete set of standards in the first positions of the tray. It is best to place two or three samples of the highest standard at the beginning since the first peak is usually low. (No explanation can be given for this phenomenon.) The first standard should not be used in any of the calculations. Remove the sample line from the demineralized wash solution when the baseline stabilizes and begin analysis.

For bed materials, weigh 100 mg or less of sample, transfer into a 100-mL volumetric flask, dilute to volume with demineralized water, and analyze as above. When the analyses are complete, the tubes in the manifold and separator column should be cleaned if any sediment is present. The cleaning is accomplished by circulating 6 M hydrochloric acid and demineralized water through all the tubes.

RESULTS AND DISCUSSION

Two automated digestion procedures are incorporated into the above described arsenic methods: (1) ultraviolet radiation and (2) acid–persulfate digestion. Both procedures degraded the organic arsenic compounds, in demineralized water matrix, to about the same degree (Table I). Without digestion, recovery of arsenic from these compounds was low. The arsenic recovery was also low when the standard nitric–sulfuric manual digestion procedure was used. The loss of organic arsenic compounds in the standard nitric–sulfuric acid digestion method cannot be explained. It was first thought that the organic arsenic compounds were partially volatilized during the manual digestion process, whereas in the automated processes there could be no loss because the compounds were confined in a closed system. To determine if this were the case, the same organic arsenic compounds as well as inorganic arsenic were digested to fumes of sulfur trioxide in distillation apparatus and the distillates were collected in both weakly acidic and basic solutions. The concentrations of arsenic found in the distillates were negligible. Recoveries of arsenic in the digests, except for the inorganic arsenic solutions, were similarly low as is shown in Table I. It appears that the arsenic has been converted to some unreactive form in the digest. Further investigation is warranted and planned.

Table IV. Precision of Automated Methods on Standard Reference Water Samples (SRWS) (All results in μg/L)

			Acid–persulfate digestion[a]			Ultraviolet radiation[b]		
Sample No.	Mean	Std dev	Range	Mean	Std dev	Range	Mean	Std dev
SRWS 52	9.1	3.7	9.5–11.0	10.4	0.5	9.0–11.2	10.4	1.0
SRWS 53	55.5	12.8	55.0–64.0	59.6	2.8	55.5–66.0	61.4	4.4
SRWS 56	14.3	4.9	14.6–16.6	15.5	0.7	13.2–14.5	13.8	0.6
SRWS 57	5.4	1.3	5.3–6.3	5.8	0.3	4.3–5.3	5.0	0.5
D[c]			4.6–5.1	4.8	0.2	4.3–5.2	4.7	0.4

[a] Values based on seven replicate determinations. [b] Values based on four replicate determinations. [c] Sample solution contains 5.0 μg/L of arsenic from phenylarsonic acid.

Table V. Recovery of Organic Arsenic Compounds in Water-Suspended Sediment Mixtures (All Results in μg/L)

				Found[a]	
Sample No.	Amount present[a]	Amount added	Total	Ultraviolet radiation	Acid–persulfate digestion
1	3.2	10 (as phenylarsonic acid)	13.2	9.3	13.3
2	1.4	10 (as phenylarsonic acid)	11.4	7.4	10.2
3	1.0	10 (as phenylarsonic acid)	11.0	8.2	11.0
4	0.8	10 (as phenylarsonic acid)	10.8	7.7	9.8
1	3.1	10 (as cacodylic acid)	13.1	12.6	12.0
2	1.4	10 (as cacodylic acid)	11.4	9.9	10.0
3	1.0	10 (as cacodylic acid)	11.0	10.3	10.7
4	0.8	10 (as cacodylic acid)	10.8	10.6	10.2

[a] Based on duplicate values of both automated procedures.

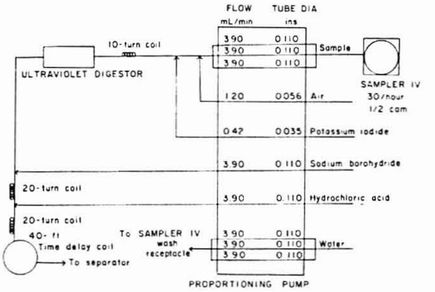

Figure 2. Ultraviolet radiation digestion manifold

Table VI. Comparison of Automated and Manual Analyses on Water-Suspended Sediment Mixtures (All results in μg/L)

	Automated methods		Manual method
Sample	Acid-persulfate digestion	Ultraviolet radiation	Nitric-sulfuric acid digestion
1	...	0.8	1.0
2	...	1.0	2
3	...	1.4	2
4	...	3.1	5
5	3.1	...	2
6	3.2	...	4
7	10.0	...	7
8	18.0	...	15
9	143	28	140

Table II shows results found for arsenic on filtered natural water samples (0.45-μm membrane filter) by both automated and manual methods. There is excellent agreement between results found by the ultraviolet radiation and acid–persulfate automated methods. The results generally agree with those found by the manual nitric–sulfuric acid digestion procedure followed by manual generation of the hydride and measurement by atomic absorption.

The almost identical and linear arsenic working curves for the two automated methods based on replicate analyses are shown in Table III.

Table IV gives the precision and an indication of the accuracy of the automated methods. Several Standard Reference Water Samples used by the Geological Survey and one organic compound, phenylarsonic acid, were used for this purpose. The precision of both digestion procedures is about the same.

The method for water-suspended sediment mixtures and bed materials (less than 2 mm) incorporates only the acid–persulfate digestion. The study showed that recovery of arsenic from organic compounds was lower when ultraviolet radiation was used (Table V). This is caused by the loss in penetration of ultraviolet radiation in the samples in which suspended material was present. This was especially apparent for sample 9 in Table VI. The quantity of suspended material was also a problem in the acid–persulfate method. Samples containing sediment concentrations above 1 g/L caused various problems. First, sediment collected at various points in the manifold; second, the baseline drifted considerably and arsenic peaks became very ragged.

It is suggested that the ultraviolet radiation procedure be used if only dissolved arsenic is to be determined; however, if a laboratory is also analyzing water-suspended sediment mixtures and bed materials, the acid–persulfate method should be used. This would eliminate the need of converting the manifold from one system to another or from having a separate manifold, for dissolved arsenic.

The quartz tubes have a limited life. Over a period of time, the voltage applied to the tube furnace was increased gradually in order to maintain a temperature of 800 °C. When it became impossible to obtain a temperature of 800 °C with the voltage regulator, the tube and nickel-chrome wire were replaced.

An interference study was not conducted since the arsine is freed from the original sample matrix. Also, a detailed inorganic interference study by Pierce and Brown (8) showed that most trace elements below 300 μg/L do not interfere.

LITERATURE CITED

(1) P. D. Goulden and P. Brooksbank, *Anal. Chem.*, **46**, 1431 (1974).
(2) F. D. Pierce, T. C. Lamoreaux, H. R. Brown, and R. S. Fraser, *Appl. Spectrosc.*, **30**, 38 (1976).
(3) R. S. Braman and C. C. Foreback, *Science*, **182**, 1247 (1973).
(4) Y. Talmi and D. T. Bostick, *Anal. Chem.*, **47**, 2145 (1975).
(5) J. S. Edmonds and K. A. Francesconi, *Anal. Chem.*, **48**, 2019 (1976).
(6) A. A. El-Awady, R. B. Miller, and M. J. Carter, *Anal. Chem.*, **48**, 110 (1976).
(7) P. D. Goulden, B. K. Afghan, and P. Brooksbank, *Anal. Chem.*, **44**, 1845 (1972).
(8) F. D. Pierce and H. R. Brown, *Anal. Chem.*, **48**, 693 (1976).

RECEIVED for review May 2, 1977. Accepted June 29, 1977. The use of the brand name in this report is for identification purposes only and does not imply endorsement by the U.S. Geological Survey.

Determination of Ethylene Oxide in Gas Sterilants by Fourier Transform Infrared Spectrometry

P. V. Allen and A. J. Vanderwielen*

Control Analytical Research and Development, The Upjohn Company, Kalamazoo, Michigan 49001

A quantitative infrared determination of ethylene oxide in dichlorodifluoromethane has been described. The method was developed on a computerized single beam Fourier Transform Infrared (FTIR) system to overcome some of the problems associated with dispersive infrared spectrometers. The FTIR method gave accurate results between 5 and 25%, calculated on a weight basis. A comparison was made between a gas chromatographic method, an infrared analysis on a dispersive infrared spectrophotometer, and the FTIR determination. A brief study on difference spectrometry has been made and showed promise as a quality control technique.

Gas sterilization using ethylene oxide or propylene oxide as the active ingredient has become a preferred method for treating a wide variety of foodstuffs, drugs, and medical supplies and equipment. Basically, gas sterilization is used because certain materials cannot be readily sterilized with dry heat, steam, or chemical soaks without damage (*1*, *2*).

Present analytical methods utilize gas chromatography to determine the amount of active ingredient present in the sterilizing gas mixture. Gas chromatography using a flame ionization detector has been investigated (*3*–*5*) and satisfactory results were obtained by using a gas-sampling loop as verified by two independent methods (*5*). However, a large fraction of some gas sterilants consists of halocarbons (e.g., CCl_2F_2 is a common inert propellant) and flame ionization detectors are not well suited for halocarbon analysis. To date, there have been no studies that have examined the possibility of utilizing infrared spectrometry as an analytical method to identify and quantitate the amount of ethylene oxide in gas sterilants, although infrared analyzers have been used to monitor the amount of ethylene oxide in sterilization units (*1*). The objective of the present research was to examine the viability of using infrared spectrometry as an analytical method for determining the ethylene oxide content in dichlorodifluoromethane (Freon 12) in cylinders of sterilizing gas using Fourier Transform Infrared spectrometry.

In this paper we describe a quantitative infrared method for determining the ethylene oxide concentration in cylinders of sterilizing gas containing ethylene oxide and Freon-12. Procedures for taking samples from the gas cylinders and analyzing these gas mixtures have been established. The results are compared to quantitative methods using a conventional double-beam grating spectrophotometer and an analytical gas chromatograph. We also report the results of a brief study to determine the usefulness of difference spectrometry as a quality control method (*6*).

EXPERIMENTAL

Infrared. Spectra were obtained on a Digilab Model FTS-10M Fourier Transform Infrared Spectrophotometer (FTIR) and on a Perkin-Elmer 421 grating spectrophotometer. The P-E 421 was set to scan at approximately 9 cm^{-1}/s using a fivefold gain and no suppression. These conditions give a nominal resolution of about 6 cm^{-1}. Calibration curves were constructed using standard mixtures which were prepared in a vacuum line by combining pure Linde ethylene oxide and dichlorodifluoromethane.

Spectra measured on the FTS-10M were collected in a single beam mode and ratioed against a stored spectrum of the empty gas cell. The spectrophotometer was purged using dry nitrogen. From 50 to 500 scans were co-added to obtain an acceptable signal to noise ratio at 4 cm^{-1} nominal resolution (as given by the FTS-10M instrument settings). All calculations (except one as will be indicated later) were carried out in single precision without apodization of the interferograms. Except for the difference spectra obtained using the absorbance subtraction technique, spectra were plotted on the transmittance scale and the intensities of the peaks were measured by the baseline method. This worked very well since the empty gas cell provides the ideal reference and flat baselines were obtained for the ratioed spectra.

Gas Chromatography. The sterilizing gas mixture was also analyzed by gas chromatography (GC) using a Hewlett-Packard Model 402 instrument with a flame ionization detector. The GC conditions used were those adapted by P. B. Bowman and P. A. Hartman (*7*) for headspace analysis (*8*) and are as follows: (i) Column: 4 ft × 0.25 inch o.d. glass, packed with Porapak R; (ii) Temperatures: Oven at 67 °C, injector at 64 °C, detector at 120 °C; Carrier Gas: Helium at 40 mL/min. A 100-μL gas tight syringe was used to withdraw samples from the cylinder (method discussed under Sampling Procedures) and inject approximately 30 μL of gas onto the GC column.

Sampling Technique. We attached a two-stage regulator to the tanks of sterilizing gas and assembled the sampling apparatus shown in the diagram depicted in Figure 1. The regulator was adjusted to deliver 5–10 psi of gas to the 250-mL sampling bulb. Special care must be taken in sampling to prevent fractionation of the gas mixture. The sampling apparatus was purged six times in a stepwise fashion so that there was never a dynamic flow through the system which could cool the regulator enough to cause fractionation (whenever practical, a heat gun or heating tape should be used to keep the regulator at or above room temperature). The sample was then trapped in a small bulb on a vacuum system using liquid nitrogen, warmed to ambient

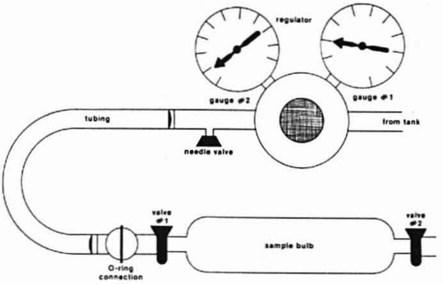

Figure 1. Sampling apparatus for collecting gas samples for infrared analysis. First stage pressure is approximately 50 psi at ambient temperature. Second stage pressure is set at 5–10 psi

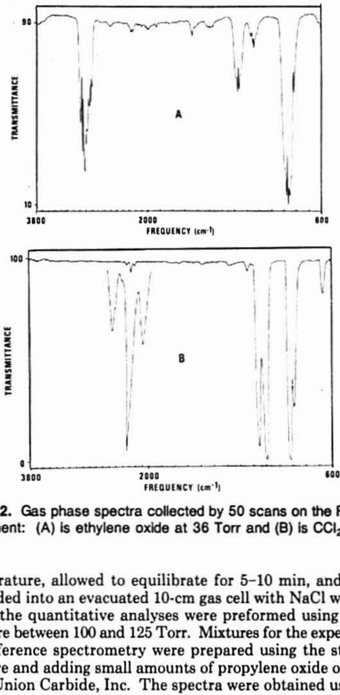

Figure 2. Gas phase spectra collected by 50 scans on the FTS-10M instrument: (A) is ethylene oxide at 36 Torr and (B) is CCl_2F_2 at 12 Torr

temperature, allowed to equilibrate for 5–10 min, and finally expanded into an evacuated 10-cm gas cell with NaCl windows. All of the quantitative analyses were preformed using sample pressure between 100 and 125 Torr. Mixtures for the experiments on difference spectrometry were prepared using the standard mixture and adding small amounts of propylene oxide obtained from Union Carbide, Inc. The spectra were obtained using the same 10-cm cell filled to a pressure between 20 and 50 Torr of gas mixture.

For the gas chromatographic analyses, the method of sampling was altered; for this experiment a septum and two needle valves were attached to the regulator and the gas was sampled with a gas-tight syringe. The same precautions as noted above were taken during purging.

RESULTS

Spectra were obtained of pure ethylene oxide (ETO) and CCl_2F_2 (Figure 2, A and B, respectively) and the peaks of interest were found to be a C–H stretching band between 3150 cm^{-1} and 2850 cm^{-1} and a CF_2 overtone between 2350 cm^{-1} and 2150 cm^{-1} (Figure 3A and 3B). A calibration curve of the ratio of the peak intensities vs. % ETO (by weight) was constructed. The weight percent of ETO was calculated according to:

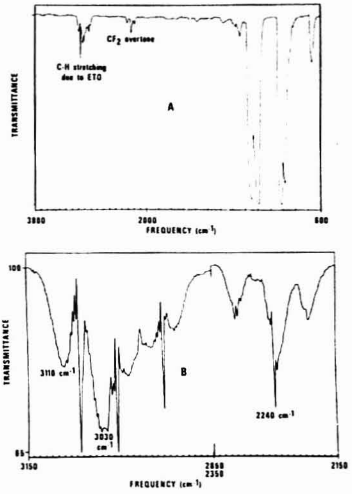

Figure 3. Gas phase spectrum of (A) ethylene oxide (9% w/w) in CCl_2F_2 (cell pressure, 24 Torr, 500 scans), and (B) the scale expanded spectrum of the region of interest

$$\% \text{ ETO}\left(\frac{\text{w}}{\text{w}}\right) = \frac{P_{\text{ETO}} \times MW_{\text{ETO}} \times 100}{(P_{\text{ETO}} \times MW_{\text{ETO}}) + (P_{\text{CCl}_2\text{F}_2} \times MW_{\text{CCl}_2\text{F}_2})} \quad (1)$$

where P and MW refer to the pressure in mm of Hg (torr) and molecular weight in g/mol of each gas. A plot of the ratio of the peak intensities ($I_{\text{C-H}}/I_{\text{CF}_2}$) vs. the % ETO (w/w) gave a slope of 0.052 and an intercept of 0.256 using the FTS-10M FTIR and somewhat different values on the P-E 421 instrument (Slope, 0.070, intercept, 0.619). The correlation coefficient in both cases was found to be 0.998.

At 10–15% ETO the 95% confidence limits were found to be ±0.8% when a linear regression analysis was performed. Plotting the ratio of absorbances vs. the ratio of weights in general would be expected to produce a linear calibration curve over a wide range of values. However, as is indicated by our data, the ratio of the peak intensities vs. the weight percent was linear over the region from 5 to 25% ETO by weight. This method of presentation was best suited for our needs in terms of data collection and ease of calculation by the laboratory analyst. Using absorbance values would be advised for general application to give a wider range. Plots of the absorbance ratio vs. % ETO by weight were linear, but a non-zero intercept (0.2) was still observed. This would indicate that Beer's law is not strictly obeyed or that there is a low intensity band of the CCl_2F_2 under the ETO peaks of interest. The weight percentages of samples then calculated according to:

$$\% \text{ ETO}\left(\frac{\text{w}}{\text{w}}\right) = m \times \left[\text{Ratio } \frac{I_{\text{C-H}}}{I_{\text{CF}_2}} - b\right] \quad (2)$$

where b = Intercept and m = 1/slope. $I_{\text{C-H}}$ = Peak intensity at 3110 cm^{-1} for FTS-10M and at 3030 cm^{-1} for the P-E 421. I_{CF_2} = Peak intensity at 2240 cm^{-1} for the FTS-10M and a shoulder on the 2240 cm^{-1} peak for the PE-421.

Table I. Multiple Samples from One Tank

Results on FTS-10M

Sample	Intensity of peak at 3110 cm^{-1}, cm	Intensity of peak at 2240 cm^{-1}, cm	Ratio	% ETO by weight
A	14.43	15.27	0.945	13.25
B	13.61	13.64	0.998	14.27
C	13.08	13.39	0.977	13.87
D	12.55	13.26	0.946	13.28
E	12.88	13.74	0.937	13.10
F	12.65	12.78	0.990	14.16
			Av =	13.7%
			Std dev =	0.5

Results on P-E 421

Sample	Intensity of peak at 3030 cm^{-1}, cm	Intensity of shoulder at 2240 cm^{-1}, cm	Ratio	% ETO by weight
A	9.30	5.54	1.678	15.13
B	9.42	5.60	1.682	15.18
C	9.18	5.48	1.675	15.08
D	9.48	5.58	1.699	15.32
E	9.25	5.79	1.598	13.97
F	9.50	5.69	1.670	15.00
			Av =	15.0%
			Std dev =	0.5

Table II. Duplicate Samples from Four Tanks

Sample	Intensity of peak at 3110 cm^{-1}, cm	Intensity of peak at 2240 cm^{-1}, cm	Ratio	%ETO by weight	Av, %
Tank No. 1					
A	11.68	12.78	0.914	12.66	12.8
B	13.21	14.22	0.929	12.93	
Tank No. 2					
C	13.72	14.40	0.953	13.41	13.2
D	13.21	14.22	0.929	12.93	
Tank No. 3					
E	14.33	13.74	1.043	15.13	15.2
F	14.58	13.89	1.050	15.27	
Tank No. 4					
G	13.72	14.22	0.965	13.63	13.6
H	13.89	14.48	0.959	13.53	

Table III. Gas Chromatography Results[a]

Sample	ETO area	CCl_2F_2 area	% ETO by weight
A	1 205	1 295	19.6
B	1 076	1 307	12.4
C	1 060	1 266	12.6
D	1 274	1 250	14.9
E	2 577	1 797	19.8
F	1 860	1 827	14.9
		Mean	15.7
		Std dev	3.3

[a] Samples taken from the same tank used during the infrared analysis listed in Table I.

Multiple samples were taken from one tank of sterilizing gas and analyzed using the FTS-10M. The same samples were also run on the P-E 421 for comparison. The results are given in Table I and typical spectra are shown in Figures 3–5.

Duplicate samples of four other cylinders were run on the FTS-10M. The results listed in Table II show good agreement between the various duplicate experiments. The reproducibility of the results indicates that our sampling procedure is adequate for this gas mixture. Table I reveals that while the FTS-10M and P-E 421 have nearly identical precision, the average obtained on the PE-421 is significantly higher (significant difference = 0.8% ETO at the 95% confidence level).

For the chromatographic analysis of the sterilant mixtures, areas under the curve were obtained by using a ball and disc integrator. The percent ethylene oxide was calculated from the peak areas by normalization with response factors (*5*):

$$\% \text{ ETO}\left(\frac{\text{w}}{\text{w}}\right) = \frac{100\, A_1}{A_1 + (R_2 \times A_2)} \qquad (3)$$

where A_1 is the area of the ETO peak, A_2 is the area of the CCl_2F_2 peak, and R_2 is the correction factor for CCl_2F_2 to ETO ($R_2 = 5.8$ was used). The results (Table III) indicate that there are several problems associated with the gas chromatographic assay when a gas syringe is used; (i) the large variability indicates that it is very difficult to obtain representative samples using a gas syringe, and (ii) the results may be biased high due to gas fractionation (CCl_2F_2 has a higher vapor pressure than ETO).

The results of the absorbance subtraction experiments (Figure 6) indicate that a 0.7% impurity is easily detectable. The spectral data for the difference spectrum depicted in Figure 6B was collected by 100 double precision scans (resolution = 4 cm^{-1}) on the FTS-10M FTIR. The Fourier Transform calculations were carried out in double precision and used a rectangular apodization function (this results in essentially no weighing of data points of the interferogram during the transform calculation).

DISCUSSION

As is so often the case, sampling is the most critical aspect in the analysis of the sterilizing gas mixture. Sampling and subsequent use of the sterilizing "gas" is facilitated by withdrawing the liquid mixture (tank is under pressure and liquid is forced out through a tube that extends to the bottom) and vaporizing it. By using the apparatus (Figure 1) and the sampling procedure outlined in the Experimental section, liquid samples are permitted to vaporize completely (no fractionation), and the gas mixture, therefore, is representative of the liquid.

When the ratio of peak intensities is to be used to determine the relative concentrations of two gas phase components by infrared spectrometry, it would be desirable to choose a peak for each component which is distinct, reproducible, and totally free of interference from peaks due to other components. The C–H stretching band at 3110 cm^{-1} and the CF_2 overtone at 2240 cm^{-1} adequately fulfill these conditions. As Figures 2A and 2B show, the peak at 3110 cm^{-1} is quite distinct, essentially independent of any peak from CCl_2F_2 and nearly free of interference from rotational spikes (unlike the slightly more intense peak at 3030 cm^{-1}). The CF_2 overtone at 2240 cm^{-1} is reproducible, very sharp, and despite the fact that it falls in the midst of some weak ETO peaks, sufficiently independent of ETO to be useful.

The band at 3110 cm^{-1} and the peak at 2240 cm^{-1} which were used when the analysis was done on the FTS-10M could not be used on the PE-421 because of the lack of reproducibility for these sharp peaks. It was necessary to use the broader peak at 3030 cm^{-1} and the shoulder on the 2240 cm^{-1} peak during analyses with the PE-421.

We chose to use a rectangular (box car) apodization function to calculate the Fourier Transform of the interferogram to obtain a signal to noise ratio of approximately 200 in a reasonable time (*9*) and to avoid the possible error than can occur in the absorbance measurement when a triangular apodization function is used (*10*). Anderson and Griffiths indicate that for a 4-cm^{-1} wide band measured with a nominal resolution of 2 cm^{-1}, the measured peak absorbance will be

Table IV. Pressure Effects

Pressure, mm Hg	Ratio, I_{CH}/I_{CF_2}	Ethylene oxide,[a] % by weight
150	0.768	9.85
125	0.766	9.81[b]
100	0.752	9.55[b]
75	0.719	8.91
50	0.708	8.69

[a] Standard provided by Union Carbide was 10.1% (w/w) ethylene oxide in CCl_2F_2. [b] Average obtained under normal experimental conditions was 9.68% ETO (w/w).

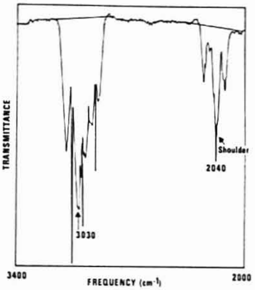

Figure 4. Scale expanded spectrum of ethylene oxide (13.6% by weight in CCl_2F_2) obtained on a Perkin-Elmer 421 at 120-Torr pressure

at least 16% low if triangular apodization is used. They also suggest that apodization somewhere between triangular and rectangular might be an excellent compromise for analytical work. However, we feel that rectangular apodization gave us accurate results in this case with no interference from the secondary lobes due to neighboring peaks.

The widths of absorption bands in gas phase spectra can be affected by the total sample pressure. A study was performed on the FTIR instrument to examine these pressure effects on the ratio of the band intensities. A standard (10.1% w/w ethylene oxide) was prepared for us by the Linde Division of Union Carbide. The analysis was performed at pressures ranging from 50 to 150 Torr and the % ETO was calculated using the calibration curves obtained under the normal experimental conditions (100–125 Torr). The results (Table IV) indicate that there is a pressure effect; however, only the results at 50 and 75 Torr differ from the actual value by more than 0.8% (ETO 95% confidence limit).

It is of interest to compare the results obtained on the FTS-10M to those obtained on the PE-421. As mentioned previously, the latter gives ethylene oxide concentrations that are higher (Table I) than those obtained on the FTIR instrument. The accuracy of the FTIR result was verified during the study on pressure effects (9.7% ETO measured vs. 10.1% ETO actual). There are several possible reasons for this anomaly. The bias could be caused by the uncertain baseline (see Figure 4) or by cell effects (e.g., NaCl window fogged). The problem is corrected on the FTIR instrument since the empty cell is used as the reference. On the P-E 421, excessive scanning time was necessary to minimize anomalies due to pen response and even then it was necessary to use the shoulder of the CF_2 overtone at 2240 cm^{-1} to obtain reproducible results. The instrument line shape of a dispersion spectrophotometer is approximately represented by a triangle (*11*). Therefore, it is quite possible that the resolution and absorbance errors observed with triangular apodized FTIR spectra (*9*) are likely to occur in spectra obtained on conventional dispersion spectrometers. The C–F_2 band is considerably narrower than the C–H band. The decrease in absorbance due to triangular apodization should, therefore, be expected to have a greater effect on I_{C-F_2} than on I_{C-H}, causing a net increase in the apparent concentration of ETO as calculated from I_{C-H}/I_{C-F_2}. However, this effect should be accounted for in the calibration curve. It is more likely that the higher values for ETO concentration obtained on the P-E 421 are due to uncertainties in the baseline, a problem not encountered with the FTS-10M.

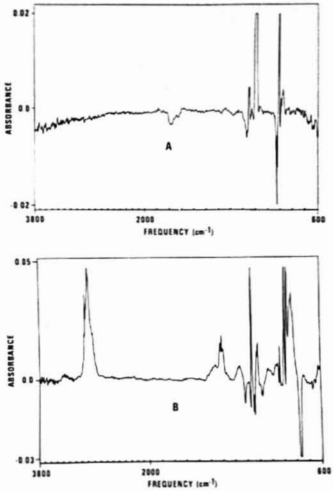

Figure 5. Results of the absorbance subtraction of (A) two gas mixtures (both consisting of 89% (w/w) CCl_2F_2 + 11% ethylene oxide) and (B) mixture minus (mixture + 0.7% (w/w) propylene oxide). Cell pressure of Sample A approximately 22 Torr and Sample B approximately 50 Torr

Infrared analysis of ethylene oxide concentration is only one of many techniques available today (*12, 13*), but we feel that this method offers several advantages (speed, accuracy, and easy sample handling) and will be useful for many applications.

It has been suggested that difference spectrometry on Fourier Transform instruments could be used as a quality control method (*6*). When the spectrum of an acceptable product or material is recorded and stored, it can be compared with any subsequent spectra. The difference spectrum in Figure 5A shows that when the absorbance spectra of two acceptable samples of sterilizing gas (11% ETO in each case) are subtracted from each other, the difference is less than 0.005 absorbance unit (AU) in the region 3800 cm^{-1} to 1200 cm^{-1}. The peaks observed at lower wavenumbers are due to the difficulty in subtracting peaks due to strongly or totally absorbing vibrational modes. Figure 5B is the difference between two samples of gas sterilant (9% ETO), one of which contains 0.7% (w/w) of propylene oxide as an impurity. The difference in this case is 0.05 AU in the region 3800 cm^{-1} to 1200 cm^{-1}. A comparison of the resulting spectrum to that of pure propylene oxide (Figure 6) shows that there would be little difficulty in identifying the impurity. These results indicate that it is certainly plausible to utilize the capabilities of FTIR instruments for quality control decisions. In our example case, we might require that the difference in the region 1500 cm^{-1} to 1300 cm^{-1} be no greater than 0.01 AU (this corresponds to approximately 0.5% propylene oxide) and a different specification for the region 3200 cm^{-1} to 2800 cm^{-1}

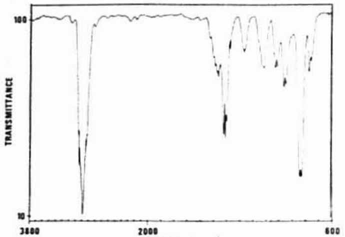

Figure 6. Gas phase spectrum of propylene oxide (50 scans, cell pressure is 30 Torr)

to allow for acceptable variations in ethylene oxide concentration.

The results of our study on difference spectrometry indicate that the method can be developed as a quality control technique. However, computer programs will have to be written to automate the data manipulation before it can become a viable technique.

ACKNOWLEDGMENT

We thank M. F. Fuller for her help in obtaining the gas chromatographic data and R. W. Brink for the experimental work for the studies on pressure effects.

LITERATURE CITED

(1) John J. Perkins, "Principles and Methods for Sterilization in Health Sciences", Charles C Thomas, Springfield, Ill., pp 501–530.
(2) Allan Claghorn, *Inhalation Therapy*, **11**, 77–84 (1966).
(3) B. Warren, *J. Pharm. Pharmacol.*, **23**, 1705–1755 (1971).
(4) Ben Berck, *J. Chromatogr. Sci.*, **13**, 256–267 (1975).
(5) R. G. Williams, Upjohn Fine Chemicals Division, unpublished work, February 1976.
(6) J. L. Koenig, *Appl. Spectrosc.*, **29**, 293–308, (1975).
(7) P. B. Bowman and P. A. Hartman, Upjohn, Product Control Division, "Determination of Residues of Gaseous Sterilants", to be published.
(8) S. J. Romano, J. A. Renner, and P. M. Leitner, *Anal. Chem.*, **45**, 2327–2330 (1973).
(9) Peter R. Griffiths, "Chemical Infrared Fourier Transform Spectroscopy", John Wiley and Sons, New York, N.Y., 1975, Chapter 8.
(10) R. J. Anderson and P. R. Griffiths, *Anal. Chem.*, **47**, 2339–2347 (1975).
(11) K. S. Seshadri and R. N. Jones, *Spectrochim. Acta.*, **19**, 1013 (1963).
(12) S. J. Romano and J. A. Renner, *J. Pharm. Sci.*, **64**, 1412–1417 (1975).
(13) N. A. Kolchina, *Zh. Anal. Chim.*, **20**, 380–387 (1965).

RECEIVED for review January 12, 1977. Accepted June 20, 1977.

Enhancement of the Fluorescence Intensity of Derivatives of Amino Acids in Mixed Solvent Systems

Peter M. Froehlich* and Larry D. Murphy

Department of Chemistry, North Texas State University, Denton, Texas 76203

A number of reagents are known to react with amino acids to form fluorescent derivatives and it has been shown that the fluorescence intensity of the derivatives can be increased by consideration of the solvent system used for its formation. The use of mixed solvent systems such as DMSO/water in place of water for the formation and detection of *o*-phthaldehyde (opt) derivatives of amino acids was found to raise the fluorescence intensity significantly (e.g., 64% for tryptophan–opt in 17% DMSO (v/v) compared to the case where DMSO was absent). Similar observations were found with dansyl amino acids and fluorescamine amino acids.

Table I. Relative Fluorescence Intensity of *o*-Phthaldehyde Derivatives of Amino Acids in Mixed DMSO[a]

	% DMSO						
Amino acid	0	7	10	13.5	17	20	27
Alanine	1.00	1.00	1.34	1.72	1.91	1.57	1.66
Phenylalanine	1.00	1.11	1.15	1.20	1.23	1.34	1.40
Histidine	1.00	1.50	1.70	2.15	2.20	2.45	
Tryptophan	1.00	1.40	1.69	1.63	1.64	1.58	1.7

[a] All data relative to the fluorescence of the derivative in 0% DMSO.

In an analytical procedure where the detection is performed by fluorometry, the ultimate sensitivity is directly related to the fluorescence quantum yield of the analyte (or of a derivative directly related to the analyte). The fluorescence quantum yield of many compounds is very sensitive to the environment of the excited state (*1*). It has been determined, for example, that water is capable of interacting with the excited state of indole (*2*), tryptophan and its metabolites (*3*), and tryrosine (*4*) to form an excited state complex (exciplex). The formation of an exciplex is competitive with fluorescence; hence the fluorescence quantum yield is reduced, thus raising the minimum detection limit of an analytical procedure. A reasonable approach to the problem of exciplex formation in fluorometric analyses might be to perform the analysis under nonaqueous conditions. In theory, this would serve the analyst quite nicely; however, the removal of water may be time consuming. In those cases, the removal of water is not a viable procedure for the analysis.

We have recently shown that the fluorescence of various indoles, tryptophan metabolites, and tyrosine metabolites (*3*) is considerably higher in mixed DMSO/water or ethanol/water than in neat water; this indicates that it may be very useful to consider the overall solvent system used in the analysis of these compounds.

A common tactic in analytical chemistry is the formation of a derivative of the compound of interest. The final solvent system in such an analysis is a composite of the original solvent of the sample, solvents used to isolate the compound of interest from the matrix, and solvents used in the formation of

Table II. Relative Fluorescence Intensity of Dansyl Chloride Derivatives of Amino Acids in Mixed Solvent Systems[a]

Amino acid	% DMSO								
	0	4	8	12	16	20	24	28	32
Alanine	1.00	1.70	2.00	2.20	2.42	2.46	2.54	2.68	2.58
Tryptophan	1.00	1.65	2.03	2.23	2.41	2.61	2.85	3.00	3.08
Lysine	1.00	1.04	1.85	2.00	2.15	2.30	2.30	2.52	2.48
Histidine	1.00	1.34	1.44	1.56	1.75	1.81	2.06	2.12	2.12

[a] All data relative to the fluorescence intensity of the derivative in 0% DMSO.

the derivative. This strongly suggests that a consideration of the solvents used in various steps of such an analysis may lead to an enhancement of the fluorescence intensity of the derivative.

We have studied two analytical procedures which involve the formation of fluorescent derivatives of amino acids and find that the use of DMSO in the place of water or acetone in the formation process may be quite useful in improving the luminescent intensity of the derivative.

EXPERIMENTAL

Salts used to prepare buffers (ACS grade or better) and DMSO (certified ACS grade) were received from Fisher Scientific Co. (Fairlawn, N.J.). Amino acids were obtained from Sigma Chemical Co. (St. Louis, Mo.). *o*-Phthaldehyde, *N*,*N*-dimethylaminonaphthalenesulfonyl chloride (dansyl chloride) and 2-mercaptoethanol were received from Eastman Organic Chemicals (Rochester, N.Y.). All reagents were used as received. Distilled water was doubly distilled from a glass still and used on the day of distillation.

Fluorometric measurements were made on an Aminco-Bowman Spectrophotofluorometer (American Instrument Co., Silver Spring, Md.) equipped with a Hamamatsu 1P21 photomultiplier, a Hanovia 901C Mercury–Xenon arc and an ellipsoidal condensing system.

Preparation of *o*-Phthaldehyde Derivatives. The *o*-phthaldehyde derivatives were made via a modification of Roth's procedure (*5*). A borate buffer (approximately 0.05 M sodium tetraborate) was prepared and the pH was adjusted to 9.5 with concentrated NaOH. A solution of 2-mercaptoethanol (5 mg/mL) in ethanol and a solution of *o*-phthaldehyde (10 mg/mL) in ethanol were prepared daily. The derivatives were prepared by mixing 0.166 mL of the *o*-phthaldehyde solution, 0.166 mL of the 2-mercaptoethanol solution, 4.40 mL of a solution of the amino acid (1×10^{-5} M in water), and 10.00 mL of a mixture of the borate buffer and DMSO. After a 5-min incubation period, the fluorescence was read at 455 nm, upon excitation at 340 nm.

Preparation of Dansyl Chloride Derivatives. One-tenth mL of a solution of the amino acid was mixed with 1.5 mL of a solution of dansyl chloride (1 mg/mL in acetone) and 0.1 mL of 20% Na_2CO_3. A total of 0.8 mL of DMSO and acetone was added to change the % DMSO in the final mixture. The solution was heated for 2.5 h at 35 °C. The fluorescence was measured at 514 nm, upon excitation at 335 nm.

RESULTS AND DISCUSSION

The relative fluorescence of the *o*-phthaldehyde derivatives of several amino acids may be seen in Table I. The corresponding data for the dansyl chloride derivatives appear in Table II. We observe a definite enhancement in fluorescence as the fraction of DMSO in the solvent system increases.

A small red shift in the λ_{max} for fluorescence was observed for the dansyl amino acids as the DMSO concentration was increased. A blue shift was observed for the fluorescence maxima for the *o*-phthaldehyde derivatives as the % DMSO was increased. These observations are consistent with Lippert's (*6*) theory relating the wavelength of maximum fluorescence intensity with the dielectric constant of the solvent. All fluorometric measurements for a given derivative (e.g., all the dansyl amino acids) were taken at the same wavelength. The error that is introduced by the shift in luminescence maxima will be small (ca. 2–4%) as the maximum shifted only 2–4 nm in 30% DMSO/70% water (or 30% DMSO/70% acetone) and this will not affect the results of this work.

Table III. Comparison of the Fluorescence Enhancement from 30% DMSO with Various Fluorescent Derivatives[c]

	Fluorescamine	Dansyl chloride[a]	*o*-Phthaldehyde[b]
Alanine	1.38	2.63	1.7
Tryptophan	1.98	3.04	1.8

[a] Average from 28 and 32% taken from Table II.
[b] Extrapolation from 27% DMSO shown on Table I.
[c] Each entry is the relative fluorescence of that derivative in 30% DMSO, compared to 0% DMSO.

Our data clearly indicate that the optimum sensitivity of fluorometric assays may be improved by careful consideration of the overall solvent system. This work, in conjunction with our recent investigation on the effect of using mixed solvent systems to enhance the luminescence of fluorescamine derivatives (*7*) shows that DMSO is a useful solvent for assays which involve the measurement of the fluorescence of a derivative. The greatest enhancement by DMSO is for the dansyl derivatives, as indicated in Table III. Chen (*8*) has indicated that the intense fluorescence of the dansyl derivatives leads to extremely low minimum detectable limits, and the use of DMSO should lead to an enhancement of sensitivity.

We observe that an upper limit to the level of DMSO present in the final solvent system does exist. In the case of the *o*-phthaldehyde derivatives, buffer salts begin to precipitate out at approximately 40% DMSO. The fluorescence of the dansyl derivatives and the fluorescamine derivatives increases with the addition of DMSO but a plateau in the intensity may be observed. In some cases, a decrease in the intensity may be observed (e.g., the fluorescamine derivative of alanine (*7*)). This suggests that the analyst should determine the optimum fraction of DMSO for the derivative of interest.

The enhancement of fluorescence by the use of mixed solvent systems is very useful for analytical work. For example, the fluorescence of a solution of the dansyl chloride derivative of tryptophan which has been prepared using 8% DMSO is double that of a solution of the derivative with no DMSO. If the derivative is made by a different procedure than we have outlined, it may still be useful to add DMSO to enhance the fluorescence. As an example, if 9% (by volume) DMSO is added to a solution of dansyltryptophan in acetone, the effect of the added DMSO will raise the fluorescence by 85% (not the 100% indicated in Table II as the dilution will have a small effect; the data in Tables I and II are for equivolume solutions).

Our work strongly suggests that it should be very useful for the analyst to carefully consider the overall solvent system used in fluorometric analysis, as a small change in solvent composition may lead to a very useful enhancement in sensitivity.

LITERATURE CITED

(1) E. L. Wehry, in "Practical Fluorescence Theory, Methods and Techniques", G. G. Guilbault, Ed., Marcel Dekker, New York, N.Y., 1973, pp 79–136.
(2) T. R. Hopkins and R. Lumry, *Photochem. Photobiol.*, **15**, 555 (1972).
(3) P. M. Froehlich and M. Yeats, *Anal. Chim. Acta*, **87**, 185 (1976).
(4) R. McGuire and I. Feldman, *Photochem. Photobiol.*, **18**, 119 (1973).
(5) M. Roth, *Anal. Chem.*, **43**, 880 (1971).
(6) E. Lippert, *Z. Electrochem.*, **61**, 962 (1957).
(7) P. M. Froehlich and T. D. Cunningham, *Anal. Chim. Acta*, **84**, 427 (1976).
(8) R. F. Chen, *Arch. Biochem. Biophys.*, **120**, 609 (1967).

RECEIVED for review April 14, 1977. Accepted June 30, 1977. We would like to thank the Faculty Research Committee of North Texas State University for support of this work. This work was presented at the 173rd National Meeting of the American Chemical Society, New Orleans, La., March 1977.

Multichannel Pipet for Parallel Aliquoting of Samples and Reagents into Centrifugal Analyzer Minidiscs

R. P. Gregory IV, J. D. Lowry,[1] and H. V. Malmstadt*

School of Chemical Sciences, University of Illinois, Urbana, Illinois 61801

A multichannel pipet system has been developed for the parallel dispensing of samples and reagents into centrifugal analyzer minidiscs. The present pipet has eight channels; four channels for sample solutions and four channels for composite reagents. Each channel has a nominal volume of 67 μL and the reproducibility of delivery is within 0.5% RSD. The multichannel nature of the pipet allows the sample solutions and composite reagents to be simultaneously aliquoted and delivered within 30 s. A microprocessor (8080A, Intel Corporation) is used to control the hardware associated with the pipet, to control the timing necessary for proper operation and sequencing, and to monitor the operation of the pipet. The concepts, design, advantages, and disadvantages of the multichannel pipet are discussed and evaluation data are presented.

Minidisc Centrifugal Analyzers utilize centrifugal force in spinning disc to gain several analytical advantages. These include the parallel transfer and mixing of micro samples with composite reagent into multiple observation cells, the use of a single optical channel for encoding the quantitative chemical information for all samples, and the automatic degassing of the solutions. The measurements for all samples on the minidisc can be considered to be done in parallel because the sequential measurements are very rapid and, typically, measurements from several rotations of the minidisc are averaged to obtain the absorbance value for each sample. To maintain the high throughput advantage of essentially simultaneous measurements of many samples, a multichannel pipet has been developed for the parallel aliquoting and delivery of solutions into the minidiscs. The introduction of this parallel loading system can improve the overall sample throughput of the minidisc centrifugal analyzer.

Sample-Handling Considerations. Sample throughput is limited for centrifugal analyzers by the time required to load the sample discs. To improve throughput, this loading time must be reduced.

The minidisc used in this work, similar in size and volume capacity to that developed at Oak Ridge (*1*), is shown in Figure 1. This minidisc consists of three 3.49-in. diameter pieces, a $^{3}/_{16}$-in. Plexiglas central body and two $^{1}/_{10}$-in. UVT Plexiglas windows, sealed together using Dow Corning 3145 RTV Adhesive/Sealtant (Dow Corning Corp., Midland, Mich.). It contains eight measurement cuvettes which have optical entrance and exit ports formed along an outer ring of 1.50-in. radius. Associated with each measurement cuvette are the sample and reagent cuvettes which are 0.125-in. deep depressions machined into the central body. This 8-position minidisc is more compatible with the multichannel pipet reported here and its design helped ease the complexity of the initial design, construction, and implementation of the pipet.

A new X-Y mixer configuration has been incorporated into this minidisc by machining $^{3}/_{64}$-in. deep channels from the sample and reagent cuvettes to the measurement cuvettes. This geometry provides immediate mixing of sample and reagent as they travel out to the measurement cuvettes.

The sample-handling problem of the minidisc centrifugal analyzer is the filling of the sample and reagent cuvettes (nominal 67 μL each) before an analysis. Access to these cuvettes is through a 3-mm opening in the top plate of the minidisc (see Figure 1). For accurate and precise results, it is necessary to deliver 67-μL aliquots of solution through these small openings. Further, to improve the sample throughput, the entire minidisc, i.e., all the sample and reagent cuvettes, must be filled rapidly. Thus, in designing any delivery system for centrifugal analyzer minidiscs, it is necessary to provide reproducible delivery of small volumes either in rapid sequence or simultaneously to load the entire minidisc in a short period of time.

Some laboratories which have centrifugal analyzers use various types of manual pipets. A Pipetmen 200-μL adjustable pipet (Rainin Instrument Co., Brighton, Mass.) has often been used in our laboratory. Although these pipets are sometimes convenient, they do not solve the sample-handling problems for high throughput. The reproducibility and time required to manually load minidiscs are greatly dependent on the technician.

To eliminate the dependence upon a given technician for reliable results, various mechanized delivery systems have been reported. These include "Gemeni, the Miniature Centrifugal Analyzer" (Electro-Nucleonics, Inc., 368 Passaic Ave., Fairfield, N.J. 07006), "Automatic Gemsaec Fast Analyzer" (Electro-Nucleonics, Inc.), "Rotochem II, Parallel Fast Analyzer" (Aminco, American Instrument Co., Silver Spring, Md.), "Centrifichem" (Clinical Diagnostics, Union Carbide, Tar-

---

[1] Present address E. I. DuPont de Nemours & Co., Wilmington, Del. 19898.

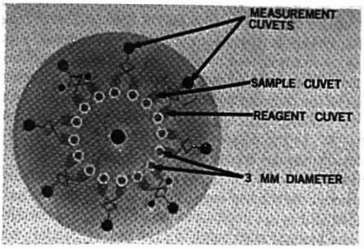
MEASUREMENT CUVETS
SAMPLE CUVET
REAGENT CUVET
3 MM DIAMETER

Figure 1. Centrifugal analyzer minidisc

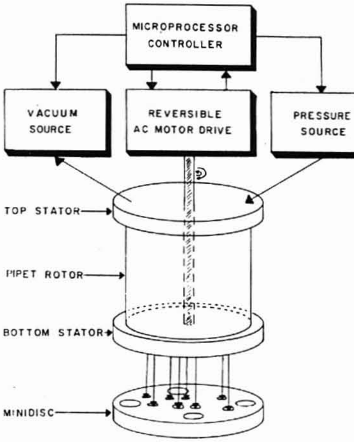
MICROPROCESSOR CONTROLLER
VACUUM SOURCE
REVERSIBLE AC MOTOR DRIVE
PRESSURE SOURCE
TOP STATOR
PIPET ROTOR
BOTTOM STATOR
MINIDISC

Figure 2. Block diagram of multichannel pipet system

rytown, N.Y.), and the system described in Ref. 1. These systems mimic a technician in loading the sample discs. That is, sample and reagent cuvettes are filled sequentially until the complete sample disc is loaded. Since the system is mechanized, the reproducibility and time required for loading the sample discs are no longer technician dependent. Thus, improvements in precision and loading time are realized as compared to manual methods.

However, the sample-handling still remains the sample throughput rate-limiting step with these sequential delivery systems. The time for loading the sample and reagent cuvettes with these systems varies from 7–18 s/cuvette and thus 3–5 minutes are needed to load a 16-position disc. The multichannel pipet discussed here loads 4 sample cuvettes and 4 reagent cuvettes (8 total) in 30 s. By using the principles of this pipet and including additional aliquoting channels, an entire 16-position disc (16 sample and 16 reagent cuvettes) could be loaded in 30 s.

INSTRUMENTATION

The basic components of the multichannel pipet system are shown in Figure 2. Eight solutions are simultaneously aliquoted in a pipet rotor which moves between two stators. The pipet rotor is connected to a reversible, ac motor which turns the rotor back and forth between the aliquot and delivery positions, located 45° apart. In the aliquot position, solutions are drawn into the pipet rotor via a partial vacuum applied at the top stator. After the solutions have been aliquoted, the pipet rotor moves to the delivery position and pressure

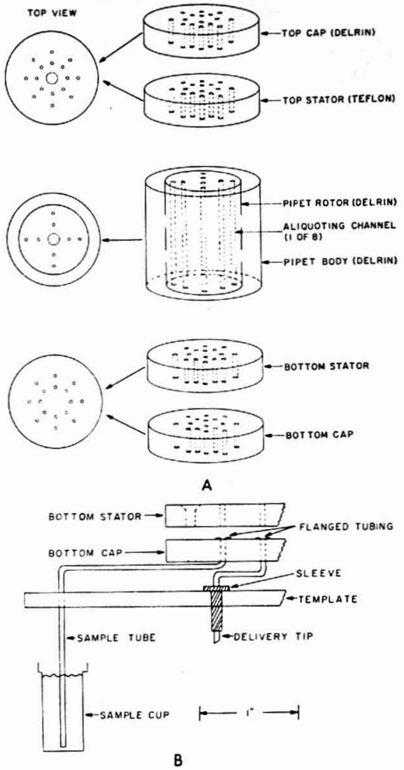
TOP VIEW
TOP CAP (DELRIN)
TOP STATOR (TEFLON)
PIPET ROTOR (DELRIN)
ALIQUOTING CHANNEL (1 OF 8)
PIPET BODY (DELRIN)
BOTTOM STATOR
BOTTOM CAP
A
BOTTOM STATOR
FLANGED TUBING
BOTTOM CAP
SLEEVE
TEMPLATE
SAMPLE TUBE
DELIVERY TIP
SAMPLE CUP
1"
B

Figure 3. (A) Exploded view of multichannel pipet. (B) Close-up view of tubing alignment

is applied to simultaneously deliver the solutions into the minidisc sample and reagent cuvettes. The microprocessor controls the motor drive, activates the pressure and vacuum sources at the proper time, and handles all the timing and sequencing necessary for proper operation of the pipet. Four operator options are switch-selectable on the front panel of the microprocessor. Each of the components of the multichannel pipet system is discussed in detail.

Multichannel Pipet. The present pipet contains only eight aliquoting channels. It was decided to have eight channels to simplify the design and construction of the pipet. However, the extension of the principles to a pipet with additional aliquoting channels would not increase the time for aliquoting and delivering the solutions. To do this, it is necessary only to drill additional channels and to realign the encoders; all other hardware can be used as described. As shown in Figure 2, eight aliquoting channels enable the pipet to simultaneously load four positions of a minidisc.

An exploded view of the multichannel pipet is shown in Figure 3A. It consists of a pipet rotor and body both made of Delrin, two Teflon stators, and two Delrin caps. Each of these pieces contains two concentric rings of 1.5-mm holes. These are spaced 45° apart in the caps and stators and 90° apart in the pipet rotor (see Figure 3A, Top View). The holes in the pipet rotor are the aliquoting channels, each with a nominal volume of 67 μL.

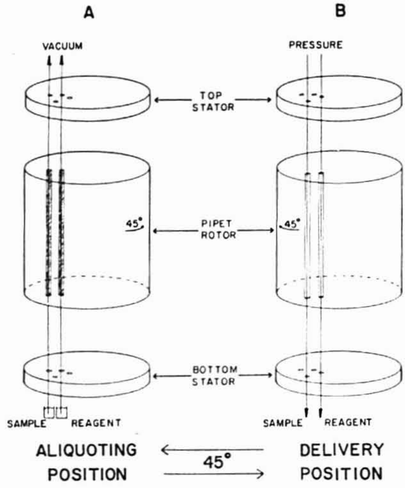

Figure 4. Functional diagram of multichannel pipet

The caps are needed to seal flanged Teflon tubing against the stators as shown in Figure 3B. The Teflon tubing is flanged in our laboratory using the Durrum Flarefit flanging tool, placed in the appropriate holes in the caps and then the cap and stator are screwed together to form one unit. There are 16 lines of tubing in the top cap/stator unit forming eight vacuum lines for pulling solution into each aliquoting channel of the pipet rotor and eight pressure lines for delivering the eight solutions into the minidisc cuvettes. There are also 16 lines of tubing in the bottom cap/stator unit. These form eight lines for picking up solutions from sample and reagent cups and eight lines for delivering solutions into the minidisc. A template located below the bottom cap is used to align these tubes with the sample and reagent cups and the entrance ports to the sample and reagent cuvettes in the minidisc. This is illustrated for two tubes in Figure 3B. Each sample tube is located in the center of a sample cup and is measured to extend down to just above the bottom of the cup. This ensures that each tube is always below solution level. The delivery tips are positioned directly in the center of the cuvette entrance ports on the minidisc. They are held stationary within stainless steel sleeves.

The minidisc and sample cups are placed on a tray which has vertical movement. In the lower position, the minidisc can easily be placed on or removed from the tray, while in the upper position the sample/reagent tubes are in the sample cups and the delivery tips are in the entrance ports of the sample and reagent cuvettes. This enables solutions from each of eight cups to be drawn into the pipet, aliquoted, and delivered directly into the sample and reagent cuvettes of the minidisc.

The pipet rotor is pinned to a shaft coupled to the drive shaft of a high torque, synchronous, reversible ac motor (SLO-SYN Driving Motor, Type SS-150P2, Superior Electric Co., Bristol, Conn.). This motor moves the rotor back and forth between the aliquoting and delivery positions of the pipet. In operation, the only external moving part of the pipet is the rotor shaft since the pipet rotor is enclosed within the pipet body and between the stators.

The functional operation of the multichannel pipet is shown in Figure 4. For illustration, only one pair of channels is shown, one for the sample and one for the composite reagent. The other channels (three sample and three reagent) operate in the same manner and at the same time as the channels described. The rotor begins in the ready position which is the same as the delivery position shown in Figure 4B. A start pulse from the microprocessor activates the motor which turns the rotor 45° to the aliquoting position (Figure 4A). Here, a continuous channel exists from the sample and reagent cups through the aliquoting channels of the rotor to the vacuum lines attached to the top cap/stator unit. Since the sample and reagent tubes are positioned below the liquid level in the sample and reagent cups, applying the proper partial vacuum will pull the solutions uniformly through the proper aliquoting channel, as shown in Figure 4A. When these solutions travel above the top cap/stator unit, the rotor is turned, simultaneously aliquoting sample and reagent via a knife-edge action between the top and bottom stators. The volume aliquoted is equal to the volume of the channel in the rotor. The rotor continues turning until it has moved 45° back to the delivery position. Now a continuous channel exists from the pressure lines attached to the top cap/stator unit through the aliquoting channels in the rotor to the delivery tips positioned in the sample and reagent cuvettes of the minidisc. The proper pressure is applied to deliver the sample and reagent solutions into the minidisc cuvettes. The minidisc is removed for analysis and the rinse solution is pulled through the pipet channels using full vacuum from the vacuum source (house vacuum in this work). The rinse solution is then removed and the pipet channels are dried by the full vacuum.

Control Circuitry. The ac motor is controlled by the circuitry shown in Figure 5. The motor must turn through an angle of 45°, first counterclockwise (CCW) and then clockwise (CW). The 45° travel is determined by two encoders mounted 45° apart near the motor shaft. Each encoder consists of an infrared light-emitting diode (LED) and phototransistor mounted at an angle of 15° from each other. A reflective surface placed between the LED and phototransistor will reflect light from the LED to the phototransistor and turn it on. Attached to the motor shaft is a blackened aluminum disc with one vertical silver line on its circumference, which serves as the reflective surface for the two encoders.

The motor is turned on and off using two optically isolated, zero crossing switches (MSR 100, Monsanto, St. Louis, Mo.) which are activated by TTL signals. Two switches are needed to be able to reverse the direction of the motor. Since only one switch can be on at any one time to prevent shorting out the motor, three cases are possible: both switches off; switch #1 on, switch #2 off; and switch #1 off, switch #2 on. The triacs in parallel with each of the switches give the isolation necessary for switching the highly inductive ac motor. The switches are turned off by a HIGH logic-level signal and turned on by a LOW signal. The operational amplifier and Schmitt trigger (ST) associated with each encoder, NAND gates 1–4, and the monostable (Figure 5) are used to produce the necessary TTL signals to control the motor. Table I lists the logic level signals during operation of the pipet. Refer to both Figure 5 and Table I for the following discussion.

In the ready position, encoder #1 is ON and encoder #2 is OFF. The output of ST 1 is HIGH and ST 2 is LOW. This LOW signal is input to NAND gate 2 producing a HIGH output. The result is that both inputs to NAND gate 1 are HIGH producing a LOW output. This is input to NAND gate 4 forcing it HIGH. The *Q* output of the monostable is normally LOW which forces NAND gate 3 HIGH. Since the outputs of both NAND gates 3 and 4 are HIGH, switches 1 and 2 are both off and the motor is off.

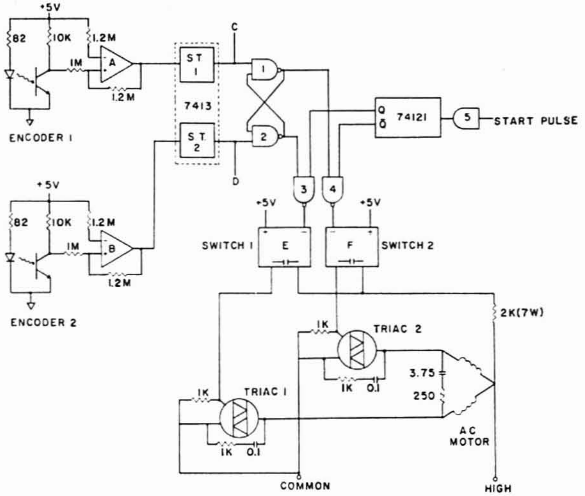

Figure 5. Control and drive circuitry for reversible, ac motor. Capacitance values in μF and resistance values in ohms unless otherwise noted. A, B are LM3900. C is delivery position status. D is aliquot position status. E, F are MSR 100

A start pulse from the microprocessor controller produces a negative-going edge at the monostable inverting Q and $\bar{Q}$. Switch 2 remains off because the $\bar{Q}$ input keeps NAND gate 4 HIGH. However, both inputs to NAND gate 3 are now HIGH producing a LOW output. This activates switch 1 which turns on triac 1 activating the motor. As soon as the motor turns, encoder #1 is turned off because the reflective surface attached to the motor shaft has moved. When the motor has turned through 45°, the reflective surface reaches encoder #2 turning on its phototransistor and the output of ST 2 goes HIGH. Both inputs to NAND gate 2 are now HIGH producing a LOW output forcing both NAND gate 1 and NAND gate 3 HIGH. NAND gate 4 is still held HIGH by Q. Both inputs to switches 1 and 2 are HIGH and the motor is stopped. This is the aliquot position and the sample and reagent solutions are pulled into the pipet. The motor remains in this position for a time equal to the adjustable delay time of the monostable (typically 5 s.).

After the delay time, the monostable returns to its original state and Q is again LOW and $\bar{Q}$ is HIGH. Switch 1 remains off because the Q input keeps NAND gate 3 HIGH. However, both inputs to NAND gate 4 are now HIGH producing a LOW input to switch 2. This turns on triac 2 and the motor is turned on, moving in the opposite direction as before. The motor turns through 45° until the reflective surface reaches encoder #1 turning on its phototransistor. The output of ST 1 is HIGH and ST 2 is LOW forcing NAND gate 2 HIGH. Both inputs to NAND gate 1 are HIGH forcing its output LOW. The output of both NAND gates 3 and 4 are now HIGH turning off the motor. This is the delivery position of the pipet and the sample and reagent solutions are delivered into the minidisc. The motor will remain in this position until another start pulse is received.

Vacuum/Pressure Module. The vacuum source has two functions in this system: to uniformly pull solutions into the pipet aliquoting channels and to wash and dry the pipet. The former function requires a finely adjusted partial vacuum while the latter requires a strong vacuum. Thus the vacuum source must be switched between partial and full vacuum quickly and easily. The pressure source is used to deliver the aliquoted solutions into the sample and reagent cuvettes of the minidisc. Both the vacuum and pressure must be properly adjusted, applied at the proper time and applied for the proper length of time. It is especially important for the pressure source to be immediately turned off when the solutions have been delivered. This is because air blowing over the solutions after delivery can enhance evaporation and bubbling of the solutions causing significant errors in volume reproducibility.

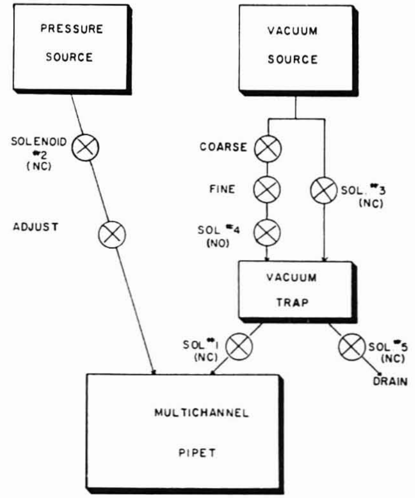

Figure 6. Block diagram of vacuum/pressure module

The components of the vacuum/pressure module are given in Figure 6. The present design requires five solenoids and three needle valves. Under microprocessor control, the solenoids (6 volt, Angar Scientific Corp., East Hanover, N.J.)

Table I. Logic Level Signals

	Ready position	CCW motor movement	Aliquot position	CW motor movement	Delivery position
ST #1[a]	H	L	L	L	H
ST #2[a]	L	L	H	L	L
Gate #1[b]	L	H	H	H	L
Gate #2[b]	H	H	L	H	H
Q of MS[c]	L	H	H	L	L
Q of MS[c]	H	L	L	H	H
Gate #3[b,d]	H	H	H	L	H
Gate #4[b,d]	H	L	H	H	H

[a] ST #1 and #2 are 7413. [b] Gates 1-4 are 7400. [c] MS is 74121. [d] Gates #3 and #4 are control inputs to switches #1 and #2 (see Figure 5).

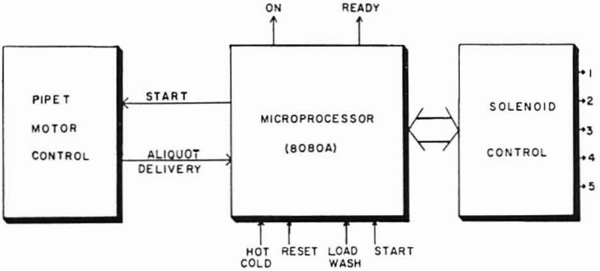

Figure 7. Block diagram of microprocessor controller

are used to open and close the vacuum and pressure lines. The needle valves in the vacuum line are used to adjust the house vacuum down to a slightly negative pressure, while the valve in the pressure line acts as a ballast for the air pressure tank regulated at 3 psi. These manual adjustments are made once daily prior to using the pipet.

For illustration, one complete cycle of the pipet is described. In the ready position all solenoids are off. After a start pulse is given, the motor turns the pipet to the aliquoting position. Here, solenoid #1 is activated applying a partial vacuum to the multichannel pipet. After aliquoting occurs, solenoid #1 is deactivated and the motor turns to the delivery position. Solenoid #2 is activated opening the pressure line to the pipet. After all solutions have been delivered, solenoid #2 is deactivated and the minidisc is ready for analysis.

The multichannel pipet must be washed and dried before another minidisc can be loaded. This is necessary to prevent any significant errors due to possible solution carry-over, which is quite possible in the delivery tips. The sample/reagent tubes are positioned in a wash solution (usually water), the WASH cycle is selected, and a start pulse is given to the microprocessor. The wash solution is aliquoted and delivered to a waste reservoir to clean the aliquoting channels and delivery tips. The delivery tips are first dried by blowing air through them for 30 s following the delivery of the wash solution. Then, solenoids #1 and #3 are simultaneously activated which applies a full house vacuum to the pipet. This rapidly pulls the wash solution through the sample/reagent tubes and the aliquoting channels. After a delay time, the wash solution is removed and the full vacuum is used to dry the pipet. This is required so that all aliquoting channels and associated tubing are clear of any drops of solution. After drying is complete solenoids #1 and #3 are deactivated and the pipet is ready to load another minidisc. This entire wash and dry cycle requires a minimum of $2^{1}/_{2}$ min.

When the vacuum trap is filled, it must be drained. Solenoid #4 is activated which isolates the vacuum source from the trap, then solenoid #5 is activated opening the trap to the drain. After draining is complete, solenoids #4 and #5 are deactivated. The vacuum trap is sufficiently large that it needs to be drained only after 20–30 minidiscs have been loaded.

Microprocessor Controller. The operations of the multichannel pipet system are handled by the microprocessor controller based on the Intel 8080A (Intel Corp., Santa Clara, Calif.). The basic system is shown in Figure 7. Located on the front panel of the microprocessor are four switches and two lights. The ON light indicates that the microprocessor is operating and the READY light indicates that the microprocessor is waiting for a start pulse. If the READY light is off, the microprocessor ignores all front panel switches except the RESET, which restarts the program.

The flow diagram in Figure 8 indicates the function of the four switches. The HOT/COLD switch refers to the start-up procedure. In a COLD start, usually a power-on start, the first step is to drain the vacuum trap. The HOT start saves time by allowing this step to be omitted. The LOAD/WASH switch determines the mode of operation: to load a minidisc with sample and reagents or to wash and dry the pipet. The START switch initiates the action of the pipet.

The program for operating the multichannel pipet consists of a main program and five subroutines and is contained in one 256 × 8 Programmable Read Only Memory (PROM) Chip (1702). As shown in Figure 8, the main program monitors the front panel switches for the mode of operation and the start pulse. When a start pulse is detected, the microprocessor reads the mode of operation (load or wash) from the front panel and goes to the appropriate subroutine. The other three subroutines are check the solenoids, drain the trap, and a timing loop. The microprocessor checks the status of all the solenoids to be certain that all are off. If they are not off or cannot be turned off, the microprocessor halts. This prevents the pipet from attempting to operate with improper solenoid control. The vacuum trap is drained by the drain the trap subroutine. The timing loop enables variable delay times to be pro-

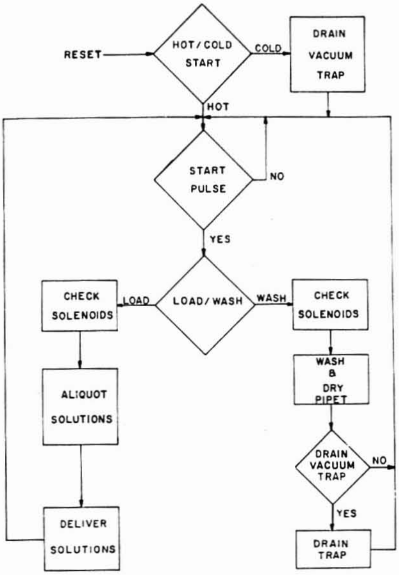

Figure 8. Flow chart of program used by microprocessor to control multichannel pipet system

grammed into the pipet operation.

The two main subroutines are the load and wash routines. If a minidisc is to be filled, the LOAD/WASH switch is set to load and the START switch is pushed. All the solenoids are checked and if all are off, a start pulse is given to the motor control circuitry (see Figures 5 and 7). The pipet moves to the aliquoting position. When the microprocessor detects that the aliquoting position has been reached, it sends a pulse to activate solenoid #1 (see Figures 6 and 7). The microprocessor deactivates solenoid #1 as soon as the pipet leaves the aliquoting position. When the delivery position is reached, the microprocessor activates solenoid #2. After a programmed delay time, solenoid #2 is deactivated and the minidisc is ready for analysis. Control of the program is returned to the main program to await another start pulse.

To wash the pipet, the wash mode is selected and a start pulse given. Again the microprocessor checks the solenoids. The delivery tips are first washed and dried as described earlier, then solenoids #1 and #3 are activated to wash and dry the pipet via a full vacuum. After a programmed delay, both solenoids are deactivated. If the vacuum trap is full, the drain the trap subroutine is called which controls solenoids #4 and #5. Control of the program is then returned to the main program as before.

The microprocessor interface is shown in Figure 9. It requires only six chips: one 74154 chip, a four-line to sixteen line decoder for the generation of the device select codes; three 74279 chips, RS flip-flops to control the five solenoids and two front panel lights; and two 8095 tri-state buffers to input status information into the microprocessor from the solenoids, the front panel switches, and the aliquot and delivery positions. Since only one tri-state buffer can be activated at one time, both inputs $\bar{G}1$ and $\bar{G}2$ are needed.

RESULTS

The multichannel pipet system has been experimentally evaluated. For the application of this pipet system to a minidisc centrifugal analyzer, the absolute volume of each channel is unimportant as long as the delivered relative volume of each pair of channels is known and is reproducible. Therefore, only relative volume and reproducibility studies have been made. The initial test of the pipet was a gravimetric evaluation using a solution of 0.1 mM paranitrophenol in 0.1 M tris(hydroxymethyl)aminomethane, pH 10.6. This solution was used because it more closely resembles the serum samples used in our laboratory. This solution was aliquoted by the multichannel pipet, delivered into four weighing bottles, and weighed. Thus results were obtained for four pairs of channels simultaneously. This experiment was repeated over a ten-day period and the reproducibility of delivery of each pair of channels is within 0.3% for both within-day and day-to-day studies. These results show the precision of aliquoting and delivery of solutions with the multichannel pipet.

Table II. Spectrophotometric Evaluation of Multichannel Pipet

Cuvet position[a]	Method[b]	N	Absorbance[c]	RSD, %
1	A	15	0.913	0.48
2	A	15	0.912	0.67
3	A	15	0.911	0.57
		Average:	0.912	0.57
		% RSD:	0.10	
4	B	15	0.911	0.46
5	B	15	0.914	0.34
6	B	15	0.913	0.37
		Average:	0.913	0.39
		%RSD:	0.16	

[a] Cuvette position refers to measurement cuvette number on minidisc. [b] Pipetting method used: A = Multichannel pipet; B = Pipetman manual pipet. [c] Absorbing solution: 10 ppm Fe, 0.1% $H_2NOH \cdot HCl$, 0.02% 1,10-phenanthroline, 1% sodium acetate.

To evaluate the performance of the multichannel pipet in normal operation and to determine relative volumes, the multichannel pipet was used to load an absorbing solution as the sample and deionized water as the reagent into the minidisc (see Figure 1). For the cuvettes not filled by the multichannel pipet, a Pipetman manual pipet, adjusted to deliver 67 μL, was used to load iron and water solutions into sample and reagent cuvettes, respectively. Thus data for both pipetting methods were obtained simultaneously on the same minidisc. The absorbing solution, measured at 509 nm, was 10 ppm iron, 0.1% hydroxylamine hydrochloride, 0.02% 1,10-phenanthroline, and 1% sodium acetate. The sequence followed was to load the minidisc with the iron solution in the sample cuvettes and water in the corresponding reagent cuvettes (first manually, then using the multichannel pipet), measure the resulting absorbance in each measurement cuvette with our centrifugal analyzer (2), clean the minidisc, and repeat. This was done 15 times and the results are given in Table II. These results show the good reproducibility of aliquoting and delivery for both methods of pipetting. Further these data show that the relative volume of each pair of channels is the same. Since the absorbance resulting from manual pipetting is known to be from an exact 1:1 dilution of the iron solution to water (67 μL:67 μL) and the absorbance determined from the multichannel pipet is nearly identical to that obtained manually, each pair of channels in the multichannel pipet must also have a 1:1 volume ratio. It should be noted that the data obtained manually are representative of an experienced technician while the multichannel pipet is technician-independent. Further, the multichannel pipet can handle eight solutions simultaneously, while only one solution at a time can be handled manually.

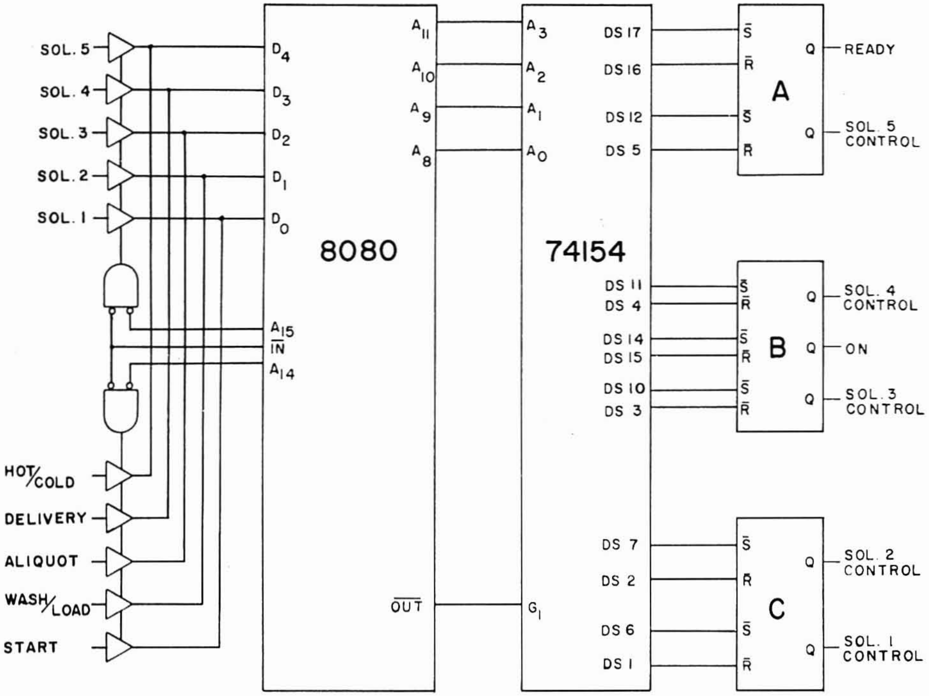

Figure 9. Microprocessor interface circuitry for control of multichannel pipet system. A, B, C are 74279. The two tri-state buffers are 8095 (54365)

The multichannel pipet was also evaluated by a rate method analysis of glucose. Aqueous glucose standards were prepared in the range of 40–200 mg/dL and analyzed by a modified glucose oxidase–peroxidase procedure (*3*). These standards were used to calculate a working curve based on several loadings of the minidisc with both manual and multichannel pipetting. Then a 50 mg/dL aqueous standard was analyzed several times via this averaged working curve. The concentration determined with the multichannel pipet was 50.9 mg/dL with a precision of 1.00% while that determined manually was 50.5 mg/dL with a precision of 1.15%. These results further demonstrate the performance of the multichannel pipet. The multichannel pipet and manual pipet data are almost identical. However, the multichannel pipet is significantly faster than the manual, sequential pipetting method.

The results obtained with the multichannel pipet show that the parallel aliquoting and delivery of solutions into minidiscs is a viable and reliable approach to the sample-handling problem. This pipet has been in use in our lab for over two years. The present design of eight aliquoting channels has improved sample throughput with no loss in precision. Further, the design of the multichannel pipet has the advantages of minimal sample carry-over and elimination of aliquoting with the delivery tips. The carry-over for a pair of aliquoting channels is less than 0.9% and is not significant after one aliquoting and delivery cycle. Sample carry-over is limited to the delivery tips because for proper aliquoting, solution must travel above the aliquoting channel and is discarded. This discarded solution cleans out the channel as it travels upward. Aliquoting is done inside the pipet body eliminating design constraints on the delivery tips. Further, these aliquoting channels remain stationary and all aliquoting and delivery is done from the same position. This avoids problems of gravity effects associated with aliquoting and delivery from different positions.

There are some disadvantages of the current design. The solution volumes are fixed by the volume of the aliquoting channels. It is time-consuming and impractical to change the volume. However, the volume of the sample and reagent cuvettes in our minidiscs is also fixed and determines the volume needed. The solution waste of the pipet is about 50 μL per channel. This is due to the discarded solution which travels above the aliquoting channels. However, this solution does minimize carry-over by priming the channels.

Only having eight aliquoting channels has limited the application of the pipet. However, this pipet has demonstrated that the concept of parallel aliquoting and delivery of solutions is sound and deserves further work.

Presently the concepts described here are being applied to the design and construction of a 24-channel pipet. A method of optically encoding the solution travel in each channel of the pipet has been tested and will be used with the new pipet. This will provide positive feedback for each channel and improve the reliability and performance of the pipet.

ACKNOWLEDGMENT

The authors express their gratitude to Jim Perry for his valuable assistance with the design of the microprocessor

system.

LITERATURE CITED

(1) C. A. Burtis, W. F. Johnson, and J. B. Overton, *Anal. Chem.*, **46**, 786 (1974).
(2) J. Avery, R. P. Gregory IV, B. W. Renoe, T. Woodruff, and H. V. Malmstadt, *Clin. Chem.* (*Winston-Salem, N.C.*), **20**, 942 (1974).
(3) L. Morin and J. Prox, *Clin. Chem.* (*Winston-Salem, N.C.*), **19**, 959 (1973).

RECEIVED for review February 10, 1977. Accepted June 27, 1977. Presented in part at the Third Annual FACSS meeting, Philadelphia, Pa., November, 1976. This work was supported in part by NIH Grant HEW PHS GM 21984-02.

Determination of Low Levels of Sulfur in Organics by Combustion Microcoulometry

D. C. White

British Petroleum Company Limited, Group Research and Development Department, Analytical Branch, Sunbury-on-Thames, Middlesex, England

A combustion system for the determination of sulfur by oxidative combustion-microcoulometry is described. The conditions have been selected so that the conversion of organic sulfur to SO_2 is close to 100%, the conversion being largely independent of matrix and sulfur function type. The technique has been applied to a wide range of petroleum products (residual fuel and wax to low boiling products), and to natural gas. In addition, coking problems sometimes encountered with higher boiling products are avoided. The limit of detection is 0.2 ppm by weight and the standard deviation at the 1 to 2 ppm level is 0.1 ppm by weight.

The use of combustion-microcoulometry for the determination of traces of sulfur, nitrogen, and chlorine is now quite familiar, mainly as the Dohrmann system. Such a system was used for the determination of trace amounts of chlorine (*1–4*). Applications to the determination of trace amounts of sulfur are more numerous, finding considerable use in the petroleum industry (*5–17*).

From the literature, it is evident that the oxidative route has been strongly favored in practice (*7–17*) but the performance has never been entirely satisfactory, especially in correlative work. It was considered, however, on the basis of the work by Dixon (*11*) and Cedergren (*13*), that considerable improvements in the efficiency of conversion of organic sulfur to sulfur dioxide should be possible by proper choice of combustion conditions.

Consideration of the equilibria involved in the reaction $SO_2 + {}^1/_2O_2 \rightleftharpoons SO_3$ show that a high sulfur dioxide yield is favored by high temperature and low partial oxygen pressure. At high enough temperatures, the sulfur dioxide yield is largely independent of oxygen partial pressure, e.g., combustion at 1420 °C with an oxygen partial pressure of 1 atm gives a yield of 98%, compared with about 75% at 930 °C (*18*). At lower temperatures, the yield is increasingly dependent on oxygen partial pressure. The relationship can be seen in Figure 1 (*13*). It is evident that unless very high furnace temperatures are used, high sulfur dioxide yields can be obtained only practically by the maintenance of low oxygen partial pressure.

Combustion conditions have commonly employed pyrolysis and volatilization of the sample in an inert gas (nitrogen, helium, argon) at 400–700 °C, which gas stream is then passed into an oxygen atmosphere in a main furnace at about 700–950 °C where sample oxidation takes place. The oxygen/inert gas ratio varies from 1:4 to 4:1. Under these various conditions, the sulfur dioxide yield lies typically between 70 and 85%.

The problem with using a low oxygen partial pressure in the oxidation zone in conjunction with a furnace temperature no greater than 950 °C is that of ensuring complete oxidation of the organic material. Incomplete oxidation leads to the formation of olefins or aldehydes etc. which react with iodine in the cell to give spurious values (*7, 8*), and carbonaceous deposits may also form in the inlet or outlet portion of the combustion tube.

These problems have been overcome in the system developed and described here which uses a combination of the methods of Dixon (*11*) and Cedergren (*13*). It involves injection of the sample into an oxygen–helium mixture in an injection section at 700 °C where complete or nearly complete oxidation occurs at a high flame temperature followed by dilution with a large flow of helium in a combustion/equilibration zone. About 100% recoveries of organic sulfur as sulfur dioxide are obtained, largely independent of sample type or matrix.

EXPERIMENTAL

Apparatus and Reagents. A diagram of the apparatus is shown in Figure 2. A Dohrmann S-350 pyrolysis furnace is used with three separately controlled sections, inlet, center, and outlet, together with valves and flowmeters for the carrier and combustion gases. The temperatures are shown in Figure 3. The combustion tube is made in clear quartz and is detailed in Figure 4.

A cooling chamber is provided, made exactly as the water absorber described by Lädrach (*3*) except that the side entry for filling is omitted. Initially in the measurement of sulfur it was used purely for convenience in linking the combustion tube and cell. It was, however, permanently retained because it was thought to perform the useful function of cooling the gases before entry to the cell. The inlet tube to the absorber was heated to ca. 70 °C as before.

The titration cell used is similar to the Dohrmann T-300-P titration cell, except that the multicapillary glass barriers between the various compartments are replaced by specially cut glass sinters. The reference electrode is a platinum wire immersed in the cell electrolyte saturated with iodine. An excess of solid iodine is also present. The indicating and generating electrodes are pure platinum foil (ca. 7 mm square).

The cell is supported on a 250-rpm synchronous magnetic stirrer (Grant Instruments, Cambridge, England). Cell plus stirrer are enclosed in an aluminum cabinet (30 × 16 × 16 cm). This, as well as protecting from drafts, provides electrical screening by connecting the cabinet to the amplifier chassis earth.

The coulometer produces pulses of titrating current of constant amplitude and length. The number of pulses is recorded by a digital counter and is proportional to the amount of substance

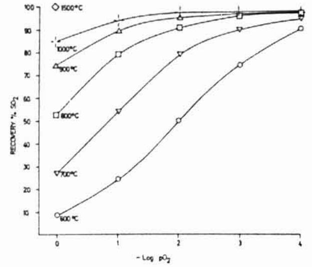

Figure 1. Theoretical recovery of SO_2 in equilibrium with O_2 and SO_3 as function of temperature and oxygen pressure

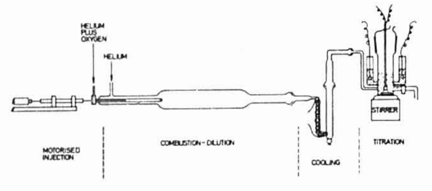

HELIUM PLUS OXYGEN
HELIUM
STIRRER
MOTORISED INJECTION
COMBUSTION - DILUTION
COOLING
TITRATION

Figure 2. Diagram of apparatus

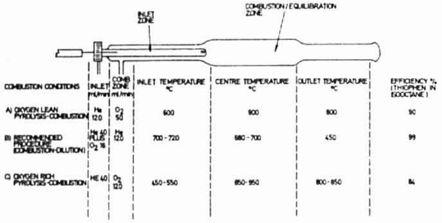

INLET ZONE
COMBUSTION / EQUILIBRATION ZONE

COMBUSTION CONDITIONS	INLET ml/min	COMB ZONE ml/min	INLET TEMPERATURE °C	CENTRE TEMPERATURE °C	OUTLET TEMPERATURE °C	EFFICIENCY % (THIOPHEN IN ISOOCTANE)
A) OXYGEN LEAN PYROLYSIS-COMBUSTION	He 120	O_2 50	600	900	800	90
B) RECOMMENDED PROCEDURE (COMBUSTION-DILUTION)	He 40 PLUS O_2 16	He 120	700 - 720	680 - 700	450	99
C) OXYGEN RICH PYROLYSIS-COMBUSTION	HE 40	O_2 120	450 - 550	850 - 950	800 - 850	84

Figure 3. Gas flows, furnace temperatures, and efficiencies for various combustion conditions

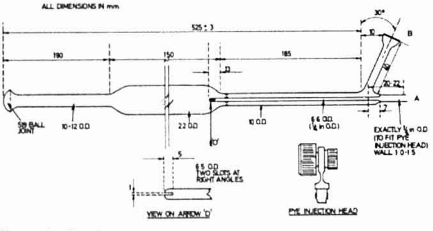

ALL DIMENSIONS IN mm
525 ± 3
190
150
185
30°
10
B
A
20-22
7
S18 BALL JOINT
10-12 O.D.
22 O.D.
10 O.D.
6.6 O.D. (¼ in O.D.)
EXACTLY ¼ in O.D. (TO FIT PYE INJECTION HEAD) WALL 1.0-1.5
D
5
6.5 O.D. TWO SLOTS AT RIGHT ANGLES
VIEW ON ARROW 'D'
PYE INJECTION HEAD

Figure 4. Combustion tube

titrated. The mean current is proportional to the frequency of the pulses and an analogue voltage output to which the pulse frequency is proportional is provided for continous recording. A supplementary current unit bleeds a small, variable, nonintegrated continuous current into the cell to compensate for cell drift and so maintain a near zero titration baseline. Since the amount of titrating current produced is related to the digital output by the pulse amplitude and width, in practice the system is calibrated by injecting known amounts of standards into the furnace. Such a coulometer is easier to design for stable operation and less expensive to make than those employing a continuous titrating current, avoiding as it does the need for a current integrating device. Certain features of the coulometer are the subject of Patent Cover. A block diagram is shown in Figure 5.

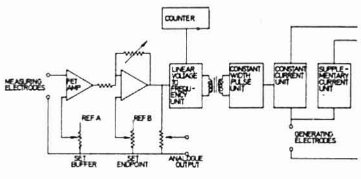

COUNTER
MEASURING ELECTRODES
FET AMP
REF A
REF B
LINEAR VOLTAGE TO FREQUENCY UNIT
CONSTANT WIDTH PULSE UNIT
CONSTANT CURRENT UNIT
SUPPLEMENTARY CURRENT UNIT
GENERATING ELECTRODES
SET BUFFER
SET ENDPOINT
ANALOGUE OUTPUT

Figure 5. Pulse coulometer

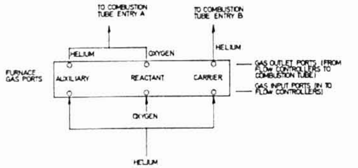

TO COMBUSTION TUBE ENTRY A
TO COMBUSTION TUBE ENTRY B
HELIUM
OXYGEN
HELIUM
FURNACE GAS PORTS
AUXILIARY
REACTANT
CARRIER
GAS OUTLET PORTS (FROM FLOW CONTROLLERS TO COMBUSTION TUBE)
GAS INPUT PORTS (IN TO FLOW CONTROLLERS)
OXYGEN
HELIUM

Figure 6. Gas supplies to Dohrmann furnace and combustion tube

Helium and oxygen are supplied to Negretti-Zambra pressure regulators (set at 10-psi output pressure) and thence to the gas entry ports of the furnace. The configurations used are shown in Figure 6.

A Hamilton 10-μL syringe 701 with 3-inch needle is most suitable for liquid samples.

For gas samples, a 20 μL Summit all-glass syringe is used fitted with a 2-inch detachable needle.

It is essential that a slow and controlled rate of sample injection be used. A hand operated device comprises a cradle in which the syringe lies. A plate travelling on a threaded rod engages the plunger and pushes it forward. A hand operated crank on the threaded rod provides the necessary forward travel. The threaded rod has a pitch such that one complete turn of the handle per second provides an injection rate of ca. 1 μL/s.

A motor driven device is based on the same principle. The push rod is driven by a 30-rpm synchronous motor to give an injection rate from a 10-μL Hamilton syringe of 1 μL/11 s. By changing to a larger cradle to accommodate the 20-mL syringe and exchanging the drive motor to a 15-rpm motor, gases are injected at a rate of 1 mL/11 s. The cradle and motor are quickly interchangeable.

The preferred electrolyte is that described by Clare (*9*), made up of potassium iodide AR (0.001 g), potassium bromide AR (0.20 g), and acetic acid AR (0.05 g) dissolved in 100 mL distilled water.

If nitrogen or chlorine are present in the sample, an azide-containing electrolyte may be used instead (*5*).

Recommended Procedure. The gas connections are shown in Figure 6 and the flows and furnace temperatures in Figures 3B. High temperature combustion takes place in the inlet zone of the combustion tube in the 1 to $2^1/_2$ mixture of oxygen and helium (16 mL/min oxygen plus 40 mL/min helium). On entry to the combustion/equilibration zone, rapid dilution with helium (120 mL/min) then takes place, together with cooling to 680–700 °C, at which temperature the oxidation of sulfur dioxide to trioxide is slow (*13*). At the same time it is considered that the temperature in the combustion/equilibration zone is high enough to ensure oxidation of any residual organic fragments. Assuming that a liquid hydrocarbon (e.g., heptane, toluene) is injected at the rate of 1 μL/11 s or a gaseous hydrocarbon (e.g., methane) injected at the rate of 1 mL/11 s, then the oxygen concentration in the combustion/equilibration zone will be 2 to 3% by volume so that in the equilibrium $SO_2 + {}^1/_2O_2 \rightleftharpoons SO_3$ formation of SO_2 is favored, see Figure 1. When a sample has been taken into a syringe, the needle is inserted fully through the septum into the furnace until the "needle peak" has completely emerged. This peak is due to liquid or material from the septum on the inside or outside of the needle.

Although rapid deterioration of the needle of the injection syringe might be expected in the oxidative conditions of the combustion tube inlet, in fact this is not so, and prolonged use of a stainless steel needle for sample injection in this mode has

Table I. Effect of Matrix and Sulfur Function Type on Combustion Efficiency-Recommended Procedure

	Solvent					
	Isooctane		Toluene		Methanol	
Compound	Efficiency, %	No. of Expts.	Efficiency, %	No. of Expts.	Efficiency, %	No. of Expts.
Butyl ethyl sulfide	91.2	4	98.8	3	98.1	4
$(C_4H_9)(C_2H_5)S$	99.4	3			98.2	1
Phenyl sulfide	96.3	4	100.1	3	99.1	4
$(C_6H_5)_2S$	98.1	2			94.9	3
Butyl mercaptan	97.0	4	98.5	3	94.6	2
C_4H_9SH						
Thiophene	99.4	37	101.9	4	100.9	4
$CH{=}CHCH{=}CHS$		std dev,	102.6	4	97.4	3
		2.2%	99.1	4		
Dimethyl sulfoxide			97.2	3	96.6	3
CH_3SOCH_3			99.2	5		
Dimethyl sulfolane			102.3	3	99.2	3
$CH_3CHCH_2CH(CH_3)CH_2SO_2$					99.5	2

had no adverse effect. If pure oxygen is used for the inlet gas, then it is essential to use a platinum needle (*11*).

RESULTS AND DISCUSSION

The term pyrolysis is used to refer to the process occurring in the inlet section when a sample is injected into inert gas, and where it is considered that pyrolysis as well as volatilization takes place. When oxygen is added to these organic products at a later stage, the process then occurring is referred to as oxidation rather than oxidative pyrolysis.

Initial work was carried out using pyrolysis in helium in the inlet section with subsequent oxidation by addition of oxygen into the center oxidation section, this being the most commonly used procedure (cf. introduction). This procedure is referred to as "pyrolysis-combustion." The gas flows (helium 120 mL/min, oxygen 50 mL/min) and furnace temperatures (Figure 3A) were similar to those specified in the ASTM procedure (*15*). The efficiency (conversion of organic sulfur to sulfur dioxide) was 90% for thiophen in isooctane but results were not as repeatable as would be desired. A slow sample injection rate (1 μL/10 s) was employed.

In view of the work of Dixon (*11*) and Cedergren (*13*), it was decided to attempt bringing the conversion of organic sulfur to sulfur dioxide nearer to 100% by application of the principle of high temperature combustion in oxygen followed by dilution with helium to a low oxygen concentration mixture. This procedure is referred to as "combustion-dilution". A center furnace temperature of 800 °C was initially used; however an improvement in recovery was found on reducing this to 700 °C.

Although the formation of carbonaceous deposits is a problem associated with the pyrolysis-combustion technique, provided a proper rate of sample injection is observed in the combustion-dilution technique, this cannot occur, and in fact no such deposits have been observed over a long period of operation. The fear has also been expressed that the high recovery using these conditions may be due in part to products of incomplete oxidation reaching the cell and resulting in spuriously large titration. This possibility is rendered extremely unlikely by the negligible responses obtained from the combustion of sulfur-free hydrocarbon samples such as isooctane, toluene, and methane.

Calibration of Titration Cell and Combustion Efficiency. Cell calibration by direct introduction of sulfur dioxide in water was carried out, replicate measurements being made on each occasion, and having a relative standard deviation of 1% or better. Comparison between the response factor obtained in this way, and also by combustion of a thiophen in isooctane standard gave a measure of the combustion/absorption efficiency. The mean value for combustion efficiency obtained in this way was 99.4% with a standard deviation of 0.9%.

Table II. Analysis of Reference Gas Samples (Ethane thiol doped natural gas)

Added S, theory		Added S, found			
ng/mL	ppm by weight	ng/mL	ppm by weight	No. of expts.	Std dev, ppm by weight
1.81	2.33	1.93	2.48	4	0.15
2.77	3.56	2.73	3.51	2	±0.04
3.88	4.99	3.89	5.01	5	0.13
7.06	9.09	7.26	9.34	5	0.09

Effect of Matrix and Sample Type. Experiments were carried out to establish the effect of solvent matrix and type of sulfur function on the combustion efficiency. Solutions of butyl ethyl sulfide, phenyl sulfide, butyl mercaptan, thiophen, dimethyl sulfoxide and dimethyl sulfolane were made up in isooctane, toluene, and methanol.

During each day, calibrations were carried out using thiophen in isooctane, and the results for other solutions referred to the mean calibration value, assuming the combustion efficiency for thiophen/isooctane to be 99.4%. The results are shown in Table I. Each value is the mean obtained on any day. From the total of 25 mean values obtained on the 16 different solutions, the mean combustion efficiency is 98.4% with a standard deviation of 2.5%. One can therefore assume that, for the solvents and compound types examined, the use of the same calibration factor irrespective of compound type or matrix would give the correct results ±5% relative for 95% of determinations.

Analysis of High Boiling Materials. Problems have been recognized in the analysis of high boiling materials, especially using pyrolysis-combustion when coke formation can occur in the inlet part of the combustion tube—although this is less likely to occur using combustion-dilution. A further cause of difficulty arises where there are components of differing boiling points in the sample of which the lighter evaporate from the injection needle leaving the residual less volatile components. When a high boiling viscous sample is diluted with a lower boiling hydrocarbon in order to reduce the sulfur level or decrease the viscosity, the same problem will arise (*5*, *11*). Thus dilution of a waxy distillate (S = 2.1%) into toluene gave results about half those expected. This problem is overcome by dilution of the high boiling sample with a sulfur-free diluent of a comparable boiling range. A suitable diluent is light liquid paraffin (*11*) (which has a suitably low

Table III. Effect of Matrix and Sulfur Function Type on Combustion Efficiency-Oxygen Rich Pyrolysis-Combustion

	Solvent					
	Isooctane		Toluene		Methanol	
Compound	Efficiency, %	No. of Expts.	Efficiency, %	No. of Expts.	Efficiency, %	No. of Expts.
Phenyl sulfide $(C_6H_5)_2S$	84.4	4				
Butyl mercaptan C_4H_9SH	76.3	2				
Thiophen CH=CHCH=CHS	83.6	8 standard deviation 1%	90.4	4	81.5	4
Dimethyl sulfoxide			80.8	3		

viscosity) and which has been successfully used for the analysis of residual fuel and waxy distillate. Residual fuel: expected, 1.97%; found, 2.09, 1.82%. Waxy distillate: expected, 2.07%; found, 1.94%.

Analysis of Gases. Some work was carried out to demonstrate the application of the method to hydrocarbon gases such as natural gas.

The motor-driven sample injection device was modified to accept a 20-mL syringe. The syringe was flushed from a flowing stream of the gas sample, filled to the 15-mL mark and the gas sample introduced into the combustion tube with minimum delay. The needle was inserted just through the rubber septum so that it remained cool and thus eliminated the needle peak.

It was considered desirable to set up hydrocarbon gas samples of known sulfur content so as to validate the procedure used. The method adopted was the permeation tube cell, using ethane thiol since the risk of condensation onto the glass syringe surfaces would then be minimal. Natural gas (ca. 95% methane), stored in a mild steel cylinder, was used as carrier.

Samples of ethane thiol doped natural gas (15 mL) were taken from the sampling point after the permeation tube and injected into the furnace, as described above. The results are shown in Table II. The sulfur content of the gas as drawn directly from the cylinder was determined in the same way and established as 0.136 ng/mL (0.175 ppm by weight) with a standard deviation (9 measurements) of 0.066 ng/mL (0.08 ppm by weight). Calibration was carried out as for liquid samples.

Comparison between Recommended Procedure and Pyrolysis-Combustion Procedure. A comparative study was made between the Recommended Procedure and pyrolysis-combustion conditions employing a large excess of oxygen over helium in the oxidation stage (oxygen rich). In this case the sample was pyrolyzed in helium at 40 mL/min at 450–550 °C and then oxidized by the addition of 120 mL/min oxygen at 900 °C. The temperature of the outlet furnace was 800–850 °C (Figure 3C). As already discussed, one would expect a reduced efficiency of conversion of organic sulfur to sulfur dioxide with this arrangement.

Some of the solutions described above were analyzed using these conditions. Again the efficiency obtained for the thiophen/isooctane solution was established by a simultaneous check measurement of the cell calibration using sulfur dioxide solution. The results are shown in Table III. The efficiency for thiophen/isooctane is seen to be 84%, as compared with 99% for the Recommended Procedure. The mean efficiency for the 6 solutions is 83% with a relative standard deviation of 5.1%. The efficiency is therefore lower and more variable. A comparison was also carried out between the Recommended Procedure, pyrolysis-combustion using an oxygen lean atmosphere in the oxidation stage (helium 120 mL/min, oxygen 50 mL/min with the furnace temperatures shown in Figure 3A), and the above pyrolysis-combustion conditions using an oxygen rich atmosphere in the oxidation stage (Figure 3C), all the experiments being carried out on the same day by appropriate adjustments of furnace temperatures and gas flow rates. All the experiments were carried out on a thiophen/isooctane solution (24 μg S/mL), and a check on the cell calibration was carried out to ascertain that no change had taken place.

The efficiences found were: oxygen lean pyrolysis-combustion, 91.5%; oxygen rich pyrolysis-combustion, 85.3%; recommended procedure, 98.6%.

A comparison between the recommended procedure and oxygen rich pyrolysis-combustion, using the azide containing electrolyte (*5*), carried out at a later date gave a recovery of 76% for the latter compared with the former.

ACKNOWLEDGMENT

The author is especially indebted to J. Martin of the Instrument Development Section of this Division for his design of and expert assistance with the optimization of the pulse coulometer.

LITERATURE CITED

(1) D. M. Coulson, and L. A. Cavanagh, *Anal. Chem.*, **32**, 1245 (1960).
(2) R. A. Hofstader, *Microchem. J.*, **11**, 87 (1966).
(3) W. Lädrach, F. van de Croots, and P. Gouverneur, *Anal. Chim. Acta*, **50**, 219 (1970).
(4) A. Cedergren and G. Johansson, *Talanta*, **18**, 917 (1971).
(5) L. D. Wallace, D. W. Kohlenberger, R. J. Joyce, R. T. Moore, M. E. Riddle, and J. A. McNulty, *Anal. Chem.*, **42**, 387 (1970).
(6) H. A. Braier, J. Eppolito, and W. C. Zemia, "The Comparison of Trace Sulfur Measurements by Microcoulometry-Oxidative vs. Reductive Mode", paper presented before the Division of Petroleum Chemistry, 165th National Meeting of the American Chemical Society, Dallas, Texas, April 8–13, 1973.
(7) H. V. Drushel, "Determination of Sulfur, Nitrogen, and Chlorine in Petroleum by Microcoulometry", paper presented before the Division of Petroleum Chemistry, 158th National Meeting of the American Chemical Society, New York, N.Y., September 7–12, 1969.
(8) F. C. A. Killer and K. E. Underhill, *Analyst (London)*, **95**, 505 (1970).
(9) F. E. Clare, "Use of the Dohrmann Coulometric Titrator for Sulfur Analysis", Shell, Stanlow, England, September 1971, private communication.
(10) D. Fraisse, *Bull. Soc. Chim. Fr.*, **4**, 1521 (1971).
(11) Jean P. Dixon, *Analyst (London)*, **97**, 612 (1972).
(12) J. M. Carter, *Analyst (London)*, **97**, 929 (1972).
(13) A. Cedergren, *Talanta*, **20**, 621 (1973).
(14) F. C. A. Killer, "Sub-ppm Sulfur Analysis by Microcoulometry", "Recent Analytical Developments in the Petroleum Industry", D. H. Hodges, Ed., Applied Science Publishers Ltd., England, 1974, Chap. 10.
(15) ASTM D3120-72T "Tentative Method of Test for Trace Quantities of Sulfur in Light Liquid Petroleum Hydrocarbons by Oxidative Microcoulometry".
(16) G. de Groot, P. A. Greve, and R. A. A. Maes, *Anal. Chim. Acta*, **79**, 279 (1975).
(17) Dohrmann Application Note M. C. 301 (7.1.71).
(18) W. G. Rice-Jones, *Anal. Chem.*, **25**, 1383 (1953).

RECEIVED for review August 2, 1976. Accepted May 16, 1977. The permission of the British Petroleum Co. Ltd. to publish this work is gratefully acknowledged.

Weak Peak Enhancement by Selective Ion Trapping in a Quadrupole Ion Storage Source

G. Lawson[1] **and J. F. J. Todd***

Chemical Laboratory, University of Kent, Canterbury, Kent, CT2 7NH, U.K.

The combination of a three-dimensional quadrupole ion storage source (QUISTOR) with a conventional quadrupole mass filter is shown to provide a means of enhancing the intensities of weak mass spectral peaks, and to be of potential use when samples are present in only trace amounts.

Current research trends, particularly in the biochemical and environmental fields have confronted chemists with the task of applying modern analytical techniques to the problem of detecting exceedingly low levels of particular species. Such concentrations may arise because the sample is either a low volatility (e.g., biochemical) compound or is in the form of trace amounts of substances in an excess of other gases, pollutants in air for example. This need to increase sensitivity has been particularly acute in mass spectrometry (*1, 2*) and although the fundamental difficulty, insufficient density of sample molecules, is the same in both applications, two separate approaches have been employed. Substances of biochemical interest are generally highly polar, have high molecular weights, and possess low vapor pressures even at elevated temperatures; the general technique for dealing with such compounds is derivatization to increase the volatility. This procedure is not only time-consuming, but may be virtually impossible if only small quantities of the original material are available. In this regard, field ionization and desorption are among the new approaches which have proved successful for a large number of compounds of low volatility (*3, 4*), as well as affording a means of reducing the extent of fragmentation, as does chemical ionization (*5, 6*). On the other hand, direct admission of an air sample containing a pollutant into a mass spectrometer ion source leads to a situation in which virtually all of the ionization products are of no interest, e.g., N_2^+, O_2^+, etc. This difficulty may be alleviated by pre-concentration techniques such as liquid nitrogen freeze-out (*7, 8*), the incorporation of a membrane separator (*9*), or more commonly the direct combination of a gas chromatograph to the mass spectrometer (*10*).

In all of the above methods there can be little or no direct control of either the ions that are formed in the source or the ions leaving the source prior to analysis, although use of different chemical ionization reagent gases does afford a degree of specificity. The ideal ion source, particularly one for monitoring pollutants, should be capable of creating, or at least preparing for analysis, only those ions of interest to the investigator. The retention of such species would allow the buildup of a sufficient number of ions to facilitate detection and analysis. The use of both the three-dimensional quadrupole ion storage (QUISTOR) (*11–13*) device and trapped ion cyclotron resonance (ICR) (*14–16*) makes it possible to retain ions of either a single or a range of m/e values. In this paper we describe the first of these techniques, in which a quadrupole ion storage device is used in place of the ion source of a conventional quadrupole mass filter. This apparatus differs from the ICR instrument (*16*) in as much that a separate analyzer is incorporated. This combination of instruments effectively produces an analyzer with a mass selective ion source capable of storing ions over extended periods. In terms of the analytical problems discussed above, the ability to reject all ions except those of interest is a considerable advantage.

THEORETICAL

In order to readily understand the chosen mode of operation of the Quistor/quadrupole combination, it is necessary to consider, in some detail, the behavior of a conventional quadrupole mass filter when scanning in the zero resolution, "total pressure mode". Despite the large volume of research data published concerning the performance of the quadrupole mass filter, it is somewhat surprising that so little attention has been paid to this aspect.

The operation of the quadrupole mass filter, comprising an array of four accurately parallel rod electrodes, can be explained (*17*) in terms of the "stability" of the ion trajectories, which themselves are described by Mathieu equations of the type

$$\frac{d^2u}{d\gamma^2} - (a + 2q \cos 2\gamma)u = 0$$

in which u represents the displacement of the ion from the origin. The values of the quantities a and q determine whether, by lying within the boundaries of the area shown in Figure 1, the trajectories are periodic such that an ion traverses the axis of the electrode structure, or whether the amplitudes of the oscillations continue to increase such that the ions collide with the electrodes. a, q, and γ are related to the physical parameters of the mass filter by

$$a = \frac{4eU}{mr_0^2\Omega^2},\ q = \frac{2eV}{mr_0^2\Omega^2},\ \text{and}\ \gamma = \Omega t/2$$

where U and V are the maximum potential differences, dc and rf, respectively, between opposing electrodes, r_0 is the radius of the inscribed circle tangential to the rods and $2\pi\Omega$ is the angular frequency of the applied rf power. Normal (i.e., mass selective) operation of the instrument is achieved by using scan line 1 (Figure 1) in which the values of U and V are scanned such that U/V remains constant. On the other hand, reference to Figure 1 suggests that operation along the q-axis (scan line 2), i.e., with zero dc field ($a = 0$), would result in a range of masses satisfying the criterion $0 \leq q \leq 0.9$ and hence that these would be transmitted by the analyzer. If we limit this argument further then for a particular ionic species, provided q has a value within this range, there appears to be no obvious reason to suppose anything other than invariant transmission efficiency through the rod structure. Thus for a system having a constant rate of sample ion generation, the expected signal output as a function of the applied rf potential should be as shown in Figure 2a. However the observed signal, for example as measured for N_2^+ formed from nitrogen containing traces

---

[1] Present address, Rubber and Plastics Research Association, Shawbury, Shrewsbury Shropshire, U.K.

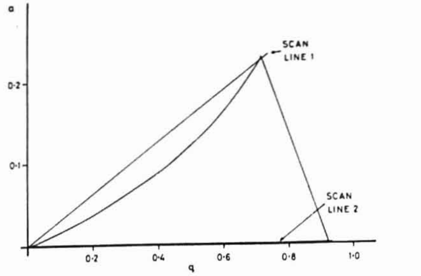

Figure 1. Stability diagram for a conventional quadrupole mass filter

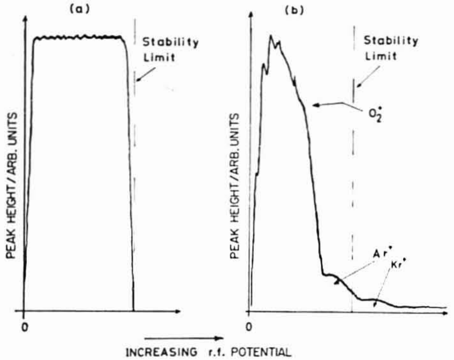

Figure 2. (a) "Expected" and (b) observed dependence of the transmission of N_2^+ ions, formed from nitrogen-containing traces of oxygen, argon, and krypton, through a quadrupole mass filter operating in the "total pressure mode" (i.e., with zero dc bias) upon the applied rf potential. With the mass filter employed in this work, an E.A.I. Quad 250A, the potential corresponding to the stability limit (indicated by the dashed line) was found to be ca. 760 V peak-peak.

of oxygen, argon, and krypton (Figure 2b), shows that a definite maximum ion transmission occurs at a potential corresponding to a q value in the range $0.3 \leq q \leq 0.4$. A further aspect of this phenomenon is that when the ion signal from a mixture of two gases of widely differing masses, e.g., nitrogen and krypton, is plotted as a function of the applied rf potential, two humps are seen, the maxima of which occur at potentials having the same ratios as the masses. Calculation shows that the maxima occur over the same range of q values for each of the gases. Thus the total pressure mode output, for equal partial pressures of nitrogen and krypton, has the form shown in Figure 3, a feature which is also apparent for O_2^+, Ar^+, and Kr^+ seen as fine structure in Figure 2b. Operation of the quadrupole at an rf potential corresponding to point A would result in only nitrogen ions being transmitted by the analyzer. Similarly for conditions corresponding to point B, only krypton ions will reach the detector despite equal numbers of both ions being created in the ion source.

An analogous effect has found to occur in the Quistor. Thus the number of ions stored within the device, as indicated by the number collected following pulsed ejection from the trap after a given storage time, exhibits a maximum at a constant value of q regardless of the m/e value of the ion concerned. An explanation of this has been advanced (*18*) on the basis that the maximum number of ions which may be contained within the Quistor (i.e., ignoring ion-loss processes) is a compromise between the probability of an ion when initially formed having a stable trajectory lying within the bounds of the electrode structure, which decreases as q increases, and the efficiency of ion trapping, which is favored at high q values (*18, 19*). This behavior inevitably, therefore, gives rise to a degree of mass selectivity in the Quistor, even in the "zero resolution" mode, and is particularly pronounced when a mixture of ions contains species of widely differing masses.

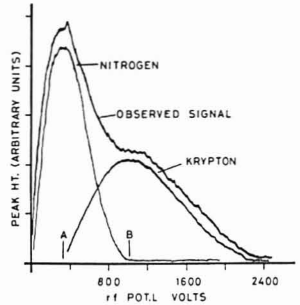

Figure 3. Observed "total pressure" signal for a quadrupole mass filter sampling a mixture of nitrogen and kryton at equal partial pressures together with the signals obtained with each gas separately

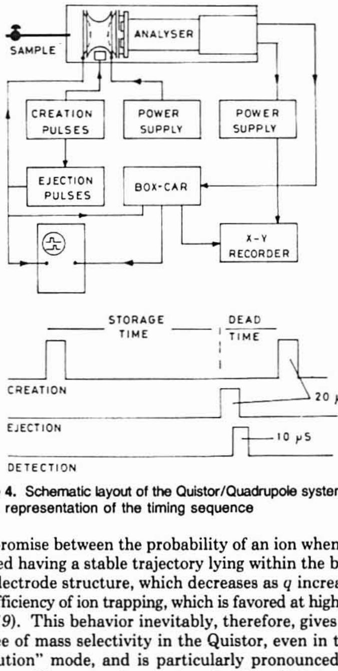

Figure 4. Schematic layout of the Quistor/Quadrupole system together with a representation of the timing sequence

EXPERIMENTAL

The experimental apparatus and timing sequence were essentially the same as that designed in this laboratory and developed over a number of years (*20–23*); they are shown schematically in Figure 4. Ions, created within the device by a pulse of nominally 50-eV electrons, are subjected to oscillating electric fields generated by applying radiofrequency power to the ring electrode only. After a predetermined storage time, the ions are ejected from the trap into the quadrupole mass filter by differentially biasing the end-cap electrodes. The ion pulse arriving from the detector is gated, at a given delay time within the boxcar amplifier, so that spuriously ejected ions from the Quistor are not recorded. The system is operated at a repetition frequency of 100 Hz and under these conditions, a slow mass sweep of the

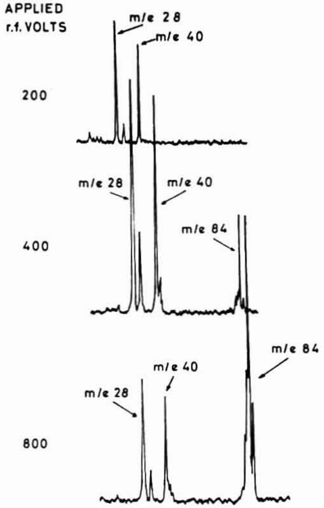

Figure 5. Mass spectra of ions ejected from the ion storage source operating at the potentials shown for a sample mixture comprising equal partial pressures of air, argon, and kryton at a total pressure of ca. 1×10^{-4} Torr

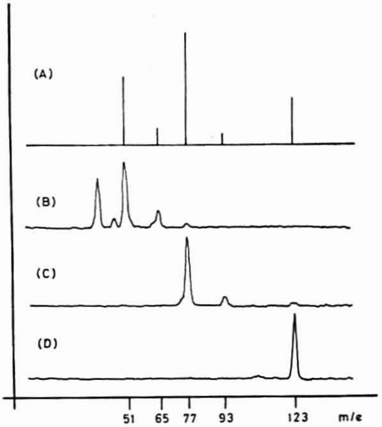

Figure 6. Mass spectra of nitrobenzene recorded with a magnetic sector instrument (A) and with the present system having peak-to-peak rf potentials applied to the Quistor of (B) 700 V, (C) 1100 V, and (D) 1750 V

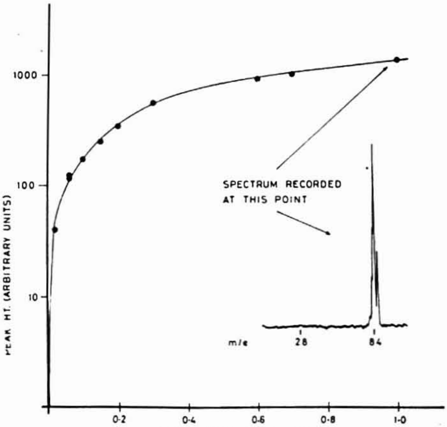

Figure 7. Curve showing the buildup of the signal from Kr^+ ions vs. ion creation time resulting from a sample of air enriched with a trace (ca. 0.1%) of krypton

quadrupole, sampling ca. 100 ion ejection events per atomic mass unit, allows the ion "beam" from the Quistor to be analyzed.

In this work the rf potential at 0.75 MHz was scanned over the range 0–2000 V (peak-to-peak) and the electron pulse width was 20 μs. The sample investigated initially consisted of equal partial pressures of air, argon, and krypton at a total pressure of ca. 1 $\times 10^{-4}$ Torr. Mass spectra of the ejected ions were recorded for the Quistor operating at different points along the rf axis of Figure 3. The data reproduced in Figure 5 do in fact show that the postulated mass selective ion storage occurs.

To emphasize the selective capability of this experimental configuration, similar spectra were recorded using nitrobenzene as the sample. Several experimental difficulties were encountered since the inlet system was designed only for gaseous sample input and as a result only a low partial pressure of nitrobenzene could be admitted. In order to compensate for this, the sensitivity of the detector was increased by operating the analyzer at very low resolving power, but the resultant spectra when compared with the conventional sector instrument data (Figure 6) do in fact show the possibility of monitoring any chosen group of peaks from a particular compound. Again the system was operated in the pulsed mode but with the storage time increased to 2 ms.

At this point it must be emphasized that in these experiments a certain degree of mass selectivity has been achieved without recourse to the use of any dc potentials as is customary in quadrupole applications. There are two advantages to be gained in this mode. The first relates to the maximum number of ions which may be stored since the application of a dc potential restricts the dimensions of the region in which ions when created remain stable within the trap and this therefore reduces the number of ions which may be retained (*19*) (cf. above). The second advantage is in the reduction in complexity of the electronic circuits required for the apparatus.

With the selective ion storage capabilities thus available, the possibility of building up an increased concentration of a particular species was investigated. The approach adopted was to set the Quistor to selectively retain krypton ions and introduce an air sample artificially enriched with a small quantity (ca. 0.1%) of krypton. Under conditions of continuous ionization and increasingly long storage times, a buildup in the number of krypton ions present in the packet of ions ejected from the Quistor is to be expected. The increase in signal observed for the krypton peak intensity (Figure 7) shows at least two orders of magnitude enhancement of the observed signal over the ionization period chosen. The degree of enhancement possible is limited by the maximum number of ions which may be stored in the device, typically 10^8 ions cm^{-3} for m/e 84 stored under these conditions, and therefore by the initial concentration of the species investigated.

The two sets of experiments described above were based on what might be termed the physical characteristics of the ion trap. Since the ionic species are retained for fairly lengthy periods (ca. 10 ms) the number of collisions experienced suggests that chemical ionization reactions may also occur within the Quistor and pioneering work in this laboratory (*22*) has indeed shown that such reactions do occur. Under these circumstances, it is possible to employ the Quistor to enhance sensitivity either by allowing the straightforward integration of ions as described above or, with the addition of a suitable reagent gas, by performing chemical

Table I. Comparison between Experimental Conditions for the Study of Chemical Ionization Reactions by Several Techniques

	This work (Quistor)	Trapped I.C.R. (*16*)	Conventional chemical ionization
Reagent gas pressure, Torr	10^{-4}	10^{-6}	1.0
Sample pressure, Torr	10^{-5}–10^{-6}	10^{-8}	10^{-3}
Ion residence time, s	5×10^{-3}	10	10^{-4}
Variety of reagent ions	Limited clustering	No clustering	Extensive clustering with polar reagents

ionization of the desired species. Thus it is worth comparing the experimental conditions employed here with those reported by McIver (*16*) and with conventional chemical ionization apparatus (*24–26*) (Table I).

DISCUSSION

The type of investigations reported in this paper are very similar to those published as a result of experiments with trapped ICR devices. The basic features of the experiments are identical, the fundamental difference being in the mode of trapping: in the Quistor the ions experience a net restoring force attracting them towards the center of the device on account of their motion in the inhomogeneous *oscillating* electric fields, while in the ICR cell, confinement occurs through the combination of a magnetic field with an inhomogeneous *static* electric field. In each case the space charge potential within the ion cloud determines the maximum density of the trapped ions, which appears to be some two to three orders of magnitude greater in the case of the Quistor. Because the mean kinetic energies of ions trapped within the Quistor are relatively large (for example it is estimated (*19*) that m/e 16 ions trapped with a potential of 800 V peak-to-peak at 2.75 MHz have a mean kinetic energy of ca. 3 eV), this prevents the formation of large cluster species characteristic of thermal ion energy systems (*27*).

LITERATURE CITED

(1) "Biochemical Applications of Mass Spectrometry", G. R. Waller, Ed., Wiley-Interscience, New York, N.Y., 1972.
(2) A. M. Lawson, *Clin. Chem.* (*Winston Salem, N.C.*), **21**, 803 (1975).
(3) H. D. Beckey, "Field Ionization Mass Spectrometry", Pergamon Press, Oxford, 1971.
(4) H. M. Fales in "Mass Spectrometry: Techniques and Applications", G. W. A. Milne, Ed., Wiley-Interscience, New York, N.Y., 1971, p 179.
(5) M. S. B. Munson and F. H. Field, *J. Am. Chem. Soc.*, **88**, 2621 (1966).
(6) D. M. Schoengold and M. S. B. Munson, *Anal. Chem.*, **42**, 1811 (1970).
(7) R. Schubert, *Anal. Chem.*, **44**, 2084 (1972).
(8) R. T. Parkinson and L. Toft, *Analyst (London)*, **90**, 220 (1965).
(9) R. Ryhage and S. Wikström in "Mass Spectrometry: Techniques and Applications", G. W. A. Milne, Ed., Wiley-Interscience, New York, N.Y. 1971, p 91.
(10) G. A. Junk, *Int. J. Mass Spectrom. Ion Phys.*, **8**, 1 (1972).
(11) E. Fischer, *Z. Phys.*, **156**, 1 (1959).
(12) G. Rettinghaus, *Angew. Phys.*, **22**, 321 (1967).
(13) R. F. Bonner, G. Lawson, J. F. J. Todd, and R. E. March in "Advances in Mass Spectrometry", A. R. West, Ed., Institute of Petroleum, London, 1974, p 377.
(14) R. T. McIver, Jr., *Rev. Sci. Instrum.*, **41**, 555 (1970).
(15) R. T. McIver, Jr., and A. D. Baranyi, *Int. J. Mass Spectrom. Ion Phys.*, **14**, 449 (1974).
(16) R. T. McIver, Jr., E. B. Ledford, Jr., and J. S. Miller, *Anal. Chem.*, **47**, 692 (1975).
(17) J. F. J. Todd and G. Lawson in "International Reviews of Science: Physical Chemistry Series Two", Volume 5, "Mass Spectrometry", A. Maccoll, Ed., Butterworths, London, 1975, pp 289–348.
(18) G. Lawson, J. F. J. Todd, and R. F. Bonner in "Dynamic Mass Spectrometry", Volume 4, D. Price and J. F. J. Todd, Ed., Heyden, London, 1976, pp 39–81.
(19) J. F. J. Todd, G. Lawson, and R. F. Bonner in "Quadrupole Mass Spectrometry and Its Application", P. H. Dawson, Ed., Elsevier, Amsterdam, 1976, pp 181–224.
(20) R. F. Bonner, G. Lawson, and J. F. J. Todd, *Int. J. Mass Spectrom. Ion Phys.*, **10**, 197 (1972/73).
(21) G. Lawson, R. F. Bonner, and J. F. J. Todd, *J. Phys. E.*, **6**, 357 (1973).
(22) R. F. Bonner, G. Lawson and J. F. J. Todd, *J. Chem. Soc., Chem. Commun.*, 1179 (1972).
(23) G. Lawson, R. F. Bonner, R. E. Mather, J. F. J. Todd, and R. E. March, *J. Chem. Soc., Faraday Trans. 1*, **72**, 545 (1976).
(24) M. S. B. Munson, *Anal. Chem.*, **43** (13), 28A (1971).
(25) F. H. Field, *Acc. Chem. Res.*, **1**, 42 (1968).
(26) G. W. A. Milne, H. M. Fales, and T. Axenrod, *Anal. Chem.*, **43**, 1815 (1971).
(27) P. Kebarle, R. H. Hayes, and J. G. Collins, *J. Am. Chem. Soc.*, **89**, 5753 (1967).

RECEIVED for review February 22, 1977. Accepted June 20, 1977.

Quantitative Comparison of Combined Gas Chromatographic/Mass Spectrometric Profiles of Complex Mixtures

Dennis H. Smith* **and Michael Achenbach**

Departments of Genetics and Chemistry, Stanford University, Stanford, California 94305

William J. Yeager, Patricia J. Anderson, William L. Fitch, and Thomas C. Rindfleisch

Department of Genetics, Stanford University, Stanford, California 94305

We describe a method, termed HISLIB, for qualitative and quantitative comparisons of complex mixtures of organic compounds. Our method compares combined gas chromatographic/mass spectrometric (GC/MS) profiles of new mixtures with historical libraries of GC/MS data on related mixtures. Co-occurrence of components is established by matching both retention indexes and mass spectra after background removal and resolution of overlapping GC components. Quantitation is achieved by comparing relative concentrations of components, calculated using internal standards. Uses include validation of analytical procedures, determination of variations among controls, and rapid detection of novel (in identity or amount) components in new mixtures.

Improvement of combined gas chromatographic/mass spectrometric (GC/MS) instrumentation, including automation of many previously manual procedures, has resulted in the routine generation of large volumes of data. There has been a steady progression of developments in computer-based procedures for analysis of these data. The first major development to assist scientists in data analysis was library search techniques (*1, 2*). These techniques are valuable not only in identification of previously observed components, but also in noting which components are not found in the library and are thus subjects for more sophisticated procedures for structure elucidation. More recently, relative retention indexes (RRI's) have been used to improve the specificity of identification in cases where related (e.g., isomeric) compounds exhibit similar mass spectra (*3–5*). To improve the quality of mass spectra obtained from GC/MS systems, which facilitates both library matching and interpretation of spectra of unknown compounds, computer programs have been developed to remove background and resolve overlapping GC components (*6, 7*).

We describe a logical synthesis and extension of the above procedures designed to automate the task of quantitative comparison of GC/MS results obtained on complex mixtures of organic compounds. A method for qualitative comparison of GC/MS profiles to detect anomalous compounds has been reported (*8*). But that method is limited to comparison of two sequential analyses and does not provide detailed quantitative information. Our developments remove these restrictions. We carry out quantitative comparisons which couple the specificity of the mass spectrum and RRI to identify each compound (*3–5*), with calculated relative concentrations to determine their relative amounts. This method, "HISLIB", is based on comparing new mixtures to "historical" libraries of previous results. It is capable of detecting new components and anomalous concentrations of previously encountered components. Applications of HISLIB include: (a) validation of analytical procedures used to isolate complex mixtures; (b) development of historical libraries which might include complete summaries of all past observations, compilations of controls, or any other selected subset of results; (c) computation of average mass spectra and RRI's of known compounds to improve the quality of existing libraries of mass spectral data; and (d) rapid comparison of new data to previously compiled library(ies) to detect differences in kind and/or amounts of individual components.

During preparation of this report, a paper appeared (*9*) which addresses some of the same issues raised in our discussions. In fact, that paper utilizes concepts and earlier programs and data from our own laboratory. The work described in our report represents the results of a maturation of these concepts and programs and the development of new programs and GC/MS procedures designed specifically to obtain reliable, quantitative results. Indeed, several of our new developments are solutions to problems discussed by Blaisdell as deficiencies of his method (*9*).

EXPERIMENTAL

We routinely collect complete GC/MS runs, including repetitively scanned mass spectra. Any system capable of providing these data is potentially adequate; we employ a Finnigan Instrument Corp. model 1015 quadrupole mass spectrometer controlled by a Digital Equipment Corp. (DEC) PDP-11/20 computer (*10*). Subsequent data processing is done on a DEC PDP-11/45 with 28K words of core memory, a 5M word disc drive, teletype, printer, CRT, and Versatek printer/plotter. Unless otherwise noted, GC and GC/MS experiments were performed on a Finnigan Instruments Corp. model 9500 gas chromatograph, employing 6-foot U-shaped $^1/_8$-inch i.d. columns, packed with 10% OV-17 on 100/120 mesh Gas-Chrom Q. Initial temperatures (usually 80 °C) were maintained for 4 min followed by temperature programming at a rate of (usually) 4 deg/min.

For optimum use of HISLIB, it is desirable to apply a number of preprocessing steps to experimental data. Because library matching, determination of RRI's and, particularly, measurements of relative concentrations depend strongly on spectra free from background and overlapping components, we first process the GC/MS data with the CLEANUP (*7*) program. Next we determine RRI's for each detected component, and compute relative concentrations based on one or more internal standards. We then match each spectrum against an existing library of mass spectral data, in our case a library of compounds of biological interest (*11*). Finally, the resulting data are combined with previous results to update the historical library or are compared against an existing historical library. The flow of data through these steps is summarized in Figure 1.

The HISLIB system can be used without applying some of the processing steps above. However, without "clean" spectra, both library search results and RRI's are compromised, especially for components of low abundance. Accurate quantitation becomes effectively impossible. RRI's are very important to increase the

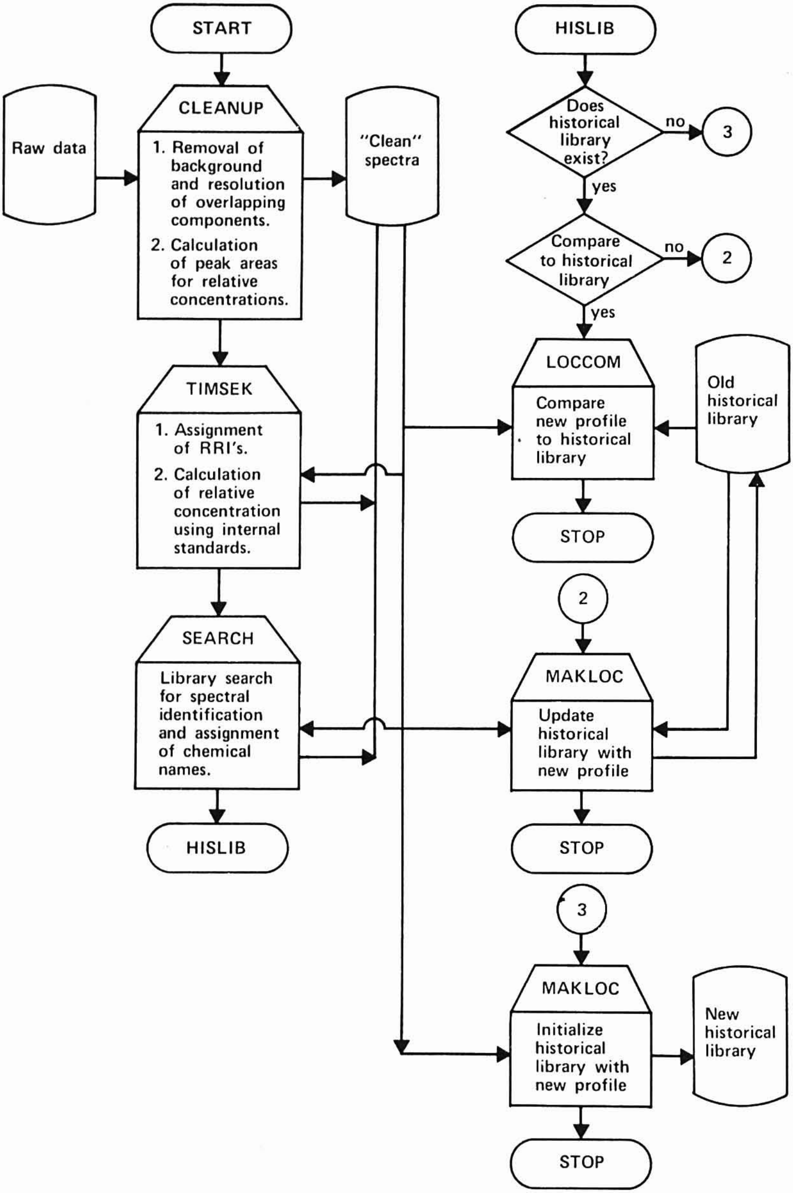
START
CLEANUP
1. Removal of background and resolution of overlapping components.
2. Calculation of peak areas for relative concentrations.
Raw data
"Clean" spectra
TIMSEK
1. Assignment of RRI's.
2. Calculation of relative concentration using internal standards.
SEARCH
Library search for spectral identification and assignment of chemical names.
HISLIB
HISLIB
Does historical library exist?
no
3
yes
Compare to historical library
no
2
yes
LOCCOM
Compare new profile to historical library
Old historical library
STOP
2
MAKLOC
Update historical library with new profile
STOP
3
MAKLOC
Initialize historical library with new profile
New historical library
STOP

Figure 1. Major steps in processing a complete set of GC/MS data to establish and search an historical library

specificity of mass spectral identifications; the combination of both is highly effective in distinguishing materials with similar spectra (*3–5*). Matching spectra against a compendium of spectra of known compounds (as opposed to the historical libraries discussed here) is also not essential, but is useful in assigning names of known compounds to their spectra as a guide in interpreting the results of comparisons to the historical library.

The following sections describe the details of our method, assuming these preprocessing steps are performed. Further information about the programs described below, including availability, may be obtained by writing the authors.

Automatic Determination of Relative Retention Indexes (RRI's). We use an extension of the method proposed by Nau and Biemann (*3, 4*) for determination of RRI's. Our procedure is automatic and calculates reproducible RRI's under variable instrumental and experimental conditions including unavoidable changes in initial GC column temperature, carrier gas flow, or temperature programming rates. It requires only three internal hydrocarbon standards for the analysis of a GC/MS run.

As previously described (*3, 4*), each column is calibrated with a mixture of hydrocarbons (we use 1 μL of an approximately 1 μg/μL solution each of n-C_{10} through n-C_{26}, and n-C_{28}). This calibration yields a file of 18 data points relating carbon numbers and mass spectrometer scan numbers. Each subsequent GC/MS experimental run using that column is processed using this calibration file as a reference (assuming that conditions of temperature programming, initial temperatures, and flow rate are approximately the same—see Results and Discussion). Three of the hydrocarbons used in the calibration run are added to each experimental mixture. The CLEANUP program is run to isolate representative spectra and to assign scan numbers corresponding to elution times for each component. The TIMSEK program (Figure 1) then locates the three added standards by matching their known spectra in windows about the expected elution scan numbers and fits the three observed hydrocarbon scan numbers to those corresponding in the calibration run using a least-squares method. We assume that differences in conditions between a given experimental run and the calibration run can be accounted for by a linear transformation of the elution time scale as given in Equation 1a. We determine the linear coefficients A and b by maximizing the correspondence between the elution times of the three standards in the experimental and calibration runs; or equivalently minimizing the error function given in Equation 1b with respect to A and b.

$$S_{\text{cal}} = AS_{\text{exp}} + b \tag{1a}$$

where S_{cal} is a scan number in the elution time scale of the calibration file, S_{exp} is a scan number in the elution time scale of the experimental run, and A and b are the linear transformation coefficients.

$$E^2 = \sum_{i=1}^{n} [S_{i(\text{cal})} - AS_{i(\text{exp})} - b]^2 \tag{1b}$$

where $S_{i(\text{cal})}$ is the scan number of the ith standard in the calibration file, $S_{i(\text{exp})}$ is the scan number of the ith standard in the experiment file, and i indexes over the internal standards used ($n = 3$ in our case).

Once A and b are determined (Equation 1b), Equation 1a is used to determine the effective scan number for elutants in the experimental run as transformed to the calibration run time scale. These effective scan numbers are converted to RRI's by a linear interpolation or extrapolation using the nearest hydrocarbons measured in the calibration file (*3, 4*). (If the GC is operated isothermally, a logarithmic interpolation/extrapolation is used.)

This method differs from that of Nau and Biemann in that the least squares fitting procedure (Equation 1b) takes explicit account of both linear offsets and expansion or contraction of the scan number/retention index curve rather than simply optimizing about the midpoint of the range (*3, 4*).

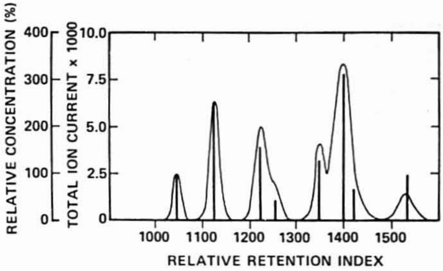

Figure 2. A schematic representation of a GC/MS profile, displaying relative concentrations of detected elutants vs. relative retention index, superimposed on the corresponding total ion current plot. For each detected elutant, the total ion current profile is effectively collapsed (Equations 2 and 3) into a line whose height represents relative concentration

Determination of Relative Concentrations. Relative concentrations are determined by TIMSEK (Figure 1) based on any one or combination of the internal standards selected by the user prior to obtaining GC/MS data. Ideally, standards should be chosen that reflect the kinds of compounds one wishes to quantitate, the variety of analytical procedures used to isolate mixtures to be analyzed, the sensitivity of spectra to changing MS conditions, and other considerations that affect accurate and reproducible quantitation using any analytical procedure. We wish only to point out that care must go into the selection and use of such standards. TIMSEK uses a pre-established library of spectra of standards together with their RRI's. The standard(s) selected is searched for in the GC/MS data by looking for the closest spectrum match (Equation 4 below) within a narrow retention index window (+/−0.2 methylene unit). This is similar to the method of Sweeley et al. (*5*). Having found the internal standard(s), the relative concentration of the ith component is calculated according to Equation 2,

$$\text{Rel Concentration} = 100 \times \frac{\text{Areal TIC of } i\text{th component}}{\text{Areal TIC of internal standard}} \tag{2}$$

The "areal" total ion current (TIC) measures the area of the GC peak of the ith component, not simply its height. The area for each GC peak is derived from the raw mass spectral data using the peak model determined for each spectrum during CLEANUP (*7*). The intensity (ion abundance expressed as peak height) of each mass in the spectrum of the ith component is determined by fitting the data-adaptive peak model to the intensity profile for each mass (fragmentogram) about the position of elution of the component (*7*). Simpson's Rule is used to determine the area of the model peak. The areal total ion current for the ith component is given by Equation 3,

$$\text{Areal TIC}_i = \frac{A_{i(\text{model})}}{h_{i(\text{model})}} \sum_m I_{im} \tag{3}$$

where $A_{i(\text{model})}$ and $h_{i(\text{model})}$ are the area and height of the peak model for the ith component and I_{im} is the ion abundance (peak height) at mass m in the mass spectrum of the ith component after processing by the CLEANUP program.

If more than one standard is used, the basis for relative concentrations is the average of the areal total ion currents for the standards. The inclusion of multiple standards provides the opportunity for a better statistical basis for computing relative concentrations since statistical fluctuations in measuring the areal TIC of one are reduced by averaging with the areal TIC's of the others. Depending on the relative quantities and reproducibility of the various standards included, a weighted average may be appropriate to account for different relative a priori uncertainties in the TIC's among them. In our case, these are comparable and a straightforward average is used. An improvement in quantitation standard reproducibility can be expected increasing approximately as the square root of the number of standards included. Results illustrating the advantages of multiple standards are presented in Results and Discussion.

Assembling an Historical Library of GC/MS Profiles. We define a "profile" for a GC/MS experiment as an assembly of data consisting of: (a) The (unnormalized) spectrum of each component after component detection, background removal and resolution of overlapping components; (b) the retention index of each component; (c) the relative concentration of each component; and (d) (optionally) a name for each component which may be a simple experiment code or a name associated with the component during routine library search (Figure 1). A GC/MS profile by this definition may be visualized as shown schematically in Figure 2. The relative concentrations are depicted as vertical bars at the appropriate elutant locations superimposed on a normal total ion current plot (total ion current vs. RRI). The height of each bar corresponds to the areal total ion current or relative concentration through Equations 2 and 3. The relative heights of the bars will approximate the relative heights of the respective peaks in the total ion current plot. However, depending on the area/height ratio of the model peak for each elutant (Equation 2), the relative concentration can differ substantially from the peak height in the total ion current plot (e.g., compare the first and last peaks in Figure 2, both of which have relative concentrations of 100%).

An historical library is assembled by HISLIB by taking the GC/MS profile from an experiment and adding it to the library (Figure 1). If the library is initially empty, the profile becomes the library. If the library already contains at least one profile, the new profile is added as follows. Each spectrum in the new profile is compared to each spectrum in the library within a narrow retention index window (e.g., +/−0.2 methylene, or +/20 RRI, units for our work). A spectral match score, in this case a cross-correlation score, is calculated by Equation 4,

$$\text{Spectral Score} = 1000 \times \frac{\left[\sum_m e_{m\,(\text{prof})}\, e_{m\,(\text{hist})}\right]^2}{\sum_m e_m{}^2{}_{(\text{prof})} \sum_m e_m{}^2{}_{(\text{hist})}} \tag{4}$$

where spectra are reduced to the two most abundant ions every 14 amu (*12*) and the spectral intensities are encoded before matching. $e_{m(\text{prof})}$ and $e_{m(\text{hist})}$ are the encoded intensities at mass m for the new profile and the historical library, respectively. They are quantized to have values 0, 1, 2, or 3 corresponding to the relative intensity ranges 0–4, 5–16, 17–64, and 65–100% of base peak, respectively.

The definition in Equation 4 has several useful properties, based on Schwartz's inequality (*13*). The spectral match score calculated is independent of the order in which spectra are compared. If two ions of the same mass are present, a positive contribution to the score results. More abundant ions are weighted more heavily because of the squared term. The score is guaranteed to be between zero and 1000, 1000 representing a perfect match. Equation 4 is similar to the "degree of coincidence" score used by Jellum et al. (*8*), except that Equation 4 uses encoded peak heights rather than just the number of peaks.

The spectral match score and the proximity of the retention indexes are combined through an heuristic evaluation function (Equation 5a) which yields the final score. This final score is the spectral match score weighted by a trapezoidal function (Equation 5b) which penalizes for disparate RRI's. The weight is unity if the difference in RRI's is less than five units and decreases linearly to a threshold weight as the absolute difference in RRI's becomes greater than 5 units up to the empirical cutoff of 20 RRI units.

$$\text{Final Score} = \text{Spectral score} \times W(\Delta\text{RRI}) \tag{5a}$$

Where $\Delta\text{RRI} = (\text{RRI}_{\text{exp}} - \text{RRI}_{\text{lib}})$ and RRI_{exp} and RRI_{lib} are the relative retention indexes for the experiment and library components respectively. The weighting function, $W(x)$, is defined by,

$$\begin{aligned} W(x) &= 1 && ;\ |x| < 5 \text{ RRI units} \\ &= 1 - \frac{(\text{Maxscore} - \text{Minscore})}{15\ \text{Maxscore}}\,x && ;\ 5 \leqslant |x| < 20 \\ &= 0 && ;\ 20 \leqslant |x| \end{aligned} \tag{5b}$$

where Maxscore = 1000 and Minscore = 400.

If this final score exceeds 400, the experiment compound is considered a potential match to the library compound. If there is more than one potential match between closely eluting experimental and library compounds, the ambiguity is resolved by a procedure (see below) that maximizes the overall correspondence between the pattern of experimental and library elutants. The Minscore value of 400 was derived empirically by examining the distribution of scores obtained by matching every *n*th spectrum in chemically related subsets of our library (*11*) with all spectra in that subset. A representative distribution of the number of matches with a given score as a function of score is shown in Figure 3. From a number of such curves a value of 400 was chosen as a threshold for distinguishing matches and non-matches (this threshold will depend to some extent on the range of compounds included in the library, derivatization procedures, etc.). Although artifactual matches may occasionally yield scores higher than the threshold, the RRI weighting (Equation 5a) significantly reduces such occurrences.

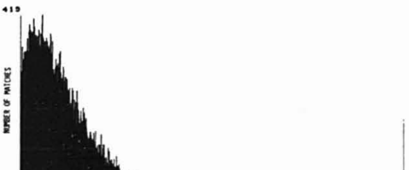

Figure 3. A histogram of the number of library comparisons with a given match score vs. score. Scores were obtained using Equation 4. Comparisons were made in two subsets of the library of Markey et al. (*11*) containing 750 compounds total. Every 5th spectrum was compared with the other spectra in each subset for a total of approximately 65 000 comparisons

Assignment of New Spectra to the Historical Library. The final step in correlating a new profile with an historical library involves selecting between alternative matchings of experimental and historical library spectra with similarly high final scores. This occurs frequently with isomeric compounds with similar spectra and retention indexes, and accidentally as, for example, with compounds whose spectra are similar due to domination of the fragmentation pattern by ions from a functionality added during derivatization.

We have implemented a pattern matching procedure to resolve such ambiguities. Briefly, the procedure attempts to maximize the consistency between a new experiment and the library, assuming they are derived from similar mixtures. In a region containing ambiguities, a matrix representing every possible assignment relating experiment and library spectra to one another is analyzed using an algorithm which can trace and rank all self-consistent "paths" through the matrix (*14*). Such paths include those which create new entries in the historical library, i.e., paths with some spectra in the new profile not being matched to any existing spectrum in the historical library. Consistency constraints on the assignments include: (a) the scoring threshold must be exceeded for a match to be considered, (b) RRI order must be preserved, and (c) a spectrum in either set can be assigned to at most one spectrum in the counterpart set. Finally, the "best" assignment is that which has the highest total score, where the total score is the summation of scores (Equation 5a) for each candidate pairing of spectra between the two sets (the score is not incremented for a spectrum found to be only in one set). This procedure is driven strongly toward maximum overlap between the two sets of spectra. This is justified when the minscore is high enough to reject dissimilar spectra and the GC/MS profiles are from related mixtures.

Once specific assignments have been made, spectra from the new profile are added to the library. New entries are created for components which scored less than minscore against library entries, or which were assigned as new entries by the above pattern-matching algorithm. When a pairing with an existing library entry is made, the new spectrum is averaged with the library spectrum for that entry, effectively weighting each contributing spectrum by its total ion current. At the same time, the new relative concentration and retention index are averaged with the previous values. Note that an important advantage of this approach is that components need not be identified by name, only by occurrence in terms of RRI and mass spectrum (*9*).

Comparing New Profiles to the Historical Library. Once a suitable historical library has been prepared, subsequent profiles can be compared to it to detect similarities and differences. In practice, we use the same program used to assemble the library to perform the comparisons, changing only a flag which prevents using the new data to update the library and which causes a summary output to be produced indicating the results of comparison. Individual users may select different formats for such a summary. The one used in our laboratory (see Results and Disucssion) was chosen to focus the attention of the user on components observed in significantly different relative concentration and on new components present in the profile regardless of relative concentration.

Manual Method of Extraction of Urinary Organic Acids. To 3 mL of freshly thawed urine is added an aliquot of *m*-chlorophenylacetic acid solution (84 μg, 0.49 μmol, in H_2O) as an internal standard for quantitation. The urine is then acidified with six drops of 3 N hydrochloric acid and extracted three times with 1:1 ether–ethyl acetate (6 mL total). The combined organic extracts are dried (Na_2SO_4) and evaporated to dryness in vacuo. The resulting residue is dissolved in methanol–ethyl acetate (1:1, 3.0 mL) and a 1.0-mL portion of this is transferred to a Teflon-capped glass vial. The solvent is blown off with a stream of nitrogen.

DEAE-Sephadex Anion Exchange Method of Extraction of Urinary Organic Acids. As in the manual method, *m*-chlorophenylacetic acid (84 μg, 0.49 μmol) is added to 3.0 mL of urine in a 12-mL centrifuge tube. Barium hydroxide solution (0.1 M, 3.0 mL) is added, the mixture is quickly stirred and centrifuged for 15 s. The supernatant is removed and treated with hydroxylamine hydrochloride (50 mg, 0.7 mmol). This mixture is heated at 60 °C for 30 min, allowed to cool, and neutralized to pH 7–8 with dilute hydrochloric acid. This solution of organic acids and oximes of keto-acids is then placed on a DEAE-Sephadex A-25 column (1.0 cm × 5.0 cm) prepared as previously described (*15*). After the acid solution is passed onto the column, the resin is washed twice with distilled water (5.0 mL) to remove neutral and basic constituents. The organic acids are then eluted with 1.5 M pyridinium acetate solution (15 mL). An aliquot of this elutant (5.0 mL) is lyophilized to dryness at 5–10 μ pressure, the residue taken up in methanol–ethyl acetate (1:1, 2 mL) and transferred to a Teflon-capped glass vial. The solvent is blown down with a stream of nitrogen.

Trimethylsilylation. The urinary acids (from either of the above procedures) are treated with *N*,*O*-bis(trimethylsilyl)trifluoroacetamide ("BSTFA", 100 μL) and heated at 60 °C for 30 min. Before analysis, a solution of hydrocarbon standards (5 μL of a 5 μg/μL solution of dodecane, octadecane, and tetracosane) is added as a reference for RRI calculations.

RESULTS AND DISCUSSION

Relative Retention Index Calculations. Because of the increasingly important role of relative retention indexes in analysis of GC/MS profiles (this study and Ref. 3, 4, and 5), we have evaluated our method, TIMSEK, for calculation of RRI's (Experimental section) in several ways. We made radical changes to temperature programming rates, starting temperatures, and carrier gas flow rates for GC/MS runs subsequent to a calibration run. These changes simulate perturbations of the system far beyond what we expect in normal operation.

We present in Figure 4*a* plots of carbon number vs. scan number for three GC temperature programming rates, 4, 6, and 8 °C/min. Using the 4 °C/min GC/MS experiment as the calibration run, we used the method described previously (see Experimental, and Equations 1a and 1b) to compute transformed scan numbers and retention indexes of hydrocarbons in the "experimental" 6 and 8 °C/min runs. For these trials we assigned the three standards C_{12}, C_{18}, and C_{24} manually because of the large discrepancies in elution times compared to the 4 °C/min calibration. The results are presented in Figure 4*b*.

The curves (Figure 4*b*) are superimposable, indicating that the method has corrected for the considerable contraction in the carbon number vs. scan number scale (Figure 4*a*). A more accurate measure is the set of RRI's calculated for the hydrocarbons in the experimental runs, which are effectively unknowns. We present in Table I the average absolute error, in RRI units, and the standard deviation of the measurements from the expected values for each programming rate based on the experiment at 4 °C/min as the calibration. These results should be evaluated considering that the determination of component elution times by the CLEANUP program to the nearest spectral scan time leaves an uncertainty of a fraction ($^1/_3$ to $^1/_2$) of a scan. Under our experimental conditions, one scan represents approximately 0.03 methylene unit (3 RRI units, Figure 4) at a temperature programming rate of 4 °C/min.

Table I. Average Absolute Error and Standard Deviations of RRI Measurements with Variation of GC Temperature Programming Rate, Based on a Four °C/min Calibration

GC programming rate, °C/min	Average absolute error, RRI units[a]	Std dev
6	4.5	4.9
8	4.4	3.4

[a] 100 times the value in methylene units.

Table II. Average Absolute Error and Standard Deviation of RRI Measurements with Variation of GC Starting Temperatures, Based on an Initial Temperature of 80 °C as the Calibration Run

GC initial temperature, °C	Average absolute error, RRI units	Std dev
60	3.1	2.6
100	21.2	36.

Table III. Average Absolute Error and Standard Deviation of RRI Measurements with Variation of GC Carrier Gas Flow Rate Based on 30 mL/min as a Calibration Run

Carrier gas flow rate, mL/min	Average absolute error, RRI units	Std dev
25	1.5	1.1
35	1.6	0.5

We next performed a similar experiment, this time varying the starting temperature beginning with 80 °C (used as the calibration run), then using 60 and 100 °C starting temperatures as experimental data. Results are presented in Table II.

Finally, we evaluated the ability of the method to cope with variation in GC carrier gas flow. Because these changes cause less extreme contractions and expansions of the scan number, or RRI, scale than variations in temperature programming, rates, TIMSEK performs very well for flow rates of 25, 30, and 35 mL/min. Using 30 mL/min as a calibration run, results are summarized in Table III. The ability of Equations 1a and 1b to adjust for variations in carrier gas flow rate is reflected in Figures 4*c* and 4*d*.

Based on these data, the initial GC colummn temperature is the most critical parameter to control to ensure accurate RRI's and, fortunately, is the easiest to control precisely. The initial isothermal period (see Experimental) at higher initial temperature distorts the linearity of the RRI vs. scan number curve at low (approximately *n*-C_{12}) carbon numbers and is responsible for the large deviations noted at higher initial temperatures (Table II).

Method for Quantitation. Areas of gas chromatographic peaks are widely used for purposes of quantitation of ma-

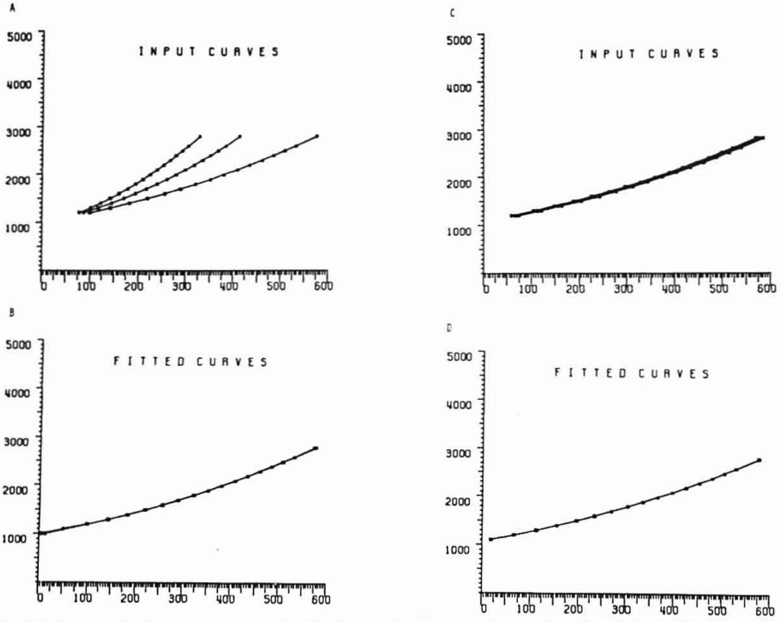

Figure 4. (*a*) Relative retention indexes vs. scan number for three hydrocarbon standard analyses (see text), at GC programming rates of 4, 6, and 8 °C/min. (*b*) Relative retention indexes vs. scan number for three analyses in Figure 4*a*, normalized to the 4 °C/min run using the linear transformation of Equation 1a. (*c*) Hydrocarbon standard analyses similar to those in Figure 4*a*, but with varying flow rates of 25, 30, and 35 mL/min. (*d*) Results of normalizing the runs in Figure 4*c* to the 30 mL/min run using the linear transformation as in Figure 4*b*

terials. When complex mixtures are analyzed by GC alone, however, there arise questions of homogeneity of GC peaks and identity of components among different analyses. RRI's and GC peak shapes are often insufficient to answer these questions, particularly when new components are observed in routine screening procedures. For these reasons GC/MS is now used extensively to analyze complex mixtures. Programs such as CLEANUP and library search techniques assist scientists in qualitative analysis of such mixtures. But much less progress has been made in obtaining quantitative results. Although workers in the petroleum industry have performed quantitative type analyses utilizing mass spectrometry for many years, such analyses depend on detailed knowledge of compound types present and careful calibration of the mass spectrometer with a suite of standards. These conditions are not met in most GC/MS analyses of mixtures.

We choose to use the areal total ion current of the internal standard(s) to compute relative concentrations of each component (Equations 2 and 3). These relative concentrations should be a better measure of the amount of material present than calculations based on single or selected ions (*5*) which are subject to greater statistical variation, given that the GC column resolution together with CLEANUP is able to remove other contributions to the spectrum. We stress that it is essential for accurate relative concentrations that the method chosen (e.g., CLEANUP) to remove background and overlapping components be able to apportion intensity of an ion common to overlapping components appropriately to the individual spectra (*7*), rather than assigning the ion to one spectrum or the other (*6*). Of course, measurement of relative concentrations provides a means for quantitative comparison of profiles but does not determine the actual amount of each component. Auxiliary methods designed for quantitation of individual components, e.g., mass fragmentography or "selected ion monitoring" (*16*), can be used to establish relationships between relative concentrations and actual amounts of materials.

We evaluated the reproducibility of relative concentrations based on areal total ion current values by analyzing five GC/MS profiles of our mixture of hydrocarbon standards. Each profile was treated as an unknown. HISLIB was used to correlate and summarize the data. We determined relative concentrations in two ways. First, we employed n-C_{18} as the internal standard. Then we employed the average of the areal total ion currents for n-C_{12}, n-C_{18} and n-C_{24} as the basis for determining the relative concentration of each component. Results are summarized in Table IV.

The results in Table IV are a measure of the reproducibility of the data acquisition and analysis procedures. They indicate the variance to be expected using this method and a single internal standard. The results also indicate significant improvement in precision of relative concentrations when multiple standards are used to smooth out statistical fluctuations in the areal total ion current of a single internal standard. The deviations in relative concentration based on n-C_{18} alone average about 6.4% of relative concentration. Using n-$C_{12,18,24}$ together, the deviations are reduced to about 4.2%, consistent with the square root of three improvement to be expected a priori for three vs. one standard.

The results, however, do not measure variations in isolation or derivatization procedures or long-term variations in performance of the GC/MS system. Results presented below indicate variations observed in a complete analytical procedure in our laboratories. Other workers must evaluate their own

Table IV. Average Relative Concentrations and Standard Deviations for Five Analyses of a Mixture of *n*-Alkanes

Carbon No.	Relative retention index		Relative concentration based on n-C_{18}		Relative concentration based on n-$C_{12,18,24}$	
	Av.	S.D.	Av.	% S.D.	Av.	% S.D.
11	1101	1.3	30.4	7.6	13.4	5.2
12	1199	0.4	40.6	7.6	17.9	6.7
13	1300	0.6	48.0	6.2	21.2	3.8
14	1400	0.4	56.4	6.6	24.9	4.0
15	1499	1.2	62.9	6.2	27.8	4.0
16	1600	0.7	75.3	4.5	33.2	1.8
17	1698	1.1	80.3	3.0	35.5	1.4
18	1801	0.7	100.0	...	44.2	3.4
19	1900	1.6	96.7	4.1	42.7	2.6
20	2000	1.3	102.0	5.3	45.0	2.9
21	2101	1.4	109.5	5.6	48.3	3.9
22	2198	0.0	109.0	5.7	48.1	3.1
23	2298	1.2	115.4	5.4	50.9	3.9
24	2399	0.7	85.8	7.9	37.8	5.0
25	2498	1.9	73.9	7.4	32.6	5.2
26	2596	2.7	75.7	7.3	33.4	4.5
28	2800	0.7	74.6	12.3	32.9	10.0

procedures similarly. One advantage of HISLIB is that such evaluations are greatly simplified.

Application Example—Comparison of Isolation Procedures. During a study of different isolation procedures for various organic fractions of human body fluids, we have used HISLIB as an aid to monitoring analytical procedures and intercomparing methods. We select as an illustrative example a comparison of two isolation procedures for the organic acid fraction of human urine, manual extraction and anion exchange (see Experimental). Data already exist in the literature for these isolation procedures, using GC methods for quantitation (*15*). To evaluate these procedures for both keto and hydroxy acids, we used aliquots of a 24-h urine sample of a patient previously diagnosed as having phenylketonuria (PKU). The patient was on a low phenylalanine diet at the time the urine was collected.

HISLIB was used to construct a library containing results from analysis of five aliquots of the above urine, using the manual extraction method. A representative total ion current plot for one of the analyses is shown in Figure 5*a*. The abundant phenylacetic, *p*-hydroxyphenylacetic, phenyllactic, and *p*-hydroxyphenyllactic acids (as TMS ethers/esters) (RRI's 1433, 1763, 1689, 1993, respectively) are notable characteristic compounds excreted in this disease; the abundance of phenylpyruvic acid is very low (in the baseline for the injected amount of the total mixture in this experiment) compared to the amount excreted prior to dietary control. The complete historical library is presented in Table V.

The reproducibility of relative concentrations is reduced relative to data presented in Table IV, because now all the variables of the isolation and derivatization procedure affect the results. However, the precision of our results is generally higher than that reported for similar analyses using a GC method for quantitation (*15*). One reason for the improved precision is, we feel, the addition of the quantitation standard at the beginning of the isolation procedure rather than just prior to derivatization (*15*). The only component with an inordinately large standard deviation is dioctylphthalate (RRI 2778). We attribute this artifact to sources other than the urine itself.

To the historical library in Table V, we compared data from an analysis of the same urine sample, but using anion exchange as the isolation method. Selected results of the comparison of a representative GC/MS profile (the total ion current plot is shown in Figure 5*b*) with the historical library are presented in Table VI.

As discussed previously (*15*), the two isolation procedures yield quite different GC/MS profiles (Figure 5). These differences are quantitated by the HISLIB output and can be quickly observed by scanning the "DISCREPANCY" column of Table VI (see footnote to the Table for explanation of terms). Some components, e.g., palmitic acid, are observed in nearly equal amounts in the two procedures. Other components, e.g., urea-diTMS and succinic acid-diTMS are observed in significantly different quantities. There are

Table V. An Historical Library Containing Organic Acid Analyses of Five Aliquots of Urine from a PKU Patient under Dietary Control

Retention index	Std dev	No. Occ.	Rel Concn	% Std dev	Chemical name
1131	...	1	9.2	...	?
1200	0.0	5	97.8	4.9	C_{12}[a]
1359	0.9	5	46.9	17.7	Urea–diTMS
1366	...	1	10.0	...	Benzoic acid–TMS
1409	1.3	5	18.9	9.0	Succinic acid–di-TMS
1433	0.6	5	243.6	17.6	Phenylacetic acid–TMS
1560	...	1	6.3	...	Erythronic acid–tetra-TMS
1596	1.0	2	11.1	21.6	Threonic acid–tetra-TMS
1620	1.5	5	100.0	...	*m*-Chlorophenylacetic acid–TMS[b]
1643	0.9	3	10.3	8.7	?
1664	1.7	3	13.9	15.8	?
1689	1.0	5	654.0	10.7	Phenyllactic acid–di-TMS
1763	1.0	5	78.7	10.4	*p*-Hydroxyphenylacetic acid–di-TMS
1798	1.0	5	343.6	7.7	C_{18}[a]
1847	1.4	5	8.1	16.0	Unknown phthalate
1887	1.1	4	17.9	16.2	Citric acid–tetra-TMS
1898	0.8	5	13.2	20.5	Unknown mixture
1991	1.2	5	76.0	3.0	*p*-Hydroxyphenyllactic acid–tri-TMS
2049	0.7	5	285.8	7.6	Unknown δ[c]
2093	1.0	5	39.1	28.1	Palmitic acid–TMS
2189	...	1	4.8	...	?
2293	0.7	5	27.3	12.8	Stearic acid–TMS
2401	0.7	5	516.0	5.2	C_{24}[a]
2778	3.8	5	83.2	86.5	Dioctylphthalate

[a] Internal RRI standard, added just prior to GC/MS analysis. [b] Internal quantitation standard, added to the urine prior to initial extraction. [c] Subsequently identified as *N*-acetylphenylalanine–TMS.

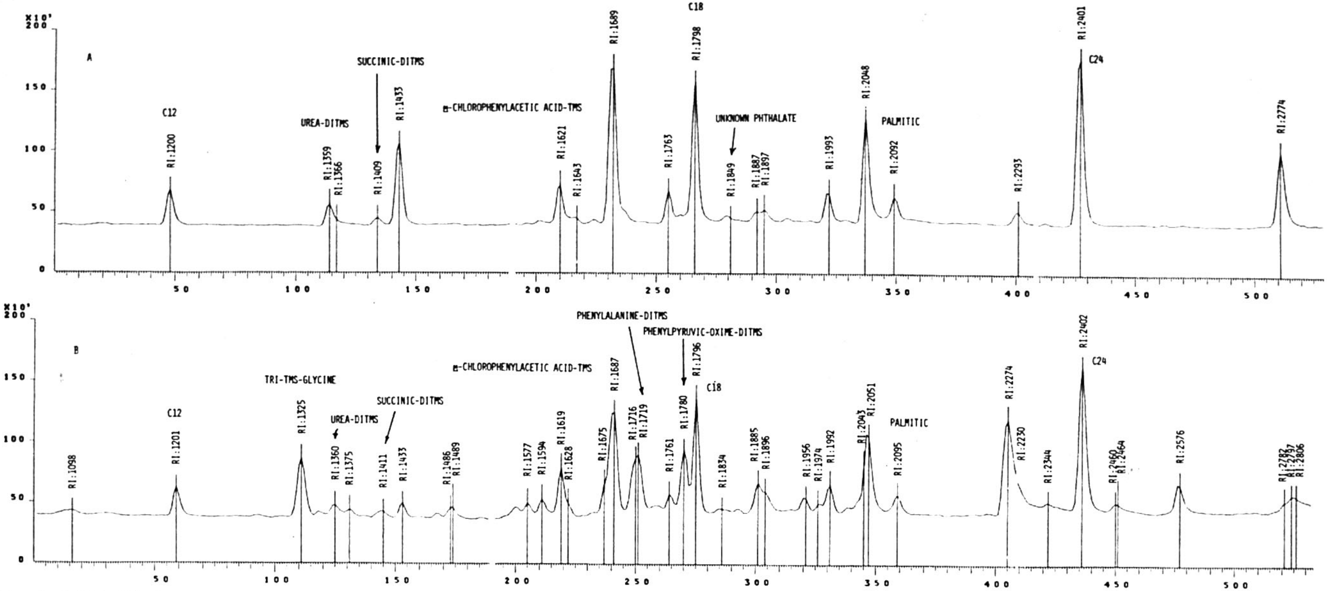

Figure 5. (*a*) Plot of total ion current vs. scan number for a representative GC/MS experiment analyzing a trimethylsilylated mixture of organic acids isolated by the manual method of extraction. (*b*) Total ion current plot of the same mixture of organic acids isolated by the anion-exchange method. *m*-Chlorophenylacetic acid–TMS is the internal quantitation standard. Minor discrepancies in RRI's between Figure 5*a* and Table VI are due to the fact that RRI's in Table VI are averages for five analyses

Table VI. Selected Results of Comparison of the GC/MS Profile of a Mixture of Urinary Organic Acids Isolated by Anion Exchange to the Historical Library of Table V. The Urine Sample was an Aliquot of the Same Urine Used to Construct the Library

Cmpd name[a]	RRI	Rel concn	HISLIB name	N[b]	RRI	Std dev	Rel concn	% Std dev	Discrepancy[c]
TRI-TMS-GLY	1325	157.5							NEW
UREA-DITMS	1360	18.3	UREA-DITMS	5	1359	0.9	46.9	17.7	-***
SUCCINIC	1411	9.3	SUCCINIC	5	1409	1.3	18.9	9.0	-******
PHENYLALA	1719	81.5							NEW
PHENYLPYRUV	1780	180.1							NEW
			?(phthalate)	5	1847	1.4	8.1	16.0	MISSING
STEARIC[d]	2095	34.9	PALMITIC	5	2093	1.0	39.1	28.1	-

[a] Names are truncated to conserve space. [b] *N* is the number of occurrences of the compound in the historical library. [c] A discrepancy of "NEW" indicates a component which was observed in the experimental GC/MS profile but is not present in the historical library. A discrepancy of "MISSING" indicates the reverse situation. The sign and number of asterisks indicate, for components present in both experiment and library, the sign and magnitude of the mismatch in relative concentration, one asterisk/standard deviation unit. [d] The best match to the library (*10*) is incorrect.

Table VII. Selected Results of Quantitative Comparison of a GC/MS Profile of Trimethylsilyl Derivatives of Urinary Organic Acids (72 h after Derivatization) with an Historical Library Composed of the Same Mixture Analyzed Repetitively at Earlier Times[a]

Cmpd name	RRI	Rel concn	HISLIB name	N	RRI	Std dev	Rel concn	% Std dev	Discrepancy
(*b*)	1323	162.3	2-AMINOETHANOL	5	1326	0.9	161.9	2.2	
GLYCERIC	1370	11.7	GLYCERIC	4	1376	0.9	12.6	23.0	-
PHENYLACETIC	1430	32.2	PHENYLACETIC	5	1433	0.6	33.6	6.5	-*
THREONIC	1592	30.8	THREONIC	5	1595	1.0	33.9	10.6	-*
PHENYLPYRUV	1781	172.2	PHENYLPYRUV	5	1781	1.1	179.5	16.4	-
4-OH-PHENYLL	1990	58.9	4-OH-PHENYLLAC	5	1992	0.8	52.1	7.3	**
PALMITIC	2093	55.7	PALMITIC	5	2095	0.7	34.8	9.2	*******

[a] See text for description. [b] Matched poorly to master library, but scored well (835) against average spectrum in historical library.

components missing in the new experiment, e.g., the unknown phthalate at RRI 1847 (Tables V and VI). There are new components, including, of course, phenylpyruvic acid–oxime–TMS (RRI 1780) because the manual extraction procedure did not include formation of oximes, and two amino acids, glycine and phenylalanine as the TMS derivatives (RRI 1325, 1719) which proved to be artifactual on a repeat analysis.

Application Example—Time Stability of Derivatives. We have also used HISLIB to monitor the long term stability of the trimethylsilyl derivatives of organic acid fractions, isolated by ion exchange, of human urine. Five samples were analyzed (from the same patient as above) 1, 2, 4, 8, and 24 h after derivative formation. The GC/MS profiles resembled each other closely enough to indicate decomposition was minimal after 24 h. After 72 h, a sixth analysis was made of the same mixture and this new GC/MS profile compared to an historical library composed of the first five experiments. We present in Table VII selected results from this comparison.

The GC/MS profile of the sixth experiment remained very similar to the previous profiles. This is established quantitatively by the strong similarity of the profiles reflected in the data of Table VII and summarized in the discrepancy column of the Table. We have no explanation for the observation of significantly greater amounts of palmitic acid–TMS and also succinic acid–diTMS; all other components compared very favorably.

Other Applications of HISLIB. From the preceding discussions, several other applications of HISLIB are suggested. We have presented examples of the use of HISLIB to check on the reproducibility of instrumentation and analytical procedures utilized to study complex mixtures. Clearly, the same technique can be used to explore other variables in an analytical scheme. HISLIB should facilitate detailed intercomparisons of complex mixtures, for example those encountered in diagnostic medicine where enhancements of GC/MS techniques are desirable (*17*).

Because the historical library can be updated at will, it is easy to maintain a long-term history of analysis of a particular type of mixture. Maintenance of several such libraries for different types of mixtures is a simple task. In fact, different historical libraries can be compared with one another, opening the possibility for comparison of results among laboratories engaged in similar research.

HISLIB averages spectra of the same compound. Thus, statistical variations in ion abundances are reduced as additional examples are encountered. The resulting average spectrum is frequently of much higher quality than a single spectrum in existing libraries. We have implemented a mechanism for adding averaged spectra to or replacing spectra in our primary library. This provides a mechanism for gradual improvement of spectral libraries with time. In addition, RRI's are included with the spectra, enabling us to improve the certainty with which subsequent spectra are matched to the primary library.

The method of comparing new profiles to an existing historical library quickly focuses attention on known materials present in abnormal quantities and on new components. The latter become subjects for more sophisticated structure elucidation procedures (*18*) which can now use the (high quality) mass spectral data directly to assist in solving the structures of unknowns (*19*).

Limitations. There are several limitations to the procedure which must be mentioned. We have not yet thoroughly investigated variations in relative concentrations with instrument operating parameters. The performance of any mass spectrometer may change as a function of time. Any change in performance which affects the ionization of the internal standard(s) relative to other mixture components will affect results of quantitation. This can be avoided in part by using several different standards in each run.

In the present implementation of the program, there are several deficiencies in the data analysis scheme. We have not included a procedure for easily deleting selected old experiments from an historical library—the library must currently be recreated excluding undesired experiments. Also the spectrum averaging scheme makes no decisions about including ions of low abundance—all are included. Ions which occur infrequently are diminished in importance as additional spectra are averaged, but they are not rejected because we have not yet developed adequate heuristics for removing such ions.

ACKNOWLEDGMENT

We thank Edwin Blaisdell, Mark Stefik, Wilfred Pereira, and Alan Duffield for their contributions to initial discussions of the problem addressed by HISLIB.

LITERATURE CITED

(1) R. G. Ridley, in "Biochemical Applications of Mass Spectrometry", G. R. Waller, Ed., John Wiley and Sons, New York, N.Y., 1972, p 177.
(2) F. W. Karasek and J. Michnowicz, *Res./Dev.*, **38**, May 1976.
(3) H. Nau and K. Biemann, *Anal. Lett.*, **6**, 1071 (1973).
(4) H. Nau and K. Biemann, *Anal. Chem.*, **46**, 426 (1974).
(5) C. C. Sweeley, N. D. Young, J. F. Holland, and S. C. Gates, *J. Chromatogr.*, **99**, 507 (1974).
(6) J. E. Biller and K. Biemann, *Anal. Lett.*, **7**, 515 (1974).
(7) R. G. Dromey, M. J. Stefik, T. C. Rindfleisch, and A. M. Duffield, *Anal. Chem.*, **48**, 1368 (1976).
(8) E. Jellum, P. Helland, L. Eldjarn, U. Markwardt, and J. Marhofer, *J. Chromatogr.*, **112**, 573 (1975).
(9) B. E. Blaisdell, *Anal. Chem.*, **49**, 180 (1977).
(10) W. E. Reynolds, in "Biochemical Applications of Mass Spectrometry", G. R. Waller, Ed., John Wiley and Sons, New York, N.Y., 1972, p 109.
(11) S. P. Markey, W. G. Urban, and S. P. Levine, "Mass Spectra of Compounds of Biological Interest", *U.S. At. Energy Comm. Rep.*, **No. TID-26553**, National Technical Information Service, U.S. Dept. of Commerce, Springfield, Va. 22161.
(12) H. S. Hertz, R. A. Hites, and K. Biemann, *Anal. Chem.*, **43**, 681 (1971).
(13) See for example, A. N. Kolmogorov and S. V. Fomin, "Elements of the Theory of Functions and Functional Analysis, Volume 1: Metric and Normed Spaces", Graylock Press, Rochester, N.Y., 1957, p 16.
(14) E. W. Dijkstra, *Numerische Math.*, **1**, 269 (1959).
(15) J. A. Thompson and S. P. Markey, *Anal. Chem.*, **47**, 1313 (1975).
(16) C. G. Hammer, B. Holmstedt, and R. Ryhage, *Anal. Biochem.*, **25**, 532 (1968).
(17) O. Stokke, *Biomed. Mass Spectrom.*, **3**, 97 (1976).
(18) R. E. Carhart, D. H. Smith, H. Brown, and C. Djerassi, *J. Am. Chem. Soc.*, *97*, 5755 (1975).
(19) D. H. Smith and R. E. Carhart, in "Chemical Applications of High Performance Spectrometry", M. L. Gross, Ed., Proceedings in press.

RECEIVED for review April 14, 1977. Accepted June 27, 1977. Work supported by grants from the National Institutes of Health (No. RR-612 and GM-20832) and from the National Aeronautics and Space Administration (No. NGR-05-020-632).

CORRESPONDENCE

Radiofrequency Oxygen Plasma Treatment of Pyrolytic Graphite Electrode Surfaces

Sir: The formation of oxygen-containing functional groups such as carboxyl, hydroxyl, carbonyl, lactone and quinone-like groups by electrochemical (*1–5*) or air oxidation (*6–8*) on the surface of high density carbon or pyrolytic graphite has been suggested. More recently, there has been considerable interest in these groups as a means of chemical attachment of molecular species for the purpose of "chemically modifying" electrode surfaces, as exemplified by the early work of Miller and co-workers on the fabrication of a chiral electrode (*10*). They employed high temperature air oxidation for the formation of carboxyl groups for use in binding of a stereospecific species to high density, microcrystalline graphite surfaces. Other oxidations of graphite involving the use of chemical agents (permanganate, chromate, etc.) have been reported (*8, 9*). In this communication, we wish to discuss the use of a radiofrequency (rf) plasma treatment of pyrolytic graphite (PG) in an oxygen atmosphere for the formation and enhancement of the surface population of oxygen-containing functionalities believed to primarily be carboxyl and hydroquinone/quinone groups. Surface analysis by scanning electron microscopy (SEM) and x-ray photoelectron spectroscopy (ESCA), and electrochemical characterization by cyclic voltammetry and differential pulse polarography (DPP) of the PG surfaces prior to and following plasma treatment are presented as supporting evidence. The nature of these plasma oxidized PG surfaces is probed further by chemical modifications which are specific to certain oxygen functionalities followed by surface and electrochemical analysis of these reacted surfaces.

EXPERIMENTAL

Materials. Isotropic, vapor deposited pyrolytic graphite (PG) electrodes in the form of disks (0.750 or 0.375 in. diameter × 0.125 in. thick) were obtained from Ultra-Carbon Corporation (Bay City, Mich.). According to the manufacturer the ultra-pure substrate material (UT-6 grade graphite) was ground flat prior to deposition of the pyrolytic (PT-101) graphite coating (ca. 1000-μm thickness).

Dimethyl sulfate (Eastman, practical grade), *N,N'*-dicyclohexylcarbodiimide (CDI; Pierce Chemical) and benzidine (BZ; Sigma Chemical) were used as received. Methylene chloride (MCB, reagent grade) was freshly distilled from anhydrous calcium chloride; the fraction boiling at 39.0 °C was retained. Water was deionized and triply distilled. Buffer compositions were as follows: pH 2.50 and pH 2.35, Sorensen's glycine I (0.1 M glycine + 0.1 N NaCl) and modified Sorensen's glycine I (0.1 M glycine + 0.1 N $KClO_4$); pH 5.10, Sorensen's citrate II (0.1 M sodium citrate); pH 7.00, phosphate (EM "titrisol" brand concentrate). All other chemicals were reagent grade or equivalent.

Apparatus. All electrochemical measurements were made in a two-compartment cell machined from Lucite (*11*). The carbon disk electrodes were held by compression against a neoprene O-ring to provide a leak-proof seal. Electrical contact with the working electrode was accomplished by means of a brass screw embedded in the back side of the disk. Cyclic voltammetric studies were conducted using a conventional three-electrode potentiostat with circuitry for compensation of solution resistance (*12*). A Princeton Applied Research model 174 polarograph was employed for differential pulse polarographic determinations. All electrode potentials were measured vs. a Ag/AgCl (1.00 M KCl) reference electrode.

Scanning electron micrographs were recorded with a Cambridge model S4-10 Stereoscan. A Physical Electronics Industries, Inc., model 548 electron spectrometer was used to obtain ESCA spectra. Spectra were recorded at a system pressure $\leq 8 \times 10^{-9}$ Torr.

Plasma etching of the PG electrodes was carried out using a rf generater manufactured by Harrick Scientific (Ossining, N.Y.). Electrodes were centrally positioned on a quartz plate inside the quartz discharge vessel. Oxygen (anhydrous) was admitted to the discharge cell via a needle valve, and differentially pumped

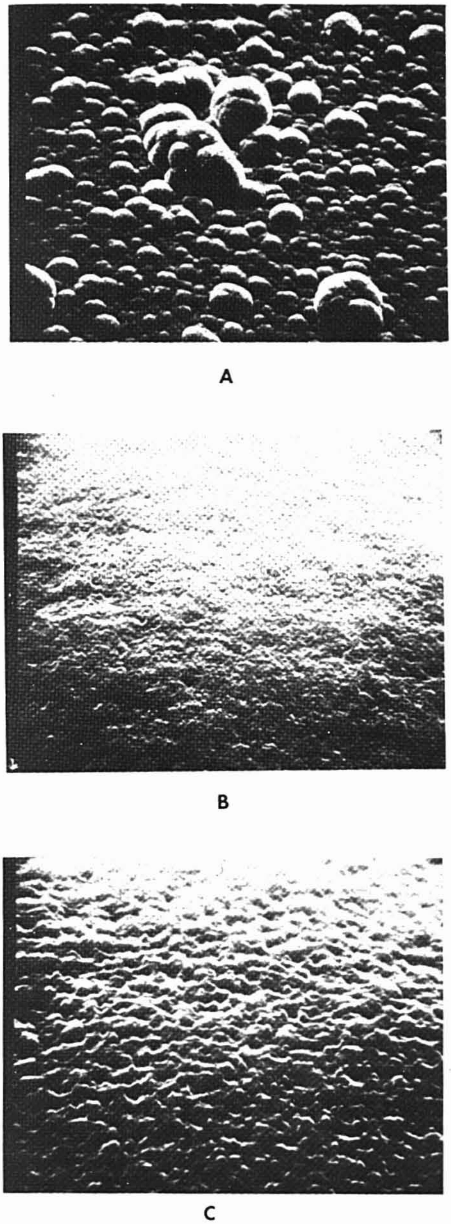

Figure 1. Scanning electron micrographs of PG electrodes: (A) untreated surface at low magnification (×200); (B) untreated surface at high magnification (×10 000); (C) plasma treated surface (1.5-h exposure) at high magnification (×10 000). Micrographs B and C are from the surface of one of the spheroids (see micrograph A)

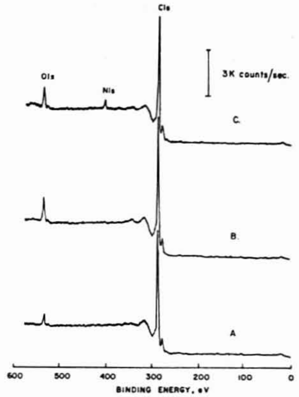

Figure 2. Low resolution ESCA spectra of PG surfaces: (A) untreated; (B) rf plasma etched (0.5-h exposure); (C) as B, with subsequent coupling of BZ. O/C atomic ratios: (A) 0.04, (B) 0.12, (C) 0.10; N/C atomic ratios: (A) nil, (B) nil, (C) 0.04

by means of a liquid nitrogen trapped mechanical vacuum pump. The constant pressure of oxygen (monitored via a thermocouple gauge) was maintained by adjustment of the needle valve during etching.

Procedures. The PG electrodes were initially extracted for 24 h in a Soxhlet apparatus using anhydrous methanol. Following extraction, residual solvent was removed by application of vacuum (<50 mTorr) for at least 4 h.

Plasma treatments (etching) were conducted at a pressure of 150 mTorr of anhydrous oxygen at ambient temperatures. With the exception of the etched specimens examined by SEM (1.5 h), exposures to the oxygen plasma were for 0.5 h.

Etched surfaces were methylated by dimethyl sulfate in refluxing methanol (10% v/v). The reaction was catalyzed by the addition of aqueous KOH to a chilled vessel (0 °C) containing the electrodes and the dimethyl sulfate solution. Following the addition of base, the solution was allowed to warm to room temperature and then refluxed for 1 h. Excess dimethyl sulfate was then hydrolyzed by the addition of water, after which the electrodes were thoroughly rinsed with water and placed in vacuum (<50 mTorr) for 4 h.

BZ (0.23 M) was coupled to the etched electrodes via the carbodiimide method of Sheehan and Hess (*13*) using CDI (0.17 M) in anhydrous methylene chloride (*14*). The coupling reaction was allowed to proceed at room temperature for 6 h. The reacted electrodes were then extracted with anhydrous methylene chloride for 12 h (Soxhlet) to remove adsorbed BZ, CDI, and dicyclohexyl urea. Following extraction, the electrodes were placed in vacuum (<50 mTorr) to remove residual solvent.

RESULTS AND DISCUSSION

The changes in the topography of the PG surfaces induced by the plasma treatment are clearly evident from examination of the SEM results shown in Figure 1. At low magnification (Figure 1A), the untreated surface appears to be comprised of spheroids. Higher magnification examination of these spheroids shows their surfaces to be relatively smooth (Figure 1B). After plasma treatment at 150 mTorr O_2 for 1.5 h., the surface is considerably roughened (Figure 1C). For the conditions employed for these treatments, the rate of removal of surface material is estimated to be ca. 100 Å/min.

The plasma treatment also increases the concentration of oxygen containing functional groups on the surface as detected by ESCA (Figure 2). Comparison of the low resolution ESCA spectrum typical of unetched speciments (Spectrum A) to that of etched electrodes (Spectrum B) shows a considerable enhancement of the O(1s) band. After correction for the O(1s)

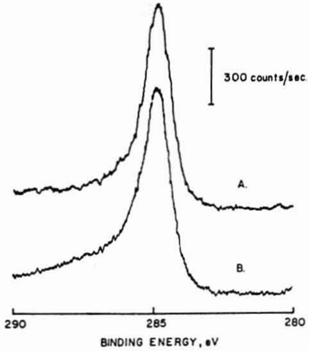

Figure 3. High resolution ESCA spectra of PG surfaces, C(1s) region: (A) untreated; (B) rf plasma etched (0.5-h exposure)

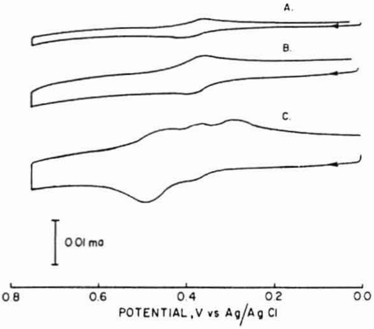

Figure 4. Cyclic voltammetry of PG surfaces in pH 2.50 glycine buffer: (A) untreated; (B) rf plasma etched (0.5-h exposure); (C) as B, with subsequent coupling of BZ. Scan rate = 50 mV/s, geometric electrode area = 1.82 cm^2

and C(1s) photoionization crosssections (*15*), the surface oxygen content (in terms of O/C atomic ratios) is increased by a factor of ca. 2.5 for the etched electrode. The high resolution C(1s) ESCA spectrum of the etched PG exhibits slight differences from the corresponding spectrum of the untreated PG (Figure 3). The C(1s) peak is noted to broaden at the high binding energy side. This is expected if surface oxides are formed, since a chemical shift for carbon has been noted for oxygen-containing compounds (*16*). The binding energy of the peak is not observed to shift (cf. Ref 17) nor is a well-defined shoulder observed on the high energy side of the carbon band. These results are taken as indication of the formation of *several* different types of surface oxygen containing functional groups arising from the plasma treatment. Resolution of the higher binding energy components (via band fitting) was not attempted primarily because the C(1s) peak of graphite basal planes (oxygen free) is noted to have similar asymmetry attributable to its metallic character (*17*). Consequently such fitting procedures would yield tenuous results (at best) in this case.

The cyclic voltammetry (background) of the untreated PB is shown in Figure 4, curve A. The quasi-reversible surface couple (*18, 19*) was present on all electrodes. The potential of this couple was dependent on solution pH (ca. 60 mV/pH unit) as noted from the data given in Table I. This pH dependence is consistent with a $2e^-/2H^+$ process such as that expected for a quinone/hydroquinone type species.

Table I. Shifts of Voltammetric Peak Potentials with Solution pH for the Electroactive Surface Species on PG Electrodes

Technique[a]	E_p (oxidation)	Solution pH
CV	+0.42	2.00[b]
	+0.41	2.35[c]
	+0.39	2.50[d]
	+0.24	5.10[e]
	—[g]	7.00[f]
DPP	+0.36	2.35[c]
	+0.39	2.50[c]
	+0.18	5.10[e]
	+0.02	7.00[f]

[a] CV: cyclic voltammetry, 50 mV/s sweep rate; DPP: differential pulse polarography, 1 mV/s sweep rate, 25-mV pulse amplitude, 2-Hz frequency. [b] Unbuffered HCl. [c] Glycine buffer, Cl$^-$ salt. [d] Glycine buffer, ClO_4^- salt. [e] Citrate buffer. [f] Phosphate buffer. [g] Cyclic voltammetric wave nearly totally attenuated in pH 7.00. In general CV and DPP peak heights were noted to be diminished with increasing pH.

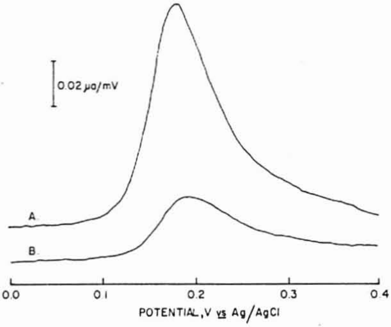

Figure 5. Differential pulse polarography of PG surfaces in pH 5.10 citrate buffer: (A) rf plasma etched surface (0.5-h exposure), (B) same electrode after methylation with dimethyl sulfate. Scan rate = 1 mV/s, pulse frequency = 2 Hz, pulse amplitude = 25 mV, geometric electrode area = 1.82 cm^2, initial potential = 0.0 V vs. Ag/AgCl

Plasma treatment affected the voltage–current curves in two ways. First, the charging current is increased overall as a result of an increase in the surface area. Second, the current in the potential region of the surface redox process increased considerably. This is interpreted as an enhancement in the number of oxygen-containing functional groups involved in the surface redox process which is in agreement with the ESCA findings.

Inferences as to the nature of the carbon surface oxides have come from examination of plasma treated samples prior to and following chemical modification by further reaction through rational chemical steps. For example, DPP curves shown in Figure 5 dramatically illustrate the decrease in peak height when the treated surface has been methylated via reaction with dimethyl sulfate. Methylation, which is expected to render the hydroxyl groups such as hydroquinone electroinactive, decreased the peak current (cf. curves A and B in Figure 5) by ca. 80%. However, the charging current at the methylated surface as examined by cyclic voltametry remained essentially unchanged.

Reaction of the untreated or high temperature air-oxidized surfaces with BZ (amidization of surface carboxyl groups) yielded no observable change in either the electrochemistry or low resolution ESCA spectrum. This result is in direct contrast to the success of coupling procedures requiring surface carboxyl groups carried out by Miller et al. on microcrystalline graphite rods (*10*) and edge planes of highly ordered pyrolytic graphite (*20*). Our attempts to generate (on PG) the carboxyl surface groups required for BZ coupling through the use of wet chemical methods (e.g. aqueous permanganate) were abandoned when surface analysis showed high contamination by oxidant. BZ coupling to plasma treated PG surfaces was found to occur readily. Both the electrochemistry of the etched PG surface (Figure 4, curve C) as well as the ESCA spectrum (Figure 2, trace C) were altered following BZ attachment indicative of the introduction of carboxyl groups by plasma treatment. The N(1s) signal observed in low resolution ESCA spectra of BZ coupled to the plasma treated PG is assigned to bound BZ. This conclusion is supported by the new peaks associated with the electrochemistry of bound BZ which are observed in the voltammogram for the coupled electrode.

No quantitation of BZ surface coverage was attempted from the ESCA data. However, surface coverage of BZ was estimated from the cyclic voltammetric responses given in Figure 4. If one assumes a $2e^-$/molecule consumption of charge for the oxidation of bound BZ (*21*); then the charge for the conversion of BZ (curve C), when corrected for background (curve B), corresponds to a coverage of $2.4(\pm0.2) \times 10^{-11}$ mol/cm^2 (geometric area).

CONCLUSIONS

Previous ESCA (*17*) and electrochemical studies (*5, 22*) on highly ordered pyrolytic graphite (HOPG) have indicated that oxygen functionalities are located exclusively on the edge planes of this material. These observations are consistent with the recent conclusions of Miller and co-workers (*20*) who found that chemical modification occurred on the edges of oxidized HOPG. The presence of significant amounts of oxygen by ESCA and of surface faradaic redox on untreated PG indicated the presence of exposed edge planes of graphite with oxygen functionalities. However, the extent of the exposed edge planes is probably relatively low in comparison to the surface area which is comprised of basal planes, since the electrochemical charging currents are only slightly larger than those reported for the basal surface of HOPG (*22*). It should be noted that the potential region at which the faradaic surface wave occurs is similar to that observed by Blurton (*23*) on pressed microcrystalline graphite, and by Randin and Yeager (*5, 22*) on the edge planes of HOPG.

Several authors have suggested a quinone/hydroquinone-type species as being responsible for the electroactive surface groups observed on various forms of carbon (*3, 5, 23, 24*). The DPP experiments on plasma treated PG before and after methylation and the attachment of silanes (*25*) and cyanuric chloride (*26*) to graphitic materials all support the presence of hydroxyl groups on the surface of conductive carbons. The existence of a quinone-like group is further implied from the chemical modifications of both glassy carbon and pressed graphite electrodes by Elliot and Murray (*25*) using 2,4-dinitrophenylhydrazine. We concur with Randin and Yeager (*5*) that the electroactive surface species is a 1,2-naphthoquinone-like structure rather than a bridgehead carbonyl, although there is no direct proof for this assignment at present.

The success of the BZ coupling to the plasma treated electrode supports the conclusion that rf etching induces the formation of carboxyl groups on PG. However, the surface coverage of carboxyl groups appears to be far less than monolayer. Due to the ambiguity in the efficiency of the coupling reaction (CDI method) and surface roughness, quantitation of the amount of carboxyl coverage is difficult. There may be other surface oxygen containing functional groups which form as a result of the plasma treatment in addition to the quinone-like and carboxyl species.

The rf plasma treatment is a rapid, reproducible, and contaminant-free procedure for the introduction and enhancement of oxygen groups. It apparently changes both the edge and basal planes of graphitic materials and appears superior to the use of chemical oxidants or high temperature, air oxidation. Indeed, the oxygen functional groups introduced on PG may be those involved in the catalysis noted previously for reduction of *p*-nitrophenol (*3*) and oxidation of nicotinamide adenine dinucleotide (*27*) at oxidized graphitic electrodes. We have also observed evidence for catalytic activity on the plasma treated PG surface (*28*). Further characterization and quantitation of these species are being pursued using various plasma treatments and physiochemical methods of analysis.

ACKNOWLEDGMENT

The authors express their gratitude to J. C. Tramontana (Xerox Corporation) and J. Swenton for helpful suggestions during the course of this work.

LITERATURE CITED

(1) G. Mamantov, D. R. Freeman, F. J. Miller, and H. E. Zittel, *J. Electroanal. Chem.*, **9**, 305 (1965).
(2) J. S. Mattson and H. B. Mark, Jr., "Activated Carbon", Marcel Dekker, New York, N.Y., 1971.
(3) B. D. Epstein, E. Dalle-Molle, and J. S. Mattson, *Carbon*, **9**, 609 (1971).
(4) W. J. Blaedel and R. A. Jenkins, *Anal. Chem.*, **46**, 1952 (1974).
(5) J. P. Randin and E. Yeager, *J. Electroanal. Chem.*, **58**, 313 (1975).
(6) H. P. Boehm, *Adv. Catal.*, **16**, 198 (1966).
(7) H. P. Boehm and M. Voll, *Carbon*, **8**, 227 (1970).
(8) B. R. Puri, in "Chemistry and Physics of Carbon", Vol. 6, P. L. Walker, Jr., Ed., Marcel Dekker, New York, N.Y., 1970.
(9) R. J. Taylor and A. A. Humffray, *J. Electroanal Chem.*, **42**, 347 (1973).
(10) B. F. Watkins, J. R. Behling, E. Kariv, and L. L. Miller, *J. Am. Chem. Soc.*, **97**, 3549 (1975).
(11) F. Hawkridge and T. Kuwana, *Anal. Chem.*, **45**, 1021 (1973).
(12) A. A. Pilla, *J. Electrochem. Soc.*, **118**, 702 (1971).
(13) J. C. Sheehan and G. P. Hess, *J. Am. Chem. Soc.*, **77**, 1067 (1955).
(14) R. B. Merrifield, J. M. Stewart, and N. Jernberg, *Anal. Chem.*, **38**, 1905 (1966).
(15) H. Berthou and K. Jorgensen, *Anal. Chem.*, **47**, 482 (1975).
(16) T. A. Carlson, "Photoelectron and Auger Spectroscopy", Plenum Press, New York, N.Y., 1975.
(17) J. M. Thomas, E. L. Evans, M. Barber, and P. Swift, *Trans. Faraday Soc.*, **67**, 1875 (1971).
(18) H. Angerstein-Kozlowska, J. Klinger, and B. E. Conway, *J. Electroanal. Chem.*, **75**, 45 (1977).
(19) H. Angerstein-Kozlowska, J. Klinger, and B. E. Conway, *J. Electroanal. Chem.*, **75**, 61 (1977).
(20) B. E. Firth, L. L. Miller, M. Mitani, T. Rogers, J. Lennox, and R. W. Murray, *J. Am. Chem. Soc.*, **98**, 8271 (1976).
(21) L. F. Oldfield and J. O'M. Bockris, *J. Phys. Chem.*, **55**, 1255 (1951).
(22) J. P. Randin and E. Yeager, *J. Electroanal. Chem.*, **36**, 257 (1972).
(23) K. F. Blurton, *Electrochim. Acta*, **18**, 869 (1973).
(24) V. A. Garten and D. E. Weiss, *Aust. J. Chem.*, **8**, 68 (1955).
(25) C. M. Elliot and R. W. Murray, *Anal. Chem.*, **48**, 1247 (1976).
(26) A. M. Yacynych and T. Kuwana, to be published.
(27) W. J. Blaedel and R. A. Jenkins, *Anal. Chem.*, **47**, 1337 (1975).
(28) J. F. Evans and T. Kuwana, *J. Electroanal. Chem.*, in press.

John F. Evans
Theodore Kuwana*

Department of Chemistry
The Ohio State University
Columbus, Ohio 43210

RECEIVED for review March 14, 1977. Accepted June 10, 1977. This work was supported by funds from NSF Grant Nos. CHE76-81591 and CHE73-04882, and US PHS Grant No. 19181.

Rate of Extraction of Copper from Aqueous Solutions

Sir: The increasing importance of the industrial production of copper by hydrometallurgical techniques has resulted in the development of a number of organic extractants under various trade names, e.g. LIX64N (General Mills), KELEX 100 (Ashland Chemical Company), and VERSATIC 911 (Shell Chemicals Ltd.). These commercial extractants are invariably kerosene solutions of organic chelating agents. The addition of a surfactant to the kerosene solution has been found to improve the phase separability and the addition of a second chelating agent has, in several instances, increased the rate of copper extraction from the aqueous phase. A definite need has arisen therefore, for a simple method that can be used routinely for the determination of the rate of copper extraction with new commercial formulations or new batches of the same extractant.

The extraction processes of industrial importance are quite rapid and it is futile to attempt to follow the kinetics of extraction by withdrawing and analyzing samples of the organic or aqueous phase at various intervals in the course of the extraction (*1*). Two general approaches have been found useful in the study of the kinetics of rapid extractions. One method that is widely employed makes use of an apparatus (AKUFVE) for the continuous measurement of the distribution of a solute in an extraction process (*2*). The apparatus consists of a mixer, a centrifuge for separation of the phases, and on-line detectors for the measurement of the solute concentration in the separated phases. Large volumes of the two phases are required and the effective interfacial area that is generated within the mixer cannot be determined. Despite these shortcomings, reliable distribution data for several liquid–liquid extraction systems have been obtained with the AKUFVE apparatus. A second method that has gained wide acceptance is the single drop technique in which droplets of known volume and surface area of one of the phases are allowed to contact the second phase for a predetermined period of time (*3, 4*). The problems that arise from the hydrodynamics of droplet systems are only moderately well characterized and the limited time of contact between the two phases restricts the amount of rate data that can be obtained. The method, however, has the advantage that the interfacial area can be treated as a variable and much useful information on the kinetics of solvent extraction has been obtained with the single drop method.

We have devised a simple and rapid method for monitoring the rate of extraction of copper ions from an aqueous phase into an organic phase containing a ligand that chelates copper ions. The concentration of copper(II) in aqueous phase can be continuously monitored without separation of the organic and aqueous phases. In addition, an experimentally reproducible interfacial area can be obtained by mixing the two phases under controlled conditions.

EXPERIMENTAL

Measured volumes of an aqueous phase containing copper(II) and an organic phase such as kerosene, containing a chelating agent, were introduced into a 150-mL jacketed vessel which was thermostated. The two phases were mixed with a variable speed magnetic stirring motor and stirring bar that was $1^1/_2$ inches long. The rate of stirring was determined by measurement of the frequency of the alternating current that was induced in a coil of coated copper wire wound around the jacketed glass vessel. At a stirring rate of 500 rpm or greater, the organic phase was uniformly dispersed in the aqueous layer and the rate of extraction was found to be independent of the stirring rate. The rate of extraction of copper(II) from the aqueous phase was monitored with an Orion Cupric Ion Selective Electrode (Model 94-29) with a double junction reference electrode. The electrodes immersed in a stirred two-phase system gave stable and reproducible potential differences for several hours at a time. Unstable readings were caused by the accumulation of the organic phase in the double junction reference electrode. This was remedied by periodically cleaning the outer compartment of the double junction and refilling it with a solution of 10% KNO_3. The potential differences were measured with an Orion Model 701 digital voltmeter and rate data were obtained from potential difference readings that were recorded as a function of time on a strip chart recorder.

The kinetic data were obtained as follows: ~75 mL of a 1.00×10^{-3} M solution of copper(II) nitrate and 25 mL of metallurgical grade kerosene were mixed in the jacketed vessel at 23.9 ± 0.1 °C and stirred at 500 rpm for several minutes until the digital voltmeter reading was constant. When the kerosene phase was evenly dispersed throughout the aqueous phase, a 2-mL sample of concentrated LIX, (obtained from General Mills) was injected into the two-phase mixture with a calibrated syringe. The potential difference between the copper ion selective electrode and the reference electrode was recorded as a function of time for about 12 min.

In one series of experiments that is discussed below, the effect of using LIX63, LIX65N, and LIX64N on the rate of extraction of copper from an aqueous solution is clearly demonstrated.

RESULTS AND DISCUSSION

The success of the method depends on the response of the cupric ion selective electrode to the aqueous phase concentration of copper(II) in the presence of the dispersed organic phase. The electrode response was Nernstian in 75 mL of an aqueous solution of Cu^{2+} (10^{-2} M–10^{-5} M) when the volume of the kerosene phase was increased from 2 to 25 mL and the rate of stirring maintained at 500 rpm. The electrode can be used over a wide range of pH and temperature. The only common transition metal ions that interfere with the electrode response are Ag^+, Hg^{2+}, and Fe^{3+}. Hence, care should be exercised in the interpretation of the rates of extraction of leach solutions that very often contain high concentrations of Fe^{3+}.

The reproducibility of the kinetic data is governed by the manner in which the kerosene phase containing the organic chelating agent (LIX) is contacted with the aqueous phase containing the copper(II). The best results were obtained by injection of a small volume (2 mL) of a concentrated solution of LIX in kerosene into the evenly dispersed two-phase system of kerosene (25 mL) in the aqueous solution (75 mL) containing Cu^{2+}, while stirring continuously at 500 rpm. Meaningful kinetic data are obtained only in the first 2 min after injection of the concentrated solution of LIX. The addition of a large volume of the kerosene solution containing the LIX to the aqueous phase containing Cu^{2+} is best avoided because the time that is required for the large volume of kerosene to be evenly dispersed, and for the electrode to attain equilibrium is at lease 30 s.

Figure 1 shows the relative rates at which Cu^{2+} is extracted by LIX63, LIX65N and LIX64N in kerosene under comparable conditions. LIX64N extracts Cu^{2+} rapidly and equilibrium is reached in a little over 2 min. The rate of extraction of Cu^{2+} with LIX63 is slower than with LIX64N and the rate of extraction is slowest with the LIX65N which has not reached equilibrium and is continuing to extract the Cu^{2+} even after 3 min have elapsed. These qualitative results have been substantiated by other workers (*3–5*). The organic chelating agent that is present in LIX63 is an α-hydroxyoxime, and in LIX65N a benzophenone oxime. LIX64N is a mixture containing LIX65N (~45%) and LIX63 (~1%). LIX64N

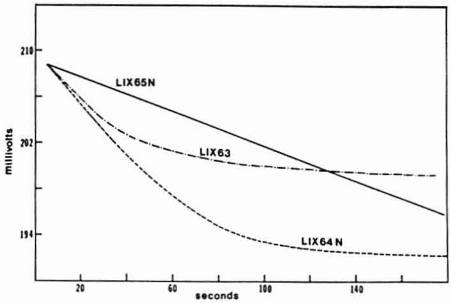

Figure 1. Variation of the rate of extraction of Cu^{2+} from an aqueous solution into kerosene solutions of LIX reagents. The solution consisted of 75 mL of 10^{-3} M $Cu(NO_3)_2$ and 25 mL of kerosene. Two mL of the concentrated LIX reagent in kerosene was injected into the solution that was being continuously stirred at 500 rpm with a magnetic stirrer. Millivolt readings were recorded 5 s after injection of the LIX

is clearly a superior extractant than either LIX63 or LIX65N; several explanations have been advanced for the synergistic effect of LIX64N, but convincing experimental evidence that supports any of these explanations is lacking. Kinetic data obtained by the single drop method and the AKUFVE apparatus for the extraction of copper(II) by LIX reagents have been reported recently (*3–5*). The results indicate that the interface plays an important role in the extraction process. It would be of interest to use the method proposed above to verify this conclusion.

ACKNOWLEDGMENT

The authors are grateful to R. N. Longwell of the Bluebird Mine, Miami, Ariz., for providing the LIX reagents used in this work.

LITERATURE CITED

(1) I. P. Alimarin, Yu. A. Zolotov, and V. A. Bodnya, *Pure Appl. Chem.*, **25**, 667 (1971).
(2) J. Rydberg, *Acta, Chem. Scand.*, **23**, 647 (1969).
(3) R. L. Atwood, D. N. Thatcher, and J. D. Miller, *Metall. Trans.*, **6B**, 465 (1975).
(4) R. J. Whewell, M. A. Hughes, and C. Hanson, *J. Inorg. Nucl. Chem.*, **37**, 2303 (1975).
(5) D. S. Flett, D. N. Okuhara, and D. R. Spink, *J. Inorg. Nucl. Chem.*, **35**, 2471 (1973).

Stephen J. Kirchner
Quintus Fernando*

Department of Chemistry
University of Arizona
Tucson, Arizona 85721

RECEIVED for review April 26, 1977. Accepted June 9, 1977. This work was supported by the Ranchers Exploration and Development Corporation, Albuquerque, N.M.

Corrosion of Stainless Steel by Organic Solvent Mixtures

Sir: In the course of conducting liquid chromatographic experiments we have noted occasional problems which arise when organic liquids are allowed to remain in contact with stainless steel materials (type 316).

Some corrosion effects are anticipated since it is known that formic, acetic, and propanoic acids are corrosive at room temperature (*1–3*). Carboxylic acids with higher molecular weight serve as corrosion inhibitors, while all organic acids are corrosive at temperatures above 300 °C (*4*). Other organic compounds, anhydrides, aldehydes, and those containing sulfur are also known to be corrosive to metals (*5*).

By contrast, most of the common organic solvents are regarded as noncorrosive. We wish to report our finding that certain of these solvents, although noncorrosive individually, may display a highly corrosive attack upon stainless steel when used in the form of mixtures.

Our findings can be summarized in terms of the following test. A 1.0-g piece of 316 stainless steel tubing, or of NBS Standard Reference Material No. 1155, was added to a glass vial containing 20 mL of a solvent or a solvent mixture—equally proportioned by volume. After 10 days of unagitated storage at 20–23 °C the samples showed the following changes. (I) No apparent change: with pure CCl_4 (this solvent is occasionally quite troublesome in HPLC, however), tetrahydrofuran, acetone, or diethylether. (II) Slight yellow coloring of the liquid with CCl_4 + acetone, CCl_4 + THF, CCl_4 + diethylether, and CCl_4 + isopropyl ether + acetone. (III) Forms viscous, brown colored liquid: CCl_4 + diethylether + acetone, CCl_4 + tetrahydrofuran + acetone. The results were not dependent on storage in room light or in darkness. Mixtures II or III produced changes that could easily be detected spectrophotometrically, by $\geq$10% transmission loss after 2 or 3 h.

The foregoing experiments were repeated using solvents of varied purity: reagent grade, those which had been commercially redistilled (in glass), and "spectroscopy" grade. The results were clearly dependent on the chemical nature of the materials and qualitatively, at least, independent of their source or purity. Since the presence of CCl_4 seemed critical to the results gathered so far, we also tested the effect of using chloroform in its place. These results were quite similar, although the reaction rates were clearly slower.

The weight loss was measured in experiments similar to II and III. After a period of time the steel was removed and rinsed with solvent. This removed a thin film from the surface of the steel. Mixed CCl_4 + THF caused weight loss that was linear with time up to 10% loss after 8 days. The loss from mixed CCl_4 + THF + acetone was also linear, but at twice the rate, up to 4 days. Then the rate accelerated to 23% loss after 24 days. The rates in III were boosted considerably by heating under boiling reflux. When the film was allowed to remain intact through gentle handling, the same experiments showed a weight gain of the dried sample of metal plus film. Gas chromatographic analysis of the liquid phase showed that a number of volatile products had formed.

In a separate experiment, mixtures of steel and solvent were stored in the dark at room temperature for 10 days. Gas chromatography showed that the reaction products contained a series of volatile compounds, as shown in Figure 1. An attempt to use GC/MS did not provide specific structure determinations, but it became clear that most of the volatile species contained more than one chlorine atom.

The volatile products in the case of the two mixtures in III, at least, seem to be quite dangerous. Severe eye irritation and headache were experienced after a single restricted exposure to test the odor. Gas evolution from any of the mixtures in

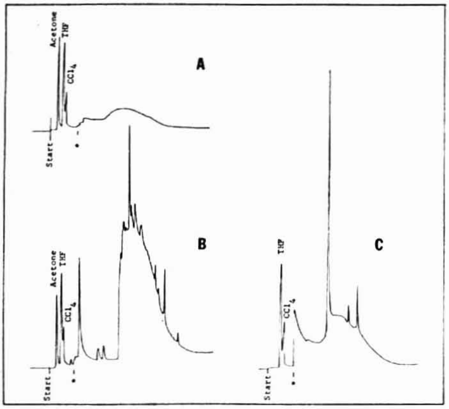

Figure 1. Gas chromatographic analysis of the following: (A) control mixture of acetone, tetrahydrofuran, and carbon tetrachloride; (B) same as A but after 10-days contact with stainless steel; and (C) after 10 days of contact with steel, tetrahydrofuran, and carbon tetrachloride. Conditions: 3% OV-101 on Chromosorb W, acid wash, DMCS treated, 50–275 °C program. At the asterisk (•), the FID amplifier gain was boosted 200-fold

III was sufficiently rapid that the vial was left unclosed to avoid pressure buildup. After three days of recirculating a mixture of CCl_4 + THF through an all-steel HPLC apparatus, the liquid stream turned dark brown and fouled the apparatus.

These results indicate a number of chemical changes which seems to be consistent with the known auto-oxidation of ethers (*6*), the ability of certain metals to form etherate complexes (*7, 8*), and the peroxide induced formation of CCl_3 radicals from CCl_4 (*9, 10*). Our experiments show that the present corrosion effects are primarily due to the presence of the halogenated hydrocarbon solvent while the other solvents may accelerate the attack and make the reactions more complicated.

It is clear that certain organic mixtures are peculiarly unstable during prolonged contact with stainless steel. For this reason we suspect that certain combinations of sample and solvent would lead to chemical changes in the components in the sample.

LITERATURE CITED

(1) C. N. Rowe, *NASA Spec., Publ.*, **NASA, JP-318**, 527–568, (1972) (Pub. 1973).
(2) U. R. Evans, "The Corrosion and Oxidation of Metals. First Supplementary Volume", Edward Arnold (Publishers), Ltd., London, 1968, p 247.
(3) E. Heitz, *Oberfläche Surf.*, **15**, 331 (1974).
(4) G. T. Paul, and J. J. Moran, "Stainless Steel, Corrosion Resistance of Metals and Alloys", 2nd ed., *ACS Monogr.*, **158**, 375 (1965).
(5) R. K. Swanby, "Corrosive, Corrosion Resistance of Metals and Alloys", 2nd ed., *ACS Monogr.*, **158**, 45 (1965).
(6) D. Elad, in "The Chemistry of the Ether Linkage", S. Patai, Ed., Interscience Publisher, London, New York, etc., 1967, p 361.
(7) W. Herwig, and H. H. Zeiss, *J. Am. Chem. Soc.*, **79**, 6561 (1957).
(8) K. J. Klabunde, *Acc. Chem. Res.*, **8**, 393 (1975).
(9) R. Hiatt, in "Organic Peroxides", D. Swern, Ed., Wiley Interscience, New York, N.Y., 1970, p 802.
(10) M. S. Kharasch, E. J. Jersen, and W. H. Urry, *J. Am. Chem. Soc.*, **69**, 1100 (1947).

Alice Y. Ku
David H. Freeman*

Department of Chemistry
University of Maryland
College Park, Maryland 20742

RECEIVED for review April 18, 1977. Accepted June 14, 1977. This work was supported by the National Science Foundation, Grant Number MPS 75-04802.

Sheet Resistivity Measurements of Chemically Modified Electrodes by Four-point Probe Method

Sir: Recently the use of chemically modified electrode surfaces has drawn wide attention (*1, 2*). Also photosensitization of semiconducting surfaces by dye adsorption is known (*3, 4*). Dyes have been attached to chloromethylated polymer bases via a chemical method (*5*). We decided to adsorb dyes on chemically modified electrodes, via silylation and chemical coupling. This way the monolayer coverage of the surface, rather than clusters of aggregated dyes, can be assured. The proof for surface modifications has been reported with ESCA and Auger investigations (*1, 2*). Another approach to investigate the surface modification, by measuring resistance change, is reported here. Such a method has been used to study the changes on electrochemical interphase (*6*). We used the four-point probe technique to measure the resistance changes as done by workers in the semiconductor field (*7*). The theory is given in the reference. Raman scattering study also showed some interesting aspects of the surface modification.

The effect of surface modification is more pronounced for the thin-film electrodes, as thin films possess high surface-to-mass ratio. The total free electron per unit area of the film is affected by molecular species forming bonds which change the surface scattering of electrons of the film. These perturbations of free electrons manifest strongly as a change in electrical conductance. The relative change in conductivity $\Delta\lambda/\lambda$ is shown to be

$$\frac{\Delta\lambda}{\lambda} = -\alpha\frac{n}{N}$$

where N is the total number of metal atoms present in the film, n the total number of adsorbed molecules, and α a constant characteristic of the adsorbing molecule (*8*).

Hence it is obvious that the measurement of the resistivity of thin-film electrodes will throw light on the nature of the surface modification. The four-point approach circumvents the problems of contact resistance and potential.

EXPERIMENTAL

Apparatus. Four gold-plated steel needles (sold in any fabric shop) were inserted collinearly in a Teflon block, with a distance of 0.300 cm between each. Care was taken to align them so that all the contacting needle points were at the same plane. To ensure firm contact, an insulated weight of 150 g was applied on the top of the Teflon block. Lead wires were soldered to the other ends. Later we were able to obtain a spring loaded four-point probe from government surplus (origin unknown) with a mean distance between the points, 0.064 cm. This probe had a pressure of 50 g when contacted with the surface.

Constant current was forced through the extreme two points, and the voltage between the inner two points of probe was measured. We designed the circuit shown in Figure 1, with operational amplifiers to directly measure the current–voltage characteristics in a short time. The circuit was driven with a triangular wave-generator and the I–V relationship was displayed on a x–y recorder. Values of sheet resistivities can be calculated from the slop (V–I curves, in ohms) and the dimensions of the films and the point contacts (*7*). For our purpose, for relative comparison, the measurement of the slope would suffice.

For Raman spectra, a double monochromator Spex-1401 was used with an argon ion laser.

Electrodes. The chemical modification was performed on doped tin-oxide electrodes. The plates (PE-81-E) were obtained from Libbey-Owens-Ford, Toledo, Ohio. They had electrical resistivity in the range 20–30 ohms/square. The plates were cut to 2-inch square. The experiments were run with eight such squares.

Table I. Slope (V/I) for Tin-Oxide Electrodes Obtained by Four-probe Method

No.	Before silylation, Ω	After silylation, Ω	With dye, Ω
1	13.96 ± 0.11	14.40 ± 0.10	14.70 ± 0.19
2	13.73 ± 0.06	14.02 ± 0.59	
3	14.40 ± 0.15	15.06 ± 0.19	15.18 ± 0.40
4	16.46 ± 0.04	16.62 ± 0.29	
5	14.72 ± 0.08	15.46 ± 0.70	14.86 ± 0.06
New probe			
6	11.95 ± 0.03	12.22 ± 0.09	16.86 ± 0.20
7	10.81 ± 0.09	11.67 ± 0.05	11.82 ± 0.36
Control plate			
8		11.69 ± 0.10	

Procedure. For chemical modification we essentially followed the procedure of Murray et al. (*1*). The silanization was performed with 3-chloropropyl trichloro silane on the clean tin-oxide electrode in benzene and thoroughly washed with benzene. Then silanized surfaces were refluxed with 1% solution of sodium salt of rose bengal dye in anhydrous methanol overnight. Finally the plates were refluxed in a soxhlet with methanol to remove physically adsorbed dye. All experiments were performed with the rigorous exclusion of moisture, in a glove bag in a dry nitrogen atmosphere. The control plate was refluxed with benzene without the silane. The plate was not refluxed in methanol.

RESULTS AND DISCUSSION

Data for the experimental V/I slopes are presented in Table I. Plates 1–5 were measured with the home-made probe; 6 and 7 were measured with the new probe. The standard deviation for 11 measurements is also given. We did this because the coatings were not very uniform (known by the appearance of interference pattern) and we were looking for a relatively small change in resistance. The control plate stayed constant at 11.69 ± 0.1 Ω. As one looks across the columns, one can notice the relative increase in the resistance of the plates (except plate No. 5). The changes in resistance for the nonsilylated plates to the silylated plates are more significant than those for the silylated plates to the dyed plates. One would not expect too much of a change for the dyed plates because the plates have already been modified by the silane and the dyes are attached to the silane. The effect of surface scattering loss would be less. What we are looking for here is a trend in the change in resistance, which we consider significant. It appears the dyes are bonded to the surface.

The values can be normalized by dividing the change in the conductance by the conductance of the unmodified surface ($\sim\Delta R/R$). If one assumes the thickness of the films to be uniform and the conductance to be directly related to area, the normalized values for all these plates should be the same for uniform coverage. A survey of the data shows that it is not so, indicating that the surface is not completely covered, by silanization. This confirms the observation of others (*1, 2*).

The Raman spectra of the pure silane [$Cl(CH_2)_3SiCl_3$] and the silanized electrode surface are shown in Figure 2. The peaks at 399 cm^{-1} and 423 cm^{-1} for pure silane are also seen in the reflectance Raman spectrum of the surface. We identify

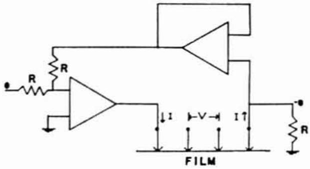

Figure 1. Circuit diagram for current-voltage measurement with four-point probe. *e* was varied with a ramp-generator. *V* and *I* were displayed on a *x–y* recorder. $I = -e/R$

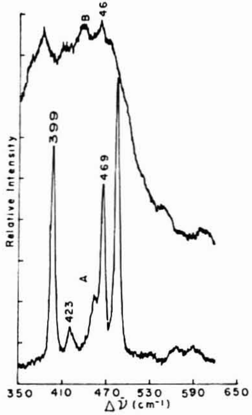

Figure 2. (A) Raman spectrum of pure $Cl(CH_2)_3SiCl_3$. (B) Raman spectrum of the modified tin-oxide electrode surface, washed in benzene only. The spectra were taken with the filter on, with an Ar ion laser

these to the Si–Cl bond (*9*). This indicates that not all the three bonds are involved in the binding of Si to the surface. It is an *experimental observation* that if there was any trace of silane on the electrode unbonded, the surface turned immediately "frosty" on exposure to atmosphere because of hydrolysis with water vapor. Our plates were clear despite the existence of some Si–Cl on the modified surface. The peak at 469 cm^{-1} is identified with C–Cl which could also be seen on the surface spectrum. We were surprised to see the Si–Cl bond even in the atmospheric air, as one would expect the Si–Cl to be hydrolyzed. Once again this corroborates Murray's interpretation of the silyl group extending away from the surface with C–Cl the farthest.

In conclusion, our results obtained from an independent technique confirm earlier observations by others.

ACKNOWLEDGMENT

We want to thank William Scovell for his assistance in obtaining the Raman spectra.

LITERATURE CITED

(1) P. R. Moses, L. Wier, and R. W. Murray, *Anal. Chem.*, **47**, 1882 (1975).
(2) N. R. Armstrong, A. W. C. Lin, M. Fujihara, and T. Kuwana, *Anal. Chem.*, **48**, 741 (1976).
(3) H. Gerischer, *Photochem. Photobiol.*, **16**, 243 (1972).
(4) R. Memming, *Photochem. Photobiol.*, **16**, 325 (1972).
(5) A. P. Schapp, A. L. Thayer, E. C. Blossey, and D. C. Neckers, *J. Am. Chem. Soc.*, **95**, 5820 (1973).
(6) W. J. Anderson and W. N. Hansen, *J. Electronal. Chem.*, **43**, 329 (1973).
(7) F. M. Smits, *Bell Syst. Tech. J.*, **37**, 711 (1958).
(8) P. Zwietering, H. L. T. Koks, and C. Van Heerden, *J. Phys. Chem. Solids*, **11**, 18 (1959).
(9) J. E. Griffiths, *Spectrochim. Acta, Part A*, **30**, 169 (1974).

Vakula S. Srinivasan*
Walter J. Lamb

Department of Chemistry
Bowling Green State University
Bowling Green, Ohio 43403

RECEIVED for review February 22, 1977. Accepted June 9, 1977. Acknowledgment is made to the donors of the Petroleum Research Fund, administered by the American Chemical Society, for support of this work. Presented in 1976 at the Pacific Conference on Chemistry and Spectroscopy, Phoenix, Ariz.

AIDS FOR ANALYTICAL CHEMISTS

Photographic Techniques for Fluorescent Spots on Thin-Layer Chromatographic Plates

P. W. Rulon* and M. J. Cardone

Norwich Pharmacal Company, Norwich, New York 13815

Documentation is a critical part of good laboratory practices and, in thin-layer chromatography (TLC) analysis, the documentation can be improved by using photographs to augment the written description of visual observations. To serve most effectively, the photographs must reproduce the visual observations as closely as possible. The following technique covers the color photography of UV activated fluorescent spots on TLC plates.

When attempting to photograph UV activated fluorescent spots, two problems become apparent. First, instant color print films are relatively slow (i.e., Polaroid type 58 film ASA 75) requiring long exposure times. Second, the film is extremely sensitive to the UV light used to activate the fluorescence, causing an overall blue cast in the final print. This blue cast affects the colors of the fluorescent spots causing them to appear too blue. The analyst can use color correction filters to remove the blue cast; however, the amount of filtration required results in exposure times of such length (over 5 min) that the film suffers reciprocity failure which further adds to the complexity of the problem.

Another way to circumvent the problem of film sensitivity to UV light is to use a UV cut-off filter over the lens of the camera. A Wratten 2E filter will eliminate both long wave 365- and short wave 254-nm light from exposing the film. The resultant photograph will be fluorescent spots, seemingly suspended in mid air, with true color rendition of the spots. This procedure is not acceptable since there is no frame of reference for the spots. In fact, when the analyst visually inspects a TLC plate in a view box, he can see the plate because of the eyes' limited sensitivity to UV. Other UV filters are available that cut off the UV light (i.e. 2A, 2B), but are not as efficient as the 2E. The residual UV light transmitted results in a blue appearance of the print, and spot color is not true.

EXPERIMENTAL

Photography was carried out on a Camag MP-4 Camera system, equipped with Foto-UV lighting system using Polaroid Type 58 film. The Foto-UV system consists of two 8-W mercury short wave lamps, 8-W black lite long wave lamps, and two Corning 9863 filters. WARNING: Do not view UV lights without proper eye protection! Four 150-W photofloods Type B provide the white light source.

Procedure. Place a TLC plate on the copy stand base, center, frame, and bring into proper focus. Place an 80B filter in the filter drawer, set the *f*-stop for 5.6, and set shutter speed at $^1/_{60}$ s. Switch on the photofloods and allow to come to proper temperature for 5 s before the exposure is made. Trip the shutter, turn the lights off without moving anything. Replace the 80B with a 2E filter, reset the *f*-stop to 4.5 and allow the long wave UV (short wave may also be used) lamps to warm up for 5 s. Make a second exposure for 1 full minute by holding down the shutter release. Turn off the lamps, remove the film from the camera, and process as recommended.

RESULTS AND DISCUSSION

The result is a photograph that has the proper color rendition and is taken using reasonable exposure times. Each part of the intentional double exposure serves a different function. The first exposure sets a frame of reference for the spots. The 80B filter provides the proper color correction to allow the use of photofloods with a daylight type film. The proper result of this exposure should be a dim plate that is gray in color. The plate should be light enough to be able to read any notations written on the plate, but as dark as possible to retain contrast in final print. If the plate is not gray, a color correction filter may be used (this is usually unnecessary).

The second exposure photographs the spots. The 2E filter is a UV cut off filter, preventing any of the UV light that is used to activate the fluorescence from exposing the film. This filter prevents the blue cast from appearing on the film, resulting in proper color of the spots. Color correction filters at this point are unnecessary.

An important benefit from this procedure is that the film speed is effectively increased for the second exposure. The first exposure serves to "preflash" the film for the second exposure. The technique of "preflashing" film to get higher effective film speeds has been used by photographers for many years.

CONCLUSIONS

The procedure outlined above allows the analyst to photograph UV activated fluorescent spots on TLC plates with the following three advantages: (1) The exposure times are shorter than with other techniques; (2) the use of color-correcting filters is usually not necessary; (3) the colors of the fluorescent spots in the final print closely match those seen by the eye. Since the prints obtained by this procedure reasonably represent what is seen by the eye, they can be valuable documents for the TLC analysis.

The technique outlined above is not limited to the specific camera system indicated under Experimental. The only requirement is that the copy stand has both a UV and white light source and can accommodate filters. The first exposure can be determined experimentally by installing the proper filter for the light source, and adjusting exposure until the print shows a dark gray plate. The second exposure uses the 2E filter and exposure time is adjusted until the intensity of the fluorescent spot in the prints matches that seen by the eye.

RECEIVED for review April 11, 1977. Accepted June 6, 1977.

Determination of Mercury in Edible Oils by Combustion and Atomic Absorption Spectrophotometry

Wei-Chong Tsai and Lih-Jiuan Shiau

Food Industry Research and Development Institute, P.O. Box 246, Hsinchu, Taiwan, Republic of China

In recent years, the environmental mercury contamination has been recognized as a health problem. Accurate and reliable methods of analysis of a wide variety of materials, which may contain trace amounts of mercury in both organic and inorganic forms, are needed. Alkyl or aryl forms of mercury may be determined by gas–liquid chromatography (*1–3*). After wet digestion or combustion, total mercury could be quantitatively determined by using various methods, of which the application of flameless atomic absorption spectrophotometry is perhaps the most common and convenient one. Although much has been studied on the occurrence of mercury in biological materials, such as fish and grain, by acid digestion followed by reduction and aeration (*4*, *5*), by amalgamation and heating (*6*, *7*), by direct combustion (*8*, *9*), or by various combinations of these and other less common techniques (*10–14*), little has been known about the mercury contamination in vegetable oils.

Knauer et al. (*15*) determined mercury in petroleum and petroleum products by burning the sample in a Wickbold oxy-hydrogen combustion apparatus and collecting the vaporized mercury in an acidic permanganate solution, and essentially quantitative recoveries were obtained. This paper describes a rapid and reliable method that can be carried out with equipment available in most laboratories. The method, which is a modification of the Schöniger combustion technique (*8*, *9*), includes pretreatment of the sample by burning and collection of the vaporized mercury in an acidic permanganate solution. The closed-system combustion apparatus, in which the sample was burned with the aid of oxygen stream, is different from Wickbold's combustion apparatus.

EXPERIMENTAL

Reagents. (a) Acidic potassium permanganate oxidizing solution was prepared daily by dissolving 5 g of reagent-grade potassium permanganate in 1 L of 3 N H_2SO_4 solution. (b) Stannous chloride reducing solution (*16*) was prepared by dissolving 1 g of reagent-grade hydrazine dichloride, 20 g of sodium chloride, 20 g of hydroxylamine hydrochloride, and 33 g of stannous chloride in 25 mL of 18 N H_2SO_4 and diluting to the volume of 1 L with deionized distilled water. (c) Stock solution of $HgCl_2$ (1000 μg Hg/mL) was prepared from E. Merck standard

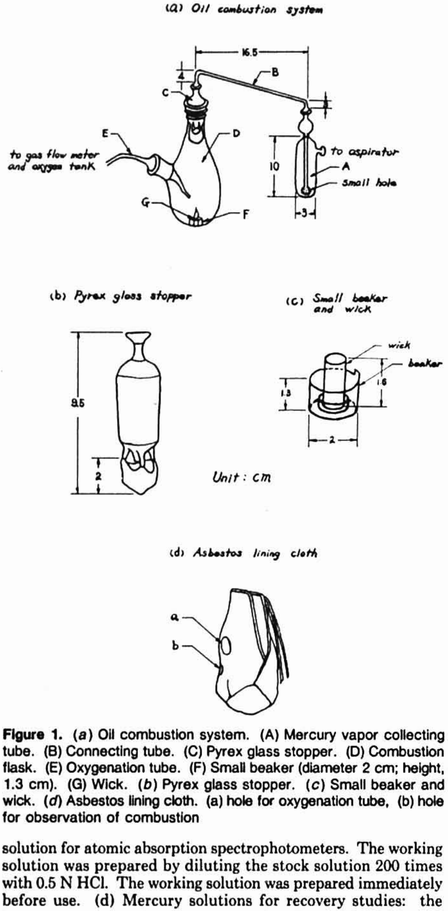
(a) Oil combustion system
16.5
B
4
C
E
D
to gas flow meter and oxygen tank
10
to aspirator
A
Small hole
G
F
3
(b) Pyrex glass stopper
9.5
2
(c) Small beaker and wick
wick
beaker
1.3
1.6
2
Unit: cm
(d) Asbestos lining cloth
a
b

Figure 1. (*a*) Oil combustion system. (A) Mercury vapor collecting tube. (B) Connecting tube. (C) Pyrex glass stopper. (D) Combustion flask. (E) Oxygenation tube. (F) Small beaker (diameter 2 cm; height, 1.3 cm). (G) Wick. (*b*) Pyrex glass stopper. (*c*) Small beaker and wick. (*d*) Asbestos lining cloth. (a) hole for oxygenation tube, (b) hole for observation of combustion

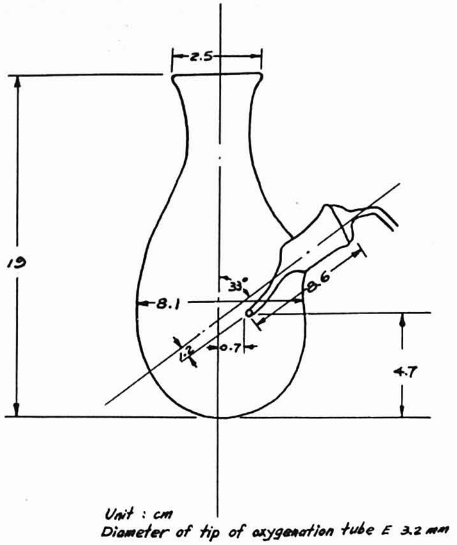

Figure 2. Combustion flask (D) and oxygenation tube (E) of Figure 1

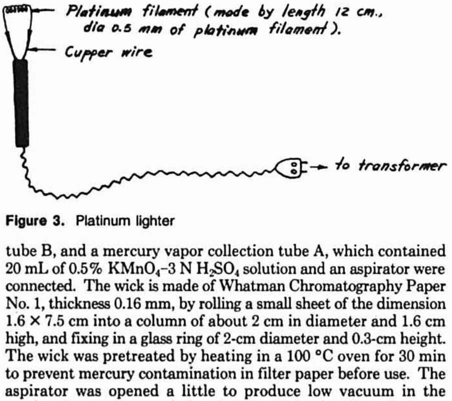
Platinum filament (made by length 12 cm., dia 0.5 mm of platinum filament).
Cupper wire
to transformer

Figure 3. Platinum lighter

solution for atomic absorption spectrophotometers. The working solution was prepared by diluting the stock solution 200 times with 0.5 N HCl. The working solution was prepared immediately before use. (d) Mercury solutions for recovery studies: the inorganic mercury solution was prepared by diluting the inorganic mercury standard stock solution (1000 μg Hg/mL) 100 times with acetone; phenylmercuric acetate solution was prepared by dissolving 1.70 mg of phenylmercuric acetate in 100 mL of acetone, and the concentration of mercury is about 10 μg/mL; and methylmercuric chloride solution was prepared by dissolving 1.25 mg of methylmercuric chloride in 100 mL of acetone, and the concentration of mercury is about 10 μg/mL.

The accurate mercury concentrations of the three solutions were standardized against a water solution of mercury standard and were rechecked every time they were used. Samples were pretreated by mixing with 20 mL of the acidic permanganate solution and incubated in a boiling water bath for 10 min to decompose acetone and other organic compounds.

Apparatus. The combustion system is shown in Figures 1, 2, and 3 and the Mercury Analyzer, Coleman MAS-50, was used for cold vapor mercury determination. All glassware used for experiments was decontaminated from mercury by soaking in a cleaning solution overnight and then rinsing thoroughly with deionized distilled water and oven-drying.

Procedure. About 2 g of edible oil was precisely weighed into a small beaker F and put into the flask D, which was encapsulated with asbestos lining cloth for insulation. A wick was set at the center of the beaker F, and a Pyrex glass stopper C, a connection tube B, and a mercury vapor collection tube A, which contained 20 mL of 0.5% $KMnO_4$–3 N H_2SO_4 solution and an aspirator were connected. The wick is made of Whatman Chromatography Paper No. 1, thickness 0.16 mm, by rolling a small sheet of the dimension 1.6 × 7.5 cm into a column of about 2 cm in diameter and 1.6 cm high, and fixing in a glass ring of 2-cm diameter and 0.3-cm height. The wick was pretreated by heating in a 100 °C oven for 30 min to prevent mercury contamination in filter paper before use. The aspirator was opened a little to produce low vacuum in the combustion system, and the wick was lighted with a platinum electric lighter (Figure 3). The oxygenation tube E was immediately attached, and the oxygen flow rate was first adjusted to about 200 mL/min and then to about 600 mL/min, and soot formation should be avoided. After 12–14 min of combustion, the sample oil and the wick would be burned out. The oxygen flow was kept for 2 more minutes to drive out the residual mercury vapor from the flask D. The mercury vapor collection tube A was put in boiling water for 10 min (this step could be omitted if the sample contains no organic mercury), and then the solution was transferred into a BOD bottle. A small amount of hydroxylamine–hydrochloride was added to reduce $KMnO_4$ before 10 mL of the stannous chloride solution was added. Total mercury in the sample was determined by the mercury analyzer, Coleman MAS 50.

RESULTS AND DISCUSSION

In order to decompose solvent acetone and organic forms of mercury for accurate determination of mercury concentration, the mercury solution was incubated with 20 mL of

Table I. Oxidative Decomposition Effect of 0.5% $KMnO_4$-3 N H_2SO_4 Solution on Acetone and Mercuric Compounds after Incubation for Different Periods of Time in a Boiling Water Bath

Mercuric compound[a]	Meter reading (μg Hg) after incubation 0 min	5 min	10 min	20 min	40 min	60 min
$HgCl_2$	0.151	0.134	0.128	0.137	0.135	
CH_3ClHg	0.043	0.134	0.141	0.137	0.142	0.141
$C_6H_5HgOCOCH_3$	0.071	0.098	0.096	0.096	0.097	0.100

[a] All three mercuric compounds were dissolved in acetone to about 10 μg Hg mL, and 0.01 mL of the solutions were taken for incubation with 20 mL of 0.5% $KMnO_4$-3 N H_2SO_4. Each datum was the average of two determinations.

Table II. Recovery of Mercury Added in the Forms of Various Mercury Compounds to Soybean Oil by the Proposed Method

Mercury compound	$HgCl_2$			CH_3HgCl		$C_6H_5HgOCOCH_3$	
Hg added, μg/mL	0	0.033	0.068	0	0.063	0	0.052
Hg found, μg/mL	0.007	0.041	0.074	0.006	0.071	0.007	0.060
	0.008	0.042	0.075	0.007	0.066	0.008	0.058
	0.008	0.039	0.075	0.006	0.068	0.006	0.059
	0.007	0.040	0.076	0.006	0.068	0.008	0.059
Mean, μg/mL	0.008	0.041	0.075	0.006	0.068	0.007	0.059
Corrected for blanks		0.033	0.067		0.062		0.052
Recovery, %		100	99		99		100

Table III. Reproducibility of Mercury Analysis by the Proposed Method on Mercuric(II) Chloride Added at Various Concentrations

	I	II	III
Hg found, μg/mL	0.045	0.081	0.153
	0.046	0.080	0.160
	0.044	0.081	0.163
	0.045	0.080	0.160
	0.045	0.080	0.160
	0.046	0.084	0.165
Mean ± S.D.	0.045 ± 0.64%	0.081 ± 0.90%	0.160 ± 0.95%

Table IV. Effects of Temperature of Combustion Flask before Burning, Amounts of Oxygen Supply, and Time Length of Burning on the Determination of Mercury in Soybean Oil

Oxygen flow rate	Temperature of flask before burning, °C[a]	Time length of burning	Hg found, μg
620 mL/min	26	14 min, 20 s	0.090
	30	13 min, 28 s	0.090
	70	12 min, 21 s	0.090
	85	10 min, 45 s	0.090
420 mL/min	24	15 min, 56 s	0.087
	36	18 min, 44 s	0.090
	70	17 min, 28 s	0.090
	121	18 min, 15 s	0.085

[a] Temperature of outside bottom of flask D was measured with a Type J Iron Constantan Thermocouple.

0.5% $KMnO_4$-3 N H_2SO_4 in a boiling water bath. Five minutes of incubation was sufficient to digest organic matters contained in the incubation mixture, and further incubation did not change the mercury analytic results (Table I). Ten minutes of incubation was taken to ensure complete decomposition of all organic matters in the sample solution. For recovery studies on mercuric(II) chloride, methylmercuric chloride, and phenylmercuric acetate by the proposed method, known amounts of the mercury solution were added to soybean oil. The results in Table II showed that recoveries of $HgCl_2$ in levels of 0.033 ppm and 0.068 ppm were 100% and 99%, respectively, and of methylmercuric chloride and phenylmercuric acetate in levels of 0.063 ppm and 0.052 ppm were 99% and 100%, respectively. Reproducibility of analysis by the combustion techniques was good at low levels of mercury in 2.0 g of soybean oil. Table III showed the results with standard deviations of 0.64%, 0.90%, and 0.95% for six repeated analyses at levels of 0.045, 0.081, and 0.160 ppm, respectively. This recovery experiment was carried out by weighing 2-g samples to which different amounts of mercuric chloride were premixed. Therefore, there were no errors caused by micropipetting variation, which was associated with the experimental results of Table I and II.

The temperature of flask D before burning, amounts of oxygen supply (in the range of 420 mL/min to 620 mL/min without soot formation), and the time length of burning (in the range of 11–19 min) had no significant effect on the determination of mercury in soybean oil (Table IV). Therefore, the apparatus can be continuously used by changing the small beaker F charged with a new sample.

Satisfactory results of mercury determination depend on the conditions of sample burning. The soot formation during sample burning caused low recoveries. To prevent soot formation, the diameter of the tip and the angle or slope of the oxygen flow tube, as well as the distance between the tip of oxygen flow tube and the wick should be kept in such a fashion as shown in Figure 2, and the oxygen flow rate should be kept at about 600 mL/min in order to avoid overoxygenation, which will cause soot formation. Such a special alignment is very important for obtaining ideal combustion without soot formation. A few times of practice was needed to find the best conditions. It is essential to insulate the flask D with asbestos lining cloth. Partial insulation by putting some glass fiber underneath the flask D resulted in recoveries in a range of about 70–80%, which were dependent on burning conditions. For a sample containing organic mercuric compounds, after collecting mercury vapor in 0.5% $KMnO_4$-3 N H_2SO_4 in tube A, it is advisable to incubate the solution in tube A in boiling water for 10 min in order to decompose the residual organic mercury compounds possibly remained unburned. Without further incubation in boiling water, the recoveries of inorganic mercury, phenylmercuric acetate, and methylmercuric chloride were about 100%, 90%, and 80%, respectively, while they were all about 100% with further incubation.

LITERATURE CITED

(1) G. Westöö, *Acta Chem. Scand.*, **22**, 2277 (1968).
(2) S. Nishi and Y. Horimoto, *Bunseki Kagaku*, **17**, 75 (1968).
(3) P. Zarnegar and P. Mushak, *Anal. Chim. Acta*, **69**, 389 (1974).
(4) W. R. Hatch and W. L. Ott, *Anal. Chem.*, **40**, 2085 (1968).

(5) R. K. Munns and D. C. Holland, *J. Assoc. Off. Anal. Chem.*, **54**, 202 (1971).
(6) M. J. Fishman, *Anal. Chem.*, **42**, 1462 (1970).
(7) I. Okuno, R. A. Wilson, and R. E. White, *J. Assoc. Off. Anal. Chem.*, **55**, 96 (1972).
(8) W. J. Herrmann, Jr., J. W. Butler, and R. G. Smith, in "Laboratory Diagnosis of Diseases Caused by Toxic Agents", F. W. Sunderman and F. W. Sunderman, Jr., Ed., Warren H. Green, Inc., St. Louis, Mo., 1970, p 379.
(9) R. J. Thomas, R. A. Hagstrom, and E. Kuchar, *Anal. Chem.*, **44**, 512 (1972).
(10) G. Thilliez, *Chem. Anal. Part.*, **50**, 226 (1968).
(11) V. Lidums and U. Ulfvarson, *Acta Chem. Scand.*, **22**, 2150 (1968).
(12) G. W. Kalb, *At. Absorp. Newsl.*, **9**, 84 (1970).
(13) T. Ukita, T. Osawa, N. Imura, M. Tonomura, Y. Sayato, K. Nakamura, S. Kanno, S. Fudui, M. Kaneko, S. Ishikura, M. Yonaba, and T. Nakamura, *J. Hyg. Chem.*, **16**, 258 (1970).
(14) O. I. Joensuu, *Appl. Spectrosc.*, **25**, 526 (1971).
(15) H. E. Knauer and G. E. Milliman, *Anal. Chem.*, **47**, 1263 (1975).
(16) W. L. Hoover, J. R. Melton, and R. A. Howard, *J. Assoc. Off. Anal. Chem.*, **54**, 860 (1971).

RECEIVED for review February 15, 1977. Accepted June 1, 1977. This research was supported by the National Council of Science (Republic of China) NSC-65B-0409-18(02).

Dry Ashing of Animal Tissues for Atomic Absorption Spectrometric Determination of Zinc, Copper, Cadmium, Lead, Iron, Manganese, Magnesium and Calcium

E. E. Menden, D. Brockman, H. Choudhury, and H. G. Petering*

Kettering Laboratory, Department of Environmental Health, University of Cincinnati College of Medicine, Cincinnati, Ohio 45267

In the course of a study of the toxicity of heavy metal ingestion to the offspring of pregnant rats, we were faced with the task of analyzing a single sample by flame atomic absorption for zinc, copper, iron, manganese, magnesium, calcium, and cadmium or lead in a difficult matrix containing bone in addition to other tissues.

Wet ashing was initially employed. It was observed then that a large part of the sample residue resulting from ashing and evaporation of the remaining acid could not be dissolved in hot 10% or concentrated nitric acids prior to dilution of the samples for atomic absorption spectrophotometry. This prompted a decision to investigate dry ashing as a suitable alternate method of sample preparation.

A survey of literature indicated that there were several dry ashing methods with possible application to the kind of samples being investigated, although none described the determination of all of the eight metals of interest to us (*1*). It was also evident that the recovery of metals, such as cadmium (*2*), lead (*3*), iron and calcium (*4*) and to a lesser degree zinc and copper, could be affected by sample matrix composition, temperature of ashing, interaction with the sample vessel and by incomplete solubility of the ash.

Therefore, in the dry ashing method which was subsequently developed and which is described in this publication it was necessary to incorporate optimal dry ashing conditions and an effective solubilization procedure so that these obstacles were overcome and maximum recoveries of all metals were achieved.

EXPERIMENTAL

Apparatus. A Perkin-Elmer Model 403 atomic absorption spectrophotometer was used as equipped with a strip chart recorder, air–acetylene and nitrous oxide–acetylene burners, and a deuterium arc lamp for background correction.

A large hot plate with regulated temperature settings was used for evaporating and dissolving. Dry ashing took place in a Thermolyne Model F-6020 muffle furnace equipped with a close tolerance temperature controller (Furnatrol 133).

Reagents and Standards. Reagent grade Fisher Scientific hydrochloric and perchloric acids and potassium sulfate, and J. T. Baker nitric acid were sufficiently pure for direct use.

Ash-aid (*5*) consisted of potassium sulfate dissolved in hot concentrated nitric acid (0.25 g/mL).

Atomic absorption mixed metal standards, covering the range of 0.01 to 100 ppm were made in a solution consisting of 10% nitric acid, 0.85% hydrochloric acid, and 2.5 g of potassium sulfate per liter.

Single metal standards, from which aliquots were added to tissue samples for recovery tests, were prepared in a solution containing 2.4% nitric acid, 0.18% hydrochloric acid, and 0.05% perchloric acid. An equal volume of this blank solution was added to each tissue serving as control.

Procedure. Bodies of day-old rat pups of 5–7 g fresh weight, one-half of which were from cadmium-exposed mothers, were used in the experiments. Variable surface contamination of the bodies was removed by soaking them for several minutes in 1% EDTA (*6*) solution and rinsing with deionized water. Chromium plated surgical instruments also immersed in the EDTA solution, were used to cut up and mince the tissues. Each tissue sample was then distributed in equal weights between two 50-mL metal-free Pyrex beakers, one serving as the control and the other as the recovery test sample.

The duplicate samples were oven dried until constant weight was attained and weighed. Standard aliquots containing 70 μg of zinc, 26 μg of copper, 3 μg of cadmium and lead, 300 μg of iron, 10 μg of manganese, 1000 μg of magnesium, and 8000 μg of calcium were added to the test samples. An equal volume of the solution in which single standards were prepared was added to each control sample and all samples were taken to dryness at ca. 120 °C. The added metals amounted to between 40 and 200% of the metal levels usually contained by such tissue samples (except for manganese, which was in 9-fold excess).

The dried tissue was subjected to charring in the furnace at 300 °C for 5 h. The samples were placed in a cold furnace and the charring temperature was reached in approximately 40 min. One milliliter of ash-aid and 3 mL of concentrated nitric acid were added to each sample and the char was broken up and roughly ground with a thick glass rod while in contact with the liquid. The samples were taken to dryness at the ca. 120 °C temperature, which was used for all evaporation and dissolution treatments on the hot plate.

The ashing took place at 400 °C in the furnace, over 20–24 h. Then the samples were treated with 3 mL of concentrated nitric acid and the acid was evaporated. Ashing was completed at the same temperature over 2–4 h, resulting in a white to yellow ash.

At this point the samples were divided into groups of 5 test/control pairs per group, each group including 2–3 pairs of tissue samples from cadmium exposed animals. A different ash solubilization method was tested on each group. One method which produced good results for all metals and two other ones which gave poor or inconsistent recoveries of calcium only, are further described.

Method A consisted of successive additions and evaporations of two 5-mL volumes of aqua regia. The ash residue was then dissolved by adding a third volume of aqua regia, heating until vapors appeared, agitating the beaker contents, adding 5 mL of water, reheating and again mixing the contents. Water was

Table I. Recoveries of Added Metals, Mean ± Relative Standard Deviation (Percent, $n = 5$)

Metal	Method A	Method B	Method C
Zn	100.1 ± 6.8	95.1 ± 4.4	100.2 ± 6.1
Cu	99.9 ± 6.3	95.6 ± 7.7	96.5 ± 7.0
Cd	95.9 ± 2.2	97.4 ± 3.6	99.8 ± 3.7
Pb	96.0 ± 8.5	96.4 ± 8.1	98.9 ± 9.8
Fe	94.7 ± 8.2	96.2 ± 9.0	97.8 ± 5.9
Mn	99.8 ± 3.5	102.8 ± 5.9	102.1 ± 7.1
Mg	98.7 ± 7.6	99.6 ± 7.1	102.3 ± 6.2
Ca	96.0 ± 7.3	51.0 ± 24.0	101.8 ± 26.8

replenished if a volume reduction occurred upon longer heating, and the contents were transferred to a 10-mL volumetric flask and readjusted to 10.0 mL with water upon cooling.

Method B was somewhat similar to Method A. The first two treatments were with concentrated hydrochloric acid and the third one was with concentrated nitric acid. The nitric acid was evaporated to ca. 1.5 mL. Water was added not to exceed a total volume of 10 mL, and the contents reheated and transferred to a 10-mL volumetric flask.

Method C followed the procedure of Method B, except for two treatments with aqua regia after the hydrochloric acid ones, and before the final nitric acid one.

Background compensation was used with the atomic absorption instrument when determining cadmium, lead, manganese, magnesium, and calcium, and 100-fold dilutions were required to read magnesium and calcium.

RESULTS AND DISCUSSION

Table I depicts the recoveries of zinc, copper, cadmium, lead, iron, manganese, magnesium, and calcium, expressed as a percentage of the added standard metal amount. The dry ashing procedure is identical for the three methods, which only differ at the ash solubilization stage. Of these methods, only Method A produced good results with calcium, since Method B had low recovery and Method C a relative standard deviation of ca. 27%.

The average total micrograms of the reagent blank metal levels for zinc, copper, cadmium, lead, iron, manganese, magnesium, and calcium were, respectively, for Method A: 0.11, 0.06, 0.03, 0.10, 0.22, 0.01, 0.60, and 0.37. For Method B, they were 0.12, 0.05, 0.03, 0.10, 0.25, 0.01, 0.63, and 0.40, and for Method C, they were 0.16, 0.08, 0.05, 0.15, 0.34, 0.02, 0.85 and 0.64.

The somewhat large relative standard deviations of the recoveries of most metals can be attributed to the fact that since the amount of recovered metal is obtained as the difference between two determined values, experimental errors reflected in both are cumulative. Such effect is especially pronounced in cases where the control tissue sample metal level is high in comparison with the amount added for the recovery test. See Table I.

Dry ashing conditions were selected with the aim of minimizing metal losses and achieving complete oxidation at the same time. Since no losses occur at 300 °C (*7*), this temperature was employed to reduce through charring the amount of organic matter in the sample, and thus eliminate the often vigorous reaction during treatment with nitric acid.

Since the chloride salts of some metals (*8*) are prone to losses during dry ashing, the chloride anion was eliminated by heating with nitric acid and evaporating it to dryness. The generated hydrogen chloride volatilizes (*9*) before all nitric acid is evaporated.

The addition of potassium sulfate permits the formation of nonvolatile cadmium sulfate and possibly other low volatility metal sulfates, which minimizes their loss at the ashing temperature. Moreover, potassium sulfate provided a matrix with a large air-exposed surface facilitating oxidation during the mild ashing at 400 °C and reduced any chemical interaction (*10*) of metals such as copper and iron with the vessel surface by limiting their contact with it. The low ashing temperature may also have contributed to reduction in metal–vessel surface interaction. Although such temperature necessitated longer ashing, the furnace was conveniently left in operation overnight. Further work can then be continued the next day with little extra time needed.

A second treatment with nitric acid is necessary to complete the ashing. The acid is evaporated and the sample heated at 400 °C in the furnace, which completes the oxidation. Evidently, occluded carbonaceous particles are exposed and further oxidation during heating in the furnace is accelerated. The ash, due to the presence of sulfates, phosphates, and pyrophosphates, did dissolve completely only in aqua regia, after two pretreatments with it—as indicated by the calcium results.

The above described dry ashing method has also been found to be useful in our laboratory for the preparation of microsamples of tissue and milk for anodic stripping voltammetry. Here, the ash is not dissolved in acids but is directly taken up in hot, pH 9 citrate-based supporting electrolyte (*11*) for the determination of cadmium, lead, zinc, and copper.

Preliminary results indicate that with suitable scale-up, larger samples or samples with more bone in them can be prepared by Method A. Similarly, we have also found that by heating the ash in aqua regia, adding sufficient water and reheating, the samples can be solubilized and the first two treatments with aqua regia used in Method A can be eliminated.

ACKNOWLEDGMENT

We thank Leslie W. Michael and Bernard Meiners of the Analytical Section for a helpful discussion.

LITERATURE CITED

(1) T. T. Gorsuch, "The Destruction of Organic Matter" Pergamon Press, New York, N.Y., 1970, pp 60–79, 93–99, 116–117, 121–129.
(2) Society for Analytical Chemistry, Analytical Methods Committee, *Analyst (London)*, **94**, 1153 (1969).
(3) T. T. Gorsuch, *Analyst (London)*, **84**, 135 (1959).
(4) J. E. Allen, "Agricultural Analysis", Varian Techtron Pty. Ltd., Springvale, Victoria, Australia, 1970, p 6.
(5) D. W. Yeager, J. Cholak, and B. G. Meiners, *J. Am. Ind. Hyg. Assoc.*, **34**, 450 (1973).
(6) E. E. Menden, L. Murthy, and H. G. Petering, unpublished data (1971).
(7) Ref. 1, pp 34–35, 78–79.
(8) Ref. 1, pp 35–36, 75–77, 97–99, 128.
(9) E. E. Menden and H. G. Petering, unpublished data (1976).
(10) Ref. 1, pp 35–39, 62–65, 77, 117, 128.
(11) E. E. Menden and H. G. Petering, unpublished data (1976).

RECEIVED for review April 15, 1977. Accepted June 13, 1977. Financial support for this work was provided by U.S. Public Health Service Grant No. ES-00159.

Small Volume, High Performance Cell for Nonaqueous Spectroelectrochemistry

Fred M. Hawkridge*

Department of Chemistry, Virginia Commonwealth University, Richmond, Virginia 23284

Jeanne E. Pemberton and Henry N. Blount*

Brown Chemical Laboratory, The University of Delaware, Newark, Delaware 19711

The growing need to reduce cell volumes while maintaining favorable cell transfer functions for aqueous spectroelectrochemical studies is being met by novel cell designs (*1*) and modifications thereon (*2*, *3*). The utility of such cells in nonaqueous work is most often limited by solvent attack of cell body material (e.g., Lucite). While cell bodies for nonaqueous work may be fabricated from Kel-F, Teflon, or high density polyethylene, newly available machinable glass-ceramic (Macor, Corning Glass Works, Corning, N.Y.) affords cell bodies for nonaqueous spectroelectrochemistry which have superior thermal and mechanical properties. This report describes the fabrication of such a cell and the comparison of its performance with that of a conventional glass spectroelectrochemical cell.

EXPERIMENTAL

Macor machinable glass-ceramic was obtained from Corning Glass Works. Conventional metal machining equipment and techniques (*4*) were employed in fabrication of a Macor cell similar in design to a previously described small volume Lucite spectroelectrochemical cell (*1*). The cell described here differed significantly from the previous one in that a circular platinum auxiliary electrode was located adjacent to the quartz rear window and encircled the optical beam. This auxiliary electrode placement afforded a much improved transfer function relative to the previously described cell. The volume of the Macor cell was 0.80 mL and had a working electrode area of 0.38 cm².

RESULTS

The electrochemical response of the Macor cell as evidenced by the oxidative cyclic voltammetry of 9,10-diphenylanthracene (DPA) was found to be identical to that of a conventional spectroelectrochemical cell (5) over a broad range of sweep rates.

Identical single potential step spectroelectrochemical (chronoabsorptometry) experiments were conducted using each cell wherein DPA was oxidized to the cation radical at a platinum OTE. The absorbance-time response predicted for such potential step perturbations is that given by Equation 1 (*6*)

$$A_{\mathrm{DPA}^{+\cdot}}(\lambda,t) = \frac{2}{\sqrt{\pi}}\, \epsilon_{\mathrm{DPA}^{+\cdot}}(\lambda) D^{1/2}{}_{\mathrm{DPA}} C^{\circ}{}_{\mathrm{DPA}}\, t^{1/2} \qquad (1)$$

where all terms have their usual meanings (6). Representative absorbance–time responses for the Macor and the conventional cells are shown in Figure 1, A and B, respectively, and the corresponding absorbance–time$^{1/2}$ behavior is shown in Figure 1, C and D. For eight independent trials using each cell, values of 27.38(±0.14) $M^{-1}\ s^{-1/2}$ and 27.09(±0.20) $M^{-1}\ s^{-1/2}$ were obtained for $\epsilon_{\mathrm{DPA}^{+\cdot}} D^{1/2}{}_{\mathrm{DPA}}$ in the Macor and conventional cells, respectively.

The removal of oxygen and its long-term exclusion from the Macor cell which is necessary for reductive work was demonstrated. Oxygen was vacuum outgassed from a pH 7.0 buffer (0.10 M phosphate, 0.10 M NaCl) and its subsequent presence in solution as a function of time was monitored voltammetrically at a tin oxide electrode. No oxygen was in evidence for a period of 3 h. The behavior of the Macor cell in this regard is superior to that of Lucite (*11*).

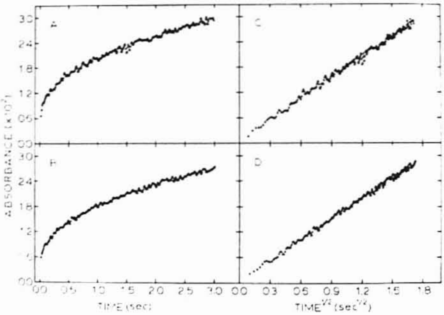

Figure 1. Spectroelectrochemical responses for potential step oxidation of DPA at Pt-OTE. Experimental techniques and instrumentation (*7*), electrode preparation (*8*), and materials (*9*, *10*) have been described. (A) absorbance–time response for potential step of +0.70 to +1.35 V vs. SCE in Macor cell. (B) Absorbance–time response for potential step of +0.70 to +1.35 V vs. SCE in conventional cell. (C) Fit of absorbance–time data from curve A (Macor cell) to Equation 1. Slope = 1.624(±0.008) × 10^{-2}; intercept = 6.1(±0.9) × 10^{-5}; coefficient of correlation = 0.9979. (D) Fit of absorbance–time data from curve B (conventional cell) to Equation 1. Slope = 1.601(±0.006) × 10^{-2}; intercept = 6.3(±0.7) × 10^{-5}; coefficient of correlation = 0.9981

DISCUSSION

The use of Macor as a material for the fabrication of small-volume cells for nonaqueous spectroelectrochemical work affords many advantages over other popular materials. The modest cost of this glass-ceramic (ca. $6 for the Macor used in the cell described here), the ease of machining (conventional metal machining techniques, water cooling), and the tolerances routinely obtained (±0.0005 in.) (*4*) permit the inexpensive fabrication of a wide variety of spectroelectrochemical cells. Unlike many ceramic materials, Macor does not require firing to insure nonporous surfaces. The dimensional stability of this material is superior to Kel-F, Teflon, and high density polyethylene such that high-torque screwing into tapped holes and high-stress clamping and similar manipulative operations can be easily executed.

Although cell volume minimization was not the thrust of the work reported here, smaller volume cells can be readily constructed which permit the electrochemical and spectroscopic characterization of minute amounts of material. This feature coupled with the extremely low gas permeability of this material gives rise to cells which are ideally suited for the vacuum outgassing necessary in bioelectrochemical work where anaerobic, hydrophobic conditions are required.

The temperature stability of Macor and its small coefficient of thermal expansion (*4*) make it an ideal cell body material both for the spectroelectrochemical examination of the temperature dependences of various electrochemically induced kinetic processes and for spectroelectrochemistry in fused salts, especially those of higher fusion temperatures. The inertness of this glass-ceramic toward acidic and basic materials (*4*) permits the use of less common electrochemical solvents such as trifluoroacetic acid or fluorosulfonic acid (*12*). No cell memory effects (e.g., adsorption, absorption) have been observed with the material.

Platinum is reported to adhere to Macor with excellent mechanical stability (*4*). This suggests the vapor deposition of auxiliary electrodes *within the cell body* in order to obtain electrode configurations necessary for optimal cell transfer functions. Moreover, in the course of this work it has been found that other materials can be readily attached to this glass-ceramic by conventional epoxy cement as well as high-vacuum epoxy-ceramic materials.

Like all small-volume cells used in spectroelectrochemical work, the contents of the cell described here are subject to infrared heating if allowed to remain in the spectral beam for extended periods. Use of an infrared filter in the optical path prior to the cell alleviates this problem, as does interruption of the analyzing beam by means of a shutter when no experiment is in progress.

LITERATURE CITED

(1) F. M. Hawkridge and T. Kuwana, *Anal. Chem.*, **45**, 1021 (1973).
(2) M. Fujihira and T. Kuwana, private communication, 1975.
(3) F. R. Shu and G. S. Wilson, *Anal. Chem.*, **48**, 1676 (1976).
(4) Corning Glass Works Technical Bulletin 9658, "Machining Instructions, MACOR Machinable Glass-Ceramic", Corning, N.Y. 14830.
(5) See, for example, T. Kuwana and N. Winograd in "Electroanalytical Chemistry", Vol. 7, A. J. Bard, Ed., Marcel Dekker, New York, N.Y., 1974, Figure 7, p 25.
(6) N. Winograd, H. N. Blount, and T. Kuwana, *J. Phys. Chem.*, **73**, 3456 (1969).
(7) J. F. Evans and H. N. Blount, *J. Phys. Chem.*, **80**, 1011 (1976).
(8) W. von Benken and T. Kuwana, *Anal. Chem.*, **42**, 1114 (1970).
(9) J. F. Evans, H. N. Blount, and C. R. Ginnard, *J. Electroanal. Chem.*, **59**, 169 (1975).
(10) T. Osa and T. Kuwana, *J. Electroanal. Chem.*, **22**, 389 (1969).
(11) F. M. Hawkridge, unpublished results.
(12) H. N. Blount et al., to be published.

RECEIVED for review March 14, 1977. Accepted June 20, 1977.

CORRECTION

Studies on the Mechanism of Atom Formation in Graphite Furnace Atomic Absorption Spectrometry

In this article by R. E. Sturgeon, C. L. Chakrabarti, and C. H. Langford, *Anal. Chem.*, 48, 1792 (1976), the proposed mechanism of formation of aluminum atoms given on p 1804 is wrong because of a miscalculation of thermodynamic data. However, this does not change the measured E_a values. Although no self-consistent mechanism for $Al_{(g)}$ formation that accounts for the observed E_a values can be advanced, it seems reasonable to postulate that one or more oxide species (AlO, Al_2O, Al_2O_2) may be involved, and also that $Al_{(g)}$ may be formed by direct thermal decomposition of $Al_2O_{3(s)}$.

CORRECTION

Gel Permeation Chromatography of Low Molecular Weight Materials with High Efficiency Columns

In this article by Anoop Krishen and Ralph G. Tucker (*Anal. Chem.*, **49**, 898 (1977)) the equation on page 899, column 2, should read:

$$\text{Molar Volume (mL/mol at 20 °C)} = 33.02 + 16.18\,(\text{CAU}) + 0.0041\,(\text{CAU})^2$$

CORRECTION

Determination of Thorium and Uranium in Ores and Mill Tailings by Alpha Spectrometry

In the paper by C. W. Sill, *Anal. Chem.*, **49**, 618 (1977), part of a sentence was omitted. On page 619, the sentence beginning on the tenth line from the bottom in the right-hand column should read as follows: "When dry, place the plate first on a hot plate covered with a piece of asbestos cloth for 1 min, then on an uncovered hot plate for about 5 min and cool."

Also, it now seems necessary to call attention to the need to correct the thorium-234 tracer recovered for that contributed by the sample itself when relatively large samples of uranium ores, uranium concentrates, or fresh mill tailings are being analyzed for thorium-230. With ores, or with concentrates older than a few months since the last chemical separations were made, the correction can be determined from the uranium-238 activity, if known. However, with concentrates in which the ingrowth of thorium-234 is unknown, with tailings less than a few months old from which the thorium-234 will not have decayed sufficiently, or if uranium-238 is not being determined, the correction must be determined by other means. The simplest way is to increase the thorium-234 added to about 10^5 dpm instead of the "at least 10^4 dpm" recommended previously. Because 0.27% uranium ore contains 2×10^3 dpm/g of thorium-234, the error will be less than 2% for samples up to 1 g, even if no corrections are applied. Similar arguments can be made for uranium concentrates and tailings. With larger samples or higher-grade ore, corrections will have to be made.

It should also be emphasized that this method for the determination of thorium-230 in uranium ore is not applicable to ores containing relatively high concentrations of natural thorium and/or the light lanthanides, e.g., uraniferous monazites. Unless the total quantity of these elements in the aliquot taken for analysis is kept less than about 1 mg, they will so saturate the barium sulfate lattice positions that precipitation of thorium-230 will be grossly incomplete. See *Anal. Chem.*, **41**, 1624 (1969) for effects of these elements on precipitations with barium sulfate. Also, the thorium, cerium, lanthanum, etc., carried in the barium sulfate form complexes with the potassium sulfate also present that are very insoluble in even hot 72% perchloric acid, making it appear that the barium sulfate fails to dissolve in the perchloric acid. Because of their solubility in water, however, the insoluble precipitates dissolve readily on addition of the strong aluminum nitrate solution.

Author Index

Achenbach, M. 1623
Allen, P. V. 1602
Anderson, P. J. 1623
Andrew, J. 1482
Andrews, J. E. 1536
Anson, F. C. 1589
Arguello, M. D. 1595
Arvanitis, S. 1567
Atsuya, I. 1489

Bicknell, R. 1551
Birks, L. S. 1505
Blaedel, W. J. 1563
Blount, H. N. 1646
Brockman, D. 1644
Brown, A. P. 1589
Bury, R. 1573
Buttrill, S. E., Jr. 1497

Campana, J. E. 1501
Cardone, M. J. 1640
Carmack, G. D. 1577
Choudhury, H. 1644

Dresbach, D. 1551
Duhamel, A. P. 1536

Erdtmann, G. 1510
Evans, C. A., Jr. 1514
Evans, J. F. 1632

Fernando, Q. 1636
Fishman, M. 1599
Fitch, W. L. 1623
Forrest, J. 1579
Freed, D. J. 1544
Freeman, D. H. 1637
Freiser, H. 1577
Fritz, J. S. 1595
Froehlich, P. M. 1606
Furr, A. K. 1507

Giam, C. S. 1540
Giam, P. Y. 1540
Goodwin, T. E. 1540
Gregory, R. P., IV 1608
Gunn, A. M. 1492
Gustafson, F. J. 1474

Hannaker, P. 1485
Hawkridge, F. M. 1646
Hirsch, R. F. 1549
Hughes, T. C. 1485

Ikeda, M. 1494
Iverson, D. G. 1563

Johansson, M. 1545
Jordan, J. 1573

Kawaguchi, H. 1489
Kira, S. 1494
Kirchner, S. J. 1636
Kirkbright, G. F. 1492
Knight, H. G. 1507
Krottinger, D. L. 1586
Ku, A. Y. 1637
Kuwana, T. 1632

Lamb, W. J. 1639
Laurence, D. F. 1557
Lavallee, D. K. 1482
Lawson, G. 1619
Linton, R. W. 1514
Littlejohn, M. A. 1536
Lowry, J. D. 1608

McCracken, M. S. 1586
McIntyre, N. S. 1521
Magnusson, P. 1545
Malmstadt, H. V. 1586, 1608
Menden, E. E. 1644
Miller, M. P. 1474
Morf, W. E. 1567
Morrison, G. H. 1529
Mujsce, A. M. 1544
Murphy, L. D. 1606

Natusch, D. F. S. 1514
Newman, L. 1579

Ogata, M. 1494
Ohmori, S. 1494
Opheim, L. N. 1492
Oteiza, R. M. 1586

Parkinson, T. F. 1507
Paschal, D. C. 1551
Pemberton, J. E. 1646
Petering, H. G. 1644
Petri, H. 1510
Phillips, C. S. G. 1549
Prescott, S. R. 1501
Price, P. C. 1497

Rindfleisch, T. C. 1623
Rion, K. F. 1540
Risby, T. H. 1501
Rulon, P. W. 1640

Sastri, C. S. 1510
Scilla, G. J. 1529
Sepaniak, M. J. 1554
Shiau, L-J. 1641
Siegfried, R. 1584
Simon, W. 1567
Smith, D. H. 1623
Smith, S. G. 1540
Spencer, R. 1599
Srinivasan, V. S. 1639
Stromberg, S. 1545
Swofford, H. S., Jr. 1497

Tallant, D. R. 1474
Thoma, A. P. 1567
Todd, J. F. J. 1619
Tsai, W-C. 1641

Vanderwielen, A. J. 1602
Vallee, B. L. 1489
Veillon, C. 1489
Vessman, J. 1545
Viviani-Nauer, A. 1567

White, D. C. 1615
Williams, P. 1514
Wright, J. C. 1474

Yeager, W. J. 1623
Yeung, E. S. 1554

Zetaruk, D. G. 1521
Zetlmeisl, M. J. 1557

Future Articles

Ultra-Trace Method for Lanthanide Ion Determination by Selective Laser Excitation

F. J. Gustafson and J. C. Wright

Trace Analysis of Nonfluorescent Ions by Selective Laser Excitation of Lanthanide Ions

J. C. Wright

Peak Broadening Factors in Thermal Field-Flow Fractionation

L. Smith, M. N. Myers, and J. C. Giddings

Square Wave Voltammetry at the Dropping Mercury Electrode: Theory

J. H. Christie, J. A. Turner, and R. A. Osteryoung

Determination of Sulfur in Environmental Materials by Thermal Neutron Capture Prompt Gamma-Ray Spectrometry

E. T. Jurney, D. B. Curtis, and E. S. Gladney

Combined Retrieval System for Infrared, Mass, and Carbon-13 Nuclear Magnetic Resonance Spectra

J. Zupan, D. Hadzi, M. Penca, and J. Marsel

Solution of General Equilibrium Systems by the System Equation

J. Blaha

Amperometric Measurement of Enzyme Reactions with an Oxygen Electrode Using Air Oxidation of Nicotinamide Adenine Dinucleotide

F. S. Cheng and G. D. Christian

Microprocessor-Controlled, Scanning Dye Laser for Spectrometric Analytical Systems

J. A. Perry, M. F. Bryant, and H. V. Malmstadt

Isotopic Assay of Nanomole Amounts of Nitrogen-15 Labeled Amino Acids by Collision Induced Dissociation Mass Spectrometry

J. H. McReynolds and M. Anbar

Determination of Nitrite by Direct Injection Enthalpimetry

L. D. Hansen, B. E. Richter, and D. J. Eatough

Determination of Sub-Microgram per Cubic Meter Levels of *N*-Nitrosodimethylamine in Air

R. L. Fisher, B. A. Lasoski, and R. W. Reiser

Computer Assignment of Elemental Compositions of Mass Spectral Peaks from Isotopic Abundances

I. K. Mun, R. Venkataraghavan, and F. W. McLafferty

Just flip a switch and do an entire titration automatically, even the calculations.

It could be just one, or as many as 44 acid/base, redox, colorimetric, conductometric or coulometric titrations.

It could be an end point, a pH stat or a Karl Fischer titration.

It could be a recording of the titration curve, or its first derivative.

Whatever the titration, Metrohm Titrators have the versatility and sensitivity to perform it automatically right to the final calculation at the touch of a switch.

In fact, there is hardly a titration procedure which Metrohm equipment, using appropriate accessories, cannot do more efficiently and conveniently. (A standard convenience feature of all Metrohm Titrators are the interchangeable 'snap-in' buret units, which permit repeated, non-stop change of titrants).

For a new 16-page brochure describing the complete line of Metrohm Recording Titrators and accessories, just write: Metrohm Division, Brinkmann Instruments, Cantiague Road, Westbury, N.Y. 11590. In Canada: 50 Galaxy Boulevard, Rexdale (Toronto), Ont.

A DIVISION OF
BRINKMANN
Metrohm Titrators

CIRCLE 20 ON READER SERVICE CARD

Dosimat E 535
Potentiog E 536
Metrohm
Brinkmann